

Christopher Jekeli

# Inertial Navigation Systems with Geodetic Applications



Walter de Gruyter · Berlin · New York 2001

**Author**

Dr. Christopher Jekeli  
Department of Civil & Environmental  
Engineering & Geodetic Science  
The Ohio State University  
470 Hitchcock Hall, 2070 Neil Avenue  
Columbus, Ohio 43210-1275  
USA

@Printed on acid-free paper which falls within the guidelines of the ANSI to ensure permanence and durability.

***Library of Congress Cataloging-in-Publication Data***

Jekeli, Christopher, 1953–  
Inertial navigation systems with geodetic applications / Christopher Jekeli.  
p. cm.  
Includes bibliographical references and index.  
ISBN 3110159031  
1. Earth – Figure – Measurement. 2. Inertial navigation – Mathematics. I. Title.  
QB283 .J45 2001  
526'.1–dc21

00-03 1644

***Die Deutsche Bibliothek – Cataloging-in-Publication Data***

Jekeli, Christopher:  
Inertial navigation systems with geodetic applications / Christopher Jekeli. – Berlin ; New York : de Gruyter, 2001  
ISBN 3-11-015903-1

© Copyright 2000 by Walter de Gruyter GmbH & Co. KG, 10785 Berlin, Germany

All rights reserved, including those of translation into foreign languages. No part of this book may be reproduced or transmitted in any form or by any means, electronic or mechanical, including photocopy, recording or any information storage and retrieval system, without permission in writing from the publisher.

Cover design: Rudolf Hübner, Berlin

Typesetting: ASCO Trade Typesetting Ltd., Hong Kong

Printing: Werner Hildebrand, Berlin

Binding: Lüderitz & Bauer-GmbH, Berlin

To my Mother and Father



## Preface

*It is amazing that gyros perform as well as they do.*

Wallace E Vander Velde, M.I.T., 1983.

The quote above is a beautiful expression and tribute to the engineering triumph in the latter half of the twentieth century of the mechanical gyroscope that is an integral part of the traditional inertial navigation system (INS). In today's technological age of lasers and digital electronics, having also benefited inertial sensors, high performance is almost expected; yet the most accurate navigation and guidance systems still rely on the mechanical predecessors of the modern optical gyro. On the other hand, robustness, reliability, efficiency, and, above all, cost-effectiveness belong to the new generation of sensors and open the opportunity for increased utility and wider application in commercial, industrial, and scientific endeavors. Concurrent with the technological innovations came new analytical tools, specifically the Kalman filter, that is tailor-made for the analysis, calibration, and integration of the inertial navigation system. In the last two decades, the Global Positioning System (GPS) has come to dominate the wide range of positioning and navigation applications, but the new inertial sensor technology has enabled a continuing and growing utilization of these marvelous instruments and has motivated a revival from a number of different perspectives, the geodetic one in the present case, especially in regard to their integration with GPS.

Geodesy, the science of the measurement and determination of the Earth's surface, now routinely relies on the exquisite accuracy extractable from GPS, but equally recognizes the advantages and opportunities afforded by including INS in several applications. Although the present book is ultimately dedicated to this goal, it should prove to be of equal value to non-geodesists who desire a thorough understanding of the mathematics behind the INS and its general use for precision navigation and positioning. In particular, an attempt is made with this book to join the principles of inertial technology and estimation theory that applies not only to an understanding of the dynamics of the sensors and their errors, but to the integration of INS with other systems such as GPS. The text is written by a geodesist who loves the application of mathematics and believes that an appreciation of these topics comes best with illustrative formulas that are derived from first principles. As such, considerable effort is devoted to establishing preliminary concepts in coordinate systems, linear differential equations, and stochastic processes, which can also be found readily in other eminent texts, but whose inclusion makes the present text essentially self-contained. With the mathematical details, and occasional numerical considerations, it is also hoped that the reader will obtain an appreciation for Vander Velde's statement, above, that may well be extended to the navigation system and further to its entire technological development—the achievements in inertial technology are truly amazing.

The text assumes that the reader is fluent in the differential and integral calculus, as well as the basic vector and matrix algebras. Undergraduate courses in calculus,

including the traditional advanced calculus, and linear algebra are, therefore, prerequisites to this text. Further minimal background in complex variables, differential equations, and numerical and statistical analyses, though not essential, would provide the reader with additional mathematical maturity to fully benefit from the material. The book may be used as a text for a college semester course at the senior or graduate level. Although mathematical derivations are given in detail, the old adage that mathematics is not a spectator sport should be followed by serious readers.

This text would not have materialized without the significant inspiration derived from my colleagues while working at the Air Force and at the Ohio State University. I would like to thank, in particular (affiliations are not necessarily current): Warren Heller, Jim White, Jacob Goldstein, Robert Shipp (TASC); Triveni Upadhyay, Jorge Galdos (Mayflower Communications, Inc.); David Gleason, Gerald Shaw (Air Force Geophysics Laboratory); Jim Huddle (Litton Guidance and Control, Inc.); Alyson Brown (NAVSYS Corp.); Klaus-Peter Schwarz (University of Calgary); Clyde Goad, Burkhard Schaffrin, Dorota Grejner-Brzezinska, C.K. Shum, Ren Da, Jin Wang, Jay Kwon (Ohio State University). In addition, several outstanding lecture notes by W. Vander Velde and A. Willsky (both at M.I.T.) have motivated key aspects of the mathematical understanding embodied in this text.

Columbus, Ohio; July 2000

C. Jekeli

# Contents

|           |   |    |
|-----------|---|----|
| <b>1</b>  | <b>Coordinate Frames and Transformations</b>      | 1  |
| 1.1       | Introduction                                      | 1  |
| 1.2       | Coordinate Frames                                 | 3  |
| 1.2.1     | Inertial Frame                                    | 3  |
| 1.2.2     | Earth-Centered-Earth-Fixed Frame                  | 6  |
| 1.2.3     | Navigation Frame                                  | 6  |
| 1.3       | Transformations                                   | 9  |
| 1.3.1     | Direction Cosines                                 | 10 |
| 1.3.2     | Euler Angles                                      | 11 |
| 1.3.3     | Quaternions                                       | 13 |
| 1.3.4     | Axial Vectors                                     | 18 |
| 1.3.5     | Angular Rates                                     | 19 |
| 1.4       | Differential Equation of the Transformation       | 20 |
| 1.5       | Specific Coordinate Transformations               | 22 |
| 1.6       | Fourier Transforms                                | 27 |
| <b>2</b>  | <b>Ordinary Differential Equations</b>            | 31 |
| 2.1       | Introduction                                      | 31 |
| 2.2       | Linear Differential Equations                     | 32 |
| 2.3       | General Solution of Linear Differential Equations | 33 |
| 2.3.1     | Homogeneous Solution                              | 35 |
| 2.3.1.1   | An Example  | 38 |
| 2.3.1.2   | Fundamental Set of Solutions                      | 39 |
| 2.3.2     | Particular Solution                               | 40 |
| 2.3.2.1   | The Example, Continued                            | 42 |
| 2.4       | Numerical Methods                                 | 44 |
| 2.4.1     | Runge-Kutta Methods                               | 45 |
| 2.4.2     | Numerical Integration of Functions                | 50 |
| <b>3</b>  | <b>Inertial Measurement Units</b>                 | 51 |
| 3.1       | Introduction                                      | 51 |
| 3.2       | Gyroscopes  | 53 |
| 3.2.1     | Mechanical Gyroscopes                             | 54 |
| 3.2.1.1   | SDF Gyro  | 56 |
| 3.2.1.1.1 | Principal Error Terms                             | 63 |
| 3.2.1.2   | TDF Gyro  | 65 |
| 3.2.2     | Optical Gyroscopes                                | 70 |

|           |  |     |
|-----------|--|-----|
| 3.2.2.1   | Ring Laser Gyro                                      | 73  |
| 3.2.2.1.1 | RLG Error Sources                                    | 77  |
| 3.2.2.2   | Fiber-Optic Gyro                                     | 81  |
| 3.2.2.2.1 | FOG Error Sources                                    | 85  |
| 3.3       | Accelerometer  | 86  |
| 3.3.1     | Accelerations in Non-Inertial Frames                 | 89  |
| 3.3.2     | Force-Rebalance Dynamics                             | 90  |
| 3.3.3     | Pendulous Accelerometer Examples                     | 93  |
| 3.3.4     | Vibrating Element Dynamics                           | 96  |
| 3.3.5     | Error Sources  | 99  |
| <b>4</b>  | <b>Inertial Navigation System</b>                    | 101 |
| 4.1       | Introduction   | 101 |
| 4.2       | Mechanizations                                       | 104 |
| 4.2.1     | Space-Stabilized Mechanization                       | 106 |
| 4.2.2     | Local-Level Mechanization                            | 106 |
| 4.2.2.1   | Schuler Tuning                                       | 107 |
| 4.2.2.2   | Wander Azimuth Mechanization                         | 110 |
| 4.2.3     | Strapdown Mechanization                              | 112 |
| 4.2.3.1   | Numerical Determination of the Transformation Matrix | 114 |
| 4.2.3.1.1 | A Second-Order Algorithm                             | 115 |
| 4.2.4.1.2 | A Third-Order Algorithm                              | 118 |
| 4.2.3.2   | Specializations                                      | 122 |
| 4.3       | Navigation Equations                                 | 123 |
| 4.3.1     | Unified Approach                                     | 124 |
| 4.3.2     | Navigation Equations in i-Frame                      | 126 |
| 4.3.3     | Navigation Equations in e-Frame                      | 126 |
| 4.3.4     | Navigation Equations in n-Frame                      | 126 |
| 4.3.5     | Navigation Equations in w-Frame                      | 131 |
| 4.3.6     | Numerical Integration of Navigation Equations        | 134 |
| <b>5</b>  | <b>System Error Dynamics</b>                         | 139 |
| 5.1       | Introduction   | 139 |
| 5.2       | Simplified Analysis                                  | 140 |
| 5.3       | Linearized Error Equations                           | 147 |
| 5.3.1     | Error Dynamics Equations in i-Frame                  | 151 |
| 5.3.2     | Error Dynamics Equations in e-Frame                  | 152 |
| 5.3.3     | Error Dynamics Equations in n-Frame                  | 153 |
| 5.4       | Approximate Analysis                                 | 157 |
| 5.4.1     | Effects of Accelerometer and Gyro Errors             | 159 |
| 5.4.2     | Vertical Velocity and Position Error Effects         | 161 |
| 5.4.3     | Essential Error Modes                                | 162 |

|          |  |     |
|----------|--|-----|
| <b>6</b> | <b>Stochastic Processes and Error Models</b> | 165 |
| 6.1      | Introduction                                 | 165 |
| 6.2      | Probability Theory                           | 165 |
| 6.2.1    | Gaussian Distribution                        | 170 |
| 6.3      | Stochastic Processes                         | 172 |
| 6.3.1    | Covariance Functions                         | 173 |
| 6.3.2    | Power Spectral density                       | 175 |
| 6.3.3    | Ergodic Processes                            | 176 |
| 6.4      | White Noise                                  | 177 |
| 6.5      | Stochastic Error Models                      | 179 |
| 6.5.1    | Random Constant                              | 180 |
| 6.5.2    | Random Walk                                  | 181 |
| 6.5.3    | Gauss-Markov Model                           | 182 |
| 6.6      | Gravity Models                               | 186 |
| 6.6.1    | Normal Gravity Field                         | 186 |
| 6.6.2    | Deterministic Gravity Models                 | 190 |
| 6.6.3    | Stochastic Gravity Models                    | 192 |
| 6.7      | Examples of IMU Error Processes              | 195 |
| <b>7</b> | <b>Linear Estimation</b>                     | 197 |
| 7.1      | Introduction                                 | 197 |
| 7.2      | Bayesian Estimation                          | 199 |
| 7.2.1    | Optimal Estimation Criteria                  | 200 |
| 7.2.2    | Estimation with Observations                 | 202 |
| 7.2.2.1  | A Posteriori Density Function                | 203 |
| 7.2.2.2  | A Posteriori Estimate and Covariance         | 205 |
| 7.3      | Discrete Kalman Filter                       | 207 |
| 7.3.1    | Observation Model                            | 209 |
| 7.3.2    | Optimal State Vector Estimation              | 210 |
| 7.3.2.1  | Prediction                                   | 212 |
| 7.3.2.2  | Filtering                                    | 213 |
| 7.3.2.3  | Smoothing                                    | 215 |
| 7.4      | Discrete Linear Dynamics Model               | 220 |
| 7.5      | Modifications                                | 223 |
| 7.5.1    | Augmented State Vector                       | 223 |
| 7.5.2    | Closed-Loop Estimation                       | 225 |
| 7.6      | A Simple Example                             | 227 |
| 7.7      | Continuous Kalman Filter                     | 230 |
| 7.7.1    | Covariance Function                          | 233 |
| 7.7.2    | Solution to Matrix Riccati Equation          | 235 |
| 7.7.2.1  | Constant Coefficient Matrices                | 235 |
| 7.7.2.2  | No System Process Noise                      | 236 |
| 7.7.2.3  | No Observations                              | 237 |

|           |  |     |
|-----------|--|-----|
| <b>8</b>  | <b>INS Initialization and Alignment</b>    | 238 |
| 8.1       | Introduction                               | 238 |
| 8.2       | Coarse Alignment                           | 240 |
| 8.3       | Fine Alignment and Calibration             | 243 |
| 8.3.1     | Acceleration Observations                  | 244 |
| 8.3.2     | Velocity and Azimuth Observations          | 246 |
| 8.3.3     | Kinematic Alignment                        | 252 |
| <b>9</b>  | <b>The Global Positioning System (GPS)</b> | 255 |
| 9.1       | Introduction                               | 255 |
| 9.2       | Global Positioning System                  | 259 |
| 9.2.1     | Clocks and Time                            | 259 |
| 9.2.2     | GPS Signals                                | 261 |
| 9.2.3     | GPS Receiver                               | 263 |
| 9.3       | GPS Observables                            | 266 |
| 9.4       | GPS Errors                                 | 269 |
| 9.5       | Combinations of Observations               | 273 |
| 9.5.1     | Dual-Frequency Pseudorange and Phase       | 275 |
| 9.5.2     | Single and Double Differences              | 278 |
| 9.6       | Kinematic Positioning                      | 282 |
| 9.6.1     | Dynamics Model                             | 284 |
| 9.6.2     | Observation Equations                      | 287 |
| 9.6.3     | Single-Receiver Case                       | 288 |
| 9.6.4     | Multiple-Receiver Case                     | 292 |
| <b>10</b> | <b>Geodetic Application</b>                | 295 |
| 10.1      | Introduction                               | 295 |
| 10.2      | Inertial Survey System                     | 297 |
| 10.2.1    | Historical Developments                    | 297 |
| 10.2.2    | Estimation Methods                         | 300 |
| 10.2.2.1  | Models and Observations                    | 300 |
| 10.2.2.2  | Parameter Estimation                       | 302 |
| 10.2.3    | Final Adjustments                          | 303 |
| 10.2.4    | Typical Results                            | 305 |
| 10.3      | GPS/INS Integration                        | 306 |
| 10.3.1    | Integration Modes                          | 308 |
| 10.3.1.1  | Decentralized Integration                  | 310 |
| 10.3.1.2  | Centralized Integration                    | 314 |
| 10.3.2    | Cycle Ambiguity Determination              | 318 |
| 10.4      | Moving-Base Gravimetry                     | 320 |
| 10.4.1    | Gravitation from Inertial Positioning      | 323 |

|                   |                                |     |
|-------------------|--------------------------------|-----|
| 10.4.2            | Gravitation from Accelerometry | 327 |
| 10.4.2.1          | Kalman Filter Approaches       | 330 |
| 10.4.2.2          | Scalar Gravimetry              | 334 |
| <i>References</i> |                                | 336 |
| <i>Index</i>      |                                | 343 |

## About the Author

Christopher Jekeli received his Ph.D. degree in Geodetic Science at the Ohio State University in 1981, after which he was employed as research scientist at the Air Force Geophysics Laboratory, Bedford, Massachusetts, until 1993. There he led analysis teams associated with the airborne gravity gradiometer projects sponsored by the Defense Mapping Agency (now National Imagery and Mapping Agency) and non-Newtonian gravity experiments. In 1993 he became associate professor at Ohio State University (professor since 1998) in the Department of Geodetic Science and Surveying, now the Department of Civil and Environmental Engineering and Geodetic Science. His teaching and research interests and specializations include global and local gravity modeling and measurement, geoid determination, gravimetric spectral analysis, satellite geodesy, inertial navigation systems, GPS, and geodetic reference systems.

He is a Fellow of the International Association of Geodesy (IAG) and serves on its executive committee and as president of study groups in airborne gravimetry and the theory of height systems. Christopher Jekeli was a member of the National Research Council Committee on Geodesy and holds membership with the American Geophysical Union and the Institute of Navigation. He was associate editor of the *Journal of Geodesy* (formerly *Bulletin Géodésique* and *Manuscripta Geodaetica*) and publishes regularly in the fields of gravimetric geodesy and theory.

# 1 Coordinate Frames and Transformations

## 1.1 Introduction

When describing locations of points on or near the Earth's surface, we most naturally turn to a system of coordinates. Although one could imagine devising a relational or synthetic data base to describe the whereabouts of objects and places, it is of necessity that we assign an algebraic system of coordinates if we wish to go beyond mere location information and obtain measures of distance, area, volume, and direction. And, likewise with navigation, we need to define a coordinate system in which we can measure our progress and easily determine our course and destination. There are several coordinate systems from which to choose. Each has its own unique utility depending on the particular application in a particular discipline. In geodesy we deal with determining positions, or the mathematics of map projections, or the navigation of a vehicle, or its guidance along a predefined path. Specific coordinate systems must be defined in each case.

We will be concerned primarily with the *Cartesian*, or *rectangular*, coordinates, whose axes are mutually orthogonal by definition, but this triad of axes, as shown in Figure 1.1, may assume a variety of orientations in space. The axes of any coordinate system are designated here generally in numerical order as the 1-axis, the 2-axis, and the 3-axis. Each system of axes is defined to be right-handed in the sense that a  $90^\circ$ -counterclockwise (positive) rotation about the 1-axis, as viewed along the 1-axis toward the origin, rotates the 2-axis into the 3-axis. Also, a  $90^\circ$  rotation about the 2-axis rotates the 3-axis into the 1-axis; and, a  $90^\circ$  rotation about the 3-axis rotates the 1-axis into the 2-axis.

We will denote the set of Cartesian coordinates by a lower-case subscripted letter, such as  $x_j$ ,  $j = 1, 2, 3$ . The corresponding bold letter,  $\mathbf{x}$ , will denote a vector with  $x_j$  as components (see Figure 1.1). Also shown in Figure 1.1 is a set of special vectors, called *unit vectors*, denoted by  $\mathbf{e}_j$ ,  $j = 1, 2, 3$ . Each unit vector has only one non-zero component, namely the  $j$ -th component equals 1; that is,  $\mathbf{e}_j$  is directed along its respective axis and has unit length.

The vector representation of  $\mathbf{x}$  as an ordered triplet of coordinates is

$$\mathbf{x} = \begin{pmatrix} x_1 \\ x_2 \\ x_3 \end{pmatrix}. \quad (1.1)$$

Or, using the unit vectors, we may also write:

$$\mathbf{x} = x_1 \mathbf{e}_1 + x_2 \mathbf{e}_2 + x_3 \mathbf{e}_3, \quad (1.2)$$

where it is clear that the coordinates,  $x_j$ , are the orthogonal projections of  $\mathbf{x}$  onto the respective axes. It is assumed that the reader is familiar with vector (and matrix) algebra, including the usual operations of addition, subtraction, and multiplication

## 2 1 Coordinate Frames and Transformations

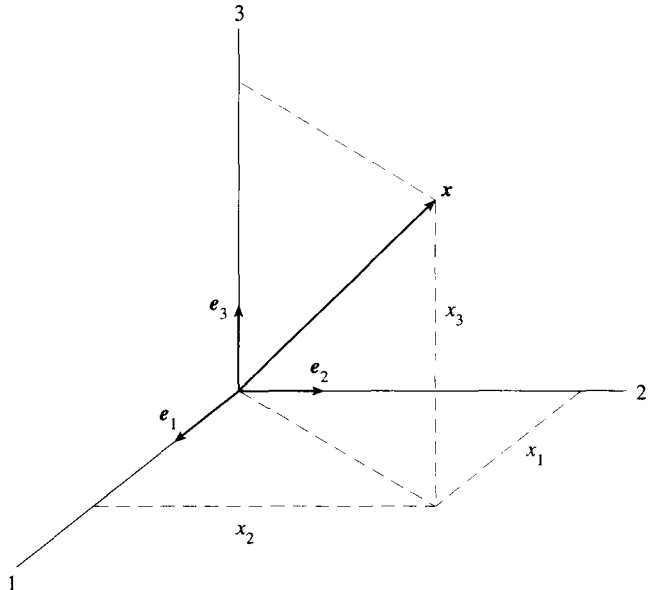


Figure 1.1: Cartesian coordinates of vector  $\mathbf{x}$ , and unit vectors  $e_j$ .

(scalar or dot product, vector or cross product, as well as matrix multiplication and inversion). For a review of these algebras, see Lang (1971).

Before proceeding, a few additional introductory remarks are in order. The geodetic/astronomic conventional usage of the terms coordinate *system* and coordinate *frame* will be followed (Moritz and Mueller, 1987). The *system* includes the conventions and physical theories, or their approximations and models, that are used to define the triad of coordinate axes; while a *frame* denotes the accessible realization of the system through a set of points whose coordinates are monumented or otherwise observable. The general principles and methodologies of determining a coordinate (or, reference) system are beyond the scope of this text, and it is enough to know for present purposes that each set of coordinate axes is well-defined and accessible, and represents a coordinate frame. In the navigation literature reference is often made to frames instead of systems, a convention also adhered to in this text, where we will understand that for each frame there is a system in the background.

The frames that we will deal with are either global or local in extent, where the “extent” is largely defined by the application and the accuracies desired. The global Cartesian coordinates are tied either to the rotating Earth or to the celestial sphere (“fixed” stars); the local Cartesian coordinates are defined by local directions, such as north, east, and down. In addition, we consider curvilinear coordinates as alternative descriptors of points in space—we do not use these to characterize the intrinsic properties of surfaces (or space) which is perhaps their more pertinent

mathematical (differential geometric) application; rather, their use is motivated by the fact that our motions and positions are generally close to being on a spherical or ellipsoidal surface. These coordinates are still three-dimensional and serve mostly to facilitate computations and derivations, besides having their own historical significance. The curvilinear coordinates are either the spherical polar coordinates, or more appropriately, the geodetic coordinates latitude, longitude, and height (these will be defined precisely in Section 1.2).

When considering inertial navigation systems, various additional coordinate frames enter; for example, those of the navigation instruments, of the platform on which they are mounted, and of the vehicle carrying the platform. Each of these is almost always a Cartesian frame. One of the main problems, as might already be apparent, is to relate each frame to all other relevant frames so that measurements in one frame can be transferred, or formulated, in the frame most appropriate to the end use of the information they provide. This entails the topic of *transformations* (Section 1.3). First, we define each coordinate frame more explicitly.

## 1.2 Coordinate Frames

Our application of coordinate frames centers on *geodesy*, the science of the measurement, determination, and mapping of coordinates of points on or near the Earth's surface. We extend this abbreviated, formal definition, paraphrased from a definition due to F.R. Helmert (1880), by including the kinematic and dynamic positioning of points along a trajectory, that is, *navigation*. By navigation we usually mean positioning in real time, or almost instantaneously; but, navigation systems clearly can be used for positioning in a post-mission application. In either case, by concerning ourselves with motion, we immediately invoke certain basic physical laws; and, as we will see, *gravitational* acceleration plays a significant role.

### 1.2.1 Inertial Frame

We start with the most fundamental coordinate system in geodesy, appropriately, the *inertial system*, defined classically as that system in which Isaac Newton's laws of motion hold. The Newtonian definition of the inertial system implies a Euclidean (Galilean) system, defined as a system with coordinates satisfying Euclidean geometry. In such a system, a body at rest (or, in uniform rectilinear motion) will remain at rest (respectively, in uniform rectilinear motion) in the absence of applied forces. This is Newton's *First Law of Motion*.

In addition, the dynamics of the motion in this system can be formulated on the basis of Newton's Second and Third Laws of Motion. Specifically, Newton's *Second Law of Motion* (Goldstein, 1950) states that the time-rate of change of the linear momentum of a particle equals the sum of applied forces,  $\mathbf{F}$ :

$$\mathbf{F} = \frac{d}{dt}(m_i \dot{\mathbf{x}}), \quad (1.3)$$

## 4 1 Coordinate Frames and Transformations

where  $m_i\ddot{\mathbf{x}}$  is the particle's linear momentum, being the product of  $\dot{\mathbf{x}}$ , its velocity, and  $m_i$ , its inertial mass. (Dots above a variable denote differentiation with respect to time—once with one dot, twice with two dots, etc.) If no forces act on the particle, its linear momentum is a constant (*Law of Conservation of Linear Momentum*).

Assuming the mass is a constant, we also have a slightly more familiar, though less correct form of Newton's Second Law,

$$m_i\ddot{\mathbf{x}} = \mathbf{F}, \quad (1.4)$$

showing that the acceleration,  $\ddot{\mathbf{x}}$ , of a particle in an inertial system is directly proportional to  $\mathbf{F}$ . Besides providing the foundation for the inertial coordinate system, these classical laws of Newton's form the basis for describing the dynamics of the inertial measurement units (Chapter 3).

In our world, a global inertial system is at best an abstraction, since any frame in the vicinity of the solar system is permeated by a gravitational field that possesses spatially varying gradients. For example, in the frame attached to the center of mass of the solar system and assumed to be non-rotating, a body initially at rest or in uniform rectilinear motion will accelerate under the gravitational influence of the sun and planets (thus violating Newton's First Law); and therefore, this frame is not inertial. The gravitational acceleration, like the centrifugal or coriolis acceleration, is not due to an externally applied physical action as meant by  $\mathbf{F}$  in (1.3), but rather it is a consequence of a field, in this case, the gravitational field, and belongs to the class of *kinematic forces* (Martin, 1988) that cause accelerations that are independent of the mass being accelerated.

In order to proceed, then, with the classical approach, it is necessary to modify Newton's Second Law (just as it is sometimes modified in a rotating frame to account for centrifugal and coriolis accelerations). Equation (1.4) is changed to account for the acceleration due to an ambient gravitational field:

$$m_i\ddot{\mathbf{x}} = \mathbf{F} + m_g\mathbf{g}. \quad (1.5)$$

The gravitational acceleration vector,  $\mathbf{g}$ , can be thought of as the “proportionality factor” between the gravitational mass,  $m_g$ , and the resulting gravitational force,  $\mathbf{F}_g$ , as formulated by Newton's *Law of Gravitation* (inverse square law):

$$\mathbf{F}_g = k \frac{m_g M}{\ell^2} \mathbf{e}_\ell = g m_g, \quad (1.6)$$

where the gravitational field is generated by the particle mass,  $M$ , a distance  $\ell$  from  $m_g$ , and where  $\mathbf{e}_\ell$  is the unit vector along the line joining the two particles and  $k$  is a constant (Newton's gravitational constant) that accommodates our particular choice of units.

With the (weak) Principle of Equivalence one may speak of just one kind of mass,  $m_i = m_g = m$ , and we have

$$\ddot{\mathbf{x}} = \mathbf{a} + \mathbf{g}, \quad (1.7)$$

where  $\mathbf{a} = \mathbf{F}/m$  is the acceleration due to an applied force, or a force of physical action;  $\mathbf{a}$  is also known as the *specific force* (force per unit mass). Examples of specific forces include atmospheric drag, the lift provided by an aircraft wing, and the “reaction force” the Earth’s surface exerts on us to keep us from falling toward its center.

A note on terminology is in order here. Appearing in the geodetic literature (e.g., Moritz and Mueller, 1987) is the designation *quasi-inertial* frame, referred to as the Earth-centered frame accelerating, but not rotating, around the sun, being “practically inertial” because, relativistically speaking, the gravitational field of the solar system is relatively weak and the curvature of space-time is very small so that classical Newtonian dynamics hold. While this nomenclature may be adequate for the frame itself, it is unsatisfactory when considering objects moving in this frame. For clearly, if inertial frames are defined by Newton’s First Law of Motion, as was done at the beginning of this section, and since gravitational attraction is *not* an applied force—it is a field, or a part of the space we live in, then even in an approximate sense, we generally do not encounter inertial frames, as illustrated above. If we wish to continue with classical methods (as we do here), we must always modify Newton’s laws to account for gravitation. Fortunately, because of the Principle of Equivalence, this is easy to do. But, strictly speaking these frames are not inertial, nor quasi-inertial. Perhaps a better nomenclature is *pseudo-inertial* frame (much like the pseudorange in the glossary of the Global Positioning System (GPS, see Chapter 9) that means a measured range containing the effect of a clock bias).

Recognizing and understanding its origins, we will retain the name *inertial frame* (or, *i-frame*) for the frame that is attached to the Earth’s center, is in *free-fall*, and is not rotating. The frame is freely falling in the gravitational fields of the sun, moon, and planets. The  $\mathbf{g}$  in (1.7) includes the Earth’s gravitational acceleration, as well as the differences in solar, lunar, and planetary gravitational accelerations (tidal accelerations) relative to the Earth’s center. The frame’s orientation is fixed to the celestial sphere as realized by the observed directions of *quasars*, extremely distant celestial objects that have not shown any evidence of changing their relative orientation. The coordinates of a point in the *i-frame* are components of the vector designated  $\mathbf{x}^i$ . The superscript denotes the frame in which the coordinates are expressed.

The International Earth Rotation Service (IERS) establishes the “*inertial*” system, or the International Celestial Reference System (ICRS), using an adopted set of directions defined by extragalactic radio sources (McCarthy, 1996; Feissel and Mignard, 1998), such that the 3-axis (the North Celestial Pole) and the 1-axis (on the celestial equator) are close to traditional definitions. The system is realized by a catalogue of 608 quasars whose directions are determined using the technique of Very Long Baseline Interferometry and by the coordinates of some 120,000 stars published in the Hipparcos Catalogue. The ITRS (Section 1.2.2) is connected to the ICRS using adopted theories and conventions for the nutation and precession of the Earth’s spin axis and orbit in space, as well as the motion of the pole with respect to the Earth’s surface. Formally, the origin of the ICRS is the center of mass of the solar system in order to be consistent with the definition of dynamic time which is the

time argument in the theories of planetary motion. This difference of origins for the  $i$ -frame has no practical consequence in this presentation.

### 1.2.2 Earth-Centered-Earth-Fixed Frame

Next we consider a frame that is fixed to the Earth; its origin is also at the Earth's center of mass. Its coordinate axes are defined by convention such that the 3-axis is a mean, fixed, polar axis; and, on the corresponding equator a zero-longitude is defined that specifies the location of the 1-axis (and the mean Greenwich meridian). The mean polar axis intersects the Earth's surface at the *Conventional International Origin* (CIO) and is close to the spin axis that deviates variously from this fixed point due to *polar motion* (Moritz and Mueller, 1987).

The designation of a coordinate vector in the so-called *Earth-centered-Earth-fixed* (ECEF) frame, or *e-frame*, is  $\mathbf{x}^e$ . Historically, Earth-fixed coordinate systems (not necessarily geocentric) were realized through the definition of a *geodetic datum* (Torge, 1991), whereby the adopted coordinates of one or more points (in the sense of an adjusted minimal constraint) on the Earth's surface served the function of defining the origin. Today, the IERS establishes the so-called *International Terrestrial Reference System* (ITRS), which is realized through satellite laser ranging systems, as well as GPS and other satellite systems; therefore, it is geocentric. The International Terrestrial Reference Frame (ITRF) is based on a set of globally distributed observatories whose coordinates are corrected also for crustal motion due to plate tectonics (McCarthy, 1996).

### 1.2.3 Navigation Frame

The frame that is commonly used to describe the navigation of a vehicle is a *local* coordinate frame. To define this properly, we first consider global (or, historically, also regional) geodetic reference systems. Conventional geodetic reference systems consist of curvilinear coordinates  $(\phi, \lambda)$  that define the direction of the normal (i.e., the perpendicular) to an adopted ellipsoid of revolution (see Figure 1.2). The parameters of this ellipsoid, defining its scale and shape, are chosen so that it approximates the zero-height level surface (the *geoid*) of the Earth.

The *geodetic latitude*,  $\phi$ , of a point is the angle in the meridian plane of the normal through the point, with respect to the equator, positive northward or negative southward. The *geodetic longitude*,  $\lambda$ , is the angle in the equatorial plane from the Greenwich meridian (containing the  $1^e$ -axis) to the meridian plane of the point. The *ellipsoid height*,  $h$ , is the distance from the ellipsoid along the normal to the point. The coordinates  $(\phi, \lambda, h)$  constitute an orthogonal set of coordinates. They could be used in place of the Cartesian coordinates,  $\mathbf{x}^e$ , to describe positions in the *e-frame*, provided that a particular ellipsoid has been specified and that it is geocentric (i.e., its origin is the Earth's center of mass). The transformation between  $(\phi, \lambda, h)$  and  $\mathbf{x}^e$  is given in Section 1.5.

The local system of coordinates may now be defined as a set of Cartesian coordinate axes, where the third axis is aligned with the ellipsoidal normal at a point, in the "down" direction, the first axis points due north (parallel to the tangent to the

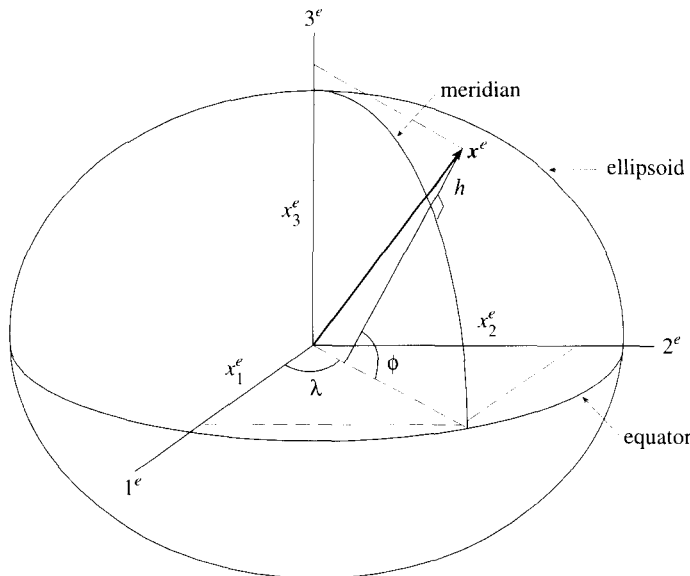


Figure 1.2: Earth-fixed-Earth-centered coordinates and geodetic coordinates with respect to an Earth Ellipsoid.

meridian), and the second axis points east (Figure 1.3). An alternative to north-east-down (NED) is south-east-up, where the positive 3-axis points up, and the frame is again right-handed. In contrast, geodesists often use local north-east-up frames for astronomic-geodetic observations; these are left-handed frames and will not be considered. The north-east-down frame, adopted here and conventionally implemented in the field of inertial navigation, is known as the *navigation frame*, or the *n-frame*. The origin of the *n*-frame is local, either on the ellipsoid, or at the location of the navigation system (as shown in Figure 1.3).

Note that the 3-axis of the *n*-frame does not pass through the Earth's center of mass. This adds a complication to the transformation of coordinates of points between the *n*-frame and the *e*-frame. But more important, the *n*-frame is not used generally to coordinatize a vehicle's *position*. Instead, one should visualize the *n*-frame such that the 3-axis always moves with the vehicle carrying the navigation system. The purpose of the *n*-frame primarily is to provide local directions, north, east, down, along which *velocities* may be indicated. This is particularly useful in those navigation systems that are mechanized such that the sensors are always aligned with the local horizon and vertical. As we will see, the same utility of the *n*-frame is offered through computational means to systems that are arbitrarily mechanized. In addition, the *n*-frame also serves as a common reference frame to which platform and sensor frames may be related.

With this special consideration of the *n*-frame, its relative *orientations* with respect to the *e*-frame and the *i*-frame are of primary importance. The vector  $x^n$  is not used to coordinatize the vehicle's position except in a formal sense because by definition only its third component might be non-zero.

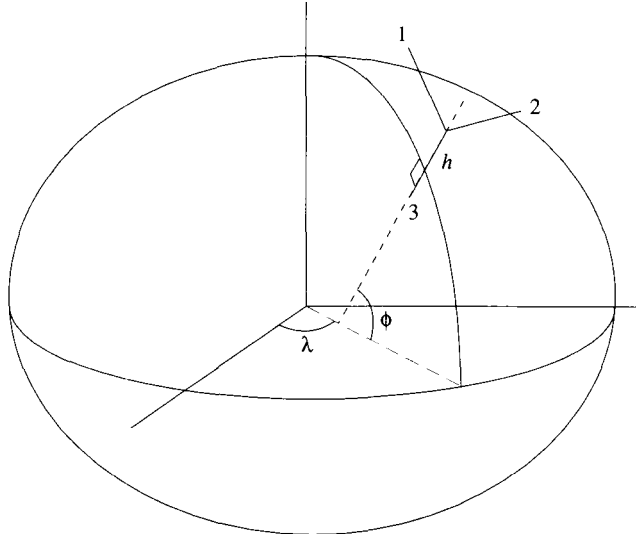


Figure 1.3: Local north-east-down coordinate frame.

In addition to these basic frames, one can associate, as already mentioned, Cartesian (orthogonal) coordinate frames with each of the various components of the measurement system and the vehicle carrying it (AFSC, 1992). The *body frame*, or *b-frame*, generally refers to the vehicle to be navigated. The axes conventionally are defined along the forward, right, and through-the-floor directions (see Figure 1.4, also Figure 1.8). The *sensor frame* is a single representative, analytic frame for the navigation system. It is used to model and identify instrument errors in a unified frame for analytical purposes like filtering. In the case of a strapdown system (Section 4.2.4) the sensor frame may be identified with the body frame, and in the case of a local-level gimbaled system (Section 4.2.2) the sensor frame usually corresponds to the navigation frame.

The instruments of an inertial navigation system (INS) are accelerometers and gyroscopes; the accelerometers measure accelerations that are integrated to yield positions and the gyroscopes provide information on the orientation of the accelerometers (see Chapter 3). Each set of instruments, accelerometers and gyroscopes, has its own coordinate system. The *accelerometer frame* is taken to be orthogonal, but with the realization that the sensitive axis of only one accelerometer will be aligned with a frame axis (1-axis), while the others may be misaligned with respect to the corresponding frame axes. This non-orthogonality of the instruments is determined with special calibration procedures. The origin of the accelerometer frame is the point of specific force computation for the accelerometers. The *gyro frame* similarly is orthogonal with only one of the input axes aligned along a frame axis (1-axis). The origin of the gyro frame is the same as the accelerometer frame. For purposes of understanding the operation of each instrument, we introduce

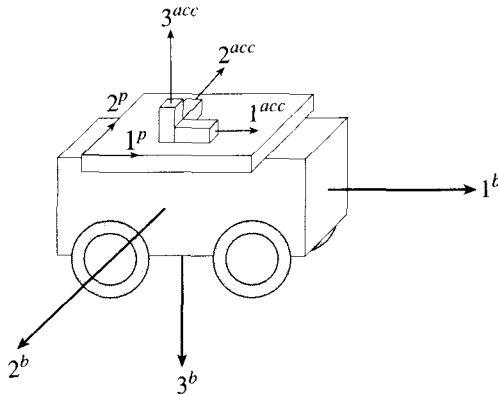


Figure 1.4: Typical relationships between body, platform, and IMU frames.

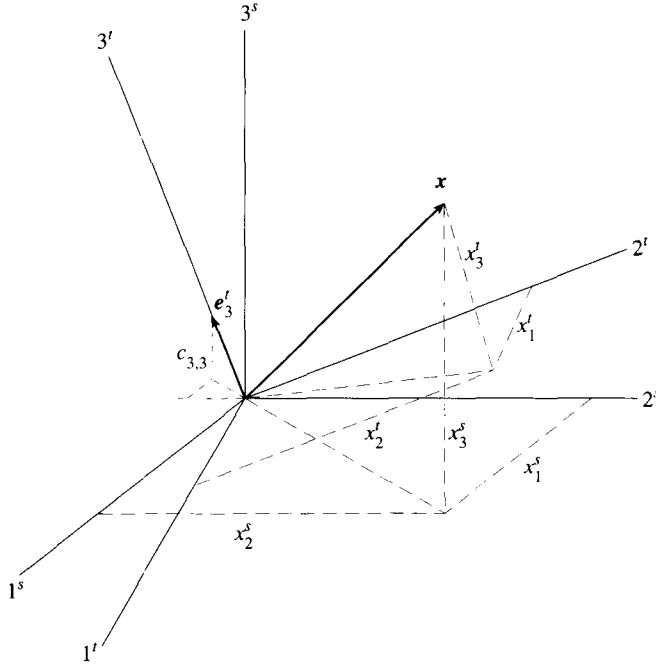
individual *instrument frames* that serve also to define the input and output axes for each accelerometer and gyroscope. Finally, the *platform frame* (or, chassis frame) provides a physical set of fiducial axes that provide a common origin for the instrument cluster.

In each case the coordinates of a point in the respective frame are the components of a corresponding vector with an appropriate superscript. Ultimately, to perform inertial navigation, the measurements coordinatized in the instrument frames must be transformed into useful data in an Earth-fixed frame. This requires, first of all, the development of transformations among coordinate frames, which is the topic of the next sections.

### 1.3 Transformations

Several possibilities exist to define the transformation of coordinates from one frame to another. Of primary concern is their relative orientation. There may also be a translation between corresponding origins, but this is described simply by a vector of coordinate differences that is applied equally to all points in a frame. There will, in general, be no need to consider different scales, the scale being universally defined for all systems by convention such as by the *Bureau International des Poids et Mesures* (BIPM, 1991). (One sensor of a particular type may yield differently scaled data than another of the same or different type, but rather than endowing each coordinate frame with its own scale, the data themselves are associated with a scale parameter.)

Because the coordinate frames under consideration are orthogonal, three angles suffice to describe their relative orientation. The transformation is linear and can be achieved with direction cosines, rotation (Euler) angles, or quaternions (where four dependent parameters are used). Although quaternions will be discussed in some detail in this chapter and will be used in Chapter 4, analyses and investigations of

Figure 1.5: Coordinate frames  $s$  and  $t$ .

applications in inertial geodesy will mostly concern the use of direction cosines and rotation angles, since they are entirely adequate in these considerations, referring generally to dynamically benign environments.

### 1.3.1 Direction Cosines

Consider two concentric frames, say, the  $s$ -frame and the  $t$ -frame, whose relative orientation is arbitrary (Figure 1.5). Let the coordinates of a point be represented by the vector,  $\mathbf{x}^s$ , in the  $s$ -frame, and by the vector,  $\mathbf{x}^t$ , in the  $t$ -frame:

$$\mathbf{x}^s = \begin{pmatrix} x_1^s \\ x_2^s \\ x_3^s \end{pmatrix}; \quad \mathbf{x}^t = \begin{pmatrix} x_1^t \\ x_2^t \\ x_3^t \end{pmatrix}. \quad (1.8)$$

The coordinates of the point in either frame are the orthogonal projections of the vector onto the respective axes of the frame, as in (1.2):

$$\mathbf{x}^s = x_1^s \mathbf{e}_1^s + x_2^s \mathbf{e}_2^s + x_3^s \mathbf{e}_3^s, \quad (1.9)$$

$$\mathbf{x}^t = x_1^t \mathbf{e}_1^t + x_2^t \mathbf{e}_2^t + x_3^t \mathbf{e}_3^t, \quad (1.10)$$

where, e.g.,  $x_j^s = \mathbf{e}_j^s \cdot \mathbf{x}^s$ ,  $j = 1, 2, 3$  are the coordinates in the  $s$ -frame and  $\mathbf{e}_j^s$ ,

$j = 1, 2, 3$  are corresponding unit vectors along the axes of the frame; similarly for the  $t$ -frame.

Analogously, the coordinates of the  $t$ -frame unit vector,  $\mathbf{e}_k^t$ , in the  $s$ -frame are

$$c_{j,k} = \mathbf{e}_j^s \cdot \mathbf{e}_k^t, \quad (1.11)$$

so that:

$$\mathbf{e}_k^t = c_{1,k} \mathbf{e}_1^s + c_{2,k} \mathbf{e}_2^s + c_{3,k} \mathbf{e}_3^s. \quad (1.12)$$

If we substitute (1.12) for each  $k$  into (1.10) and compare the result with (1.9), we obtain the transformation between coordinates, written in vector form as

$$\mathbf{x}^s = C_t^s \mathbf{x}^t, \quad (1.13)$$

where the *transformation matrix* is given by

$$C_t^s = \begin{pmatrix} c_{1,1} & c_{1,2} & c_{1,3} \\ c_{2,1} & c_{2,2} & c_{2,3} \\ c_{3,1} & c_{3,2} & c_{3,3} \end{pmatrix}. \quad (1.14)$$

Note how the particular index notation on  $C_t^s$  signifies the original frame (lower index) and the transformed frame (upper index). We may say that the lower index of  $C_t^s$  “cancels” and the upper index “replaces” the frame index of the vector.

From (1.11) and the property of the scalar product of vectors, we see that the coefficient,  $c_{j,k}$ , is the cosine of the angle between the  $j^{\text{th}}$   $s$ -frame axis and the  $k^{\text{th}}$   $t$ -frame axis.  $C_t^s$  may be called more specifically the *direction cosine matrix*. Note also that the  $k^{\text{th}}$  column of  $C_t^s$  represents the unit vector  $\mathbf{e}_k^t$  in the  $s$ -frame; and the  $j^{\text{th}}$  row of  $C_t^s$  represents the unit vector  $\mathbf{e}_j^s$  in the  $t$ -frame. Hence the columns are mutually orthogonal, as are the rows; and the matrix,  $C_t^s$ , is an orthogonal matrix:

$$C_t^s (C_t^s)^T = I \Rightarrow C_s^t \equiv (C_t^s)^{-1} = (C_t^s)^T. \quad (1.15)$$

The orthogonalities imply that the nine elements in  $C$  are dependent, that is, the relative orientation is governed by only three degrees of freedom.

The transformation of any 3-by-3 matrix,  $A$ , under an orthogonal frame transformation can now be derived as follows. Let  $\mathbf{y}^t = A^t \mathbf{x}^t$ . Then, using (1.13) and (1.15), we have

$$\mathbf{y}^t = A^t \mathbf{x}^t \Rightarrow C_s^t \mathbf{y}^s = A^t C_s^t \mathbf{x}^s \Rightarrow \mathbf{y}^s = C_t^s A^t C_s^t \mathbf{x}^s. \quad (1.16)$$

From this, it follows that

$$A^s = C_t^s A^t C_s^t. \quad (1.17)$$

### 1.3.2 Euler Angles

The relative orientation of the  $s$ - and  $t$ -frames could also be described by a sequence of rotations. Therefore, an alternative to the direction cosine matrix transformation is the successive application of rotation matrices about specific axes. The rotation

matrices for each of the axes are given by

$$R_1(\theta) = \begin{pmatrix} 1 & 0 & 0 \\ 0 & \cos \theta & \sin \theta \\ 0 & -\sin \theta & \cos \theta \end{pmatrix}; \quad R_2(\theta) = \begin{pmatrix} \cos \theta & 0 & -\sin \theta \\ 0 & 1 & 0 \\ \sin \theta & 0 & \cos \theta \end{pmatrix};$$

$$R_3(\theta) = \begin{pmatrix} \cos \theta & \sin \theta & 0 \\ -\sin \theta & \cos \theta & 0 \\ 0 & 0 & 1 \end{pmatrix}. \quad (1.18)$$

$R_j(\theta)$  represents the rotation about the  $j$ -th axis by the angle  $\theta$ , positive in the counterclockwise sense as viewed along the axis toward the origin (right-hand rule). Clearly, each  $R_j(\theta)$  is a specialized direction cosine matrix. It is orthogonal:  $R_j^{-1}(\theta) = R_j^T(\theta)$ ; and, the inverse is also the “reverse rotation”:  $R_j^{-1}(\theta) = R_j(-\theta)$ . Now, for example, if the  $s$ -frame is the result of rotating the  $t$ -frame, first about the 1-axis by  $\alpha$ , then about the (new) 2-axis by  $\beta$ , and finally about the (even newer) 3-axis by  $\gamma$ , the total transformation matrix from the  $t$ -frame to the  $s$ -frame is  $R_3(\gamma)R_2(\beta)R_1(\alpha)$ ; and

$$\mathbf{x}^s = R_3(\gamma)R_2(\beta)R_1(\alpha)\mathbf{x}^t. \quad (1.19)$$

The total transformation matrix is again orthogonal, since each individual rotation matrix is orthogonal:

$$(R_3(\gamma)R_2(\beta)R_1(\alpha))^{-1} = (R_3(\gamma)R_2(\beta)R_1(\alpha))^T = R_1(-\alpha)R_2(-\beta)R_3(-\gamma). \quad (1.20)$$

It is particularly important to note that the transformation also depends on the order of the applied rotations. This is easily verified with an example like  $R_1(\alpha)R_2(\beta) \neq R_2(\beta)R_1(\alpha)$ .

The choices of axes about which the rotation occurs depend entirely on the problem at hand. Different sequences can yield the same final transformation, but the convenience of one may surpass that of another. A prevalent sequence of rotations used in group theory, physics, and related fields is  $R_3R_2R_3$ , and the corresponding angles ordinarily are known as *Euler angles* (although some authors define the sequence as  $R_3R_1R_3$ ). In fact, however, as noted in (O'Donnell, 1964) and (Arfken, 1970), the nomenclature for these angles is not connected invariably to any particular sequence of rotations, and in this spirit we refer to the rotation angles, in general, as Euler angles. The sequence (1.19) is preferred in reference to the inertial navigation system since its angular degrees of freedom are often identified with the rotations about the three independent coordinate axes. This reflects the construction of stabilized platforms (Section 4.2) and the types of rotations executed by aircraft (roll, pitch, yaw; see Section 1.5).

Finally, it is evident that whether we use direction cosines or Euler angles, the net result for a given transformation must be the same; that is, in this case:

$$C_t^s = R_3(\gamma)R_2(\beta)R_1(\alpha). \quad (1.21)$$

Explicitly, we have

$$R_3(\gamma)R_2(\beta)R_1(\alpha) = \begin{pmatrix} \cos\gamma\cos\beta & \cos\gamma\sin\beta\sin\alpha + \sin\gamma\cos\alpha & -\cos\gamma\sin\beta\cos\alpha + \sin\gamma\sin\alpha \\ -\sin\gamma\cos\beta & -\sin\gamma\sin\beta\sin\alpha + \cos\gamma\cos\alpha & \sin\gamma\sin\beta\cos\alpha + \cos\gamma\sin\alpha \\ \sin\beta & -\cos\beta\sin\alpha & \cos\beta\cos\alpha \end{pmatrix}. \quad (1.22)$$

This clearly shows the relationship between the Euler angles and the direction cosines; of course, this relationship depends on the choice of Euler angles and the order of rotations. In this case, given the transformation in terms of Euler angles as in (1.19), the direction cosines  $c_{j,k}$  are simply the elements of the matrix in (1.22). Conversely, given the direction cosines, the Euler angles, *in this case*, are given by

$$\alpha = \tan^{-1}\left(\frac{-c_{3,2}}{c_{3,3}}\right); \quad \beta = \sin^{-1}(c_{3,1}); \quad \gamma = \tan^{-1}\left(\frac{-c_{2,1}}{c_{1,1}}\right). \quad (1.23)$$

For small angles,  $\alpha, \beta, \gamma$ , we may approximate  $\cos\alpha \approx 1$ ,  $\sin\alpha \approx \alpha$ , etc.; and, retaining only first-order terms, (1.22) becomes

$$R_3(\gamma)R_2(\beta)R_1(\alpha) \approx \begin{pmatrix} 1 & \gamma & -\beta \\ -\gamma & 1 & \alpha \\ \beta & -\alpha & 1 \end{pmatrix} = \begin{pmatrix} 1 & 0 & 0 \\ 0 & 1 & 0 \\ 0 & 0 & 1 \end{pmatrix} - \begin{pmatrix} 0 & -\gamma & \beta \\ \gamma & 0 & -\alpha \\ -\beta & \alpha & 0 \end{pmatrix} = I - \Psi, \quad (1.24)$$

where  $\Psi$ , defined in (1.24), is a skew symmetric matrix of the small rotation angles. From (1.21) we also have (for small angles,  $\alpha, \beta, \gamma$ )

$$C_t^s \approx I - \Psi = \begin{pmatrix} 1 & \gamma & -\beta \\ -\gamma & 1 & \alpha \\ \beta & -\alpha & 1 \end{pmatrix}. \quad (1.25)$$

Since the small rotation angles are the angles between the respective axes of the *s*-frame and *t*-frame, it is clear that in this approximation the order of rotations about the axes is irrelevant; the result is always (1.25). Also, the reverse transformation is given by

$$C_s^t \approx \begin{pmatrix} 1 & \gamma & -\beta \\ -\gamma & 1 & \alpha \\ \beta & -\alpha & 1 \end{pmatrix}^T = \begin{pmatrix} 1 & 0 & 0 \\ 0 & 1 & 0 \\ 0 & 0 & 1 \end{pmatrix} - \begin{pmatrix} 0 & \gamma & -\beta \\ -\gamma & 0 & \alpha \\ \beta & -\alpha & 0 \end{pmatrix} = I - \Psi^T \quad (\text{small angles, } \alpha, \beta, \gamma). \quad (1.26)$$

### 1.3.3 Quaternions

In a sense, quaternions are a generalization of complex numbers. This does not reflect a need in algebra to invent new kinds of numbers (the way that complex numbers are needed to find all the roots of arbitrary polynomials). Rather, just as a complex number may be used to represent a vector in two dimensions, a quaternion is a number that represents a vector in four dimensions (quaternions are attributed

usually to Hamilton and form part of an arsenal of operators for vector fields (Morse and Feschbach, 1953), though in modern physics they now have only historical value).

The complex number,  $z$ , is the sum of real and imaginary parts:

$$z = x + iy, \quad (1.27)$$

where  $x$  and  $y$  are real numbers and  $i$  represents the imaginary unit (and the implied 1, antecedent to  $x$ , represents the real unit). The imaginary unit satisfies the equation:  $i^2 = -1$ . The representation of two-dimensional vectors using complex numbers arises by defining 1 and  $i$  to be units along two mutually orthogonal axes, so that  $x$  and  $y$  are the coordinates of the vector, analogous to (1.2). An equivalent form of the complex number is

$$z = \rho e^{i\theta}, \quad (1.28)$$

where  $\rho$  may be interpreted as the magnitude of the vector and  $\theta$  as the angle the vector makes with the 1-axis. The equivalence of (1.27) and (1.28) is easily shown by substituting *Euler's equation*:

$$e^{i\theta} = \cos \theta + i \sin \theta. \quad (1.29)$$

This equation, in turn, can be proved using the series expansions for  $e^{i\theta}$ ,  $\cos \theta$ , and  $\sin \theta$ :

$$\begin{aligned} e^p &= 1 + \frac{1}{1!} p + \frac{1}{2!} p^2 + \frac{1}{3!} p^3 + \dots, \\ \sin(p) &= p - \frac{1}{3!} p^3 + \frac{1}{5!} p^5 - \frac{1}{7!} p^7 + \dots, \\ \cos(p) &= 1 - \frac{1}{2!} p^2 + \frac{1}{4!} p^4 - \frac{1}{6!} p^6 + \dots, \end{aligned} \quad (1.30)$$

which hold for any  $p$ .

For quaternions, we introduce two additional “imaginary units”,  $j$  and  $k$ , that together with  $i$  represent the units along three mutually orthogonal axes. The unit 1 represents the unit along the fourth axis, that may be considered orthogonal to the other three in a formal sense. The units  $j$  and  $k$  are defined like  $i$ :

$$i^2 = -1; \quad j^2 = -1; \quad k^2 = -1. \quad (1.31)$$

In addition, we define the products:

$$ij = -ji = k; \quad jk = -kj = i; \quad ki = -ik = j; \quad (1.32)$$

where we note the non-commutativity of unlike units (e.g.,  $ij \neq ji$ ).

Now, a quaternion is given by the sum:

$$q = a + ib + jc + kd, \quad (1.33)$$

where  $a, b, c, d$  are real numbers. The conjugate of  $q$  (like the complex conjugate of

$z$ ) is obtained by reversing the sign of all imaginary units:

$$q^* = a - ib - jc - kd. \quad (1.34)$$

With (1.30) and (1.31), the square of the magnitude of  $q$  is easily shown to be, analogous to complex numbers:

$$qq^* = q^*q = a^2 + b^2 + c^2 + d^2. \quad (1.35)$$

In general, both the product and the sum of two quaternions are again quaternions. However, because of (1.32) multiplication is not commutative as it is with complex numbers. That is, if  $q_1$  and  $q_2$  are two arbitrary quaternions, then generally

$$q_1q_2 \neq q_2q_1. \quad (1.36)$$

The complex number  $e^{i\theta}$ , when it multiplies an arbitrary complex number,  $z = \rho e^{i\phi}$  (representing a two-dimensional vector), rotates that vector by the angle  $\theta$ :

$$w = e^{i\theta}z = e^{i\theta}\rho e^{i\phi} = \rho e^{i(\theta+\phi)}, \quad (1.37)$$

so that the angle between the vector represented by  $w$  and the 1-axis is  $\theta + \phi$ . Analogously, a certain type of quaternion can be used to describe rotations of three-dimensional vectors. Consider the quaternion

$$q_\zeta = \cos \frac{\zeta}{2} + \sin \frac{\zeta}{2}(ib + jc + kd) = a_\zeta + ib_\zeta + jc_\zeta + kd_\zeta, \quad (1.38)$$

where the numbers  $b, c$ , and  $d$  satisfy the constraint

$$b^2 + c^2 + d^2 = 1. \quad (1.39)$$

Also, of course, we have the constraint among the numbers  $a_\zeta, b_\zeta, c_\zeta, d_\zeta$ :

$$a_\zeta^2 + b_\zeta^2 + c_\zeta^2 + d_\zeta^2 = 1. \quad (1.40)$$

This particular quaternion may be represented, analogous to Euler's equation (1.29), by an exponential involving the angle,  $\zeta/2$ :

$$q_\zeta = e^{(\zeta/2)(ib+jc+kd)}. \quad (1.41)$$

The validity of this equation, again, can be demonstrated using infinite series expansions.

The magnitude of the quaternion  $q_\zeta$  is unity by (1.35), and the exponent  $\zeta(ib + jc + kd)/2$  in (1.41) represents a three-dimensional space vector with magnitude  $\zeta/2$  and direction cosines  $b, c$ , and  $d$  (indeed, the sum  $ib + jc + kd$  represents a unit vector with coordinates, or direction cosines according to (1.12),  $b, c$ , and  $d$ ). It happens that the quaternion triple product

$$x' = q_\zeta x q_\zeta^* \quad (1.42)$$

rotates the arbitrary three-dimensional vector represented by  $x = ix_1 + jx_2 + kx_3$  about the direction  $ib + jc + kd$  by the angle  $\zeta$  (not  $\zeta/2!$ ) into the vector  $x'$ . This can be verified after the following development with our usual rotation matrices.

Although the formulation (1.41) for the rotation quaternion is appealing because of the analogy to the rotation obtained by the complex number,  $e^{i\theta}$ , the use of (1.41) is restricted to mere operator notation since the exponent, because of (1.32), cannot be manipulated (added, subtracted) like a quaternion. For example, the product of two rotation quaternions is not formed by adding their respective exponents in the exponential function (as this would imply commutativity!).

Instead of performing rotations of vectors as described by (1.42) we use the standard and more intuitive rotation matrix. However, rotation quaternions are extremely useful in the numerical integration of rotation *rates*, as will be seen in Sections 1.4 and 1.5. Therefore, it is important to find the relationship between elements of the rotation quaternion and elements of the direction cosine matrix. To begin, we assume that any particular rotation between frames may be defined by the rotation about a single *rotation vector*. This (three-dimensional) rotation vector specifies the single axis about which one rotation transforms one frame to another. That such a rotation vector always exists follows from its construction in terms of direction cosines, as shown below.

Consider two frames, the t-frame and the s-frame, and suppose they are related by the usual orthogonal transformation  $C_t^s$ , the result of a sequence of standard rotations about coordinate axes. We wish to describe this transformation by an equivalent single rotation through the angle,  $\zeta$ , about the appropriate direction. Let this direction be specified by the unit rotation vector,  $e_\zeta^t$ , whose direction cosines (i.e., coordinates) in the t-frame are  $b, c, d$ . These may be used to define the numbers associated with the rotation quaternion (1.41); and, without loss in generality, they also may be represented in terms of spherical polar coordinates,  $\theta, \lambda$ :

$$e_\zeta^t = \begin{pmatrix} b \\ c \\ d \end{pmatrix} = \begin{pmatrix} \sin \theta \cos \lambda \\ \sin \theta \sin \lambda \\ \cos \theta \end{pmatrix}. \quad (1.43)$$

To describe a rotation about this direction, we first define a new frame, the i-frame, whose 3-axis lies along the direction of  $e_\zeta^t$ , and whose 1-axis is in the plane formed by  $e_\zeta^t$  and the 3-axis of the t-frame (see Figure 1.6). The transformation from the t-frame to the c-frame is given by

$$C_t^\zeta = R_2(-\theta)R_3(-\pi + \lambda) = \begin{pmatrix} -\cos \theta \cos \lambda & \cos \theta \sin \lambda & \sin \theta \\ \sin \lambda & -\cos \lambda & 0 \\ \sin \theta \cos \lambda & \sin \theta \sin \lambda & \cos \theta \end{pmatrix}. \quad (1.44)$$

The matrix that performs the c-rotation in the c-frame is  $R_3(\zeta)$ . In the t-frame that same rotation is given, according to (1.17), by  $C_\zeta^t R_3(\zeta) C_t^\zeta$ . Subsequently, we impose the condition that this rotation should be  $C_t^s$ :

$$C_t^s = C_\zeta^t R_3(\zeta) C_t^\zeta. \quad (1.45)$$

We can write the transformation  $C_t^\zeta$  in terms of the quaternion elements using (1.43) and (1.44):

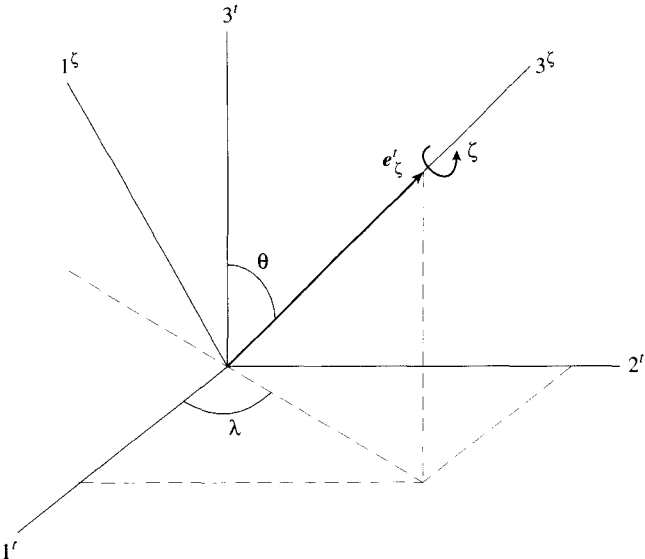


Figure 1.6: The unit rotation vector  $e_\zeta^t$ ; and the  $\zeta$ - and  $t$ -frames.

$$C_t^\zeta = \begin{pmatrix} -db & -dc & \sqrt{1-d^2} \\ \frac{c}{\sqrt{1-d^2}} & \frac{-b}{\sqrt{1-d^2}} & 0 \\ \frac{b}{\sqrt{1-d^2}} & \frac{c}{\sqrt{1-d^2}} & d \end{pmatrix}. \quad (1.46)$$

Introducing the alternative form of the elements,  $a_\zeta, b_\zeta, c_\zeta, d_\zeta$ , as defined in (1.38), one obtains from (1.45),

$$C_t^s = \begin{pmatrix} a_\zeta^2 + b_\zeta^2 - c_\zeta^2 - d_\zeta^2 & 2(b_\zeta c_\zeta + d_\zeta a_\zeta) & 2(b_\zeta d_\zeta - c_\zeta a_\zeta) \\ 2(b_\zeta c_\zeta - d_\zeta a_\zeta) & a_\zeta^2 + c_\zeta^2 - b_\zeta^2 - d_\zeta^2 & 2(c_\zeta d_\zeta + a_\zeta b_\zeta) \\ 2(b_\zeta d_\zeta + c_\zeta a_\zeta) & 2(c_\zeta d_\zeta - a_\zeta b_\zeta) & a_\zeta^2 + d_\zeta^2 - b_\zeta^2 - c_\zeta^2 \end{pmatrix}. \quad (1.47)$$

This demonstrates the relationship between the direction cosines of the transformation (1.14) in terms of the quaternion elements (1.38). (With straightforward algebraic manipulations using (1.31) and (1.32), one can show that (1.42) yields the same result.) It is noted that there are at most three independent elements that define an orthogonal transformation; and while the rotation quaternion has four elements, one degree of freedom is eliminated by the constraint (1.39). The constraint (1.40) allowed  $C_t^s$  in (1.47) to be developed, through (1.44) and (1.45), as an orthogonal matrix. The converse is also true; namely, given an orthogonal matrix with elements as arranged in (1.47), then the constraint (1.40) is satisfied. It is left to the reader to verify this, showing that the constraint (1.40) is a necessary and sufficient condition for the orthogonality of (1.47).

The inverse relationship from direction cosines to quaternions is obtained by noting first that the trace (i.e., the sum of diagonal elements) of  $C_t^s$ , as expressed by (1.47), is given with (1.40) by

$$\text{tr } C_t^s = 4a_\zeta^2 - 1. \quad (1.48)$$

Hence,

$$a_\zeta = \frac{1}{2} \sqrt{1 + c_{1,1} + c_{2,2} + c_{3,3}}, \quad (1.49)$$

where  $c_{j,j}$  is a direction cosine; see (1.14). Subtracting corresponding off-diagonal elements in (1.47) similarly leads to

$$b_\zeta = \frac{1}{4a_\zeta} (c_{2,3} - c_{3,2}), \quad (1.50)$$

$$c_\zeta = \frac{1}{4a_\zeta} (c_{3,1} - c_{1,3}), \quad (1.51)$$

$$d_\zeta = \frac{1}{4a_\zeta} (c_{1,2} - c_{2,1}). \quad (1.52)$$

Thus, given a set of direction cosines, the corresponding rotation quaternion can be computed using (1.49)–(1.52); and vice versa, using (1.14) and (1.47).

### 1.3.4 Axial Vectors

Because the angular data provided by inertial measurement units are related to angular rates of the instrument or body frame, we need to derive equations that express these sensed rates in terms of rates of angles in, say, the navigation frame. These equations are differential equations that can then be integrated to yield the navigation frame angles at any time from the sensed angular rates.

To develop the differential equations, it is necessary, first, to define what is meant by an axial vector. The *axial vector* (also known as pseudo-vector) is the ordered triple of Eulerian angles  $(\alpha, \beta, \gamma)$ . It is not a true vector, except under special circumstances. Specifically two such axial “vectors”, in general, do not obey the commutativity property of vectors:

$$\psi_1 = \begin{pmatrix} \alpha_1 \\ \beta_1 \\ \gamma_1 \end{pmatrix}, \quad \psi_2 = \begin{pmatrix} \alpha_2 \\ \beta_2 \\ \gamma_2 \end{pmatrix} \quad \Rightarrow \quad \psi_1 + \psi_2 \neq \psi_2 + \psi_1 \quad (\text{in general}). \quad (1.53)$$

This is related to the dependence of the rotational transformation on the order of axis-rotations. On the other hand, if the angles are small, then  $\psi$  behaves more like a vector, although not completely (it satisfies commutativity to a first order approximation). The true test of a vector is whether it transforms like a vector under *arbitrary* orthogonal transformations. It can be shown (Goldstein, 1950) that  $\psi$ , if it is a triple of small angles, is a vector only if such a transformation is a proper rotation, i.e., if no axis inversions, e.g., changing from left-handed to right-handed systems,

are allowed. For our purposes,  $\psi = (\alpha, \beta, \gamma)^T$ , always assumed to be a triple of small angles, will be treated as a vector that enjoys all the properties of being a vector. (Smallness obviously is in the eye of the beholder, and the property of being a vector formally holds only for infinitesimal angles.)

The transformation of the  $t$ -frame to the  $s$ -frame under *small-angle* rotations can then also be written with (1.25) as

$$\begin{aligned} \mathbf{x}^s &= C_t^s \mathbf{x}^t = (I - \Psi) \mathbf{x}^t = \mathbf{x}^t - \Psi \mathbf{x}^t \\ &= \mathbf{x}^t - \psi \times \mathbf{x}^t. \end{aligned} \quad (1.54)$$

The equivalence of the matrix multiplication of  $\Psi$  to the cross-product with  $\psi$  can be verified from the definition of  $\Psi$  in (1.24). Formally, we may write

$$[\psi \times] = \Psi \quad \text{or} \quad \left[ \begin{pmatrix} \alpha \\ \beta \\ \gamma \end{pmatrix} \times \right] = \begin{pmatrix} 0 & -\gamma & \beta \\ \gamma & 0 & -\alpha \\ -\beta & \alpha & 0 \end{pmatrix}. \quad (1.55)$$

Under our restrictions, the “coordinates” of the axial vector  $\psi$  under a rotational transformation change like those of a vector. Let  $\psi'$  be a small rotation of the  $t$ -frame. The question is: what is the corresponding small rotation of the  $s$ -frame if the two frames are related by an arbitrary rotational transformation  $C_t^s$ ? The answer is that  $\psi'$ , being a vector, transforms according to (1.13):

$$\psi^s = C_t^s \psi'. \quad (1.56)$$

The alternative to (1.56), in view of (1.17), is then also

$$\Psi^s = C_t^s \Psi' C_s^t. \quad (1.57)$$

Equations (1.56) and (1.57) are equivalent in the sense of (1.55).

### 1.3.5 Angular Rates

Before leaving this section and as an introduction to the next section, a systematic notation for angular rates is introduced. It conforms to the notation used by Britting (1971). Here, we consider that the frames are rotating with respect to each other and that the rotations are functions of time. That is, the angles have velocities (and accelerations) associated with them. Let  $\omega = (\omega_1 \ \omega_2 \ \omega_3)^T$  be a vector of rotational rates about the three respective, instantaneous axes of a frame. These rates need not be small because rates, by definition, are infinitesimal angles in the ratio to infinitesimal increments of time. But, strictly,  $\omega$  is still only an axial vector, because it transforms as a vector only under proper rotations. A simple example is the rotation vector associated with the Earth's rotation. If the 3-axis is aligned with the Earth's spin axis, then  $\omega = (0 \ 0 \ \omega_e)^T$ , where  $\omega_e$  is the angular rate of the Earth's rotation.

In general, consider the  $t$ -frame rotating with respect to the  $s$ -frame. We denote:

$$\begin{aligned} \omega'_{st} &= \text{the angular velocity of the } t\text{-frame with respect to the } s\text{-frame,} \\ &\quad \text{with coordinates in the } t\text{-frame.} \end{aligned} \quad (1.58)$$

The angular velocity of the  $s$ -frame with respect to the  $t$ -frame, having coordinates in the  $s$ -frame, is  $\omega_{ts}^s$ . Again, because angular velocities are considered to be vectors, in different frames they are related by the corresponding rotational transformation matrix (its elements also depend on time). We have

$$\omega_{st}^t = C_s^t \omega_{st}^s = -C_s^t \omega_{ts}^s, \quad (1.59)$$

because, clearly,

$$\omega_{st}^s = -\omega_{ts}^s. \quad (1.60)$$

As vectors, relative angular rates can be added component-wise (satisfying also commutativity):

$$\omega_{st}^t = \omega_{st}^t + \omega_{ut}^t. \quad (1.61)$$

Note, however, that the addition must be performed in a single frame. In terms of a skew-symmetric matrix, there is the equivalence

$$[\omega_{st}^t \times] = \Omega_{st}^t; \quad \text{where } \Omega_{st}^t = \begin{pmatrix} 0 & -\omega_3 & \omega_2 \\ \omega_3 & 0 & -\omega_1 \\ -\omega_2 & \omega_1 & 0 \end{pmatrix}. \quad (1.62)$$

Again, it is emphasized that the components of  $\omega = (\omega_1 \ \omega_2 \ \omega_3)^T$  can have any value even though  $\omega$  is sometimes written in the skew-symmetric form as was the vector,  $\psi$ , of small rotation angles.

## 1.4 Differential Equation of the Transformation

Usually, we consider two frames that are rotating with respect to each other; that is, their relative orientation changes with time. To describe this in terms of rotational transformations, it is necessary to find an expression for the derivative of the transformation with respect to time, namely  $\dot{C}_t^s$ . In general, if frames are rotating with respect to each other, it is important to identify the frame in which the time-differentiation takes place. Unless otherwise indicated, *the time-differentiation is done in the frame designated by the superscript of the variable*.

The time derivative of the rotational transformation,  $C_t^s$ , being a function of time,  $\tau$ , formally is given by:

$$\dot{C}_t^s = \lim_{\delta\tau \rightarrow 0} \frac{C_t^s(\tau + \delta\tau) - C_t^s(\tau)}{\delta\tau}. \quad (1.63)$$

The transformation at time  $\tau + \delta\tau$  is the result of the transformation up to time  $\tau$  followed by a small change of the  $s$ -frame during the interval,  $\delta\tau$ . This is expressed as

$$C_t^s(\tau + \delta\tau) = \delta C^s C_t^s(\tau), \quad (1.64)$$

where the words “followed by” mean “successive application of” in the sense of transformations, as in (1.13). The small-angle transformation can also be written as

(see (1.25))

$$\delta C^s = I - \Psi^s. \quad (1.65)$$

Substituting (1.64) and (1.65) into (1.63) yields

$$\begin{aligned} \dot{C}_t^s &= \lim_{\delta\tau \rightarrow 0} \frac{(I - \Psi^s)C_t^s(\tau) - C_t^s(\tau)}{\delta\tau} \\ &= \lim_{\delta\tau \rightarrow 0} \frac{-\Psi^s C_t^s(\tau)}{\delta\tau} = -\lim_{\delta\tau \rightarrow 0} \frac{\Psi^s}{\delta\tau} C_t^s(\tau) \\ &= -\Omega_{ts}^s C_t^s, \end{aligned} \quad (1.66)$$

where the last equality follows from the fact that, in the limit, a small rotation of the  $s$ -frame with respect to the time,  $\delta\tau$ , represents the angular velocity of the  $s$ -frame with respect to the  $t$ -frame as coordinatized in the  $s$ -frame (see (1.58)). Using (1.17) and (1.60), we have

$$\Omega_{ts}^s = -\Omega_{st}^s = -C_t^s \Omega_{st}^t C_s^t. \quad (1.67)$$

Therefore, the time derivative of the transformation matrix is given by

$$\dot{C}_t^s = C_t^s \Omega_{st}^t. \quad (1.68)$$

Taking the time-derivative of (1.13) yields:

$$\begin{aligned} \dot{x}^s &= C_t^s \dot{x}^t + \dot{C}_t^s x^t \\ &= C_t^s (\dot{x}^t + \Omega_{st}^t x^t), \end{aligned} \quad (1.69)$$

or

$$C_s^t \dot{x}^s = \dot{x}^t + \omega_{st}^t \times x^t, \quad (1.70)$$

which is the *Law of Coriolis* (named after Gaspard G. de Coriolis (1792–1843)). The left side is a vector in the  $t$ -frame, but the time-differentiation takes place in the  $s$ -frame; while on the right side the time-differentiation is in the  $t$ -frame. This important equation clearly shows that proper care is needed when defining the frame of the time-differentiation.

Analogous to (1.70) we can derive the differential equations for the quaternion elements. Solving (1.48) for  $a_\zeta^2$  and differentiating:

$$2a_\zeta \dot{a}_\zeta = \frac{1}{4} \text{tr}(\dot{C}_t^s) = \frac{1}{4} \text{tr}(C_t^s \Omega_{st}^t). \quad (1.71)$$

After substituting from (1.47) and (1.62), this yields

$$\dot{a}_\zeta = \frac{1}{2} (b_\zeta \omega_1 + c_\zeta \omega_2 + d_\zeta \omega_3), \quad (1.72)$$

where  $\omega_{st}^t = (\omega_1, \omega_2, \omega_3)^T$ .

Also, we have from (1.50)

$$\begin{aligned} 4a_\zeta b_\zeta &= c_{23} - c_{32} \\ \Rightarrow 4(\dot{a}_\zeta b_\zeta + a_\zeta \dot{b}_\zeta) &= \dot{c}_{23} - \dot{c}_{32} = c_{21}\omega_2 - c_{22}\omega_1 + c_{31}\omega_3 - c_{33}\omega_1 \\ \Rightarrow \dot{b}_\zeta &= \frac{1}{2}(-a_\zeta\omega_1 - d_\zeta\omega_2 + c_\zeta\omega_3). \end{aligned} \quad (1.73)$$

Similarly, the differential equations for  $\dot{c}_\zeta$  and  $\dot{d}_\zeta$  are easily found from (1.51) and (1.52). Putting them all together, we have:

$$\begin{aligned} \dot{a}_\zeta &= \frac{1}{2}(b_\zeta\omega_1 + c_\zeta\omega_2 + d_\zeta\omega_3), \\ \dot{b}_\zeta &= \frac{1}{2}(-a_\zeta\omega_1 - d_\zeta\omega_2 + c_\zeta\omega_3), \\ \dot{c}_\zeta &= \frac{1}{2}(d_\zeta\omega_1 - a_\zeta\omega_2 - b_\zeta\omega_3), \\ \dot{d}_\zeta &= \frac{1}{2}(-c_\zeta\omega_1 + b_\zeta\omega_2 - a_\zeta\omega_3), \end{aligned} \quad (1.74)$$

or, succinctly:

$$\dot{\mathbf{q}}_\zeta = \frac{1}{2}A\mathbf{q}_\zeta, \quad (1.75)$$

where  $A$  is the  $4 \times 4$  skew symmetric matrix

$$A = \begin{pmatrix} 0 & \omega_1 & \omega_2 & \omega_3 \\ -\omega_1 & 0 & \omega_3 & -\omega_2 \\ -\omega_2 & -\omega_3 & 0 & \omega_1 \\ -\omega_3 & \omega_2 & -\omega_1 & 0 \end{pmatrix}. \quad (1.76)$$

## 1.5 Specific Coordinate Transformations

The transformations among the external coordinate frames ( $i$ - and  $e$ -frames) and the body frame are detailed below. The transformation between frames internal to the navigation system are treated together with the respective inertial instruments in Chapter 3.

Figure 1.7 shows the relationship between the  $i$ -frame and  $e$ -frame coordinates, as well as the geodetic coordinates with respect to a rotationally symmetric ellipsoid; all coordinate origins are coincident. It is assumed that the  $e$ -frame and  $i$ -frame differ by a rotation only about the  $x_3$ -axis; thus polar motion as well as precession and nutation of the Earth's instantaneous spin axis are ignored. If  $\omega_e$  is the (presumably uniform) rate of Earth rotation, then  $\omega_e t$ , where  $t$  denotes time, is the angle

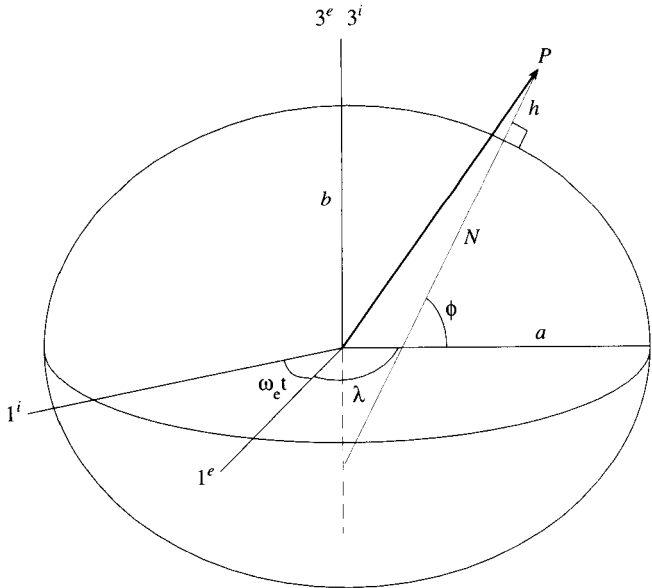


Figure 1.7: *i*-frame, *e*-frame, and geodetic coordinates.

that rotates the *i*-frame into the *e*-frame; and (see (1.58))

$$\omega_{ie}^e = (0 \quad 0 \quad \omega_e)^T. \quad (1.77)$$

The transformation matrix from the *i*-frame to the *e*-frame is simply a rotation about the 3-axis:

$$C_i^e = \begin{pmatrix} \cos \omega_e t & \sin \omega_e t & 0 \\ -\sin \omega_e t & \cos \omega_e t & 0 \\ 0 & 0 & 1 \end{pmatrix}, \quad (1.78)$$

which shows also that

$$\omega_{ie}^e = \omega_{ie}^i. \quad (1.79)$$

The geodetic coordinates of a point, *P*, are specific to a predefined rotationally symmetric ellipsoid with known semi-major axis (*a*) and flattening (*f*), where *f* = (*a* − *b*)/*a* and *b* = semi-minor axis. The coordinates of *P* are the geodetic latitude, geodetic longitude, and height above the ellipsoid (see Section 1.2.3). The relationship between the  $\mathbf{x}^e = (x_1^e, x_2^e, x_3^e)^T$  and  $(\phi, \lambda, h)$  coordinates is (see Torge, 1991, for further details)

$$\begin{pmatrix} x_1^e \\ x_2^e \\ x_3^e \end{pmatrix} = \begin{pmatrix} (N + h) \cos \phi \cos \lambda \\ (N + h) \cos \phi \sin \lambda \\ (N(1 - e^2) + h) \sin \phi \end{pmatrix}, \quad (1.80)$$

where *N* is the radius of curvature of the ellipsoid in the prime vertical plane, i.e.,

## 24 1 Coordinate Frames and Transformations

the plane containing the normal at  $P$  and perpendicular to the meridian:

$$N = \frac{a}{\sqrt{1 - e^2 \sin^2 \phi}}, \quad (1.81)$$

and  $e^2 = 2f - f^2$  is the square of the first eccentricity of the ellipsoid. For future reference, we give the radius of curvature in the meridian,  $M$ :

$$M = \frac{a(1 - e^2)}{(1 - e^2 \sin^2 \phi)^{3/2}}. \quad (1.82)$$

Both  $N$  and  $M$  are distances along the ellipsoid normal through  $P$ , with  $N$  the distance from the ellipsoid to the polar (minor) axis.

Earth-approximating ellipsoids abound in geodetic history, where values of the parameters  $(a, f)$  are adopted based on observational data. We will use the current internationally adopted values for the Geodetic Reference System 1980 (GRS80) (Moritz, 1992):

$$\begin{aligned} a &= 6378137, \\ f &= 1/298.257222101. \end{aligned} \quad (1.83)$$

These values are almost identical to those used for the GPS reference ellipsoid established by the U.S. Department of Defense: World Geodetic System 1984 (WGS84; NIMA, 1997). Given geodetic coordinates with respect to a specified ellipsoid, it is straightforward to compute the corresponding Cartesian coordinates using (1.80) and (1.81).

The reverse relationship from  $\mathbf{x}^e = (x_1^e, x_2^e, x_3^e)^T$  to  $(\phi, \lambda, h)$  is often presented in iterative form, although closed expressions exist (yet, computationally they are not necessarily more efficient). It is readily verified that

$$\begin{pmatrix} \phi \\ \lambda \\ h \end{pmatrix} = \begin{pmatrix} \tan^{-1} \left( \frac{x_3^e}{\sqrt{(x_1^e)^2 + (x_2^e)^2}} \left( 1 + \frac{e^2 N \sin \phi}{x_3^e} \right) \right) \\ \tan^{-1} \left( \frac{x_2^e}{x_1^e} \right) \\ \frac{\sqrt{(x_1^e)^2 + (x_2^e)^2}}{\cos \phi} - N \end{pmatrix}. \quad (1.84)$$

The equation for  $\phi$  is iterated to convergence starting with the initial assumption that  $h = 0$ , in which case, from (1.84) and (1.80):

$$\phi_0 \equiv \phi(h = 0) = \tan^{-1} \left( \frac{x_3^e}{\sqrt{(x_1^e)^2 + (x_2^e)^2}} \left( \frac{1}{1 - e^2} \right) \right). \quad (1.85)$$

Other iterative formulations of this inverse problem exist which may converge faster

or may be more stable. However, for most practical situations, (1.84) is quite robust and the iterations of the first equation in (1.84) converge to better than  $10^{-3}$  arc-seconds in  $\phi$  after two steps. A closed (non-iterative) solution was obtained by Borkowski (1989).

The transformations between the  $n$ -frame (NED) and the  $e$ -frame is complicated by the fact that they are not concentric. However, we can derive their relative orientation using Euler angles (see Figure 1.3). First, rotate about the local east axis by the angle  $(\pi/2 + \phi)$ , then rotate about the new 3-axis by the angle  $-\lambda$ :

$$C_n^e = R_3(-\lambda)R_2(\pi/2 + \phi). \quad (1.86)$$

The result is

$$C_n^e = \begin{pmatrix} -\sin \phi \cos \lambda & -\sin \lambda & -\cos \phi \cos \lambda \\ -\sin \phi \sin \lambda & \cos \lambda & -\cos \phi \sin \lambda \\ \cos \phi & 0 & -\sin \phi \end{pmatrix}. \quad (1.87)$$

The angular rates may be derived from (1.68),  $\Omega_{en}^n = C_e^n \dot{C}_n^e$ , and with (1.62):

$$\omega_{en}^n = (\dot{\lambda} \cos \phi \quad -\dot{\phi} \quad -\dot{\lambda} \sin \phi)^T. \quad (1.88)$$

These angular rates,  $\dot{\phi}, \dot{\lambda}$ , are the changes in latitude and longitude of a vehicle traveling parallel to the ellipsoidal surface. They can be changed to north and east velocities using the local radii of curvature of the ellipsoid (see Chapter 4). For future reference, we include the angular rate of the  $n$ -frame with respect to the  $i$ -frame, which follows immediately from (1.88) and simple geometric considerations (Figure 1.7):

$$\omega_{in}^n = ((\dot{\lambda} + \omega_e) \cos \phi \quad -\dot{\phi} \quad -(\dot{\lambda} + \omega_e) \sin \phi)^T \quad (1.89)$$

We consider one additional transformation particularly relevant in navigation: the  $b$ -frame to  $n$ -frame transformation, where the body is the vehicle (in practice, additional transformations may be required to go from the frame of the instruments (accelerometers and gyroscopes) to the  $b$ -frame). The  $b$ -frame axes, fixed to the vehicle, point forward, to the right, and down (through the floor) as naturally defined by the geometry of the vehicle. Again, Euler angles define the transformation; they are the *roll* (or, bank), *pitch* (or, elevation), and *yaw* (or, heading) angles, respectively,  $\eta, \chi, \alpha$ , of the body axes with respect to the NED axes, as shown in Figure 1.8.

The transformation matrix from  $b$ -frame to  $n$ -frame is, for example, the composite of a rotation about the 1-axis by the negative roll angle,  $-\eta$ , followed by a rotation about the 2-axis by the negative pitch angle,  $-\chi$ , ending with the rotation about the 3-axis by the negative yaw angle,  $-\alpha$ . Note that this sequence is constructed by definition and, in practice, may depend on the mechanized configuration of the gyroscopes. We have

$$C_b^n = R_3(-\alpha)R_2(-\chi)R_1(-\eta). \quad (1.90)$$

Now, as before, one could use (1.68) and the time-derivative of (1.90) to obtain a relationship between the angular rates  $\omega_{nb}^b$  and the attitude rates  $\dot{\eta}, \dot{\chi}, \dot{\alpha}$ . A simpler, alternative derivation comes from the realization that (1.90) may be written generi-

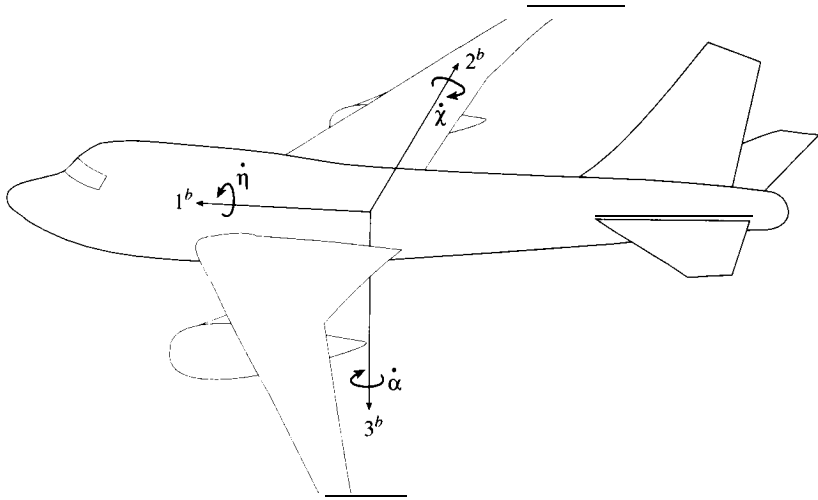


Figure 1.8: Body frame and angular rates with respect to n-frame.

cally as

$$C_b^n = R_3(-\alpha)R_2(-\chi)R_1(-\eta) = C_{b_2}^n C_{b_1}^{b_2} C_b^{b_1}, \quad (1.91)$$

where the  $b_1$  and  $b_2$  frames are intermediate frames established by the  $\eta$ - and  $\chi$ -rotations. All frames,  $b$ ,  $b_1$ , and  $b_2$ , rotate in time with respect to each other and relative to the n-frame. Therefore, we can also write from (1.61) and (1.59)

$$\begin{aligned} \omega_{nb}^b &= \omega_{nb_2}^b + \omega_{b_2 b_1}^b + \omega_{b_1 b}^b \\ &= C_{b_1}^{b_2} C_{b_2}^{b_1} \omega_{nb_2}^{b_2} + C_{b_1}^{b_2} \omega_{b_2 b_1}^{b_1} + \omega_{b_1 b}^b. \end{aligned} \quad (1.92)$$

The second equality follows from the usual transformation of vectors. Now, clearly (with reference to (1.58)), we have

$$\omega_{b_1 b}^b = \begin{pmatrix} \dot{\eta} \\ 0 \\ 0 \end{pmatrix}; \quad \omega_{b_2 b_1}^{b_1} = \begin{pmatrix} 0 \\ \dot{\chi} \\ 0 \end{pmatrix}; \quad \omega_{nb_2}^{b_2} = \begin{pmatrix} 0 \\ 0 \\ \dot{\alpha} \end{pmatrix}. \quad (1.93)$$

Finally, with (1.91), equation (1.92) becomes

$$\begin{aligned} \omega_{nb}^b &= R_1(\eta)R_2(\chi)\begin{pmatrix} 0 \\ 0 \\ \dot{\alpha} \end{pmatrix} + R_1(\eta)\begin{pmatrix} 0 \\ \dot{\chi} \\ 0 \end{pmatrix} + \begin{pmatrix} \dot{\eta} \\ 0 \\ 0 \end{pmatrix} \\ &= \begin{pmatrix} 1 & 0 & -\sin \chi \\ 0 & \cos \eta & \cos \chi \sin \eta \\ 0 & -\sin \eta & \cos \chi \cos \eta \end{pmatrix} \begin{pmatrix} \dot{\eta} \\ \dot{\chi} \\ \dot{\alpha} \end{pmatrix}. \end{aligned} \quad (1.94)$$

Solving for the attitude rates, it can be verified that

$$\begin{pmatrix} \dot{\eta} \\ \dot{\chi} \\ \dot{\alpha} \end{pmatrix} = \begin{pmatrix} 1 & \sin \eta \tan \chi & \cos \eta \tan \chi \\ 0 & \cos \eta & -\sin \eta \\ 0 & \sin \eta \sec \chi & \cos \eta \sec \chi \end{pmatrix} \omega_{nb}^b. \quad (1.95)$$

These are the differential equations that may be integrated to obtain the attitude angles of the vehicle as a function of time, given the body-to-navigation frame rates,  $\omega_{nb}^b$  (it is noted that the gyroscopes do not sense these directly, but they could be computed from the gyro data; see Chapter 4). Clearly, these equations become singular for pitch angles of  $\pm 90^\circ$ , due to the  $\tan \chi$  and  $\sec \chi$  terms.

The alternative differential equations in terms of quaternions are given by (1.74) or (1.75). Their relative simplicity in the numerical solution compared to (1.95) is evident and they avoid all possibility of singularities in the integration. It is the preferred scheme for inertial navigation systems. The numerical integration of (1.75) will be given in Chapter 4.

## 1.6 Fourier Transforms

Formally, expressing a vector as an ordered triple of coordinates, equation (1.1), may also be interpreted as transforming the vector from one type of representation (a directed magnitude) to another (a set of coordinates). The transformation is accomplished by performing the scalar product:

$$x_j = \mathbf{e}_j \cdot \mathbf{x}. \quad (1.96)$$

This type of transformation manifestly differs from the previously discussed transformations (i.e., the rotations). It is the idea behind the Fourier transform that applies to functions rather than vectors, where the objective is to resolve a function into its fundamental constituents according to some basis. The analogy to vectors is complete, being distinct only in that vectors are finite dimensional while the functions in the class to be considered here have infinite dimension (in the sense that they are variable at all scales of the independent variable). Since we will have only limited need for Fourier transforms, the present treatment is quite superficial and just sufficient for our later purposes. For more rigorous treatments, the interested reader may consult such classics as (Bracewell, 1965) and (Papoulis, 1962), or any of a number of texts oriented towards specific applications.

Consider a function defined over the real line and integrable, meaning that the integration will not result in singularities or that the function is piecewise continuous. The function is either periodic or non-periodic. The Fourier transform is defined differently for these two cases. Suppose  $\tilde{g}(t)$  is a function of the independent variable,  $t$ , and it is periodic with period  $T$ . Then, it is completely defined by its values over just a single interval, say  $[0, T]$ , and we have  $\tilde{g}(t + T) = \tilde{g}(t)$ . We would like

to express  $\tilde{g}(t)$  as a sum of sinusoidal functions (the basis functions). One way to accomplish this is by writing:

$$\tilde{g}(t) = a_0 + 2 \sum_{k=1}^{\infty} a_k \cos \frac{2\pi}{T} kt + 2 \sum_{k=1}^{\infty} b_k \sin \frac{2\pi}{T} kt, \quad (1.97)$$

where  $a_k$  and  $b_k$  are constant coefficients. Note that each sinusoid has period equal to an integral fraction of  $T$ , and thus,  $\tilde{g}(t)$  is decomposed into a sum of waves oscillating at different frequencies. A relatively large coefficient for a particular sinusoid implies a relatively large amplitude of the function at that frequency; just like a relatively large coordinate of a vector implies greater directionality of the vector toward the corresponding coordinate axis.

It is preferred for notational and mathematical economy to utilize Euler's equation (1.29) and express the series of sinusoids in terms of the complex exponential:

$$\tilde{g}(t) = \frac{1}{T} \sum_{k=-\infty}^{\infty} G_k e^{i(2\pi/T)kt}, \quad (1.98)$$

where the coefficients  $G_k$  are (in general) complex numbers. The relationship between the coefficient sets  $\{a_k, b_k\}$  in (1.97) and  $\{G_k\}$  is given by:

$$G_k = T \begin{cases} (a_k - ib_k), & k > 0; \\ a_0, & k = 0; \\ (a_{-k} + ib_{-k}), & k < 0. \end{cases} \quad (1.99)$$

The inverse relationship is left as an exercise for the reader.

The series (1.98) or (1.97) is called a *Fourier series*. The quantities  $k/T$  appearing in the arguments of the sinusoids are the harmonic *frequencies* of the function thus expressed. The fact that there is an infinity of such frequencies is due to the assumed (piecewise) continuity of the function—there are oscillations of infinitely many possible frequencies inherent in the function. The fundamental frequency is  $1/T(k = 1)$ . Frequency is the inverse of *wavelength*—high frequency (large  $k$ ) implies short wavelength; low frequency (small  $k$ ) implies long wavelength. Usually, frequency refers to the inverse of time, but we retain the use of the term frequency even if  $t$  is any other independent variable, although *wavenumber* (referring to the integers  $k$ ) is also used. When associated with time, frequency has units of *cycle per unit of time*, e.g., cycle per second, or Hz (*Hertz*). Generally, the units of frequency are cycles per unit of  $t$ .

The set of coefficients,  $\{G_k\}$ , is known as the *Fourier (series) transform* of  $\tilde{g}$ , or also the *(Fourier) spectrum* of  $\tilde{g}$ . Given  $\tilde{g}$ , one can compute the Fourier transform using the orthogonality of the sines and cosines on the interval  $[0, T]$ . For the complex exponential, we have the following orthogonality relationship:

$$\begin{aligned}
\int_0^T e^{i(2\pi/T)kt} e^{-i(2\pi/T)\ell t} dt &= \int_0^T e^{i(2\pi/T)(k-\ell)t} dt \\
&= \int_0^T \cos\left(\frac{2\pi}{T}(k-\ell)t\right) dt + i \int_0^T \sin\left(\frac{2\pi}{T}(k-\ell)t\right) dt \\
&= \begin{cases} 0, & k \neq \ell; \\ T, & k = \ell. \end{cases}
\end{aligned} \tag{1.100}$$

Therefore, multiplying (1.98) on both sides by  $e^{-i(2\pi/T)\ell t}$  and integrating yields, in view of (1.100),

$$G_k = \int_0^T \tilde{g}(t) e^{-i(2\pi/T)kt} dt. \tag{1.101}$$

The analogy to vectors is now apparent. The basis functions,  $e^{-i(2\pi/T)kt}$ , are like the unit vectors and the coefficients,  $G_k$ , are like coordinates. They are obtained by (1.101) which is completely analogous to (1.96).

The function and its Fourier transform are *dual* representations of the same information—one is equivalent to the other (as long as the function is continuous). The transform of a function displays the same information, but in a different domain—the *frequency domain*, where it is often more insightful than in the domain of  $t$ . The two relationships (1.98) and (1.101) constitute a *Fourier Transform pair* for periodic functions. The Fourier series, that is,  $\tilde{g}$ , may also formally be called the *inverse Fourier transform* of  $G_k$ . It is noted only in passing that the often encountered Fast Fourier transform (FFT) is a transform that applies only to periodic functions defined on a *discrete*, evenly spaced, finite set of values of the independent variable.

For non-periodic, piecewise continuous functions the Fourier transform may be defined similarly. However, we require the additional condition of square-integrability. For the function  $g$  defined on the real line this means that

$$\int_{-\infty}^{\infty} (g(t))^2 dt < \infty. \tag{1.102}$$

Generally, the function must approach zero sufficiently fast as  $|t| \rightarrow \infty$ . Then, its *Fourier transform*, also a square-integrable function, is defined by

$$\mathcal{F}(g) \equiv G(f) = \int_{-\infty}^{\infty} g(t) e^{-i2\pi ft} dt. \tag{1.103}$$

Note that *periodic* functions are *not* included here, because they are not square-integrable. In addition, the *inverse Fourier transform* is given by

$$\mathcal{F}^{-1}(G) \equiv g(t) = \int_{-\infty}^{\infty} G(f) e^{i2\pi ft} df. \tag{1.104}$$

$G(f)$  is a complex function of the frequency,  $f$ , and is also known as the *spectrum* (or *spectral density*) of  $g$ . The units of  $G(f)$  are the units of  $g$  per unit of frequency, whence its alternative name, spectral density.

Transforms (1.103) and (1.104) are mutually consistent, provided the function,  $g$ , is continuous. Each provides as much information about the function as the other. If  $g(t)$  is real-valued, that is, it equals its own complex conjugate, then from (1.103) we find that  $G(f)$  is *Hermitian* (its real part is even, or symmetric about  $f = 0$ , and its imaginary part is odd, or anti-symmetric):

$$g(t) = g^*(t) \Leftrightarrow G(-f) = G^*(f), \quad (1.105)$$

where  $*$  denotes complex conjugate. Furthermore, if  $g(t)$  is real-valued and an even function, then its spectrum also is real and even:

$$\begin{cases} g(t) = g^*(t) \\ g(t) = g(-t) \end{cases} \Leftrightarrow \begin{cases} G(f) = G^*(f) \\ G(f) = G(-f) \end{cases}. \quad (1.106)$$

This is proved easily using (1.103). Properties (1.105) and (1.106) are just two of many special cases useful in Fourier analysis.

## 2 Ordinary Differential Equations

### 2.1 Introduction

Inertial navigation systems (INS) yield the position vector,  $\mathbf{x}$ , and the velocity vector,  $\dot{\mathbf{x}}$ , by integrating measured accelerations, essentially, according to equation (1.7). Such an equation is known as a *differential equation*: an equation that expresses a relationship between the derivative(s) of a function and possibly the independent variable(s) and the function itself.

The general form of a differential equation, of order  $m$ , may be written as

$$F(t, y, \dot{y}, \ddot{y}, \dots, y^{(m)}) = 0, \quad (2.1)$$

where, first, we consider arbitrary, scalar functions  $y(t)$  that are  $m$  times differentiable. Later we will consider differentiable vector and matrix functions. Without loss in generality and apropos of inertial navigation systems the independent variable,  $t$ , is time. The derivative operator is denoted either, as before, by a dot over the function, or by a parenthetical superscript. Since the function depends on only one independent variable in this case, the derivatives are total derivatives rather than partial derivatives, and (2.1) is known more accurately as an *ordinary differential equation*, distinct from *partial differential equations* that involve multivariate functions. Since our applications concern mostly functions in time, we restrict the discussion to the former.

Given the differential equation (2.1), it is desired to solve for the function  $y(t)$ , which involves integrating the equation with respect to  $t$ . Certain classes of differential equations have solutions that can be found analytically using various rules or formulas, and others have no analytic solution. In the general case of arbitrary equations, if an analytic solution exists, it must be guessed and checked by back-substitution (that is, a putative solution certainly must satisfy the differential equation). With today's modern computational capabilities, numerical methods are more common than in the past, and often are the only viable course to follow.

Since solving a differential equation, in essence, involves an integration, it is important to note that the solution is incomplete without a constant of integration. The solution to a differential equation of order  $m$  requires  $m$  integrations, implying that  $m$  constants must be specified. These constants are also known as initial conditions and we may think of them as indicating the values of the function and its  $m - 1$  derivatives at some (usually) initial time,  $t_0$ . Thus (2.1) should include the following statement:

$$y^{(j-1)}(t_0) = \mu_j, \quad j = 1, \dots, m, \quad (2.2)$$

where the  $\mu_j$  are constants with given values.

Differential equations pervade the study of inertial navigation systems, from the dynamics of the sensors to the determination of a navigation solution and the

analysis of the associated errors. In particular, the differential equations associated with coordinate transformations that we already encountered in Section 1.4 play an essential role in the navigation solution. However, it is clearly not the intent here to develop fully the theory of differential equations. Only results useful to our exposition of INS and its applications will be derived. This includes a general treatment of linear ordinary differential equations with discussion of analytic solutions and one method of numerical solution.

## 2.2 Linear Differential Equations

A *linear* differential equation is one where the relationship  $F$  in (2.1) is linear in the function  $y$  and all its derivatives, allowing (2.1) to be written as

$$y^{(m)}(t) + a_1(t)y^{(m-1)}(t) + \cdots + a_{m-1}(t)\dot{y}(t) + a_m(t)y(t) = c(t), \quad (2.3)$$

where the  $a_j(t)$  and  $c(t)$  are functions of  $t$ . The antecedent coefficient function of  $y^{(m)}(t)$  is assumed to be  $a_0(t) = 1$  without loss in generality, since any non-zero coefficient may be divided out, changing the other coefficients but not the form of the equation. A differential equation that cannot be expressed as (2.2) is *nonlinear*. Of course, the initial conditions (2.2) still must accompany (2.3).

Differential equations naturally generalize to vector functions, where an  $m^{\text{th}}$ -order, linear differential equation in the vector function,  $\mathbf{y}(t)$ , may be written as

$$\mathbf{y}^{(m)}(t) + A_1(t)\mathbf{y}^{(m-1)}(t) + \cdots + A_{m-1}(t)\dot{\mathbf{y}}(t) + A_m(t)\mathbf{y}(t) = \mathbf{c}(t), \quad (2.4)$$

with initial values

$$\mathbf{y}^{(j-1)}(t_0) = \boldsymbol{\mu}_j, \quad j = 1, \dots, m. \quad (2.5)$$

The  $A_j(t)$  are square matrices whose elements are functions of  $t$ ,  $\mathbf{c}(t)$  is a vector function of  $t$ , and the  $\boldsymbol{\mu}_j$  are constant vectors of given values. Again, with no loss in generality,  $A_0(t) = I$ . Equation (2.4) constitutes a *system* of linear,  $m^{\text{th}}$ -order, differential equations for the component functions of the vector,  $\mathbf{y}(t)$ . That is, let

$$\mathbf{y}(t) = \begin{pmatrix} y_1(t) \\ \vdots \\ y_n(t) \end{pmatrix}, \quad (2.6)$$

then

$$\dot{\mathbf{y}}(t) = \begin{pmatrix} \dot{y}_1(t) \\ \vdots \\ \dot{y}_n(t) \end{pmatrix}, \quad (2.7)$$

and (2.4) can be expanded to yield a set of  $n$  *coupled*, scalar, linear differential equations in the functions  $y_1(t), \dots, y_n(t)$ . An example of such a coupled set is the set of first-order equations (1.74) for the quaternions, whose vector equivalent is (1.75). Incidentally, it is worth noting that the corresponding differential equation (1.95) for the roll, pitch, and yaw angles is non-linear.

A scalar, linear differential equation of any order  $m$ , such as (2.3), may be written as a system of  $m$  *first-order* linear differential equations by letting

$$y_j(t) = y^{(j-1)}(t), \quad j = 1, \dots, m. \quad (2.8)$$

With this definition, it is easy to verify that (2.3) is equivalent to

$$\frac{d}{dt} \begin{pmatrix} y_1(t) \\ y_2(t) \\ \vdots \\ y_{m-1}(t) \\ y_m(t) \end{pmatrix} + \begin{pmatrix} 0 & -1 & 0 & \cdots & 0 \\ 0 & 0 & -1 & \cdots & 0 \\ \vdots & \vdots & \vdots & \ddots & \vdots \\ 0 & 0 & 0 & \cdots & -1 \\ a_m(t) & a_{m-1}(t) & a_{m-2}(t) & \cdots & a_1(t) \end{pmatrix} \begin{pmatrix} y_1(t) \\ y_2(t) \\ \vdots \\ y_{m-1}(t) \\ y_m(t) \end{pmatrix} = \begin{pmatrix} 0 \\ 0 \\ \vdots \\ 0 \\ c(t) \end{pmatrix}, \quad (2.9)$$

which is exactly of the type (2.4) with  $m = 1$ . It is left as an exercise to the reader to show that any higher ( $m > 1$ ) order system of linear differential equations, such as (2.4), may be reduced to a first-order system using an artifice like (2.8).

One further generalization of linear differential equations may be considered. Instead of vector functions, suppose the differential equation is for a matrix function, as was introduced for the rotation transformation matrices, equation (1.66). The general equation for the  $n \times p$  matrix function  $Y(t)$ ,

$$Y^{(m)}(t) + A_1(t)Y^{(m-1)}(t) + \cdots + A_{m-1}(t)\dot{Y}(t) + A_m(t)Y(t) = C(t), \quad (2.10)$$

where  $C(t)$  is an  $n \times p$  matrix also with functions of  $t$  as elements, may be thought of as a separable collection of differential equations of the type (2.4), since we may write  $Y(t)$  as a collection of column vectors:

$$Y(t) = [y_1(t) \cdots y_p(t)]. \quad (2.11)$$

The solutions for individual vectors,  $y_k(t)$ ,  $k = 1, \dots, p$ , are similar, with differences arising only from the different columns of  $C(t)$ .

With these arguments, we may reduce a general treatment of linear differential equations (scalar, vector, or matrix) of arbitrary order to a study of linear, first-order, differential equations of vectors. Thus, consider a system of linear differential equations expressed succinctly, including initial values, as:

$$\dot{y}(t) + A(t)y(t) = c(t), \quad (2.12)$$

$$y(t_0) = \mu, \quad (2.13)$$

where  $A(t)$  is a general square matrix function of  $t$ . We will assume the dimension of  $A$  is  $n \times n$ ; that is, there are  $n$  equations in the system and  $n$  components of  $y(t)$  with  $n$  initial values, contained in the vector,  $\mu$ .

## 2.3 General Solution of Linear Differential Equations

The solution to a differential equation from a theoretical viewpoint hinges in the first place on two important types of theorems: an existence theorem and a unique-

ness theorem. An existence theorem for any particular class of differential equations specifies the conditions on the functions involved that will guarantee the existence of a solution. Often, the existence theorem will not actually show how the solution is to be constructed, but knowing that a solution exists at least allows one to pursue it. If a uniqueness theorem can be proved for the class of differential equations, then having found a solution to a certain differential equation with initial conditions means that no different solution exists.

For the system of linear, first-order, differential equations (2.12), one has, in fact, very strong existence and uniqueness theorems (Boyce and DiPrima, 1969). In essence, they state that if the component functions of the matrix,  $A(t)$ , and of the vector,  $c(t)$ , are continuous in an interval containing the initial point,  $t_0$ , then there exists a unique solution,  $y(t)$ , that satisfies the differential equation (2.12) in that interval and also the initial conditions, (2.13).

In constructing a solution to (2.12), it is convenient to consider first the corresponding differential equation that excludes the term not depending on the function,  $y(t)$ , that is, the vector  $c(t)$ . This is called the *homogeneous* differential equation given by

$$\dot{y}(t) + A(t)y(t) = \mathbf{0}, \quad (2.14)$$

where the right-hand side is the zero vector. A solution to (2.14) is known as a *homogeneous solution*. Let  $y_H(t)$  denote such a solution. If  $y_P(t)$  is any solution of the original, non-homogeneous, differential equation (often known as the *particular solution*), then the sum  $y_H(t) + y_P(t)$  is also a solution of the original equation. Indeed:

$$\begin{aligned} & \frac{d}{dt}(y_H(t) + y_P(t)) + A(t)(y_H(t) + y_P(t)) \\ &= (\dot{y}_H(t) + A(t)y_H(t)) + (\dot{y}_P(t) + A(t)y_P(t)) \\ &= \mathbf{0} + c(t) = c(t), \end{aligned} \quad (2.15)$$

which shows that the sum of homogeneous and particular solutions satisfies the differential equation (2.12). Moreover, without loss in generality, we may impose the condition that the homogeneous solution should satisfy the initial conditions (2.13). Then clearly

$$y_H(t_0) = \mu, \quad (2.16)$$

$$y_P(t_0) = \mathbf{0}, \quad (2.17)$$

which specifies the initial condition for the particular solution. It is often easier to find a general solution of the homogeneous equation, including the initial condition, than to deal with the non-homogeneous part in a general way.

Before proceeding, we mention that a general method of solving these differential equations can also be developed on the basis of the Laplace transform. That is, the differential equation is first transformed into a corresponding algebraic equation where the independent variable is in a different domain (analogous to the frequency

domain associated with the Fourier transform, see Section 1.6). This method has the advantage of more crisply distinguishing the contributions to the solution due to  $A(t)$  (i.e., the system function) and due to  $c(t)$  and  $\mu$  (i.e., the excitation function and initial condition), at least in the transformed domain. However, it operates under the same restrictions that we must impose on  $A(t)$  in the following exposition. We will not use Laplace transforms here; and the interested reader is referred to (Thomson, 1960) for the general treatment and application of Laplace transforms, as well as to any comprehensive text on differential equations.

### 2.3.1 Homogeneous Solution

We consider first the homogeneous differential equation (2.14), where we temporarily dispense with the special subscript, H. In addition, we make the fundamental assumption that the coefficient matrix,  $A(t)$ , in fact, is a *constant* matrix. This will allow us to construct a solution in a general analytic sense. Standard analytic solutions for variable matrices,  $A(t)$ , are restricted to special cases, such as periodic functions (e.g., see Wilson, 1971), or so-called reducible systems (Goursat, 1945). Thus, suppose that

$$\dot{\mathbf{y}}(t) + A\mathbf{y}(t) = \mathbf{0}, \quad (2.18)$$

whose solution satisfies the initial condition (2.13). It is known that solutions to (2.18) have the form

$$\mathbf{y}(t) = \rho e^{-\lambda(t-t_0)}, \quad (2.19)$$

where  $\rho$  is a constant vector and  $\lambda$  is a number (positive or negative; real or complex). Formally, one would say that (2.19) is a reasonable guess at a solution and then verify this conjecture by substitution. We have, in fact,

$$\frac{d}{dt}(\rho e^{-\lambda(t-t_0)}) + A\rho e^{-\lambda(t-t_0)} = (A - \lambda I)\rho e^{-\lambda(t-t_0)}; \quad (2.20)$$

and the function (2.19) is a solution to (2.18) if and only if (2.20) is zero. This is zero if and only if

$$(A - \lambda I)\rho = \mathbf{0}, \quad (2.21)$$

since the exponential function cannot be zero. If we are seeking only non-trivial, that is, non-zero solutions, then clearly we require that  $\rho \neq \mathbf{0}$ . In order for this to hold, the matrix,  $A - \lambda I$ , must not be invertible; for if it were, then multiplying both sides of (2.21) by its inverse would imply the undesired  $\rho = \mathbf{0}$ .

The singularity of  $A - \lambda I$  is guaranteed for those values,  $\lambda$ , that make its determinant vanish:

$$\det(A - \lambda I) = 0, \quad (2.22)$$

The left-hand side is a polynomial of degree  $n$  in the variable,  $\lambda$ :

$$\lambda^n + \alpha_1\lambda^{n-1} + \cdots + \alpha_n = 0, \quad (2.23)$$

where the  $\alpha_j$  are constants and the values,  $\lambda$ , that satisfy this equation, or equation

(2.22), are the roots of the polynomial. Since the polynomial, which is called the *characteristic polynomial* of  $A$ , is of degree  $n$ , it has exactly  $n$  roots. These roots are called *eigenvalues* of the matrix,  $A$ ; and for each such eigenvalue,  $\lambda_j$ , there is an *eigenvector*,  $\rho_j$ , such that, from (2.21),

$$A\rho_j = \lambda_j \rho_j. \quad (2.24)$$

In summary, a guess at a solution, (2.19), with constant quantities,  $\lambda$  and  $\rho$ , has led us to the condition (2.24) among these constant quantities, so that the solutions to (2.18) are, more specifically, given by

$$y_j(t) = \rho_j e^{-\lambda_j(t-t_0)}. \quad (2.25)$$

If the eigenvalues are all different, then it can be shown that the eigenvectors are all independent (Lange, 1971). The eigenvectors can be determined by solving the set of linear equations (2.21) for  $\rho_j$ , with  $\lambda_j$  substituted. Thus, we may assume that the eigenvalues and eigenvectors are known and a general solution to (2.18) is given by a linear combination of the solutions (2.25):

$$y(t) = \sum_{j=1}^n \eta_j y_j(t) = \sum_{j=1}^n \eta_j \rho_j e^{-\lambda_j(t-t_0)}, \quad (2.26)$$

where the  $\eta_j$  are arbitrary numbers. With  $\boldsymbol{\eta} = [\eta_1 \cdots \eta_n]^T$  and defining the matrix,  $T = [\rho_1 \cdots \rho_n]$ , this may be written as

$$y(t) = T \operatorname{diag}(e^{-\lambda_j(t-t_0)}) \boldsymbol{\eta}, \quad (2.27)$$

where  $\operatorname{diag}(e^{-\lambda_j(t-t_0)})$  represents a diagonal matrix with  $j$ -th diagonal element as indicated.

The numbers,  $\eta_j$ , are determined from the initial condition (2.13). Substituting (2.27) with  $t = t_0$  into (2.13), we have

$$T \boldsymbol{\eta} = \boldsymbol{\mu}. \quad (2.28)$$

The constant vector,  $\boldsymbol{\eta}$ , can then be determined from

$$\boldsymbol{\eta} = T^{-1} \boldsymbol{\mu}, \quad (2.29)$$

since the eigenvectors are independent (assuming distinct eigenvalues) and, therefore, the matrix,  $T$ , is nonsingular. The solution (2.27), with initial conditions (2.29) substituted, is finally given by

$$y(t) = T \operatorname{diag}(e^{-\lambda_j(t-t_0)}) T^{-1} \boldsymbol{\mu}. \quad (2.30)$$

An alternate form of this solution derives from the power series for the exponential. Substituting the first equation of (1.30) with  $p = -\lambda_j(t - t_0)$  into (2.26), we find

$$y(t) = \sum_{j=1}^n \eta_j \rho_j \sum_{k=0}^{\infty} \frac{(-1)^k}{k!} \lambda_j^k (t - t_0)^k. \quad (2.31)$$

Now, from (2.24) it is easily verified that for any  $k \geq 0$

$$\lambda_j^k \rho_j = \lambda_j^{k-1} A \rho_j = \lambda_j^{k-2} A^2 \rho_j = \cdots = A^k \rho_j. \quad (2.32)$$

Then, interchanging summations in (2.31) and substituting (2.32) yields

$$\mathbf{y}(t) = \sum_{k=0}^{\infty} \frac{(-1)^k}{k!} (t - t_0)^k A^k \sum_{j=1}^n \eta_j \rho_j. \quad (2.33)$$

Noting from (2.28) that  $\sum \eta_j \rho_j = \mu$ , we find that

$$\mathbf{y}(t) = \sum_{k=0}^{\infty} \frac{(-1)^k}{k!} (t - t_0)^k A^k \mu. \quad (2.34)$$

Formally, one may now write the series in powers of the matrix,  $A$ , in exponential fashion:

$$e^{-A(t-t_0)} = \sum_{k=0}^{\infty} \frac{(-1)^k}{k!} (t - t_0)^k A^k. \quad (2.35)$$

Using this convenient notation, the solution to the homogeneous differential equation (2.18), with initial condition (2.16), may be written as

$$\mathbf{y}(t) = e^{-A(t-t_0)} \mu. \quad (2.36)$$

In this form the solution avoids the determination of eigenvalues and eigenvectors, but, in principle, all powers of the matrix,  $A$ , must be determined and summed as indicated by (2.35). Although it may be obscure and rather complicated, an analytic form always results from this labor because (2.36) is identical to (2.30).

On the basis of our previous discussion in Section 2.2, we easily find the solution to the matrix differential equation

$$\dot{\mathbf{Y}}(t) + A \mathbf{Y}(t) = 0, \quad (2.37)$$

with initial condition,  $\mathbf{Y}(t_0) = \mathbf{M}$ ; it is given by

$$\mathbf{Y}(t) = e^{-A(t-t_0)} \mathbf{M}. \quad (2.38)$$

If the eigenvalues of  $A$  are not all distinct, then the general form (2.26) (or 2.30) may no longer be valid, but (2.36) still does represent the solution, since from (2.35) it is readily shown that

$$\frac{d}{dt} e^{-A(t-t_0)} = -A e^{-A(t-t_0)}, \quad (2.39)$$

and, therefore, (2.36) satisfies (2.18) as well as the initial condition (2.16).

We return now to the solution in terms of the eigenvalues, again assumed distinct. Each component of the solution vector,  $\mathbf{y}(t)$ , according to (2.26) or (2.30), is a linear combination of exponential functions,  $e^{-\lambda_j(t-t_0)}$ ; and, hence, the eigenvalues,  $\lambda_j$ , of the coefficient matrix,  $A$ , determine the behavior of the solution. In particular, if one of the eigenvalues is zero, then the components of  $\mathbf{y}(t)$  include a constant term, since  $e^0 = 1$ . If an eigenvalue is real and positive, then the corresponding part of the solution exponentially approaches zero with increasing  $t$ ; if it is real and negative, the solution (in absolute value) increases exponentially.

If an eigenvalue is a complex number,  $\lambda_j = \alpha_j + i\beta_j$ , where  $i$  is the imaginary unit ( $i^2 = -1$ ), and  $\alpha_j, \beta_j$  are real numbers, then with Euler's equation (1.29) the corresponding part of the solution varies according to

$$e^{-\lambda_j(t-t_0)} = e^{-\alpha_j(t-t_0)}(\cos(\beta_j(t-t_0)) - i \sin(\beta_j(t-t_0))). \quad (2.40)$$

That is, the solution is oscillatory with period  $2\pi/\beta_j$  and amplitude  $e^{-\alpha_j(t-t_0)}$ . Again, depending on whether  $\alpha_j$  is positive, zero, or negative, the amplitude of the oscillations will decay to zero, remain constant, or become unbounded.

If the matrix,  $A$ , is real (which, in our practice, will always be the case), then for each complex eigenvalue, there is another that is its conjugate, for otherwise the polynomial (2.23) would not be real. Furthermore, the oscillatory solutions for each pair of conjugate eigenvalues will combine to yield a real solution, as required.

### 2.3.1.1 An Example

To illustrate the solutions arising from a linear, homogeneous, differential equation, consider the second-order equation with constant coefficients:

$$\ddot{y} + \beta y = 0; \quad y(0) = \mu_1; \quad \dot{y}(0) = \mu_2; \quad (2.41)$$

where  $\beta$  and  $\mu_j$  are real numbers and  $t_0 = 0$ . First, we recast this equation as a first-order system of equations, as in (2.9):

$$\frac{d}{dt} \begin{pmatrix} y_1 \\ y_2 \end{pmatrix} + \begin{pmatrix} 0 & -1 \\ \beta & 0 \end{pmatrix} \begin{pmatrix} y_1 \\ y_2 \end{pmatrix} = \begin{pmatrix} 0 \\ 0 \end{pmatrix}; \quad y_1(0) = \mu_1; \quad y_2(0) = \mu_2; \quad (2.42)$$

where, according to (2.8), we let  $y_1 = y$  and  $y_2 = \dot{y}$ .

Using (2.22), the eigenvalues of the coefficient matrix are the roots of

$$\lambda^2 + \beta = 0. \quad (2.43)$$

They are

$$\lambda_1 = +\sqrt{-\beta}; \quad \lambda_2 = -\sqrt{-\beta}; \quad (2.44)$$

and it can be verified using (2.20) that the corresponding eigenvectors are

$$\rho_1 = \begin{pmatrix} 1 \\ -\sqrt{-\beta} \end{pmatrix}; \quad \rho_2 = \begin{pmatrix} 1 \\ \sqrt{-\beta} \end{pmatrix}. \quad (2.45)$$

The solution to (2.42) according to the form (2.30) is given by

$$\begin{pmatrix} y_1(t) \\ y_2(t) \end{pmatrix} = \frac{1}{2\sqrt{-\beta}} \begin{pmatrix} 1 & 1 \\ -\sqrt{-\beta} & \sqrt{-\beta} \end{pmatrix} \begin{pmatrix} e^{-\sqrt{-\beta}t} & 0 \\ 0 & e^{\sqrt{-\beta}t} \end{pmatrix} \begin{pmatrix} \sqrt{-\beta} & -1 \\ \sqrt{-\beta} & 1 \end{pmatrix} \begin{pmatrix} \mu_1 \\ \mu_2 \end{pmatrix}. \quad (2.46)$$

From this the solution to (2.41) may be extracted:

$$y(t) = \frac{1}{2\sqrt{-\beta}} [(\sqrt{-\beta}\mu_1 + \mu_2)e^{\sqrt{-\beta}t} + (\sqrt{-\beta}\mu_1 - \mu_2)e^{-\sqrt{-\beta}t}]. \quad (2.47)$$

If  $\beta < 0$ , then the eigenvalues are real and we have

$$y(t) = \frac{1}{2\sqrt{|\beta|}} [(\sqrt{|\beta|}\mu_1 + \mu_2)e^{\sqrt{|\beta|}t} + (\sqrt{|\beta|}\mu_1 - \mu_2)e^{-\sqrt{|\beta|}t}], \quad (2.48)$$

showing that the solution increases without bound as  $t \rightarrow \pm\infty$ . If  $\beta > 0$ , then the eigenvalues are imaginary numbers; and, with (1.29), we write the solution in terms of sinusoids to obtain:

$$y(t) = \mu_1 \cos(\sqrt{\beta}t) + \frac{\mu_2}{\sqrt{\beta}} \sin(\sqrt{\beta}t). \quad (2.49)$$

This is the solution to the classic harmonic oscillator with period given by  $2\pi/\sqrt{\beta}$ .

If  $\beta = 0$ , then the solution does not have the form (2.30), since in this case the eigenvalues are not distinct, as presumed in the development leading to (2.26). However, we find that the powers of the coefficient matrix are given by:

$$\begin{pmatrix} 0 & -1 \\ 0 & 0 \end{pmatrix}^k = \begin{pmatrix} 0 & 0 \\ 0 & 0 \end{pmatrix}; \quad k \geq 2. \quad (2.50)$$

Substituting this into (2.35), we easily determine the solution in the form (2.36), where the first component is our desired result:

$$y(t) = \mu_1 + \mu_2(t - t_0). \quad (2.51)$$

This is the familiar solution to the position of a body undergoing no acceleration:  $\ddot{y}(t) = 0$ .

The last case in this example shows what happens when an eigenvalue is repeated; i.e., when it has *multiplicity* greater than one. In general, if the coefficient matrix,  $A$ , is symmetric, then even if some eigenvalues are repeated, the form of the solution is still given by (2.26) or (2.30), since  $n$  linearly independent eigenvectors can be found. For other matrices whose eigenvalues have multiplicity  $q > 1$ , it may not be possible to find  $q$  corresponding linearly independent eigenvectors. The interested reader is referred to (Boyce and DiPrima, 1969) for further development of this situation using matrix theory. It is noted, again, that (2.36) holds regardless of the multiplicity of the eigenvalues.

### 2.3.1.2 Fundamental Set of Solutions

The construction of a solution for the homogeneous equation was developed explicitly for the case that the coefficient matrix,  $A$ , is a constant. In the case that it is a function of  $t$ , a solution may still be obtained, however, there are no standard techniques that apply to all situations. Nevertheless, it can be proved (Boyce and DiPrima, 1969) that if the elements of the  $n \times n$  matrix,  $A(t)$ , are continuous functions, then there exists a set of  $n$  linearly independent solutions; let these be denoted  $y_1(t), \dots, y_n(t)$ . Furthermore, any solution of (2.14) can be written as a linear combination of the  $y_j(t)$ :

$$\mathbf{y}(t) = \sum_{j=1}^n c_j y_j(t). \quad (2.52)$$

The set of linearly independent solutions is called a *fundamental set of solutions*. They may be combined to form the columns of the *fundamental matrix*,  $\Psi(t) = [y_1(t) \cdots y_n(t)]$ ; and the solution (2.52) has the form

$$\mathbf{y}(t) = \Psi(t)\mathbf{c}, \quad (2.53)$$

where  $\mathbf{c}$  is the vector of constants,  $c_j$ .

The fundamental matrix,  $\Psi(t)$ , because of the linear independence of its columns is nonsingular. Therefore, with initial conditions (2.16), we have  $\mathbf{c} = \Psi^{-1}(t_0)\boldsymbol{\mu}$ , and

$$\mathbf{y}(t) = \Phi(t, t_0)\boldsymbol{\mu}, \quad (2.54)$$

where

$$\Phi(t, t_0) = \Psi(t)\Psi^{-1}(t_0). \quad (2.55)$$

Substituting (2.54) into (2.14), we see that

$$\left[ \frac{d}{dt} \Phi(t, t_0) + A(t)\Phi(t, t_0) \right] \boldsymbol{\mu} = 0. \quad (2.56)$$

Since we wish to put no restrictions on the value of  $\boldsymbol{\mu}$  (it is arbitrary), the bracketed term must be the zero matrix. Therefore,  $\Phi(t, t_0)$ , satisfies the following differential equation, with initial condition:

$$\frac{d}{dt} \Phi(t, t_0) + A(t)\Phi(t, t_0) = 0; \quad \Phi(t_0, t_0) = I. \quad (2.57)$$

For the special case that the coefficient matrix is a constant, the solution is given by (2.38):

$$\Phi(t, t_0) = e^{-A(t-t_0)}, \quad (2.58)$$

which, when substituted into (2.54), yields the solution for  $\mathbf{y}(t)$ , in agreement with (2.36).

The matrix  $\Phi(t, t_0)$  has the interpretation of a “transition matrix” that takes the solution from its initial value to the value at some arbitrary  $t$ . Hence, this form of the solution will be especially useful in connection with the Kalman filter (Chapter 7) because of its recursive nature. Also, (2.54) is the starting point for determining a particular solution, as shown in the next section.

### 2.3.2 Particular Solution

Although a solution to the homogenous, linear differential equation with variable coefficient matrix,  $A(t)$ , may not be determined using standard techniques, if such a solution has been found, the particular solution may be obtained using the method of *variation of parameters*. Therefore, consider the non-homogeneous, first-order, linear differential equation (2.12) with initial conditions (2.13), repeated for convenience:

$$\dot{\mathbf{y}}(t) + A(t)\mathbf{y}(t) = \mathbf{c}(t), \quad (2.59)$$

$$\mathbf{y}(t_0) = \boldsymbol{\mu}. \quad (2.60)$$

The functions contained in the coefficient matrix, as well as in the vector,  $\mathbf{c}(t)$ , are assumed to be continuous. Also, we suppose that a solution to the corresponding homogeneous equation has been found, as in (2.54):

$$\mathbf{y}_H(t) = \Phi(t, t_0)\boldsymbol{\mu}. \quad (2.61)$$

The method of variation of parameters seeks a particular solution of the form

$$\mathbf{y}_P(t) = \Phi(t, t_0)\mathbf{v}(t), \quad (2.62)$$

$$\mathbf{y}_P(t_0) = \mathbf{0}, \quad (2.63)$$

where  $\mathbf{v}(t)$  is a vector function to be determined, and the initial condition is in accordance with (2.17).

We proceed in a straightforward manner, first substituting  $\mathbf{y}_P$ , as given by (2.62), back into equation (2.59) of which it is supposed to be a solution:

$$\frac{d}{dt}\Phi(t, t_0)\mathbf{v}(t) + \Phi(t, t_0)\frac{d}{dt}\mathbf{v}(t) + A(t)\Phi(t, t_0)\mathbf{v}(t) = \mathbf{c}(t). \quad (2.64)$$

Then, making use of (2.57), we find

$$\Phi(t, t_0)\frac{d}{dt}\mathbf{v}(t) = \mathbf{c}(t), \quad (2.65)$$

or

$$\frac{d}{dt}\mathbf{v}(t) = \Phi^{-1}(t, t_0)\mathbf{c}(t), \quad (2.66)$$

since  $\Phi(t, t_0)$ , like  $\Psi(t)$ , is invertible. The integral of (2.66) yields the desired vector function,  $\mathbf{v}(t)$ :

$$\mathbf{v}(t) = \int_{t_0}^t \Phi^{-1}(\tau, t_0)\mathbf{c}(\tau) d\tau, \quad (2.67)$$

where the corresponding constant of integration has been chosen equal to zero to ensure the condition (2.63).

Combining (2.67) with (2.62) and (2.61) leads to the total solution:

$$\mathbf{y}(t) = \Phi(t, t_0)\boldsymbol{\mu} + \Phi(t, t_0) \int_{t_0}^t \Phi^{-1}(\tau, t_0)\mathbf{c}(\tau) d\tau. \quad (2.68)$$

Now, using (2.55), we deduce:

$$\Phi(t, t_0)\Phi^{-1}(\tau, t_0) = \Psi(t)\Psi^{-1}(t_0)\Psi(t_0)\Psi^{-1}(\tau) = \Phi(t, \tau). \quad (2.69)$$

With this, (2.68) may be simplified to yield the final form of the solution to the non-homogeneous equation (2.59):

$$\mathbf{y}(t) = \Phi(t, t_0)\boldsymbol{\mu} + \int_{t_0}^t \Phi(t, \tau)\mathbf{c}(\tau) d\tau. \quad (2.70)$$

The corresponding total solution to the first-order matrix differential equation,

$$\dot{Y}(t) + A(t)Y(t) = C(t), \quad Y(t_0) = M, \quad (2.71)$$

is the straightforward extension of (2.70):

$$Y(t) = \Phi(t, t_0)M + \int_{t_0}^t \Phi(t, \tau)C(\tau) d\tau. \quad (2.72)$$

In Chapter 7, we will also encounter a first-order, linear, matrix differential equation of slightly different form:

$$\dot{Y}(t) + A(t)Y(t) + Y(t)B(t) = C(t), \quad Y(t_0) = M. \quad (2.73)$$

Its solution is given by

$$Y(t) = \Phi(t, t_0)M\Theta(t, t_0) + \int_{t_0}^t \Phi(t, \tau)C(\tau)\Theta(t, \tau) d\tau, \quad (2.74)$$

where, analogous to (2.57),

$$\frac{d}{dt}\Theta(t, t_0) + \Theta(t, t_0)B(t) = 0; \quad \Theta(t_0, t_0) = I. \quad (2.75)$$

We prove (2.74) by back-substitution. That is, we show that (2.74) indeed satisfies the initial condition and its derivative satisfies the differential equation (2.73).

The first task is easy since  $\Phi(t_0, t_0) = I$  and  $\Theta(t_0, t_0) = I$  imply that when  $t = t_0$  is substituted into (2.74) we obtain  $Y(t_0) = M$ . Taking the derivative of (2.74) yields

$$\begin{aligned} \dot{Y}(t) &= \dot{\Phi}(t, t_0)M\Theta(t, t_0) + \Phi(t, t_0)M\dot{\Theta}(t, t_0) \\ &\quad + \int_{t_0}^t [\dot{\Phi}(t, \tau)C(\tau)\Theta(t, \tau) + \Phi(t, \tau)C(\tau)\dot{\Theta}(t, \tau)] d\tau \\ &\quad + \Phi(t, t)C(t)\Theta(t, t)\frac{dt}{dt}, \end{aligned} \quad (2.76)$$

with due application of Leibnitz's rule for differentiating an integral. Now substitute (2.57) and (2.75) to obtain

$$\begin{aligned} \dot{Y}(t) &= -A(t)\Phi(t, t_0)M\Theta(t, t_0) - \Phi(t, t_0)M\Theta(t, t_0)B(t) \\ &\quad - A(t) \int_{t_0}^t \Phi(t, \tau)C(\tau)\Theta(t, \tau) d\tau - \int_{t_0}^t \Phi(t, \tau)C(\tau)\Theta(t, \tau) d\tau B(t) + C(t). \end{aligned} \quad (2.77)$$

Each integral term above can be replaced with  $Y(t) - \Phi(t, t_0)M\Theta(t, t_0)$  from (2.74); and the result is (2.73), as was to be shown.

### 2.3.2.1 The Example, Continued

We obtain the same homogeneous solution for the differential equation (2.42) in the example of Section 2.3.1.1 using the formulas (2.54) and (2.58). Identifying the

coefficient matrix in (2.42) by  $A$ , it is readily verified that

$$\begin{aligned} A^2 &= \begin{pmatrix} -\beta & 0 \\ 0 & -\beta \end{pmatrix}, \quad A^3 = \begin{pmatrix} 0 & \beta \\ -\beta^2 & 0 \end{pmatrix}, \quad A^4 = \begin{pmatrix} \beta^2 & 0 \\ 0 & \beta^2 \end{pmatrix}, \\ A^5 &= \begin{pmatrix} 0 & -\beta^2 \\ \beta^3 & 0 \end{pmatrix}, \dots \end{aligned} \quad (2.78)$$

Therefore, from (2.35), we have with  $\Delta t = t - t_0$ :

$$e^{-A\Delta t} = \begin{pmatrix} 1 - \frac{\beta}{2!}\Delta t^2 + \frac{\beta^2}{4!}\Delta t^4 - \frac{\beta^3}{6!}\Delta t^6 + \dots & \Delta t - \frac{\beta}{3!}\Delta t^3 + \frac{\beta^2}{5!}\Delta t^5 - \frac{\beta^3}{7!}\Delta t^7 + \dots \\ -\beta\Delta t + \frac{\beta^2}{3!}\Delta t^3 - \frac{\beta^3}{5!}\Delta t^5 + \dots & 1 - \frac{\beta}{2!}\Delta t^2 + \frac{\beta^2}{4!}\Delta t^4 - \frac{\beta^3}{6!}\Delta t^6 + \dots \end{pmatrix}. \quad (2.79)$$

If  $\beta > 0$ , then the transition matrix,  $\Phi(t, t_0)$ , is found with the help of (1.30) to be:

$$\Phi(t, t_0) = \begin{pmatrix} \cos(\sqrt{\beta}\Delta t) & \frac{1}{\sqrt{\beta}} \sin(\sqrt{\beta}\Delta t) \\ -\sqrt{\beta} \sin(\sqrt{\beta}\Delta t) & \cos(\sqrt{\beta}\Delta t) \end{pmatrix}, \quad (2.80)$$

thus yielding, through (2.54), the usual harmonic oscillator solution already shown in (2.49) for the first component,  $y_1$ , as well as its derivative,  $y_2$ .

If  $\beta < 0$ , then  $-\beta = |\beta| > 0$ ; and the series in (2.79) sum to hyperbolic sines and cosines:

$$\Phi(t, t_0) = \begin{pmatrix} \cosh(\sqrt{|\beta|}\Delta t) & \frac{1}{\sqrt{|\beta|}} \sinh(\sqrt{|\beta|}\Delta t) \\ \sqrt{|\beta|} \sinh(\sqrt{|\beta|}\Delta t) & \cosh(\sqrt{|\beta|}\Delta t) \end{pmatrix}, \quad (2.81)$$

which yields the solution, according to (2.54), that is identical to (2.48).

Consider now the non-homogeneous differential equation, generalized from (2.41):

$$\ddot{y} + \beta y = c(t); \quad y(0) = \mu_1; \quad \dot{y}(0) = \mu_2; \quad (2.82)$$

where  $c(t)$  is called the *forcing function*, assumed to be integrable. With  $\beta > 0$ , this describes the dynamics of a *forced harmonic oscillator*. Equation (2.82) can be re-written as a system of non-homogeneous, first-order differential equations:

$$\frac{d}{dt} \begin{pmatrix} y_1 \\ y_2 \end{pmatrix} + \begin{pmatrix} 0 & -1 \\ \beta & 0 \end{pmatrix} \begin{pmatrix} y_1 \\ y_2 \end{pmatrix} = \begin{pmatrix} 0 \\ c(t) \end{pmatrix}; \quad y_1(0) = \mu_1; \quad y_2(0) = \mu_2. \quad (2.83)$$

Its total solution (homogeneous plus particular parts) is given by (2.70). Extracting just the first component for  $y \equiv y_1$ , we get with  $\beta > 0$ :

$$\begin{aligned} y(t) &= \mu_1 \cos(\sqrt{\beta}(t - t_0)) + \frac{\mu_2}{\sqrt{\beta}} \sin(\sqrt{\beta}(t - t_0)) \\ &\quad + \frac{1}{\sqrt{\beta}} \int_{t_0}^t \sin(\sqrt{\beta}(t - \tau)) c(\tau) d\tau; \end{aligned} \quad (2.84)$$

and with  $\beta < 0$ :

$$\begin{aligned} y(t) = & \mu_1 \cosh(\sqrt{|\beta|}(t - t_0)) + \frac{\mu_2}{\sqrt{|\beta|}} \sinh(\sqrt{|\beta|}(t - t_0)) \\ & + \frac{1}{\sqrt{|\beta|}} \int_{t_0}^t \sinh(\sqrt{|\beta|}(t - \tau)) c(\tau) d\tau. \end{aligned} \quad (2.85)$$

We note that if  $c(\tau)$  is a sinusoidal function with the same frequency,  $\sqrt{\beta}$ , then the integration in (2.84) results in a linear term in  $t$  and the solution becomes unbounded with increasing  $t$ —the forcing function in this case excites the system at its resonant frequency.

## 2.4 Numerical Methods

When analytic solutions to differential equations can be found, they provide not only a ready formula to be evaluated, but also immediate insight into the behavior of the solution. As such they are, of course, always preferred over purely numerical solutions. But, in many cases, such as when the coefficient matrix,  $A(t)$ , in (2.8) is neither constant nor of a limited class of special forms that would admit to an analytic solution, the solution can be found, if at all, only by numerical means. That is, we calculate approximate values of  $y(t)$  for a discrete and finite set of values of  $t$ . The numerical technique may be formulated as an algorithm, but the result is always only a set (or table) of calculated values; and, one must be wary of the associated algorithm error which is usually known only in terms of orders of magnitude.

There are many numerical techniques to solve differential equations, such as (2.1). We will limit the discussion to so-called single-step methods. That is, a solution is obtained successively for each value of  $t$  based on an evaluation of the functional relationship,  $F$ , at that particular  $t$  and on the solution  $y(t)$  obtained for the immediately previous value of  $t$ . This procedure is especially suited to the type of initial value problem defined in this chapter. The alternative methods, known as multi-step or difference methods, while often faster computationally, require evaluations of  $F$  at a number of successive values of  $t$ . They can be used to solve initial value problems, if a single-step method is used to obtain the first few required values of the solution. In other words, they are not self starting and care must be used to obtain the starting values with sufficient accuracy.

The single-step methods under consideration assume that the solution may be approximated by a truncated Taylor series. As such, the usual requirements on the differentiability of the solution and its derivatives must be assumed. We will also assume that the numerical solution is sufficiently stable. This will, in general, depend on the smoothness and regularity of  $F$  in the interval of  $t$  that is of interest. These questions of stability as well as convergence are left to other more comprehensive texts on differential equations and their numerical solution (e.g., Gear, 1971).

It is noted that the following discussion is not restricted to linear equations nor first-order equations. However, using the definitions (2.8), we see that any ordinary differential equation of the type (2.1) may be reduced to a *system* of first-order differential equations:

$$\dot{y}(t) = f(t, y(t)), \quad (2.86)$$

with initial conditions (2.13). And similarly a *system* of higher-order differential equations may be thus reduced. On the other hand, there is no intrinsic difference in the numerical algorithms to be derived for the vector equation (2.86) and the corresponding scalar equation:

$$\dot{y}(t) = f(t, y(t)). \quad (2.87)$$

Therefore, we start with the latter in order to simplify the notation in the derivations.

### 2.4.1 Runge-Kutta Methods

The general idea behind the Runge-Kutta numerical techniques is based on a Taylor series expansion of the solution:

$$\begin{aligned} y(t) &= y(t_0) + \dot{y}(t_0)(t - t_0) + \frac{1}{2!} \ddot{y}(t_0)(t - t_0)^2 + \dots \\ &\quad + \frac{1}{m!} y^{(m)}(t_0)(t - t_0)^m + \dots, \end{aligned} \quad (2.88)$$

where the first derivative is already given by (2.87) and subsequent derivatives of  $y$  can be obtained analytically from the given function,  $f$ . Up to third order we have:

$$\begin{aligned} \dot{y}(t_0) &= f, \\ \ddot{y}(t_0) &= f_t + f_y f, \\ \dddot{y}(t_0) &= f_{tt} + 2f_{ty}f + f_{yy}f^2 + f_t f_y + f_y^2 f, \end{aligned} \quad (2.89)$$

where the subscripted variables on the function indicate partial differentiation; and furthermore, in this case,  $f$  and its derivatives are evaluated at  $t = t_0$ ,  $y = y_0$ , e.g.:

$$f_{ty} = \left. \frac{\partial^2 f}{\partial t \partial y} \right|_{t=t_0, y=y_0}. \quad (2.90)$$

Since  $y(t_0) = y_0$  is given, the first derivative,  $f(t_0, y_0)$ , and all subsequent derivatives can be evaluated at  $t_0$ . Substituting (2.89) into (2.88) then yields an approximation to the solution for  $t$  in a neighborhood of  $t_0$ , provided the series converges in this neighborhood.

However, to circumvent the usually cumbersome, if not difficult, determination of these higher derivatives, the Runge-Kutta methods seek to approximate the solution by a polynomial in  $(t - t_0)$  that agrees with the Taylor series up to some specified degree, but is derived from a different geometric argument. Instead of predicting

the value of the solution at  $t$ , according to the Taylor series, from values of its derivatives of several orders at the initial point, the prediction is based on a suitably weighted average of slopes, or first derivatives, at several points in the neighborhood of  $t_0$ .

In the general formulation, the solution for a sequence of discrete values of  $t$  is obtained iteratively, where the solution at  $t_n$  is based on the solution already obtained at  $t_{n-1}$  and serves as initial value for the solution to be obtained at  $t_{n+1}$ , etc. The interval between successive steps in  $t$  need not be constant, although in practice it is often so organized. Thus, let

$$h = t_{n+1} - t_n \quad (2.91)$$

be the step size of the algorithm. (If  $h$  is not constant, replace  $h$  in the following formulas by an appropriately defined  $h_{n+1}$ .) We seek an approximation to the solution having the form

$$y_{n+1} = y_n + h(\alpha_1 k_1 + \alpha_2 k_2 + \dots + \alpha_m k_m), \quad (2.92)$$

where each of the  $k_j$  is a slope of  $y$  (i.e., the first derivative,  $f$ ) at some point in the closed interval  $[t_n, t_{n+1}]$ :

$$\begin{aligned} k_1 &= f(t_n, y_n), \\ k_2 &= f(t_n + \beta_2 h, y_n + \xi_{2,1} h k_1), \\ k_3 &= f(t_n + \beta_3 h, y_n + \xi_{3,1} h k_1 + \xi_{3,2} h k_2), \end{aligned} \quad (2.93)$$

The constants  $\alpha_j$ ,  $\beta_j$ , and  $\xi_{j,p}$  are to be determined such that the approximation,  $y_{n+1}$ , agrees with the true value,  $y(t_{n+1})$ , up to a certain power in  $h$ . For a Runge-Kutta algorithm of order  $m$ , their difference is then:

$$|y_{n+1} - y(t_{n+1})| = O(h^{m+1}), \quad (2.94)$$

where  $O(h^{m+1})$  stands for a term “of order  $h^{m+1}$ ”, in this case. It is understood with our notation that the subscripted values,  $y_n$ , appearing in (2.92), as well as in (2.93), are all approximations to the true values,  $y(t_n)$ , in the sense of (2.94). Clearly, the algorithm (2.92), (2.93) also requires only a single initial value,  $y_0 \equiv y(t_0)$ . Each successive  $k_j$  at points between  $t_n$  and  $t_{n+1}$  is defined for corresponding  $y$ -values propagated using previous slopes,  $k_p$ ,  $p < j$ .

It happens that up to fourth order ( $m \leq 4$ ), the  $m^{\text{th}}$ -order Runge-Kutta algorithm requires only  $m$  weighted slopes,  $k_j$ . But, for example, a sixth-order algorithm approximates the solution by a weighted sum of eight slopes (Babuska et al., 1966). The algebra becomes quite complicated for orders higher than  $m = 3$ ; and we will derive the algorithms only up to the third order, whereupon derivations of higher orders will be evident. Therefore, we wish to find an approximate solution of the form

$$y_{n+1} = y_n + h(\alpha_1 k_1 + \alpha_2 k_2 + \alpha_3 k_3), \quad (2.95)$$

where the functions  $k_j$ ,  $j = 1, 2, 3$ , are given by (2.93), and the constants  $\alpha_j$ ,  $\beta_j$ , and  $\xi_{j,p}$  are to be determined such that the error of approximation is of second, third, or fourth order.

Assuming that the function  $f(t, y)$  is continuously differentiable in a neighborhood of  $t_n$ , it may be expanded as a bivariate Taylor series with respect to the variables  $t$  and  $y$ :

$$\begin{aligned} f(t, y) &= f(t_n, y_n) + (f_t(t - t_n) + f_y(y - y_n)) \\ &\quad + \frac{1}{2!} (f_{tt}(t - t_n)^2 + 2f_{ty}(t - t_n)(y - y_n) + f_{yy}(y - y_n)^2) \\ &\quad + \dots, \end{aligned} \tag{2.96}$$

where, as before, the subscripted functions are evaluated at  $(t_n, y_n)$ . Applying this with  $t - t_n = \beta_2 h$  and  $y - y_n = \xi_{2,1} h k_1$  to  $k_2$  in (2.93), and noting that  $k_1 = f$ , we find

$$\begin{aligned} k_2 &= f + h(\beta_2 f_t + \xi_{2,1} f_y f) \\ &\quad + \frac{h^2}{2!} (\beta_2^2 f_{tt} + \xi_{2,1}^2 f_{yy} f^2 + 2\beta_2 \xi_{2,1} f_{ty} f) + O(h^3), \end{aligned} \tag{2.97}$$

where only terms up to second order in  $h$  are included explicitly. Similarly, again applying (2.96) with  $t - t_n = \beta_3 h$  and  $y - y_n = \xi_{3,1} h k_1 + \xi_{3,2} h k_2$  to  $k_3$  in (2.93), and now with (2.97), it is readily verified that

$$\begin{aligned} k_3 &= f + h(\beta_3 f_t + (\xi_{3,1} + \xi_{3,2}) f_y f) \\ &\quad + \frac{h^2}{2!} [\beta_3^2 f_{tt} + (\xi_{3,1} + \xi_{3,2})^2 f_{yy} f^2 + 2\beta_3 (\xi_{3,1} + \xi_{3,2}) f_{ty} f \\ &\quad + 2\beta_2 \xi_{3,2} f_t f_y + 2\xi_{2,1} \xi_{3,2} f_y^2 f] + O(h^3). \end{aligned} \tag{2.98}$$

Substituting (2.97) and (2.98) into (2.95) we obtain

$$\begin{aligned} y_{n+1} &= Y_{n+1} + h(\alpha_1 + \alpha_2 + \alpha_3) f \\ &\quad + h^2 [\alpha_2 (\beta_2 f_t + \xi_{2,1} f_y f) + \alpha_3 (\beta_3 f_t + (\xi_{3,1} + \xi_{3,2}) f_y f)] \\ &\quad + \frac{h^3}{2} [\alpha_2 (\beta_2^2 f_{tt} + \xi_{2,1}^2 f_{yy} f^2 + 2\beta_2 \xi_{2,1} f_{ty} f) \\ &\quad + \alpha_3 [\beta_3^2 f_{tt} + (\xi_{3,1} + \xi_{3,2})^2 f_{yy} f^2 + 2\beta_3 (\xi_{3,1} + \xi_{3,2}) f_{ty} f \\ &\quad + 2\beta_2 \xi_{3,2} f_t f_y + 2\xi_{2,1} \xi_{3,2} f_y^2 f]] \\ &\quad + O(h^4). \end{aligned} \tag{2.99}$$

Now from (2.88), the true value of the solution at  $t_{n+1}$  is given by

$$y(t_{n+1}) = y(t_n) + h\dot{y}(t_n) + \frac{h^2}{2!} \ddot{y}(t_n) + \frac{h^3}{3!} \dddot{y}(t_n) + O(h^4), \tag{2.100}$$

which, with the derivatives expressed as in (2.89), yields

$$\begin{aligned} y(t_{n+1}) &= y(t_n) + hf + \frac{h^2}{2}(f_t + f_y f) \\ &\quad + \frac{h^3}{6}(f_{tt} + 2f_{ty}f + f_{yy}f^2 + f_tf_y + f_y^2f) + O(h^4). \end{aligned} \quad (2.101)$$

Comparing coefficients of corresponding powers of  $h$  in (2.99) and (2.101), we find the following conditions on the parameters:

$$h: \quad \alpha_1 + \alpha_2 + \alpha_3 = 1, \quad (2.102)$$

$$\begin{aligned} h^2: \quad 2(\alpha_2\beta_2 + \alpha_3\beta_3) &= 1, \\ 2(\alpha_2\xi_{2,1} + \alpha_3(\xi_{3,1} + \xi_{3,2})) &= 1, \end{aligned} \quad (2.103)$$

$$\begin{aligned} 3(\alpha_2\beta_2^2 + \alpha_3\beta_3^2) &= 1, \\ 3(\alpha_2\xi_{2,1}^2 + \alpha_3(\xi_{3,1} + \xi_{3,2})^2) &= 1, \\ h^3: \quad 3(\alpha_2\beta_2\xi_{2,1} + \alpha_3\beta_3(\xi_{3,1} + \xi_{3,2})) &= 1, \\ 6\alpha_3\beta_2\xi_{3,2} &= 1, \\ 6\alpha_3\xi_{2,1}\xi_{3,2} &= 1. \end{aligned} \quad (2.104)$$

These 8 conditions are not all independent, and therefore they allow some degree of freedom in choosing the values for the 8 parameters.

For the first-order method, we require that the estimate from the algorithm agree with the true solution up to the first power in the integration interval,  $h$ . Thus we set  $\alpha_2 = 0$  and  $\alpha_3 = 0$ ; hence, from (2.102),  $\alpha_1 = 1$ . All other parameters are immaterial; and the algorithm (2.95) is given by

$$y_{n+1} = y_n + hf(t_n, y_n). \quad (2.105)$$

This is also known as the *Euler method*.

For the second-order algorithm, we consider the conditions (2.102) and (2.103) and set  $\alpha_3 = 0$ . Immediately, we see that  $\beta_2 = \xi_{2,1}$ . If we choose  $\alpha_1 = 1/2$ , then  $\beta_2 = \xi_{2,1} = 1$  and the algorithm becomes

$$\begin{aligned} y_{n+1} &= y_n + \frac{h}{2}(k_1 + k_2), \\ k_1 &= f(t_n, y_n), \\ k_2 &= f(t_n + h, y_n + hk_1). \end{aligned} \quad (2.106)$$

All three sets of conditions (2.102)–(2.104) must be fulfilled for the third-order algorithm. From the last two in (2.104), we find, again, that  $\beta_2 = \xi_{2,1}$ , which implies from (2.103) that

$$\beta_3 = \xi_{3,1} + \xi_{3,2}, \quad (2.107)$$

and consequently makes the first three conditions in (2.104) identical. We may choose  $\alpha_1 = 1/6$ ,  $\alpha_2 = 4/6$ ,  $\alpha_3 = 1/6$ , thus satisfying (2.102). Then the first con-

ditions, respectively, of (2.103) and of (2.104) together yield  $\beta_2 = 1/2$  and  $\beta_3 = 1$ . Hence,  $\xi_{2,1} = 1/2$ , and the last condition of (2.104) implies  $\xi_{3,2} = 2$ , which further implies from (2.107) that  $\xi_{3,1} = -1$ . We have constructed one possibility for a third-order Runge-Kutta algorithm:

$$\begin{aligned} y_{n+1} &= y_n + \frac{h}{6}(k_1 + 4k_2 + k_3), \\ k_1 &= f(t_n, y_n), \\ k_2 &= f\left(t_n + \frac{h}{2}, y_n + \frac{h}{2}k_1\right), \\ k_3 &= f(t_n + h, y_n - hk_1 + 2hk_2). \end{aligned} \tag{2.108}$$

Other possibilities may be derived similarly (e.g., we could choose  $\alpha_1 = 1/4$ ,  $\alpha_2 = 1/2$ ,  $\alpha_3 = 1/4$ ); as long as conditions (2.102)–(2.104) are satisfied, it is a third-order algorithm.

We give the popular fourth-order Runge-Kutta algorithm without proof:

$$\begin{aligned} y_{n+1} &= y_n + \frac{h}{6}(k_1 + 2k_2 + 2k_3 + k_4), \\ k_1 &= f(t_n, y_n), \\ k_2 &= f\left(t_n + \frac{h}{2}, y_n + \frac{h}{2}k_1\right), \\ k_3 &= f\left(t_n + \frac{h}{2}, y_n + \frac{h}{2}k_2\right), \\ k_4 &= f(t_n + h, y_n + hk_3). \end{aligned} \tag{2.109}$$

Variations of the fourth-order algorithm and a six-order algorithm are given by Babuska et al. (1966).

As a final note, while the developments of these numerical techniques were restricted to the scalar case, all could be duplicated for the case that  $f$  is a vector function, as in (2.86). In fact, the results would be the same algorithms with vector quantities,  $\mathbf{y}_n, \mathbf{f}, \mathbf{k}_m$ , replacing corresponding scalar quantities,  $y_n, f, k_m$ . Only the independent variable,  $t$ , remains a scalar. For example, the third-order Runge-Kutta algorithm becomes:

$$\begin{aligned} \mathbf{y}_{n+1} &= \mathbf{y}_n + \frac{h}{6}(\mathbf{k}_1 + 4\mathbf{k}_2 + \mathbf{k}_3), \\ \mathbf{k}_1 &= \mathbf{f}(t_n, \mathbf{y}_n), \\ \mathbf{k}_2 &= \mathbf{f}\left(t_n + \frac{h}{2}, \mathbf{y}_n + \frac{h}{2}\mathbf{k}_1\right), \\ \mathbf{k}_3 &= \mathbf{f}(t_n + h, \mathbf{y}_n - h\mathbf{k}_1 + 2h\mathbf{k}_2). \end{aligned} \tag{2.110}$$

Clearly, the vector dimensions of  $\mathbf{y}_n$  and  $\mathbf{f}$ , and hence of  $\mathbf{k}_m$ , are all equal.

### 2.4.2 Numerical Integration of Functions

Having developed general single-step algorithms for the solution of linear, first-order differential equations of the type (2.87), it is straightforward to specialize these to integrations of

$$\dot{y}(t) = f(t), \quad (2.111)$$

where the function,  $f$ , does not depend on  $y(t)$ . Corresponding to first, second, third, and fourth order algorithms (2.105), (2.106), (2.108), and (2.109), the integration rules of respective order are obtained by omitting the dependence of  $f$  on its second argument everywhere on the right-hand sides:

first-order (rectangle rule):

$$y_{n+1} = y_n + hf(t_n); \quad (2.112)$$

second-order (trapezoid rule):

$$y_{n+1} = y_n + \frac{h}{2} (f(t_n) + f(t_n + h)); \quad (2.113)$$

fourth-order (Simpson's rule):

$$y_{n+1} = y_n + \frac{h}{6} \left( f(t_n) + 4f\left(t_n + \frac{h}{2}\right) + f(t_n + h) \right). \quad (2.114)$$

The third-order and fourth-order algorithms in this case are, in fact, identical. In each case the error of the algorithm is on the order of the neglected power of the integration step,  $h$ . More definitive error analyses and other rules are treated in most elementary books on numerical analysis (e.g., Conte and de Boor, 1965). The generalization to vector functions is obvious, following procedures exemplified by (2.110).

## 3 Inertial Measurement Units

### 3.1 Introduction

*Inertial navigation* may be defined as the indication, in real time, of position and velocity of a moving vehicle using sensors that react on the basis of Newton's laws of motion. As noted in Chapter 1, the coordinate frame in which Newton's laws hold is the inertial frame (*i*-frame). The sensors or instruments of an inertial navigation system generally are called *inertial measurement units* (IMU's); and, it is not only reasonable, but also to a certain extent necessary, to define their function in the *i*-frame. There are two types of motion, translational and rotational motion; and conventionally, two types of IMU exist: the *accelerometer* that senses linear accelerations, and the *gyroscope* that senses angular rate. Angular accelerometers also exist; however, for purposes of navigation, gyroscopes have proved more accurate. We note from the Newtonian perspective that gyroscopes sense only *rotation* with respect to inertial space and not curvilinear translation such as experienced by a satellite orbiting in free-fall around the Earth.

Each device, whether accelerometer or gyroscope, has three axes associated with it: the *input axis* (1-axis), the *output axis* (2-axis), and a third axis particular to the instrument in some way. These three axes are mutually perpendicular, at least, in theory, and they form the instrument frame. The input axis is always the sensing axis; for example, the accelerometer's input axis is aligned with the direction of the instrument that is sensitive to acceleration. The output axis can usually be identified with the corresponding data quantity.

Although one traditionally associates the name gyroscope ("gyro", for short) with an instrument that measures the reactions of a spinning proof mass (the original principle of operation), the name has been adopted for modern, optical devices whose principle of operation is not associated with spinning mass elements but rests with a particular property of light in a rotating frame known as the *Sagnac effect* (Section 3.2.2). Though dynamical laws of motion are not invoked in the optical gyroscope, the *i*-frame is of principal importance. The fundamental technologies of the gyroscope are quite diverse and to an extent still evolutionary, where, for example, micro-machined devices are based primarily on vibrating mechanical elements (Burdess et al., 1994). The principle of operation of the accelerometer, in contrast, has largely remained unchanged, based essentially on the laws of dynamics of an inertial proof mass, although technological advances have changed the sensor configuration, as well as the particular method of measurement.

Indeed, the design of accelerometers has burgeoned in the last few decades, facilitated by new technologies in manufacturing, and driven by a broad range of applications in vibration and shock determination in commercial and manufacturing systems (Meydan, 1997; Walter, 1997), in test and evaluation of military and aerospace systems (Walter, 1999), as well as in gravimetry for exploration geophysics

and geodesy (Chapin, 1998). Single-axis and multi-axis instruments have been devised; even a six-axis cryogenic accelerometer was invented (Paik, 1996) that senses the three translational, as well as the three angular accelerations with a single proof mass. Similarly, the result of significant developments in sensor technology has affected the range of applications of gyroscopes. Emerging mostly from uses in military navigation, guidance, and attitude determination, as well as commercial aviation (Savet, 1961; Stieler and Winter, 1982; Greenspan, 1995; Barbour and Schmidt, 1998), they can now be found routinely in commercial vehicles, as well as space systems of all kinds and science experiments, such as the exquisite test of the Lense-Thirring (frame-dragging) effect of general relativity (Everitt, 1988; Lipa and Keiser, 1988).

Most importantly, the recent advances in micro-machining of mechanical systems have led to the development and manufacture of small, inexpensive inertial sensors for a variety of other applications that require any kind of linear and angular motion detection, such as safety and stability devices in automobiles, motion sensors and stabilization mechanisms in electronic and other consumer products (e.g., virtual reality computer systems and video cameras), control of industrial and construction equipment (robotics, crane control, vibration determination, etc.), and biomedical uses involving activity monitoring. These sensors, based on the technologies of micro-electro-mechanical systems (MEMS) and micro-opto-electro-mechanical systems (MOEMS) typically have sensitivities much less than required for inertial navigation, but continuing improvements in design and manufacturing processes are yielding devices which rival the traditional macro-sensors. For a good review, the reader is directed to (Yazdi et al., 1998).

Inertial sensors fall into three general categories of application performance, which is characterized by the stability of the inherent biases in their output, measured in degrees per hour for the gyroscope and meters per second-squared for the accelerometer, and by the stability in their scale factors, measured in parts per million. With the exception of some recent advancements for scientific purposes, as noted above, the most accurate gyros and accelerometers were developed primarily for strategic military applications involving the guidance of intercontinental ballistic missiles. The bias stability in these gyros is better than  $0.0001\text{ }^{\circ}/\text{hr}$  with a scale factor stability better than 50 ppm, and the bias and scale factor stabilities in the accelerometers are better than  $10^{-6}\text{ m/s}^2$  ( $\approx 1\text{ micro-}g = 1\text{ }\mu\text{g}$ ) and 2 ppm, respectively. The next class of IMU's belongs largely to the navigation-grade category with respective bias stabilities covering roughly  $(0.0001 - 0.1)^{\circ}/\text{hr}$  and  $(1 - 1000) \times 10^{-6}\text{ m/s}^2$ . Scale factor stability for both types of sensors in this application range approximately from 1 to 100 ppm. Finally, the commercial grade (also tactical grade in military applications) comprises sensors that are designed for economy in cost, size, and power consumption or short-term accuracy; and corresponds to bias stabilities generally in the ranges  $(0.1 - 10000)^{\circ}/\text{hr}$  and  $(50 - 10000) \times 10^{-6}\text{ m/s}^2$ , and scale factor stabilities larger than 100 ppm. The present text is confined to the genre of modern and classical IMU's conventionally deployed for navigation and, by extension, for nominal geodetic purposes. These devices will be treated in detail in this chapter.

The essence of inertial navigation is the integration with respect to time of the sensed acceleration to obtain velocity and the subsequent integration, again with respect to time, to obtain position. Depending on the number of degrees of freedom associated with the vehicle motion (usually, at least the two horizontal motions), a corresponding number of accelerometers is needed with their input axes appropriately aligned. For example, a vehicle navigating in the horizontal directions would have two accelerometers, one pointing forward and one pointing to the side. To obtain the position of a vehicle that has three-dimensional (i.e., arbitrary freedom in) motion requires three accelerometers whose input axes for practical reasons should be mutually orthogonal.

Simply installing a set of accelerometers on a vehicle is inadequate for most navigation purposes because the accelerometers will not be aligned with the principal directions of the navigation frame (north, east, down). Furthermore, the navigation frame, itself, is generally non-inertial and one must account for the well known centrifugal and Coriolis accelerations due to Earth's rotation with respect to the inertial frame. Both of these orientation transformations (between the navigation frame and the body and inertial frames) are performed with measurements from gyroscopes. Three directions (or, integrated angular rates) suffice to fully orient the accelerometers in the most general case. Thus, in total, there are six IMU's associated with the most general inertial navigator: three accelerometers and three gyroscopes (later, we will see that so-called two-degree-of-freedom gyros also exist, which reduces the number of required gyros to two).

We begin with a discussion of the gyroscope, in particular the mechanical gyro, since its dynamics and that of today's pendulous accelerometer are related.

## 3.2 Gyroscopes

The term “gyroscope” originates with *J.B.L. Foucault*, who in 1850, using a spinning disc, demonstrated that the Earth rotates. His demonstration was based on the fact that since the rotation axis of the disc must remain fixed in inertial space in the absence of applied torques (constant angular momentum, see below), its direction with respect to the Earth changes as the Earth rotates underneath it. Gyroscopes provide a means to determine relative attitude, or orientation, as well as absolute direction in a number of applications, including, of course, inertial navigation, where traditionally the primary application of gyros is to isolate the vehicle motion from the platform holding the accelerometers. Viewed generally as measuring angles or angular rates, the gyro has also found utility as an auxiliary device in such science and engineering endeavors as remote sensing, photogrammetry (Schwarz et al., 1993), terrestrial surveying (see Chapter 10), and terrain profiling using synthetic aperture radar (SAR) (Madsen and Zebker, 1993). Gyros of one or another kind play an important part where rotational stability or accurate angular registration is required, not only for navigation and positioning, but for any platform of instruments or devices on any vehicle (ground vehicles, aircraft, ships, or satellites)

or portable system for military, civil, commercial, consumer, science, and engineering purposes.

We will be concerned with inertial navigation systems and their use in geodesy, but the analyses can easily be carried to the many other applications. As such, the gyros are regarded as orientation devices for platforms that may have accelerometers (our primary focus in subsequent chapters) for navigation, positioning, surveying, or gravimetry, or a set of sensors (e.g., cameras) for photogrammetry, remote sensing, or geographic information science.

Although one might say that their function is only secondary to accelerometers in inertial navigation, gyros are considerably more complex sensors. The first instruments were mechanical devices based on the concept of preservation of angular momentum of a spinning proof mass in inertial space. For ease of implementation (minimum computations, optimal control of error sources, and natural self-calibration), the accelerometers were mechanized on a *gimbaled* platform, that is, a platform generally maintained in a local-level frame so that the accelerometers were naturally oriented in the navigation frame (north-east-down). The *local-level stabilization* is accomplished by gyros whose orientation with respect to inertial space can be changed in concert with Earth's rotation and vehicle motion (see Chapter 4). The complexity of the mechanical gyros and the gimbal system kept the cost of these inertial navigation systems very high.

The cost could be driven down substantially with the use of the so-called *strapdown* mechanization. As the name implies, a strapdown inertial navigation system is physically bolted to the frame of the vehicle to be navigated. The orientation must now be accomplished completely by computations, using gyro data, that transform the accelerometer output from the sensor frame to the navigation frame. In addition, calibration requires special vehicle maneuvers or external references, and care must still be exercised in the placement of the INS in the vehicle to avoid the coupling of certain error sources. With the invention of optical gyros and more accurate accelerometers, as well as faster computers, most of these concerns are becoming secondary to the savings in cost.

### 3.2.1 Mechanical Gyroscopes

A mechanical gyroscope functions on the basis of a rapidly spinning mass whose angular momentum provides a well defined direction in inertial space. The physical law governing the operating principle of this type of gyroscope is the equation of rotational motion of a body, comparable to Newton's Second Law of Motion. It says that the time-rate of change of the angular momentum of a rotating body is equal to the applied torque:

$$\mathbf{L} = \frac{d}{dt}(I\boldsymbol{\omega}), \quad (3.1)$$

where  $\mathbf{L}$  is the torque,  $\boldsymbol{\omega}$  is the angular rate (both are axial vectors, by previous stipulations, see Chapter 1), and  $I$  is called the inertia tensor. The product of  $I$  and

$\omega$  is defined as the angular momentum vector,  $\mathbf{H}$ :

$$\mathbf{H} = I\omega. \quad (3.2)$$

Equation (3.1) is completely analogous to the formulation (1.3) for the linear motion of a point mass; and it applies only in an inertial (i.e., non-rotating) frame. The torque is related to the force,  $\mathbf{F}$ , through the “lever-arm” equation:

$$\mathbf{L} = \mathbf{r} \times \mathbf{F}, \quad (3.3)$$

where  $\mathbf{r}$  is a vector that represents the lever-arm. Applying a force to one end of the lever-arm creates a torque, or moment of force, about the other (hinged) end that, according to (3.3), is perpendicular to both  $\mathbf{r}$  and  $\mathbf{F}$ .

The inertia tensor,  $I$ , is the analogue of (inertial) mass in (1.3). It is a  $3 \times 3$  matrix of elements,  $I_{j,k}$ , that are the second-order moments of the mass distribution of a body with respect to the coordinate axes. Specifically, the *moments of inertia* occupy the diagonal of the matrix and are given by

$$I_{j,j} = \int_{\text{mass}} (r^2 - x_j^2) dm, \quad j = 1, 2, 3; \quad (3.4)$$

where  $r^2 = x_1^2 + x_2^2 + x_3^2$ ; and the *products of inertia* are the off-diagonal elements expressed as

$$I_{j,k} = - \int_{\text{mass}} x_j x_k dm, \quad j \neq k. \quad (3.5)$$

The products of inertia vanish if the coordinate axes coincide with the *principal axes of inertia* for the body. This happens with a suitable rotation of the coordinate system (with origin assumed to be at the center of mass) that diagonalizes the inertia tensor according to (1.17). In fact, a tensor is a generalization of the vector (in our case, to second order); and, like a vector, is defined in terms of its transformation properties under coordinate rotations (in this case, it should transform according to (1.17)).

Combining (3.1) and (3.2), now explicitly written for the  $i$ -frame, we have:

$$\mathbf{L}^i = \dot{\mathbf{H}}^i. \quad (3.6)$$

If  $\mathbf{L} = \mathbf{0}$  (no applied torques), then the angular momentum is a constant; that is, it is conserved (*Law of Conservation of Angular Momentum*), meaning that both the magnitude and direction of  $\mathbf{H}$  remain unchanged in the  $i$ -frame.

Equation (3.2) is given more explicitly by

$$\mathbf{H}^i = I^i \omega_{ia}^i. \quad (3.7)$$

$\mathbf{H}^i$  is the angular momentum of a body and its coordinates are in the  $i$ -frame. The body, itself, is endowed with an arbitrary, body-fixed frame, say the  $a$ -frame; and  $\omega_{ia}^i$  is the angular velocity of the  $a$ -frame (the body) with respect to the  $i$ -frame, co-ordinatized in the  $i$ -frame (see (1.58)). Transforming the inertia tensor according to (1.17), we obtain

$$\begin{aligned}\mathbf{H}^i &= C_a^i I^a C_i^a \omega_{ia}^i = C_a^i I^a \omega_{ia}^a \\ &= C_a^i \mathbf{H}^a,\end{aligned}\quad (3.8)$$

where the angular momentum vector coordinatized in the  $a$ -frame is given by

$$\mathbf{H}^a = I^a \omega_{ia}^a. \quad (3.9)$$

It should be noted that the vectors  $\mathbf{H}^a$  and  $\omega_{ia}^a$  are not parallel, in general.

Since it is rotating, the  $a$ -frame is not inertial, and with respect to it, the equation of rotational motion (3.1) becomes, according to the Coriolis Law (1.70):

$$\begin{aligned}\mathbf{L}^a &= C_i^a \mathbf{L}^i = C_i^a \dot{\mathbf{H}}^i \\ &= \dot{\mathbf{H}}^a + \omega_{ia}^a \times \mathbf{H}^a.\end{aligned}\quad (3.10)$$

Differentiating (3.9) with respect to time in the  $a$ -frame, we get for (3.10)

$$\mathbf{L}^a = I^a \dot{\omega}_{ia}^a + \omega_{ia}^a \times (I^a \omega_{ia}^a), \quad (3.11)$$

where we assume that the body is rigid, so that the inertia tensor,  $I^a$ , expressed in the body-fixed  $a$ -frame is constant:  $\dot{I}^a = 0$ . With the further assumption that the products of inertia are zero in the  $a$ -frame (the coordinate axes are the principal axes of inertia), equation (3.11) is the well known *Euler equation* for rotational motion (about a fixed point) of a rigid body. The matrix  $I^a$ , in this case, is diagonal with elements being the moments of inertia (3.4) with respect to each of the coordinate axes.

### 3.2.1.1 SDF Gyro

A gyro whose inertial element (spinning mass) has its spin axis restrained to rotate about a single axis is called a *single-degree-of-freedom* (SDF) gyro, as depicted schematically in Figure 3.1. It consists of a spinning proof mass (*rotor*) supported by a *gimbal* that can rotate about an axis with respect to the outer case. The three supposedly orthogonal axes associated with this instrument (the case) are the input axis, output axis, and spin reference axis. The reason for the name of the latter is that it identifies a reference for the spin axis of the rotor; for the others the nomenclature will be evident later. The gimbal provides freedom of rotation about the output axis, as indicated by the angle,  $\eta$ . Ideally, the bearings of the spinning rotor and of the gimbal are frictionless with zero compliance (allowing no displacements) in the respective orthogonal axes. The supports of the gimbal are furnished with devices, the *signal generator*, at one end to sense the angle of rotation, and a *torque generator* at the other end to create torques about the output axis. The signal generator is an electrical pick-off device that measures a voltage corresponding to the turned angle about the output axis. The torque generator is a motor driven by a current proportional to the amount of torque to be applied. The need for these generators will be discussed in connection with the performance equations.

Suppose the case of the gyroscope defines a coordinate frame ( $c$ -frame) and is rotating in the inertial frame with angular velocity  $\omega_{ic}^c$ . Consider also the frame of

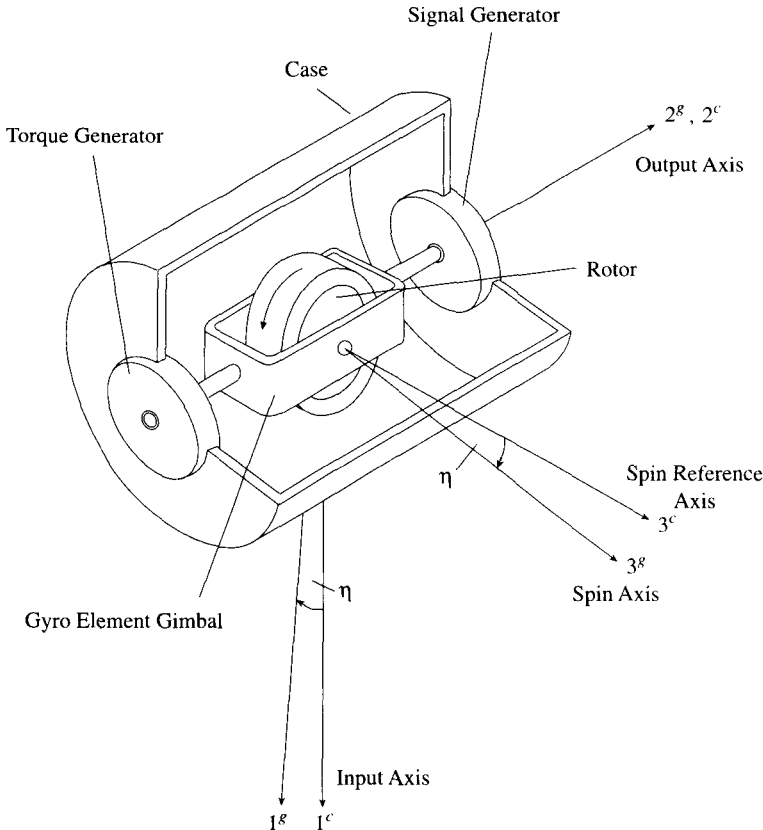


Figure 3.1: Single-degree-of-freedom gyroscope.

the gimbal ( $g$ -frame), and let the angular velocity of the gimbal, coordinatized in the  $g$ -frame, with respect to the case be denoted  $\omega_{cg}^g$ . Then the angular velocity of the gimbal with respect to inertial space is given in terms of  $g$ -frame coordinates by (cf. (1.61))

$$\omega_{ig}^g = \omega_{ic}^g + \omega_{cg}^g. \quad (3.12)$$

For the moment we consider the dynamics of the sensing element (the rotor) within the frame of the gimbal. Then (3.12) will be used later to relate these rotations to rotations of the case with respect to the  $i$ -frame.

The total angular momentum of the gimbal/rotor assembly is given, using (3.9), by the sum

$$\begin{aligned} \mathbf{H}^g &= \mathbf{H}_{\text{gimbal}}^g + \mathbf{H}_{\text{rotor}}^g \\ &= I_{\text{gimbal}}^g \boldsymbol{\omega}_{ig}^g + I_{\text{rotor}}^g \boldsymbol{\omega}_{ir}^g, \end{aligned} \quad (3.13)$$

where  $\omega_{ir}^g$  is the angular rate of the rotor with respect to the  $i$ -frame, but coordinate-ized in the  $g$ -frame. We assume that the corresponding lines of mass symmetry of the gimbal and the rotor coincide and thus define the principal axes of inertia of the gimbal/rotor assembly. By defining the coordinate axes to lie along these axes, the inertia tensors  $I_{\text{gimbal}}^g$  and  $I_{\text{rotor}}^g$  both become diagonal matrices. Furthermore, since the rotor is (supposedly) rigidly supported by the gimbal, the angular rates about the 1- and 2-axes with respect to the  $i$ -frame are the same for gimbal and rotor; and, by decoupling the angular rate of the spinning rotor, we obtain:

$$\boldsymbol{\omega}_{ir}^g = \begin{pmatrix} (\omega_{ig}^g)_1 \\ (\omega_{ig}^g)_2 \\ (\omega_{ig}^g)_3 + (\omega_{gr}^g)_3 \end{pmatrix}. \quad (3.14)$$

Thus,

$$\begin{aligned} \mathbf{H}^g &= \begin{pmatrix} (I_{\text{gimbal}}^g)_1 & 0 & 0 \\ 0 & (I_{\text{gimbal}}^g)_2 & 0 \\ 0 & 0 & (I_{\text{gimbal}}^g)_3 \end{pmatrix} \begin{pmatrix} (\omega_{ig}^g)_1 \\ (\omega_{ig}^g)_2 \\ (\omega_{ig}^g)_3 \end{pmatrix} \\ &\quad + \begin{pmatrix} (I_{\text{rotor}}^g)_1 & 0 & 0 \\ 0 & (I_{\text{rotor}}^g)_2 & 0 \\ 0 & 0 & (I_{\text{rotor}}^g)_3 \end{pmatrix} \begin{pmatrix} (\omega_{ig}^g)_1 \\ (\omega_{ig}^g)_2 \\ (\omega_{ig}^g)_3 + (\omega_{gr}^g)_3 \end{pmatrix} \\ &= I^g \boldsymbol{\omega}_{ig}^g + \begin{pmatrix} 0 \\ 0 \\ I_s \omega_s \end{pmatrix}, \end{aligned} \quad (3.15)$$

where  $I^g$  is the inertia tensor for the combined gimbal/rotor assembly:

$$I^g = \begin{pmatrix} I_1^g & 0 & 0 \\ 0 & I_2^g & 0 \\ 0 & 0 & I_3^g \end{pmatrix}, \quad (3.16)$$

that is,

$$I_j^g = (I_{\text{gimbal}}^g)_j + (I_{\text{rotor}}^g)_j. \quad (3.17)$$

$I_s \equiv (I_{\text{rotor}}^g)_3$  is the moment of inertia of the rotor with respect to the rotor spin axis, and the spin rate of the rotor is  $\omega_s \equiv (\omega_{gr}^g)_3$ .

We apply the equations of rotational motion (3.10) to the  $g$ -frame and with (3.15) obtain equations, again, analogous to Euler's equations:

$$\mathbf{L}^g = I^g \dot{\boldsymbol{\omega}}_{ig}^g + \begin{pmatrix} 0 \\ 0 \\ I_s \dot{\omega}_s \end{pmatrix} + \boldsymbol{\omega}_{ig}^g \times \left( I^g \boldsymbol{\omega}_{ig}^g + \begin{pmatrix} 0 \\ 0 \\ I_s \omega_s \end{pmatrix} \right). \quad (3.18)$$

Equation (3.18) is the relationship between applied torques,  $\mathbf{L}^g$ , and the angular

rate of the gimbal with respect to inertial space,  $\omega_{ig}^g$ . We note that  $\omega_s$  is a large number, typically hundreds of revolutions per second, and presumed constant; it is certainly much larger than any component of  $\omega_{ig}^g$ . Therefore, for simple analyses, we may approximate:

$$\mathbf{H}^g \approx \begin{pmatrix} 0 \\ 0 \\ I_s \omega_s \end{pmatrix} \Rightarrow \dot{\mathbf{H}}^g \approx \begin{pmatrix} 0 \\ 0 \\ 0 \end{pmatrix}, \quad (3.19)$$

which leads to

$$\mathbf{L}^g \approx \omega_{ig}^g \times \mathbf{H}^g. \quad (3.20)$$

From (3.19) the vector  $\mathbf{H}^g$  points roughly along the spin axis. Approximately, then, if  $\omega_{ig}^g$  is a vector pointing along the positive input axis, the vector  $\mathbf{L}^g$  according to (3.20) points along the *negative* output axis.

It remains to express the angular rate of the gimbal,  $\omega_{ig}^g$ , in terms of the angular rate of the gyro case. Toward this end we consider the gimbal angle,  $\eta$ , about the output axis that rotates the *c*-frame into the *g*-frame (Figure 3.1). It is constrained to be small by torques applied to the gimbal (see below). Then, by (1.25):

$$C_c^g = \begin{pmatrix} 1 & 0 & -\eta \\ 0 & 1 & 0 \\ \eta & 0 & 1 \end{pmatrix}; \quad (3.21)$$

and, from (3.12) and (1.59):

$$\begin{aligned} \omega_{ig}^g &= C_c^g \omega_{ic}^c + \omega_{cg}^g = C_c^g \omega_{ic}^c + \begin{pmatrix} 0 \\ \dot{\eta} \\ 0 \end{pmatrix} \\ &= \begin{pmatrix} \omega_1^c - \eta \omega_3^c \\ \omega_2^c + \dot{\eta} \\ \omega_3^c + \eta \omega_1^c \end{pmatrix}, \end{aligned} \quad (3.22)$$

where  $\omega_{cg}^g = (0 \ \dot{\eta} \ 0)^T$  is the angular rate of the gimbal with respect to the case, and we have defined the angular rate of the case with respect to the *i*-frame to be:

$$\omega_{ic}^c = \begin{pmatrix} \omega_1^c \\ \omega_2^c \\ \omega_3^c \end{pmatrix}. \quad (3.23)$$

Equation (3.18) with (3.22) then expresses the dynamics of the gimbal for a case rotating with angular velocity given by (3.23).

We are interested only in the dynamics of the gimbal about the output axis; the dynamics about the other axes concern the constraints provided by the support bearings of the gimbal with respect to the case or of the rotor with respect to the gimbal. These are less important for the understanding of the sensing principles of

the gyro and will not be dealt with explicitly. (They are important in a comprehensive analysis of instrument errors.) Therefore, it is simpler at this point to abandon the vector notation as only the second component of (3.18) will be considered. Using (3.16) and (3.22), this is found to be, upon performing the cross product:

$$\begin{aligned} L_2^g &= I_2^g(\dot{\omega}_2^c + \ddot{\eta}) + (\omega_3^c + \eta\omega_1^c)I_1^g(\omega_1^c - \eta\omega_3^c) \\ &\quad - (\omega_1^c - \eta\omega_3^c)(I_3^g(\omega_3^c + \eta\omega_1^c) + I_s\omega_s). \end{aligned} \quad (3.24)$$

Rearranging terms, we obtain:

$$\begin{aligned} I_2^g\ddot{\eta} &+ [(I_3^g - I_1^g)((\omega_3^c)^2 - (\omega_1^c)^2) + I_s\omega_s\omega_3^c]\eta + (I_3^g - I_1^g)\omega_1^c\omega_3^c\eta^2 \\ &= L_2^g + I_s\omega_s\omega_1^c - I_2^g\dot{\omega}_2^c + (I_3^g - I_1^g)\omega_3^c\omega_1^c. \end{aligned} \quad (3.25)$$

Since  $\omega_3^c \ll \omega_s$  and the gimbal angle,  $\eta$ , is small, so that its square can be neglected (as already done in (3.21)), equation (3.25) may be approximated by

$$I_2^g\ddot{\eta} + H_s\omega_3^c\eta = L_2^g + H_s\omega_1^c - I_2^g\dot{\omega}_2^c + (I_3^g - I_1^g)\omega_3^c\omega_1^c, \quad (3.26)$$

where the angular momentum of the rotor is

$$H_s = I_s\omega_s. \quad (3.27)$$

Equation (3.26), called the *output axis equation*, is a second-order, linear, non-homogeneous, differential equation for the gimbal angle. It refers to an idealized gyro and describes the dynamic behavior of  $\eta$  in a general sense, with forcing function represented by the terms on the right side. However, the dynamics of the gimbal angle are restrained and the angle, itself, is kept small in a feedback manner by the applied torque,  $L_2^g$ . Hence, the analysis of the gyro performance can be restricted to the steady-state condition, where the short-term variations in  $\eta$  may be viewed as averaged out; that is, we assume for the steady state that  $\ddot{\eta} \approx 0$ .

Again, noting that the angular rates,  $\omega_1^c$  and  $\omega_3^c$ , are relatively small compared to the spin rate,  $\omega_s$ , the predominant terms in (3.26) are the applied torque and the input angular rate term,  $H_s\omega_1^c$ . Considering the discussion above, with  $\eta \approx 0$ , we have approximately:

$$L_2^g \approx -H_s\omega_1^c, \quad (3.28)$$

where  $H_s = I_s\omega_s \geq 0$ . This fundamental equation may be interpreted in two different ways. In the first case, it says that a torque applied about the negative output axis of the gimbal ( $L_2^g < 0$ ) gives rise to a positive angular rate,  $\omega_1^c$ , of the case about the input axis:

$$\omega_1^c = \frac{-L_2^g}{H_s}, \quad (3.29)$$

which, therefore, induces a *precession* of the spin axis (3-axis). Likewise, a positive torque creates a negative input axis rotation of the case. Thus, by applying an appropriate torque the direction of the spin axis may be changed with respect to inertial space.

In the second interpretation, a rotation of the case about the input axis causes a torque about the output axis of the gimbal; that is, the product  $H_s\omega_1^c$  represents a torque due to an input rotation rate. But it is a torque opposite in sign to an applied torque; it is a *reaction* torque:

$$L_2^e = H_s\omega_1^c = -L_2^g. \quad (3.30)$$

For example, if  $\omega_1^c > 0$ , then  $L_2^e > 0$  is a reaction torque generated along the positive output axis and creates the angle,  $\eta$ , of the gimbal with respect to the case. It means that input axis rotations will be sensed along the positive output axis.

The gimbal angle is kept small (it is nulled) either by torquing the gimbal relative to the case or the case relative to the gimbal, or both. In the first manner, torques are applied (at the negative output axis) using a torque motor powered by electrical currents generated from pick-off voltages obtained at the positive output axis (signal generator). These applied torques balance the reaction torques caused by the rotation rate of the case about the input axis. Some gyros have a restraining spring on the output axis that has the same desired torquing effect; however, it is generally a less accurate balancing method. Alternatively, the case, mounted on a platform, is connected to the vehicle through a set of gimbals; and the output signal is used to power servo motors at the gimbal mounts, thus torquing the platform. In this way, the platform is maintained in a particular orientation as specified by the gyros. The mechanism of nulling the gimbal angle through feedback is known as a *rebalance loop*, which also belongs to the more general class of *closed-loop* operations that will be encountered many times in the design of other inertial instruments (accelerometers and optical gyros in this chapter) as well as analysis methods (extended Kalman filter, Section 7.5.2). By keeping the signal obtained from a measuring device small the sensing dynamics of the system are shifted as much as possible to its “linear” region (cf., equation (3.21)), which usually maximizes its sensitivity and stability.

The applied torque,  $L_2^g$ , in equation (3.26) arises from one or more sources, depending on the type of gyro and its application. Already we mentioned the restoring torque applied through the rebalance loop. These and other types of torques applied directly to the gimbal using a torque motor are called *commanded torques*. They may include compensation torques that attempt to negate the extraneous forcing terms depending on the moments of inertia on the right side of (3.26). The latter can be calibrated to some extent in the laboratory. This is particularly critical for the strapdown applications.

Applying a commanded rebalance torque is typical of the *rate* gyro, a gyro that directly indicates the angular rate about its input axis. The rate is given by the rebalance torque. That is, let the commanded rebalance torque be  $L_{reb}$ , and denote by  $L_c$  the error compensation torque that includes various computable drift effects, and by  $v_0$  any residual torque error. The total applied torque is then

$$L_2^g = L_{reb} + L_c + v_0. \quad (3.31)$$

In the steady state (average) condition, where  $\dot{\eta} \approx 0$  and  $\eta = 0$ , the expression for

angular rate about the input axis of the rate gyro is thus given by (3.26):

$$\omega_1^c = -\frac{1}{H_s} (L_{\text{reb}} + v_0). \quad (3.32)$$

The applied commanded rebalance torque,  $L_{\text{reb}}$ , is determined directly from the negative of the gimbal angle indicated by the signal generator:

$$L_{\text{reb}} = -K_t \eta, \quad (3.33)$$

where  $K_t$  is the torquer scale factor. Rate gyros are used mostly in the strapdown mechanization (Section 4.2.4); and, since the full rotational dynamics of the vehicle are thus imposed on the gyros, the scale factor must be known very accurately. Note that some of the terms in (3.25) are torques of the same type as (3.33), proportional to  $\eta$ . To reduce this cross-coupling effect on the scale factor requires a high gain on the rebalance loop.

In order to capture the high-frequency rotational dynamics of the vehicle carrying the rate gyro, the torques are usually summed digitally over a short time interval,  $\delta t$ , to yield a change in *angle*:

$$\delta\theta = \int_{\delta t} \omega_1^c dt. \quad (3.34)$$

In this way, in the case of digital processing, the sampling interval,  $\delta t$ , may be set comparatively long without losing the higher-frequency information (bandwidth) of the rotational dynamics, which accumulates in the output angle.

Another important commanded torque is associated with the mechanization that stabilizes a platform in the local level (Section 4.2.4). As noted above, the orientation of a gimballed platform is determined through servo motors according to the directions defined by the gyros mounted on it. We can change (command) the orientation of the gyro rotor, and hence, of the platform, with respect to inertial space only by applying a torque to the gimbal of the gyro, as indicated with equation (3.29). In this way, for example, the platform can be aligned continually with the local level. Rate gyros are not suitable to stabilize a platform since the indicated rates would first require integration to angles to be applied to the servo motors of the platform gimbals. Instead, platforms used for inertial navigation generally are stabilized with *rate-integrating* gyros, meaning that they measure the integral of angular rate, or the gimbal angle, itself. It is noted that rate-integrating gyros can also be used in strapdown applications (Savage, 1978).

In one common type of rate-integrating gyro the rebalance torque is produced by the damping effect of a dense, viscous fluid that is used to float the gimbal with neutral buoyancy inside the case. The buoyancy relieves the weight of the gimbal on its support bearings and reduces the friction and corresponding gyro drift of these *floated* gyros. The applied torque, due to the viscosity of the fluid, is proportional to the rate of the gimbal angle,  $-C\dot{\eta}$ , where  $C$  is the coefficient of viscous damping. In some gyros the fluid may just serve as a damper on the dynamics of the gimbal angle, but is not used for flotation. Other gyros are “dry” with air dampers.

In these cases, the applied torque is given by

$$L_2^g = L_{\text{lev}} + L_c - C\dot{\eta} + v_0, \quad (3.35)$$

where  $L_{\text{lev}}$  is the commanded torque needed to maintain the level on a vehicle moving in an Earth-fixed frame, and  $L_c$  accounts for compensable errors. The dynamics equation (3.26) now becomes

$$I_2^g \ddot{\eta} + C\dot{\eta} = L_{\text{lev}} + H_s \omega_1^c + v_0. \quad (3.36)$$

The homogeneous solution (Section 2.3.1) for the gimbal angle is given by

$$\eta_h = e^{-(C/I_2^g)t}, \quad (3.37)$$

which can be checked most easily by back-substitution. This shows that the gyro *time constant* (the time required for a significant reduction in the angle, that is, to  $1/e$ ) is  $I_2^g/C$ ; while the steady state solution ( $\ddot{\eta} \approx 0$ ) is approximately given by

$$\eta \approx \frac{1}{C} \int (L_{\text{lev}} + H_s \omega_1^c + v_0) dt. \quad (3.38)$$

Uncommanded ( $L_{\text{lev}} = 0$ ), and neglecting the error torques, the only restraining torque comes from the damping effect of the fluid; and, the rate-integrating gyro yields the angle of the platform with respect to inertial space. That is, the measured gimbal angle is proportional to the integrated angular rate:

$$\eta \approx \frac{H_s}{C} \int \omega_1^c dt. \quad (3.39)$$

To increase the response (reduce the time constant) of the rebalance loop, the damping constant,  $C$ , due to the viscosity of the fluid, is made large by designing the gap between the case and gimbal float to be narrow (typically, 0.02 mm). The gain,  $H_s/C$ , has values typically on the order of 1.

### 3.2.1.1.1 Principal Error Terms

We return now to the error sources expressed in equation (3.26). The term with  $\dot{\omega}_2^c$  is called the *output axis rotation error* and is due to angular acceleration of the case about the output axis. The term involving  $I_3^g - I_1^g$  is called the *anisoinertia error* and is due to the inequality of the moments of inertia of the gimbal/rotor assembly with respect to the input and spin axes. Lastly, the term with  $H_s \omega_3^c$  is called the *cross-coupling error* due to rotations of the case about the spin axis which are coupled to the gimbal angle. These systematic errors could be compensated ( $L_c$ ) to some extent by determining the moments of inertia of the gimbal/rotor in the laboratory and using angular rates of the case as measured by other (orthogonal) gyros.

The error term,  $v_0$ , includes other effects such as bias drift; drifts depending on acceleration, temperature changes, and magnetic fields; and scale factor errors, nonlinearities, as well as purely random noise in the determination of the commanded torques  $L_{\text{reb}}$ ,  $L_{\text{lev}}$ , and  $L_c$ . The bias drift is due to torques relative to the case caused by the suspension of the rotor and gimbal and those induced by reaction torques exerted by the electrical pick-offs. Also, vibration of the vehicle will cause torques

on the output axis that cause it to oscillate (also, known as a type of coning). This has a rectifying effect through cross-coupling with the input signal. The combined drift has a constant and a randomly fluctuating component. The constant part may vary from turn-on to turn-on of the gyro.

The acceleration-dependent drifts are due to mass unbalances and unequal compliances of the gimbal support structure, as well as buoyancy unbalance in the floated gyro. A mass unbalance along one axis together with an acceleration along another axis causes a torque about the remaining axis (cf. pendulous accelerometer, Section 3.3.2). The mass unbalance errors, therefore, are directly proportional to the acceleration. One can show that *differences* in the compliance (*anisoelasticity*) in the support bearings of the axes of the rotor or gimbal cause torques that are proportional to the products of accelerations along corresponding axes (particularly between the input and spin axes).

To appreciate the seriousness of the mass unbalance effect, consider the precision with which the center of mass of the rotor must lie on the output axis. Movement of the rotor along the spin axis by a small distance,  $\Delta\ell$ , causes its mass center to be offset from the output axis. Then, an acceleration,  $a$ , along the input axis induces an applied torque along the output axis (due to the inertia of the mass unbalance) given by  $+m \cdot a \cdot \Delta\ell$ , where  $m \cdot a$  is the force associated with the acceleration and  $m$  is the mass of the rotor. This, according to (3.29), yields an angular rate (error):

$$\delta\omega_1 = -\frac{m \cdot \Delta\ell \cdot a}{H_s}. \quad (3.40)$$

If  $H_s = 6 \cdot 10^5 \text{ gm cm}^2/\text{s}$ ,  $m = 100 \text{ gm}$ , and the allowable drift error is  $\delta\omega_1 \leq 0.01^\circ/\text{hr}$ , the tolerance on the off-center distance for the rotor must be  $\Delta\ell = 3 \cdot 10^{-7} \text{ cm per g}$ , where 1 g is the acceleration of gravity. An analogous output error (but opposite in sign) comes from the converse: a mass offset along the input axis with an acceleration along the spin axis. To minimize the mass unbalance errors, the output axis of a SDF gyro is usually oriented in the vertical (except for the azimuth gyro) to avoid the reaction to the large gravity acceleration.

Additional errors in the gyro output are caused by scale factor errors arising through the rebalance loop electronics, see (3.33); and misalignments from non-orthogonal mounting of the rotor and gimbal with respect to the case. Calibration functions can be determined in the laboratory for some of the errors associated with an individual gyroscope (Chatfield, 1997). Then, given approximate values for the environmental factors, such as acceleration, temperature, and magnetics, appropriate compensations can be calculated and applied to the output data. The extent to which these calibrations hold over time characterizes the long-term stability of the instrument. Periodic re-calibration may be done in real time, or as part of the post mission data processing (Chapter 8).

A general model for the error of a single gyro axis has the form

$$\delta\omega = \delta\omega_d + \kappa_\omega \omega_1^c + v_\omega, \quad (3.41)$$

where  $\kappa_\omega$  is the scale factor error,  $v_\omega$  is the white noise, and  $\delta\omega_d$  represents drift rate.

The scale factor error, itself, may contain linear and non-linear terms, depending on higher powers of the angular rate. A typical model for the total drift rate is given by

$$\begin{aligned}\delta\omega_d = & \delta\omega_0 + c_1 a_1 + c_2 a_2 + c_3 a_3 + c_4 a_1 a_3 + c_5 a_1 a_2 + c_6 a_2 a_3 \\ & + c_7 \delta T + c_8 B_1 + c_9 B_2 + c_{10} B_3,\end{aligned}\quad (3.42)$$

where  $\delta\omega_0$  is the drift bias (constant),  $a_j$  is the acceleration along the  $j$ -th case axis,  $\delta T$  is the temperature difference with respect to some calibration value, and  $B_j$  is a component of the magnetic field. An example of calibrated values for the bias drift, the mass-unbalance drift coefficients ( $c_1, c_2, c_3$ ), the anisoelastic drift coefficients ( $c_4, c_5, c_6$ ), the temperature coefficient ( $c_7$ ), and the magnetic field coefficients ( $c_8, c_9, c_{10}$ ) of a navigation-grade gyro are given by Kayton and Fried (1997):

$$\begin{aligned}\delta\omega_0 &= 0.1^\circ/\text{hr} \quad (0.02^\circ/\text{hr stability for weeks}) \\ c_1, c_2, c_3 &= 0.5^\circ/(\text{hr g}) \quad (0.1^\circ/(\text{hr g}) \text{ stability for weeks}) \\ c_4, c_5, c_6 &= 0.1^\circ/(\text{hr g}^2) \\ c_7 &= 0.02^\circ/(\text{hr }^\circ\text{C}) \\ c_8, c_9, c_{10} &= 0.005^\circ/(\text{hr gauss})\end{aligned}\quad (3.43)$$

Scale factor errors typically range from less than 1 ppm (part per million) to 100 ppm. Any uncompensated errors can be modeled as (3.41) with additional error terms as warranted by the particular gyro and its operational environment. More thorough and further discussions and analyses related to errors of a mechanical gyro can be found in (Stieler and Winter, 1982), (Kayton and Fried, 1969, 1997), (Britting, 1971), and (Lawrence, 1998).

### 3.2.1.2 TDF Gyro

The discussion for the single-degree-of-freedom gyro can be extended to a gyro whose rotor has two degrees of freedom (TDF). One possible design of a TDF gyro is the generalization of the single gimbal instrument, as indicated in Figure 3.2, where a second gimbal supports the rotor gimbal and provides the connection to the case. Each axis orthogonal to the spin axis serves both as an input and an output axis. A three-dimensional orientation reference system then requires only two gyros (either two TDF gyros, with one redundant angle indication, or one TDF gyro and one SDF gyro).

An alternative design concept has yielded superior performance characteristics; this is the *dry, tuned gyro*. By the nature of its design it is a TDF gyro, where the rotor (the inertial element) is attached through a universal joint to the shaft of the driving motor such that the rotor is free to roll about the two axes orthogonal to the shaft, while the motor supplying the spin is fixed to the case (Figure 3.3). The rotor is not floating in a liquid, hence this gyro is “dry”. The universal joint consists of a gimbal with two half-axial connections to the shaft of the motor and, orthogonal to these, two half-axial connections to the rotor. Additional gimbals, connected successively in analogous fashion, are sometimes included to reduce rectifying error torques. The

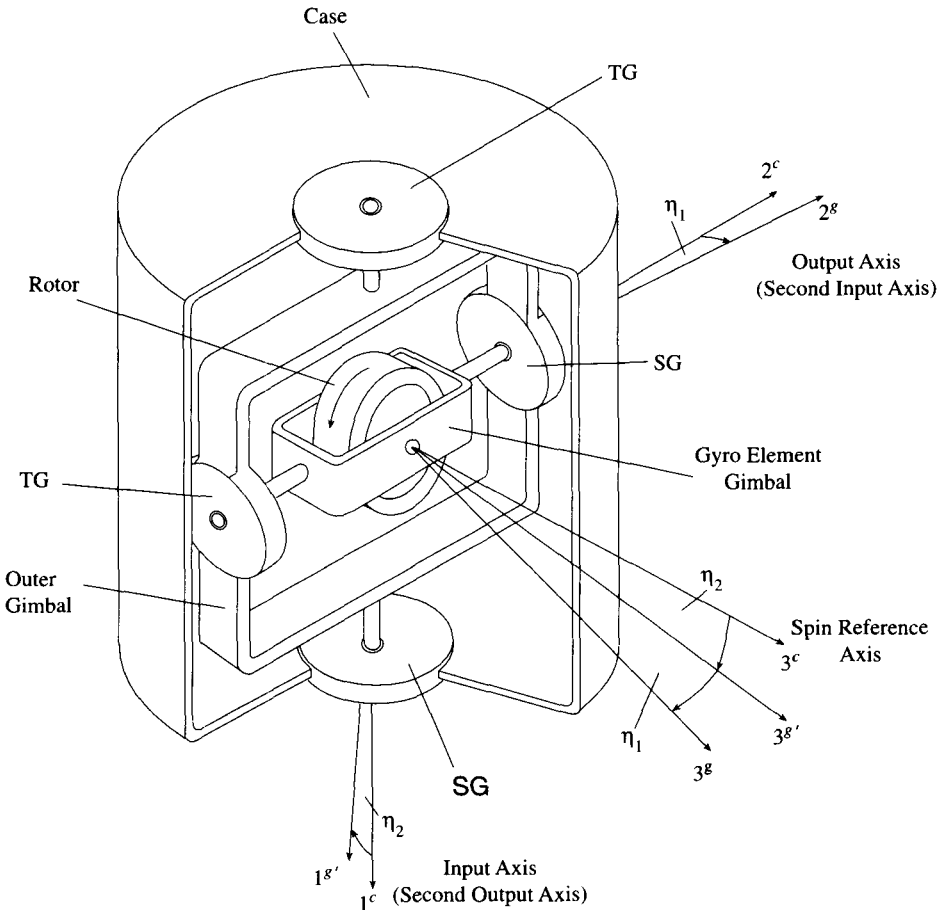


Figure 3.2: Two-degree-of-freedom gyroscope.

key to the rotor's suspension, however, lies in the axial connections of the gimbal. Instead of being rigidly supported in ball bearings (or a similar suspension), the bars are connected with torsional springs that can be set to a specific spring rate. If there is a small rotation of the case in space, then reaction torques in the gimbal support connections due to friction tend to return the rotor to its original attitude relative to the case. This dynamically induced torsion, which depends on the angular speed and inertia of the rotor and produces a *negative* spring rate effect, can be cancelled with appropriate settings of the spring rate in the flexure bars. With this dynamical *tuning*, the rotor becomes a freely rotating element in space, insensitive to case rotations.

However, the gimbal angles that define the orientation of the rotor with respect to the shaft are kept close to zero, as in the SDF rate gyro, with a rebalance loop in

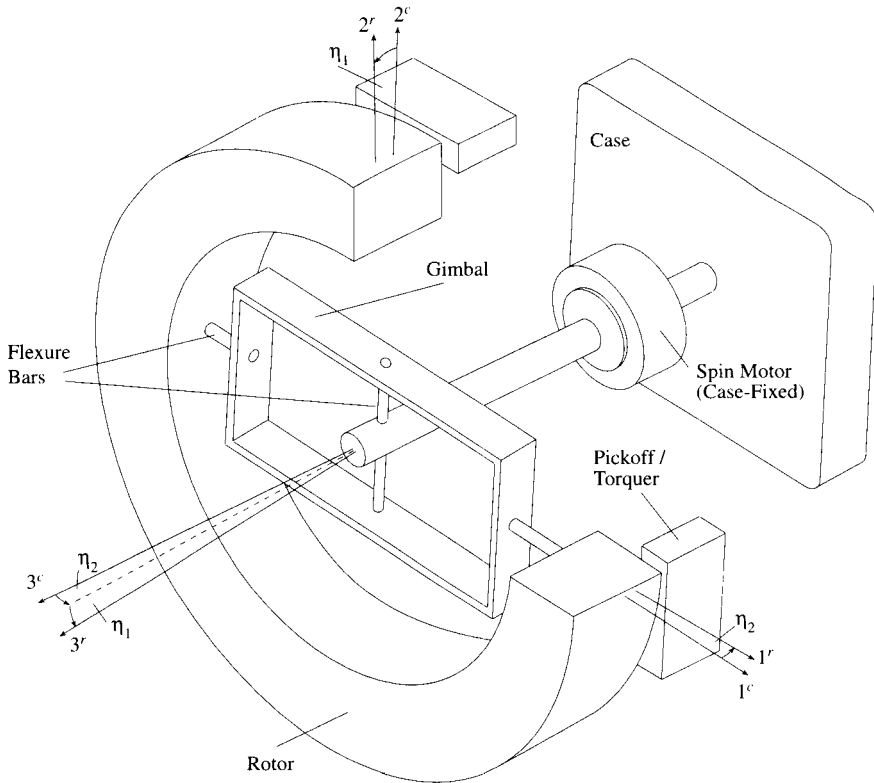


Figure 3.3: Schematic of the tuned-rotor gyro.

which pickoff signals are used to generate restoring torques on the rotor. A simplified derivation of the dynamics of the tuned TDF gyro is based on a coordinate frame aligned with the rotor (but not spinning with it) whose orientation with respect to the case frame is defined by the two small angles,  $\eta_1$  and  $\eta_2$ , as shown in Figure 3.3. Initially, however, consider the frame fixed to the rotor, with its 3-axis along the spin axis of the rotor (not the motor shaft); call this the  $r'$ -frame. In this frame, the angular momentum of the rotor/gimbal assembly is given, according to (3.9), by:

$$\mathbf{H}^{r'} = I^{r'} \boldsymbol{\omega}_{ir'}, \quad (3.44)$$

where we assume that the inertia tensor is diagonal, constant, and moments of inertia about the 1-axis and 2-axis are equal:

$$I^{r'} = \begin{pmatrix} I_1^{r'} & 0 & 0 \\ 0 & I_1^{r'} & 0 \\ 0 & 0 & I_3^{r'} \end{pmatrix}; \quad (3.45)$$

that is, we neglect the small rotations of the gimbal with respect to the rotor, as well as the non-circular symmetry in the masses of the flexure bars. Transforming (3.44) to the non-spinning rotor frame, the  $r$ -frame, which involves a rotational transformation,  $C_r^r$ , about the 3-axis by the angle,  $\omega_s t$ , where  $\omega_s$  is the spin rate and  $t$  is time, we find from (1.17) that  $I' = I^{r'}$ . With  $\omega_{ir'}^r = \omega_{ir}^r + \omega_{rr'}^r$  and  $\omega_{rr'}^r = (0 \ 0 \ \omega_s)^T$ , the angular momentum becomes

$$\begin{aligned} \mathbf{H}^r &= C_r^r \mathbf{H}^{r'} \\ &= C_r^r I^{r'} C_r^{r'} C_r^r \omega_{ir'}^r, \\ &= I' \omega_{ir'}^r \\ &= I' \omega_{ir}^r + \begin{pmatrix} 0 \\ 0 \\ I_3' \omega_s \end{pmatrix}. \end{aligned} \quad (3.46)$$

The relationship between the angular rate,  $\omega_{ir}^r$ , and the angular rate of the case,  $\omega_{ic}^c$  is:

$$\omega_{ir}^r = \omega_{ic}^c + \omega_{cr}^r = C_c^r \omega_{ic}^c + \omega_{cr}^r. \quad (3.47)$$

From Figure 3.3 and referring to equation (1.25), we find the transformation matrix,  $C_c^r$ , for small angular displacements of the rotor from the case:

$$C_c^r = R_2(\eta_2)R_1(\eta_1) \approx \begin{pmatrix} 1 & 0 & -\eta_2 \\ 0 & 1 & \eta_1 \\ \eta_2 & -\eta_1 & 1 \end{pmatrix}, \quad (3.48)$$

where second-order terms have been neglected, as usual. Then, from (1.68), we have

$$\Omega_{cr}^r = C_c^r \dot{C}_r^c, \quad (3.49)$$

which means that from (1.62), again neglecting second-order terms:

$$\omega_{cr}^r = \begin{pmatrix} \dot{\eta}_1 \\ \dot{\eta}_2 \\ 0 \end{pmatrix}. \quad (3.50)$$

Substituting this and (3.48) into (3.47) yields, explicitly:

$$\omega_{ir}^r = \begin{pmatrix} \omega_1^c - \eta_2 \omega_3^c + \dot{\eta}_1 \\ \omega_2^c + \eta_1 \omega_3^c + \dot{\eta}_2 \\ \omega_3^c + \eta_2 \omega_1^c - \eta_1 \omega_2^c \end{pmatrix}, \quad (3.51)$$

where case rotations are defined by (3.23). Now, we put (3.46) and its derivative into the torque equation (3.9) to obtain:

$$\begin{aligned}
\begin{pmatrix} L'_1 \\ L'_2 \\ L'_3 \end{pmatrix} = & \begin{pmatrix} I'_1 & 0 & 0 \\ 0 & I'_1 & 0 \\ 0 & 0 & I'_3 \end{pmatrix} \begin{pmatrix} \dot{\omega}_1^c - \dot{\eta}_2 \omega_3^c - \eta_2 \dot{\omega}_3^c + \ddot{\eta}_1 \\ \dot{\omega}_2^c + \dot{\eta}_1 \omega_3^c + \eta_1 \dot{\omega}_3^c + \ddot{\eta}_2 \\ \dot{\omega}_3^c + \dot{\eta}_2 \omega_1^c + \eta_2 \dot{\omega}_1^c - \dot{\eta}_1 \omega_2^c - \eta_1 \dot{\omega}_2^c \end{pmatrix} \\
& + \begin{pmatrix} 0 \\ 0 \\ I'_3 \dot{\omega}_s \end{pmatrix} + \begin{pmatrix} \omega_1^c - \eta_2 \omega_3^c + \dot{\eta}_1 \\ \omega_2^c + \eta_1 \omega_3^c + \dot{\eta}_2 \\ \omega_3^c + \eta_2 \omega_1^c - \eta_1 \omega_2^c \end{pmatrix} \\
& \times \left[ \begin{pmatrix} I'_1 & 0 & 0 \\ 0 & I'_1 & 0 \\ 0 & 0 & I'_3 \end{pmatrix} \begin{pmatrix} \omega_1^c - \eta_2 \omega_3^c + \dot{\eta}_1 \\ \omega_2^c + \eta_1 \omega_3^c + \dot{\eta}_2 \\ \omega_3^c + \eta_2 \omega_1^c - \eta_1 \omega_2^c \end{pmatrix} + \begin{pmatrix} 0 \\ 0 \\ I'_3 \dot{\omega}_s \end{pmatrix} \right]. \quad (3.52)
\end{aligned}$$

Grouping terms common to the gimbal angles, the first two components of this vector differential equation are given by:

$$\begin{aligned}
L'_1 = & I'_1 \ddot{\eta}_1 + (I'_3(\omega_3^c + \omega_s) - 2I'_1 \omega_3^c) \dot{\eta}_2 + [\omega_1^c(I'_3 - I'_1)(\omega_2^c + \eta_1 \omega_3^c + \dot{\eta}_2) - I'_1 \dot{\omega}_3^c] \eta_2 \\
& + [I'_3 \omega_s \omega_3^c - (I'_3 - I'_1)((\omega_2^c)^2 - (\omega_3^c)^2 + \omega_2^c(\eta_1 \omega_3^c + \dot{\eta}_2))] \eta_1 \\
& + I'_1 \dot{\omega}_1^c + (I'_3 - I'_1) \omega_2^c \omega_3^c + I'_3 \omega_s \omega_2^c,
\end{aligned} \quad (3.53)$$

and

$$\begin{aligned}
L'_2 = & I'_1 \ddot{\eta}_2 + (2I'_1 \omega_3^c - I'_3(\omega_3^c + \omega_s)) \dot{\eta}_1 + [\omega_2^c(I'_3 - I'_1)(\omega_1^c - \eta_2 \omega_3^c + \dot{\eta}_1) + I'_1 \dot{\omega}_3^c] \eta_1 \\
& + [I'_3 \omega_s \omega_3^c - (I'_3 - I'_1)((\omega_1^c)^2 - (\omega_3^c)^2 + \omega_1^c(\eta_2 \omega_3^c - \dot{\eta}_1))] \eta_2 \\
& + I'_1 \dot{\omega}_2^c - (I'_3 - I'_1) \omega_1^c \omega_3^c - I'_3 \omega_s \omega_1^c.
\end{aligned} \quad (3.54)$$

Now,  $\omega_3^c \ll \omega_s$  and the coefficients of the small gimbal angles,  $\eta_1$  and  $\eta_2$ , are dominated by the angular momentum due to the spin of the rotor,  $H_s = I'_3 \omega_s$ . We then obtain approximately:

$$L'_1 = I'_1 \ddot{\eta}_1 + H_s \dot{\eta}_2 + H_s \omega_3^c \eta_1 + I'_1 \dot{\omega}_1^c + (I'_3 - I'_1) \omega_1^c \omega_3^c + H_s \omega_2^c, \quad (3.55)$$

$$L'_2 = I'_1 \ddot{\eta}_2 - H_s \dot{\eta}_1 + H_s \omega_3^c \eta_2 + I'_1 \dot{\omega}_2^c - (I'_3 - I'_1) \omega_1^c \omega_3^c - H_s \omega_1^c. \quad (3.56)$$

These second-order differential equations for the gimbal angles are similar to (3.26) for the SDF gyro, although they are cross-coupled through the second terms on the right side. However, in the steady state, the indicated outputs, when used as a rate gyro, are given analogous to (3.32) for each axis:

$$\omega_1^c = -\frac{1}{H_s} (L_{\text{reb},2} + v_{0,2}), \quad (3.57)$$

$$\omega_2^c = \frac{1}{H_s} (L_{\text{reb},1} + v_{0,1}). \quad (3.58)$$

where  $L_{\text{reb},1}$  and  $L_{\text{reb},2}$  are commanded rebalance torques,  $v_{0,1}$  and  $v_{0,2}$  are corre-

sponding residual error torques, and appropriately defined compensation torques are included in the applied torques,  $L'_{1,2}$ . The TDF gyro exhibits the same rotation-induced errors in each axis as the SDF, namely, due to anisoinertia, cross coupling, and output axis rotation.

A more thorough derivation of the dynamics of the TDF gyro may be found in (Craig, 1972a), and Mansour and Lacchini (1993) offer a good review. This gyro may be used in both strapdown and stabilized mechanizations, hence both as a rate gyro and as an attitude and heading reference device. It is generally more reliable and simpler in design than the floated gyro, although, the torquer loops are more complex and the lack of a damping fluid requires additional electronics to provide stability in performance. We note that because of the dynamic tuning of the gyro, torques about the shaft axis do not couple into the 1- and 2-axes of the rotor, and thus the outputs are not seriously affected by the quality of the shaft support bearings. There is also excellent mass stability as the rotor/gimbal assembly is equally affected by longitudinal shifts in the spin-motor shaft. Error models such as (3.41) and (3.42) may be formulated for each axis of the TDF gyro. Complete error analyses are given in (Stieler and Winter, 1982) and (Craig, 1972b).

Another type of suspension of the spinning mass is achieved with the electrostatic gyro. In this case the rotor is spherical, rotating at high speed, and is suspended in a vacuum by an electrostatic or electromagnetic field. The rotor and case are completely isolated; there are no bearings of any kind resulting in the elimination of associated error torques. The angles are sensed using electrical or optical pick-offs. This type of TDF gyro can only be used to determine attitude since there is no provision for torquing to keep the pick-off angles near zero; it is primarily suited for strapdown mechanization.

### 3.2.2 Optical Gyroscopes

Optical gyroscopes are based on entirely different sensing principles, being kinematic rather than dynamic. Although there is no spinning proof mass, the nomenclature “gyroscope”, or “gyro”, is retained in deference to convention. Light acts as the sensor element in the optical gyro, and since it has no mass, it is not be affected by the dynamics of the environment in which the gyro finds itself. It is thus the natural alternative to the mechanical gyro in a non-stabilized deployment, that is, the strapdown mechanization (see Section 4.2.3). On the other hand, the optical gyro cannot be torqued or commanded like the mechanical gyro and, therefore, is not as suitable for providing local-level stabilization of a platform (Section 4.2.2). The optical gyro is a single degree-of-freedom device, which means that three gyros are needed with sensitive axes mutually perpendicular in order to measure all three angular rates or to provide a three-dimensional reference for attitude.

The rotational sensitivity of the optical gyros is based on the *Sagnac effect* (Sagnac, 1913; Post, 1967) which occurs when a light beam propagates around a closed path in a frame that rotates with respect to the inertial frame. Consider a light beam traversing an arbitrary circuitous planar conduit, as shown in Figure 3.4, having

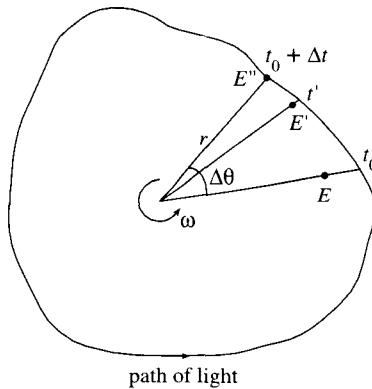


Figure 3.4: The Sagnac effect. During time interval  $\Delta t$ , light traverses a complete closed path in the rotating frame, and the emitter travels from  $E$  to  $E'$  to  $E''$ .

total path length equal to  $L$ . Suppose that the planar conduit in which this light beam travels is rotating with respect to inertial space about an axis perpendicular to its plane; the angular rate is denoted  $\omega$ . If the path is rotating in the counterclockwise direction ( $\omega > 0$ ), as shown, then a counterclockwise-travelling beam of light, starting and ending at the emitter (that travels with the conduit), will traverse a total distance  $L + \Delta L$ , where  $\Delta L$  is the apparent *lengthening* of the path during the travel time of the light. That is, if the light beam leaves the emitter,  $E$ , at time  $t_0$ , it will return to that same angular, inertial-frame position (where the emitter used to be) at time  $t_0 + \Delta t$  when the light has caught up with the emitter, having completed a full circuit in the rotating frame, the emitter is at  $E''$ . The extra path traversed during the time interval  $\Delta t$  is  $\Delta L$ .

To determine  $\Delta L$ , consider the differential change in path length during a differential time interval  $dt$ . During that time interval the light travels a distance  $rd\theta$ , hence

$$dt = \frac{rd\theta}{c}, \quad (3.59)$$

where  $d\theta$  is a differential angle increment,  $c$  is the speed of light, and  $(r, \theta)$  are polar coordinates (see Figure 3.4); while the conduit rotates by

$$d(\Delta L) = r\omega dt. \quad (3.60)$$

That the speed of light is a constant,  $c$ , even though it was emitted from a source in a rotating frame, is a fundamental tenet of the theories of special and general relativity. The total apparent lengthening of the path occurs while the light travels through an angle of  $2\pi + \Delta\theta$  radians, where  $\Delta\theta$  is the angle corresponding to  $\Delta t$ . Therefore,  $\Delta L$  is given by the following integral of (3.60) with (3.59) substituted:

$$\Delta L = \int_{t_0}^{t_0 + \Delta t} r\omega dt = \int_0^{2\pi} \frac{r^2\omega}{c} d\theta + \int_0^{\Delta\theta} \frac{r^2\omega}{c} d\theta. \quad (3.61)$$

The integral on the left-hand side describes the total change in path length in inertial space due to rotation of the conduit during the time interval,  $\Delta t$ . Changing the time variable to the angle,  $\theta$ , swept out by the light yields the two integrals on the right-hand side of the equation.

Now, one can further change the variable of integration from angle to area,  $A$ , swept out by the light, where it is assumed that the rate of rotation is much smaller than the speed of light ( $\omega r \ll c$ ), so that special relativistic effects can be ignored. The change of variables is given according to the formula for a differential element of area:

$$dA = \frac{1}{2} r \cdot r d\theta. \quad (3.62)$$

Therefore, since the total area has not been covered when the light returns to point  $E$ , having completed an angle of  $2\pi$  radians in inertial space, we have from (3.61)

$$\begin{aligned} \Delta L &= \int_{A-\Delta A}^{A} \frac{2\omega}{c} dA + \int_{\Delta A}^{2\pi} \frac{2\omega}{c} dA \\ &= \frac{2\omega}{c} A. \end{aligned} \quad (3.63)$$

Implicitly, we assume that during the interval,  $\Delta t$ , (typically,  $10^{-9}$  s) the angular rate,  $\omega$ , is constant. The area  $A$  represents the area enclosed by the conduit of the light beam and directly determines the change in length,  $\Delta L$ .

A similar derivation leads to the apparent *shortening* of the path for a light beam travelling the same conduit in the clockwise direction:

$$\begin{aligned} \Delta \ell &= \int_{t_0}^{t_0 + \Delta t} r\omega dt = \int_0^{2\pi - \Delta\theta} \frac{r^2\omega}{c} (-d\theta) = - \int_A^{2\pi} \frac{2\omega}{c} dA \\ &= - \frac{2\omega}{c} A. \end{aligned} \quad (3.64)$$

The negative sign signifies an integration in the clockwise (negative) direction and the apparent change in path length is negative.

In either case, the apparent lengthening or shortening of the path is directly proportional to the area enclosed by the path; and, already we see that the sensitivity of the optical gyroscope depends in some way on its size. Note, however, that it does not depend on the shape of the path. Furthermore, the center of rotation (or the coordinate origin) is arbitrary within the plane of the path as shown by our derivation, which implies that also the location of the input axis is arbitrary as long as it is

perpendicular to the plane of rotation. The Sagnac effect, therefore, is sensitive only to the intrinsic rotation with respect to inertial space, not to any translation. In fact, as mentioned at the beginning of the chapter, gyroscopes (mechanical or optical) ideally sense only pure rotation with respect to inertial space. Thus, for example, a gyro on a satellite orbiting the Earth does not sense the orbital motion (the free-fall acceleration), but does sense any rotation of the satellite with respect to the fixed stars (quasars) that define the inertial frame.

Consider a conduit defined by a circle with radius equal to 10 cm, rotating at  $2\pi$  rad/s (1 revolution per second). With  $c \approx 3 \times 10^{-8}$  m/s, the apparent path lengthening from (3.63) is  $\Delta L \approx 1.3 \times 10^{-9}$  m. This is roughly 1000 times shorter than the wavelength of visible light ( $\lambda_{\text{light}} \approx 3 \times 10^{-7} - 3 \times 10^{-6}$  m).

### 3.2.2.1 Ring Laser Gyro

As the numerical example above illustrates, it is extremely difficult to detect typical rotations (fractions of the value used) using reasonably sized instruments by just measuring the additional fractional part of the waves, i.e., the phase, of the light in a closed path (see, however, the fiber optic gyro, Section 3.2.2.2). On the other hand, by letting the closed conduit for the light beam be the resonant optical cavity of a *laser*, one can take advantage of the fundamental property in this case that the number of wavelengths in the conduit must remain constant, even under rotation, which means that the frequency must change if the apparent length of the conduit changes. Then, two counter-traveling light beams will create a fringe pattern that represents the interference of the waves due to their different frequencies. Counting the fringes directly indicates input *angular rate*. This is the basic concept of the ring laser gyro (RLG) that will be fully developed below.

Typical constructions for the closed path include the three-mirror and four-mirror ring resonators, as shown in Figure 3.5 (similar design used by Honeywell, Inc.) and Figure 3.6 (design used by Litton Guidance and Control Systems). Two oppositely traveling light beams with the same frequency are generated from the lasing action of a gas discharge (He-Ne gas,  $\lambda = 0.633$  μm). The ionization of the gas is achieved by applying a high voltage (e.g., 1000–1500 volts) across the anode-cathode pair of electrodes. The light beams are reflected by mirrors such that each traverses the same optical path in a closed loop. The beams are reflected completely at all mirrors, except at one corner where a partially reflecting mirror allows some of the light from each beam to pass to a detector through an assembly of prisms that combine the beams. At the detector the beams interfere to form a fringe pattern.

In addition to these basic components the RLG contains various optical and electro-mechanical devices that are used to compensate or eliminate major sources of errors. These will be discussed in Section 3.2.2.1.1. The key to a laser is that the number,  $N$ , of wavelengths,  $\lambda$ , inside the resonant cavity of length  $L$  is a constant, where  $N$  is always an integer:

$$L = N\lambda. \quad (3.65)$$

No matter what the length, the lasing of the light ensures a constant integer number

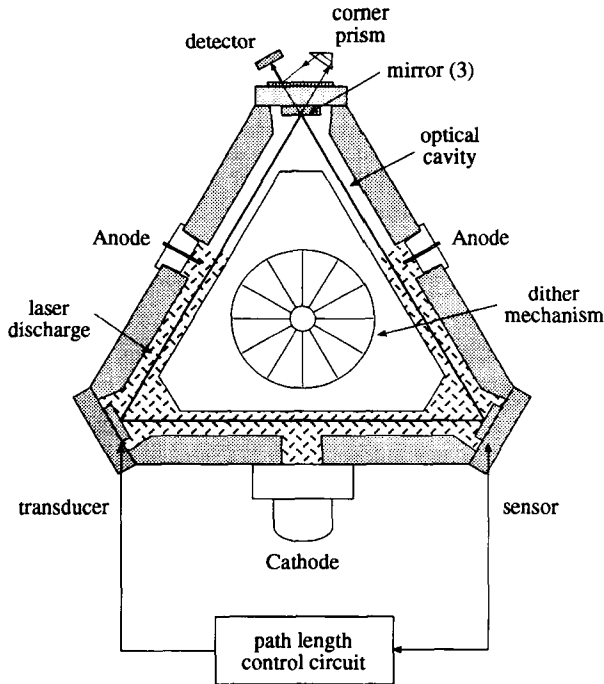


Figure 3.5: Schematic of three-mirror ring laser gyro.

of wavelengths within the cavity (coherent light). This means that a change in apparent length of the resonant cavity, i.e., the Sagnac effect (or any real change in path length, such as caused by thermal expansion), can only be accommodated by a change in the wavelength:

$$\Delta L = N\Delta\lambda. \quad (3.66)$$

The change in wavelength is converted to a change in frequency using the relationship between frequency,  $f$ , and wavelength:

$$f = \frac{c}{\lambda}. \quad (3.67)$$

According to the theory of general relativity, the speed of light,  $c$ , is a universal constant in vacuum. Here and in subsequent discussions, we omit the fact that the speed of light in a gas discharge medium clearly depends on the index of refraction. But if the medium is homogeneous and isotropic (constant index of refraction), the following arguments still apply. Specifically, we have approximately (neglecting non-linear terms):

$$\Delta f\lambda + f\Delta\lambda = \Delta c = 0, \quad (3.68)$$

which leads to

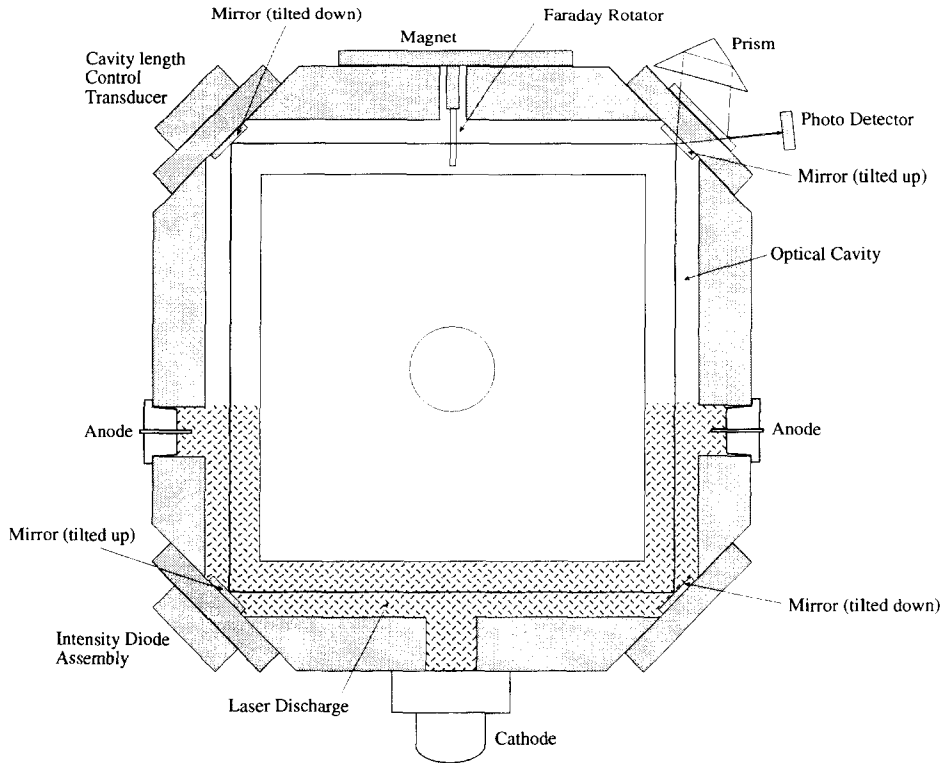


Figure 3.6: Schematic of multioscillator ring laser gyro with out-of-plane optical path.

$$\begin{aligned}\Delta f &= -\frac{f}{\lambda} \Delta\lambda = -\frac{f}{N\lambda} \Delta L \\ &= -\frac{f}{L} \Delta L.\end{aligned}\quad (3.69)$$

This equation holds for positive or negative  $\Delta L$ . An apparent change in path length (due to rotation) directly implies a change in frequency of the propagating light. To measure the frequency change the conduit is set up as an interferometer using two counter-propagating beams.

Let  $f_1 = f_0 + \Delta f_1$  and  $f_2 = f_0 + \Delta f_2$  be the respective frequencies of the counter-clockwise and clockwise propagating beams, with respect to some frequency,  $f_0$ , for the non-rotating path. That is, the changes in frequency  $\Delta f_1$  and  $\Delta f_2$  are due to rotation. From (3.69), (3.63), and (3.64), the difference in the frequencies of the counter-propagating beams is

$$\begin{aligned}\delta f &= f_2 - f_1 = \Delta f_2 - \Delta f_1 = -\frac{f_0}{L} \Delta\ell + \frac{f_0}{L} \Delta L = \frac{4Af_0}{Lc} \omega \\ &= \frac{4A}{\lambda L} \omega,\end{aligned}\quad (3.70)$$

where  $\lambda$  is the nominal wavelength corresponding to  $f_0$ . Integrating this with respect to time yields the phase change (since the time-derivative of phase is frequency):

$$\begin{aligned}\delta\phi &= \int_{\delta t} \delta f dt = \frac{4A}{\lambda L} \int_{\delta t} \omega dt \\ &= \frac{4A}{\lambda L} \delta\theta,\end{aligned}\quad (3.71)$$

where  $\delta\phi$  is in units of cycles, and the change in the angle,  $\delta\theta$ , due to rotation during a time interval,  $\delta t$ , is (in radians)

$$\delta\theta = \int_{\delta t} \omega dt \quad (3.72)$$

Note, again, that the phase change depends directly on the area enclosed by the path, but also inversely on the length of the path; that is, the sensitivity of the RLG depends only linearly on its physical dimension.

The interference fringe pattern produced by the combining optics at one corner of the RLG is sensed at the detector by two photodiodes. The phase change,  $\delta\phi$ , is measured by detecting the transitions from light to dark in the pattern. The fringe pattern is stationary ( $\delta\phi = 0$ ) if there is no rotation in inertial space. But, it migrates in the presence of rotation; and counting the number of fringes passing the detector provides a digitized measure of the change in angle per unit time.

Two detectors, a quarter cycle apart, are used to count the number of passing fringes; thus,  $\delta\phi$  is quantized to a quarter cycle (Figure 3.7) which represents the resolution of the instrument. The quarter cycles of phase change are detected as the detectors change from both on, to one or the other on, to both off, etc., as shown in the Figure. This arrangement of two detectors also provides for the determination

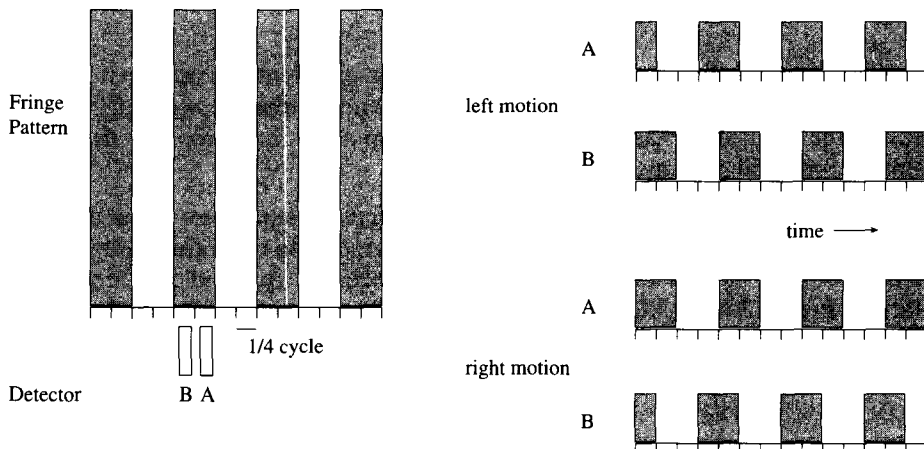


Figure 3.7: Fringe pattern of RLG as seen by detectors *A* and *B*.

of the direction of rotation. As an example, consider a triangular RLG with side lengths of 10 cm. Then we have  $L = 0.3$  m and  $A = 0.0043$  m<sup>2</sup>; and with  $\lambda = 0.6 \mu\text{m/cy}$  (He-Ne laser) the angular resolution per unit time is

$$\begin{aligned}\delta\theta &= \frac{\lambda L}{4A} \delta\phi = \frac{(0.6 \times 10^{-6} \text{ m/cy})(0.3 \text{ m})}{4(0.0043 \text{ m}^2)} \left(\frac{1}{4} \text{ cy}\right) = 2.6 \times 10^{-6} \text{ rad} \\ &= 0.5 \text{ arcsec.}\end{aligned}\quad (3.73)$$

The actual output of the RLG is the number of pulses at a particular data rate, e.g. 256 Hz, implying  $\delta t = 0.00390625$  s, and represents the accumulated rotation,  $\delta\theta$ , of the instrument in inertial space over this interval, according to (3.72). Since only a whole number of pulses can be counted during each interval, the output is affected by a *quantization error*, being the remainder of rotation not included in the output during  $\delta t$ . The remainder is not lost since it is part of the pulse count during the next interval, but the output value for each interval is slightly erroneous, which has the net effect of adding noise to the measurement.

### 3.2.2.1.1 RLG Error Sources

As mentioned, optical gyros, like the RLG, are not subject to the kind of dynamical error sources associated with the mechanical gyro. Nevertheless, sophisticated technologies had to be developed to isolate the sensitivity to rotation from the sundry effects that distort the optical path from the ideal or that cause unequal path lengths (*non-reciprocity*) for the two counter-propagating beams. In the past these technological challenges have largely kept the RLG from competing with the mechanical gyros in terms of accuracy, although in terms of cost, reliability, and maintainability, they are far superior. Whereas the most precise gyros are still of the mechanical kind, optical gyros are now routinely being used for commercial and non-strategic military navigation and attitude purposes.

Foremost, the accuracy of the RLG depends on the stability of the path length. Thus the construction material for the basic frame must have a very low coefficient of thermal expansion; a type of glass/ceramic block is often used. Further path stability is achieved by implementing a path length control loop whereby one of the mirrors is adjusted by a piezoelectric transducer such that the detected intensity of the laser beam is maximized (the intensity varies with the length of the path, with peaks of intensity (resonances) occurring at frequency intervals defined by the so-called free spectral range,  $c/L$ ), thus also ensuring maximal energy in the output.

The electric field set up by the high voltage across the anode-cathode pair causes the gas to flow within the laser cavity (*Langmuir flow*). This results in a differential change in the index of refraction for the two counter-traveling beams and a consequent shift in frequency, thus mimicking an angular input rate. To counter this phenomenon, two anodes and one cathode (or, vice versa) are used to create a dual-leg gas discharge such that the two associated flows are balanced.

One of the more significant problems of the ring laser gyro is its susceptibility to a phenomenon called *frequency lock-in* that precludes its sensitivity to low angular

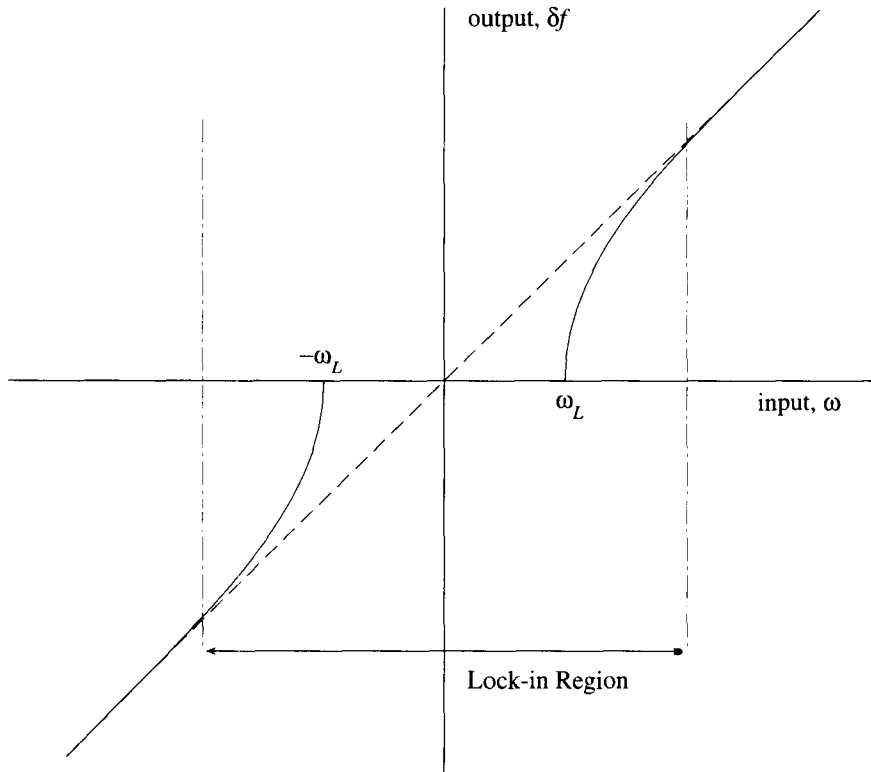


Figure 3.8: Response of ring laser gyro to input angular rate.

rates. Imperfections in the various components of the resonant cavity, including the gas medium and, in particular, the mirrors, cause light to scatter, and the two counter-traveling beams, oscillating at nearly the same frequency, interact in such a way that they lock together at the same frequency over a range of input rotations, typically up to several hundred degrees per hour. As such, the indicated rotation is zero even when the actual rotation is not. For example, Earth rate, being 15 °/hr, would not be detected. Figure 3.8 shows the response of the ring laser gyro to rotational frequency. For  $|\omega| < \omega_L$ , the fringe pattern is stationary.

The frequency lock-in problem can be solved by deliberately designing asymmetries into the device which affect one light beam differently (oppositely) than the other. This causes an artificial, but presumably known bias in the sensed angular rate. To obtain the true rate, the sensed rate must be corrected by the effect of the designed asymmetry. Options available to introduce this bias include mechanical motions and magnetically induced biases, of either a monotonic or a periodic nature, as well as optical techniques. Imposing a monotonic rate means physically rotating the RLG about its sensitive axis with some constant rate, thus moving the sensed rate, that now includes this bias, away from the lock-in range. The bias rate must be

sufficiently large to exceed the maximum actual range of inertial rate that might be encountered (e.g.,  $\pm 100^\circ/\text{s}$ ). This turns out to be technically unfeasible since the stability of this bias cannot be controlled to high accuracy.

The alternative is to superimpose a bias in the form of an alternating rotation, i.e., a dithering or oscillation (tens to hundreds of Hz) of the gyro about the sensitive axis (Figure 3.5). In this way, knowing the precise magnitude of the bias is not important since the output (see equation (3.72)) integrates any uniform oscillation to zero in the average. On the other hand, the gyro will spend a small amount of time, twice per dither period, within the lock-in range when the bias changes from the clockwise to the counterclockwise rate and vice versa. During this time the RLG will not sense actual rotation, and this contributes to an error that can be characterized as a random walk (Section 6.5.2). In addition, the accuracy of the instrument now depends on the accuracy of the mutual alignment of the dither axis and the sensitive axis of the RLG. Furthermore, the compliance of the dither spring, itself, causes misalignments of the sensitive axis when subjected to accelerations.

The other approaches to the lock-in problem involve magnetic-induced or combined optical/magnetic-induced biases that altogether eliminate moving parts from the gyro. This avoids the self induced vibration and misalignment errors in the sensed angular rates and also the associated cross-coupling vibrational effects on the accelerometers, and it reduces the overall random noise of the system.

These techniques make use of the *Faraday effect*, whereby a magnetic field with field lines parallel to the direction of beam propagation rotates the plane of polarization of polarized light. As a consequence of this rotation, the phase of circularly polarized light is either advanced or retarded depending on the direction of the magnetic field lines (parallel or anti-parallel), or, depending on the direction of propagation through a given field. Moreover, the phase of left-circularly polarized light is advanced while that of right-circularly polarized light is retarded as each propagates in the direction of the field lines. The phase difference between two counter-propagating beams of like polarization implies a difference in apparent optical path length, which can only be accommodated by a difference in frequency between the two resonant beams. Therefore, the placement of a so-called *Faraday cell* or *Faraday rotator* in the path of polarized light beams adds a frequency bias to the signal generated by the Sagnac effect, moving the range of sensed rotations away from the lock-in region. With alternating magnetic field directions, the bias, again, is periodic, but the time spent in the lock-in range is much shorter, corresponding to the switching time of the field.

Another use of magnetic fields is to apply a ferromagnetic film in one of the mirrors and with an alternating magnetic field create a relative phase shift between the two beams (*Kerr effect*). This technique is less susceptible to stray magnetic fields than the Faraday cell approach. The switching time in both cases is limited since large magnetic fields are required, and this limits the bandwidth of the output.

A scheme that has found commercial success is the *multioscillator RLG*, or *differential laser gyro* (DILAG). Instead of two beams, consider four light beams brought to resonance within the same laser cavity, two left-circularly polarized (lcp) counter-

propagating beams and two right-circularly polarized (rcp) counter-propagating beams. With a single Faraday rotator for all four beams, each set of polarized beams is biased away from the lock-in range, but the biases, being equal in magnitude, have opposite sign because of the opposite polarizations. If  $\delta f_{lcp}$  and  $\delta f_{rcp}$  denote the frequency differences for the two pairs of beams, then from (3.69)

$$\begin{aligned}\delta f_{lcp} &= K\omega + f_F \\ \delta f_{rcp} &= K\omega - f_F,\end{aligned}\quad (3.74)$$

where  $f_F$  is the Faraday bias, and  $K = 4A/(\lambda L)$  is the scale factor. Adding, we obtain

$$\Delta f = \delta f_{lcp} + \delta f_{rcp} = 2K\omega, \quad (3.75)$$

showing that the bias (and associated errors) cancels, while the output (and the sensitivity) is doubled.

In practice, the circularly polarized beams are susceptible to a multitude of phase rotations due to anisotropies along the optical path, differential losses at the mirrors, and backscattering, which could have the net effect of neutralizing the bias and returning the frequency differences to the lock-in region. To circumvent this type of lock-in, the two polarized counter-propagating beam pairs are split in frequency by half the free spectral range with a relative 180°-rotation of the phases between the lcp and rcp beams:  $\delta f_{rcp} = \delta f_{lcp} + c/(2L)$ . In order to avoid placing another optical element (a reciprocal polarization rotator) in the path of the beams, creating losses due to additional backscattering and thermal expansion of the element, the relative rotation of the phases of the polarized beams can be achieved by appropriately tilting the mirrors such that the total optical path does not lie in one plane (but closes on itself). This out-of-plane configuration (Figure 3.6), requiring more than three mirrors, is used with success in Litton's differential "zero-lock gyro". For additional details and other biasing approaches see (Chow et al., 1985) and (Lawrence, 1998).

The uncompensated error model for the RLG comprises terms similar to those in the error model for the SDF mechanical gyro, except for those depending directly on the dynamics of the proof mass. The general model may be expressed as in (3.41) in terms of drift error, scale factor error, and random (white) noise,  $v_\omega$ , repeated here for convenience:

$$\delta\omega = \delta\omega_d + \kappa\omega + v_\omega. \quad (3.76)$$

The scale factor error,  $\kappa$ , may include a constant part and linearly varying parts that also depend on the sign of the input rate. The uncompensated drift bias may comprise residual temperature and magnetic sensitivity terms and a constant part due to medium flow and optical backscattering effects, to lock-in (deadband), and hysteresis resulting from thermal cycling of the unit:

$$\delta\omega_d = \delta\omega_0 + c_T\delta T + c_1B_1 + c_2B_2 + c_3B_3, \quad (3.77)$$

similar to (3.42). Other terms may also be added to account for uncompensated alignment errors (for the mechanically dithered RLG) and time-correlated noise.

Kayton and Fried (1997) give the following values as an example of the uncompensated errors:

$$\begin{aligned}
 \text{gyro bias} &= 0.005^\circ/\text{hr} \\
 \text{residual deadband} &= 0.003^\circ/\text{hr} \\
 \text{thermal hysteresis} &= 0.003^\circ/\text{hr} \\
 \text{thermal bias sensitivity} &= 5 \times 10^{-5}^\circ/(\text{hr }^\circ\text{C}) \\
 \text{scale factor error} &= 2 \times 10^{-6} \\
 \text{alignment error} &= 5 \times 10^{-6} \text{ rad} \\
 \text{magnetic sensitivity} &= 0.002^\circ/(\text{hr gauss}). 
 \end{aligned} \tag{3.78}$$

### 3.2.2.2 Fiber-Optic Gyro

Another class of optical gyros is that of the fiber-optic gyro (FOG), where in this case the light-wave guide is optical fiber. Fiber-optic gyros are solid-state devices (no moving parts) that require low power, are very rugged and reliable, and thus are suitable to harsh dynamic environments. The optical fiber, itself, is maintenance free, low in cost, and has long shelf life. Furthermore, the drift of the FOG theoretically can be as low as that of a high-accuracy ring-laser gyro (0.001°/hr). Several concepts are being developed, with the *interferometric* type now in commercial production and operation. Analogous to GPS satellite ranging (Chapter 9), the interferometric FOG (I-FOG) measures the difference in phases of two light beams traveling through a loop of optical fiber, where, ideally, the phase difference is due to rotation of the plane of the loop according to the Sagnac effect. Other types of FOG's are based on passive ring resonators (laser outside the resonant optical fiber cavity) or on Brillouin scattering that induces lasing within the fiber wave-guide. These are described in more detail by Chow et al. (1985), Lefèvre (1993), and Hotate (1997).

We limit the present discussion to the I-FOG (Figure 3.9), where light from a broad-spectrum source (superluminescent diode) passes through a coupler to a polarizer and is split into two beams that propagate in opposite directions through the optical fiber loop. Upon exiting the loop, the two light waves are recombined and the resulting wave is now sent to a photodetector that generates an electrical voltage proportional to the optical power of the wave. Figure 3.10 gives an impression of the I-FOG manufactured by Fibersense Technologies Corporation.

Again, due to the Sagnac effect, the rotation of the loop about an axis perpendicular to the plane of the loop causes a light beam to travel an extra distance  $\Delta L$ , given by (3.63). For two propagating beams the net relative distance is the difference (see also (3.64))

$$\Delta L - \Delta \ell = \frac{4\omega}{c} A. \tag{3.79}$$

Recall that the Sagnac effect is independent of the shape of the conduit. Therefore,

82 3 Inertial Measurement Units

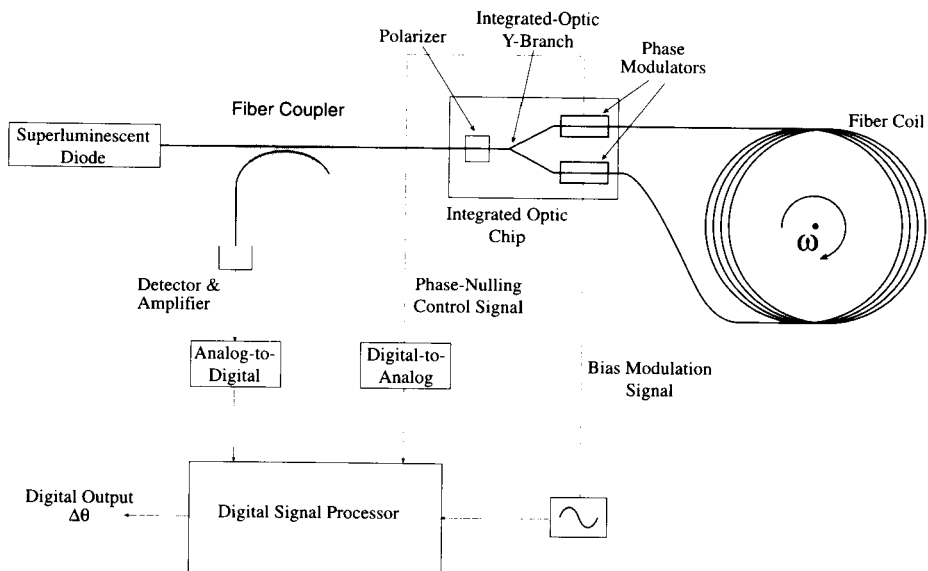


Figure 3.9: Schematic of the interferometric fiber-optic gyro.

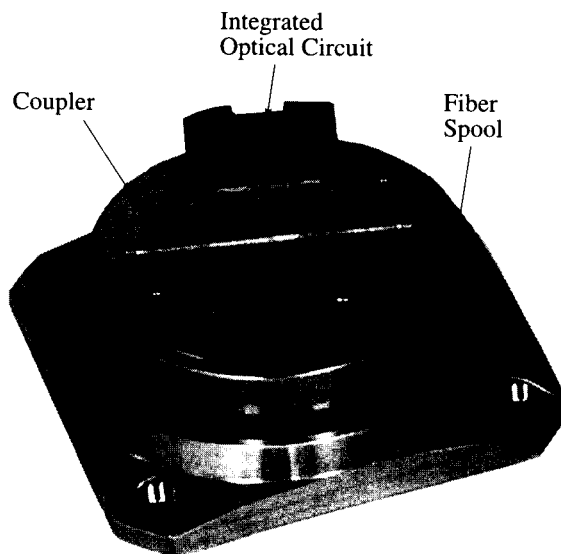


Figure 3.10: Interior of the FOG 200/45 (courtesy Fibersense Technologies Corporation).

the fiber is coiled to increase the actual enclosed area,  $A$ , of the loop, thus increasing the phase difference for a given rotation and hence the sensitivity of the gyro. Let  $n$  be the number of optical fiber windings of the coil. The effective total area covered by the beams is

$$A = n\pi \frac{d^2}{4} = \frac{1}{4} Ld, \quad (3.80)$$

where  $d$  is the diameter of the coils and  $L$  is the total length of the fiber. Substituting (3.80) into (3.79) and converting to phase difference, we find the phase change, in radians, due to rotation:

$$\Delta\phi = \frac{\Delta L - \Delta\ell}{\lambda} = \frac{Ld}{\lambda c} \omega. \quad (3.81)$$

where  $\Delta\phi$  is in units of cycle.

Using the large value,  $\omega = 0.01 \text{ rad/s} \approx 2000^\circ/\text{hr}$ , and  $d = 10 \text{ cm}$ ,  $\lambda = 0.8 \mu\text{m/cy}$ , we see that a single winding ( $L = \pi d$ ) yields a phase difference between the light waves of about  $1.3 \times 10^{-6}$  cy, the measurement of which would already represent a technological challenge. The increase in sensitivity is achieved typically with fiber lengths of several hundred meters, up to 1 km, where the scale factor between rotation rate and phase difference increases linearly with the length of the fiber. To yield the same phase difference of  $1.3 \times 10^{-6}$  cy, but corresponding to a sensitivity of  $1^\circ/\text{hr}$  (a good I-FOG) requires 640 m of fiber.

While the relationship between  $\omega$  and  $\Delta\phi$  is linear, the detection of  $\Delta\phi$  using a voltage response, at first glance, is not. Consider the amplitude,  $b$ , of the light beam as it enters the ideal optical fiber coil. As the beam is split in two, the clockwise and counterclockwise amplitudes are halved. Subsequently, they are shifted in phase due to the rotation,  $\omega$ , of the sensor; one by  $-\Delta\phi/2$ , the other by  $\Delta\phi/2$ . This can be represented as “rotation” of the amplitude in phase space, mathematically denoted with a complex exponential, as in (1.37). The recombined amplitude is then given by

$$\tilde{b} = \frac{1}{2} b e^{i\Delta\phi/2} + \frac{1}{2} b e^{-i\Delta\phi/2}. \quad (3.82)$$

The square of this is the power which is converted to voltage using a photodetector, yielding the result:

$$V(\Delta\phi) = V_0 \cos^2 \frac{\Delta\phi}{2} = \frac{V_0}{2} (1 + \cos(\Delta\phi)), \quad (3.83)$$

where  $V_0$  is a constant depending on the input light intensity. If the two beams combine constructively, then  $\Delta\phi = 0$  and  $V$  is maximum; if they combine destructively,  $\Delta\phi = \pi$ , and  $V = 0$ . The sensitivity to  $\Delta\phi$ , and thus to angular rate because of (3.81), is given by

$$\frac{dV(\Delta\phi)}{d(\Delta\phi)} = -\frac{V_0}{2} \sin(\Delta\phi). \quad (3.84)$$

This is zero for small phase differences; that is, small angular rates can hardly be detected. This can also be seen in Figure 3.11a showing the nonlinear relationship between  $\Delta\phi$  and  $V$  near  $\Delta\phi = 0$ .

Linearizing the relationship for small rates and matching the signs on  $\Delta\phi$  and  $V$  (so that a negative rotation is indicated by a negative voltage) can be accomplished by introducing a phase modulator at one end of the coiled fiber, as shown in Figure 3.9. One type of modulator is a piezoelectric cylinder wound a few times with the fiber. The fiber is stretched slightly according to a sinusoidal signal applied to the piezoelectric device, thus causing its actual length, and consequently the phase, to oscillate. If the sinusoidal signal, varying with time,  $t$ , is given by  $-\theta \cos(2\pi f_m t)$ , having amplitude,  $-\theta$ , and frequency,  $f_m$ , then the total phase shift in one beam is  $\Delta\phi/2 - \theta \cos(2\pi f_m t)$ . The other beam, first having to travel through the coil, encounters the phase modulator at a later time,  $t+T$ , and its phase shift is  $-\Delta\phi/2 - \theta \cos(2\pi f_m(t+T))$ . The combined beam amplitude, analogous to (3.82) is then given by

$$\tilde{\tilde{b}} = \frac{1}{2} b e^{i[\Delta\phi/2 - \theta \cos(2\pi f_m t)]} + \frac{1}{2} b e^{-i[\Delta\phi/2 + \theta \cos(2\pi f_m(t+T))].} \quad (3.85)$$

Introducing a shift in the time argument (without loss in generality),  $t' = t + T/2$ , we obtain

$$\tilde{\tilde{b}} = \frac{b}{2} e^{-i\theta\sqrt{1-\mu^2} \cos(2\pi f_m t')} [e^{i[\Delta\phi/2 - \theta\mu \sin(2\pi f_m t')]} + e^{-i[\Delta\phi/2 - \theta\mu \sin(2\pi f_m t')]}], \quad (3.86)$$

where  $\mu = \sin(2\pi f_m T/2)$ . The voltage generated from the power is now expressed as

$$\begin{aligned} \tilde{V}(\Delta\phi) &= \frac{\tilde{V}_0}{2} [1 + \cos(\Delta\phi - 2\theta\mu \sin(2\pi f_m t'))] \\ &= \frac{\tilde{V}_0}{2} [1 + \cos\Delta\phi \cos(2\theta\mu \sin(2\pi f_m t')) + \sin\Delta\phi \sin(2\theta\mu \sin(2\pi f_m t'))] \\ &= \frac{\tilde{V}_0}{2} [1 + \cos\Delta\phi + 2\theta\mu \sin\Delta\phi \sin(2\pi f_m t') + \text{higher powers of } \sin(2\pi f_m t')]. \end{aligned} \quad (3.87)$$

We see from the third term in the last equation of (3.87) that  $\sin\Delta\phi$  is modulated by the frequency,  $f_m$ . That is, if we demodulate the voltage at this frequency (in other words, obtain the Fourier transform coefficient corresponding to the first harmonic of  $V$ , see Section 1.6), then the result is proportional to  $\sin\Delta\phi$ :

$$\mathcal{F}(\tilde{V}(\Delta\phi))_1 \sim \sin\Delta\phi. \quad (3.88)$$

This gives a linear relationship between the output and the phase (rotation rate) for small  $\Delta\phi$ . Furthermore, the sign of the output also indicates the sign of  $\Delta\phi$  and of the rotation rate (see Figure 3.11b).

Other phase biasing techniques have also been developed by incorporating phase modulators on integrated optical circuits (see Hotake, 1997). In summary, we note

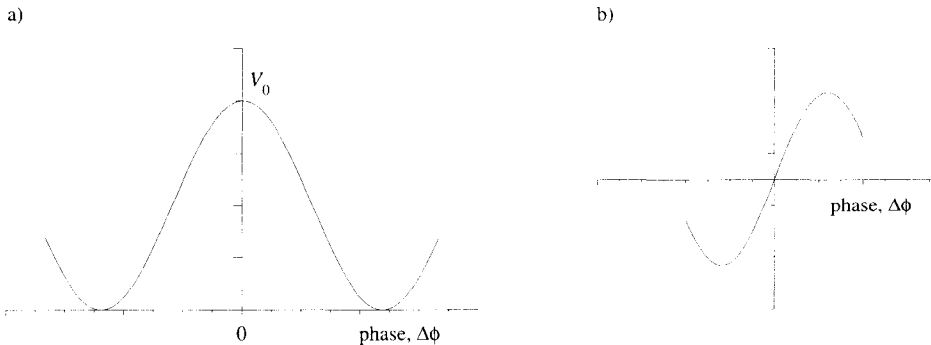


Figure 3.11: I-FOG output versus input phase difference,  $\Delta\phi$ , a) without bias modulation, and b) with bias modulation.

that just as in the RLG (but for a different reason), the phases of the light beams must be biased so that the sensor operates in the region of maximum sensitivity.

To benefit from the linearity in the output, the dynamic range of the sensor configuration so far is limited to small  $\Delta\phi$ . To increase the dynamic range, the Sagnac phase difference is removed from the exiting light through a feedback loop (closed-loop operation) again using a (higher band width) phase modulator (see Figure 3.9). Of course, the amount “removed” through this phase-nulling technique is a measure of the input angular rate. This is analogous to the torque rebalance loop used to null the gimbal angle of the mechanical gyro and maintains the linearity between input and output. Other control loops may be added to remove known phase shifts due to environmental factors such as temperature variations. The closed-loop operation produces excellent scale factor stability for the FOG.

Open-loop configurations have also been developed, where the linearity in the output is obtained electronically by using the higher harmonics of the demodulated signal. However, although involving fewer components, it is expected that these devices may not achieve the same dynamic range or quality.

### 3.2.2.2.1 FOG Error Sources

The errors associated with the FOG derive from the fact that the two light beam do not propagate identically through the fiber, that is, the optical path is not *reciprocal*. Nonreciprocity is caused by different polarizations of the two beams, thus requiring that they first pass through a polarizer. As they travel through the coil, their polarization will change, but identically. Even so, any magnetic fields will induce non-reciprocal phase changes according to the *Faraday effect*. This is usually countered by using special (costly) polarization maintaining optical fiber. Other nonreciprocity factors include *Rayleigh scattering* due to fluctuations in the refractive index of the fiber and the *Kerr effect* caused by the dependence of the velocity of the wave on its intensity. The limit in performance is ultimately dictated by photon shot noise and noise in the intensity of the light source. Various counter-measures have been designed to reduce these effects (Kim and Shaw, 1986; Hotate, 1997).

A typical error model for the FOG can be expressed similar to that given by (3.76), consisting of a scale factor error, drift error, and random noise. Typical uncompensated drift values (bias stability) for commercial grade I-FOG's range from 0.5 °/hr to 150 °/hr, and uncompensated scale factor errors from 100 ppm to over 1000 ppm. The development of the FOG is rapid and bias stability better than 0.001 °/hr is already demonstrated in the laboratory and widely anticipated in commercial markets, thus rivaling the RLG. Scale factor stability, however, is still dominated by the RLG (Barbour and Schmidt, 1998).

### 3.3 Accelerometer

In one sense, the first accelerometer was actually a gravity meter, a pendulum (in fact, gravity meters of all kinds are accelerometers), dating back to Christiaan Huygen's seventeenth century. Of course, it could measure only one type of acceleration and was useless on a moving vehicle. Knowing the length of the pendulum arm and measuring the period of the pendulum, one can deduce the value of the total gravity acceleration. It was in this way first demonstrated, by comparing measurements of the pendulum period to accurate clocks, that the gravity acceleration varies on the Earth's surface with respect to latitude (as predicted by Newton).

Today's field gravity meter (or, gravimeter) is based almost exclusively on the concept of a proof mass on a spring, where the mechanical principles correspond to the rotational degree-of-freedom of the mass on the end of a rod that is connected to the housing at one end by a hinge and at the mass-end by a spring (Torge, 1989). A very common accelerometer design is based on similar principles where the mechanical spring is replaced by electromagnetically induced torques. Both types of instruments use the nulling method (closed-loop operation analogous to the rebalance loop of the mechanical gyro, Section 3.2.1.1) whereby the force needed to restore the proof mass to a state of equilibrium is a measure of the (change in) acceleration. Another common type of accelerometer is based on the change in resonant frequency of a vibrating element with change in applied tension due to a change in acceleration of the proof mass. In both types, the response to acceleration is effected by an inertial mass and Newton's laws of motion ultimately dictate the dynamics of the sensing mechanism.

A distinction is made between linear and angular accelerometers, where the focus of the present treatment is the linear variety since these are used in inertial navigation systems, while gyros have much better performance than angular accelerometers, at least in the case of low frequency motions. Furthermore, it is noted that accelerometer development covers a much larger field in commercial applications related to shock and vibration monitoring and determination not discussed in the present text; see Walter (1997) and Meydan (1997).

For illustrative purposes and with results applying to linear accelerometers of any kind, we consider first the simple case of a proof mass on an ideal spring. This has strong intuitive appeal as it provides a conceptual view of what an accelerometer

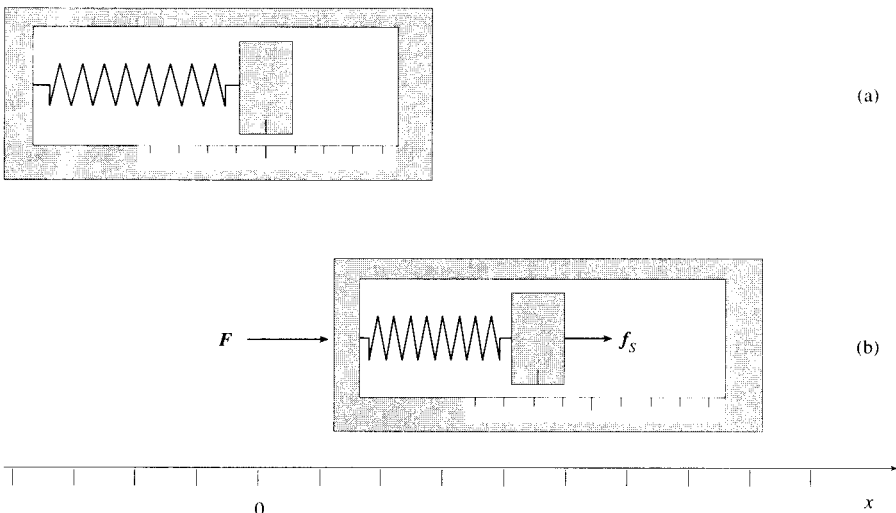


Figure 3.12: Accelerometer in an inertial frame without (a) and with (b) an applied force,  $F$ .

senses, even though it is only a translational analogy for the case of a rotational (pendulum-type) sensing mechanism. The triviality of stating that an accelerometer senses an acceleration is confounded by the *Equivalence Principle*. One sometimes finds in the geodetic literature statements to the effect that the accelerometer senses both kinematic and gravitational acceleration. This imprecise wording should be replaced with “*the accelerometer senses only specific force*,” as the following shows.

As depicted in Figure 3.12, the idealized accelerometer consists of a proof mass attached to a spring, which in turn is attached to a box. The proof mass is permitted to move (without friction) only in the direction defined by the spring and the box has graduations to indicate its relative position. The stiffness,  $k > 0$ , of the spring is assumed constant. The reference frame in this first case is truly inertial as discussed in Chapter 1, that is, with no gravitational field. In Figure 3.12a, the accelerometer is at rest (or in uniform rectilinear motion); and, consequently, the spring is unstressed since no forces are acting on the proof mass (the proof mass remains at  $x = 0$ ).

In Figure 3.12b, a force,  $F$ , (i.e., a contact force, or a physical action) is applied to the box causing it to accelerate with constant acceleration,  $a$ , within the reference frame (along the  $x$ -axis). A manifestation of this force is transmitted to the proof mass via the spring which compresses (initially) and imparts a force,  $f_s$ , on the proof mass. Let  $X$  denote the position of the proof mass relative to the box and let  $x_b$  be the position of the box in the external reference frame. Then, the position of the proof mass in the external reference frame is

$$x = x_b + X. \quad (3.89)$$

The (only) force acting on the proof mass is due to the compression of the spring

and is given by *Hooke's Law*:  $f_s = -kX$ ; therefore, the equation of motion (in the inertial frame) is, according to Newton's Second Law of Motion, (1.3),

$$m\ddot{x} = f_s = -kX, \quad (3.90)$$

where  $m$  is the mass of the proof mass. Substituting (3.89) into the left-hand side of (3.90) and noting that  $\ddot{x}_b = a$ , yields

$$\ddot{X} + \frac{k}{m} X = -a. \quad (3.91)$$

This is the differential equation of a forced harmonic oscillator with the well known solution given by (2.84):

$$X(t) = \frac{-ma}{k} \left( 1 - \cos \left( t\sqrt{\frac{k}{m}} \right) \right), \quad (3.92)$$

assuming the following initial conditions

$$X(t=0) = 0, \quad \dot{X}(t=0) = 0. \quad (3.93)$$

Clearly, the average position of the proof mass relative to the box is directly proportional to the applied acceleration with proportionality constant  $m/k$ ; and therefore, the device is, indeed, an accelerometer. For this to be a practical accelerometer, some form of damping would have to be introduced to attenuate the oscillations.

Now, suppose a gravitational field pervades the (otherwise inertial) reference frame. In this case, gravitation acts to accelerate the box and the proof mass (and the spring). The gravitational acceleration is the same for the proof mass and the box (by Newton's Law of Gravitation, (1.6)), if the gravitational acceleration,  $g$ , is assumed constant over the length of the box. Equation (1.7) now defines the motion of the proof mass; and, with no applied force,  $\ddot{x} = g$ . Similarly for the box,  $\ddot{x}_b = g$ . Hence, by equation (3.89), the motion of the proof mass relative to the box is given by

$$\ddot{X} = 0 \quad \Rightarrow \quad X(t) = 0, \quad (3.94)$$

where conditions (3.93) apply. The accelerometer is accelerating (falling) in the gravitational field, but it indicates no acceleration. This trivial derivation, consistent with the previous development, shows that, in principle, *the accelerometer does not directly sense the presence of a gravitational field*. As a final example, an accelerometer in orbit around Earth, though always accelerating (falling) towards Earth, senses only atmospheric drag and solar (and other) radiation pressure, but not gravitation.

In summary, an accelerometer senses only specific forces (the “ $a$ ” in equation (1.7)), that is, accelerations resulting from *real* (i.e., applied, action, or contact) forces. This complies with the IEEE Standards (IEEE, 1984) definition of an accelerometer as “a device that senses the inertial reaction of a proof mass for the purpose of measuring ... acceleration”. It senses neither gravitational acceleration nor the acceleration of other types of kinematic forces (due to rotation, see the discussion in

Chapter 1). It does sense the *reactions* to these, if there are any, because the reaction (the lift provided by the wing of an aircraft, the resistance of the Earth's surface acting on objects at rest) is a real force. In accordance with the Principle of Equivalence, the measurement cannot distinguish whether the *reaction* is a consequence of gravitation or rotation or an applied force.

### 3.3.1 Accelerations in Non-Inertial Frames

Transformed from the inertial frame, the *sensed* acceleration vector coordinatized in an arbitrary frame, say the *a*-frame, is given simply by

$$\mathbf{a}^a = C_i^a \mathbf{a}^i. \quad (3.95)$$

The transformation,  $C_i^a$ , is a rotation about the center of the sensor that redirects the components of the vector,  $\mathbf{a}^i$ , along directions defined by the *a*-frame. The *a*-frame could be rotating (then it is non-inertial), but no additional terms, such as centrifugal or Coriolis accelerations, enter the transformation as long as the sensing point of the accelerometer is at the frame origin.

On the other hand, consider a case containing an array of accelerometers that is rotating with respect to the *i*-frame. Let the frame of the case be the *c*-frame and suppose that the frames of the accelerometers (the *a*-frames) are rigidly connected and parallel to the *c*-frame. For a particular accelerometer, the translation between *a*- and *c*-frames is given by the vector (see Figure 3.13):

$$\mathbf{b}^i = \mathbf{x}_{\text{accel}}^i - \mathbf{x}_{\text{case}}^i, \quad (3.96)$$

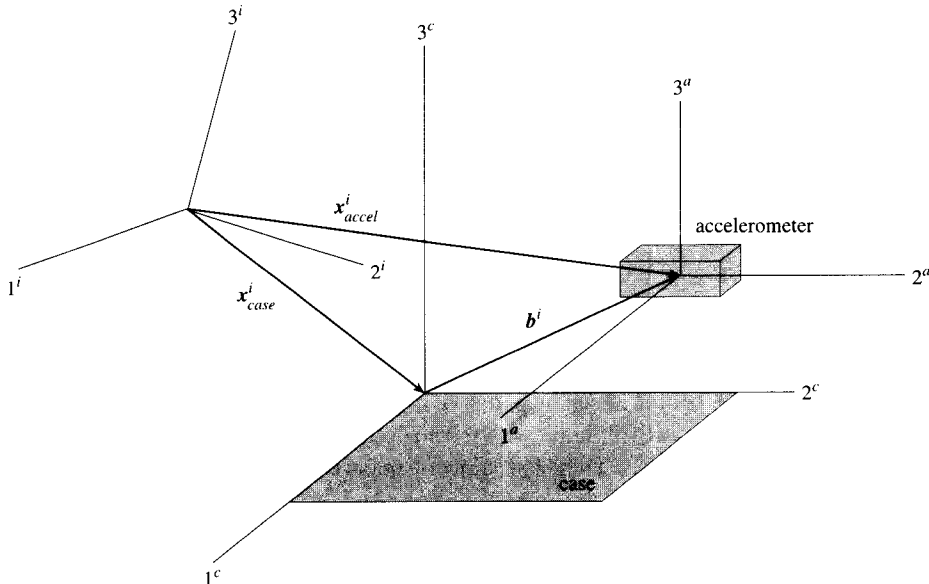


Figure 3.13: Accelerometer and case frames relative to the *i*-frame.

where all coordinates are in the  $i$ -frame. We wish to express the acceleration of the  $c$ -frame in terms of the sensed acceleration in the  $a$ -frame. By the Coriolis law (1.70) and with  $\dot{\mathbf{b}}^c = \mathbf{0}$ , we have

$$\ddot{\mathbf{x}}_{\text{accel}}^i = \ddot{\mathbf{x}}_{\text{case}}^i + \dot{\mathbf{b}}^i = \ddot{\mathbf{x}}_{\text{case}}^i + C_c^i \boldsymbol{\omega}_{ic}^c \times \mathbf{b}^c, \quad (3.97)$$

and, differentiating again, using (1.68) and (1.62),

$$\begin{aligned} \ddot{\mathbf{x}}_{\text{accel}}^i &= \ddot{\mathbf{x}}_{\text{case}}^i + (\dot{C}_c^i \boldsymbol{\omega}_{ic}^c + C_c^i \dot{\boldsymbol{\omega}}_{ic}^c) \times \mathbf{b}^c \\ &= \ddot{\mathbf{x}}_{\text{case}}^i + C_c^i \dot{\boldsymbol{\omega}}_{ic}^c \times \mathbf{b}^c + C_c^i \boldsymbol{\omega}_{ic}^c \times (\boldsymbol{\omega}_{ic}^c \times \mathbf{b}^c). \end{aligned} \quad (3.98)$$

Assume that there is a gravitational field, then from (1.7)

$$\mathbf{a}_{\text{accel}}^i = \ddot{\mathbf{x}}_{\text{accel}}^i - \mathbf{g}_{\text{accel}}^i, \quad \mathbf{a}_{\text{case}}^i = \ddot{\mathbf{x}}_{\text{case}}^i - \mathbf{g}_{\text{case}}^i. \quad (3.99)$$

Let  $C_i^c$  represent the rotation from the  $i$ -frame to the  $c$ -frame. Then with (3.99) and (3.98), we have:

$$\begin{aligned} \mathbf{a}_{\text{accel}}^c &= C_i^c(\ddot{\mathbf{x}}_{\text{accel}}^i - \mathbf{g}_{\text{accel}}^i) \\ &= C_i^c(\ddot{\mathbf{x}}_{\text{case}}^i + C_c^i \dot{\boldsymbol{\omega}}_{ic}^c \times \mathbf{b}^c + C_c^i \boldsymbol{\omega}_{ic}^c \times (\boldsymbol{\omega}_{ic}^c \times \mathbf{b}^c) - \mathbf{g}_{\text{accel}}^i) \\ &= \mathbf{a}_{\text{case}}^c + \mathbf{g}_{\text{case}}^c - \mathbf{g}_{\text{accel}}^i + \dot{\boldsymbol{\omega}}_{ic}^c \times \mathbf{b}^c + \boldsymbol{\omega}_{ic}^c \times (\boldsymbol{\omega}_{ic}^c \times \mathbf{b}^c). \end{aligned} \quad (3.100)$$

This says that the acceleration sensed in the  $a$ -frame, but coordinatized in a parallel frame, the  $c$ -frame of the case, to which it is rigidly attached, is equal to the acceleration of the case plus various reaction forces supplied by the rigid support of the  $a$ -frame to the  $c$ -frame. The first of these is due to the gravitational difference between locations of the accelerometer and case frame origins, and the others are associated with the rotation of the case in the  $i$ -frame. They constitute the *lever-arm effect* that results whenever the acceleration sensor is not at the center of motion of the vehicle.

We will make use of equation (3.100) when considering the fact that while an accelerometer senses the inertial acceleration in its own frame, the  $a$ -frame, the sensed acceleration is interpreted to be with respect to a defined reference point of the accelerometer case, the  $c$ -frame. The error of this interpretation is given by all but the gravitational terms on the right side of (3.100) (because  $\mathbf{b}^c$  is on the order of a few centimeters or less, the gravitational difference can be neglected).

### 3.3.2 Force-Rebalance Dynamics

The motion of the proof mass in today's high-quality, navigation-grade accelerometers is pendulous rather than strictly translational as depicted for the mass on a linear spring (Figure 3.12). That is, the proof mass is the arm of a pendulum that is hinged to the case of the accelerometer and responds to applied accelerations with a rotation about the hinge point. However, using an appropriate feed-back loop (closed-loop operation), the mass is forced always into its null position thus maintaining the linearity of the instrument's sensitivity to applied accelerations. To conceptualize the dynamics of this *force-rebalance accelerometer*, we allude to the

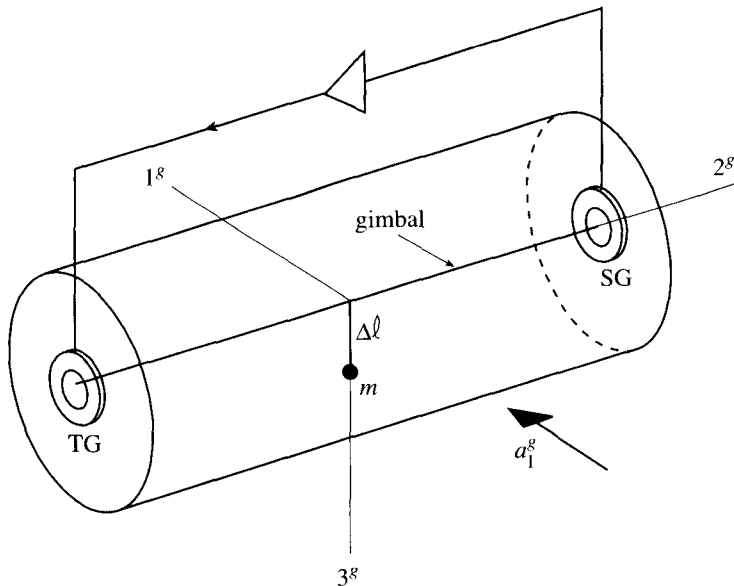


Figure 3.14: Concept of force (torque)—rebalance pendulous accelerometer.

mechanical SDF gyro, as depicted schematically in Figure 3.14. The proof mass in this case is *asymmetric*, as shown, with mass,  $m$ , and its center displaced a distance,  $\Delta\ell$ , along the 3-axis. In response to an acceleration along the 1-axis, the mass is allowed to pivot about the 2-axis which represents the “hinge” of the pendulum. Indeed, this is similar to the mass imbalance that was discussed for the mechanical gyro, only here it is intentional because the instrument should be sensitive to accelerations. The 1-axis is the *input axis*, the 2-axis is the *output axis*, and the 3-axis containing the proof mass is called the *pendulous axis*.

Suppose a specific force vector,  $\mathbf{a}$ , is acting on the accelerometer case, causing the gimbal to rotate, and suppose the case, itself, is rotating with respect to inertial space (the  $i$ -frame) with angular rate  $\omega_i^c$ , whose components are given by (3.23). Due to the specific force component along the 1<sup>g</sup>-axis,  $a_1^g$ , the pendulous axis of the proof mass will deviate from a reference axis by the angle  $\eta$  (Figure 3.15). Let this *pendulous reference axis* be the 3-axis of the  $c$ -frame. Also, we define the 2<sup>c</sup>-axis to be parallel to the 2<sup>g</sup>-axis, but for reasons that will be apparent, we locate the origin of the  $c$ -frame a distance,  $\ell$ , from the  $g$ -frame origin along the pendulous reference axis.

To derive the dynamics equation, we start with that of the mechanical gyro (3.24) with  $H_s = I_s\omega_s = 0$  (there is no spinning rotor) and a rearrangement of terms:

$$I_2^g \ddot{\eta} = L_2^g - I_2^g \dot{\omega}_2^c + (\omega_3^c + \eta \omega_1^c)(I_3^g - I_1^g)(\omega_1^c - \eta \omega_3^c), \quad (3.101)$$

where the total applied torque about the output axis is due to the commanded rebalance torque,  $L_{reb}$ , and the torque applied by the output axis suspension in

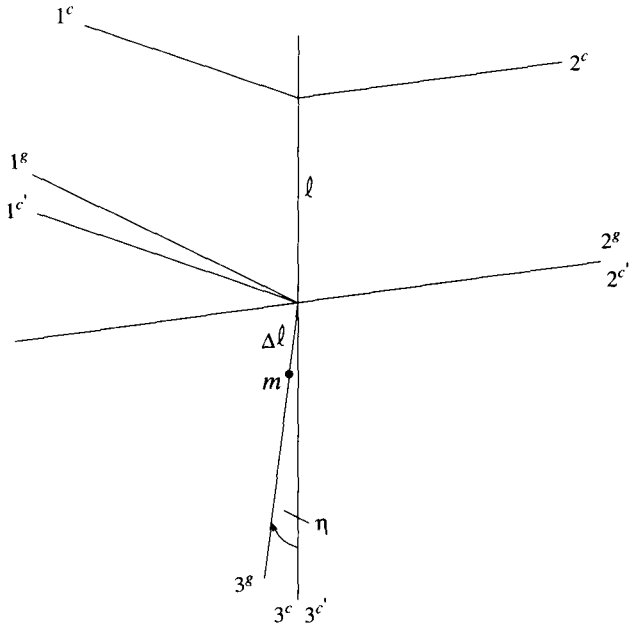


Figure 3.15: Coordinate frames for pendulous force-rebalance accelerometer.

reaction to the acceleration,  $a_1^g m \Delta\ell$  (see (3.40)). We also include a spring torque,  $-K\eta$ , that is exercised by the hinge of our conceptual pendulum accelerometer, and a damping torque,  $-C\dot{\eta}$ , so that the total applied torque is

$$L_2^g = L_{\text{reb}} + a_1^g m \Delta\ell - C\dot{\eta} - K\eta. \quad (3.102)$$

Note that the moments of inertia in (3.99) refer to the axes as depicted in Figure 3.14, which, unlike the SDF gyro, do not define the axes of mass symmetry; however, the products of inertia are still zero. Also, note that the input acceleration,  $a_1^g$ , in (3.102) refers to an acceleration along the  $1^g$ -axis, with reference point at the origin of the  $g$ -frame. Ultimately, we would like to measure the acceleration along the  $1^c$ -axis, the *reference input axis*.

Moreover, we wish to refer the sensed acceleration to the origin of the  $c$ -frame. Let the  $c'$ -frame be parallel to the  $c$ -frame, sharing its origin with the  $g$ -frame. Using (3.21) for  $\mathbf{C}_{c'}^g$ , the acceleration in the  $g$ -frame along the  $1^g$ -axis is given by

$$a_1^g = a_1^{c'} - \eta a_3^{c'}. \quad (3.103)$$

According to (3.100), with gravitational effects neglected and  $\mathbf{b}^c = (0, 0, \ell)^T$ , the component,  $a_1^c$ , is given in terms of the corresponding component in the displaced  $c$ -frame by

$$a_1^{c'} = a_1^c + \dot{\omega}_2^c \ell + \omega_1^c \omega_3^c \ell. \quad (3.104)$$

Substituting this into (3.103) and subsequently into (3.102) yields the applied torque

in the g-frame, which, put into (3.101), produces the following differential equation in the angle,  $\eta$ :

$$\begin{aligned} L_{\text{reb}} = & I_2^g(\ddot{\eta} + \dot{\omega}_2^c) + (I_1^g - I_3^g)\omega_1^c\omega_3^c \\ & - (a_1^c + \dot{\omega}_2^c\ell + \omega_1^c\omega_3^c\ell - \eta a_3^{c'})m\Delta\ell + C\dot{\eta} + K\eta, \end{aligned} \quad (3.105)$$

where the anisoinertia terms depending on the small angle,  $\eta$ , have been neglected. The product  $m\Delta\ell$  is called the *pendulosity*,  $p$ , and is a known quantity of the instrument. Dividing by  $p$ , (3.105) becomes

$$\frac{L_{\text{reb}}}{p} = -a_1^c + \frac{I_2^g\ddot{\eta}}{p} + \dot{\omega}_2^c\left(\frac{I_2^g}{p} - \ell\right) + \left(\frac{I_1^g - I_3^g}{p} - \ell\right)\omega_1^c\omega_3^c + \frac{C}{p}\dot{\eta} + \frac{K}{p}\eta + a_3^{c'}. \quad (3.106)$$

We now choose the origin point of the c-frame such that

$$\ell = \frac{I_2^g}{p}, \quad (3.107)$$

thus eliminating the error due to the output axis rotation,  $\dot{\omega}_2^c$ . Then (3.106) becomes

$$\frac{L_{\text{reb}}}{p} = -a_1^c + \frac{I_2^g\ddot{\eta}}{p} + \left(\frac{I_1^g - I_2^g - I_3^g}{p}\right)\omega_1^c\omega_3^c + \frac{C}{p}\dot{\eta} + \left(\frac{K}{p} + a_3^{c'}\right)\eta, \quad (3.108)$$

which is the dynamics equation for the pendulous, force-rebalance accelerometer in final form. The last term is known as the *vibropendulous error* which cross-couples the pendulous axis acceleration,  $a_3^{c'}$ , into the input and can be a serious source of bias if  $a_3^{c'}$  and  $\eta$  oscillate in phase.

The torque  $L_{\text{reb}}$  is applied to the output axis so that the deflection angle,  $\eta$ , is adjusted back to null ( $\eta = 0$ ). The indicated specific force is given by the measured electric current needed to apply this restoring torque. In the steady state ( $\dot{\eta} = 0$ ) and neglecting the anisoinertia error (which can be calibrated), we have with  $\eta \approx 0$ :

$$a_1^c = -\frac{1}{p}L_{\text{reb}}, \quad (3.109)$$

where, by definition,  $L_{\text{reb}}$  is the component of applied torque along the output axis (note, as for the gyro,  $L_{\text{reb}} < 0$  implies  $a_1^c > 0$ ). The rotational dynamics equations of the pendulous accelerometer (3.108) is similar to the translational dynamics equation of the spring accelerometer (3.91). However, in the usual design of the force-rebalance accelerometer, forces are applied directly to the proof mass, rather than in the form of a torque on the hinge.

### 3.3.3 Pendulous Accelerometer Examples

The design of the rebalanced pendulum principle is manifested in today's hinged pendulous accelerometer; the dynamics are identical to the rotational system above. A schematic of the hinged pendulum accelerometer, exemplified by the A-4 accelerometer found in Litton's RLG inertial navigators, is shown in Figure 3.16. An

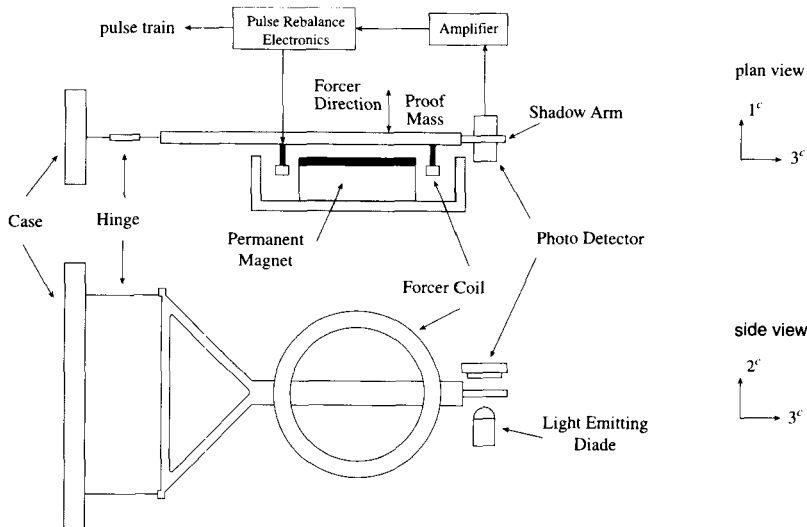


Figure 3.16: Schematic of hinged pendulous force rebalance accelerometer.

electrical current from an optical pickoff is generated when the hinged proof mass responds to an acceleration along the input axis. Torquing pulses obtained from this signal through the electronics module are used to restrain the proof mass in its null position and also provide a pulse train whose rate is a direct measure of the change in velocity (or of acceleration).

Similar configurations are used in the Bell Aerospace Model VII accelerometer, shown in Figure 3.17, and the QA2000 (also the QA3000) by Allied Signal (Sundstrand) in Figures 3.18a and 3.18b, which is used in Honeywell's RLG inertial navigator. The pendulum design (among many others) can now also be used in the manufacture of solid state accelerometers that are micro-machined from a silicon wafer. The entire assembly including proof mass, hinges, and support structure is etched out of a single crystal of silicon using methods employed by integrated circuit manufacturers. These methods are also amenable to batch fabrication, where hundreds of accelerometers can be etched onto a single silicon wafer. The micro-machined accelerometers are not as accurate as their "macro-cousins", but they are very inexpensive, particularly in terms of obtaining sets of sensors having matched performance characteristics.

Another type of pendulous accelerometer is the pendulous integrating gyro accelerometer (PIGA) which includes a gyroscopic element whose spin axis is along the axis that has the mass imbalance (Figure 3.19). The support of the sensor assembly to the case is now provided by the trunnion along the input axis. An acceleration along the input axis produces a deflection of the spin axis,  $3^g$ , causing a torque to be applied about the 2-axis (output axis); and this is equivalent to a rotational rate

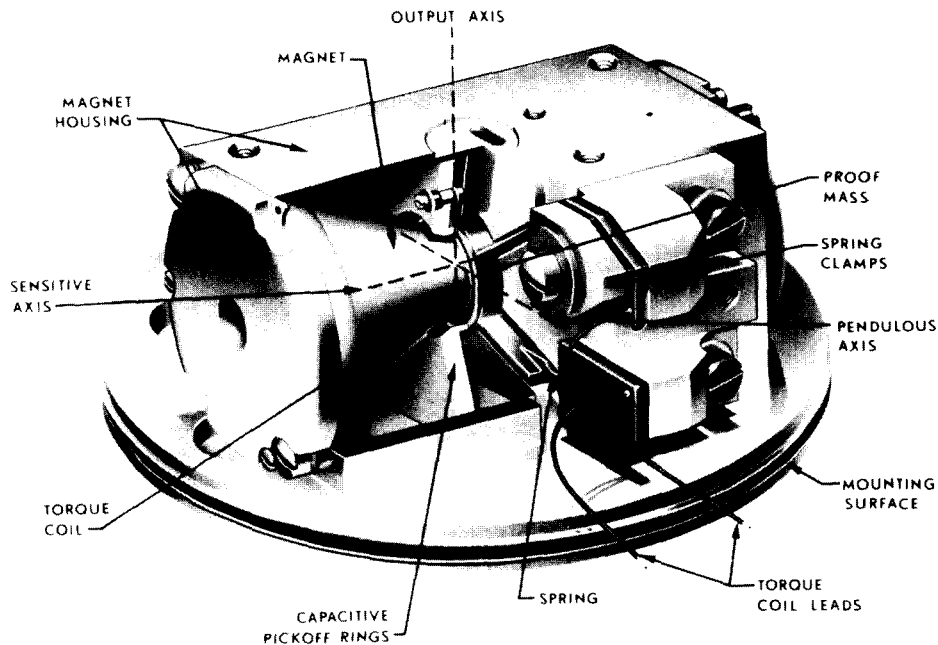


Figure 3.17: Bell Aerospace model VII force-rebalance accelerometer.

about the input axis according to (3.28):

$$L_2^g = -H_s \omega_1^c, \quad (3.110)$$

where  $H_s = I_s \omega_s$ . In this case, also, the relationship between the applied torque and the specific force is given by (3.109). Therefore,

$$pa_1^c = H_s \omega_1^c. \quad (3.111)$$

The angular rate  $\omega_1^c$  is the rate of the trunnion with respect to the case, say  $\dot{\eta}$ , plus the rate of the case with respect to the inertial frame. The latter is practically zero if the case is on a stabilized platform, in which case  $\omega_1^c \approx \dot{\eta}$ , and we can integrate (3.111) to obtain:

$$\Delta\eta = \frac{p}{H_s} \int a_1^c dt = \frac{p}{H_s} \Delta v, \quad (3.112)$$

where  $\Delta v$  is the integral of the specific force, i.e. velocity. The servo motor rotates the gimbal to create a torque on the gyro element thus balancing the pendulous torque. The PIGA is less suitable for strapdown applications where the case angular rate has to be accounted for in the calculation of the acceleration.

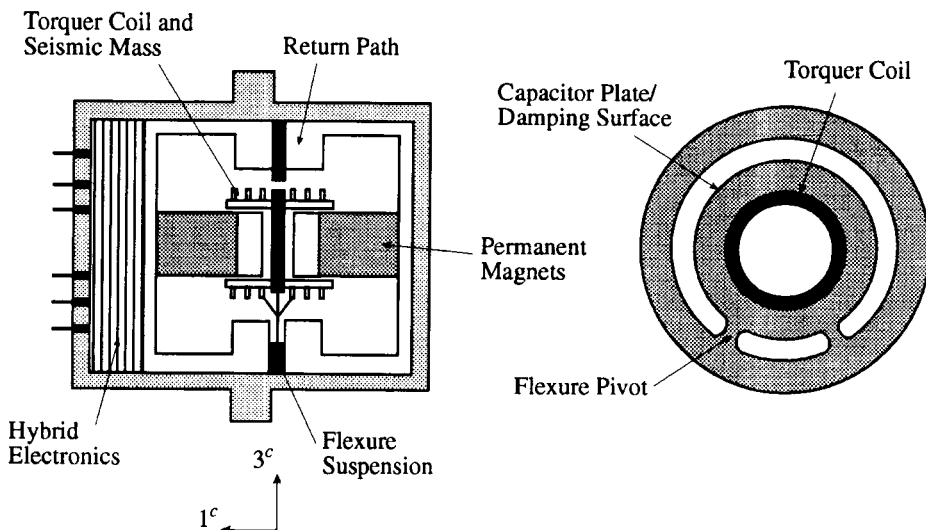


Figure 3.18a: Pendulous force rebalance accelerometer based on quartz-flexure suspension.

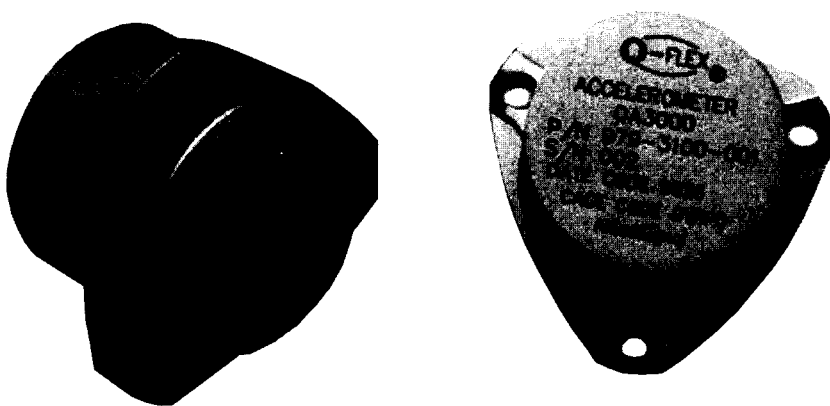


Figure 3.18b: Allied Signal (Sundstrand) QA3000 accelerometer.

### 3.3.4 Vibrating Element Dynamics

The sensing principle of the resonant accelerometer, or *vibrating-beam* accelerometer, is based on the dependence of the resonant frequency of a vibrating element, such as a wire or tape or bar, on the tensile force applied to it. Using a string for illustrative purposes (like that of a violin; see also Figure 3.20), there is the following relationship that holds for small-amplitude waves:

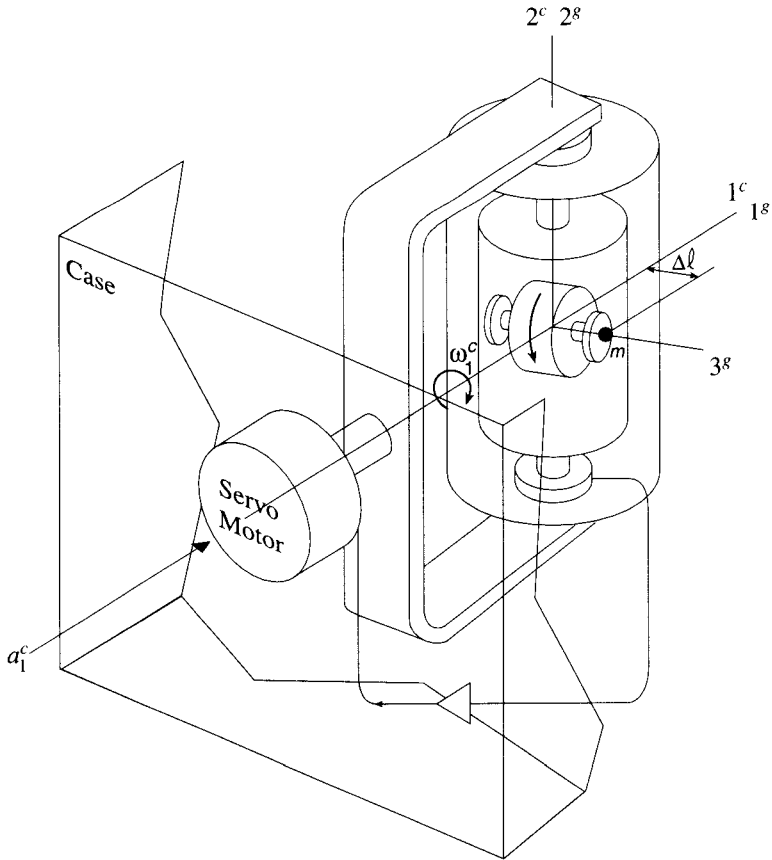


Figure 3.19: Schematic of the pendulous integrating gyro accelerometer.

$$v = \sqrt{\frac{F}{\mu}}, \quad (3.113)$$

which is another way of stating that the longitudinal force or tension,  $F$ , on a vibrating string equals the product of the square of the velocity,  $v$ , of a transverse wave in the string and the string's mass per unit length,  $\mu$ . This can be derived by applying Newton's laws to the motion of the string as described by the classical differential equation for waves (see any book on elementary physics, such as (Shortley and Williams, 1971)). The relationship between the velocity and frequency,  $f$ , of the wave is easily obtained from the fact that one cycle of the wave per unit time corresponds to its velocity divided by its wavelength,  $\lambda$ ; thus

$$f = \frac{v}{\lambda}. \quad (3.114)$$

Combining (3.113) and (3.114) and using  $F = ma$ , from (1.4), where  $a$  is an applied

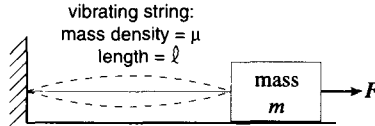


Figure 3.20: Vibrating string.

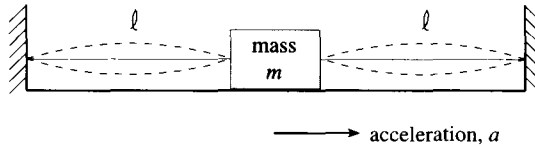


Figure 3.21: Vibrating string accelerometer.

acceleration in the direction of  $F$  and  $m$  is the mass of the proof mass, we obtain

$$f = \frac{1}{2\ell} \sqrt{\frac{ma}{\mu}}, \quad (3.115)$$

where, for a standing wave, such as in Figure 3.20, we have  $\ell = \lambda/2$ . A change in tension in the string, or equivalently a change in applied acceleration, produces a change in frequency (like tuning a string on a violin).

To measure changes in frequency, one constructs a differential device as shown in Figure 3.21. The added benefits of two strings or beams in tension include the cancellation of many mechanical and temperature-induced errors common to both halves of the configuration, and the doubling of the scale factor. With an applied acceleration, as indicated, the proof mass stretches the left string, changing its tension to  $F_1 = F_0 + ma$ , and relaxes the right string, changing its tension to  $F_2 = F_0 - ma$ , where  $F_0$  is the initial tension on both strings. Corresponding frequencies change to  $f_1$  and  $f_2$ ; and, assuming that the two strings have the same mass density and that their lengths do not change appreciably, we apply (3.115) to each half and get

$$\begin{aligned} \mu(2\ell f_1)^2 &= F_0 + ma, \\ \mu(2\ell f_2)^2 &= F_0 - ma. \end{aligned} \quad (3.116)$$

Solving for the acceleration by eliminating  $F_0$  yields

$$a \approx \frac{4m_s \ell f_0}{m} \Delta f, \quad (3.117)$$

where  $f_0$  is a nominal frequency and  $m_s = \mu\ell$  is the total mass of each string. The measured output is inherently digital, similar to the RLG (Section 3.2.2.1), thus requiring no additional A/D conversion electronics. Also, unlike the force-rebalance accelerometer, the operation is in the open-loop mode. This means that the scale

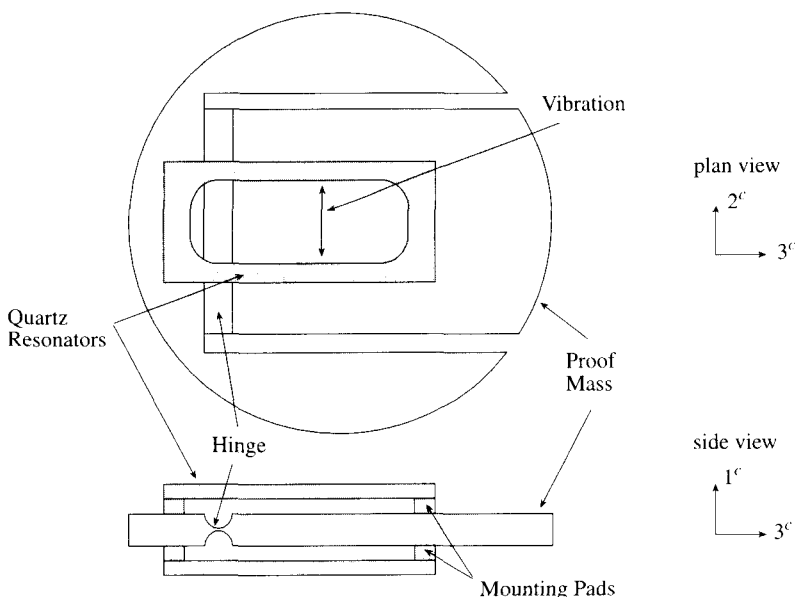


Figure 3.22: Schematic of quartz resonator vibrating beam accelerometer (Accelerex design, Allied Signal, after Lawrence, 1998)

factor,  $4m_s\ell f_0/m$ , shown in (3.117), must be very stable; and principal errors result from changes in the mechanical properties of the structural components.

Instead of strings, practical resonant accelerometers use crystalline quartz which is thermally and mechanically much more stable, and the sliding proof mass is replaced with a hinged pendulum, as shown schematically in Figure 3.22. The quartz resonators are attached to both the instrument frame and the pendulum, and the latter, in turn, applies tension or compression to the vibrating crystals in response to applied accelerations. The entire sensor (resonators, pendulum, and support structures) is also being constructed as a micro-machined device from a single quartz crystal, yielding high thermal stability and reliability, as well as low cost.

### 3.3.5 Error Sources

The errors affecting the accelerometer measurement are analogous to those for the mechanical gyro. The general model includes a bias term consisting of a constant, a dependence on temperature changes, and thermally induced hysteresis; and anisotropic effects due to unequal compliance in the pivots of the pendulum and depending on the accelerations along the input and pendulum axes, as well as other cross-coupling terms, such as the vibropendulous error. Also included is a scale factor error that consists of a constant, as well as linear and quadratic dependencies on the input acceleration. This scale factor error occurs in the torque rebalance

electronics. In addition, the reference axes of the pendulum assembly may not coincide with the axes of the case and this introduces misalignments that couple accelerations along all three axes into the input axis. The latter, in particular, and other error terms can be included in the dynamics model (3.108) for calibration purposes in the laboratory (Chatfield, 1997). A model for the remaining uncompensated error has the form:

$$\delta a = \delta a_b + \kappa a_1 + v_a, \quad (3.118)$$

where  $\delta a_b$  is the bias,  $\kappa$  is the scale factor error (higher-order terms can be neglected in dynamically benign environments), and  $v_a$  is the random (white) noise of the accelerometer. The bias may be decomposed analogous to (3.42) into the following:

$$\delta a_b = \delta a_0 + c_2 a_2 + c_3 a_3 + c_T \delta T, \quad (3.119)$$

with terms of higher order, depending on products of acceleration, added if necessary. As an example, Kayton and Fried (1997) give the following values for the uncompensated errors:

$$\begin{aligned} \delta a_0 &= 25 \times 10^{-5} \text{ m/s}^2 \\ c_T &= 0.5 \times 10^{-5} \text{ m/s}^2/\text{°C} \\ c_2, c_3 &= 25 \times 10^{-6} \text{ rad} \\ \kappa &= 50 \times 10^{-6}. \end{aligned} \quad (3.120)$$

## 4 Inertial Navigation System

### 4.1 Introduction

Although an individual inertial measurement unit (IMU), by itself, could provide useful information about the platform on which it is mounted (its acceleration, rotational rate, or orientation), only the concerted signals from a collection of suitably arranged, or *mechanized*, inertial measurement units provide the necessary data to perform inertial navigation. In general, an *inertial navigation system* (INS) comprises a set of IMU's, both accelerometers and gyros, the platform on which they are mounted, including the stabilization mechanism if so provided, and the computer that performs the calculations needed to transform sensed accelerations and, in some mechanizations, angles or angular rates into navigationally useful information: position, velocity, and attitude. Figure 4.1 schematically shows the components of an INS in the strapdown mechanization. The inertial sensor assembly for Honeywell's H-423 strapdown INS is shown in Figure 4.2 where the three gyros (RLG's) and three accelerometers (figuratively) occupy the six faces of a right rectangular prism; the INS, itself, is shown in Figure 4.3. Finally, for gimbaled mechanizations, the hardware becomes more complicated as seen in Figure 4.4 (Section 4.2).

The development of inertial navigation systems has its origins at the beginning of the twentieth century when gyroscope-based compasses were invented in Germany and used in ship navigation. Early concepts or analogues of navigation systems were developed before and during World War II principally by J. Gievers in Germany for marine and land use (Stieler and Winter, 1982). Aircraft navigation did not benefit until after the War when systems for high speed vehicles were designed, particularly by Charles Draper at the Massachusetts Institute of Technology. As accuracies in gyros steadily improved and digital electronic computers arrived, their application quickly spread to commercial and military aviation in the 1960's and 1970's, including missile guidance, and also space navigation, notably the famed manned lunar flights. Also marine navigation (*SINS*, ship's inertial navigation system) continued to utilize these systems, especially submarine navigation that still today relies significantly on inertial navigation. Aside from aircraft inertial navigation systems (*AINS*), aviation has a long history in radio navigation aids (Loran, Omega, Doppler systems, VHF Omni-directional range (VOR), among others; see (Beck, 1971; Kayton and Fried, 1969, 1997)). Both INS and terrestrial radio navigation, today, are overshadowed by the satellite navigation system: the Global Positioning System (GPS). However, INS continues to play an important role in submarine navigation, aiding satellite and radio navigation and precision aircraft landing, and autonomous (jam-proof) military navigation and guidance.

In Chapter 3 we saw that gyro errors are basically drift errors (they do not average away with time); and therefore, INS errors generally accumulate, as discussed more

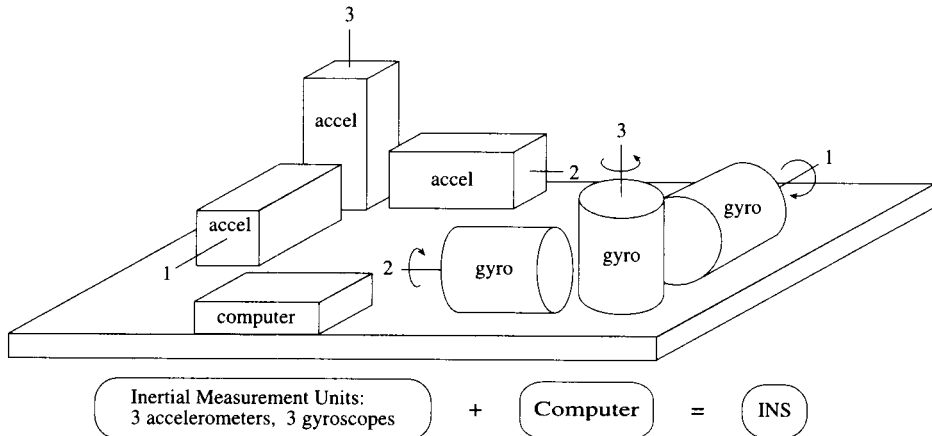


*Figure 4.1:* Basic inertial navigation system comprising IMU's and a navigation computer.

throughly in Chapter 5. The accuracy of an INS may be categorized as low, medium, and high in terms of the error (indicated minus actual position) per unit time. Thus, a low-accuracy system deviates by (for some, substantially) more than 1–2 nautical miles (nmi) per hour ( $>2\text{--}4 \text{ km/hr}$ ); a medium-accuracy, or navigation-grade system may be characterized as performing at 0.5–2 nmi/hr (1–4 km/hr); and a high-accuracy system typically is rated at 0.1–0.2 nmi/hr (0.2–0.4 km/hr), or

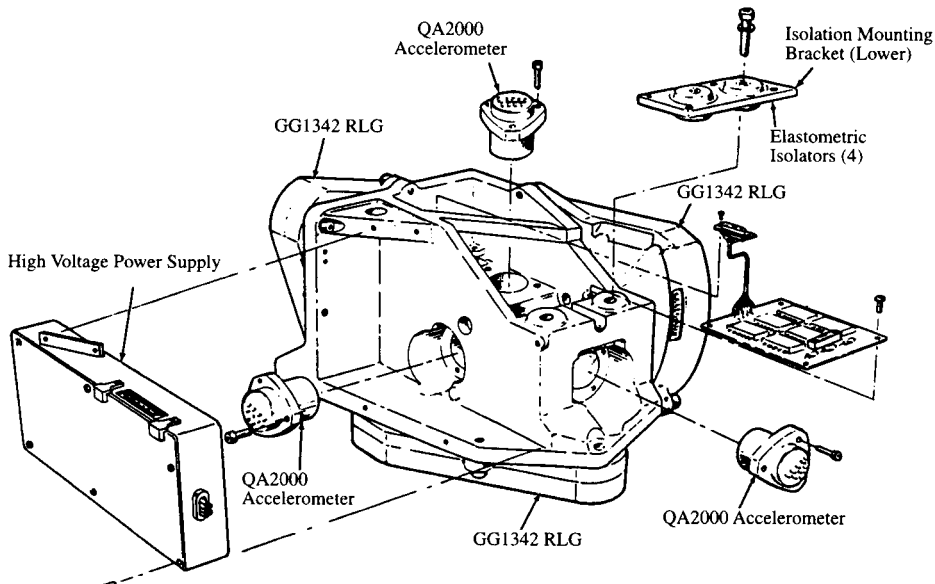


*Figure 4.2:* Inertial sensor assembly for the Honeywell H-423 INS (courtesy Honeywell, Inc.)

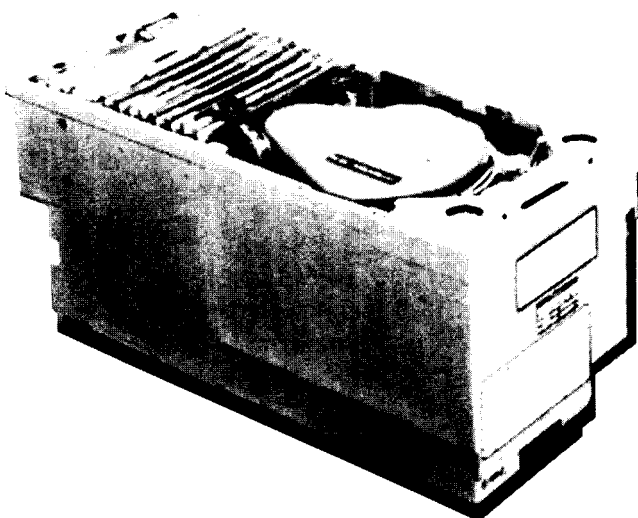


Figure 4.3: H-423 showing inertial sensor assembly and supporting sensor and navigation processor electronics.

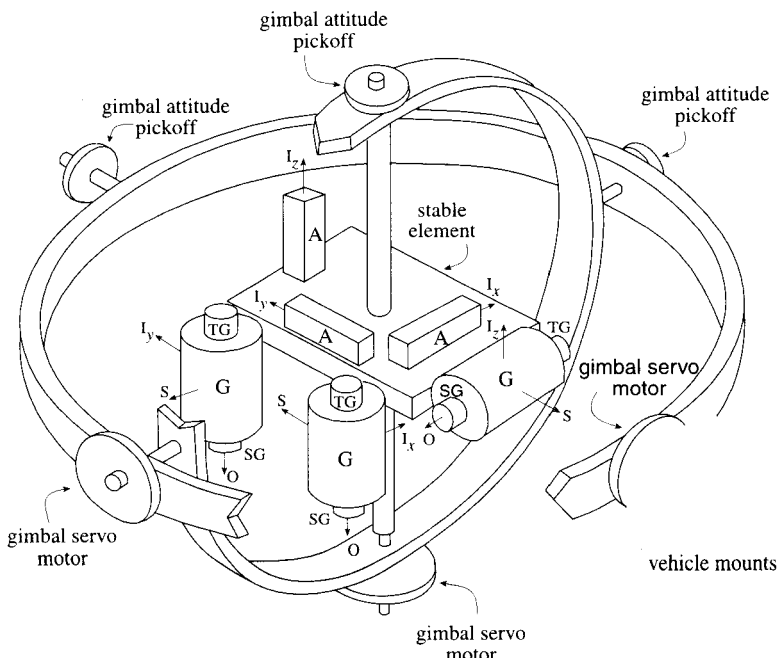


Figure 4.4: Schematic of three-gimbal stabilized platform ( $G = SDF$  gyro,  $A =$  accelerometer).

better. These specifications are only general performance indicators, are not linear, and should not be used for statistical analyses.

We distinguish between inertial navigation systems and *attitude and heading reference systems* (AHRS). The latter are used only to provide a vertical reference (attitude) and a reference to north (heading) for flight control, to orient platforms, mostly for flight test and other military applications, and as aid in Doppler radar navigation systems. AHRS often employ gyros of lower than navigation quality, usually on stabilized platforms also of lower grade. Three-dimensional orientation (attitude and heading) is, likewise, provided by an INS, but at higher cost and usually greater accuracy. AHRS belong in a larger class of attitude and heading reference systems and will not be discussed further here (see, e.g., Kayton and Fried, 1997).

There is also a conceptual difference between an inertial navigation system and an inertial guidance system, although an INS is used to perform either function. Navigation is the real-time determination of the current position and velocity of a vehicle; whereas, guidance refers to the determination and implementation of the procedures needed to take the vehicle from its current state to a pre-specified state, where the state encompasses both position and velocity. A discussion of guidance system is also left to other texts (e.g., Leondes, 1963).

## 4.2 Mechanizations

In one sense, the *mechanization* of the inertial navigation system describes the physical arrangement of the inertial sensors relative to the vehicle and to the inertial, navigation, and/or body coordinate frames. However, the choice of mechanization is not merely a matter of design convenience; rather it is intimately concerned with the error propagation of the sensors and how this affects the intended application. Different mechanizations offer a variety of modes of isolating the system from vehicle motion, as well as optimal tuning to particular frames of navigation. Isolation systems may represent a large part of the cost of an INS. Also, as noted in Chapter 3, the character of the sensor errors of mechanical systems depends to a certain extent on the acceleration environment of the instrument, and therefore, on their orientation with respect to one of the more dominant accelerations, the gravity vector, in addition to other larger linear and angular acceleration directions of the vehicle.

The mechanization of an INS may also refer to the frame in which the navigation equations are solved, regardless of the physical construction of the system. In this sense, a particular mechanization reflects the complexity of the solution to these equations, as well as the suitability of the coordinate frame to the application.

There are two general types of mechanization: the *stabilized platform* and the *strapdown* configuration. Stabilized platforms provide angular motion isolation from the vehicle; while strapdown systems are just what the name implies: the platform holding the IMU's is attached firmly to the vehicle. In the stabilized

system, the platform consists of a *stable element* that is connected to the vehicle through a set of gimbals, each allowing rotation about a particular axis (Figure 4.4). To a large extent, the isolation could be achieved by the gimbals themselves and the inertia of the stable element (like a hammock in a ship on gently rolling waves), but the bearings are not absolutely frictionless and the stabilization is better controlled by purposely creating appropriate rotations about the gimbal axes using servo motors.

The amount of rotation needed to isolate the platform from the vehicle motion is obtained from the output of the gyros mounted on the stable element. Usually, the gyros are of the integrating-rate type whose output consists of small angles. That is, the case of the gyro rotates as the vehicle rotates and causes an output in the form of an indicated gimbal angle, e.g., according to (3.36). The value of this angle is measured as a voltage using an electrical pickoff device and generates a current that drives the servo motor of the platform gimbal so as to null the gimbal angle of the gyro. With this feedback arrangement, the accelerometers and gyros, mounted on the stable element of the platform, are isolated from the rotational dynamics of the vehicle. This not only protects complex instruments like the mechanical gyro from physical failure, but also leads to better performance than in a strapdown system. Furthermore, the stabilized platform conveniently yields attitude and heading values at the gimbals for monitoring the rotational dynamics of the vehicle, as needed in flight control.

In the strapdown mode, the accelerometers and gyros are physically bolted to the vehicle (possibly, with some shock/vibration isolation mounts), where all instruments are contained within a single box. Consequently, these sensors are subjected to the entire range of dynamics of the vehicle, which degrades their performance. For example, mechanical gyro errors depend in part on torques generated by angular accelerations and cross-coupling terms involving angular rates; see equation (3.26). Also, accelerometers are subject to lever-arm effects due to vehicle rotations and expressed analogously as in Section 3.3. These dynamics-induced errors are partly compensable based on laboratory calibrations.

In addition, certain modeling errors in the computed navigation solution are caused by numerically integrating the accelerations and angular rates in the body frame of the rotating vehicle. At each discrete step of the numerical integration, the frame is assumed to be non-rotating, when in fact it is rotating, resulting in *coning errors* for the gyroscope and *sculling errors* for the accelerometers. These will be treated analytically in more detail in Section 4.2.3.1.

With the strapdown mechanization, the particular attitude of the physical mounting of the INS is somewhat arbitrary because, as opposed to the stabilized mechanization, the transformation of the accelerometer and gyro data from the body frame to the navigation frame is done computationally. Nevertheless, in benign environments one strives also to position and orient the box so as to minimize sensor errors. The main advantage of strapdown systems is smaller size, weight, and power consumption, and lower cost (there are no mechanically complex set of gimbals as in the stabilized system). Though the highest accuracy of a strapdown system is worse

than that of the best stabilized system, the recent technological developments in optical gyroscopes have brought the strapdown system close to par with its gimbaled cousin. With virtually no moving parts, the strapdown system based on optical gyros is also far superior in maintenance and in the mean time between failures. Being also much less expensive, the latter has the greater potential for future geodetic application and, therefore, is also the focus in subsequent sections on data processing.

#### 4.2.1 Space-Stabilized Mechanization

By rotating the stabilized platform relative to the vehicle in order to null the gyro gimbal angles, the spin axis of the gyro rotor, and consequently the platform itself, remains fixed in orientation with respect to inertial space. Hence, this type of stabilization is called *space stabilization*, or also *inertial* stabilization; the system is said to be space-stabilized.

The accelerometers and gyros on a space-stabilized platform ideally are completely isolated from the rotational dynamics of the system and, therefore, tend to have better performance than in the case of strapdown systems. The rotation-induced errors associated with the mechanical gyros are essentially eliminated as are the lever-arm effects of accelerometers. On the other hand, the sensors' orientation with respect to the gravity vector changes in time due to the motion of the vehicle and Earth's rotation, and this can lead to variations in scale factor errors in the accelerations and in drift errors in the orientation angles. This problem is eliminated with the local-level stabilization discussed in the next section.

#### 4.2.2 Local-Level Mechanization

For vehicles navigating primarily in the horizontal directions, near the Earth's surface (land vehicles, ships, aircraft), the most prevalent stabilization is that which keeps the platform tangent to the local horizon; this is called *local-level stabilization* and requires knowing where the plane of the horizon (or vertical direction) is. The object of the local-level mechanization is to maintain a frame for the accelerometers in which their output can be integrated directly to yield (after correcting for Coriolis and gravity effects) position and velocity in local coordinates. That is, the input axes of two accelerometers are situated orthogonally in the horizontal plane, and optionally, a third one is aligned with the local vertical. As will be seen in Chapter 5 on system error dynamics, this type of mechanization is particularly advantageous for navigation since it specializes the navigation problem to the two directions (the horizontal directions) in which unaided inertial navigation is at all possible over longer periods of time. It will be shown that inertial navigation errors in the vertical direction quickly become unbounded in the presence of system errors and without external positioning aids.

In order to sense only the horizontal acceleration (to be integrated into horizontal velocity and position), the platform carrying the accelerometers should be always parallel to the local horizon. Since a gyro, if left undisturbed, maintains a fixed

orientation in inertial space, it will not provide the needed frame of reference for the accelerometers. However, if torqued at an appropriate rate, corresponding to the motion of the vehicle relative to the Earth and the rotation of the Earth relative to inertial space, the gyros on the platform can be commanded to maintain a reference associated always with the horizon.

Moreover, it may be desirable to place the horizontal accelerometers directly in the  $n$ -frame, where the input axis of one accelerometer is always pointing northward, and the other eastward. The north direction is established during the initialization phase of inertial navigation, while the vehicle is stationary (fixed to the Earth), by leveling the platform (such that horizontal accelerometers sense no acceleration) and slewing the platform about the vertical until the gyro with east-pointing input axis senses no rotation. This is called *gyrocompassing* and will be described in more detail in Chapter 8. Ideally the platform remains aligned with the  $n$ -frame under the commands issued to the gyros based on the computed motion of the vehicle and known rotation of the Earth. In this case we have the *north-slaved*, local-level mechanization, distinguished from the *wander-azimuth*, local-level mechanization, in which the horizontal accelerometers do not remain fixed in azimuth (see Section 4.2.2.2).

#### 4.2.2.1 Schuler Tuning

The concept of local-level stabilization is illustrated with the idealization depicted in Figure 4.5. It is known as *Schuler tuning*; that is, tuning or adjusting the platform so that it remains level. It is based on Schuler's (1923) assertion that if a device (such as a pendulum) has a natural period of about 84 minutes, then accelerations of the device on the Earth's surface (sphere) will not cause it to oscillate. This principle lies behind the boundedness of accumulated errors in (horizontal) inertial navigation. To simplify the discussion, consider just one (the northward) horizontal dimension, and suppose the accelerometer is mounted on a stabilized platform with its sensitive axis parallel to the plane of the platform. The vehicle is travelling on the Earth, and the (northward) horizontal acceleration is  $\ddot{x}$ . As it travels, the platform, if initially level, will come out of level and attempt to maintain a fixed direction in inertial space as dictated by the gyro signals that drive the servo motor on the platform gimbal. The corresponding angular acceleration of the vehicle in the  $i$ -frame is

$$\ddot{\eta} = \frac{\ddot{x}}{R}, \quad (4.1)$$

where  $\eta$  is the tilt angle by which the platform is out of level, and  $R$  is the mean radius of the Earth. Therefore, in order to return the platform to level alignment, the platform must be slewed by the angle  $-\eta$ . This is accomplished by appropriately torquing the reference direction maintained by the gyro. The amount of torquing is proportional to the angular rate:

$$-\dot{\eta} = \frac{\dot{x}}{R}, \quad (4.2)$$

where  $\dot{x}$  is the velocity obtained by integrating the acceleration of the platform in the horizontal direction.

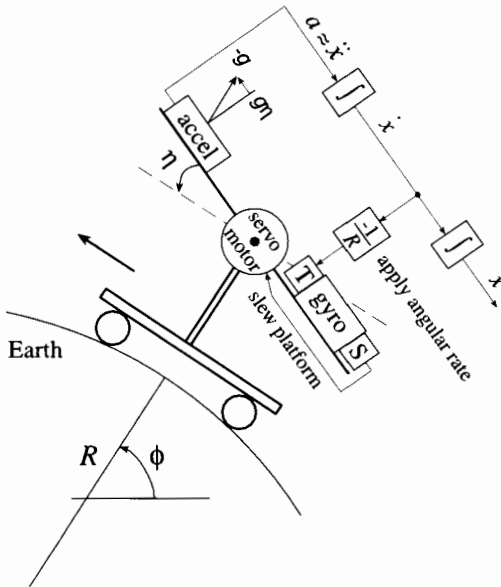


Figure 4.5: The concept of Schuler tuning.

During an increment of time,  $\Delta t$ , the vehicle moves a distance  $\Delta x = \eta R$  in inertial space due to self-propelled motion (and, in general, also due to Earth's rotation). If initially aligned in the horizontal, after a time  $\Delta t$ , the accelerometer senses both the acceleration,  $\ddot{x}$ , and the *reaction* (positive, in Figure 4.5) of the gravity component due to the misalignment,  $\eta$ , as a result of the motion on a sphere (see (1.7) and Figure 4.3):

$$a = \ddot{x} + g\eta, \quad (4.3)$$

where  $a$  is the sensed acceleration and  $g$  is the magnitude of gravity. Substituting  $\ddot{x}$  given by (4.1) into (4.3), we find the differential equation that describes the dynamics of the platform tilt angle:

$$\ddot{\eta} + \frac{g}{R}\eta = \frac{a}{R}, \quad (4.4)$$

under the assumption that  $\eta$  is small, so that (4.3) approximately holds, i.e.,  $\ddot{x}$  is the horizontal acceleration of the vehicle.

From the example in Section 2.3.1.1, we know that equation (4.4) represents a harmonic oscillator, equation (2.49), with resonant frequency given by

$$\omega_S = \sqrt{\frac{g}{R}}. \quad (4.5)$$

$\omega_S$  is known as the *Schuler* frequency. Commanding the platform to follow the local horizon by torquing the gyros endows the system with a natural (resonant)

oscillation that has amplitude, say  $\eta_0$ , being the initial tilt (error) of the platform, and a period equal to the *Schuler period*:

$$\frac{2\pi}{\omega_S} \approx 84.4 \text{ minutes.} \quad (4.6)$$

Ideally,  $\eta_0 = 0$ , but there are always initial errors due to misalignments (see Chapter 8), and subsequent errors in the commanded torques.

If  $\eta$  represents the tilt error of the platform, then this could be interpreted as a corresponding position error given by  $R\eta$ , and we already see, since  $R$  is essentially a constant, that the horizontal position error satisfies the same harmonic oscillator equation. The differential equation for the position error will be rederived in Chapter 5 from first principles independent of the mechanization. It will be shown, in agreement with this simplified argument, that the error, due to a constant forcing error term, such as an accelerometer bias, oscillates at the Schuler frequency and is bounded. This contrasts with the vertical position error that does not enjoy this bounding property.

Thus, it is worth noting that *horizontal* inertial navigation would be impossible for longer periods if the Earth were flat. If the level (horizontal) surface did not have curvature in inertial space, instrument biases would quickly overwhelm the navigation solution with unacceptable errors. For example, accelerometer biases would simply integrate into position error with the square of time. Similarly, since the gyros' primary function is to ensure the proper alignment of the accelerometers along the appropriate coordinate axes, indicated accelerations contain errors due to platform misalignment caused by gyro errors. Therefore, a drift error in the gyro-indicated *rate* implies an acceleration error *rate*. This, in turn, gets integrated into a position error that grows with the cube of time (see also Chapter 5). The Earth's spherical shape bounds or at least reduces the growth rate of the errors, thus making horizontal inertial navigation feasible over longer periods.

The commanded angular rate of the local-level stabilized platform should be such that its angular rate (generally, in all three dimensions) with respect to the navigation frame is zero:  $\omega_{np}^p = 0$ ; the subscript  $p$  refers to the platform frame. (We tacitly ignore all differences between the platform frame and the instrument frame as defined in Chapter 1.)

For any local-level stabilized platform, we may write the angular rate of the platform with respect to the  $i$ -frame as

$$\omega_{ip}^p = \omega_{in}^p + \omega_{np}^p, \quad (4.7)$$

being the sum of the relative rates between the  $n$ - and  $i$ -frames and between the  $p$ - and  $n$ -frames. It is also given by

$$\omega_{ip}^p = \omega_{com} + \delta\omega_d, \quad (4.8)$$

where  $\omega_{com}$  is the rate commanded by the platform gimbal servo motor, as a result of the change in reference direction effected by the gyro torque generator; therefore, it is also the rate corresponding to the torque applied to the gyro.  $\delta\omega_d$  comprises the

drift errors of the gyros as similarly transmitted to the servo motors. Without commanded gyro torques and gyro errors, the platform would be space-stabilized, i.e.,  $\omega_{ip}^p = 0$ . Since the drift can be partly compensated based on the dynamics model of the gyro (e.g., (3.26)), even mechanical gyros (that can be torqued) on a space stabilized platform are commanded by  $\omega_{com} = -\delta\omega_d$  to balance the known systematic errors.

If, in addition to being local-level stabilized, the platform is north-slaved (its l-axis is commanded to point north), then the platform frame is always parallel to the n-frame; and we have  $\omega_{in}^p = \omega_{in}^n$  and  $\omega_{np}^p = 0$ . Putting these into the right side of (4.7) and equating to (4.8), we see that the commanded rate is given by

$$\omega_{com} = \omega_{in}^n - \delta\omega_d. \quad (4.9)$$

With (1.89), it is also expressed in terms of geodetic angular rates as:

$$\omega_{com} = ((\dot{\lambda} + \omega_e) \cos \phi \ - \dot{\phi} \ - (\dot{\lambda} + \omega_e) \sin \phi)^T \ - \delta\omega_d, \quad (4.10)$$

where  $\dot{\phi}$  and  $\dot{\lambda}$  are the rates in latitude and longitude of the platform, and are related to north and east velocities that are obtained by integrating the accelerometer signals (see Section 4.3);  $\omega_e$  is Earth's spin rate.

#### 4.2.2.2 Wander Azimuth Mechanization

There are situations where the n-frame is not the most suitable local-level frame in which to integrate the accelerations. Consider the case of navigating near the polar areas. Due to the convergence of the meridians, the longitude rate is given approximately by  $\dot{\lambda} = v_E / (R \cos \phi)$ , where  $v_E$  is east velocity (see also (4.103)). Substituting this into (4.10), we see that the third component of the commanded angular rate includes the term  $v_E \tan \phi / R$ . The dependence on  $\tan \phi$  causes the commanded rate to become infinite at the poles. A solution to this problem is to slew the platform about the vertical by a rate different from the vehicle's longitudinal velocity. This has the effect of letting the platform "wander in azimuth"; it will not maintain a north-pointing orientation.

We define a new frame, the wander-azimuth frame, or w-frame, that is related to the n-frame by a rotation in azimuth (Figure 4.6):

$$C_n^w = \begin{pmatrix} \cos \alpha & \sin \alpha & 0 \\ -\sin \alpha & \cos \alpha & 0 \\ 0 & 0 & 1 \end{pmatrix}. \quad (4.11)$$

The wander angle,  $\alpha$ , is the (positive) angle from the l-axis of the n-frame to the l-axis to the w-frame. In our case, it is the azimuth of the w-frame's l-axis. (In those conventions where the navigation frame is not NED, the wander angle may not be the positive azimuth, e.g., if the n-frame is north-west-up, the wander angle is defined westward from north.) Also, the corresponding angular rate vector is given by

$$\omega_{nw}^n = \omega_{nw}^w = (0 \ 0 \ \dot{\alpha})^T. \quad (4.12)$$

The commanded angular rate should now ensure that the platform is aligned with

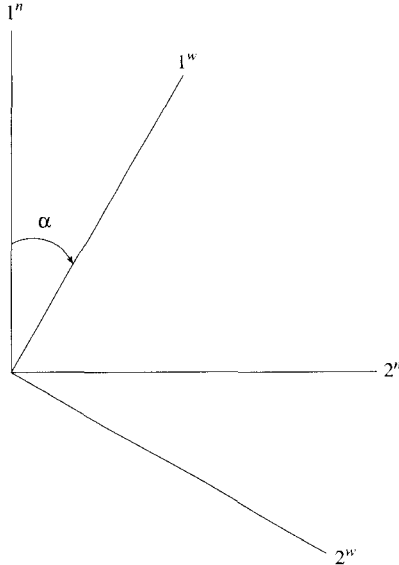


Figure 4.6: Wander azimuth frame.

the wander frame:  $\omega_{wp}^p = 0$ . And, analogous to (4.8), we now have  $\omega_{bw}^w = \omega_{com} + \delta\omega_d$ . Therefore, with  $\omega_{bw}^w = \omega_{in}^w + \omega_{nw}^w$  and (4.12), the commanded rate is

$$\begin{aligned}\omega_{com} &= C_n^w \omega_{in}^w + \omega_{nw}^w - \delta\omega_d \\ &= \begin{pmatrix} (\dot{\lambda} + \omega_e) \cos \phi \cos \alpha - \dot{\phi} \sin \alpha \\ -(\dot{\lambda} + \omega_e) \cos \phi \sin \alpha - \dot{\phi} \cos \alpha \\ -(\dot{\lambda} + \omega_e) \sin \phi + \dot{\alpha} \end{pmatrix} - \delta\omega_d.\end{aligned}\quad (4.13)$$

One option to avoid the singularity at the poles is to command the platform not at all about the vertical:

$$\omega_{com} = \begin{pmatrix} (\dot{\lambda} + \omega_e) \cos \phi \cos \alpha - \dot{\phi} \sin \alpha \\ -(\dot{\lambda} + \omega_e) \cos \phi \sin \alpha - \dot{\phi} \cos \alpha \\ 0 \end{pmatrix} - \delta\omega_d.\quad (4.14)$$

Disregarding the drift correction, this implies from (4.13) that

$$\dot{\alpha} = (\dot{\lambda} + \omega_e) \sin \phi,\quad (4.15)$$

which may be integrated to obtain the wander azimuth of the platform with respect to the  $n$ -frame that is also needed in the first two components of the commanded rate.

### 4.2.3 Strapdown Mechanization

In the strapdown configuration, the accelerometer output, indicating the inertial acceleration of the vehicle, is coordinatized in the frame of the vehicle (body frame). Though they are important in actual operations, we will ignore the lever-arm effects given by (3.100) and any transformations between the reference frame of each accelerometer and the platform or instrument frames. It is convenient for an understanding of the strapdown mechanization to think of the accelerations and angular rates as being sensed in the body frame, or  $b$ -frame. The sensed accelerations,  $\mathbf{a}^b$ , cannot be integrated directly to obtain velocity and position as in the case of the stabilized system that mechanically defines the navigation frame for the accelerometers. Instead, the inertial accelerations for a particular frame must be *computed* by applying a transformation to the acceleration data according to:

$$\mathbf{a}^a = C_b^a \mathbf{a}^b, \quad (4.16)$$

where  $C_b^a$  is the orthogonal transformation from the  $b$ -frame to some arbitrary  $a$ -frame that should serve as navigation frame. The  $a$ -frame could be the  $i$ -frame, analogous to the space-stabilized mechanization, or the  $n$ -frame (or  $w$ -frame), analogous to the local-level stabilization.

To illustrate the needed computations, consider the case where the navigation frame is, in fact, the  $n$ -frame ( $C_b^n \equiv C_b^w$ ). The angles of the transformation,  $C_b^n$ , may be defined as the roll ( $\eta$ ), pitch ( $\chi$ ), and yaw ( $\alpha$ ) angles; and, the transformation itself may be defined according to the specific order of angle rotations given by (1.90), repeated here for convenience:

$$C_b^n = R_3(-\alpha)R_2(-\chi)R_1(-\eta). \quad (4.17)$$

The angles,  $\eta$ ,  $\chi$ ,  $\alpha$ , could be obtained by integrating their differential equation (1.95). It remains to express the rates,  $\omega_{nb}^b$ , appearing in (1.95), in terms of the gyro-indicated rates,  $\omega_{ib}^b$ . Using (1.61), we have

$$\begin{aligned} \omega_{nb}^b &= \omega_{ni}^b + \omega_{ib}^b \\ &= \omega_{ib}^b - C_n^b \omega_{in}^n, \end{aligned} \quad (4.18)$$

where  $\omega_{in}^n$  is given by (1.89).

Substituting (4.18) and (1.90) into (1.95) yields

$$\begin{pmatrix} \dot{\eta} \\ \dot{\chi} \\ \dot{\alpha} \end{pmatrix} = \begin{pmatrix} 1 & \sin \eta & \tan \chi & \cos \eta & \tan \chi \\ 0 & \cos \eta & \cos \chi & -\sin \eta & -\sin \chi \\ 0 & \sin \eta & \sec \chi & \cos \eta & \sec \chi \end{pmatrix} (\omega_{ib}^b - R_1(\eta)R_2(\chi)R_3(\alpha)\omega_{in}^n). \quad (4.19)$$

Establishing the initial conditions for these differential equations involves the initialization of the INS and will be discussed in Chapter 8.

The essential difference between the strapdown and the stabilized mechanizations concerns the transformation from the accelerometer frame to the navigation frame. With the stabilized mechanization the transformation is done mechanically with torque commands to the servos of the platform gimbals and to the gyros (for the

local-level stabilization, as specified by (4.10), or by (4.14) in the case of the wander-azimuth mechanization). In concert, these torque-induced rotations stabilize the platform so that it is always parallel to the desired frame. Then  $\mathbf{a}^i = \mathbf{a}^p$  for space-stabilization, and  $\mathbf{a}^n = \mathbf{a}^p$  (alternatively,  $\mathbf{a}^w = \mathbf{a}^p$ ) for local-level stabilization.

In the strapdown mode, the transformation is accomplished computationally, where the rates sensed by the gyros are combined with the computed rates of the  $a$ -frame,  $\omega_{ia}^a$  (e.g.,  $\omega_m^n$ ), to yield the transformation  $C_b^a$  that converts the sensed accelerations to the desired navigation frame:  $\mathbf{a}^a = C_b^a \mathbf{a}^b$  (which can be specialized to any particular  $a$ -frame). The details of this computation are given in Section 4.2.3.1. Clearly, the strapdown mechanization is easily (at least in theory) amenable to navigation in any frame by simply computing the necessary transformation. The corresponding navigation equations (see Section 4.3) would utilize the accelerations then coordinatized in that frame.

Although the mechanizations are different physically and computationally, for the given set of navigation equations the net result is the same. In both cases the Schuler feedback loop is the same and characterizes the resonant behavior of the system. Therefore, generally speaking, the effects on the navigation solution of errors associated with the gyros and accelerometers are independent of the mechanization since in both cases these sensors ultimately determine the position and velocity in the frame of the navigation equations.

But at the sensor level, a particular mechanization may cause certain errors to dominate. For example, the orientation of mechanical gyros and accelerometers relative to the typical acceleration environment of the vehicle is judiciously selected to minimize the acceleration-dependent systematic errors. This makes the local-level stabilized platform particularly attractive since the horizontal accelerometers have acceleration-dependent errors coming primarily from the horizontal sensor axes along which the specific forces usually are much less than along the vertical (where it is  $-g$ ).

Furthermore, the sensor biases of the stabilized platform system are much more easily calibrated before and after a sortie. When the vehicle is stationary, the sensors, both accelerometers and gyros, can be slewed by rotating the gimbals into different orientations with respect to the gravity vector and Earth's spin axis, thus exposing biases that are unaffected by this orientation change (Chapter 8). Clearly, a similar calibration procedure of the strapdown system would require changing the orientation of the vehicle, which is impractical, in general. Finally, we will see in Chapter 5 that accelerometer biases in the north-slaved, local-level mechanization tend to be cancelled by corresponding tilt errors, a phenomenon not shared by the strapdown mechanization.

A significant advantage of the strapdown INS is the additional sensor measurements directly available, particularly the attitude angular rates sensed by the gyros. In the stabilized platform system, the roll, pitch, and heading of the vehicle are obtained via the servos at the platform gimbals that slew the platform to the local horizon and north. But, compared to the gyro, these devices typically are lower

in accuracy, resolution, and data rate. In the strapdown system, the quality of the angular rates of the vehicle is limited by the gyro, itself.

It is noted that with today's advanced computer technology, the computational limitations that once loomed for the strapdown system are diminishing in importance. Furthermore, the strapdown system is ideally suited to the use of optical gyroscopes whose errors are independent of the acceleration environment and which cannot, anyway, be used to stabilize a platform in the local horizon because they cannot be torqued.

#### 4.2.3.1 Numerical Determination of the Transformation Matrix

One procedure to determine the transformation matrix, such as (4.17), is to solve the differential equation for the associated Euler angles. In the case of  $C_b^a$ , we could solve (4.19) for the roll, pitch, and yaw angles  $(\eta, \chi, \alpha)$ , and then substitute them into (4.17). The solution to this equation may be performed numerically using an integrator such as the Runge-Kutta algorithm of Chapter 2. It was already indicated in Chapter 1, however, that this procedure can lead to difficulties if the pitch angle approaches  $\pm 90^\circ$ , since the differential equation then becomes singular. In fact, most inertial navigation algorithms employ quaternions to solve the equation, not only to avoid this singularity (which geodesists need hardly worry about), but also to eliminate the more time-consuming evaluations of trigonometric functions in the integrator. The use of quaternions offers a very robust method to compute the transformation matrix under any circumstances and corresponding algorithms will be developed here. It is left to the interested reader to develop an appropriate integration algorithm based on (4.19).

We may formulate the problem generally as determining the transformation matrix,  $C_b^a$ , from the body frame to an arbitrary frame, the  $a$ -frame, that may be the  $i$ -frame, the  $e$ -frame, the  $n$ -frame, the  $w$ -frame, or any other frame, depending on the application. As before, no distinction is made between the instrument frame and the body frame. The differential equation to be solved is given by (1.68)

$$\dot{C}_b^a = C_b^a \Omega_{ab}^b, \quad (4.20)$$

where the off-diagonal elements of  $\Omega_{ab}^b$  are the components of the angular rates,  $\omega_{ab}^b$ , in accordance with (1.62).

The equivalent differential equation in terms of quaternions is given by (1.75):

$$\dot{\mathbf{q}} = \frac{1}{2} A \mathbf{q}, \quad (4.21)$$

where  $\mathbf{q} = (a, b, c, d)^T$  is a four-vector of time-dependent quantities,  $a, b, c, d$ , that satisfy (1.47):

$$C_b^a = \begin{pmatrix} a^2 + b^2 - c^2 - d^2 & 2(bc + ad) & 2(bd - ac) \\ 2(bc - ad) & a^2 - b^2 + c^2 - d^2 & 2(cd + ab) \\ 2(bd + ac) & 2(cd - ab) & a^2 - b^2 - c^2 + d^2 \end{pmatrix}. \quad (4.22)$$

The matrix  $A$  is a  $4 \times 4$  skew-symmetric matrix of time-dependent angular rates, (1.76):

$$A = \begin{pmatrix} 0 & \omega_1 & \omega_2 & \omega_3 \\ -\omega_1 & 0 & \omega_3 & -\omega_2 \\ -\omega_2 & -\omega_3 & 0 & \omega_1 \\ -\omega_3 & \omega_2 & -\omega_1 & 0 \end{pmatrix}, \quad (4.23)$$

where  $\omega_{ab}^b = (\omega_1, \omega_2, \omega_3)^T$ . The integration of  $\mathbf{q}$  according to (4.21) is done incrementally over a time interval, such as  $\delta t$ , or a multiple of  $\delta t$ ; and, this gives the elements of  $C_a^a$  for each step.

A minor difficulty in this procedure is that the angular rates,  $\omega_{ab}^b$ , are not obtained directly from the gyros. Instead, the gyros provide only rates with respect to inertial space,  $\omega_{ib}^b$ , and we must compute, using (1.61) and (1.59):

$$\omega_{ab}^b = \omega_{ib}^b - C_a^b \omega_{ia}^a, \quad (4.24)$$

which clearly involves the transformation that is to be determined. Furthermore, we note that the digital readout of gyros consists of pulses representing angular increments per unit time (e.g., (3.72)). Combining the pulses from all three gyros into a single vector, we define  $\delta\theta_\ell$  as the vector of body-frame angle increments, for the  $\ell^{\text{th}}$  time increment,  $\ell = 1, 2, \dots$ . With corresponding time increments,  $\delta t = t_\ell - t_{\ell-1}$ , assumed constant, the data from the gyros are given exactly by:

$$\delta\theta_\ell = \int_{\delta t} \omega_{ib}^b(t) dt. \quad (4.25)$$

Considering (4.24) we also define the incremental angles

$$\delta\beta_\ell = \int_{\delta t} \omega_{ab}^b(t) dt = \int_{\delta t} (\omega_{ib}^b(t) - C_a^b(t) \omega_{ia}^a(t)) dt. \quad (4.26)$$

Both (4.25) and (4.26) are exact equations, and it is noted that the integration takes place in the  $b$ -frame, which is rotating with respect to the inertial frame.

#### 4.2.3.1.1 A Second-Order Algorithm

Since the time increment, or sampling interval, for an IMU is usually very small (e.g., the data rate may be 256 Hz, so that  $\delta t = 0.00390625$  s), it *may* be sufficient to approximate  $\omega_{ib}^b$  as constant over this time interval. It is not necessary to rely on this approximation; however, more accurate representations obviously increase the complexity of the integration formulas, as seen in the subsequent section. It is, however, clear that, for the  $a$ -frames to be considered, the rates  $\omega_{ia}^a$  are much smaller than  $\omega_{ib}^b$  and, consequently, the term  $C_a^b \omega_{ia}^a$  may be treated as constant over the sampling interval.

Assuming constant angular rates over  $\delta t$ , we have the approximate observation, from (4.25), for the  $\ell^{\text{th}}$  sampling interval:

$$\delta\hat{\theta}_\ell = \omega_{ib}^b(t_\ell) \delta t. \quad (4.27)$$

For the previous interval, we obtain from the solved angles the matrix,  $C_a^b(t_{\ell-1})$ , and from the navigation solution, the rates,  $\omega_{ia}^a(t_{\ell-1})$ . Therefore, we can compute:

$$\delta\hat{\beta}_\ell = \omega_{ab}^b(t_\ell) \delta t \approx \delta\theta_\ell - C_a^b(t_{\ell-1}) \omega_{ia}^a(t_{\ell-1}) \delta t. \quad (4.28)$$

Moreover, the matrix  $A$ , equation (4.23), with elements from the vector,  $\omega_{ab}^b(t_\ell)$ , may also be assumed constant over the interval,  $\delta t$ . Denoting it  $\hat{A}_\ell$ , we readily find an analytic form of the solution to (4.21), since it is a differential equation of the type (2.18). From (2.36) with (2.13), we have

$$\hat{\mathbf{q}}(t) = e^{1/2\hat{A}_\ell(t-t_{\ell-1})} \hat{\mathbf{q}}(t_{\ell-1}), \quad 0 \leq t - t_{\ell-1} \leq \delta t, \quad (4.29)$$

which, using the series form (2.35), yields the following iterative solution:

$$\hat{\mathbf{q}}(t_\ell) = \left( I + \frac{1}{2} \hat{A}_\ell \delta t + \frac{1}{8} \hat{A}_\ell^2 \delta t^2 + \frac{1}{48} \hat{A}_\ell^3 \delta t^3 + \dots \right) \hat{\mathbf{q}}(t_{\ell-1}), \quad \ell = 1, 2, \dots, \quad (4.30)$$

where a single initial condition,  $\hat{\mathbf{q}}(t_0)$ , must be specified. A corresponding closed form may be found by noting that the powers of the matrix  $\hat{A}_\ell$  are either proportional to the identity matrix,  $I$ , (even powers) or proportional to  $\hat{A}_\ell$  itself (odd powers):

$$\begin{aligned} \hat{A}_\ell^{2n} &= (-\omega_1^2(t_\ell) - \omega_2^2(t_\ell) - \omega_3^2(t_\ell))^n I, \\ \hat{A}_\ell^{2n+1} &= (-\omega_1^2(t_\ell) - \omega_2^2(t_\ell) - \omega_3^2(t_\ell))^n \hat{A}_\ell. \end{aligned} \quad (4.31)$$

Substituting these into (4.30) and using the series expressions for sine and cosine, equations (1.30), one then has:

$$\hat{\mathbf{q}}(t_\ell) = \left[ \cos\left(\frac{1}{2} |\delta\hat{\beta}_\ell| \right) I + \frac{1}{|\delta\hat{\beta}_\ell|} \sin\left(\frac{1}{2} |\delta\hat{\beta}_\ell| \right) \hat{B}_\ell \right] \hat{\mathbf{q}}(t_{\ell-1}), \quad (4.32)$$

where  $|\delta\hat{\beta}_\ell| = \sqrt{\delta\hat{\beta}_\ell^T \delta\hat{\beta}_\ell}$ , and

$$\hat{B}_\ell = \hat{A}_\ell \delta t. \quad (4.33)$$

The solution (4.29), or equivalently (4.32), in principle, contains two types of errors that are due to the assumption of constant angular rates over the interval,  $\delta t$ . One is the data error, where (4.27) is used instead of (4.25); and the other is an algorithm error, since solution (4.29) holds only for a constant matrix,  $A$ . However, the data error can be eliminated by noting that  $\hat{B}_\ell$  is an unnecessary approximation of the integral of  $\hat{A}_\ell$ . That is, we do not really need the angular rates in (4.30) or (4.32), just their integrals, as defined in (4.25). Thus, the matrices

$$B_\ell = \int_{t_{\ell-1}}^{t_\ell} A(t) dt \quad (4.34)$$

should be used instead of  $\hat{B}_\ell$ , where, according to (4.23), the elements of  $B_\ell$  are the components of the vector

$$\delta\beta_\ell = \delta\theta_\ell - C_a^b(t_{\ell-1}) \omega_{ia}^a(t_{\ell-1}) \delta t, \quad (4.35)$$

still assuming that the integration errors in the second term are negligible. More explicitly, with reference to (4.23):

$$B_\ell = \begin{pmatrix} 0 & (\delta\beta_1)_\ell & (\delta\beta_2)_\ell & (\delta\beta_3)_\ell \\ -(\delta\beta_1)_\ell & 0 & (\delta\beta_3)_\ell & -(\delta\beta_2)_\ell \\ -(\delta\beta_2)_\ell & -(\delta\beta_3)_\ell & 0 & (\delta\beta_1)_\ell \\ -(\delta\beta_3)_\ell & (\delta\beta_2)_\ell & -(\delta\beta_1)_\ell & 0 \end{pmatrix}. \quad (4.36)$$

With  $B_\ell$  substituted for  $\hat{A}_\ell/\delta t$  in (4.30) or for  $\hat{B}_\ell$  in (4.32), the final algorithm becomes

$$\hat{\mathbf{q}}(t_\ell) = \left( I + \frac{1}{2} B_\ell + \frac{1}{8} B_\ell^2 + \frac{1}{48} B_\ell^3 + \dots \right) \hat{\mathbf{q}}(t_{\ell-1}), \quad \ell = 1, 2, \dots; \quad (4.37)$$

or, with  $|\delta\boldsymbol{\beta}_\ell| = \sqrt{\delta\boldsymbol{\beta}_\ell^T \delta\boldsymbol{\beta}_\ell}$ ,

$$\hat{\mathbf{q}}(t_\ell) = \left[ \cos\left(\frac{1}{2} |\delta\boldsymbol{\beta}_\ell|\right) I + \frac{1}{|\delta\boldsymbol{\beta}_\ell|} \sin\left(\frac{1}{2} |\delta\boldsymbol{\beta}_\ell|\right) B_\ell \right] \hat{\mathbf{q}}(t_{\ell-1}). \quad (4.38)$$

Formulas (4.37) or (4.38), however, still contain the algorithm error.

The algorithm error is of the order  $\delta t^3$ . Indeed, let the true quaternion be represented over the integration interval by the series

$$\mathbf{q}(t_\ell) = \mathbf{q}(t_{\ell-1}) + \dot{\mathbf{q}}(t_{\ell-1}) \delta t + \frac{1}{2!} \ddot{\mathbf{q}}(t_{\ell-1}) \delta t^2 + \frac{1}{3!} \dddot{\mathbf{q}}(t_{\ell-1}) \delta t^3 + \dots \quad (4.39)$$

Substituting (4.21) yields

$$\begin{aligned} \mathbf{q}_\ell = & \left[ I + \frac{1}{2} A_{\ell-1} \delta t + \frac{1}{4} \left( \dot{A}_{\ell-1} + \frac{1}{2} A_{\ell-1}^2 \right) \delta t^2 \right. \\ & \left. + \frac{1}{12} \left( \ddot{A}_{\ell-1} + \dot{A}_{\ell-1} A_{\ell-1} + \frac{1}{2} A_{\ell-1} \dot{A}_{\ell-1} + \frac{1}{4} A_{\ell-1}^3 \right) \delta t^3 + \dots \right] \mathbf{q}_{\ell-1}, \end{aligned} \quad (4.40)$$

where all quantities are true, not approximate, and subscripts denote the time epoch at which they are defined. Similarly, from (4.34) we may write in terms of true quantities (again, we ignore the integration error associated with (4.35)):

$$B_\ell = A_{\ell-1} \delta t + \frac{1}{2} \dot{A}_{\ell-1} \delta t^2 + \frac{1}{6} \ddot{A}_{\ell-1} \delta t^3 + \dots \quad (4.41)$$

Substituting (4.41) into (4.37) and comparing with (4.40) yields the algorithm error. One may easily verify that it is

$$\hat{\mathbf{q}}_\ell - \mathbf{q}_\ell = \left[ \frac{1}{48} (A_{\ell-1} \dot{A}_{\ell-1} - \dot{A}_{\ell-1} A_{\ell-1}) \delta t^3 + \dots \right] \mathbf{q}_{\ell-1}, \quad (4.42)$$

based on the error,  $\hat{\mathbf{q}}_{\ell-1} - \mathbf{q}_{\ell-1}$ , for the previous interval being likewise of third order.

The off-diagonal elements of the matrix product,  $A_\ell \dot{A}_\ell$ , are the components of the vector,  $\omega_{ab}^b \times \dot{\omega}_{ab}^b$ . If the rotational velocity vector,  $\omega_{ab}^b$ , changes with time at most in

magnitude, and not in direction, then it remains parallel to its time derivative and the off-diagonal elements of  $A_t A_t$  and  $\dot{A}_t \dot{A}_t$  vanish. In that case, the matrix,  $A$ , and its first time-derivative commute, thus eliminating the third-order error term in (4.42). That is why the algorithm (4.37) is said to have *commutativity error*, or *coning error*. In other words, if the angular rate vector *does* change direction, the system is “coning” and causes third-order errors in this algorithm. We see also that the coning error is really just the algorithm error associated with the numerical integration of the linear first-order differential equation (4.21). It is the error committed by formulating the integration in a non-rotating frame that is, in fact, rotating. An analogous error occurs in mechanically stabilized systems if the vehicle experiences vibrations in roll and pitch at frequencies too high for the controlling servo motors that maintain the orientation of the platform. The resulting coning motion of the yaw axis implies a steady-state variation in the azimuth rate and a consequent drift in the azimuth angle (Broxmeyer, 1964).

#### 4.2.4.1.2 A Third-Order Algorithm

One method to reduce the coning error in strapdown systems is to decrease the step size of the numerical integration of (4.21), thus more closely approximating linear motion within the time increment,  $\delta t$ . This clearly increases the computational load on the system which usually is a critical parameter in real-time navigation. Various other numerical and algorithmic artifices have been developed to maximize the capture of rotational motion and to improve the integration of the gyro data (see, for example, Bortz, 1971; Ignagni, 1990; Jiang and Lin, 1992), while at the same time minimizing the computational burden. This section gives a natural improvement to the algorithm presented above that incorporates higher-order terms in the numerical integration of the quaternions in (4.21) that is required to compute the transformation matrix,  $C_b^a$ . No consideration of the computational cost is made.

The simple approximation, (4.27), being the rectangle rule of integration, led to an exact solution of the differential equation (4.21), at the expense of algorithm errors of the third order of the sampling interval. Better numerical integrators, however, require more evaluations of the function being integrated; in other words, the integration interval will span more sampling intervals. On the other hand, our gyro data are not really evaluations of the function to be integrated, in this case the angular rates. Instead, they are already the integrals of these rates. It is necessary, therefore, to build a model for the rates on the basis of the data.

The Runge-Kutta (R.K.) algorithm (see Section 2.4.1) is the numerical integrator used here. It is very stable for our problem and relatively easy to implement. It happens that the third-order R.K. method with a linear model for the angular rates yields an algorithm for the quaternions with fourth-order algorithm error. The third-order R.K. method requires that the function being integrated is evaluated at either end of the integration interval and half-way in between (see equations (2.108)). Therefore, in this case the integration interval is twice the data sampling interval:

$$\Delta t = 2\delta t. \quad (4.43)$$

To simplify the notation, we dispense with the index notation for the frames since there is only one objective, and that is to determine the quaternions for the transformation matrix,  $C_h^a$ . Therefore, let

$$\omega_{ab}^b(t) \equiv \omega(t), \quad (4.44)$$

and assume that over the integration interval,  $\Delta t$ , we may write:

$$\omega(t) = \omega_{\ell-2} + \dot{\omega}_{\ell-2}(t - t_{\ell-2}) + O(\Delta t^2), \quad |t - t_{\ell-2}| \leq \Delta t; \quad (4.45)$$

where the subscript,  $\ell$ , as before, denotes evaluation of the (true) quantity at the corresponding epochs spanning the sampling intervals  $\delta t$ , *not*  $\Delta t$ . The notation  $O(\Delta t^2)$  stands for terms of order two and higher in  $\Delta t$ . Substituting (4.45) into the first equation of (4.26) yields for two consecutive sampling epochs:

$$\delta\beta_{\ell-1} = \int_{t_{\ell-2}}^{t_{\ell-1}} \omega(t') dt' = \omega_{\ell-2}\delta t + \frac{1}{2}\dot{\omega}_{\ell-2}\delta t^2 + O(\Delta t^3), \quad (4.46)$$

$$\delta\beta_\ell = \int_{t_{\ell-1}}^{t_\ell} \omega(t') dt' = \omega_{\ell-2}\delta t + \frac{3}{2}\dot{\omega}_{\ell-2}\delta t^2 + O(\Delta t^3). \quad (4.47)$$

For each of these sampling epochs, the incremental angle,  $\delta\beta_\ell$ , strictly given by (4.26), is approximated, analogous to (4.35), by

$$\delta\beta_{\ell-1} = \delta\theta_{\ell-1} - C_a^b(t_{\ell-1})\omega_{ia}^a(t_{\ell-1})\frac{\Delta t}{2}, \quad (4.48)$$

$$\delta\beta_\ell = \delta\theta_\ell - C_a^b(t_{\ell-1})\omega_{ia}^a(t_{\ell-1})\frac{\Delta t}{2}, \quad (4.49)$$

where  $\delta\theta_\ell$  is the vector of output values indicated by the gyros. Again, the second term in each case is an approximation with negligible error since the rates,  $\omega_{ia}^a$ , are comparatively small. Note, however, that the evaluation of this term in both cases is at the center of the integration interval, and requires that the quaternions be solved for every epoch,  $t_\ell$ , associated with the sampling interval. (We also note that the basic length of the sampling interval,  $\delta t$ , can be made equal to a multiple of the gyro sampling interval. Then  $\delta\theta_\ell$  is by simply the *sum* of the corresponding number of output values.)

Solving (4.46) and (4.47) for  $\omega_{\ell-2}$  and  $\dot{\omega}_{\ell-2}$ , it is readily verified that

$$\begin{aligned} \omega_{\ell-2} &= \frac{1}{2\delta t}(3\delta\beta_{\ell-1} - \delta\beta_\ell) + O(\Delta t^2), \\ \dot{\omega}_{\ell-2} &= \frac{1}{\delta t^2}(\delta\beta_\ell - \delta\beta_{\ell-1}) + O(\Delta t). \end{aligned} \quad (4.50)$$

Using these expressions in (4.45) yields for three consecutive sampling epochs:

$$\begin{aligned}\omega_{\ell-2} \Delta t &= 3\delta\beta_{\ell-1} - \delta\beta_\ell + O(\Delta t^3), \\ \omega_{\ell-1} \Delta t &= \delta\beta_{\ell-1} + \delta\beta_\ell + O(\Delta t^3), \\ \omega_\ell \Delta t &= 3\delta\beta_\ell - \delta\beta_{\ell-1} + O(\Delta t^3).\end{aligned}\quad (4.51)$$

Therefore, with an accuracy of second order in the model for the angular rates, we have the following observed quantities (i.e., neglect  $O(\Delta t^3)$  in (4.51)):

$$\begin{aligned}\hat{\omega}_{\ell-2} \Delta t &= 3\delta\beta_{\ell-1} - \delta\beta_\ell, \\ \hat{\omega}_{\ell-1} \Delta t &= \delta\beta_{\ell-1} + \delta\beta_\ell, \\ \hat{\omega}_\ell \Delta t &= 3\delta\beta_\ell - \delta\beta_{\ell-1}.\end{aligned}\quad (4.52)$$

With the Taylor expansions (4.46) and (4.47) substituted into the right sides, we also obtain for later use:

$$\begin{aligned}\hat{\omega}_{\ell-2} \Delta t &= \omega_{\ell-2} \Delta t + O(\Delta t^3), \\ \hat{\omega}_{\ell-1} \Delta t &= \omega_{\ell-2} \Delta t + \frac{1}{2}\dot{\omega}_{\ell-2} \Delta t^2 + O(\Delta t^3), \\ \hat{\omega}_\ell \Delta t &= \omega_{\ell-2} \Delta t + \dot{\omega}_{\ell-2} \Delta t^2 + O(\Delta t^3).\end{aligned}\quad (4.53)$$

The third-order R.K. algorithm, given by (2.108), may be adapted to the differential equation presently under consideration, namely (4.21), where

$$\dot{\mathbf{q}} = f(t, \mathbf{q}), \quad (4.54)$$

with

$$f(t, \mathbf{q}) = \frac{1}{2} A(t) \mathbf{q}. \quad (4.55)$$

We have the following recursive algorithm for the quaternions:

$$\hat{\mathbf{q}}_\ell = \hat{\mathbf{q}}_{\ell-2} + \frac{\Delta t}{6} (\Delta \mathbf{q}_0 + 4\Delta \mathbf{q}_1 + \Delta \mathbf{q}_2), \quad (4.56)$$

where

$$\begin{aligned}\Delta \mathbf{q}_0 &= f(t_{\ell-2}, \hat{\mathbf{q}}_{\ell-2}), \\ \Delta \mathbf{q}_1 &= f\left(t_{\ell-1}, \hat{\mathbf{q}}_{\ell-2} + \frac{\Delta t}{2} \Delta \mathbf{q}_0\right), \\ \Delta \mathbf{q}_2 &= f(t_\ell, \hat{\mathbf{q}}_{\ell-2} - \Delta t \Delta \mathbf{q}_0 + 2 \Delta t \Delta \mathbf{q}_1).\end{aligned}\quad (4.57)$$

This iterative integration algorithm provides an approximate solution at intervals of  $\Delta t$ ; but one could do a second iteration, using the same data, on the in-between points—it just depends on the starting value:  $\hat{\mathbf{q}}_0$  or  $\hat{\mathbf{q}}_1$ . Note that only one starting value for the quaternion is required for each iteration, since the R.K. algorithm is a single-step method.

The implementation of the algorithm according to (4.56) and (4.57) requires the evaluation of the function (4.55). This can be done approximately using the estimate of the previous quaternion and the approximate “observed” values (4.52) for  $A(t_{\ell-2})$ ,  $A(t_{\ell-1})$ ,  $A(t_\ell)$ . Denote these  $\hat{A}(t_{\ell-2})$ , etc., and let, e.g.,

$$\hat{B}_{\ell-2} = \hat{A}_{\ell-2} \Delta t \quad (4.58)$$

where the elements of  $\hat{B}_{\ell-2}$ ,  $\hat{B}_{\ell-1}$ ,  $\hat{B}_\ell$  now are, respectively, the components of the vectors defined by equations (4.52). For example, analogous to (4.36):

$$\hat{B}_\ell = \begin{pmatrix} 0 & 3(\delta\beta_1)_\ell - (\delta\beta_1)_{\ell-1} & 3(\delta\beta_2)_\ell - (\delta\beta_2)_{\ell-1} & 3(\delta\beta_3)_\ell - (\delta\beta_3)_{\ell-1} \\ -3(\delta\beta_1)_\ell + (\delta\beta_1)_{\ell-1} & 0 & 3(\delta\beta_3)_\ell - (\delta\beta_3)_{\ell-1} & -3(\delta\beta_2)_\ell + (\delta\beta_2)_{\ell-1} \\ -3(\delta\beta_2)_\ell + (\delta\beta_2)_{\ell-1} & -3(\delta\beta_3)_\ell + (\delta\beta_3)_{\ell-1} & 0 & 3(\delta\beta_1)_\ell - (\delta\beta_1)_{\ell-1} \\ -3(\delta\beta_3)_\ell + (\delta\beta_3)_{\ell-1} & 3(\delta\beta_2)_\ell - (\delta\beta_2)_{\ell-1} & -3(\delta\beta_1)_\ell + (\delta\beta_1)_{\ell-1} & 0 \end{pmatrix}. \quad (4.59)$$

It is readily verified that, with (4.58) put into (4.55) and with subsequent recursive substitutions, equations (4.57) become

$$\begin{aligned} \Delta q_0 &= \frac{1}{2} \hat{B}_{\ell-2} \hat{q}_{\ell-2}, \\ \Delta q_1 &= \frac{1}{2} \hat{B}_{\ell-1} \left( I + \frac{1}{4} \hat{B}_{\ell-2} \right) \hat{q}_{\ell-2}, \\ \Delta q_2 &= \frac{1}{2} \hat{B}_\ell \left[ I + \hat{B}_{\ell-1} \left( I + \frac{1}{4} \hat{B}_{\ell-2} \right) - \frac{1}{2} \hat{B}_{\ell-2} \right] \hat{q}_{\ell-2}. \end{aligned} \quad (4.60)$$

Finally, substituting these into (4.56) and simplifying the result yields

$$\begin{aligned} \hat{q}_\ell &= \left[ I + \frac{1}{12} (\hat{B}_\ell + 4\hat{B}_{\ell-1} + \hat{B}_{\ell-2}) \right. \\ &\quad \left. + \frac{1}{12} \left( I + \frac{1}{4} \hat{B}_\ell \right) \hat{B}_{\ell-1} \hat{B}_{\ell-2} + \frac{1}{12} \hat{B}_\ell \left( \hat{B}_{\ell-1} - \frac{1}{2} \hat{B}_{\ell-2} \right) \right] \hat{q}_{\ell-2}. \end{aligned} \quad (4.61)$$

The initial value for the iteration,  $\hat{q}_0$  (or,  $\hat{q}_1$ ), is obtained from the initialization (alignment) of the IMU, typically provided by the navigation computer. Or, one can determine the initial attitude externally with velocity or position updates in a Kalman filter using procedures described in Chapter 8. If the result is an initial rotation matrix,  $C_b^a$ , equations (1.49)–(1.52) can be used to get the initial quaternion:

$$\begin{aligned} a &= \frac{1}{2} (1 + (C_b^a)_{1,1} + (C_b^a)_{2,2} + (C_b^a)_{3,3})^{1/2}, \\ b &= \frac{1}{4a} ((C_b^a)_{2,3} - (C_b^a)_{3,2}), \\ c &= \frac{1}{4a} ((C_b^a)_{3,1} - (C_b^a)_{1,3}), \\ d &= \frac{1}{4a} ((C_b^a)_{1,2} - (C_b^a)_{2,1}), \end{aligned} \quad (4.62)$$

where no confusion is anticipated between the notation for the  $a$ - and  $b$ -frames and for the quaternion elements  $a, b$ .

The algorithm error associated with (4.61) is determined by substituting (4.53) into (4.58), and this into (4.61). Comparing the result to (4.40), it is readily verified that

$$\hat{\mathbf{q}}_t - \mathbf{q}_t = O(\delta t^4)\hat{\mathbf{q}}_{t-1}. \quad (4.63)$$

That is, equation (4.61) is a third-order algorithm; the algorithm error is of fourth order.

Higher order algorithms can be derived, but they will require larger integration intervals per step (if the basic data interval,  $\delta t$ , remains the same).

#### 4.2.3.2 Specializations

The numerical integration algorithms described in the previous section yield quaternions associated with the rotation matrix,  $C_b^a$ , that can be used to transform the accelerometer data from the body frame to an arbitrary frame, the  $a$ -frame. The data needed to generate the quaternions through the numerical integration algorithm are the incremental angles,  $\delta\beta_t$ , given by (4.26); and, generally, they are a combination of gyro observations ( $\delta\theta_t$ ) and rotation rates,  $\omega_{ia}^a$ , of the  $a$ -frame with respect to the  $i$ -frame that come from the navigation solution. As noted before, the values of  $\delta\beta_t$ , as determined in practice, for example, by (4.49), are exact (disregarding gyro errors) with respect to the gyro output, but approximate with respect to the navigation solution.

Clearly, if the  $a$ -frame is the  $i$ -frame, then  $\omega_{ii}^i = \mathbf{0}$ , and

$$\delta\beta_t = \delta\theta_t \quad (4.64)$$

If the  $a$ -frame is the  $e$ -frame, then the angles (4.48) and (4.49) are approximate because of the inexact integration leading to the computed transformation matrix,  $\hat{C}_e^b$ . However,  $\omega_{ie}^e$ , given by (1.77), does not depend on the solution to the navigation equations for velocity and position. On the other hand, if the  $a$ -frame is the  $n$ -frame or the  $w$ -frame, then the algorithm for the quaternions must be combined with the algorithm for the integration of the navigation equations, since  $\omega_{in}^n$ , given by (1.89), depends on the latitude and velocity of the vehicle. This will be developed in the next section.

Finally, we note that the choice of the order of the numerical integration algorithm should depend on the accuracy of the gyro data. Since computations are relatively cheap, the model error introduced by the numerical integration algorithm should always be substantially less than the data errors of the instruments. In order to obtain an approximate magnitude of the algorithm error in terms of angular error rate, we expand the transformation matrix in a Taylor series making repeated use of (4.20) and, for convenience, omitting reference to coordinate frames:

$$\begin{aligned} C(t) = C_0 &\left( I + \Omega_0 \Delta t + \frac{1}{2!} (\Omega_0^2 + \dot{\Omega}_0) \Delta t^2 \right. \\ &\left. + \frac{1}{3!} (\Omega_0^3 + 2\Omega_0\dot{\Omega}_0 + \dot{\Omega}_0\Omega_0 + \ddot{\Omega}_0) \Delta t^3 + \dots \right), \end{aligned} \quad (4.65)$$

where the zero subscript refers to evaluation at  $t = t_0$ . An  $m^{\text{th}}$ -order algorithm neglects terms of order  $\Delta t^{m+1}$ . If the angular acceleration and higher-order derivatives of the angular rate of a vehicle are small, the dominant error term is

$$\delta C \approx C(t_0) \frac{1}{(m+1)!} \Omega^{m+1} \Delta t^{m+1}, \quad (4.66)$$

or, roughly, using (1.65) and (1.62), the angular error for one integration step is  $\delta\psi \approx \omega^{m+1} \Delta t^{m+1} / (m+1)!$ . The angular error per unit time is then the angular error rate and is given by

$$\delta\omega \approx \omega^{m+1} \Delta t^m / (m+1)!. \quad (4.67)$$

To illustrate, suppose that the integration step is  $\Delta t = 1/128$  s and that vehicle rotation rates are not greater than  $|\omega| < 10^\circ/\text{s} = 0.17 \text{ rad/s}$ . Then a second-order algorithm is accurate to about  $|\delta\omega| \approx 0.01^\circ/\text{hr}$ . If the gyro drift rate is  $0.003^\circ/\text{hr}$  (medium accuracy ring-laser gyro), then a third-order algorithm is required to keep the algorithm error below the data error.

Finally, it is noted that the computed quaternions,  $\hat{\mathbf{q}}$ , from any algorithm may not satisfy the constraint (1.40), that the sum of the squares of their elements is unity. This is due to numerical round-off error, as well as model error, and causes the computed transformation matrix to become non-orthogonal. This is avoided by “re-orthogonalizing” the computed quaternions at each iteration according to

$$\hat{\mathbf{q}} \leftarrow \frac{1}{\sqrt{\hat{\mathbf{q}}^T \hat{\mathbf{q}}}} \hat{\mathbf{q}}, \quad (4.68)$$

which will ensure that  $\hat{\mathbf{q}}^T \hat{\mathbf{q}} = 1$  and that  $\hat{C}_b^a$  is orthogonal.

### 4.3 Navigation Equations

Navigation or positioning using an inertial navigation system is based fundamentally on the integration of inertially sensed accelerations with respect to time. Mathematically, it involves the solution to a differential equation that relates sensed accelerations to second-order time-derivatives of position. For example, in an inertial (i.e., non-rotating) frame, these equations are given by (1.7), repeated here more explicitly,

$$\ddot{\mathbf{x}}^i = \mathbf{g}^i(\mathbf{x}^i) + \mathbf{a}^i, \quad (4.69)$$

where  $\mathbf{x}^i$  is the position vector in the  $i$ -frame;  $\mathbf{g}^i$  is the acceleration due to the gravitational field in this frame and depends on the position vector; and  $\mathbf{a}^i$  is the specific force, being also the quantity that is sensed by the accelerometer. These equations are solved (integrated) for the position,  $\mathbf{x}^i$ , assuming that the gravitational acceleration is known. Similar differential equations can be formulated in other frames; in each case, they constitute the *navigation equations*. Obtaining positions and velocities by integrating these equations is known as *free-inertial navigation*. Except for initial conditions, it is inertial navigation free of any external information.

As soon as we consider frames rotating with respect to inertial space, then the situation is more complicated as evidenced by the Coriolis Law (1.70). In a frame such as the local level, or *n*-frame, the differential equations become nonlinear as a result of this law and because the transformation from the *i*-frame to the *n*-frame is formulated in terms of the position to be solved. Clearly, then, the formulation and subsequent method of solution of the navigation equations depend specifically on the coordinate frame in which we wish to determine positions.

Once a particular frame is decided upon, we may call this the navigation frame (although, usually the navigation frame is identified with the north-slaved, local-level frame, or *n*-frame). The choice of frame may be dictated by the type of physical mechanization of the system, or if it is a strapdown system the choice may be a matter of computational convenience. On the other hand, the particular mechanization, whether stabilized or strapdown, is immaterial in the formulation of the navigation equations, since these mechanizations differ only in how the transformation from the instrument frame to the navigation frame is effected. Moreover, the solution to the navigation equations, in whatever frame, if obtained without numerical or modeling errors, is essentially the same, differing only by a transformation from one frame to another. That is, solving the navigation equations, for example, in the *n*-frame and transforming the solution to the *i*-frame is identical to solving the corresponding navigation equations in the *i*-frame. After all, the navigation solution is based on the dynamics of motion according to laws, such as Newton's Laws, that hold universally.

Therefore, it is possible and desirable to formulate the navigation equations rigorously and in a unified way using our arbitrary frame, the *a*-frame, where the point of departure for this general formulation is equation (4.69). The resulting form may then be specialized to any particular frame, specifically the *i*-frame, *e*-frame, *n*-frame, or *w*-frame. We recall that the coordinate directions of the *n*-frame (and *w*-frame) are defined by the local horizon and by the vertical centered on the vehicle. Therefore, strictly speaking, the navigation equations are not coordinatized in the *n*-frame per se, because no horizontal motion takes place in this frame. We will refer to the *n*-frame coordinatization of the navigation equations as an Earth-referenced formulation in which the velocity components are transformed along the *n*-frame coordinate directions (a similar interpretation holds for the *w*-frame). Although this distinction is rarely articulated in the literature, it is always implicit in the development.

### 4.3.1 Unified Approach

Let the *a*-frame be a completely arbitrary frame that rotates with respect to the *i*-frame with angular rate  $\omega_{ia}^a$ . The objective is to derive an equation like (4.69), but for positions,  $\mathbf{x}^a$ , in the *a*-frame. We suppose that both the *a*-frame and the *i*-frame are concentric. This causes no loss in generalization for our applications, but it is a subtle detail in the specialization to the *n*-frame.

A vector in the *a*-frame has coordinates in the *i*-frame given by

$$\mathbf{x}^i = C_a^i \mathbf{x}^a, \quad (4.70)$$

where  $C_a^i$  is the transformation matrix from the  $a$ -frame to the  $i$ -frame. From (1.68), the time derivative of this matrix is given by

$$\dot{C}_a^i = C_a^i \Omega_{ia}^a, \quad (4.71)$$

where  $\Omega_{ia}^a$  denotes a skew-symmetric matrix with elements from  $\omega_{ia}^a$  given by (1.62):

$$[\omega_{ia}^a \times] = \Omega_{ia}^a. \quad (4.72)$$

We also need the second time derivative, which from (4.71) and the chain rule for differentiation is given by

$$\ddot{C}_a^i = C_a^i \dot{\Omega}_{ia}^a + C_a^i \Omega_{ia}^a \Omega_{ia}^a. \quad (4.73)$$

Now, differentiating (4.70) twice with respect to time yields

$$\begin{aligned} \ddot{x}^i &= \ddot{C}_a^i x^a + 2\dot{C}_a^i \dot{x}^a + C_a^i \ddot{x}^a \\ &= C_a^i \ddot{x}^a + 2C_a^i \Omega_{ia}^a \dot{x}^a + C_a^i (\dot{\Omega}_{ia}^a + \Omega_{ia}^a \Omega_{ia}^a) x^a. \end{aligned} \quad (4.74)$$

Solving for  $\ddot{x}^a$  and combining this with equation (4.69) gives the system dynamics for position in the  $a$ -frame:

$$\ddot{x}^a = -2\Omega_{ia}^a \dot{x}^a - (\dot{\Omega}_{ia}^a + \Omega_{ia}^a \Omega_{ia}^a) x^a + a^a + g^a, \quad (4.75)$$

making use of the orthogonality of  $C_a^i$ , and where

$$a^a = C_i^a a^i, \quad g^a = C_i^a g^i. \quad (4.76)$$

The system (4.75) of three second-order differential equations can be transformed into a system of six first-order differential equations (see (2.8)) by introducing three new variables, namely, the velocities,  $\dot{x}^a$ :

$$\begin{aligned} \frac{d}{dt} \dot{x}^a &= -2\Omega_{ia}^a \dot{x}^a - (\dot{\Omega}_{ia}^a + \Omega_{ia}^a \Omega_{ia}^a) x^a + a^a + g^a, \\ \frac{d}{dt} x^a &= \dot{x}^a. \end{aligned} \quad (4.77)$$

We call (4.77) the navigation equations coordinatized in the (arbitrary)  $a$ -frame. The forcing terms in these equations are the accelerations sensed by the accelerometers and the gravitational acceleration.

If the system is stabilized such that the accelerometer platform is parallel to the  $a$ -frame, then the sensed accelerations are  $a^a$ . In the strapdown mechanization, these accelerations are computed from accelerometer data sensed in the  $b$ -frame (or, sensor frame):

$$a^a = C_b^a a^b, \quad (4.78)$$

where the transformation,  $C_b^a$ , is determined by integrating the angular rates,  $\omega_{ab}^b$ , obtained from the gyro data (as discussed in Section 4.2.3.1), according to equation (4.24):

$$\omega_{ab}^b = \omega_{ib}^b - C_a^b \omega_{ia}^a. \quad (4.79)$$

The angular rates  $\omega_{ia}^a$  in (4.79) and  $\Omega_{ia}^a$  in (4.77) describing the rotation of the  $a$ -frame relative to the  $i$ -frame may also depend on the navigation solution,  $\mathbf{x}^a$ , itself, which is the case for the  $n$ - and  $w$ -frames.

### 4.3.2 Navigation Equations in $i$ -Frame

In this case, the  $a$ -frame is the  $i$ -frame; and clearly  $\Omega_{ii}^i = 0$ . Then the navigation equations (4.77) return simply to the form equivalent to (4.69):

$$\begin{aligned}\frac{d}{dt} \dot{\mathbf{x}}^i &= \mathbf{a}^i + \mathbf{g}^i, \\ \frac{d}{dt} \mathbf{x}^i &= \dot{\mathbf{x}}^i.\end{aligned}\tag{4.80}$$

For the strapdown case, the transformation matrix,  $C_b^i$ , is obtained directly from the sensed angular rates,  $\omega_{ib}^b$ , by integrating (4.20) specialized to  $a \equiv i$  (see also Section 4.2.3.2):

$$\dot{C}_b^i = C_b^i \Omega_{ib}^b.\tag{4.81}$$

Equations (4.80) and (4.81) represent the total dynamics of the (strapdown) system in terms of a set of differential equations in the  $i$ -frame.

### 4.3.3 Navigation Equations in $e$ -Frame

If the  $a$ -frame is defined to be the  $e$ -frame, then because  $\dot{\Omega}_{ie}^e = 0$ , we obtain from (4.77) the navigation equations in the  $e$ -frame:

$$\begin{aligned}\frac{d}{dt} \dot{\mathbf{x}}^e &= -2\Omega_{ie}^e \dot{\mathbf{x}}^e - \Omega_{ie}^e \Omega_{ie}^e \mathbf{x}^e + \mathbf{a}^e + \mathbf{g}^e, \\ \frac{d}{dt} \mathbf{x}^e &= \dot{\mathbf{x}}^e,\end{aligned}\tag{4.82}$$

where  $\Omega_{ie}^e$  is known from (1.77). Again, as with the  $i$ -frame coordinatization, the determination of the transformation matrix,  $C_b^e$ , in the strapdown case is completely decoupled from the navigation solution, being obtained from the integration of (4.20) with  $a \equiv e$  (see also Section 4.2.3.2):

$$\dot{C}_b^e = C_b^e \Omega_{eb}^b,\tag{4.83}$$

where, in terms of the sensed angular rates,  $\omega_{ib}^b$ , we have:

$$\omega_{eb}^b = \omega_{ib}^b - C_e^b \omega_{ie}^e.\tag{4.84}$$

As in the  $i$ -frame formulation, the navigation equations cast in the  $e$ -frame are linear differential equations with constant coefficients.

### 4.3.4 Navigation Equations in $n$ -Frame

To obtain the navigation equations in the  $n$ -frame, one might be tempted simply to substitute “ $n$ ” for “ $a$ ” in equations (4.77). However, this would not give the desired

result, because the integration would take place in a fixed frame; whereas, the desired velocities should be always in the (rotating) local horizon frame. By our definition of the  $n$ -frame, the vehicle does not move (horizontally) in this frame. The  $n$ -frame serves to define local directions for the velocity vector determined in a frame in which the vehicle has motion (e.g., the  $e$ -frame).

Thus, the desired velocity vector is the  $e$ -frame (Earth-referenced) velocity vector coordinatized in a frame parallel to the  $n$ -frame, which we denote as  $\mathbf{v}^n$ , and it is given by

$$\mathbf{v}^n = C_e^n \dot{\mathbf{x}}^e. \quad (4.85)$$

It should be noted strenuously that  $\mathbf{v}^n \neq \dot{\mathbf{x}}^n$ .  $\mathbf{v}^n$  is a notation we use for a vector, in this case a vector of velocity components; while  $\dot{\mathbf{x}}^n$  is the *time-derivative* of a vector. Similarly,  $\mathbf{a}^n$  is a vector, while  $\ddot{\mathbf{x}}^n$  is the second time-derivative of a vector. We know that these derivatives are not ordinary vectors since, according to the Coriolis Law, (1.70), they do not transform as vectors.

Formally we could obtain the navigation equations in the  $n$ -frame through (4.77) by replacing “ $a$ ” with “ $n$ ”, and with the implicit modification of putting the  $n$ -frame origin at the Earth’s center ( $e$ -frame origin). Subsequently, however, it is necessary to substitute for  $\dot{\mathbf{x}}^n$  using the relation

$$\dot{\mathbf{x}}^n = \mathbf{v}^n - \Omega_{en}^n \mathbf{x}^n, \quad (4.86)$$

that comes from differentiating  $\mathbf{x}^n = C_e^n \mathbf{x}^e$  (the Coriolis Law!) and (4.85). The remaining derivation and simplifications are left as an exercise to the reader, who will find agreement with the result (4.88).

We follow a simpler approach that clearly emphasizes the Earth-referenced frame in which the integration of the resulting navigation equations takes place. That is, we merely transform the navigation equations, given in the  $e$ -frame, (4.82), into the  $n$ -frame by the direct substitution of  $\dot{\mathbf{x}}^e = C_n^e \mathbf{v}^n$  from (4.85). Making use of  $\dot{C}_n^e = C_n^e \Omega_{en}^n$  from (1.68), we have for the left-hand side of the first equation of (4.82):

$$\frac{d}{dt} C_n^e \mathbf{v}^n = C_n^e \left( \frac{d}{dt} \mathbf{v}^n + \Omega_{en}^n \mathbf{v}^n \right). \quad (4.87)$$

On the right-hand side of (4.82), we use (4.85) and  $\Omega_{ie}^n = C_e^n \Omega_{ie}^e C_n^e$  from (1.17), and the result is:

$$\frac{d}{dt} \mathbf{v}^n = \mathbf{a}^n - (2\Omega_{ie}^n + \Omega_{en}^n) \mathbf{v}^n + \mathbf{g}^n - C_e^n \Omega_{ie}^e \Omega_{ie}^e \mathbf{x}^e. \quad (4.88)$$

The last two terms are, respectively, the gravitational vector and the centrifugal acceleration due to Earth’s rotation, coordinatized in the  $n$ -frame. Together they define the *gravity* vector:

$$\bar{\mathbf{g}}^n = \mathbf{g}^n - C_e^n \Omega_{ie}^e \Omega_{ie}^e \mathbf{x}^e. \quad (4.89)$$

The distinction between the terms gravitation and gravity, commonly made in geodesy, refers to the difference between the acceleration due to mass attraction,

alone, and the total acceleration, gravitational and centrifugal, that is measured at a fixed point on the rotating Earth. Finally, by suitably manipulating the subscripts with the aid of (1.61), we also obtain

$$2\Omega_{ie}^n + \Omega_{en}^n = \Omega_{in}^n + \Omega_{ie}^n. \quad (4.90)$$

Substituting (4.89) and (4.90) into (4.88) then yields the desired form of the  $n$ -frame navigation equations:

$$\frac{d}{dt} \mathbf{v}^n = \mathbf{a}^n - (\Omega_{in}^n + \Omega_{ie}^n) \mathbf{v}^n + \bar{\mathbf{g}}^n, \quad (4.91)$$

where equation (4.85) could serve as the differential equation for the position vector, written as

$$\frac{d}{dt} \mathbf{x}^e = C_n^e \mathbf{v}^n. \quad (4.92)$$

Usually, however, (4.92) is formulated in terms of the geodetic latitude,  $\phi$ , longitude,  $\lambda$ , and height,  $h$ , instead of the Cartesian coordinates in the  $e$ -frame. To express the velocity components in terms of *rates* of geodetic coordinates, we start with (1.80), repeated here for convenience:

$$\mathbf{x}^e = \begin{pmatrix} (N+h)\cos\phi\cos\lambda \\ (N+h)\cos\phi\sin\lambda \\ (N(1-e^2)+h)\sin\phi \end{pmatrix}, \quad (4.93)$$

where  $e^2$  is the square of the eccentricity of the ellipsoid associated with the geodetic coordinates, and  $N$  is the radius of curvature of the ellipsoid in the prime vertical, (1.81). Now, it is readily shown that

$$\frac{d}{d\phi} ((N+h)\cos\phi) = -(M+h)\sin\phi, \quad (4.94)$$

and

$$\frac{d}{d\phi} ((N(1-e^2)+h)\sin\phi) = (M+h)\cos\phi, \quad (4.95)$$

where  $M$  is the radius of curvature in the meridian (1.82). Therefore, with  $d/dt = (d/d\phi)\dot{\phi}$ , etc., we have from (4.93)

$$\dot{\mathbf{x}}^e = \begin{pmatrix} -\dot{\phi}(M+h)\sin\phi\cos\lambda - \dot{\lambda}(N+h)\cos\phi\sin\lambda + \dot{h}\cos\phi\cos\lambda \\ -\dot{\phi}(M+h)\sin\phi\sin\lambda + \dot{\lambda}(N+h)\cos\phi\cos\lambda + \dot{h}\cos\phi\sin\lambda \\ \dot{\phi}(M+h)\cos\phi + \dot{h}\sin\phi \end{pmatrix}. \quad (4.96)$$

And, with the transformation matrix  $C_e^n$  from (1.87), it is easily verified that (4.85) becomes

$$\mathbf{v}^n = \begin{pmatrix} \dot{\phi}(M+h) \\ \dot{\lambda}(N+h)\cos\phi \\ -\dot{h} \end{pmatrix}. \quad (4.97)$$

Again, it is clear that the velocity components of  $\mathbf{v}^n$  refer to the Earth-fixed vector,  $\dot{\mathbf{x}}^e$ , but oriented along directions defined by the  $n$ -frame. For example, the first component is the north velocity, being the local rate of change in position along the tangent to the meridian, northward.

Finally, the angular rates in (4.91) are also expressed readily in terms of latitude and longitude rates. From (1.89) and (1.62), we have

$$\Omega_{in}^n = \begin{pmatrix} 0 & (\dot{\lambda} + \omega_e) \sin \phi & -\dot{\phi} \\ -(\dot{\lambda} + \omega_e) \sin \phi & 0 & -(\dot{\lambda} + \omega_e) \cos \phi \\ \dot{\phi} & (\dot{\lambda} + \omega_e) \cos \phi & 0 \end{pmatrix}. \quad (4.98)$$

In addition, using (1.77) and (1.87), we have, with reference to (1.17),

$$\Omega_{ie}^n = C_e^n \Omega_{ie}^e C_n^e = \begin{pmatrix} 0 & \omega_e \sin \phi & 0 \\ -\omega_e \sin \phi & 0 & -\omega_e \cos \phi \\ 0 & \omega_e \cos \phi & 0 \end{pmatrix}. \quad (4.99)$$

Therefore, the explicit form of the angular rate coefficient matrix of  $\mathbf{v}^n$  in (4.91) is given by:

$$\Omega_{in}^n + \Omega_{ie}^n = \begin{pmatrix} 0 & (\dot{\lambda} + 2\omega_e) \sin \phi & -\dot{\phi} \\ -(\dot{\lambda} + 2\omega_e) \sin \phi & 0 & -(\dot{\lambda} + 2\omega_e) \cos \phi \\ \dot{\phi} & (\dot{\lambda} + 2\omega_e) \cos \phi & 0 \end{pmatrix}. \quad (4.100)$$

Now let the components of the Earth-referenced velocity,  $\mathbf{v}^n$ , the sensed acceleration,  $\mathbf{a}^n$ , and the *gravity* vector,  $\bar{\mathbf{g}}^n$ , be denoted more descriptively by their north, east, and down components, as follows:

$$\mathbf{v}^n = \begin{pmatrix} v_N \\ v_E \\ v_D \end{pmatrix}; \quad \mathbf{a}^n = \begin{pmatrix} a_N \\ a_E \\ a_D \end{pmatrix}; \quad \bar{\mathbf{g}}^n = \begin{pmatrix} \bar{g}_N \\ \bar{g}_E \\ \bar{g}_D \end{pmatrix}. \quad (4.101)$$

Then, substitute (4.100) into (4.91) to obtain

$$\frac{d}{dt} \begin{pmatrix} v_N \\ v_E \\ v_D \end{pmatrix} = \begin{pmatrix} a_N + \bar{g}_N - 2\omega_e \sin \phi v_E + \dot{\phi} v_D - \dot{\lambda} \sin \phi v_E \\ a_E + \bar{g}_E + 2\omega_e \sin \phi v_N + 2\omega_e \cos \phi v_D + \dot{\lambda} \sin \phi v_N + \dot{\lambda} \cos \phi v_D \\ a_D + \bar{g}_D - 2\omega_e \cos \phi v_E - \dot{\lambda} \cos \phi v_E - \dot{\phi} v_N \end{pmatrix}. \quad (4.102)$$

Equations (4.102) together with

$$\begin{pmatrix} \dot{\phi} \\ \dot{\lambda} \\ \dot{h} \end{pmatrix} = \begin{pmatrix} \frac{v_N}{M+h} \\ \frac{v_E}{(N+h) \cos \phi} \\ -\frac{v_D}{(N+h) \cos \phi} \end{pmatrix}, \quad (4.103)$$

obtained from (4.97), constitute a set of six, non-linear, differential equations in the

variables ( $v_N, v_E, v_D, \phi, \lambda, h$ ) that can be integrated to get Earth-referenced position and velocity, the latter coordinatized in the  $n$ -frame.

It is shown in Chapter 5 that the integration of (4.102) and (4.103) is unstable in the vertical channel, ( $h, v_D$ ), causing errors to grow exponentially with time due to initial height and vertical accelerometer errors. Therefore, over longer periods, the equations for the vertical components are not integrated without some form of external information that bounds the error. This information may be provided, for example, by an altimetric measurement. It is also shown that although the vertical velocity and altitude couple into the horizontal components, as seen in (4.102) and (4.103), they cause no undue error growth in these even if approximated fairly roughly. Also, the horizontal gravity values, needed for the north and east navigation equations, are small and can be neglected for many types of navigation applications.

If the platform on which the accelerometers reside is stabilized through commanded rates given by (4.9), and thus is parallel to the  $n$ -frame, then  $\mathbf{a}^p = \mathbf{a}^n$ . That is, the sensed accelerations can be used directly as  $a_N, a_E, a_D$  in the integration of differential equations (4.102) and (4.103). The torques needed to stabilize the platform in the  $n$ -frame are obtained via (4.10) from the Earth-referenced velocities of the platform, that result from the integration of the accelerations using (4.102). This feedback procedure is known as the *Schuler feedback loop*, that is implemented in the Schuler tuning of the platform, as described in Section 4.2.2.1.

In the strapdown mechanization, the situation is similar. In this case, the transformation from the body frame to the  $n$ -frame,  $C_b^n$ , is performed computationally by integrating

$$\dot{C}_b^n = C_b^n \Omega_{nb}^n, \quad (4.104)$$

using the angular rates,  $\omega_{nb}^b$ , obtained from the sensed rates,  $\omega_{ib}^b$ , according to (4.79):

$$\omega_{nb}^b = \omega_{ib}^b - C_n^b \omega_{in}^n. \quad (4.105)$$

The integration of accelerations, transformed from the body frame according to (4.78), yields velocities and positions that enable the computation of the elements of  $\omega_{in}^n$ , according to (1.89). These rates, in turn, are required to compute the orientation angles  $\eta, \chi, \alpha$ , using (4.19), or the associated quaternions (see Section 4.2.3.1), that yield the transformation,  $C_b^n$ , that is needed to compute  $\mathbf{a}^n$  from the sensed accelerations in the  $b$ -frame using (4.78). Thus, we again see the Schuler feedback loop in action, though in a computational rather than a mechanical sense. It is clear that the navigation equations (4.102) and (4.103) are independent of the type of local-level mechanization implemented, whether mechanically stabilized or computationally realized.

The extent to which this mechanization is imperfect due to unknown errors in the gyro output (affecting  $\delta\omega_d$ ) and in the navigation solution (affecting  $\omega_{in}^n$ ) will yield incorrect  $n$ -frame coordinatized inertial accelerations that further corrupt the navigation solution. Since the dominant IMU errors are unknown gyro drift biases, the navigation errors tend to grow with time. This phenomenon and methods to bound

or estimate these errors using external information are the subjects of Chapters 5 and 8.

### 4.3.5 Navigation Equations in $w$ -Frame

The navigation equations in the  $w$ -frame for the velocities are analogous to those in the  $n$ -frame, equation (4.91), with  $w$  replacing  $n$ . That is, the same derivation that led to (4.91) can be repeated for the  $w$ -frame, for which we define the wander velocity vector,  $\mathbf{v}^w$ , by

$$\mathbf{v}^w = C_e^w \dot{\mathbf{x}}^e, \quad (4.106)$$

where  $C_e^w = C_n^w C_e^n$ , and  $C_n^w$  is given by (4.11). Therefore, the navigation equations for  $\mathbf{v}^w$  are:

$$\frac{d}{dt} \mathbf{v}^w = \mathbf{a}^w - (\Omega_{iw}^w + \Omega_{ie}^w) \mathbf{v}^w + \bar{\mathbf{g}}^w. \quad (4.107)$$

The objective behind the  $w$ -frame mechanization is the elimination of singularities from the integration algorithm that occur when navigating near the poles, as happens in (4.103). Hence, the angular rate coefficient matrix in (4.107) must be written in terms of the wander frame velocities instead of the latitude and longitude rates. Toward this end, we note that, in terms of vectors,  $\Omega_{iw}^w + \Omega_{ie}^w$  is equivalent to

$$\begin{aligned} \omega_{iw}^w + \omega_{ie}^w &= \omega_{ie}^w + \omega_{ew}^w + \omega_{nw}^w \\ &= \omega_{ew}^w + 2C_e^w \omega_{ie}^e. \end{aligned} \quad (4.108)$$

The rate vector  $\omega_{ie}^e$  depends merely on Earth's spin rate and the transformation matrix,  $C_e^w$ , can be obtained by integrating

$$\dot{C}_w^e = C_n^w \Omega_{ew}^w \quad (4.109)$$

on the basis of the angular rates,  $\omega_{ew}^w$ . Therefore, it only remains to express these rates in terms of the wander frame velocities in order to find the angular rate coefficient matrix also in those terms.

From (1.88) and (4.12), we have

$$\omega_{ew}^w = \omega_{en}^n + \omega_{nw}^n = \begin{pmatrix} \dot{\lambda} \cos \phi \\ -\dot{\phi} \\ -\dot{\lambda} \sin \phi + \dot{\alpha} \end{pmatrix}, \quad (4.110)$$

and, of course,

$$\omega_{ew}^w = C_n^w \omega_{ew}^n. \quad (4.111)$$

At this point we need a more explicit definition of the wander-azimuth frame. In particular, suppose that the mechanization is prescribed (as done, e.g., for military aircraft INS) such that the  $w$ -frame does not rotate about its third axis with respect

to the  $e$ -frame. This condition is mechanized physically on a stabilized system with appropriate commanded rates on the gyros, or it is mechanized computationally for a strapdown system. In either case, it means that the third component of  $\omega_{ew}^w$  in (4.110) is zero, or that the azimuth rate is given by

$$\dot{\alpha} = \dot{\lambda} \sin \phi. \quad (4.112)$$

We note that the commanded rate in the physically mechanized wander frame is obtained according to (4.13) from

$$\omega_{com} = \omega_{hw}^w = \omega_{ew}^w + C_e^w \omega_{re}^e. \quad (4.113)$$

The angular rates,  $\omega_{ew}^w$ , and thus the transformation matrix,  $C_e^w$ , computed by integrating (4.109), are determined exclusively from the wander velocity vector,  $v^w$ . To show this, first substitute the angular rates from (4.103) into (4.110); then (4.111) becomes

$$\omega_{ew}^w = \begin{pmatrix} \frac{v_E}{N+h} \cos \alpha - \frac{v_N}{M+h} \sin \alpha \\ -\frac{v_E}{N+h} \sin \alpha - \frac{v_N}{M+h} \cos \alpha \\ 0 \end{pmatrix}. \quad (4.114)$$

Now, since

$$v^n = C_w^n v^w, \quad (4.115)$$

we obtain

$$\omega_{ew}^w = \begin{pmatrix} v_1^w \sin \alpha \cos \alpha \left( \frac{1}{N+h} - \frac{1}{M+h} \right) + v_2^w \left( \frac{\cos^2 \alpha}{N+h} + \frac{\sin^2 \alpha}{M+h} \right) \\ -v_1^w \left( \frac{\sin^2 \alpha}{N+h} + \frac{\cos^2 \alpha}{M+h} \right) - v_2^w \sin \alpha \cos \alpha \left( \frac{1}{N+h} - \frac{1}{M+h} \right) \\ 0 \end{pmatrix}. \quad (4.116)$$

From the definitions (1.81) and (1.82) of the radii of curvature,  $N$  and  $M$ , it is readily verified that

$$\frac{1}{N+h} - \frac{1}{M+h} = -\frac{e'^2 \cos^2 \phi M}{(N+h)(M+h)}, \quad (4.117)$$

$$\frac{\cos^2 \alpha}{N+h} + \frac{\sin^2 \alpha}{M+h} = \frac{M(1 + e'^2 \cos^2 \phi \sin^2 \alpha) + h}{(N+h)(M+h)}. \quad (4.118)$$

$$\frac{\sin^2 \alpha}{N+h} + \frac{\cos^2 \alpha}{M+h} = \frac{M(1 + e'^2 \cos^2 \phi \cos^2 \alpha) + h}{(N+h)(M+h)}, \quad (4.119)$$

where  $e'^2 = 1/(1 - e^2)$  is the square of the second eccentricity of the ellipsoid. Substituting (4.117) through (4.119) into (4.116), we have

$$\omega_{ew}^w = \frac{1}{(N+h)(M+h)} \times \begin{pmatrix} v_2^w(M(1+e'^2 \cos^2 \phi \sin^2 \alpha) + h) - e'^2 M v_1^w \sin \alpha \cos \alpha \cos^2 \phi \\ -v_1^w(M(1+e'^2 \cos^2 \phi \cos^2 \alpha) + h) + e'^2 M v_2^w \sin \alpha \cos \alpha \cos^2 \phi \\ 0 \end{pmatrix}. \quad (4.120)$$

This expresses  $\omega_{ew}^w$  in terms of the horizontal wander velocities,  $v_1^w$  and  $v_2^w$ , under the condition (4.112).

The terms in  $\omega_{ew}^w$  depending on latitude,  $\phi$ , and azimuth,  $\alpha$ , can be replaced by elements of  $C_e^w$ , which is given, with (4.11) and (1.87), by

$$C_e^w = C_n^w C_n^n = \begin{pmatrix} -\cos \alpha \sin \phi \cos \lambda - \sin \alpha \sin \lambda & -\cos \alpha \sin \phi \sin \lambda + \sin \alpha \cos \lambda & \cos \alpha \cos \phi \\ \sin \alpha \sin \phi \cos \lambda - \cos \alpha \sin \lambda & \sin \alpha \sin \phi \sin \lambda + \cos \alpha \cos \lambda & -\sin \alpha \cos \phi \\ -\cos \phi \cos \lambda & -\cos \phi \sin \lambda & -\sin \phi \end{pmatrix}. \quad (4.121)$$

Denoting the elements of  $C_e^w$  by  $c_{jk}$ , we see that

$$\omega_{ew}^w = \frac{1}{(N+h)(M+h)} \begin{pmatrix} v_2^w(M(1+e'^2 c_{23}^2) + h) + e'^2 M v_1^w c_{12} c_{23} \\ -v_1^w(M(1+e'^2 c_{13}^2) + h) - e'^2 M v_2^w c_{12} c_{23} \\ 0 \end{pmatrix}, \quad (4.122)$$

and, moreover,

$$N = \frac{a}{\sqrt{1-e^2 c_{3,3}^2}}, \quad M = \frac{a(1-e^2)}{(1-e^2 c_{3,3}^2)^{3/2}}. \quad (4.123)$$

Thus, since  $C_e^w$  is obtained from the rates,  $\omega_{ew}^w$ , by integrating (4.109), both depend only on the wander frame velocities. The integration (4.109) requires only a low-order algorithm (as described in Section 4.2.3.1), since the rates,  $\omega_{ew}^w$ , are small. In spherical approximation ( $e' = 0$ ), we also have

$$\omega_{ew}^w \approx \frac{1}{a+h} \begin{pmatrix} v_2^w \\ -v_1^w \\ 0 \end{pmatrix}, \quad (4.124)$$

which was to be expected.

Although all references to geodetic coordinates and the associated singularity have been removed from the integration algorithm for the wander frame velocities, ultimately, one desires the usual local-level,  $n$ -frame velocities, as well as latitude and longitude. The velocities are obtained from (4.111) and (4.11); while the azimuth and geodetic coordinates are given by

$$\begin{aligned}\phi &= \sin^{-1}(-c_{33}), \\ \lambda &= \tan^{-1}\left(\frac{c_{32}}{c_{31}}\right), \\ \alpha &= \tan^{-1}\left(\frac{-c_{23}}{c_{13}}\right),\end{aligned}\tag{4.125}$$

where  $c_{13}, c_{23}, c_{31}, c_{32}$ , and  $c_{33}$  are elements of  $C_e^w$ . Clearly, the singularity at the pole will affect the quality of  $\lambda$  and  $\alpha$ . However, this is outside the integration algorithm which is, therefore, unaffected.

Finally, as in other strapdown mechanizations, the transformation from the body frame to the  $w$ -frame,  $C_b^w$ , is realized by integrating

$$\dot{C}_b^w = C_b^w \Omega_{wb}^b,\tag{4.126}$$

where, in terms of the sensed rates,  $\omega_{ib}^b$ , the angular rates,  $\omega_{wb}^b$ , are given by (4.79):

$$\omega_{wb}^b = \omega_{ib}^b - C_w^b \omega_{iw}^w.\tag{4.127}$$

The rates,  $\omega_{iw}^w$ , needed in this integration come directly from the previous integration, according to (4.113).

In an effort to reduce the systematic errors of the IMU's, various forms of *carou-seling* of the platform have also been implemented, using either one or two gimbals. The objective is analogous to that of the initial calibration (Chapter 8), but in this case performed in real time throughout the mission. A typical rotation rate about the vertical, for example, would be  $\dot{\alpha} = 2\pi$  rad/min. As the sensors assume different orientations with respect to the acceleration and angular rate environments, one is able to solve for their long-wavelength systematic errors. Clearly, this type of mechanization is an extension of the wander azimuth principle and the navigation equations follow along similar lines.

#### 4.3.6 Numerical Integration of Navigation Equations

The navigation equations in an arbitrary frame are given by (4.77); and those for the velocity have the form

$$\frac{d}{dt} v^a = C_b^a a^b + f(x^a, v^a, \Omega_{ia}^a, \dot{\Omega}_{ia}^a, g^a).\tag{4.128}$$

Specific equations for the inertial, earth-fixed, local-level, and wander-azimuth frames were derived and are shown, respectively, in (4.80), (4.82), (4.102), and (4.107). Note that  $\dot{x}^a$  replaces  $v^a$  in the  $i$ -frame and  $e$ -frame formulations. With accelerometer data,  $a^b$ , these differential equations must be solved for the velocity,  $v^a$ , and ultimately for position. Generally, the terms collected by the vector function,  $f(\cdot)$ , are smaller and less variable than the sensed accelerations, given by the first term. This is due to the relatively slow rate of rotation of the  $a$ -frame with respect to the  $i$ -frame, as indicated by  $\Omega_{ia}^a$  that is dominated by Earth's rate of rotation for most vehicles, e.g., see (4.98). This allows integration of  $f(\cdot)$  with just a

first-order algorithm (rectangular rule, (2.103)), and requires only a calculated function value at one point (initial point or midpoint) of the integration interval. On the other hand, the integral of the first term in (4.128) requires a higher-order algorithm. However, in this way, the numerical solution of the navigation equation reduces from solving a differential equation to integrating simply a function.

Therefore, we approximate the integral of (4.128) as

$$\Delta \mathbf{v}^a = \int_{\Delta t} C_b^a(t') \mathbf{a}^b(t') dt' + \mathbf{f}(\mathbf{x}^a, \mathbf{v}^a, \Omega_{ia}^a, \dot{\Omega}_{ia}^a, \mathbf{g}^a) \Delta t, \quad (4.129)$$

where  $\Delta t$  is the integration interval. It is assumed that the transformation matrix,  $C_b^a$ , is determined concurrently with the velocities using numerical methods of sufficiently high order (see Section 4.2.3.1) to enable a high-order numerical evaluation of the first term of (4.129). As in Section 4.2.3.1, the sampling interval,  $\delta t = t_\ell - t_{\ell-1}$ ,  $\ell = 1, 2, \dots$ , is defined to correspond to the raw data rate of the IMU, or some multiple of it. The accelerometer output data arrive in the form of velocity increments, or pulses, that capture the time history of the acceleration over the sampling interval. Thus, these velocity increments are expressed exactly in terms of the body-frame acceleration as

$$\delta \mathbf{v}_\ell^b = \int_{t_{\ell-1}}^{t_\ell} \mathbf{a}^b(t') dt'. \quad (4.130)$$

The order of the adopted numerical integration algorithm determines the required number of data points. For a second-order algorithm (error  $\sim O(\Delta t^3)$ ), the integration interval may be set equal to the sampling interval; for a third-order algorithm,  $\Delta t = 2\delta t$ , as in (4.43). We consider only the third-order algorithm, which is the classic Simpson's Rule (2.105).

For the integration interval,  $[t_{\ell-2}, t_\ell]$ , we have the observations

$$\delta \mathbf{v}_{\ell-1}^b = \int_{t_{\ell-2}}^{t_{\ell-1}} \mathbf{a}^b(t') dt' \quad (4.131)$$

and

$$\delta \mathbf{v}_\ell^b = \int_{t_{\ell-1}}^{t_\ell} \mathbf{a}^b(t') dt'. \quad (4.132)$$

Following exactly the same procedure as for the angular observations in Section 4.2.3.1.2 (equations (4.45) through (4.53)), we find approximations to the accelerations at the appropriate epochs of the integration interval in terms of the observations, analogous to (4.52):

$$\begin{aligned} \hat{\mathbf{a}}_{\ell-2}^b \Delta t &= 3\delta \mathbf{v}_{\ell-1}^b - \delta \mathbf{v}_\ell^b, \\ \hat{\mathbf{a}}_{\ell-1}^b \Delta t &= \delta \mathbf{v}_{\ell-1}^b + \delta \mathbf{v}_\ell^b, \\ \hat{\mathbf{a}}_\ell^b \Delta t &= 3\delta \mathbf{v}_\ell^b - \delta \mathbf{v}_{\ell-1}^b. \end{aligned} \quad (4.133)$$

We now assume that the transformation matrix,  $C_b^a$ , has been estimated with sufficient precision at epochs  $t_{\ell-2}$ ,  $t_{\ell-1}$ , and  $t_\ell$ , according to some numerical algorithm for the quaternions, such as (4.61). For purposes of later error analyses, we assume that the model errors associated with the estimates,  $\hat{C}_b^a$ , are insignificant compared to the instrument errors. Simpson's rule (2.105) then provides the numerical algorithm for the first term in (4.129):

$$\int_{t_{\ell-2}}^{t_\ell} C_b^a(t') \mathbf{a}^b(t') dt' \approx \frac{\Delta t}{6} (\hat{C}_b^a(\ell-2) \hat{\mathbf{a}}_{\ell-2}^b + 4\hat{C}_b^a(\ell-1) \hat{\mathbf{a}}_{\ell-1}^b + \hat{C}_b^a(\ell) \hat{\mathbf{a}}_\ell^b), \quad (4.134)$$

where  $\hat{C}_b^a(\ell)$  is the estimate of  $C_b^a$  based on the estimate  $\hat{\mathbf{q}}_\ell$ . Therefore, using the acceleration estimates (4.133), the algorithm for the estimated velocity at epoch  $t_\ell$  is:

$$\begin{aligned} \hat{\mathbf{v}}_\ell^a &= \hat{\mathbf{v}}_{\ell-2}^a + \frac{1}{6} (\hat{C}_b^a(\ell-2)(3\delta\mathbf{v}_{\ell-1}^b - \delta\mathbf{v}_\ell^b) + 4\hat{C}_b^a(\ell-1)(\delta\mathbf{v}_{\ell-1}^b + \delta\mathbf{v}_\ell^b) \\ &\quad + \hat{C}_b^a(\ell)(3\delta\mathbf{v}_\ell^b - \delta\mathbf{v}_{\ell-1}^b)) + \hat{f}(\mathbf{x}^a, \mathbf{v}^a, \Omega_{ia}^a, \dot{\Omega}_{ia}^a, \mathbf{g}^a)_{t=t_{\ell-2}} \Delta t. \end{aligned} \quad (4.135)$$

Note that two separate iterations (with two sets of initial values) are required to obtain estimates at even and odd multiples of  $\Delta t$ . With deliberate interlacing of estimates the term,  $\hat{f}(\mathbf{x}^a, \mathbf{v}^a, \Omega_{ia}^a, \dot{\Omega}_{ia}^a, \mathbf{g}^a)\Delta t$ , in (4.135) could also be evaluated at  $t = t_{\ell-1}$ , with potential improvement in the integration accuracy.

Equation (4.135), in fact, represents a fourth-order algorithm for the velocity, provided the transformation matrix was obtained from a third-order algorithm. To show this, we first express the true sensed acceleration as a Taylor series (omitting coordinate-frame notation for convenience, and setting  $\ell = 2$  without loss in generality):

$$\mathbf{a}(t) = \mathbf{a}_0 + \dot{\mathbf{a}}_0(t - t_0) + \frac{1}{2!} \ddot{\mathbf{a}}_0(t - t_0)^2 + \frac{1}{3!} \dddot{\mathbf{a}}_0(t - t_0)^3 + \dots \quad (4.136)$$

Combining this with a similar true expression for the transformation matrix, (4.65), the integral on the left hand side of (4.134) is given by

$$\begin{aligned} &\int_{t_0}^{t_2} C_b^a(t') \mathbf{a}^b(t') dt' \\ &= C_0 \left[ \mathbf{a}_0 \Delta t + \frac{1}{2} (\Omega_0 \mathbf{a}_0 + \dot{\mathbf{a}}_0) \Delta t^2 + \frac{1}{6} ((\Omega_0^2 + \dot{\Omega}_0) \mathbf{a}_0 + 2\Omega_0 \dot{\mathbf{a}}_0 + \ddot{\mathbf{a}}_0) \Delta t^3 \right. \\ &\quad + \frac{1}{8} \left( \frac{1}{3} (\Omega_0^3 + 2\Omega_0 \dot{\Omega}_0 + \dot{\Omega}_0 \Omega_0 + \ddot{\Omega}_0) \mathbf{a}_0 + (\Omega_0^2 + \dot{\Omega}_0) \dot{\mathbf{a}}_0 + \Omega_0 \ddot{\mathbf{a}}_0 + \frac{1}{3} \dddot{\mathbf{a}}_0 \right) \Delta t^4 + \dots \left. \right]. \end{aligned} \quad (4.137)$$

Now, substitute (4.136) into

$$\delta v_1 = \int_{t_0}^{t_1} \mathbf{a}(t') dt', \quad \delta v_2 = \int_{t_1}^{t_2} \mathbf{a}(t') dt', \quad (4.138)$$

and integrate with respect to  $t'$ . Putting the resulting integrals into (4.133) yields

$$\begin{aligned} \hat{\mathbf{a}}_0 \Delta t &= \mathbf{a}_0 \Delta t - \frac{1}{12} \ddot{\mathbf{a}}_0 \Delta t^3 - \frac{1}{32} \dddot{\mathbf{a}}_0 \Delta t^4 + \dots, \\ \hat{\mathbf{a}}_1 \Delta t &= \mathbf{a}_0 \Delta t + \frac{1}{2} \dot{\mathbf{a}}_0 \Delta t^2 + \frac{1}{6} \ddot{\mathbf{a}}_0 \Delta t^3 + \frac{1}{24} \dddot{\mathbf{a}}_0 \Delta t^4 + \dots, \\ \hat{\mathbf{a}}_2 \Delta t &= \mathbf{a}_0 \Delta t + \dot{\mathbf{a}}_0 \Delta t^2 + \frac{5}{12} \ddot{\mathbf{a}}_0 \Delta t^3 + \frac{11}{96} \dddot{\mathbf{a}}_0 \Delta t^4 + \dots. \end{aligned} \quad (4.139)$$

Finally, we insert these into the right hand side of (4.134), together with  $\hat{C}_0$ ,  $\hat{C}_1$ , and  $\hat{C}_2$ , obtained from (4.65) (a third-order algorithm), respectively, for  $t = t_0, t_1, t_2$ . The result can be expressed as follows:

$$\int_{t_0}^{t_2} C(t') \mathbf{a}(t') dt' - \frac{\Delta t}{6} (\hat{C}_0 \hat{\mathbf{a}}_0 + 4\hat{C}_1 \hat{\mathbf{a}}_1 + \hat{C}_2 \hat{\mathbf{a}}_2) = O(\Delta t^5), \quad (4.140)$$

thus showing (4.134) to be a fourth-order algorithm for the velocities.

The error of numerical integration of the first term of (4.129) is known as the *sculling error*, in reference to the combined motion of linear acceleration and rotation, that is, sculling. As with the analogous coning error (Section 4.2.3.1.1), the sculling error can be reduced by decreasing the time increment of the numerical integration or by using a higher-order algorithm (see also Ignagni, 1998).

Assuming relatively benign vehicle dynamics, the choice of the order of the algorithm should ultimately depend on the accuracy of the instruments. From (4.137) we see that for vehicles with small derivatives of angular rate and of linear acceleration, the dominant neglected term of an  $m^{\text{th}}$ -order algorithm is

$$\delta v \approx C_0 \frac{1}{(m+1)!} \Omega_0^m \mathbf{a}_0 \Delta t^{m+1}. \quad (4.141)$$

The corresponding velocity error rate (error per unit time) is given by

$$|\delta \mathbf{a}| \approx \frac{1}{(m+1)!} \omega^m a \Delta t^m. \quad (4.142)$$

For a second-order algorithm, with  $|\omega| < 10^\circ/\text{s} = 0.17 \text{ rad/s}$ ,  $\Delta t = 1/128 \text{ s}$ , and  $a < 2g$ , the rate of algorithm error is  $\delta a \approx 6 \times 10^{-7} \text{ m/s}^2$ , just less than most accelerometer noise levels, but still high enough to warrant implementing a third-order model.

Finally, we note that the positions can be obtained from the velocities, again, by directly integrating (4.80) and (4.82), in the case of the  $i$ - and  $e$ -frames:

$$\hat{\mathbf{x}}_i^j = \hat{\mathbf{x}}_{i-2}^j + \hat{\mathbf{x}}_{i-1}^j \Delta t, \quad \hat{\mathbf{x}}_e^e = \hat{\mathbf{x}}_{e-2}^e + \hat{\mathbf{x}}_{e-1}^e \Delta t; \quad (4.143)$$

or, (4.103) for the  $n$ -frame:

$$\begin{aligned}\hat{\phi}_\ell &= \hat{\phi}_{\ell-2} + \frac{(\hat{v}_N)_{\ell-1} \Delta t}{\hat{M}_{\ell-1} + \hat{h}_{\ell-1}}, \\ \hat{\lambda}_\ell &= \hat{\lambda}_{\ell-2} + \frac{(\hat{v}_E)_{\ell-1} \Delta t}{(\hat{N}_{\ell-1} + \hat{h}_{\ell-1}) \cos \hat{\phi}_{\ell-1}}, \\ \hat{h}_\ell &= \hat{h}_{\ell-2} - (\hat{v}_D)_{\ell-1} \Delta t.\end{aligned}\tag{4.144}$$

For the  $w$ -frame, the positions are determined from (4.125) by integrating  $\dot{C}_e^w$ .

# 5 System Error Dynamics

## 5.1 Introduction

The inertial navigation system is a rather complex assemblage of up to six mechanical and/or optical sensors, each responding to physical and systematic effects extraneous to the actual desired navigation function, as well as to internal random errors of various characters and consequences. It is important, therefore, to develop the proper dynamics and stochastic models for the system errors in order to understand their effect on the navigation solution and to enable the estimation of these errors using external (i.e., independent) measurements, if available. In the following two chapters, these models will be derived and expounded. The first part, the object of this chapter, elaborates on the physical and mathematical relationships between the instrument errors, treated in a general way, and the ensuing errors in the navigation solution. The result is a mathematical model, i.e., a deterministic error dynamics model, that is rigorous to first-order approximations and is based on given physical principles. This model describes how the sensor errors propagate through the system into navigation errors. The subsequent chapter considers the stochastic nature of certain types of errors. The dynamics error model serves then also to characterize the propagation of errors from sensors to navigation solution in a stochastic setting.

In Chapter 4, the navigation equations were developed for a general frame and specialized to a number of useful coordinatizations. These equations are differential equations for the velocity and position, where the forcing functions are the sensed accelerations that are properly oriented with information provided by the gyros. How the sensor errors affect the position (and velocity) is described by the *error dynamics equations*. We derive these equations by applying a differential operator to the navigation equations. That is, the variables of the navigation equations are perturbed differentially and the differentials are then interpreted as small differences, or errors. More rigorously, one may think of analytically expanding the position, velocity, and other variables, as given by the navigation equations (4.77), in a Taylor series about their approximate values (cf. (2.96)):

$$\begin{aligned} \mathbf{0} = \mathbf{f}(\mathbf{x}^a, \dot{\mathbf{x}}^a, \Omega_{ia}^a, \dot{\Omega}_{ia}^a, \mathbf{a}^a, \mathbf{g}^a) &= \mathbf{f}(\tilde{\mathbf{x}}^a, \dot{\tilde{\mathbf{x}}}^a, \tilde{\Omega}_{ia}^a, \dot{\tilde{\Omega}}_{ia}^a, \tilde{\mathbf{a}}^a, \tilde{\mathbf{g}}^a) \\ &+ \frac{\partial \mathbf{f}}{\partial \mathbf{x}^a} (\mathbf{x}^a - \tilde{\mathbf{x}}^a) + \frac{\partial \mathbf{f}}{\partial \dot{\mathbf{x}}^a} (\dot{\mathbf{x}}^a - \dot{\tilde{\mathbf{x}}}^a) \\ &+ \frac{\partial \mathbf{f}}{\partial \Omega_{ia}^a} (\Omega_{ia}^a - \tilde{\Omega}_{ia}^a) + \frac{\partial \mathbf{f}}{\partial \dot{\Omega}_{ia}^a} (\dot{\Omega}_{ia}^a - \dot{\tilde{\Omega}}_{ia}^a) \\ &+ \frac{\partial \mathbf{f}}{\partial \mathbf{a}^a} (\mathbf{a}^a - \tilde{\mathbf{a}}^a) + \frac{\partial \mathbf{f}}{\partial \mathbf{g}^a} (\mathbf{g}^a - \tilde{\mathbf{g}}^a) + \dots \end{aligned} \quad (5.1)$$

Differences with respect to the “Taylor expansion point”,  $(\tilde{\mathbf{x}}^a, \dot{\tilde{\mathbf{x}}}^a, \tilde{\Omega}_{ia}^a, \dot{\tilde{\Omega}}_{ia}^a, \tilde{\mathbf{a}}^a, \tilde{\mathbf{g}}^a)$ ,

represent negative errors, and the partial derivatives (being represented with some notational license) are evaluated at this Taylor point. An important assumption that we will make here is  $f(\tilde{\mathbf{x}}^a, \dot{\tilde{\mathbf{x}}}^a, \tilde{\Omega}_{ia}^a, \tilde{\dot{\Omega}}_{ia}^a, \tilde{\mathbf{a}}^a, \tilde{\mathbf{g}}^a) = \mathbf{0}$ , meaning that the approximate values are not all independently determined.

In either case, using differentials or a Taylor expansion, we neglect higher than first-order terms; and thus, the error dynamics equations become *linear* models of the errors. Clearly, the underlying assumption is that the errors are small, where “smallness”, obviously, is a subjective portrayal that affects the validity, or accuracy, of the model. Should the errors be not sufficiently small, the model may require augmentation with second-order terms. It is noted that at this point the model may be a nonlinear function of time. Linearization with respect to time will be treated in Chapter 7.

The formulation of the error dynamics equation is developed in a unified way for arbitrary coordinatization which then allows specialization to specific frames. In particular, we consider the inertial (*i*-frame), ECEF (*e*-frame), and local-level (*n*-frame) constructions, where it should be recognized that the *n*-frame specialization is really the *e*-frame formulation reoriented along local-level directions. That is, no horizontal motion occurs in the *n*-frame that, by definition, moves with the navigation system over or near the Earth’s surface.

The comprehensive development of the error dynamics model tends to obfuscate the character of the navigation error dynamics. Therefore, we start with a simplified, approximate error analysis, which turns out to be, in fact, quite accurate for short-duration applications. This will be verified later by reducing the complete model to its essential components with appropriate approximations.

## 5.2 Simplified Analysis

It is most instructive to consider the error dynamics in a local coordinate frame on a non-rotating Earth, where the inertial measurement units (IMU’s) also do not rotate, so that the instrument frame and local frame are parallel. And, by restricting the motion to a local region (no rotation), we may assume that the local frame is the inertial frame. Let the coordinates be rectangular ( $x_i$ ) where the 3-axis is aligned with the local vertical (Figure 5.1). The most convenient frame for the gravitational field is Earth-centered. Therefore, while the frame is local in the horizontal directions, the vertical coordinate is reckoned from the Earth’s center, that is, the coordinate origin. The upward (radial) direction is positive and, for a right-handed system, suppose the horizontal coordinates increase in value northward and westward.

In this frame, the navigation equations for position are given by (4.69), repeated here for convenience without frame notation:

$$\ddot{\mathbf{x}} = \mathbf{g}(\mathbf{x}) + \mathbf{a}, \quad (5.2)$$

where  $\mathbf{x}$  is the position vector;  $\mathbf{g}$  is the acceleration generated by the gravitational field in this frame and depends on the position vector; and  $\mathbf{a}$  is the specific force, i.e., the quantity sensed by the accelerometer.

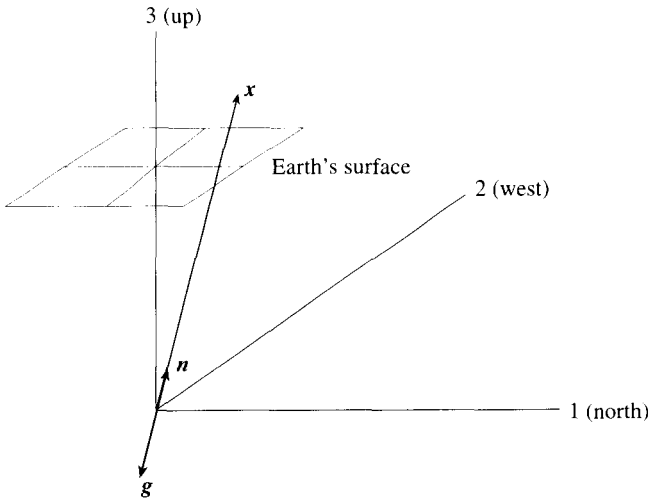


Figure 5.1: Approximate, locally inertial coordinate frame.

The position errors to first order due to errors in the system are obtained by perturbing equation (5.2), that is, by applying the differential operator,  $\delta$ . Here and subsequently we take for granted the interchangeability of the operators  $\delta$  and  $d/dt$ ; we also presume that the differential operator obeys the usual rules for differentiation. Thus

$$\delta\ddot{\mathbf{x}} = \frac{\partial \mathbf{g}}{\partial \mathbf{x}} \delta \mathbf{x} + \delta \mathbf{g} + \delta \mathbf{a}, \quad (5.3)$$

where the “derivative”  $\partial \mathbf{g} / \partial \mathbf{x}$  is a notational convenience representing the second-order tensor of partial derivatives of the gravitation vector components with respect to the coordinates:

$$\frac{\partial \mathbf{g}}{\partial \mathbf{x}} = \begin{pmatrix} \frac{\partial g_1}{\partial x_1} & \frac{\partial g_1}{\partial x_2} & \frac{\partial g_1}{\partial x_3} \\ \frac{\partial g_2}{\partial x_1} & \frac{\partial g_2}{\partial x_2} & \frac{\partial g_2}{\partial x_3} \\ \frac{\partial g_3}{\partial x_1} & \frac{\partial g_3}{\partial x_2} & \frac{\partial g_3}{\partial x_3} \end{pmatrix}. \quad (5.4)$$

Equation (5.3) is a (time-) differential equation for the position error,  $\delta \mathbf{x}$ , and accordingly describes its dynamics. Specifically, its second time derivative equals the sum of errors in the accelerometer output,  $\delta \mathbf{a}$ , plus errors in our knowledge of the gravitational acceleration,  $\delta \mathbf{g}$ , plus the change in the value of gravitation due to the positional uncertainty,  $\delta \mathbf{x}$ .

For the present purposes, the Earth’s gravitational acceleration may be approximated as that of a homogeneously dense sphere, which according to Newton’s Law

of Gravitation (1.6) is given by

$$\mathbf{g} \approx \left( \frac{-kM}{r^2} \right) \mathbf{n}, \quad (5.5)$$

where  $r^2 = x_1^2 + x_2^2 + x_3^2$  is the squared distance from the Earth's center (for points on the Earth's surface,  $r$  is approximately 6370000 m),  $\mathbf{n} = \mathbf{x}/r$  is a unit vector pointing outward along the radial direction, and  $kM$  is the gravitational constant times the mass of the Earth ( $kM \approx 3.986 \times 10^{14} \text{ m}^3/\text{s}^2$ ). The tensor  $\partial\mathbf{g}/\partial\mathbf{x}$ , (5.4), is then given by

$$\frac{\partial\mathbf{g}}{\partial\mathbf{x}} = kM \begin{pmatrix} \frac{-1}{r^3} + 3\frac{x_1^2}{r^5} & -3\frac{x_1x_2}{r^5} & -3\frac{x_1x_3}{r^5} \\ -3\frac{x_2x_1}{r^5} & \frac{-1}{r^3} + 3\frac{x_2^2}{r^5} & -3\frac{x_2x_3}{r^5} \\ -3\frac{x_3x_1}{r^5} & -3\frac{x_2x_3}{r^5} & \frac{2}{r^3} - 3\frac{x_1^2 + x_2^2}{r^5} \end{pmatrix}. \quad (5.6)$$

For local excursions of the IMU, the  $x_1$  and  $x_2$  components are small and the terms containing  $r^{-5}$  can be neglected, giving:

$$\frac{\partial\mathbf{g}}{\partial\mathbf{x}} \approx \frac{kM}{r^3} \begin{pmatrix} -1 & 0 & 0 \\ 0 & -1 & 0 \\ 0 & 0 & 2 \end{pmatrix}. \quad (5.7)$$

The approximation (5.5) together with (5.7) is quite reasonable since the approximate gravitational gradients in (5.7) deviate from the true gradients of the Earth's gravitational field typically by less than 50 E (1 E = 1 Eötvös Unit =  $10^{-9} \text{ s}^{-2}$ ) in relatively smooth terrain (anomalous gradients of up to a thousand Eötvös are possible in very mountainous terrain), while the main term of the *horizontal* gradient, included in (5.7), is about 1500 E. For small  $\delta\mathbf{x}$ , corresponding to an accumulation of position error over short duration, the gravitational gradient term in (5.3) could be neglected altogether (e.g., if  $\delta x_1 = 1 \text{ m}$ , then  $(\partial g_1/\partial x_1)\delta x_1 \approx -1.5 \times 10^{-6} \text{ m/s}^2$ , which is about an order of magnitude smaller than the noise of a typical accelerometer of medium to high quality). Clearly, the approximation (5.7) is adequate for present purposes. In fact, if one implicitly considers that the local frame moves with the system, then (5.7) is a very good approximation, even for longer times. This will be more rigorously demonstrated with the complete model development.

Substituting (5.7) into (5.3), one obtains differential equations for each component of the position error:

$$\delta\ddot{x}_1 + \frac{kM}{r^3}\delta x_1 = \delta g_1 + \delta a_1, \quad (5.8)$$

$$\delta\ddot{x}_2 + \frac{kM}{r^3}\delta x_2 = \delta g_2 + \delta a_2, \quad (5.9)$$

$$\delta\ddot{x}_3 - 2\frac{kM}{r^3}\delta x_3 = \delta g_3 + \delta a_3. \quad (5.10)$$

The differential equation for each of the *horizontal* components, (5.8) or (5.9), represents a forced harmonic oscillator, (2.82), with resonant frequency,

$$\omega_S = \sqrt{\frac{kM}{r^3}}, \quad (5.11)$$

which is the Schuler frequency (corresponding period of 84.4 minutes) already encountered in Chapter 4, equation (4.5). In fact, equation (4.4), representing the dynamics of the misalignment angle of the local-level stabilized platform, is identical to (5.8), considering that a position change  $\delta x_1$  on the Earth corresponds to a correction,  $-R\eta$ , to the misalignment of the platform.

The *homogeneous solutions* (the right sides of (5.8) and (5.9) are set equal to zero) are given according to (2.49) by:

$$\delta x_{1H}(t) = A_1 \cos(\omega_S t) + B_1 \sin(\omega_S t), \quad (5.12)$$

$$\delta x_{2H}(t) = A_2 \cos(\omega_S t) + B_2 \sin(\omega_S t), \quad (5.13)$$

where the constant coefficients of the sinusoids are determined from initial conditions (at  $t = t_0 = 0$ ):

$$\begin{aligned} A_1 &= \delta x_1(0), \quad A_2 = \delta x_2(0), \\ B_1 &= \frac{\delta \dot{x}_1(0)}{\omega_S}, \quad B_2 = \frac{\delta \dot{x}_2(0)}{\omega_S}. \end{aligned} \quad (5.14)$$

Note that initial errors in horizontal position and velocity result in bounded navigation errors oscillating at the Schuler frequency.

The homogeneous solution of the equation for the vertical component, (5.10), depends exponentially on time, as given by (2.48):

$$\begin{aligned} \delta z_H(t) &= C e^{\sqrt{2}\omega_S t} + D e^{-\sqrt{2}\omega_S t} \\ &= A_3 \cosh(\sqrt{2}\omega_S t) + B_3 \sinh(\sqrt{2}\omega_S t), \end{aligned} \quad (5.15)$$

where, again,  $C$  and  $D$ , or  $A_3$  and  $B_3$ , are constants:

$$A_3 = \delta x_3(0), \quad B_3 = \frac{\delta \dot{x}_3(0)}{\sqrt{2}\omega_S}. \quad (5.16)$$

An initial error in the vertical position causes the corresponding navigation solution to fail rapidly since the errors increase exponentially without bound. The time constant for the vertical error is  $1/(\sqrt{2}\omega_S) = 9.5$  minutes. It corresponds to the interval from the initial time during which vertical navigation errors remain below about three times the initial error; this may be considered tolerable.

Of specific interest are the *particular solutions* (non-zero right hand sides) of (5.8), (5.9), and (5.10) since they depend on the type of disturbing, or forcing, function applied to the system. As with a general harmonic oscillator, any horizontal forcing term having the resonant, or Schuler, frequency, will amplify the navigation error, while, generally, forcing terms at other frequencies will be modulated by  $\omega_S$ . Let the

forcing function be denoted by  $\mathbf{f}(t)$ ; for our simplified analysis it is given by:

$$\mathbf{f}(t) = \delta\mathbf{a} + \delta\mathbf{g}. \quad (5.17)$$

It should be noted here that the gravitational error (our lack of complete knowledge of the gravitational acceleration) depends on time because of the motion of the vehicle; more specifically, it depends on the vehicle's position which is a function of time, and we may write  $\delta\mathbf{g} \equiv \delta\mathbf{g}(\mathbf{x}(t))$ . Of course, the accelerometer error is also a function of time and the forcing function in (5.17) is, indeed, appropriately formulated.

The particular solutions of (5.8)–(5.10), extracted from (2.84) and (2.85), are given by

$$\delta x_{1_p}(t) = \frac{1}{\omega_S} \int_0^t \sin(\omega_S \tau) f_1(t - \tau) d\tau, \quad (5.18)$$

$$\delta x_{2_p}(t) = \frac{1}{\omega_S} \int_0^t \sin(\omega_S \tau) f_2(t - \tau) d\tau, \quad (5.19)$$

$$\delta x_{3_p}(t) = \frac{1}{\sqrt{2}\omega_S} \int_0^t \sinh(\sqrt{2}\omega_S \tau) f_3(t - \tau) d\tau, \quad (5.20)$$

where for convenience (and noting that  $t_0 = 0$ ) we changed integration variables,  $t - \tau \rightarrow \tau$ . Although the total horizontal position errors have an oscillatory character, whether or not they are bounded depends on the forcing function,  $f$ ; if the latter is bounded, so is the error. As in the homogeneous case, the vertical position error is unbounded, unless  $f_3$  decreases sufficiently fast to zero.

We consider several special cases of the forcing function. For actual navigation systems, a suitable model may be constructed from a linear combination of such specialized forms. The first example assumes that the components of  $\mathbf{f}$  are constants,  $c$ :  $f_j(t) = c$  (e.g., an accelerometer bias). The particular solution for the horizontal position errors is then

$$\delta x_{1_p}(t) = \frac{c}{\omega_S^2} [1 - \cos \omega_S t] \approx \frac{1}{2} ct^2, \quad (5.21)$$

where, without loss in generality, only one of the horizontal dimensions is illustrated (the same result would hold for (5.19)). For the vertical channel we have

$$\delta x_{3_p}(t) = \frac{c}{2\omega_S^2} [\cosh(\sqrt{2}\omega_S t) - 1] \approx \frac{1}{2} ct^2. \quad (5.22)$$

The approximations in (5.21) and (5.22) hold only for small  $t$ ; and they were derived using series expansions for  $\cos(p)$  (see (1.30)) and  $\cosh(p)$ . Specifically, the position errors, whether horizontal or vertical, grow approximately with the square of time, as one would expect from *Galileo's law of falling bodies* (this law expresses the distance,

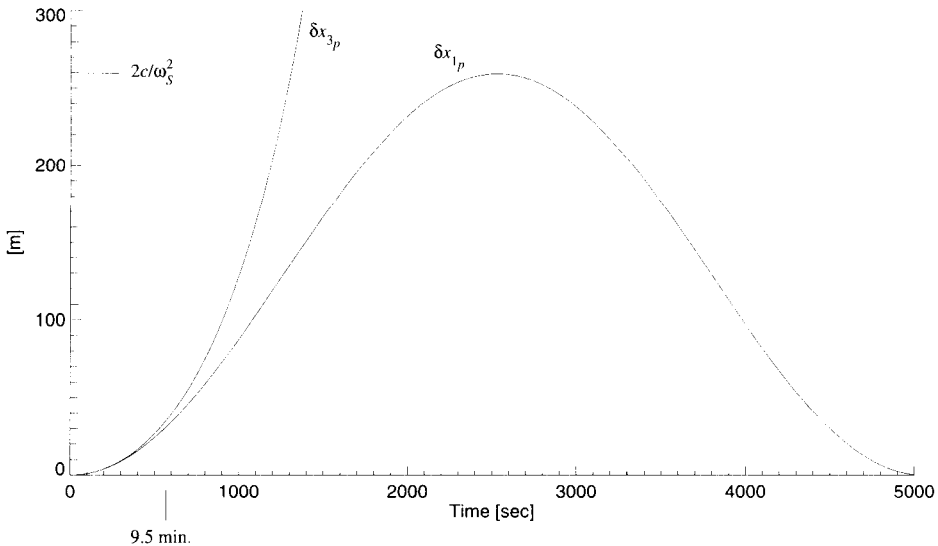


Figure 5.2: Position errors due to unknown accelerometer biases.

$x$ , travelled under the influence of acceleration,  $a$ , as depending on the square of time:  $x = at^2/2$ . As time progresses, however, the horizontal position error remains bounded by  $2c/\omega_S^2$ , while the vertical position error grows without bound. The latter may be approximated, for  $t > 20$  min, by:

$$\delta x_{3p}(t) \approx \frac{c}{4\omega_S^2} e^{\sqrt{2}\omega_S t}. \quad (5.23)$$

Figure 5.2 shows these position errors for an accelerometer bias,  $c = 2 \times 10^{-4}$  m/s<sup>2</sup>.

The boundedness of the horizontal error, even in the presence of an acceleration bias, is a consequence of navigating on a spherical surface with a central gravitational field. This was demonstrated from a more geometrical viewpoint in Chapter 4. Because of the unboundedness of the vertical position error, the INS is not used to navigate in the vertical. However, for short time intervals (few minutes), it is as accurate as in the horizontal channels; and, in the long run, the errors can be bounded by introducing external altitude information from a barometer, or altimeter, or GPS—this is called *vertical channel damping*.

For the second example, the forcing term is a linear drift:  $f_j(t) = ct$ . Then the particular solutions are

$$\delta x_{1p}(t) = \frac{c}{\omega_S^2} \left[ 1 - \frac{1}{\omega_S} \sin \omega_S t \right] \approx \frac{1}{6} c t^3 \quad (5.24)$$

and

$$\delta x_{3p}(t) = \frac{c}{2\omega_S^2} \left[ \frac{1}{\sqrt{2}\omega_S} \sinh(\sqrt{2}\omega_S t) - t \right] \approx \frac{1}{6} c t^3, \quad (5.25)$$

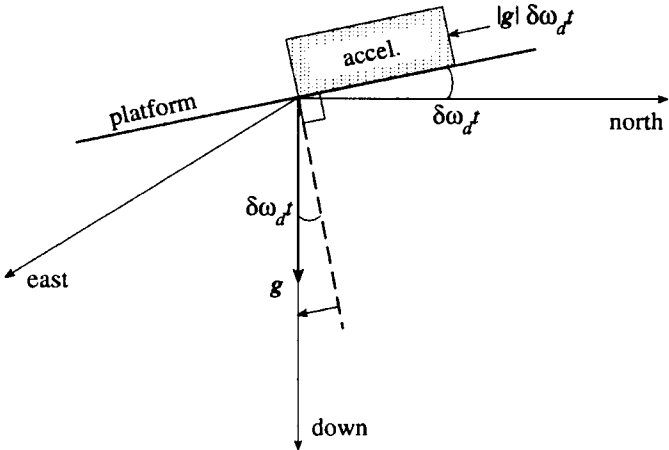


Figure 5.3: Platform tilt error causes acceleration error.

where, again, the approximations hold only for small  $t$ . We see that in this case the horizontal position errors generally grow with time, initially with the cube of time. In the long run, the drift more seriously contributes to the position error than the bias.

A drift error in the orientation of a supposedly level platform, denoted by the angular rate  $\delta\omega_d$ , causes an acceleration error as the reaction to the gravity vector couples into the horizontal acceleration. With the help of Figure 5.3, we find that this error is given by  $g\delta\omega_d t$ , where  $g \approx 9.8 \text{ m/s}^2$  is the magnitude of gravity. Hence, in this case,  $c = g\delta\omega_d$ , and the *average velocity* error in the long run (that is, considering only the non-periodic part) is determined from the derivative of the first term in (5.24) to be:

$$\frac{c}{\omega_S^2} \approx \frac{g\delta\omega_d}{g/R} = R\delta\omega_d, \quad (5.26)$$

where (4.5) was used and  $R$  is the mean radius of the Earth. Since one degree of arc on the Earth is about  $R \cdot 1^\circ \cdot (\pi/180^\circ) \approx 111 \text{ km}$ , we have a simple “rule of thumb”: *the velocity error is approximately 1 km/hr per gyro drift of 0.01 °/hr*. For example, one can roughly estimate that an inertial navigation system with gyros drifting at a rate of  $0.1^\circ/\text{hr}$  will cause (horizontal) position errors to grow to 10 km after one hour. Figure 5.4 shows the position error behavior due to this drift in more detail, demonstrating also the exponential error growth in the vertical channel.

As a final case, consider the forcing function with sinusoidal components having constant amplitude,  $c$ , frequency,  $\omega$ , and phase,  $\phi$ :  $f_j(t) = c \cos(\omega t + \phi)$ . Then it can be shown by performing the integrations in (5.18) and (5.20) that

$$\delta x_{1p}(t) = \begin{cases} \frac{c}{\omega^2 - \omega_S^2} \left[ (\cos \omega_S t - \cos \omega t) \cos \phi - \left( \frac{\omega}{\omega_S} \sin \omega_S t - \sin \omega t \right) \sin \phi \right], & \omega \neq \omega_S; \\ \frac{c}{2\omega_S^2} [\omega_S t \sin \omega_S t \cos \phi + (\omega_S t \cos \omega_S t - \sin \omega_S t) \sin \phi], & \omega = \omega_S; \end{cases} \quad (5.27)$$

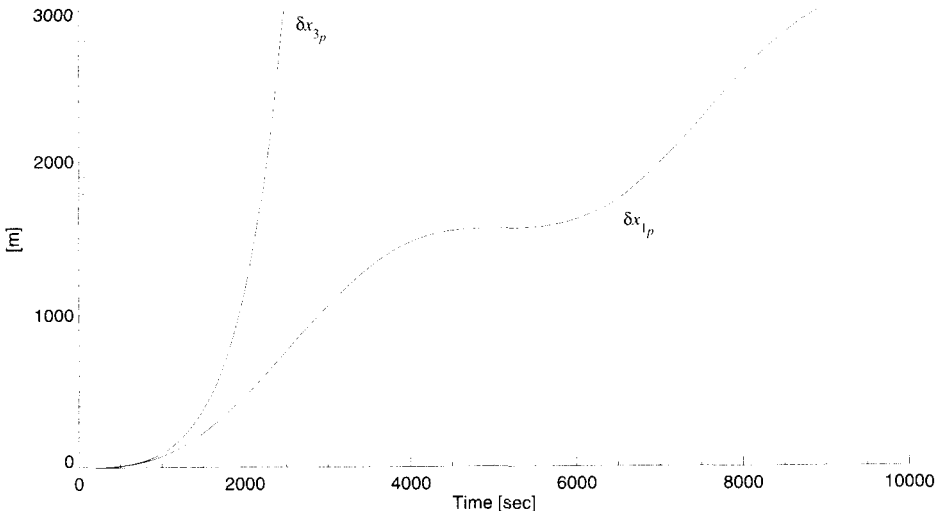


Figure 5.4: Position errors due to unknown constant gyro drifts.

and

$$\begin{aligned} \delta x_{3p}(t) = & \frac{c}{2\omega_S^2 + \omega^2} \left[ (\cosh(\sqrt{2}\omega_S t) - \cos \omega t) \cos \phi \right. \\ & \left. - \left( \frac{\omega}{\sqrt{2}\omega_S} \sinh(\sqrt{2}\omega_S t) - \sin \omega t \right) \sin \phi \right]. \end{aligned} \quad (5.28)$$

The resonance in (5.27) at  $\omega = \omega_S$  is evident as the solution increases without bound in this case. That is, if the forcing function contains significant power at the Schuler frequency, the errors will oscillate with linearly increasing amplitude. As before, the vertical position error grows without bound for all frequencies as time increases. Figure 5.5 shows how equation (5.18) translates an east horizontal gravity component ( $f_2 = g_E$ ) into an east position error. The gravity profile comes from an area of the Canadian Rockies at 5000 m flight altitude and its oscillatory character is reflected to some extent in the position error, as predicted by the first equation in (5.27).

### 5.3 Linearized Error Equations

For a unified development of the error dynamics, we begin with the navigation equations in the general  $a$ -frame coordinatization, equations (4.77). As in the previous simplified treatment, we differentially perturb these equations, again tacitly assuming the commutativity of the differential operator,  $\delta$ , and the time differentiation operator,  $d/dt$ , and then interpret the perturbations as errors (resulting in a

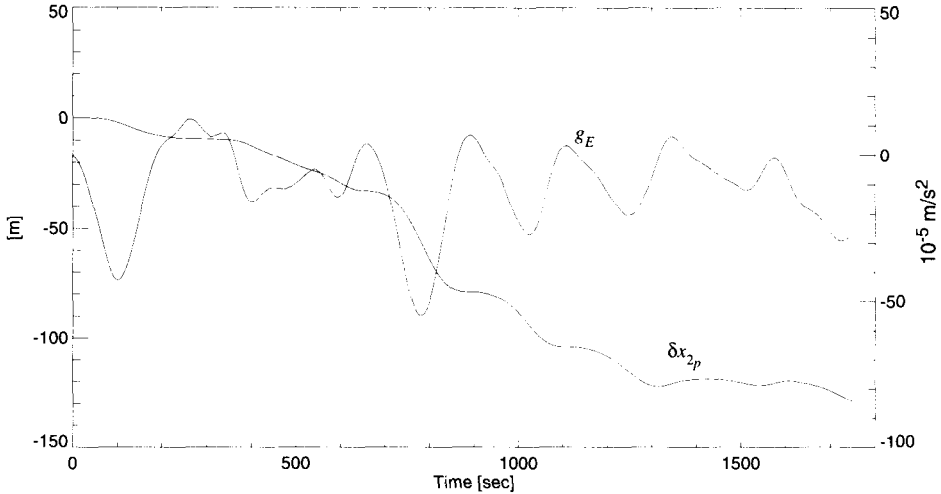


Figure 5.5: Position error due to horizontal gravity component.

linear model). The differential perturbation of (4.77) is given by

$$\begin{aligned} \frac{d}{dt} \delta \dot{x}^a &= -2\delta\Omega_{ia}^a \dot{x}^a - 2\Omega_{ia}^a \delta \dot{x}^a - (\delta\dot{\Omega}_{ia}^a + \delta\Omega_{ia}^a \Omega_{ia}^a + \Omega_{ia}^a \delta\Omega_{ia}^a) \dot{x}^a \\ &\quad - (\dot{\Omega}_{ia}^a + \Omega_{ia}^a \Omega_{ia}^a - \Gamma^a) \delta x^a + \delta a^a + \delta g^a, \end{aligned} \quad (5.29)$$

$$\frac{d}{dt} \delta x^a = \delta \dot{x}^a,$$

where  $\Gamma^a = \partial g^a / \partial x^a$  is the tensor of gravitational gradients in the  $a$ -frame. The perturbation,  $\delta g^a$ , is called the *gravitational disturbance vector*. Each of the differentials  $\delta\Omega_{ia}^a$ ,  $\delta\dot{\Omega}_{ia}^a$ , and  $\delta a^a$  may include differentials of the velocity, position, and orientation variables in the navigation solution, as well as differentials of the sensed acceleration and angular rates.

In particular, the perturbation  $\delta a^a$ , interpreted as the error in the expression in the  $a$ -frame of the sensed acceleration, represents not only accelerometer errors but also orientation errors that are committed when transforming sensed accelerations from the sensor frame ( $s$ -frame) to the  $a$ -frame. In accordance with the discussion of Section 1.2.3, we use the sensor frame in our analysis of how sensor errors affect inertial navigation. Thus, the development is independent of the mechanization of the system and applies to both stabilized and strapdown configurations with appropriate interpretations of the sensor frame. The specific constituents of the sensor-frame errors in acceleration and angular rate,  $\delta a^s$  and  $\delta \omega_{is}^s$ , may depend on the particular instrumentation and how it is mechanized. These are discussed in Chapter 3.

Taking differentials of the relation  $a^a = C_s^a a^s$ , we obtain

$$\delta a^a = \delta C_s^a a^s + C_s^a \delta a^s. \quad (5.30)$$

Furthermore, the transformation,  $C_s^a$ , from the sensor frame to the  $a$ -frame may be decomposed according to

$$C_s^a = C_i^a C_s^i. \quad (5.31)$$

Whether or not the transformation from the  $i$ -frame to the  $a$ -frame is known without error depends on our choice of the  $a$ -frame. For example, if it is the  $n$ -frame, the transformation is defined by the position (latitude and longitude) of the inertial navigation system; in this case it is not known exactly, since the position coordinates are to be determined by the INS. On the other hand, the transformation  $C_i^a$  is errorless for all times if the  $a$ -frame is the  $e$ -frame or the  $i$ -frame. The other transformation in (5.31) from the  $s$ -frame to the  $i$ -frame is determined by the output of the system gyros which always includes sensor errors. Therefore, in addition to sensor errors,  $\delta a^a$  must account for the effect of an imperfect transformation from the  $s$ -frame due to errors in the angles as indicated by the gyros, and possibly for effects due to errors in the realization of the  $a$ -frame.

We have described the orientation error in a computational setting that represents the strapdown system, but the same holds for a stabilized mechanization. In that case the transformation,  $C_s^a$ , is effected mechanically and is subject to exactly the same errors (if we neglect servo motor errors). If the  $a$ -frame is the  $n$ -frame,  $C_i^n$  corresponds to the Schuler tuning which depends on knowing the position of the system, and  $C_s^i$  corresponds essentially to the stabilization using the gyros.

In either case, the differential  $\delta C_s^a$  is caused by errors in the orientation of the  $s$ -frame with respect to the  $a$ -frame; and it is thus endowed with a dynamic character. To formulate these dynamics, it is convenient to represent  $\delta C_s^a$  in terms of small error angles, one for each of the frame axes:  $\psi^a = (\psi_1^a, \psi_2^a, \psi_3^a)^T$ . We may represent this in the equivalent form of a skew-symmetric matrix:

$$\Psi^a = \begin{pmatrix} 0 & -\psi_3^a & \psi_2^a \\ \psi_3^a & 0 & -\psi_1^a \\ -\psi_2^a & \psi_1^a & 0 \end{pmatrix}. \quad (5.32)$$

In conformity with (1.25), the matrix  $I - \Psi^a$  describes a transformation due to small-angle rotations from the true  $a$ -frame to the erroneously computed (or, otherwise realized)  $a$ -frame. That is, the *computed* (or, mechanically achieved) transformation may be represented as a sequence of two transformations comprising first the true transformation followed by an error transformation:

$$\hat{C}_s^a = (I - \Psi^a) C_s^a. \quad (5.33)$$

The computed transformation is denoted with the hat ("^"), and although it includes errors it is also *orthogonal*, by definition. That is, it is computed (or, applied) under the assumption of orthogonality. It is now evident that

$$\begin{aligned} \delta C_s^a &= \hat{C}_s^a - C_s^a \\ &= -\Psi^a C_s^a. \end{aligned} \quad (5.34)$$

Substituting (5.34) into (5.30), we obtain

$$\begin{aligned}\delta \mathbf{a}^a &= C_s^a \delta \mathbf{a}^s - \Psi^a C_s^a \mathbf{a}^s \\ &= C_s^a \delta \mathbf{a}^s + \mathbf{a}^a \times \boldsymbol{\psi}^a,\end{aligned}\quad (5.35)$$

where the second line follows from the equivalence of skew-matrix multiplication and vector cross-product (see (1.55)). Note the analogy of (5.35) with the Coriolis Law (1.70), from which it could also be derived directly.

We now establish the dynamic behavior of the error angles  $\boldsymbol{\psi}^a$  in the form of a differential equation analogous to (5.29). Toward this end, we take the differential of  $\dot{C}_s^a$  given in the form (1.68):

$$\begin{aligned}\delta \dot{C}_s^a &= \delta(C_s^a \Omega_{as}^s) \\ &= \delta C_s^a \Omega_{as}^s + C_s^a \delta \Omega_{as}^s,\end{aligned}\quad (5.36)$$

where the perturbation in angular rate,  $\delta \Omega_{as}^s$ , is interpreted as the error in the corresponding computed value, denoted by  $\hat{\Omega}_{as}^s$ :

$$\delta \Omega_{as}^s = \hat{\Omega}_{as}^s - \Omega_{as}^s. \quad (5.37)$$

Differentiating the second line of equation (5.34) with respect to time and setting the result equal to the right side of (5.36), we get

$$-\dot{\Psi}^a C_s^a - \Psi^a C_s^a \Omega_{as}^s = \delta C_s^a \Omega_{as}^s + C_s^a \delta \Omega_{as}^s. \quad (5.38)$$

Substituting for  $\Psi^a C_s^a$  from (5.34) and solving for  $\dot{\Psi}^a$  yields:

$$\dot{\Psi}^a = -C_s^a \delta \Omega_{as}^s C_a^s. \quad (5.39)$$

In terms of vectors, it is easily verified that this is equivalent to

$$\dot{\boldsymbol{\psi}}^a = -C_s^a \delta \omega_{as}^s, \quad (5.40)$$

where  $\delta \omega_{as}^s$  is the error in the rotation rate of the  $s$ -frame with respect to the  $a$ -frame (coordinatized in the  $s$ -frame). This is now separated explicitly into gyro errors and possible  $a$ -frame orientation errors as follows.

The gyros sense the inertial rates,  $\omega_{is}^s$ , of the  $s$ -frame, which is the sum, according to (1.61), of the rotation rate of the  $s$ -frame relative to the  $a$ -frame plus that of the  $a$ -frame relative to the  $i$ -frame:

$$\omega_{is}^s = \omega_{ia}^s + \omega_{as}^s. \quad (5.41)$$

A perturbation of this equation, where first we substitute  $\omega_{ia}^s = C_a^s \omega_{ia}^a$ , yields

$$\begin{aligned}\delta \omega_{is}^s &= \delta C_a^s \omega_{ia}^a + C_a^s \delta \omega_{ia}^a + \delta \omega_{ab}^s \\ &= C_a^s \Psi^a \omega_{ia}^a + C_a^s \delta \omega_{ia}^a + \delta \omega_{as}^s.\end{aligned}\quad (5.42)$$

The second line follows from the transpose of (5.34), i.e.,  $\delta C_a^s = \hat{C}_a^s - C_a^s = (\delta C_s^a)^T$ ; and hence

$$\delta C_a^s = C_a^s \Psi^a, \quad (5.43)$$

noting that  $\Psi^a$  is skew symmetric. Solving (5.42) for  $\delta\omega_{as}^s$  and substituting this into (5.40) yields the error dynamics equation for the angles in the transformation from the  $s$ -frame to the  $a$ -frame:

$$\dot{\psi}^a = -\omega_{ia}^a \times \psi^a - C_s^a \delta\omega_{is}^s + \delta\omega_{ia}^a, \quad (5.44)$$

where the cross-product term is the same as  $\Psi^a \omega_{ia}^a$ . The dynamic behavior of  $\psi^a$  depends on the vector,  $\delta\omega_{is}^s$ , that denotes the sensor error in indicated angular rates, and on  $\delta\omega_{ia}^a$  that represents the error in the orientation of the  $a$ -frame with respect to the  $i$ -frame, if applicable. These are the forcing terms in the linear differential equations for  $\psi^a$ .

### 5.3.1 Error Dynamics Equations in $i$ -Frame

We are now ready to write the complete set of error dynamics equations corresponding to the navigation equations coordinatized in any particular frame. For the  $i$ -frame, we substitute “ $i$ ” for “ $a$ ” in (5.29), that then reduces to

$$\frac{d}{dt} \delta\dot{x}^i = \Gamma^i \delta x^i + \delta a^i + \delta g^i, \quad (5.45)$$

since  $\Omega_{ii}^i = 0$  and, hence, also  $\delta\Omega_{ii}^i = 0$ , and where  $\Gamma^i = \partial g^i / \partial x^i$ . Substituting the accelerometer error, as given by (5.35) with  $a \equiv i$ , into (5.45) and combining this with (5.44), we obtain

$$\begin{aligned} \dot{\psi}^i &= -C_s^i \delta\omega_{is}^s, \\ \frac{d}{dt} \delta\dot{x}^i &= \Gamma^i \delta x^i + a^i \times \psi^i + C_s^i \delta a^s + \delta g^i, \\ \frac{d}{dt} \delta x^i &= \delta\dot{x}^i. \end{aligned} \quad (5.46)$$

This is the set of error dynamics equations in the  $i$ -frame, which may be cast in matrix form:

$$\frac{d}{dt} \begin{pmatrix} \psi^i \\ \delta\dot{x}^i \\ \delta x^i \end{pmatrix} = \begin{pmatrix} 0 & 0 & 0 \\ [a^i \times] & 0 & \Gamma^i \\ 0 & I & 0 \end{pmatrix} \begin{pmatrix} \psi^i \\ \delta\dot{x}^i \\ \delta x^i \end{pmatrix} + \begin{pmatrix} -C_s^i & 0 & 0 \\ 0 & C_s^i & I \\ 0 & 0 & 0 \end{pmatrix} \begin{pmatrix} \delta\omega_{is}^s \\ \delta a^s \\ \delta g^i \end{pmatrix}, \quad (5.47)$$

where  $I$  is the  $3 \times 3$  identity matrix; and  $0$ , as well, is a  $3 \times 3$  matrix of zeros. Also,  $[a^i \times]$  is a  $3 \times 3$  skew symmetric matrix with elements from  $a^i$ :

$$[a^i \times] = \begin{pmatrix} 0 & -a_3^i & a_2^i \\ a_3^i & 0 & -a_1^i \\ -a_2^i & a_1^i & 0 \end{pmatrix}. \quad (5.48)$$

Equation (5.47) is a set of non-homogeneous, linear differential equations for the orientation, velocity, and position errors formulated in the  $i$ -frame.

### 5.3.2 Error Dynamics Equations in $e$ -Frame

In the  $e$ -frame, we similarly have  $\delta\omega_{ie}^e = 0$  (and  $\dot{\omega}_{ie}^e = 0$ ), and therefore, the velocity perturbation in (5.29) with  $a \equiv e$  becomes

$$\frac{d}{dt}\delta\dot{x}^e = -2\Omega_{ie}^e\delta\dot{x}^e - (\Omega_{ie}^e\Omega_{ie}^e - \Gamma^e)\delta x^e + \delta a^e + \delta g^e, \quad (5.49)$$

where  $\Gamma^e = \partial g^e / \partial x^e$ . Substituting (5.35) into (5.45) and combining this with (5.44), we obtain the complete set of error dynamics equations specialized to the  $e$ -frame:

$$\begin{aligned} \dot{\psi}^e &= -\Omega_{ie}^e\psi^e - C_s^e\delta\omega_{is}^s, \\ \frac{d}{dt}\delta\dot{x}^e &= -2\Omega_{ie}^e\delta\dot{x}^e - (\Omega_{ie}^e\Omega_{ie}^e - \Gamma^e)\delta x^e + a^e \times \psi^e + C_s^e\delta a^s + \delta g^e, \\ \frac{d}{dt}\delta x^e &= \delta\dot{x}^e. \end{aligned} \quad (5.50)$$

In matrix form, this is

$$\frac{d}{dt} \begin{pmatrix} \psi^e \\ \delta\dot{x}^e \\ \delta x^e \end{pmatrix} = \left( \begin{bmatrix} -\Omega_{ie}^e & 0 & 0 \\ [a^e \times] & -2\Omega_{ie}^e & -(\Omega_{ie}^e\Omega_{ie}^e - \Gamma^e) \\ 0 & I & 0 \end{bmatrix} \right) \begin{pmatrix} \psi^e \\ \delta\dot{x}^e \\ \delta x^e \end{pmatrix} + \begin{pmatrix} -C_s^e & 0 & 0 \\ 0 & C_s^e & I \\ 0 & 0 & 0 \end{pmatrix} \begin{pmatrix} \delta\omega_{is}^s \\ \delta a^s \\ \delta g^e \end{pmatrix}. \quad (5.51)$$

In each of these formulations ( $i$ -frame,  $e$ -frame, or the following  $n$ -frame), the time history of the error could be determined by integrating the corresponding differential equations with given initial conditions if the instrument errors and the gravitational disturbance vector are known. The quantities required in the coefficient matrices on the right-hand sides of (5.47) and (5.51) are taken from the INS output, namely the sensed accelerations,  $a^s$ , and, in the case of the strapdown mechanization, from the integrated angular rates in the form of the transformation matrix,  $C_s^a$  (as given in Section 4.2.3.1). If the instrument errors and gravity disturbance are not known, only the homogeneous solution can be found, which may provide some useful information; see Section 5.4. A more systematic development of the optimal estimation of these errors is the object of Chapter 7.

It is also noted that the error dynamics formulations in the different frames are mutually consistent, meaning that the error vector determined from its dynamics equation in one frame may be transformed into any other frame using the appropriate transformation matrix (e.g.,  $\psi^e = C_i^e\psi^i$ ). The choice of frame in which to develop the error dynamics depends on the choice of navigation frame, which defines the (numerical) mechanization of the system, or how the IMU data are processed to provide navigational information. But, the magnitude of the error vectors is invariant with respect to the coordinatization.

To illustrate the alternatives that might be considered, we note that the coordinatization of the error dynamics in the  $e$ -frame by itself is much simpler than in the  $n$ -frame that will be developed in the next section. In fact, for short-term navigation

and positioning, as might be needed in the aiding of GPS positioning, the  $e$ -frame formulation is perfectly acceptable. However, for long-duration navigation, we found in Section 5.2 that the  $n$ -frame coordinatization immediately separates the unstable vertical channel from the more stable horizontal channels by mechanical or computational means. Therefore, despite the associated complexity in formulation, this represents the traditional and also a more intuitive scheme for analyzing the INS errors.

### 5.3.3 Error Dynamics Equations in $n$ -Frame

The objective in the  $n$ -frame coordinatization is to formulate the error dynamics with respect to the geodetic coordinates  $(\phi, \lambda, h)$ , corresponding to the navigation equations (4.102) and (4.103). Because of the special definition of  $\mathbf{v}^n$  (4.85), we do not specialize (5.29), but instead write the perturbation directly from the compact form of the navigation equations (4.91):

$$\frac{d}{dt} \delta \mathbf{v}^n = -\delta(\Omega_{in}^n + \Omega_{ie}^n) \mathbf{v}^n - (\Omega_{in}^n + \Omega_{ie}^n) \delta \mathbf{v}^n + \delta \mathbf{a}^n + \bar{\Gamma}^n \delta \mathbf{p}^n + \delta \bar{\mathbf{g}}^n, \quad (5.52)$$

where the gravitational and centrifugal (due to Earth-rate) accelerations are combined as in (4.89) to form the *gravity* differential,  $\delta \bar{\mathbf{g}}^n$  (however, since the centrifugal part is well known, we also have  $\delta \bar{\mathbf{g}}^n = \delta \mathbf{g}^n$ , as far as errors are concerned). Formally we identify the matrix of gravity gradients as  $\bar{\Gamma}^n = \partial \bar{\mathbf{g}}^n / \partial \mathbf{p}^n$ . Here we use another special notation,  $\delta \mathbf{p}^n$ , to represent the vector of position differentials along the axes of the  $n$ -frame (cf. (4.97)):

$$\delta \mathbf{p}^n = \begin{pmatrix} (M+h)\delta\phi \\ (N+h)\cos\phi\delta\lambda \\ -\delta h \end{pmatrix}. \quad (5.53)$$

The differential  $\delta \bar{\mathbf{g}}^n$ , construed as an error in the given gravity model, is also known as the *gravity disturbance vector* (see Section 6.6). The gravity gradients,  $\bar{\Gamma}^n$ , will require careful interpretation since the  $n$ -frame, by definition, rotates approximately with the gravity vector; this will be expounded at the end of the derivation.

The differential of  $\mathbf{v}^n$  in terms of geodetic coordinate differentials is obtained from (4.97) as follows:

$$\delta \mathbf{v}^n = \begin{pmatrix} (\delta M + \delta h)\dot{\phi} + (M+h)\delta\dot{\phi} \\ (\delta N + \delta h)\cos\phi\dot{\lambda} + (N+h)(\cos\phi\delta\dot{\lambda} - \sin\phi\dot{\lambda}\delta\phi) \\ -\delta\dot{h} \end{pmatrix}; \quad (5.54)$$

and its time-derivative is

$$\frac{d}{dt} \delta \mathbf{v}^n = \begin{pmatrix} (\delta \dot{M} + \delta \dot{h})\dot{\phi} + (\dot{M} + \dot{h})\delta\dot{\phi} + (\delta M + \delta h)\ddot{\phi} + (M+h)\delta\ddot{\phi} \\ (\delta \dot{N} + \delta \dot{h})\dot{\lambda}\cos\phi + (\dot{N} + \dot{h})(\delta\dot{\lambda}\cos\phi - \dot{\lambda}\delta\phi\sin\phi) \\ + (\delta N + \delta h)(\ddot{\lambda}\cos\phi - \dot{\lambda}\dot{\phi}\sin\phi) \\ + (N+h)((\delta\dot{\lambda} - \dot{\lambda}\delta\phi)\cos\phi - (\ddot{\lambda}\delta\phi + \delta\dot{\lambda}\phi + \dot{\lambda}\delta\dot{\phi})\sin\phi) \\ - \delta\ddot{h} \end{pmatrix}. \quad (5.55)$$

It is left to the reader to show by straightforward derivation from (1.81), (1.82), (4.94), and (4.95) that

$$\begin{aligned}\delta N &= e'^2 M \sin \phi \cos \phi \delta \phi, \\ \delta M &= 3e'^2 \frac{M^2}{N} \sin \phi \cos \phi \delta \phi, \\ \dot{\delta N} &= e'^2 M \sin \phi \cos \phi \dot{\delta \phi}, \\ \dot{\delta M} &= 3e'^2 \frac{M^2}{N} \sin \phi \cos \phi \dot{\delta \phi}, \\ \delta \dot{N} &= e'^2 M \left( \left( 1 + \left( 1 - \frac{3M}{2N} \right) \sin^2 \phi \right) \dot{\delta \phi} + \cos \phi \sin \phi \ddot{\delta \phi} \right), \\ \delta \dot{M} &= 3e'^2 \frac{M^2}{N} \left( \left( 1 + \left( 4 - \frac{M}{N} (6 + e'^2 \cos^2 \phi) \right) \sin^2 \phi \right) \dot{\delta \phi} + \cos \phi \sin \phi \ddot{\delta \phi} \right),\end{aligned}\tag{5.56}$$

where  $e'$  is the second eccentricity of the ellipsoid, already encountered in (4.117). The differential quantities  $\delta N$ ,  $\delta M$ ,  $\dot{\delta N}$ ,  $\dot{\delta M}$ , as well as  $\dot{N} \delta \dot{\lambda}$  and  $\dot{M} \delta \dot{\phi}$  are all of second- (or, higher-) order magnitude due to the approximate value  $e'^2 \approx 0.007$  for the Earth. They may be neglected in this *linear* perturbation of the system dynamics equations. To the same approximation, the principal radii of curvature,  $N$  and  $M$ , may be replaced with the *Gaussian mean radius*, defined as the azimuthal average of the ellipsoidal radius of curvature at a particular latitude,  $\phi$ :

$$\begin{aligned}R_\phi &= \frac{1}{2\pi} \int_0^{2\pi} \frac{NM}{N \cos^2 \alpha + M \sin^2 \alpha} d\alpha \\ &= \sqrt{NM} \\ &= M(1 + e'^2 \cos^2 \phi)^{1/2} = N(1 + e'^2 \cos^2 \phi)^{-1/2}.\end{aligned}\tag{5.57}$$

With these approximations, the differentials (5.54) and (5.55) become

$$\delta v^n = \begin{pmatrix} \delta h \dot{\phi} + (R_\phi + h) \delta \dot{\phi} \\ \delta h \cos \phi \dot{\lambda} + (R_\phi + h) (\cos \phi \delta \dot{\lambda} - \sin \phi \dot{\lambda} \delta \phi) \\ -\delta \dot{h} \end{pmatrix},\tag{5.58}$$

and

$$\frac{d}{dt} \delta v^n = \begin{pmatrix} \delta \dot{h} \dot{\phi} + \dot{h} \delta \dot{\phi} + \delta h \ddot{\phi} + (R_\phi + h) \delta \ddot{\phi} \\ \delta \dot{h} \dot{\lambda} \cos \phi + \dot{h} (\delta \dot{\lambda} \cos \phi - \dot{\lambda} \delta \phi \sin \phi) + \delta h (\ddot{\lambda} \cos \phi - \dot{\lambda} \dot{\phi} \sin \phi) \\ + (R_\phi + h) ((\ddot{\lambda} - \dot{\lambda} \phi \delta \phi) \cos \phi - (\ddot{\lambda} \delta \phi + \delta \dot{\lambda} \phi + \dot{\lambda} \dot{\phi}) \sin \phi) \\ -\delta \ddot{h} \end{pmatrix}.\tag{5.59}$$

This completes the expressions of the velocity perturbation terms in (5.52) cast in geodetic coordinate differentials and their time derivatives. For the angular rates,

we have from (4.100):

$$\delta(\Omega_{in}^n + \Omega_{ic}^n) = \begin{pmatrix} 0 & \delta\dot{\lambda}\sin\phi + (\dot{\lambda} + 2\omega_e)\cos\phi\delta\phi & -\delta\dot{\phi} \\ -\delta\dot{\lambda}\sin\phi - (\dot{\lambda} + 2\omega_e)\cos\phi\delta\phi & 0 & -\delta\dot{\lambda}\cos\phi + (\dot{\lambda} + 2\omega_e)\sin\phi\delta\phi \\ \delta\dot{\phi} & \delta\dot{\lambda}\cos\phi - (\dot{\lambda} + 2\omega_e)\sin\phi\delta\phi & 0 \end{pmatrix}. \quad (5.60)$$

The perturbation  $\delta\mathbf{a}^n$ , as in the previous cases, includes orientation errors. If  $\psi^n$  denotes the vector of small angles between the true  $n$ -frame and that determined from erroneous geodetic coordinates, then from (5.35):

$$\delta\mathbf{a}^n = C_s^n \delta\mathbf{a}^s + \mathbf{a}^n \times \psi^n. \quad (5.61)$$

Also, the dynamics of these orientation errors are represented by the differential equation (5.44):

$$\dot{\psi}^n = -\omega_{in}^n \times \psi^n - C_s^n \delta\omega_{is}^s + \delta\omega_{in}^n, \quad (5.62)$$

where, from (1.89),

$$\delta\omega_{in}^n = \begin{pmatrix} \delta\dot{\lambda}\cos\phi - (\dot{\lambda} + \omega_e)\delta\phi\sin\phi \\ -\delta\dot{\phi} \\ -\delta\dot{\lambda}\sin\phi - (\dot{\lambda} + \omega_e)\delta\phi\cos\phi \end{pmatrix}. \quad (5.63)$$

We now combine all the position, velocity, and orientation errors into one nine-component vector variable:

$$\boldsymbol{\varepsilon}^n = (\psi_1^n \ \psi_2^n \ \psi_3^n \ \delta\dot{\phi} \ \delta\dot{\lambda} \ \delta\dot{h} \ \delta\phi \ \delta\lambda \ \delta h)^T. \quad (5.64)$$

Also, the system errors and other forcing terms, in this case the gravity disturbance vector, are collected into a single vector:

$$\mathbf{u} = \begin{pmatrix} \delta\omega_{is}^s \\ \delta\mathbf{a}^s \\ \delta\bar{g}^n \end{pmatrix} \quad (5.65)$$

To express the total error dynamics equations in matrix form we substitute (4.97), (4.100), as well as (5.58), (5.59), (5.60), and (5.61) into (5.52). Similarly, we rewrite (5.62) by substituting (5.63) and (1.89). After several manipulations, that are left to the reader, the combined result, analogous to (5.51), and comprising equations (5.52) and (5.62) is given by

$$\frac{d}{dt} \boldsymbol{\varepsilon}^n = F^n \boldsymbol{\varepsilon}^n + G^n \mathbf{u}, \quad (5.66)$$

where, with  $r = R_\phi + h$ ,  $\dot{\ell}_1 = \dot{\lambda} + \omega_e$ , and  $\dot{\ell}_2 = \dot{\lambda} + 2\omega_e$ , we have

$F^n =$ 

$$\begin{bmatrix} 0 & -\dot{\ell}_1 \sin \phi & \dot{\phi} & 0 & \cos \phi & 0 & -\dot{\ell}_1 \sin \phi & 0 & 0 \\ \dot{\ell}_1 \sin \phi & 0 & \dot{\ell}_1 \cos \phi & -1 & 0 & 0 & 0 & 0 & 0 \\ -\dot{\phi} & -\dot{\ell}_1 \cos \phi & 0 & 0 & -\sin \phi & 0 & -\dot{\ell}_1 \cos \phi & 0 & 0 \\ 0 & \frac{-a_3^n}{r} & \frac{a_2^n}{r} & \frac{-2h}{r} & -\dot{\ell}_1 \sin 2\phi & \frac{-2\dot{\phi}}{r} & \bar{\Gamma}_{11}^n - \lambda \dot{\ell}_2 \cos 2\phi & \bar{\Gamma}_{12}^n \cos \phi & \frac{\ddot{\phi} + \frac{1}{2}\lambda \dot{\ell}_2 \sin 2\phi + \bar{\Gamma}_{13}^n}{-r} \\ \frac{a_3^n}{r \cos \phi} & 0 & \frac{-a_1^n}{r \cos \phi} & 2\dot{\ell}_1 \tan \phi & 2\left(\dot{\phi} \tan \phi - \frac{h}{r}\right) & \frac{-2\dot{\ell}_1}{r} & 2\dot{\ell}_1 \left(\dot{\phi} + \frac{h \tan \phi}{r}\right) & \bar{\Gamma}_{22}^n & \frac{2\dot{\phi} \dot{\ell}_1 \tan \phi - \ddot{\lambda} - \frac{\bar{\Gamma}_{23}^n}{\cos \phi}}{r} \\ a_2^n & -a_1^n & 0 & 2r\dot{\phi} & 2r\dot{\ell}_1 \cos^2 \phi & 0 & -r\lambda \dot{\ell}_2 \sin 2\phi - r\bar{\Gamma}_{31}^n & -r \cos \phi \bar{\Gamma}_{32}^n & \dot{\phi}^2 + \lambda \dot{\ell}_2 \cos^2 \phi + \bar{\Gamma}_{33}^n \\ 0 & 0 & 0 & 1 & 0 & 0 & 0 & 0 & 0 \\ 0 & 0 & 0 & 0 & 1 & 0 & 0 & 0 & 0 \\ 0 & 0 & 0 & 0 & 0 & 1 & 0 & 0 & 0 \end{bmatrix} \quad (5.67)$$

and

$$G^n = \begin{pmatrix} -C_s^n & 0 & 0 \\ 0 & D^{-1}C_s^n & D^{-1} \\ 0 & 0 & 0 \end{pmatrix}. \quad (5.68)$$

The matrix,  $D$ , transforms the position and velocity errors from angular to linear measure, and also inverts the vertical axis:

$$D = \begin{pmatrix} M + h & 0 & 0 \\ 0 & (N + h) \cos \phi & 0 \\ 0 & 0 & -1 \end{pmatrix} \approx \begin{pmatrix} r & 0 & 0 \\ 0 & r \cos \phi & 0 \\ 0 & 0 & -1 \end{pmatrix}. \quad (5.69)$$

In the matrices  $F^n$ , given by (5.67), and  $D$ , given by (5.69), “0” is the scalar number zero; in (5.68), “0” represents a  $3 \times 3$  matrix of zeros. It is noted that the differential equation for the geodetic-coordinatized position errors, incorporated in (5.66), is simply

$$\frac{d}{dt} \begin{pmatrix} \delta\phi \\ \delta\lambda \\ \delta h \end{pmatrix} = \begin{pmatrix} \delta\dot{\phi} \\ \delta\dot{\lambda} \\ \delta\dot{h} \end{pmatrix}. \quad (5.70)$$

But, note that  $\delta v^n$  and  $d(\delta p^n)/dt$  are not trivially related as in the case of the velocity and position errors in the  $e$ -frame coordinatization, (5.50).

Both  $F^n$  and  $G^n$  are  $9 \times 9$  matrices.  $F^n$  is called the *free-inertial dynamics matrix* of the system. Usually, all gravity gradient terms except  $\bar{\Gamma}_{33}^n$  are omitted because they are small, or of less consequence, compared to the velocity products in the corresponding matrix elements. To understand this it must be recognized that if the  $n$ -frame coordinate axes were always perfectly aligned with the tangents to the *local plumb line* and the *level surface*, then there would be no horizontal components of the gravity vector in this moving frame and its horizontal gradients also vanish. The

actual  $n$ -frame, however, is defined with respect to the ellipsoidal normal (that also moves with the vehicle). The difference in directions between the ellipsoidal normal and the plumb line is called the *deflection of the vertical*; it is generally on the order of several arcseconds in magnitude, except in rugged terrain, where it might reach tens of arcseconds, up to one arcminute. This means that the horizontal components of the gravity vector are of the order of a few  $10^{-4}$  m/s $^2$  and somewhat larger in mountainous areas. The horizontal gravity gradients are, therefore, *gradients of the gravity disturbance components*, presuming that the nominal gravity vector lies along the ellipsoid normal. These gradients typically range up to several tens of Eötvös ( $10^{-8}$  s $^{-2}$ ), although gradients of 1000 E ( $10^{-6}$  s $^{-2}$ ) or more may occur in rough terrain. However, these large gradients are extremely localized and random in character and generally would not affect appreciably the dynamics of the navigation errors. The only gradient in the dynamics matrix that has long-term systematic significance is  $\bar{\Gamma}_{33}^n$  ( $\sim 3.1 \times 10^{-6}$  s $^{-2}$ ). It is the vertical gradient of the total vertical gravity and occurs in the equation for the vertical velocity error; it is responsible for the rapid error growth in the vertical channel of an INS.

## 5.4 Approximate Analysis

It is instructive to study the error dynamics in the local-level coordinatization with some approximations. We will restrict ourselves to the horizontal components since the vertical channel, as discussed earlier is unstable and for periods longer than ten minutes is not considered without some form of damping. Returning to the equivalent formulation (5.52) in terms of  $n$ -frame coordinatized velocities, we note, in view of (5.60), that for not too large velocities (say  $\leq 200$  m/s), the term  $\delta(\Omega_{in}^n + \Omega_{ie}^n)v^n$  is of the order of a few  $10^{-5}$  m/s $^2$ . Typically, this is overshadowed by the acceleration error,  $\delta\mathbf{a}^n$ , due to accelerometer errors and platform tilt (or gyro drift) error (see (5.61)). For small velocities, the angular rates of the vehicle, contained in  $\Omega_{en}^n$ , are generally less than the angular rate of the Earth, contained in  $\Omega_{ie}^n$  and, therefore, could be neglected in the second term on the right-hand side of (5.52). Thus, for a rudimentary analysis we may let the case of zero *Earth-referenced velocity* represent the error dynamics if the vehicle has small velocities relative to the Earth ( $\leq 200$  m/s).

With  $v^n = 0$  (consequently,  $\dot{\phi} = 0$  and  $\dot{\lambda} = 0$ ) and ignoring the gravity gradient terms, the equations in (5.52) for the horizontal components then become:

$$\begin{aligned}\frac{d}{dt} \delta v_N &= -2\omega_e \sin \phi \delta v_E + \bar{g} \psi_E + \delta a_{AN} + \delta \bar{g}_N, \\ \frac{d}{dt} \delta v_E &= 2\omega_e \sin \phi \delta v_N + 2\omega_e \cos \phi \delta v_D - \bar{g} \psi_N + \delta a_{AE} + \delta \bar{g}_E,\end{aligned}\tag{5.71}$$

where also (5.61) with  $\mathbf{a}^n \approx (0 \quad 0 \quad -\bar{g})^T$  was substituted. The subscripts  $N$ ,  $E$ ,  $D$  on the variables refer to the directions of the  $n$ -frame. In addition, we use the special notation,

$$\delta\mathbf{a}_A = C_s^n \delta\mathbf{a}^s, \quad (5.72)$$

to identify the accelerometer error vector produced in the sensor frame, but coordinatized in the  $n$ -frame, where  $\delta\mathbf{a}_A = (\delta a_{AN} \ \delta a_{AE} \ \delta a_{AD})^T$ . We also have from (5.58) (with  $\dot{\phi} = 0$ ,  $\dot{\lambda} = 0$ ):

$$\delta\dot{\phi} = \frac{\delta v_N}{R + h}, \quad \delta\dot{\lambda} = \frac{\delta v_E}{(R + h) \cos \phi}. \quad (5.73)$$

The radius of curvature,  $R$ , in (5.73) is taken to be a constant without compromising the approximations already made.

The equations (5.71) are coupled to the orientation error dynamics via (5.62), specialized to the zero-velocity case:

$$\begin{aligned} \dot{\psi}_N &= -\omega_e \sin \phi \psi_E + \frac{\delta v_E}{R + h} - \omega_e \sin \phi \delta\phi - \delta\omega_{GN}, \\ \dot{\psi}_E &= \omega_e \sin \phi \psi_N - \frac{\delta v_N}{R + h} + \omega_e \cos \phi \psi_D - \delta\omega_{GE}, \\ \dot{\psi}_D &= -\omega_e \cos \phi \psi_E - \frac{\tan \phi \delta v_E}{R + h} - \omega_e \cos \phi \delta\phi - \delta\omega_{GD}, \end{aligned} \quad (5.74)$$

where (5.63) with (5.73) was used for  $\delta\omega_{in}^n$ . Again, the gyro error vector produced in the sensor frame, but coordinatized in the  $n$ -frame is denoted

$$\delta\omega_G = C_s^n \delta\omega_{is}^s, \quad (5.75)$$

where  $\delta\omega_G = (\delta\omega_{GN} \ \delta\omega_{GE} \ \delta\omega_{GD})^T$ .

Equations (5.71), (5.73), and (5.74) are depicted schematically in Figure 5.6. The Schuler loops, containing the  $g$  and  $1/r$  multipliers, illustrate the feedback mechanism inherent in the navigation errors. Also evident are the velocity cross-couplings that cause *Foucault* oscillations at the frequency,  $\omega_e \sin \phi$  (see equation (5.84)).

Alternatively, under the zero-velocity assumption, one can write the derivatives of the horizontal velocity differentials in (5.71) as differentials of the second time-derivatives of (angular) position coordinates by using (5.59) (again, with  $\dot{\phi} = 0$ ,  $\dot{\lambda} = 0$ ):

$$\delta\ddot{\phi} = \frac{d}{dt} \frac{\delta v_N}{R_\phi + h}, \quad \delta\ddot{\lambda} = \frac{d}{dt} \frac{\delta v_E}{(R_\phi + h) \cos \phi}. \quad (5.76)$$

Now substitute (5.71) into (5.76) and use (5.73) to eliminate both north and east velocity variables to get the second-order differential equations

$$\begin{aligned} r\delta\ddot{\phi} + r\omega_e \sin 2\phi \delta\dot{\lambda} - \bar{g}\psi_E &= \delta a_{AN} + \delta\bar{g}_N, \\ r\cos \phi \delta\ddot{\lambda} - 2r\omega_e \sin \phi \delta\dot{\phi} + \bar{g}\psi_N &= \delta a_{AE} + \delta\bar{g}_E + 2\omega_e \cos \phi \delta v_D, \end{aligned} \quad (5.77)$$

where  $r = R_\phi + h$ . To these equations we join the differential equations for the orientation errors (5.74), rearranged and written in terms of the latitude and longitude

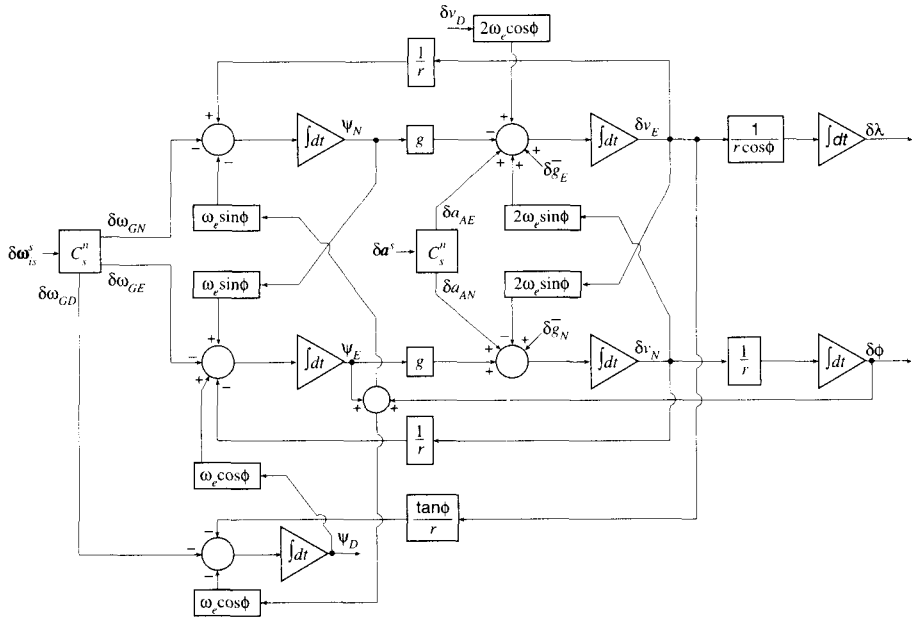


Figure 5.6: Error dynamics in the  $n$ -frame under the approximation of zero velocity.

rates:

$$\begin{aligned} \dot{\psi}_N + \omega_e \sin \phi \psi_E - \cos \phi \dot{\delta\lambda} + \omega_e \sin \phi \delta\phi &= -\delta\omega_{GN}, \\ \dot{\psi}_E - \omega_e \sin \phi \psi_N - \omega_e \cos \phi \psi_D + \dot{\delta\phi} &= -\delta\omega_{GE}, \\ \dot{\psi}_D + \omega_e \cos \phi \psi_E + \sin \phi \dot{\delta\lambda} + \omega_e \cos \phi \delta\phi &= -\delta\omega_{GD}. \end{aligned} \quad (5.78)$$

Both formulations, (5.71), (5.74) in terms of velocity errors, and (5.77), (5.78) in terms of position errors, are useful in the interpretation of the error dynamics.

We see in equations (5.77) (or, (5.71)) that the tilt (leveling) errors,  $\psi_N$  and  $\psi_E$ , integrate directly into the position (respectively, latitude and longitude) or corresponding velocity errors. Furthermore, these tilt errors and the respective accelerometer errors,  $\delta a_{AE}$  and  $\delta a_{AN}$ , enter as forcing terms in linear combination and, consequently, have the same net effect. From the point of view of estimation, these two types of errors are inseparable under usual circumstances.

#### 5.4.1 Effects of Accelerometer and Gyro Errors

We now come to an interesting phenomenon. Consider the case of a stabilized platform initially levelled, while the vehicle is stationary, by the output of accelerometers (that is, the platform is brought to the “level” by ensuring that the output of each accelerometer with input axis parallel to the platform is zero; see Chapter 8 on initialization and calibration). From Figure 5.7 and the fact that an accel-

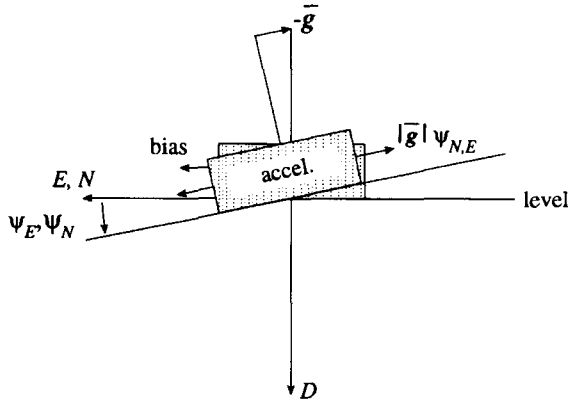


Figure 5.7: A bias in accelerometer output causes the platform to be mislevelled.

erometer senses the *reaction* to gravity, we see that a positive accelerometer bias error causes the platform to tilt from the horizontal toward the down direction so that the accelerometer picks up a reaction to the pull of gravity in order to cancel the bias. That is, the platform is thought to be level on the basis of the accelerometer output, but is, in fact, not level since the accelerometer output contains an error. For the north-pointing accelerometer, the resulting tilt is of the 1-axis toward the 3-axis and is a negative tilt error about the east axis; and for the east-pointing accelerometer the 2-axis tilts toward the 3-axis representing a positive tilt error about the north axis. We thus have

$$\begin{aligned}\delta a_{AN_{\text{bias}}} &= -\bar{g} \psi_{E_{\text{accel. bias}}}, \\ \delta a_{AE_{\text{bias}}} &= \bar{g} \psi_{N_{\text{accel. bias}}}.\end{aligned}\quad (5.79)$$

It is stressed in the notation that  $\psi_{N_{\text{accel. bias}}}$  and  $\psi_{E_{\text{accel. bias}}}$  are individual tilts directly caused *only* by accelerometer bias errors. The total tilt error consists of other errors, e.g., coming from the gyros. The two equations in (5.77) (or, (5.71)) show that the effect on position of an initial accelerometer bias error is cancelled by the effect of the consequent platform tilt error. Equations (5.79) will hold as long as the accelerometer bias errors remain constant and the platform is north-slaved and local-level stabilized, that is, as long as the biases remain *constant in the n-frame*. This is another advantage of the north-slaved, local-level mechanization as it substantially eliminates the effect on position and velocity due to constant accelerometer bias errors.

In the strapdown mechanization, the “levelling” of the platform is performed implicitly by computation, but the same effect is produced initially. However, when the vehicle begins to move and changes heading, the accelerometers change orientation with respect to the *n*-frame (and, therefore, the bias errors are not constant in the *n*-frame); the resulting “tilt error” no longer cancels the accelerometer bias. On the other hand, the tilt and accelerometer errors now become separable to some

extent. Therefore, with strapdown systems, the execution of specific vehicle maneuvers presents an opportunity to estimate the gyro and accelerometer biases since the system sees different linear combinations of these errors in relation to the  $n$ -frame, as time progresses (see Section 8.3.3).

Another important feature to note from the error dynamics equations is that the azimuth error,  $\psi_D$ , as seen in (5.78), is essentially inseparable (during shorter intervals) from the drift error,  $\delta\omega_{GE}$ , of the east-pointing gyro. Therefore, calibration of the east gyro error requires an accurate azimuth reference. Moreover, referring to (5.71) and (5.74), the down gyro error,  $\delta\omega_{GD}$ , is only weakly coupled to the velocity errors through the azimuth error,  $\psi_D$ , since the latter only affects the east leveling error; and thus also  $\delta\omega_{GD}$  is not easily calibrated (e.g., using velocity information). Only the north gyro error,  $\delta\omega_{GN}$ , feeds directly into the east velocity through the north tilt error. Consequently, the accurate calibration of the gyros is at least facilitated, if not fully possible, by allowing each gyro, in turn, to occupy the north-pointing position. (See Chapter 8 which elaborates on system calibration in full detail.)

#### 5.4.2 Vertical Velocity and Position Error Effects

We already know that free inertial navigation in the vertical is not possible for longer durations (Section 5.2). In addition, unknown errors in the vertical position and velocity couple into the horizontal position and velocity errors, as seen in the free-inertial error dynamics matrix, (5.67). Specifically, the sensitivities to vertical velocity error in the north and east acceleration errors are given by the (4, 6) and (5, 6) elements of  $F^n$ :

$$\frac{r\partial\ddot{\phi}}{\partial h} = -2\ddot{\phi}, \quad \frac{r\cos\phi\partial\ddot{\lambda}}{\partial h} = -2\cos\phi(\dot{\lambda} + \omega_e). \quad (5.80)$$

Corresponding sensitivities to vertical position error are (neglecting the gravity gradient terms)

$$\frac{r\partial\ddot{\phi}}{\partial h} = -\ddot{\phi} + \dot{\lambda}(\dot{\lambda} + 2\omega_e)\sin\phi\cos\phi, \quad \frac{r\cos\phi\partial\ddot{\lambda}}{\partial h} = 2\dot{\phi}\sin\phi(\dot{\lambda} + \omega_e) - \ddot{\lambda}\cos\phi \quad (5.81)$$

If the north velocity of a near-Earth vehicle is about 200 m/s, then  $\dot{\phi} \approx 3.1 \times 10^{-5}$  rad/s. A vertical velocity error of  $\delta\dot{h} = 3.2$  m/s yields a forcing term in the differential equation for the north position error of about  $2 \times 10^{-4}$  m/s<sup>2</sup>. If this error is a bias, we see from Figure 5.2 that the maximum effect on position within half the Schuler period is about 260 m. Somewhat greater sensitivity occurs in the east component because of Earth's angular rate, as seen in (5.80). Usually some form of damping (e.g., with a Kalman filter, see Chapter 7) from barometric altimetry is used to keep the velocity errors from unduly corrupting the position errors; however, it is not a critical source of error in low-dynamics navigation.

Performing the numerical calculations, it is readily shown that the vertical position error sensitivity is practically nonexistent, where at latitude  $45^\circ$  and assuming no persistent angular accelerations ( $\ddot{\phi} \approx 0$ ,  $\ddot{\lambda} \approx 0$ ), a constant forcing term of magni-

tude  $2 \times 10^{-4}$  m/s<sup>2</sup> arises only if the height error is of the order of 40–50 km. However, this analysis, being based on linear position error measures, does not include the effect of unknown height on the conversion to angular position coordinates. The latter is best illustrated with equation (4.144), where the effect of height error,  $\delta h$ , on latitude, for example, is  $v_N \delta h \Delta t / r^2$ . A constant height error of 500 m causes about 2" in latitude error over one hour. This is still not a significant source of error in most cases.

### 5.4.3 Essential Error Modes

We combine the five differential equations (5.77) and (5.78) into one set of linear, first-order differential equations for the vector variable  $(\psi_N \ \psi_E \ \psi_D \ \delta\dot{\phi} \ \delta\dot{\lambda} \ \delta\phi \ \delta\lambda)^T$ , excluding the forcing terms:

$$\frac{d}{dt} \begin{bmatrix} \psi_N \\ \psi_E \\ \psi_D \\ \delta\dot{\phi} \\ \delta\dot{\lambda} \\ \delta\phi \\ \delta\lambda \end{bmatrix} = \begin{bmatrix} 0 & -\omega_e \sin \phi & 0 & 0 & \cos \phi & -\omega_e \sin \phi & 0 \\ \omega_e \sin \phi & 0 & \omega_e \cos \phi & -1 & 0 & 0 & 0 \\ 0 & -\omega_e \cos \phi & 0 & 0 & -\sin \phi & -\omega_e \cos \phi & 0 \\ 0 & \frac{\bar{g}}{r} & 0 & 0 & -\omega_e \sin 2\phi & 0 & 0 \\ \frac{-\bar{g}}{r \cos \phi} & 0 & 0 & 2\omega_e \tan \phi & 0 & 0 & 0 \\ 0 & 0 & 0 & 1 & 0 & 0 & 0 \\ 0 & 0 & 0 & 0 & 1 & 0 & 0 \end{bmatrix} \begin{bmatrix} \psi_N \\ \psi_E \\ \psi_D \\ \delta\dot{\phi} \\ \delta\dot{\lambda} \\ \delta\phi \\ \delta\lambda \end{bmatrix}. \quad (5.82)$$

This is the same as the homogeneous differential equation corresponding to (5.66) under the zero-velocity assumption and with the height variables excluded. As shown in Section 2.3.1, the eigenvalues of the coefficient matrix on the right side determine the time-varying behavior of the system. Pure imaginary eigenvalues define resonances of the system. The frequencies of these natural modes are given, according to (2.40), by the square root of the eigenvalue magnitudes. If  $F_0$  denotes the coefficient matrix in (5.82), its eigenvalues are the roots of the determinant of the auxiliary matrix  $(F_0 - \mu I)$ ; see (2.22). It is left to the reader as an exercise to show using standard methods that

$$\det[F_0 - \mu I] = \begin{vmatrix} -\mu & -\omega_e \sin \phi & 0 & 0 & \cos \phi & -\omega_e \sin \phi & 0 \\ \omega_e \sin \phi & -\mu & \omega_e \cos \phi & -1 & 0 & 0 & 0 \\ 0 & -\omega_e \cos \phi & -\mu & 0 & -\sin \phi & -\omega_e \cos \phi & 0 \\ 0 & \frac{\bar{g}}{r} & 0 & -\mu & -\omega_e \sin 2\phi & 0 & 0 \\ \frac{-\bar{g}}{r \cos \phi} & 0 & 0 & 2\omega_e \tan \phi & -\mu & 0 & 0 \\ 0 & 0 & 0 & 1 & 0 & -\mu & 0 \\ 0 & 0 & 0 & 0 & 1 & 0 & -\mu \end{vmatrix} = -\mu r^2 \cos \phi (\mu^2 + \omega_e^2)(\mu^4 + 2(\omega_S^2 + 2\omega_e^2 \sin^2 \phi)\mu^2 + \omega_S^4), \quad (5.83)$$

where  $\omega_S$  is the Schuler frequency, (5.11), and  $\bar{g} \approx kM/r^2$ . Other than zero, the remaining roots of this polynomial in  $\mu$  are all pure imaginary. The zero root corresponds to a constant mode and the imaginary roots correspond to oscillations with frequencies

$$\omega_e, \quad \omega_S \pm \omega_e \sin \phi. \quad (5.84)$$

The latter frequencies in (5.84) are approximations, where terms of order  $(\omega_e \sin \phi)^2/\omega_S$  and higher have been neglected. The frequency  $\omega_e \sin \phi$  is known as the *Foucault* frequency and is associated with a period of about 34 hours at 45° latitude. Therefore, we see that the system has natural modes at Earth's spin rate and at the Schuler frequency which is modulated by the Foucault frequency. The Foucault oscillation can be traced back to the cross-coupling of velocity errors that is evident in equation (5.71) (see also Figure 5.6), which ultimately is due to the Coriolis effect.

For time intervals much less than 24 hours, say, up to a couple of hours, the errors modulated by Earth's spin rate can be ignored. The set of differential equations (5.82) with  $\omega_e = 0$  reduces to

$$\frac{d}{dt} \begin{pmatrix} \psi_N \\ \psi_E \\ \psi_D \\ \delta\phi \\ \delta\dot{\lambda} \\ \delta\ddot{\lambda} \\ \delta\phi \\ \delta\lambda \end{pmatrix} = \begin{pmatrix} 0 & 0 & 0 & 0 & \cos \phi & 0 & 0 \\ 0 & 0 & 0 & -1 & 0 & 0 & 0 \\ 0 & 0 & 0 & 0 & -\sin \phi & 0 & 0 \\ 0 & \bar{g} & 0 & 0 & 0 & 0 & 0 \\ 0 & \frac{-\bar{g}}{r} & 0 & 0 & 0 & 0 & 0 \\ \frac{-\bar{g}}{r \cos \phi} & 0 & 0 & 0 & 0 & 0 & 0 \\ 0 & 0 & 0 & 1 & 0 & 0 & 0 \\ 0 & 0 & 0 & 0 & 1 & 0 & 0 \end{pmatrix} \begin{pmatrix} \psi_N \\ \psi_E \\ \psi_D \\ \delta\phi \\ \delta\dot{\lambda} \\ \delta\ddot{\lambda} \\ \delta\phi \\ \delta\lambda \end{pmatrix}. \quad (5.85)$$

The determinant of the corresponding auxiliary matrix, from (5.83) with  $\omega_e = 0$ , is given by

$$\det[F_0 - \mu I] = -\mu^3 r^2 \cos \phi (\mu^2 + \omega_S^2)^2, \quad (5.86)$$

which shows that the system is governed essentially by the Schuler oscillation mode (for periods up to 2–3 hours, and velocities less than 200 m/s). In both cases, the solutions to (5.82) and (5.85) represent only the homogeneous components that oscillate with the modes given by (5.84). Particular solutions are determined by the forcing terms given by the right sides of (5.77) and (5.78).

Equations (5.78), with the  $\omega_e \approx 0$  and  $\dot{\phi} \approx 0$  assumptions, can be integrated to get for the horizontal tilt errors:

$$\begin{aligned} \psi_N &= \cos \phi \delta\lambda - \int \delta\omega_{GN} dt, \\ \psi_E &= -\delta\phi - \int \delta\omega_{GE} dt. \end{aligned} \quad (5.87)$$

Substituting these into (5.77) distills the error dynamics for shorter time intervals to differential equations in position error, only:

$$\begin{aligned} r\ddot{\delta\phi} + \bar{g}\delta\phi &= \delta a_{AN} + \delta\bar{g}_N - \bar{g}\int \delta\omega_{GE} dt, \\ r\cos\phi\ddot{\delta\lambda} + \bar{g}\cos\phi\delta\lambda &= \delta a_{AE} + \delta\bar{g}_E + \bar{g}\int \delta\omega_{GN} dt. \end{aligned} \quad (5.88)$$

These are identical to the equations (5.8) and (5.9) derived earlier, if the acceleration perturbations in the latter include accelerometer errors as well as tilt error effects. Note that the effect of the down orientation error does not explicitly enter here, although it may be a significant contributor to the forcing terms for the north position error. To this extent, the simple error analysis represented by (5.9) or (5.88) is somewhat oversimplified.

Finally, we consider the behavior of the errors in the very short term compared with the Schuler oscillation period of 84 minutes, say up to 8 minutes. In this case, we can neglect the Schuler feedback loop, that is, the coupling of the orientation errors to the velocity errors in the first three equations in (5.85). We write simply

$$\begin{aligned} r\ddot{\delta\phi} &= \delta a_{AN} + \delta\bar{g}_N - \bar{g}\int \delta\omega_{GE} dt, \\ r\cos\phi\ddot{\delta\lambda} &= \delta a_{AE} + \delta\bar{g}_E + \bar{g}\int \delta\omega_{GN} dt, \end{aligned} \quad (5.89)$$

which can be integrated directly and independently to yield  $r\delta\phi$  and  $r\cos\phi\delta\lambda$  with appropriate consideration of initial conditions.

# 6 Stochastic Processes and Error Models

## 6.1 Introduction

As in almost all physical systems, the instruments and sensors in inertial systems produce data that include a random component. This means that the data are not entirely describable in a deterministic sense. Often, we associate at least a part of this unpredictable part with an error. However, we may employ the theory of probability and statistics to find and use reasonable models that sufficiently describe the behavior of the system, especially the error, in some sense of expectations. In general, the statistical, or *stochastic*, models may have some deterministic structure, but the signal they describe is random, or associated with probability. The choice of model is not arbitrary and depends on the type of randomness that we believe the instruments and sensors to possess. The error models associated with measurement systems and the data they generate have a rich foundation in the theory of stochastic processes which will be reviewed briefly in the following.

To understand stochastic processes it is first necessary to be familiar with random variables, which requires a review of probability theory. Subsequently, stochastic processes can be introduced, that then serve to define our error models. It is not the intent to fully develop the theories associated with probability and stochastic processes in this text; the reader is referred to such texts as (Papoulis, 1991; Maybeck, 1979). Only the bare minimum will be covered here to enable a reasonable discussion of the estimation of INS errors using modern mathematical techniques.

## 6.2 Probability Theory

Probability formally is defined as a function operating on a collection of subsets, called *events*, comprising a *sample space*, denoted by  $\Pi$ . An event may be thought of as an outcome (or *realization*) of an experiment or a process that varies due to chance. The value of the probability function is a measure that represents the proportion of times a particular outcome, corresponding to an event, would occur with repetitions of the experiment. According to the formal definition, the *probability*,  $\mathcal{P}$ , of an event,  $A$ , denoted  $\mathcal{P}(A)$ , is a real number such that

$$0 \leq \mathcal{P}(A) \leq 1, \quad (6.1)$$

and such that  $\mathcal{P}(\Pi) = 1$ . The second condition says that if an experiment is performed, an outcome (which includes “no outcome”) will definitely occur. In addition to these two “axioms” that establish the existence of a probability function, a third one is needed to develop the theory of probability. This is: the probability of a combination of disjoint events, i.e., events that are mutually exclusive, is the sum of the probabilities of the individual events.

For two events, we can consider the probability that *both* will occur. This is the same as the product of probabilities that the first event occurs and that the second one occurs given that the first one has occurred:

$$\mathcal{P}(A_1 \text{ and } A_2) = \mathcal{P}(A_1)\mathcal{P}(A_2|A_1). \quad (6.2)$$

The latter probability, denoted  $\mathcal{P}(A_2|A_1)$ , is called a *conditional* probability. The probability that *either* of two events occurs is given by

$$\mathcal{P}(A_1 \text{ or } A_2) = \mathcal{P}(A_1) + \mathcal{P}(A_2) - \mathcal{P}(A_1 \text{ and } A_2), \quad (6.3)$$

where the probability of both events occurring is subtracted on the right-hand side because it is included in each probability of an event occurring and should not be counted twice. The two events are said to be *independent* if the conditional probability does not depend on  $A_1$  occurring:  $\mathcal{P}(A_2|A_1) = \mathcal{P}(A_2)$ ; in this case

$$\mathcal{P}(A_2 \text{ and } A_1) = \mathcal{P}(A_1)\mathcal{P}(A_2). \quad (6.4)$$

We will be concerned with two types of events:  $A_1$ , the estimation of a variable (e.g., a position coordinate); and  $A_2$ , the observation of a related variable. We presume to know the probability of the observation ( $A_2$ ), given that the estimation has occurred ( $A_1$ ), i.e.,  $\mathcal{P}(A_2|A_1)$ . We will then ask the important question: what is the probability of the (new) estimate given the result of a particular observation? This question is formulated in terms of conditional probabilities as: find  $\mathcal{P}(A_1|A_2)$ . Using (6.2) and the intuitively obvious identity,  $\mathcal{P}(A_2 \text{ and } A_1) = \mathcal{P}(A_1 \text{ and } A_2)$ , we have

$$\begin{aligned} \mathcal{P}(A_1|A_2) &= \frac{\mathcal{P}(A_1 \text{ and } A_2)}{\mathcal{P}(A_2)} \\ &= \frac{\mathcal{P}(A_1)\mathcal{P}(A_2|A_1)}{\mathcal{P}(A_2)}. \end{aligned} \quad (6.5)$$

This is the famous *Bayes' Rule*, that will form the basis of our estimation of the INS errors using external observations.

That the INS errors have particular values as estimated or measured constitutes an event of the sample space of the collection of all such possible events. The sample space is continuous in the sense that an error may take on any real value on the entire real line or in a particular (not necessarily connected) interval of values. It is convenient to define another function,  $X$ , that assigns to each outcome of the experiment (e.g., the realization of an INS error) a real number, in this case, trivially, the value of the error. This function,  $X$ , is called a *random variable*; and in our case, we will assume that the INS error as a random variable. The probability that a random variable will take on a value (or any number of values in an interval) is the probability measure of the corresponding event.

Because the real numbers are dense, formally, the probability that the random variable,  $X$ , takes on a single real number,  $x$ , is infinitesimally small or, in the limit, zero. Instead we consider intervals of values, and it is further convenient to introduce the *probability density function*,  $f(x)$ , such that

$$\mathcal{P}(x \leq X \leq x + dx) = f(x) dx, \quad (6.6)$$

or, the probability that a random variable,  $X$ , takes on a real value in the interval,  $[a, b]$ , is given, on the basis of the third axiom, by

$$\mathcal{P}(a \leq X \leq b) = \int_a^b f(x) dx. \quad (6.7)$$

Although we use the notation  $f(x)$  to identify the density function of the random variable,  $X$ , the function identified only by the letter  $f$  is ambiguous and is sometimes subscripted. We avoid this notational complication by always including the domain variable,  $x$ . It is further supposed that no undue confusion will arise between the values,  $x$ , and the coordinates of points defined in previous chapters.

Clearly, we have

$$\int_{-\infty}^{\infty} f(x) dx = 1; \quad (6.8)$$

and the probability density function must be integrable. We assume for the sake of generality that the random variable, such as an INS error, may take on any real value in the interval  $(-\infty, \infty)$ , even though the probability for most of that interval may be virtually zero. Since the probability measure is always non-negative for any event, the density function must be non-negative:  $f(x) \geq 0$ . The density function completely defines the probability measures of the random variable. An alternative definition of the probability measure of  $X$  is the *probability distribution function* related to the density by

$$F(x) = \mathcal{P}(X \leq x) = \int_{-\infty}^x f(x') dx'. \quad (6.9)$$

Two random variables,  $X$  and  $Y$ , each associated with its own density function,  $f(x)$  and  $f(y)$ , may possess a *joint density function*,  $f(x, y)$ , defined for the joint probability of both events occurring. The joint probability distribution function is given by

$$\mathcal{P}(X \leq x \text{ and } Y \leq y) = \int_{-\infty}^x \int_{-\infty}^y f(x', y') dx' dy'. \quad (6.10)$$

The *conditional* density follows from the consideration of conditional probabilities; and analogous to (6.2), we have the formula

$$f(x, y) = f(x)f(y|x). \quad (6.11)$$

Furthermore,  $X$  and  $Y$  are *independent* random variables if their joint density is the product of the individual densities:

$$f(x, y) = f(x)f(y). \quad (6.12)$$

An individual density is also known as a *marginal* density function, being the joint density with all possible outcomes of the other random variable accounted for. From (6.11), we have, e.g.,

$$f(x) = \int_{-\infty}^{\infty} f(x, y) dy, \quad (6.13)$$

since by (6.8),  $\int_{-\infty}^{\infty} f(y|x) dy = 1$  for any given  $x$ .

Often the probability density function (or the distribution function) is not known for a particular random variable,  $X$ . Then (and even if it were known), it is convenient to decompose the density function in terms of *moments* of the distribution, much like decomposing a function into a Fourier series of sinusoidal functions, or into a Taylor series of powers of the independent variable. In many cases, it suffices to work with just the first two moments of the density since they adequately describe the essential probabilities associated with the variable. The first moment specifies the value, in the domain of values for the random variable, where the density is centered—the center of mass, so to speak; it defines the *expected value*, or the *mean*, of the random variable:

$$\mu_X = \mathcal{E}(X) = \int_{-\infty}^{\infty} xf(x) dx. \quad (6.14)$$

Note that the mean value, or the expectation, is a constant with no uncertainty; it is not a random variable. We reserve the notation  $\mu_X$  for the mean value of  $X$ ; while  $\mathcal{E}$  serves as a general expectation operator, where we also have

$$\mathcal{E}(g(X)) = \int_{-\infty}^{\infty} g(x)f(x) dx. \quad (6.15)$$

Here,  $g(x)$  is the value of the random variable  $g(X)$ .

The second moment describes the amount by which the density spreads away from its center of mass. Usually, the second moment is defined with respect to the mean, and then it is called the *variance*:

$$\begin{aligned} \sigma_X^2 &= \int_{-\infty}^{\infty} (x - \mu_X)^2 f(x) dx \\ &= \mathcal{E}((X - \mu_X)^2) = \mathcal{E}(X^2) - \mu_X^2. \end{aligned} \quad (6.16)$$

The square root of the variance,  $\sigma_X$ , is called the *standard deviation*. Figure 6.1 shows an example of a density function with mean and standard deviation appropriately indicated.

For two random variables, we define the *covariance* between them as a second-order moment with respect to their means:

$$\begin{aligned} \text{cov}(X, Y) &= \mathcal{E}((X - \mu_X)(Y - \mu_Y)) \\ &= \mathcal{E}(XY) - \mu_X\mu_Y, \end{aligned} \quad (6.17)$$

where

$$\mathcal{E}(XY) = \int_{-\infty}^{\infty} \int_{-\infty}^{\infty} xyf(x, y) dx dy. \quad (6.18)$$

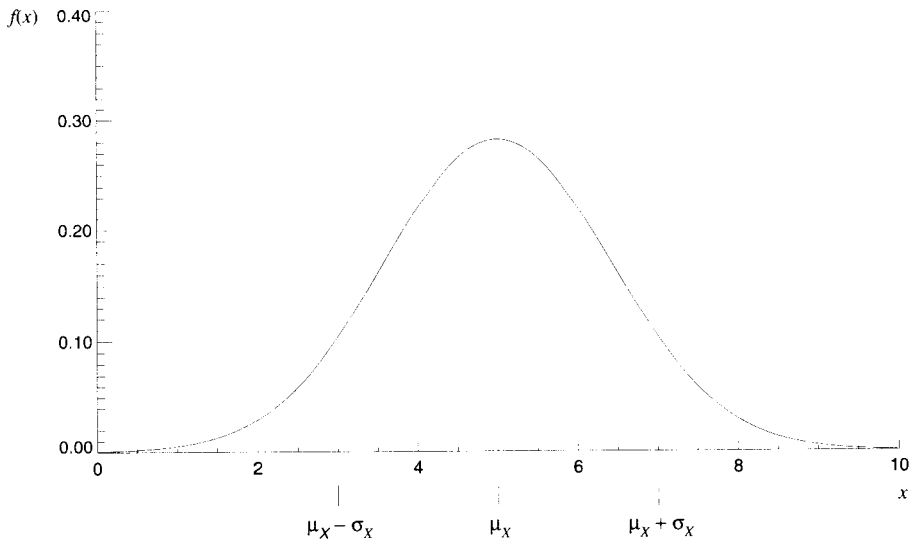


Figure 6.1: Example of a probability density function (Gaussian probability density function).

Note that  $\text{cov}(X, X) = \sigma_X^2$ . Two random variables are said to be *uncorrelated* if

$$\text{cov}(X, Y) = 0 \quad \text{or} \quad \mathcal{E}(XY) = \mathcal{E}(X)\mathcal{E}(Y). \quad (6.19)$$

We note that if  $X$  and  $Y$  are independent random variables, they are also uncorrelated, as seen from (6.12) and (6.18). The converse is not always true.

Finally, we also have *conditional* moments; for example, the conditional mean and conditional variance of  $X$ , given that  $Y$  has been realized, are

$$\mu_{X|Y} = \mathcal{E}(X|Y) = \int_{-\infty}^{\infty} xf(x|y) dx \quad (6.20)$$

and

$$\sigma_{X|Y}^2 = \mathcal{E}((X - \mu_{X|Y})^2 | Y) = \mathcal{E}(X^2 | Y) - \mu_{X|Y}^2. \quad (6.21)$$

These concepts in probability naturally extend to vectors of random variables, being simply a notational alternative to the case of a number of jointly distributed scalar random variables. The joint probability density of the *random vector* variable  $\mathbf{X}$  with  $m$  components is a scalar function  $f(\mathbf{X})$ . The mean of  $\mathbf{X}$  is the expectation given by the vector

$$\begin{pmatrix} \mathcal{E}(X_1) \\ \vdots \\ \mathcal{E}(X_m) \end{pmatrix} = \int_{-\infty}^{\infty} \cdots \int_{-\infty}^{\infty} \begin{pmatrix} x_1 \\ \vdots \\ x_m \end{pmatrix} f(x_1, \dots, x_m) dx_1 \cdots dx_m, \quad (6.22)$$

or

$$\mu_X = \mathcal{E}(X) = \int_{-\infty}^{\infty} xf(x) dx, \quad (6.23)$$

where we take some liberties in the vector notation (that is,  $\int_{-\infty}^{\infty} dx = \int_{-\infty}^{\infty} \cdots \int_{-\infty}^{\infty} dx_1 \cdots dx_m$ ). Clearly, using a generalization of (6.13), we find

$$\mu_X = \begin{pmatrix} \mu_{X_1} \\ \mu_{X_2} \\ \vdots \\ \mu_{X_m} \end{pmatrix}. \quad (6.24)$$

We can easily formulate the covariance between any two random variables in the vector,  $X$ :

$$\text{cov}(X_j, X_k) = \mathcal{E}((X_j - \mu_{X_j})(X_k - \mu_{X_k})). \quad (6.25)$$

These may be combined into an  $m \times m$  matrix,  $P_X$ , of covariances where, evidently, the diagonal elements are the variances:

$$P_X = \begin{pmatrix} \text{cov}(X_1, X_1) & \cdots & \text{cov}(X_1, X_m) \\ \vdots & \ddots & \vdots \\ \text{cov}(X_m, X_1) & \cdots & \text{cov}(X_m, X_m) \end{pmatrix}. \quad (6.26)$$

This *covariance matrix* of the random vector,  $X$ , is symmetric, and we assume that it is a non-singular matrix. It can be shown that it is then also positive definite (Koch, 1987). A more compact expression for  $P_X$  is readily verified to be:

$$\mathcal{E}((X - \mu_X)(X - \mu_X)^T) = P_X = \text{cov}(X, X). \quad (6.27)$$

$P_X$  is also known as the *auto-covariance* matrix of  $X$ , because, more generally, we have the *cross-covariance* matrix for random vectors  $X$  and  $Y$ :

$$\text{cov}(X, Y) = \mathcal{E}((X - \mu_X)(Y - \mu_Y)^T) = [\text{cov}(Y, X)]^T. \quad (6.28)$$

Corresponding elements of this matrix are the cross-covariances between elements of  $X$  and  $Y$ . We make no assumptions about the invertibility of  $\text{cov}(X, Y)$ ; in fact, it may not even be a square matrix, since its size depends on the dimensions of  $X$  and  $Y$ , as seen in the argument of the expectation in (6.28).

### 6.2.1 Gaussian Distribution

The most often used and best known probability distribution function is the *normal*, or *Gaussian*, distribution function. (We use the adjectives normal and Gaussian interchangeably, but derive the noun only from the latter: *Gaussianity*.) It has been found to serve as a suitable model for many random variables observed in nature, including, of course, our INS and observation errors, at least a component of them. Furthermore, according to the *Central Limit Theorem* of sampling theory (Dudewicz, 1976), the *average* of a sample of realizations of a random variable, whatever

its distribution, tends to be normally distributed, as the sample grows. This has significant implications in many applications, including ours.

The normal density function for one random variable is given by

$$f(x) = \frac{1}{\sigma_X \sqrt{2\pi}} e^{-(1/2)((x-\mu_X)/\sigma_X)^2}, \quad (6.29)$$

where  $\sigma_X$  and  $\mu_X$  are the standard deviation and mean of the variable,  $X$ . The density function shown in Figure 6.1 is a normal density. We use the following notation to indicate that  $X$  is normally distributed with corresponding mean and variance:

$$X \sim \mathcal{N}(\mu_X, \sigma_X^2). \quad (6.30)$$

Since, according to (6.29), the mean and variance completely define the density function, all probabilities (all higher-order moments) of a normally distributed random variable are completely determined by just these two moments. Moreover, if two normally distributed random variables are uncorrelated, they are also independent.

Again, we can readily construct the generalization for Gaussian random vectors. Let the mean and covariance matrix of a vector of  $m$  Gaussian random variables be given by (6.23) and (6.27). Then the joint density function is formulated as

$$f(\mathbf{x}) = \frac{1}{\sqrt{|P_X|(2\pi)^{m/2}}} e^{-(1/2)((\mathbf{x}-\boldsymbol{\mu}_X)^T P_X^{-1}(\mathbf{x}-\boldsymbol{\mu}_X))}, \quad (6.31)$$

where  $|P_X|$  is the determinant of  $P_X$ . Also, we write:

$$\mathbf{X} \sim \mathcal{N}(\boldsymbol{\mu}_X, P_X). \quad (6.32)$$

Normal random variables possess many useful properties, in addition to those already mentioned. A particularly applicable one is that any linear combination of normal variables is again normally distributed. The proof of this is found in most books on probability or statistics (e.g., Dudewicz, 1976). It is straightforward to extend this result to random vectors. Thus, consider the random vector

$$\mathbf{Z} = A\mathbf{X} + B\mathbf{Y} + \mathbf{C}, \quad (6.33)$$

where  $A$  and  $B$  are constant matrices and  $\mathbf{C}$  is a constant vector, and

$$\mathbf{X} \sim \mathcal{N}(\boldsymbol{\mu}_X, P_X); \quad \mathbf{Y} \sim \mathcal{N}(\boldsymbol{\mu}_Y, P_Y). \quad (6.34)$$

Then

$$\mathbf{Z} \sim \mathcal{N}(A\boldsymbol{\mu}_X + B\boldsymbol{\mu}_Y + \mathbf{C}, AP_XA^T + BP_YB^T + A \text{cov}(\mathbf{X}, \mathbf{Y})B^T + B \text{cov}(\mathbf{Y}, \mathbf{X})A^T), \quad (6.35)$$

where the expressions for  $\boldsymbol{\mu}_Z$  and  $\text{cov}(\mathbf{Z}, \mathbf{Z})$  are readily verified using (6.23) and (6.28). This important result has profound implications in our problem to estimate INS errors. Specifically, it says that if the initial error is Gaussian and our error variable transforms linearly in time, then we only need to determine the mean

and covariance of the error at one time to completely determine its probability distribution at any time (it is Gaussian); see also Section 7.2.2.1.

### 6.3 Stochastic Processes

A *stochastic* (or, *random*) process is a collection, discrete or continuous, of random variables associated with a deterministic parameter, usually a time or space coordinate. At each point in time or in space, the process is a random variable as described in the previous section. Although the stochastic process is not a determinable quantity for a given value of the time or space parameter (it depends on the outcome of an “experiment”), we will loosely speak of the process as being a function of time or space (in the present context of describing INS error models, time is the deterministic parameter). We do this because in some cases only one *realization* of the stochastic process is available, that is, the experiment at each point in time has been completed and each corresponding random variable has achieved a definite value. Then the realized process truly is a function of time. Statistical theory still allows, under appropriate circumstances, that the stochastic properties of the process can be analyzed from this single realization (*ergodicity*, see Section 6.3.3).

We denote a stochastic process by  $X(t)$ ; for any specific value of time, say  $t_k$ ,  $X(t_k)$  is a random variable with probability density function  $f(x_k)$ . Figure 6.2 shows two realizations of a (discrete) stochastic process, where at any particular time the value is the random outcome of an experiment. Examples of stochastic processes that concern us include the random errors contained in the output signals of each of

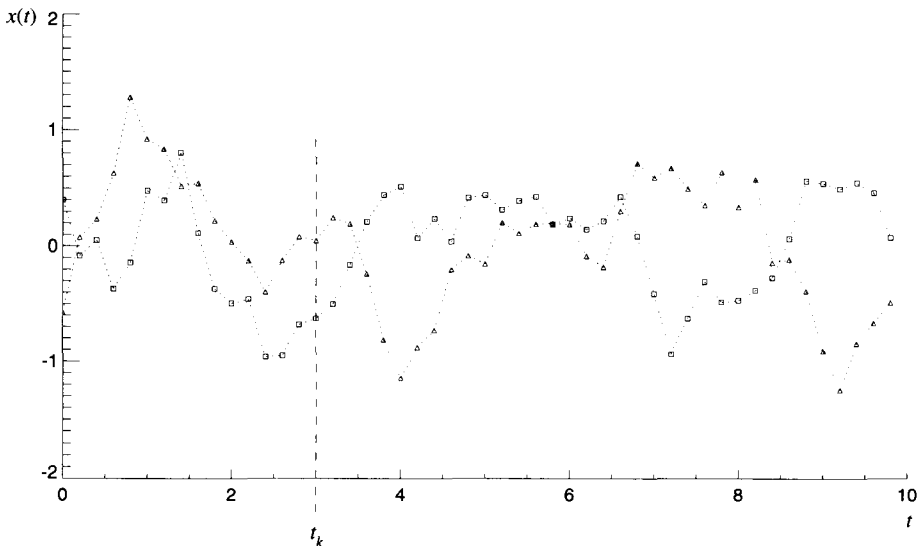


Figure 6.2: Two realizations of a (discrete) stochastic process.

the INS sensors (accelerometers and gyros). As already alluded to with INS error models such as (3.76) and (3.118), the errors may be correlated in time or they may be totally uncorrelated. It is the object of this chapter to establish adequate statistical models that describe the type and degree of correlation in these errors. In all cases, the models are only approximations that may never be realized in actuality; but from experience, they seem to serve the purpose of giving a reasonable statistical characterization of the errors. This section provides a rudimentary working basis of the fundamentals of stochastic processes.

### 6.3.1 Covariance Functions

The probabilistic treatment of the stochastic process naturally involves the consideration of jointly distributed variables, since the process comprises more than one variable. Moreover, it is equally clear that the description or formulation of the complete multivariate density function for the process is, in the most general case, beyond the realm of possibility. On the other hand, in many cases one obtains a fairly good description of the process by considering just the first- and second-order joint density functions, that is, the marginal density function of the process at any instant in time and the joint (also marginal) density function for any two instances in time.

Because the time parameter is continuous, the covariance (6.17), defined for random variables, becomes for the stochastic process the *(auto)-covariance function*, depending on two time arguments:

$$\begin{aligned}\mathcal{C}_X(t_1, t_2) &= \mathcal{E}((X(t_1) - \mu_{X_1})(X(t_2) - \mu_{X_2})) \\ &= \int_{-\infty}^{\infty} \int_{-\infty}^{\infty} (x_1 - \mu_{X_1})(x_2 - \mu_{X_2}) f(x_1, x_2) dx_1 dx_2,\end{aligned}\quad (6.36)$$

where  $\mu_{X_1}$  and  $\mu_{X_2}$  are the expected values of the process at  $t_1$  and  $t_2$ , respectively. Often one distinguishes between the covariance function and the *correlation function*; the latter describes the temporal intradependence of the process without centering the variables on their respective means:

$$\mathcal{R}_X(t_1, t_2) = \mathcal{E}(X(t_1)X(t_2)). \quad (6.37)$$

By far the most easily modeled process is the one whose probabilities do not change in time (or, space, if that is the deterministic parameter). Such a random process is called a *stationary process*; and the (marginal) joint probability density function for any subset of random variables of the process corresponding to any set of time coordinates is independent of the time origin. The stationary process is said to be time-invariant or invariant under translation of time. This means, first of all, that all marginal densities  $f(x_k)$  are identical—at each instant,  $t_k$ , the random variable  $X(t_k)$  has the same probability distribution, in particular, the same mean value and the same variance. Second, the auto-covariance function, being independent of the time origin, depends only on the time interval  $\tau = t_2 - t_1$  of two random variables of the process:

$$\mathcal{C}_X(\tau) = \int_{-\infty}^{\infty} \int_{-\infty}^{\infty} (x_t - \mu_X)(x_{t+\tau} - \mu_X) f(x_t, x_{t+\tau}) dx_t dx_{t+\tau}, \quad \text{for all } t; \quad (6.38)$$

where, of course,  $\mu_X$  is independent of time.

*Strict* stationarity of the process demands that all higher-order joint probabilities are invariant under time translation. *Wide-sense* stationarity relaxes this to just the first- and second-order probabilities, which is generally what we will assume.

We note that  $\mathcal{C}_X(0)$  is the variance of the stationary process; and the covariance is an even function:

$$\mathcal{C}_X(\tau) = \mathcal{C}_X(-\tau). \quad (6.39)$$

Also, the covariance function attains its maximum value at  $\tau = 0$ :

$$\mathcal{C}_X(|\tau|) \leq \mathcal{C}_X(0), \quad \text{for all } \tau. \quad (6.40)$$

This inequality is another way of saying that the correlation between the random variable at time  $t + \tau$  and the random variable at time  $t$  (being of the same type, probabilistically) can never be greater than the correlation of the variable with itself. A typical stationary covariance function is shown in Figure 6.3. Usually, it decreases at least for small  $\tau$ . The time interval,  $\tau_c$ , at which the covariance is a significantly reduced fraction of the variance, for example,

$$\mathcal{C}_X(\tau_c) = \frac{1}{2}\sigma_X^2, \quad (6.41)$$

is called the correlation time and identifies the interval beyond which the process may be considered decorrelated, in an approximate sense. Alternatively, the point

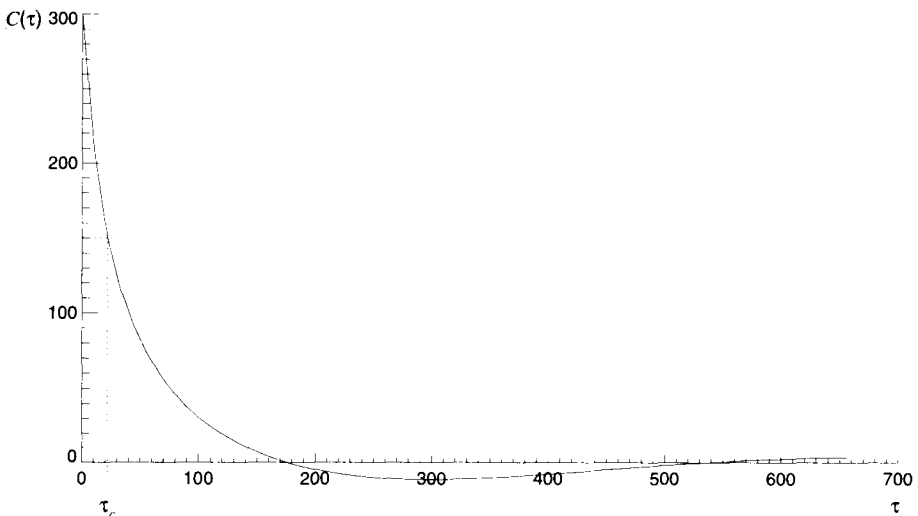


Figure 6.3: Typical covariance function.

where  $\mathcal{C}_X(\tau_c)/\mathcal{C}_X(0) = e^{-1}$  also serves to define a correlation time. It is usually assumed that in the limit as  $|\tau| \rightarrow \infty$ , the process completely decorrelates:

$$\lim_{|\tau| \rightarrow \infty} \mathcal{C}_X(\tau) = 0. \quad (6.42)$$

The extension of the concept of covariance function to more than one stochastic process follows naturally from our definitions. For example, the *cross-covariance function* of two stationary processes,  $X(t)$  and  $Y(t)$ , is given by

$$\begin{aligned} \mathcal{C}_{X,Y}(\tau) &= \mathcal{E}((X(t) - \mu_X)(Y(t + \tau) - \mu_Y)) \\ &= \int_{-\infty}^{\infty} \int_{-\infty}^{\infty} (x_t - \mu_X)(y_{t+\tau} - \mu_Y) f(x_t, y_{t+\tau}) dx_t dy_{t+\tau}, \quad \text{for all } t. \end{aligned} \quad (6.43)$$

$\mathcal{C}_{X,Y}(0)$  is called the *cross-variance* of the two processes. In general, the cross-covariance function satisfies neither (6.39) nor (6.40). Also, to avoid confusion,  $\mathcal{C}_X \equiv \mathcal{C}_{X,X}$  should be called the *auto-covariance* function.

Similarly, the cross-covariance *matrix* function between two *vectors* of stationary stochastic processes,  $X(t)$  and  $Y(t)$ , is given essentially by (6.28) with (6.43) as follows:

$$\text{cov}_{X,Y}(\tau) = \begin{pmatrix} \mathcal{C}_{X_1, Y_1}(\tau) & \cdots & \mathcal{C}_{X_1, Y_n}(\tau) \\ \vdots & \ddots & \vdots \\ \mathcal{C}_{X_m, Y_1}(\tau) & \cdots & \mathcal{C}_{X_m, Y_n}(\tau) \end{pmatrix}, \quad (6.44)$$

where  $m$  and  $n$  are the dimensions of  $X$  and  $Y$ , respectively; and  $\text{cov}_{X,Y}(\tau)$  is an  $m \times n$  matrix function. This may be specialized to the auto-covariance matrix function:  $\text{cov}_{X,X}(\tau)$ .

### 6.3.2 Power Spectral Density

It is exceedingly informative to view the auto- (or cross-) covariance function in terms of its constituent waveforms, that is, its Fourier transform. For a stationary process, the Fourier transform of the auto-covariance function,  $\mathcal{C}_X(\tau)$ , is given by (1.103):

$$\Phi_X(f) = \int_{-\infty}^{\infty} \mathcal{C}_X(\tau) e^{-i2\pi f \tau} d\tau, \quad (6.45)$$

where it is assumed that the integral exists for all frequencies,  $f$ , which happens if the process decorrelates sufficiently fast. The function,  $\Phi_X$ , is called the *power spectral density* (psd) of  $X$ . Its units are the units of the covariance function divided by the units of frequency, for the latter they are in this case [Hz] = [cy/s]. Certainly all the extensions to multiple and vector stochastic processes apply here, as well. For example, the cross-psd of the processes  $X$  and  $Y$  is

$$\Phi_{X,Y}(f) = \int_{-\infty}^{\infty} \mathcal{C}_{X,Y}(\tau) e^{-i2\pi f \tau} d\tau. \quad (6.46)$$

From the inverse Fourier transform, (1.104), we see that

$$\mathcal{C}_X(\tau) = \int_{-\infty}^{\infty} \Phi_X(f) e^{i2\pi f \tau} df. \quad (6.47)$$

And, therefore, the variance equals the area under the psd curve.

A relatively large value of the psd at a particular frequency implies high correlation of the process at that frequency; conversely, a low value implies low correlation. Because the covariance function is symmetric about the origin (see (6.39)), the power spectral density is a real function. Furthermore, it can be shown that

$$\Phi_X(f) \geq 0; \quad \text{for all } f; \quad (6.48)$$

neither is the case, necessarily, for the cross-psd.

### 6.3.3 Ergodic Processes

If the covariance function,  $\mathcal{C}_X(\tau)$ , of a stationary process decreases rapidly with increasing  $\tau$ , then the process decorrelates quickly and the random variables of the process become less predictable from one point in time to the next. If  $\mathcal{C}_X(\tau)$  decreases slowly, then the process changes less rapidly and is more predictable. That is, given the value of the process at the present time, and the covariance function, we can make a reasonable prediction of the process at some future time not too far from the present. It seems reasonable, therefore, that the converse should also hold. That is, if we have only *one realization* of the (stationary) process, i.e., values for the random variables at all instances of time, then we should be able to say something about the covariance function, even though the probability densities are not known (specifically, we do not have the luxury of repeated realizations to even guess what they are). In fact, this is precisely the idea behind the assumption of *ergodicity*. A stationary process is *ergodic* if the statistics of the process, such as the mean, the variance, and higher-order moments, associated with the underlying probabilities are equivalent to the corresponding statistics derived from time-based (space-based) averages, that is, from a single realization of the process.

A non-stationary process cannot be ergodic, because, by definition, non-stationarity implies that a single realization is the result of many different probabilities. Also, not all stationary processes are ergodic (see Section 6.5.1). Analogous to stationarity, ergodicity is defined in both the strict sense and the wide sense, where the latter means that only first and second moments of the process may be identified with their corresponding time-averages.

The statistics associated with the expectation operator,  $\mathcal{E}$ , are called *ensemble statistics*. We now define an analogous operator, the *averaging operator*,  $E$ , that operates on the realized process as a function of time:

$$E(\cdot) = \lim_{T \rightarrow \infty} \frac{1}{T} \int_{-T/2}^{T/2} (\cdot) dt, \quad (6.49)$$

where it is assumed that the limit exists. In practice, the process is realized only for a limited time interval,  $T$ , and the time averages are *approximated* without the limit. For example, the time-averaged mean is approximately given by

$$m_X \equiv E(X) \approx \frac{1}{T} \int_{-T/2}^{T/2} x(t) dt. \quad (6.50)$$

Similarly, the time-averaged (cross-) covariance function is given by

$$C_{X,Y}(\tau) = \lim_{T \rightarrow \infty} \frac{1}{T} \int_{-T/2}^{T/2} (x(t) - m_X)(y(t + \tau) - m_Y) dt, \quad (6.51)$$

which certainly includes the definition of the time-averaged auto-correlation function. Covariance functions are defined similarly, with mean values removed.

For a wide-sense ergodic process we have

$$\mu_X = m_X \quad \text{and} \quad C_{X,Y}(\tau) = C_{X,Y}(\tau). \quad (6.52)$$

Therefore, one technique to estimate the (cross-) covariance function of a realized process (or processes) is to evaluate (6.51) numerically for a given set of intervals,  $\tau$ . Such an empirical covariance function is only an approximation to the true function, even if ergodicity holds; but it is obtained without knowing the probability densities.

It can be shown that the product of the Fourier transforms of realizations of two stationary, ergodic processes is related to the (cross-) power spectral density of the process. Specifically,

$$\lim_{T \rightarrow \infty} E\left(\frac{1}{T} \mathcal{F}(X_T(t)) \mathcal{F}(Y_T(t))^*\right) = \Phi_{X,Y}(f), \quad (6.53)$$

where each process is realized over an interval of length,  $T$ , and  $(\cdot)^*$  denotes complex conjugate. This fundamental relationship provides a method with which to estimate the power spectral density, and subsequently the covariance function, of a process from Fourier transforms of the realized signal (see Brown and Hwang, 1992; also see Marple, 1987, for the estimation of covariance functions using either method).

## 6.4 White Noise

A random process,  $\mathcal{W}(t)$ , is said to be a (continuous) *white noise process* if it is a stationary process and if the random variables for any set of time instances are uncorrelated. This means that the covariance function has zero value for any non-zero time interval,  $\tau$ . Because of stationarity, the random variables of the process also have identical means and variances. We will assume from the start that the mean of the white noise process is zero. With respect to the variances, however, we

find ourselves in a dilemma when considering the power spectral density of this process. Equation (6.45) says that, because the covariance is zero everywhere (except at  $\tau = 0$ ), the psd for any continuous white noise process would be zero for all frequencies; but, clearly we would like to characterize a white noise process as having power, thus allowing us to distinguish between white noise processes having different amplitudes. The only way around this is to assign infinite variance to the process, such that the integral in (6.45) has a defined non-zero value.

This can be done with the *Dirac “delta function”*,  $\delta(t)$ , defined such that

$$\delta(t) = 0, \quad t \neq 0; \quad \text{and} \quad \int_{-\infty}^{\infty} g(t')\delta(t-t') dt' = g(t), \quad (6.54)$$

for a function,  $g(t)$ . At  $t - t' = 0$ , we may say that the delta function is infinite such that the integral in (6.54) holds. The covariance function of white noise is then defined as

$$\mathcal{E}(\mathcal{W}(t)\mathcal{W}^*(t+\tau)) = \mathcal{C}_{\mathcal{W}}(\tau) = q\delta(\tau), \quad (6.55)$$

where  $q$  is a constant; and, the psd of white noise is a constant, according to (6.45) and (6.55):

$$\Phi_{\mathcal{W}}(f) = \int_{-\infty}^{\infty} q\delta(\tau)e^{-i2\pi f\tau} d\tau = qe^0 = q; \quad \text{for all } f. \quad (6.56)$$

Thus, the psd is the same constant,  $q$ , at all frequencies, implying that power at all frequencies contributes equally to the process (whence the terminology “white” noise, alluding to white light being the combination of all equally intense optical frequencies). From (6.54) we see that the delta function in this case has units of 1/time, conventionally [Hz]; thus the units of the constant  $q$  are the units of the variance divided by Hz, consistent with the units of a psd. We also have, from (6.47) and (6.55):

$$\int_{-\infty}^{\infty} qe^{i2\pi f\tau} df = q\delta(\tau), \quad \text{for all } \tau; \quad (6.57)$$

which gives a formal definition of the delta function as an integral of the complex exponential. Changing the integration variable in (6.57) to its negative shows that the delta function is symmetric:

$$\delta(t) = \delta(-t). \quad (6.58)$$

In practice, white noise is the assumed stochastic process for signals where no correlation can be determined. Yet, it is also clear that white noise, specifically the continuous white noise defined above, theoretically having infinite variance, is physically unrealizable. Fortunately, reasonable assumptions about the physical nature of a random process allow us to use white noise concepts approximately. For example, for a presumably uncorrelated process, we may really only assume no correlation up to frequencies defined by the smallest sampling interval; for smaller time intervals (that is, higher frequencies) the process may indeed be correlated and,

therefore, will have power according to (6.45) if the variance is finite (see Section 6.5.3).

The difficulties associated with continuous white noise are absent when defining a discrete process comprising random variables at discrete points in time. The transition from the continuous to the discrete white noise process can be defined in terms of an averaging procedure, where the discrete random variable at time  $t_k$  is the average of the continuous white noise process over a small interval  $\Delta t$ :

$$W(t_k) = \frac{1}{\Delta t} \int_{t_k - \Delta t}^{t_k} \mathcal{W}(t) dt. \quad (6.59)$$

Applying the expectation operator to both sides, we find the expected value of the discrete white noise to be

$$\mathcal{E}(W(t_k)) = \mathcal{E}(\mathcal{W}(t)). \quad (6.60)$$

And, the variance is given from (6.36) and (6.55) by

$$\begin{aligned} \sigma_W^2 &= \mathcal{E}((W(t_k))^2) \\ &= \frac{1}{(\Delta t)^2} \int_{t_k - \Delta t}^{t_k} \int_{t_k - \Delta t}^{t_k} \mathcal{E}(\mathcal{W}(t)\mathcal{W}(t')) dt dt' \\ &= \frac{1}{(\Delta t)^2} \int_{t_k - \Delta t}^{t_k} \int_{t_k - \Delta t}^{t_k} q\delta(t - t') dt dt' \\ &= \frac{q}{\Delta t}, \end{aligned} \quad (6.61)$$

showing that the variance of the discrete white noise process is simply related to the psd of the corresponding continuous process. Note that the units of  $\sigma_W^2$  are the usual variance units. Figure 6.4 shows a realization of a discrete white noise process (technically, it is impossible to depict a continuous white noise process, which further underscores its abstract character).

Finally, if the distribution of each random variable of the white noise process is the Gaussian distribution with zero mean, we say that the process is *Gaussian white noise*; and it is denoted

$$W_k \sim \mathcal{N}(0, q/\Delta t), \quad \text{or} \quad \mathcal{W} \sim \mathcal{N}(0, q); \quad (6.62)$$

where it is understood that for the continuous process  $q$  is the amplitude of the psd.

## 6.5 Stochastic Error Models

Some continuous stochastic processes can be described or modeled by a stochastic linear differential equation which falls under the more general topic of autore-

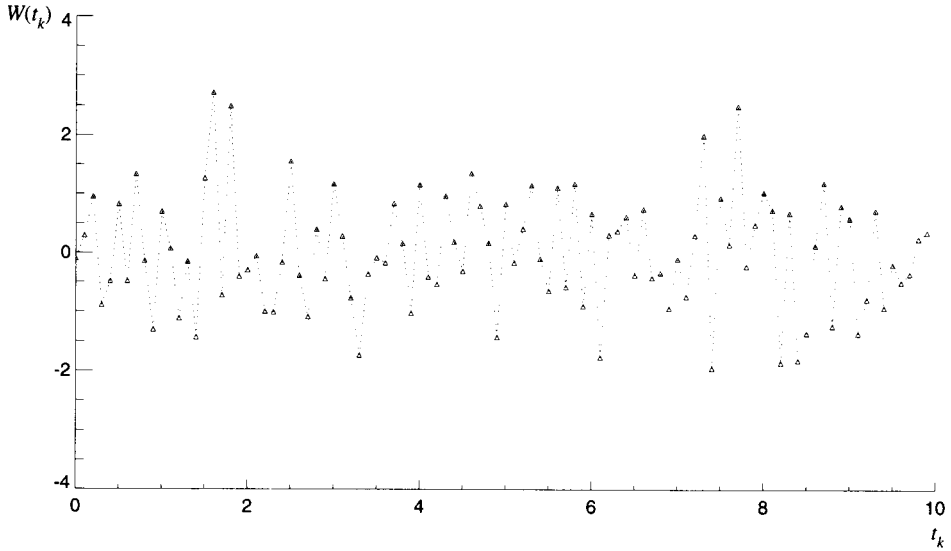


Figure 6.4: Realization of a discrete white noise process.

gressive processes. We will give brief descriptions of some of these processes that prove useful in characterizing the INS errors (in fact, they are useful in describing the stochastic nature of many physical processes). A comprehensive treatment of autoregressive processes can be found in (Priestley, 1981).

### 6.5.1 Random Constant

The random constant is a random process that takes on a constant value for all times, but the constant itself is the realization of a random variable. The differential equation, with initial condition, that describes this process is given by

$$\dot{X}(t) = 0, \quad X(t_0) = X_0. \quad (6.63)$$

Without significant loss in generality, the mean of the process may be assumed zero:  $\mathcal{E}(X_0) = 0$ . The covariance function of the process is given by

$$\mathcal{C}_X(\tau) = \sigma_X^2, \quad \text{for all } \tau, \quad (6.64)$$

where  $\sigma_X^2$  is the variance of any of the random variables of the process. Clearly, the process is fully correlated; given the value of the process at some time, it is known for all times without uncertainty. We note that the random constant, though stationary, is not an ergodic process (the time-average mean is not equal to the ensemble mean). The psd of a random constant is the delta function, according to (6.45) and (6.57):

$$\Phi_X(f) = \sigma_X^2 \delta(f), \quad (6.65)$$

where the units of this delta function are [1/Hz].

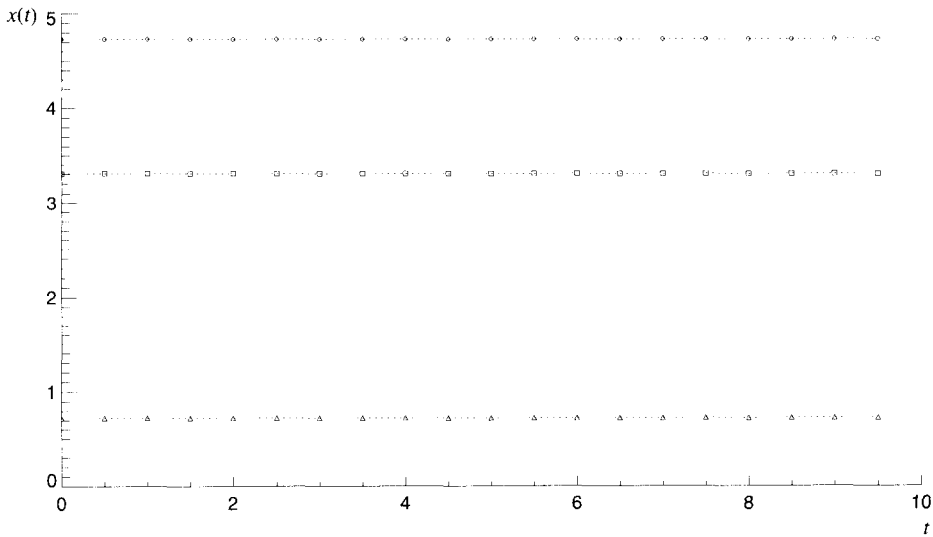


Figure 6.5: Three realizations of a (discrete) random constant stochastic process.

Output from an accelerometer or gyroscope includes an unknown bias; it may be different each time the sensor is turned on. However, from experience (i.e., from repeated laboratory and field experiments) one may know something about its mean and variance. Such biases are modeled as random constants. Figure 6.5 shows a random constant process realized three times.

### 6.5.2 Random Walk

The random walk is a process described by the differential equation and initial condition

$$\dot{X}(t) = \mathcal{W}(t), \quad \text{or} \quad X(t) = \int_{t_0}^t \mathcal{W}(t') dt'; \quad X(t_0) = 0; \quad (6.66)$$

where  $\mathcal{W}$  is a zero-mean, white noise process with covariance function,  $q\delta(t_2 - t_1)$ . The expected value of the random walk at each time is zero:

$$\mathcal{E}(X(t)) = \int_0^t \mathcal{E}(\mathcal{W}(t')) dt' = 0. \quad (6.67)$$

Also, the covariance function of  $X(t)$  is given by

$$\begin{aligned} \mathcal{C}_X(t_1, t_2) &= \mathcal{E}(X(t_1)X(t_2)) = \int_{t_0}^{t_2} \int_{t_0}^{t_1} \mathcal{E}(\mathcal{W}(t'_1)\mathcal{W}(t'_2)) dt'_1 dt'_2 = \int_{t_0}^{t_2} \int_{t_0}^{t_1} q\delta(t'_2 - t'_1) dt'_1 dt'_2 \\ &= \begin{cases} q(t_1 - t_0), & \text{if } t_2 \geq t_1 > t_0, \\ q(t_2 - t_0), & \text{if } t_1 > t_2 > t_0. \end{cases} \end{aligned} \quad (6.68)$$

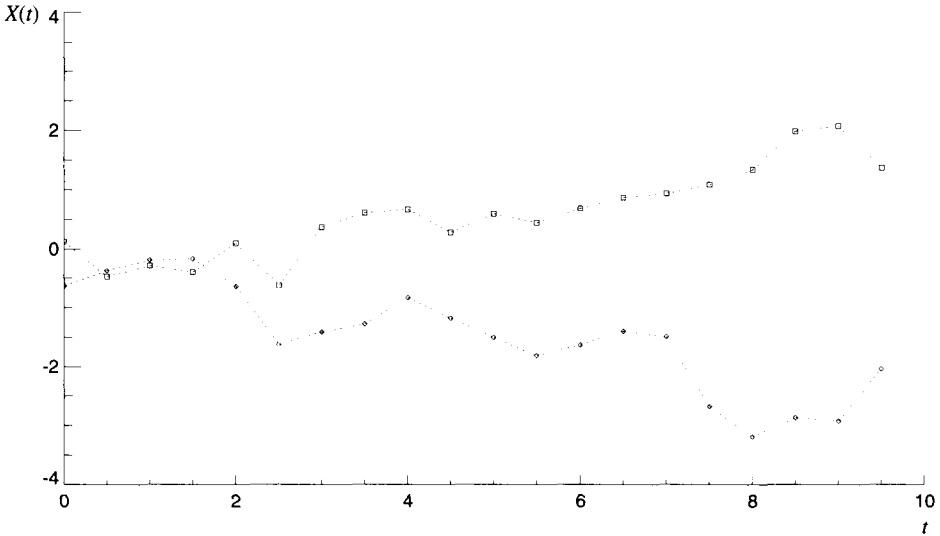


Figure 6.6: Two realizations of a (discrete) random walk process.

Clearly, the random walk is not a stationary process. Its covariance function does not depend on the difference,  $t_2 - t_1$ , and its variance,  $\sigma_X^2 = \mathcal{C}_X(t, t) = q(t - t_0)$ , grows linearly with time. If the white noise process is Gaussian, then the random walk variable,  $X$ , also is Gaussian since Gaussianity is preserved under the linear operation of integrating (summing) the Gaussian white noise variables. In this case the process is known as a *Wiener* process, or a *Brownian-motion* process. Figure 6.6 gives two realizations of a random walk process.

As seen in (6.68), the covariance function of the random walk is well defined. Therefore, just like an integral was used to define the otherwise difficult-to-define delta function, (6.54), so the random walk process often is used to define the continuous white noise process. For example, the continuous Gaussian white noise process is that process whose integral is the Wiener process.

Examples of random walk processes occur naturally in inertial navigation systems since they involve the integration of sensor data. White noise in the accelerometer output results in a velocity error that is a random walk; similarly, the orientation error is a random walk if its genesis is white noise in the sensed angular rates.

### 6.5.3 Gauss-Markov Model

Consider the linear model given by the first order differential equation

$$\dot{X}(t) = -\beta X(t) + \mathcal{W}(t), \quad (6.69)$$

where  $\beta \geq 0$  is a constant and where, in this case,  $\mathcal{W}$  is a zero-mean, Gaussian white noise process with covariance function

$$\mathcal{E}(\mathcal{W}(t_1)\mathcal{W}(t_2)) = 2\sigma^2\beta\delta(t_2 - t_1), \quad (6.70)$$

where  $\sigma^2$  is another parameter. Equation (6.69) is of the type (2.59) specialized to a scalar function. Its solution is given by (2.70) with (2.58), assuming the initial condition (2.60):

$$X(t) = X_0 e^{-\beta(t-t_0)} + \int_{t_0}^t e^{-\beta(t-t')} \mathcal{W}(t') dt', \quad (6.71)$$

where  $X_0 = X(t_0)$ .

The initial condition is designed so as to make the process stationary. The expected value is

$$\mathcal{E}(X(t)) = X_0 e^{-\beta(t-t_0)}; \quad (6.72)$$

and the covariance function, after some derivation, is found to be

$$\mathcal{C}_X(t_1, t_2) = \sigma^2 e^{-\beta|t_2-t_1|} + (X_0^2 - \sigma^2) e^{-\beta(t_1+t_2-2t_0)}. \quad (6.73)$$

Stationarity is ensured if the mean value is time invariant and the covariance depends only on the time interval,  $t_2 - t_1$ . To satisfy these requirements we must choose  $t_0 \rightarrow -\infty$ , and in that case the value,  $X_0$ , is immaterial. In other words, if we were to specify a value of the process at any point in time (i.e., give it an initial condition), the process defined by (6.69) would not be stationary.

With  $t_0 \rightarrow -\infty$  the mean is zero and the covariance function is given by

$$\mathcal{C}_X(\tau) = \sigma^2 e^{-\beta|\tau|}. \quad (6.74)$$

The parameter,  $\sigma^2$ , is the variance (we consider only non-trivial processes, where  $\sigma^2 > 0$ ). The corresponding psd is obtained from (6.45) and a Table of Integrals (e.g., Gradshteyn and Rhyzik, 1980):

$$\Phi_X(f) = \frac{2\sigma^2\beta}{4\pi^2 f^2 + \beta^2}. \quad (6.75)$$

This process is called the *first-order Gauss-Markov* process and is frequently used to describe a correlated signal, where  $\beta$  is a parameter that defines the degree of correlation. The correlation time in this case is defined to be  $1/\beta$ . If it is large, the signal is highly correlated in time; in the limit as  $\beta \rightarrow 0$ , the signal becomes a random constant. If  $1/\beta$  is small, the signal quickly decorrelates, and it resembles white noise, at least for lower frequencies. Figures 6.7(a,b) show the covariance and psd of a first-order Gauss-Markov process.

One could approximate the Gaussian white noise process by a Gauss-Markov process, thus avoiding the physical difficulty with the infinite variance. If  $\sigma^2$  is to be the variance of a signal that is uncorrelated for times greater than the sampling interval  $\Delta t$ , then choosing  $\beta = 2/\Delta t$  in (6.74) will yield correlations

$$\frac{\mathcal{C}_X(\tau)}{\sigma^2} < e^{-2} = 0.14, \quad \text{for } |\tau| > \Delta t. \quad (6.76)$$

For the frequencies of interest,  $f < 1/(2\Delta t)$  (where the limiting right-hand value is called the *Nyquist* frequency), the psd is then “approximately flat” with amplitude  $\Phi_X(0) \approx \Delta t \sigma^2$ . Although this avoids the infinite variance of the signal, the time derivative of the first-order Gauss-Markov process still has infinite variance (see (6.69)); and so it may be argued that this process is also physically unrealizable.

The name “Markov” associated with this process derives from the fact that the conditional probability density of the random variable at any time, given values of the variable at all previous times, is the same as the conditional probability of the variable, given just the most recent value of the process. This is the definition of the *Markovian property*. Higher-order ( $n^{\text{th}}$  order) Markov processes can be defined where the conditional density depends only on the  $n$  most recent values. Such processes are treated more rigorously in terms of continuous, linear, *autoregressive* models, given generally to  $k^{\text{th}}$  order by

$$X^{(k)}(t) + \alpha_1 X^{(k-1)}(t) + \cdots + \alpha_k X(t) = \mathcal{W}(t). \quad (6.77)$$

where  $X^{(j)}$  is the  $j^{\text{th}}$  derivative of  $X$ , the  $\alpha_{k-j}$  are constants, and  $\mathcal{W}$  is continuous white noise. The corresponding discrete *difference equation*, with constants,  $a_j$ , for discrete random processes,

$$X_\ell + a_1 X_{\ell-1} + \cdots + a_{\ell-k} X_{\ell-k} = W_\ell, \quad (6.78)$$

shows more clearly the dependence of the  $\ell^{\text{th}}$  random variable on the previous  $k$  variables. Deriving the discrete model from a continuous model is treated in Section 7.4. It is not the intent here to expound the theory of autoregressive models; (see, e.g., Priestley, 1981). However, we note the considerable variety of linear models available to us as we attempt to describe a particular stochastic process encountered in practical situations. Just two more frequently used models are mentioned. The derivations of the corresponding covariance functions and psd's are left to the reader.

The second- and third-order Gauss-Markov models are defined in (Gelb, 1974) on the basis of second- and third-order linear differential equations, similar to (6.77), but with only one parameter,  $\beta \geq 0$ . For the second-order model, we have

$$\ddot{X}(t) + 2\beta \dot{X}(t) + \beta^2 X(t) = \mathcal{W}(t), \quad (6.79)$$

with white noise covariance function:  $\mathcal{E}(\mathcal{W}(t_1)\mathcal{W}(t_2)) = 4\beta^3 \sigma^2 \delta(t_2 - t_1)$ , and

$$\mathcal{C}_X(\tau) = \sigma^2 e^{-\beta|\tau|} (1 + \beta|\tau|); \quad \Phi_X(f) = \frac{4\beta^3 \sigma^2}{(4\pi^2 f^2 + \beta^2)^2}. \quad (6.80)$$

And, for the third-order model, we have

$$\ddot{\ddot{X}}(t) + 3\beta \ddot{X}(t) + 3\beta^2 \dot{X}(t) + \beta^3 X(t) = \mathcal{W}(t) \quad (6.81)$$

with  $\mathcal{E}(\mathcal{W}(t_1)\mathcal{W}(t_2)) = \frac{16}{3}\beta^5 \sigma^2 \delta(t_2 - t_1)$ , and

$$\mathcal{C}_X(\tau) = \sigma^2 e^{-\beta|\tau|} \left( 1 + \beta|\tau| + \frac{1}{3}\beta^2 \tau^2 \right); \quad \Phi_X(f) = \frac{\frac{16}{3}\beta^5 \sigma^2}{(4\pi^2 f^2 + \beta^2)^3}. \quad (6.82)$$

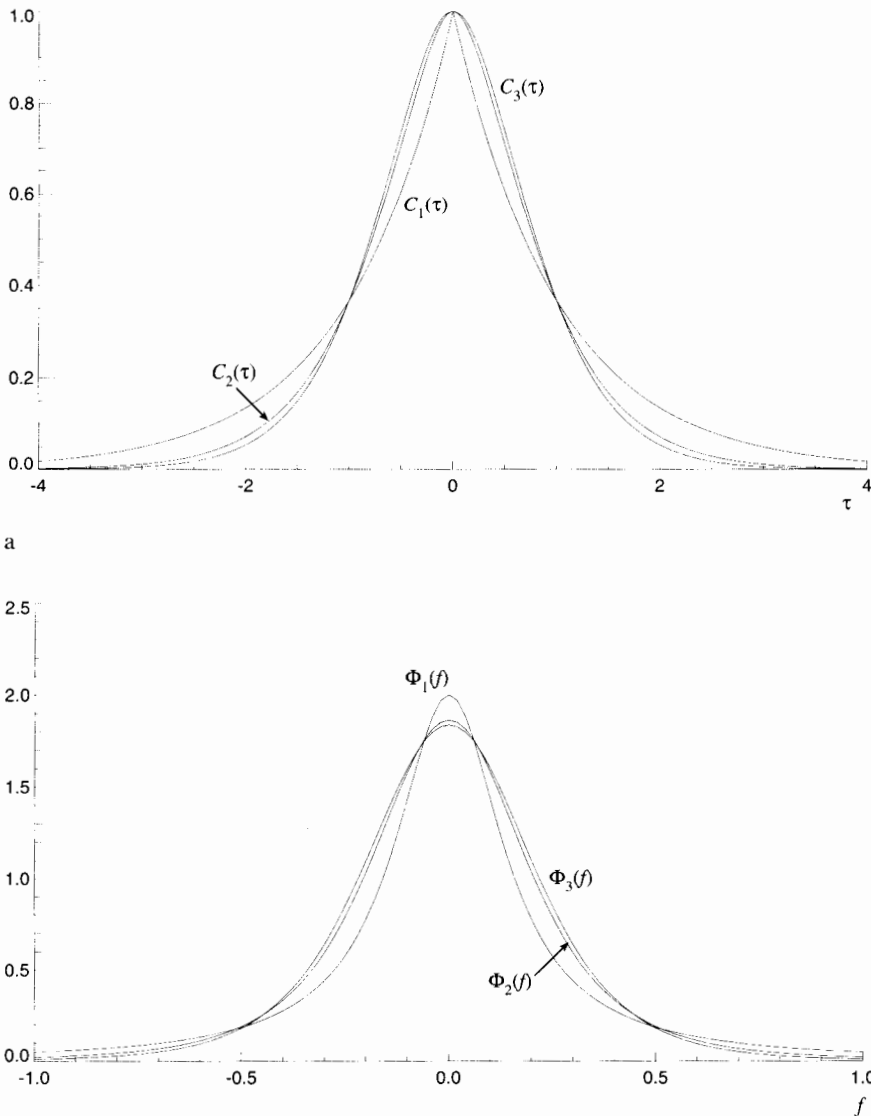


Figure 6.7: Gauss-Markov stochastic processes of first, second, and third order; a) their covariance functions; b) their power spectral densities.

Figures 6.7(a,b) show also the second- and third-order Gauss-Markov covariance functions and corresponding psd's. In each case the variance is  $\sigma^2 = 1$  and the  $\beta$ -parameter is adjusted to yield the same correlation time,  $\tau_c = 1$  (when  $\mathcal{C}_X(\tau_c) = \sigma^2 e^{-1}$ ).

## 6.6 Gravity Models

The navigation error dynamics equations (5.29) together with (5.30) and (5.44) contain, in addition to the sensor errors  $\delta\omega_{is}^s$  and  $\delta\mathbf{a}^s$ , an error in the assumed Earth's gravitation,  $\delta g^a$ . For the  $n$ -frame mechanization (5.52), it was also denoted as an error in the gravity acceleration,  $\delta\bar{g}^n$ , as conventionally defined in geodesy. The gravity error is the difference between what we presume to know about the Earth's gravity acceleration in terms of a model and the actual gravity acceleration at any point. Unlike the sensor errors, the gravity error is a function of position, either in spherical polar coordinates or geodetic coordinates (Figure 1.7). (The naturally occurring time-varying parts of the gravity field due to tides and atmospheric and oceanic mass movements are not considered, being below a few parts in  $10^7$ .) However, as seen by a moving vehicle the gravity field and its errors change in time by virtue of the vehicle's velocity; the conversion from position to time using the velocity is a trivial matter if the latter is known. We discuss gravity models and gravity errors only for the  $n$ -frame mechanization. For other mechanizations, one can simply apply the appropriate transformation to the model in the  $n$ -frame.

### 6.6.1 Normal Gravity Field

The gravity model could be as crude as equation (5.5), which is already accurate to 0.5%, even though it omits the centrifugal acceleration due to Earth's rotation, as well as the effect caused by Earth's ellipsoidal shape (polar flattening). However, it is not difficult, using classical potential theory, to define a significantly more accurate model on the basis of just four parameters (Heiskanen and Moritz, 1967). This model is the gravity potential generated by an oblate ellipsoid, circularly symmetric about the polar axis (as in Figure 1.2) and rotating with the Earth, such that the ellipsoidal surface, itself, is an *equipotential surface* of the gravitational plus centrifugal fields thus generated. (An equipotential surface is a surface on which the potential is a constant.) This ellipsoid is called the *normal ellipsoid* and the corresponding gravity field is known as the *normal gravity field*. Defined in this way, the normal ellipsoid is analogous to the *geoid*, which is an equipotential surface of the actual gravity field, that very nearly coincides with mean sea level. In fact, one of the parameters of the normal ellipsoid, the equatorial radius,  $a$ , is chosen so that the ellipsoid best fits the geoid. The fit is remarkably good, since the vertical separation between the geoid and normal ellipsoid, called the *geoid undulation*, or geoid height, amounts to just a few tens of meters, with a maximum value of  $-110$  m just south of the Indian subcontinent. Figure 6.8 shows the geometric relationship between geoid and normal ellipsoid.

The other three parameters of the normal gravity field include the Earth's rotation rate,  $\omega_e$ ; a physical scale parameter, namely, the total mass of the Earth, including its atmosphere, multiplied by the Newtonian gravitational constant,  $kM$ ; and a shape-related parameter, the dynamical flattening,  $J_2$ , being the relative difference between the polar and equatorial moments of inertia of the Earth. Values of these parameters for the Earth are readily determined from astronomic observations (for

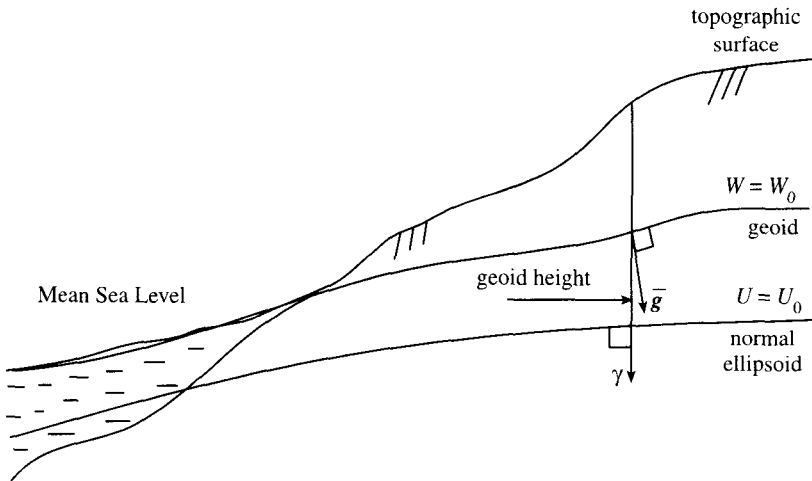


Figure 6.8: Relationship between geoid, normal ellipsoid and topographic surface.

$\omega_e$ ) and by observing the trajectories of Earth-orbiting satellites (for  $kM$ ,  $J_2$ ). The currently adopted normal gravity field, known as the Geodetic Reference System 1980 (GRS80; Torge, 1991) is defined by the following constants:

$$\begin{aligned} a &= 6378137 \text{ m}, \\ J_2 &= 1.08263 \times 10^{-3}, \\ kM &= 3.986005 \times 10^{14} \text{ m}^3/\text{s}^2, \\ \omega_e &= 7.292115 \times 10^{-5} \text{ rad/s}. \end{aligned} \quad (6.83)$$

The geometric flattening of the ellipsoid can be derived rigorously from these four parameters and is given by  $f = 1/298.257222101$ .

Once values for the four parameters, as in (6.83), have been adopted, the normal gravity potential anywhere outside the ellipsoid or any quantity related to the normal potential is completely and unambiguously defined. The potential may be represented in closed form in terms of ellipsoidal coordinates, or more conventionally in spherical polar coordinates by the following series:

$$U(r, \theta) = \frac{kM}{r} \left( 1 - \sum_{n=1}^{\infty} \left( \frac{a}{r} \right)^{2n} J_{2n} P_{2n}(\cos \theta) \right) + \frac{1}{2} \omega_e^2 r^2 \sin^2 \theta, \quad (6.84)$$

where  $P_{2n}$  is an even-degree Legendre polynomial (Hobson, 1965), and the coefficients of the series with degree,  $2n$ , greater than 2 are all related to the given parameters:

$$J_{2n} = (-1)^{n+1} \frac{3e^{2n-2}}{(2n+1)(2n+3)} ((1-n)e^2 + 5nJ_2), \quad (6.85)$$

where  $e$  is the first eccentricity of the ellipsoid ( $e \approx 0.0818$ ). The first part of (6.84), the bracketed series, represents the gravitational potential (due only to mass attraction), and the second part is the centrifugal potential due to Earth's rotation. Note also the polar and equatorial symmetry of the potential, reflecting the geometry of the normal ellipsoid. Often just the first three or four terms in the series are needed for sufficient accuracy because of the factor  $e^{2n-2}$  in (6.85).

The normal gravity (acceleration) vector is the gradient of the normal gravity potential:

$$\gamma = \nabla U, \quad (6.86)$$

where  $\nabla$  is the gradient operator; e.g., in spherical polar coordinates it is

$$\nabla = \left( \frac{\partial}{r\partial\phi}, \frac{\partial}{r\sin\phi\partial\lambda}, \frac{\partial}{\partial r} \right)^T. \quad (6.87)$$

On the normal ellipsoid, the potential varies only in the direction of the perpendicular to the ellipsoid, since the latter is an equipotential surface. That is another way of saying that the gradient of a field is always perpendicular to its field lines, or in this case, surfaces. The normal gravity vector is perpendicular to the normal ellipsoid at points on the ellipsoid. Its magnitude on the ellipsoid, thus equal to the component of  $\gamma$  along the perpendicular, is given by the Somigliana formula (Heiskanen and Moritz, 1967):

$$\gamma(\phi) = \frac{a\gamma_a \cos^2 \phi + b\gamma_b \sin^2 \phi}{\sqrt{a^2 \cos^2 \phi + b^2 \sin^2 \phi}}, \quad (6.88)$$

where  $\phi$  is the *geodetic* latitude;  $b$  is the semi-minor axis of the ellipsoid; and  $\gamma_a$ ,  $\gamma_b$  are the normal gravity values, respectively, at the equator and pole. These parameters can be derived rigorously from the four basic defined constants, and for GRS80 they are given by

$$\begin{aligned} b &= 6356752.3141 \text{ m}, \\ \gamma_a &= 9.7803267715 \text{ m/s}^2, \\ \gamma_b &= 9.8321863685 \text{ m/s}^2. \end{aligned} \quad (6.89)$$

Normal gravity given by (6.88) is an exact formula that holds only for points on the ellipsoid. For points at height,  $h$ , above the ellipsoid, we have the following approximate formula for the magnitude of  $\gamma$  (Heiskanen and Moritz, 1967):

$$\gamma(h, \phi) = \gamma(\phi) \left( 1 - \frac{2}{a} (1 + f + m - 2f \sin^2 \phi) h + \frac{3}{a^2} h^2 \right), \quad (6.90)$$

where

$$m = \frac{\omega_e^2 a^2 b}{kM}. \quad (6.91)$$

Formula (6.90) is in error by not more than  $1.45 \times 10^{-6} \text{ m/s}^2$  at  $h = 20 \text{ km}$ ; the

error is smaller for all points at lower elevations (see (NIMA, 1997) for an exact formulation of the components of the normal gravity vector and its magnitude at any altitude). With the same accuracy,  $\gamma(h, \phi)$ , given by (6.90), also approximates the down component of normal gravity in the  $n$ -frame.

For points at altitude, the normal gravity vector,  $\gamma$ , is only approximately aligned with the perpendicular to the ellipsoid, since the equipotential surfaces of the normal field are not parallel. This deviation from the perpendicular is in the meridian plane and yields a (north) horizontal component of normal gravity given approximately by (Heiskanen and Moritz, 1967, p. 196):

$$\gamma_N(\phi) \approx -8.08 \times 10^{-6} h_{\text{km}} \sin 2\phi \quad [\text{m/s}^2], \quad (6.92)$$

where  $h_{\text{km}}$  is the height of the point in units of km. This formula is accurate to better than  $1 \times 10^{-6}$  m/s<sup>2</sup> at an altitude of 20 km and more accurate at lower altitudes. In most cases, this component is much smaller than the horizontal component of the actual gravity vector,  $\bar{g}_N$ . However, at higher altitudes it can represent a significant fraction of  $\bar{g}_N$ . The normal gravity vector is thus expressed in the  $n$ -frame as

$$\gamma = (\gamma_N \quad 0 \quad \gamma_D)^T, \quad (6.93)$$

where  $-\gamma_D \approx \gamma(\phi, h)$  is computed from (6.90).

The difference between the actual gravity potential,  $W$ , and the normal gravity potential, (6.84), is known as the *disturbing potential*,  $T$ :

$$T = W - U. \quad (6.94)$$

Its gradient is the difference between the actual and normal gravity vectors, called the *gravity disturbance vector*:

$$\delta\bar{g} = \nabla T = \bar{g} - \gamma. \quad (6.95)$$

We use the more conventional  $\delta$ -notation for the gravity disturbance vector and assume that no conflict will arise with the notation for the gravity error used in (5.52) and subsequently. In fact, the gravity error in navigation systems compensated only for normal gravity is equal to the gravity disturbance vector.

More precisely, with (6.93) and  $\bar{g}$  in the  $n$ -frame given by (4.101), we have

$$\delta\bar{g} = (\bar{g}_N - \gamma_N \quad \bar{g}_E \quad g_D - \gamma_D)^T. \quad (6.96)$$

If the system is not compensated for gravity, then the gravity errors in horizontal inertial navigation are  $\bar{g}_N$  and  $\bar{g}_E$ , as inferred from (4.102). If we estimate the gravity disturbance components,  $\delta\bar{g}_N$ ,  $\delta\bar{g}_E$ , on the basis of potential theory (e.g., using (6.94) and gravity measurements; see (6.98) and (6.101)) in order to correct inertial navigation systems, then the gravity compensation terms that would enter (4.102) are

$$\begin{aligned} \hat{\bar{g}}_N &= \delta\hat{\bar{g}}_N + \gamma_N, \\ \hat{\bar{g}}_E &= \delta\hat{\bar{g}}_E, \end{aligned} \quad (6.97)$$

where “ $\hat{\cdot}$ ” signifies an estimated quantity. The corresponding errors in this com-

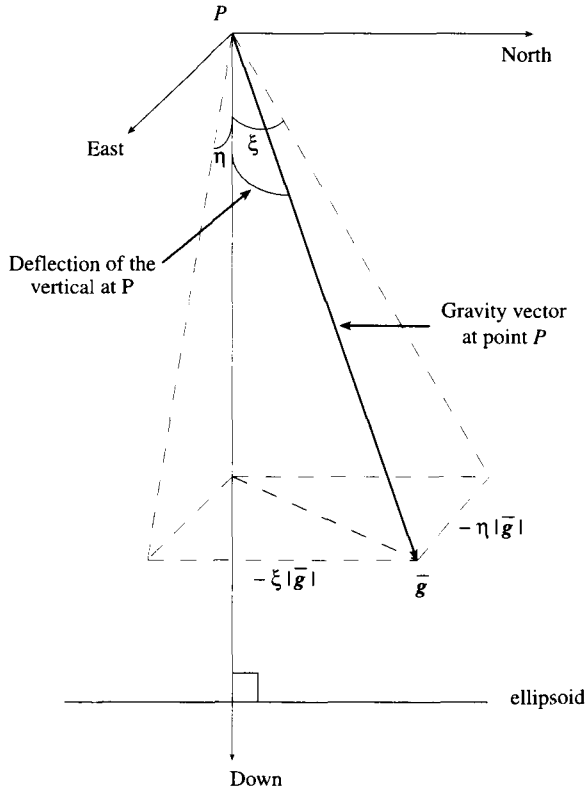


Figure 6.9: Deflection of the vertical.

pensation are the errors in the gravity disturbance estimation (and the north component of normal gravity, if it is neglected).

It is noted that the horizontal gravity components are related to the angular components of the *deflection of the vertical*,  $\xi$ ,  $\eta$ , (see Figure 6.9); to first order in these angles we have:

$$\bar{g} \approx (-\xi \bar{g} \quad -\eta \bar{g} \quad \bar{g})^T, \quad (6.98)$$

where  $\bar{g}$  is the magnitude of gravity, and the signs of the first two terms are consistent with the definition of the vertical deflection as the difference between the outward directions of gravity and the perpendicular to the ellipsoid. Therefore, direct observations of these angles on the Earth's surface (using astronomic determinations of latitude and longitude) also yield compensations for gravity (but only for systems near the Earth's surface since the direction of  $\bar{g}$  changes with altitude).

### 6.6.2 Deterministic Gravity Models

Today we have global and regional gravity models that with reasonable or even fairly high accuracy approximate the Earth's gravity field, including the horizontal

components given by (6.96). Global models of the gravitational potential are formulated as truncated series of spherical harmonic functions,  $\bar{Y}_{nm}$ :

$$\hat{V}(r, \theta, \lambda) = \frac{kM}{a} \sum_{n=0}^{n_{\max}} \sum_{m=-n}^n \left(\frac{a}{r}\right)^{n+1} C_{nm} \bar{Y}_{nm}(\theta, \lambda), \quad (6.99)$$

where  $(r, \theta, \lambda)$  are spherical polar coordinates and the coefficients,  $C_{nm}$ , are determined by observing the trajectories of Earth-orbiting satellites and analyzing ground gravity and satellite altimetry data (Nerem et al., 1995). In (6.99),

$$\bar{Y}_{nm}(\theta, \lambda) = \bar{P}_{n|m|}(\cos \theta) \begin{cases} \cos m\lambda, & m \geq 0 \\ \sin |m|\lambda, & m < 0 \end{cases}, \quad (6.100)$$

where  $\bar{P}_{nm}$  is the fully normalized associated Legendre function of the first kind (Heiskanen and Moritz, 1967; see also (Abramowitz and Stegun, 1970) that has a slightly different normalization). The higher the degree,  $n_{\max}$ , of truncation of the series, the more detail or resolution can be represented by the model.

All of these models have errors resulting from observational error and from the lack of complete global data coverage. The models are least accurate at the high degrees,  $n$ , and require a nontrivial amount of computational capability to calculate a gravitational component at any arbitrary point. A recent model, EGM96 (Lemoine et al., 1998), was derived up to degree  $n_{\max} = 360$ , representing resolution in the field as high as 50 km. This model, containing  $(360 + 1)^2 = 130,321$  coefficients, approximates the horizontal gravity components better in areas of smooth gravity variation, such as the eastern U.S., than in mountainous areas where gravity has much stronger variation, as shown in Figure 6.10.

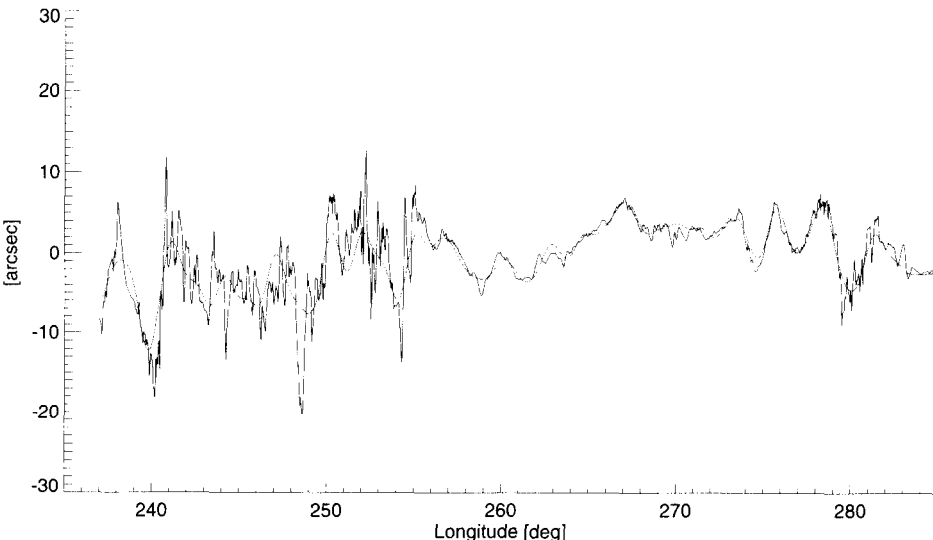


Figure 6.10: North deflection of the vertical at 2-arcminute resolution (jagged line) and according to EGM96 (smooth line) in a profile across the U.S.

We note that inertial navigation systems are sensitive to horizontal gravity components *relative* to the initial calibration point. This is because any acceleration error at the initial point, whether due to accelerometer bias or a reaction to the vertical deflection, is cancelled by an associated tilt according to (5.79). Thus, inertial systems are sensitive to the more regional components of the field, at least for shorter flights. Because of this and the computational expense, high-degree models have not been implemented in navigation systems. Instead, detailed data bases of the vertical deflections are generated for the general area of a flight trajectory using local and regional gravity data. The inertial navigator is then provided with this data base and a fast interpolation routine.

The deflection of the vertical may be determined locally from gravity measurements using the *Vening-Meinesz* equations, given in (Heiskanen and Moritz, 1967):

$$\begin{Bmatrix} \xi(r, \theta, \lambda) \\ \eta(r, \theta, \lambda) \end{Bmatrix} = \frac{1}{4\pi\gamma} \iint_{\sigma} \Delta g(\theta', \lambda') \frac{dS(r, \psi)}{d\psi} \begin{Bmatrix} \cos \alpha \\ \sin \alpha \end{Bmatrix} d\sigma, \quad (6.101)$$

where  $\Delta g$  is the *gravity anomaly* (gravity on the geoid minus normal gravity on the ellipsoid), the geoid is approximated by a sphere of radius  $R$ ,  $\sigma$  represents the unit sphere, and  $\alpha$  is the azimuth of the integration point  $(R, \theta', \lambda')$  with respect to the computation point  $(r, \theta, \lambda)$ .  $S(r, \psi)$  is *Stokes' function* given by

$$S(r, \psi) = \frac{2R}{\ell} + \frac{R}{r} - 3 \frac{R\ell}{r^2} - \frac{R^2}{r^2} \cos \psi \left( 5 + 3 \ln \frac{r - R \cos \psi + \ell}{2r} \right), \quad (6.102)$$

where  $\cos \psi = \cos \theta \cos \theta' + \sin \theta \sin \theta' \cos(\lambda - \lambda')$ , that is,  $\psi$  is the central angle between  $(R, \theta', \lambda')$  and  $(r, \theta, \lambda)$ ; and  $\ell$  is the distance between these points:  $\ell = \sqrt{r^2 + R^2 - 2rR \cos \psi}$ .

Although in coarse navigation applications the deflection of the vertical can be neglected, in precise free-inertial navigation, even for short intervals, it can be a significant source of error, amounting to several hundred meters in just two to three hours, as illustrated in Figure 5.5. It is the reason why precise navigation or guidance systems in long-range military aircraft, missiles, and submarines require a detailed gravity model.

### 6.6.3 Stochastic Gravity Models

Consider the integration of an inertial navigation system with some external source of updating information that attempts to correct, or at least account for the inherent errors of the system (see Chapter 7). If no actual gravity data are available and the horizontal gravity disturbance components are treated as errors, it may prove beneficial to model these components as stochastic processes. The situation can be inverted, leading to one method of actually estimating the gravity disturbance components, represented as stochastic processes, using an INS integrated with the Global Positioning System (see Section 10.4). Stochastic gravity models are also useful in conducting error analyses of inertial navigation systems under different types of applications.

The basis for stochastic modeling is the fact that the horizontal gravity disturbance components generally fluctuate in a random-like fashion, with respect to the regional mean value, in concert with the more or less arbitrary distribution of topographic and crustal mass densities. This stochastic interpretation of the field has been rigorously developed from a theoretical viewpoint in discrete optimal estimation (Moritz, 1980). The method known in physical geodesy as *least-squares collocation* (and as *kriging* in the wider discipline of spatial data statistics; Cressie, 1993) is used successfully to interpolate, extrapolate, or, in general, predict various components of the field from any finite set of gravity field measurements; and it forms one of the principal tenets of gravimetric geodesy.

Many forms of stochastic models have been devised to represent the presumed random nature of the field; a sampling of developments includes references to Heller and Jordan (1979), Moritz (1980), Vassiliou and Schwarz (1987), Forsberg (1987), and Eissfeller and Spietz (1989). The deterministic parameters of the random process in this case are the coordinates of space rather than time. The models are two-dimensional, representing the random character in the horizontal extent, but some include a purely deterministic continuation, based on potential theory, into the vertical dimension. That is, the gravity disturbance at altitude depends rigorously, through a convolution integral (Poisson's integral), on the gravity disturbances distributed on the Earth's surface; and thus, in the vertical dimension the gravity disturbance could hardly be considered stochastically varying.

To simplify the modeling and also to apply the models in estimation algorithms, like the Kalman filter (Chapter 7), we assume stationarity of the gravity disturbance field. Clearly, this may be a highly questionable assumption considering that the single realization of the process available to us often is ostensibly punctuated with areas of rough and smooth variation. Furthermore, since we cannot repeat the experiment of creating the Earth, we must assume ergodicity of the field in order to infer the statistics of the process, e.g., its covariance function, from this one realization. One additional assumption, often imposed, is *isotropy* of the covariance function. In essence any azimuthal correlation is ignored and the covariance becomes simply a function only of distances between points. Certainly any or all of these assumptions are at the core of most criticisms of the stochastic interpretation, and ultimately it is up to the user to decide if a method so founded will yield acceptable results.

The covariance function may be either *empirical*, based on a given distribution of data and computed on the basis of (6.51) or (6.53), or it may be modeled in functional form containing usually at least two parameters: the variance and the correlation distance. It is not the purpose here to elaborate the myriad sophistications to which stochastic gravity modeling has evolved, but simply to illustrate the use of one model and discuss some of the pitfalls and limitations that might be encountered.

If we had some idea of the variance and correlation distance of the horizontal gravity disturbance components along a trajectory, then a Gauss-Markov model might be a suitable choice to describe the along-track correlations. The parameters

could be determined by fitting the Gauss-Markov model to an empirically determined covariance function (it is usually assumed that the mean of the disturbance field is zero; if not, its non-zero mean should first be subtracted and treated as a known bias). For example, a third-order Gauss-Markov model for the covariance of the east gravity disturbance component might be

$$\begin{aligned}\mathcal{C}_{\delta\bar{g}_E}(s) &= \sigma^2 e^{-\beta|s|} \left( 1 + \beta|s| + \frac{1}{3}\beta^2 s^2 \right); \\ \sigma &= 21.8 \times 10^{-5} \text{ m/s}^2; \quad \beta = \frac{1}{8800 \text{ m}};\end{aligned}\quad (6.103)$$

where  $s$  is distance along the trajectory and can be converted to time using the velocity of the vehicle. The correlation distance (see equation (6.41)) for this model turns out to be about 26 km.

The dynamics of the east gravity disturbance component are then modeled by differential equation (6.81), that can be converted to a set of first-order equations:

$$\frac{d}{dt} \begin{pmatrix} \delta\bar{g}_E \\ X_2 \\ X_3 \end{pmatrix} = \begin{pmatrix} 0 & 1 & 0 \\ 0 & 0 & 1 \\ -(\beta v)^3 & -3(\beta v)^2 & -3\beta v \end{pmatrix} \begin{pmatrix} \delta\bar{g}_E \\ X_2 \\ X_3 \end{pmatrix} + \begin{pmatrix} 0 \\ 0 \\ \mathcal{W} \end{pmatrix}, \quad (6.104)$$

where  $X_2$  and  $X_3$  are intermediate variables, and  $v$  is the presumably constant velocity. With the values of  $\beta$  and  $\sigma$  given by (6.103) and  $v = 100 \text{ m/s}$ , we have for the white noise:

$$\mathcal{E}(\mathcal{W}(t)\mathcal{W}(t')) = \frac{16}{3}(\beta v)^5 \sigma^2 \delta(t - t') = 4.8 \times 10^{-17} \left[ \frac{\text{m}^2}{\text{s}^{10}} \right] \delta(t - t'). \quad (6.105)$$

Another such set of equations, with corresponding values for the variance and correlation distance, would serve as model for the north gravity component. This type of formulation, as a linear differential equation with white noise excitation, is required to include the gravity components as permissible error processes in the linear error estimation algorithm to be developed in Chapter 7. However, such a model of the gravity disturbance field is highly contrived. Even if one accepts the stochastic interpretation, a component of the actual field is neither linear, nor finite-order (as modeled above, it is supposed to be a third-order process). In addition, one should note that the components of the gravity disturbance are physically, and therefore by our assumptions, stochastically correlated. That is, the east gravity component at a point is correlated with the down and north components at some distance away from the point (at the point, they are independent). The model (6.104) for the east component is *not self-consistent* with a similar model for the north component. Self-consistency in the models can be ensured by stochastic modeling of the disturbing potential, (6.94). Since the gravity disturbance vector is the gradient of the disturbing potential, stochastic models of the former can be *derived* from the disturbing potential model by appropriate differentiations (Jordan, 1972; Moritz, 1980). In this way all gravity disturbance components (and other higher-order derivatives) have mutually self-consistent stochastic properties.

We note that these correlations among the various components may change as the trajectory of the vehicle rotates in azimuth. That is, although one might assume that the disturbing potential covariance function is isotropic, the derived covariances for the horizontal components are not isotropic and, therefore, may not adequately model their stochastic behavior as the vehicle changes its heading. With the additional non-stochastic nature of the gravity field in the vertical dimension it is clear that no single stochastic model may suffice for trajectories that have significant changes in heading or altitude.

These several shortcomings do not preclude approximating the gravity disturbance components as random processes with practical covariance models if the resulting mismodeling errors have no deleterious effects on the desired INS application. These effects can usually be investigated using simulations and covariance analyses.

## 6.7 Examples of IMU Error Processes

As an illustration of the kind of stochastic modeling that might be considered in the estimation of INS errors, we consider the error models usually associated with (optical) gyros and accelerometers. These are analogous to equations (3.76) and (3.118), respectively, with some specific (and not atypical) noise processes added for purposes of demonstration. The units of measure often cause the most difficulty. A particular manufacturer may provide a specification for the errors, based on laboratory or field test experience, as shown in Table 6.1. The acceleration units may be  $[m/s^2]$  or, as shown here, [mgal]. The latter are usually used in geodesy and geophysics to quantify gravity (in honor of Galileo) and are defined by

$$1 \text{ gal} = 10^{-2} \text{ m/s}^2; \quad 1 \text{ mgal} = 10^{-5} \text{ m/s}^2. \quad (6.106)$$

The second column in Table 6.1 identifies the type of error, and from the specific numerical values and their units in the third column, one may infer the specific dynamics model associated with each error, assumed to be a random process.

The error models for the  $j^{\text{th}}$  accelerometer would then be given by the following:

$$\delta a_j^s(t) = B_j + \kappa_{A_j} a_j^s(t) + C_{A_j}(t) + T_j e^{-t/(100\text{s})} + \mathcal{W}_{A_j}(t), \quad (6.107)$$

Table 6.1: Example of accelerometer and gyro error specifications.

|                |                    |                                     |
|----------------|--------------------|-------------------------------------|
| Accelerometer: | bias repeatability | 220 mgal                            |
|                | scale factor error | 300 ppm                             |
|                | white noise        | 40 mgal/ $\sqrt{\text{Hz}}$         |
|                | correlated noise   | 75 mgal, 12 min correlation time    |
|                | thermal transient  | 90 mgal, 100 s time constant        |
| Gyro:          | bias repeatability | 0.005 °/hr                          |
|                | scale factor error | 10 ppm                              |
|                | white noise        | 0.002 °/ $\sqrt{\text{hr}}$         |
|                | correlated noise   | 0.004 °/hr, 60 min correlation time |

where the dynamics of the various constituent processes and their statistics are given, in this case, by

$$\begin{aligned}
 \dot{B}_j &= 0, & \sigma_{B_j}^2 &= (220 \text{ mgal})^2; \\
 \dot{\kappa}_{A_j} &= 0, & \sigma_{\kappa_{A_j}}^2 &= (300 \times 10^{-6})^2; \\
 \dot{T}_j &= 0, & \sigma_{T_j}^2 &= (90 \text{ mgal})^2; \\
 \dot{C}_{A_j}(t) &= -\frac{1}{720 \text{ s}} C_{A_j}(t) + \mathcal{W}_{C_{A_j}}(t), & \mathcal{E}(\mathcal{W}_{C_{A_j}}(t)\mathcal{W}_{C_{A_j}}(t')) &= 15.6 \left( \frac{\text{mgal}}{\text{s}} \right)^2 \Bigg|_{\text{Hz}} \delta(t-t'); \\
 & & \mathcal{E}(\mathcal{W}_{A_j}(t)\mathcal{W}_{A_j}(t')) &= (40 \text{ mgal})^2 / \text{Hz} \delta(t-t').
 \end{aligned} \tag{6.108}$$

The mean value of each random variable is assumed to be zero. The constants in (6.107) are modeled as random constants (6.63), with variance (6.64). The thermal transient is modeled simply as a (non-stationary) exponentially decaying process with random initial amplitude; while the correlated noise is assumed to behave like a first-order Gauss-Markov process (6.69). The covariance of the white noise associated with this process is given by (6.70). The white noise,  $\mathcal{W}_{A_j}$ , is assumed formally to be a continuous process with covariance function given by (6.55).

Similarly, for the  $j^{\text{th}}$  gyro we have the model

$$(\delta\omega_{is}^s)_j(t) = D_j + \kappa_{G_j}(\omega_{is}^s)_j(t) + C_{G_j}(t) + \mathcal{W}_{G_j}(t), \tag{6.109}$$

where the dynamics and the statistics of the processes, analogous to (6.108), are given by

$$\begin{aligned}
 \dot{D}_j &= 0, & \sigma_{D_j}^2 &= 5.9 \times 10^{-16} \left( \frac{\text{rad}}{\text{s}} \right)^2; \\
 \dot{\kappa}_{G_j} &= 0, & \sigma_{\kappa_{G_j}}^2 &= (10 \times 10^{-6})^2; \\
 \dot{C}_{G_j}(t) &= -\frac{1}{3600 \text{ s}} C_{G_j}(t) + \mathcal{W}_{C_{G_j}}(t), & \mathcal{E}(\mathcal{W}_{C_{G_j}}(t)\mathcal{W}_{C_{G_j}}(t')) &= 2.1 \times 10^{-19} \left( \frac{\text{rad}}{\text{s}^2} \right)^2 \Bigg|_{\text{Hz}} \delta(t-t'); \\
 & & \mathcal{E}(\mathcal{W}_{G_j}(t)\mathcal{W}_{G_j}(t')) &= 3.4 \times 10^{-13} \left( \frac{\text{rad}}{\text{s}} \right)^2 \Bigg|_{\text{Hz}} \delta(t-t').
 \end{aligned} \tag{6.110}$$

Note that the specification for the white noise in the angular rates has units  $[\text{°}/\text{hr}] = [60 \text{ °}/\text{hr}/\sqrt{\text{Hz}}]$ , which are also the units for the square root of the variance per unit time for the angle errors, treated as random walk processes (see (6.68)).

## 7 Linear Estimation

### 7.1 Introduction

The previous chapters developed the dynamics equations for the system errors, that is, a set of differential equations that model the behavior of the system errors as time progresses. These equations are linear under the assumption that the errors are small enough to be represented by differential perturbations of the system dynamics or navigation equations; in other words, second and higher-order powers of the errors were neglected. Given initial conditions, the differential equations could be integrated to determine the error at any time after the initial time. In some cases, this is readily done and also has conceptual value (as demonstrated in Chapter 5); but generally the problem is more complicated. In the first place, the forcing terms of the differential equations contain a random part, a stochastic process, which implies that the error cannot be determined exactly. Only some statistical aspects, such as the mean and variance, can be estimated, and even then we must know or assume something about the probability distribution of the stochastic process. Secondly, we often have information about our system errors from external sources, that is, from presumably independent observations, that themselves may have a stochastic component. We would like to include these external observations to quantify better the system errors (e.g., calibration and initialization) and to correct them to the extent possible in order to preserve the validity of our linear model. If the system errors are allowed to grow too large, the linear perturbation development may no longer represent an adequate model. To summarize, we have a system of errors associated with the operation of the inertial navigation system, namely errors in position, velocity, and orientation. Under certain specifications, these errors will be identified as the *state* of the system, representing the departure of the indicated inertial navigation quantities from their true values. We would like to estimate the state of the system at any time with (or without) external knowledge about this state, where this external information is given in the form of independent *observations* of the system.

This problem belongs to the general theory of estimation. Rather than provide a full development of this theory (which can be found in many good textbooks, e.g., by Maybeck (1979), Gelb (1974), and Brown and Hwang (1992)), this text presents only the essential ingredients needed for our problem. The theory of estimation is built on three essential objectives. One is to provide a unified framework in which the data may be interpreted and combined. This is the theory of probability and stochastic processes that was reviewed in the previous chapter and that sets the foundation for developing the necessary tools to estimate the system state, assumed to be a set of random variables. The second objective, then, is to formulate these algorithms or *estimators* that operate on the data obtained from the system and external observations. Depending on what and how much is known about their statistical behavior, alternative approaches may be considered. We proceed on the

basis of the *Bayesian* approach where the probability densities of the observations and of the system states are presumed known. Finally, methods should be developed to measure the quality of these algorithms. The assessment of a particular estimation procedure involves the establishment of a truth model against which the procedure can be tested. Usually, the aim is to economize the computational load of the estimation where possible, primarily for the benefit of real-time applications. The present chapter concentrates on the second objective and the reader is directed to Maybeck (1979) for a discussion of algorithm assessment.

The estimation problem may be divided into three distinct processes: *filtering*—estimating the value of a state based on observations up to some time (e.g., the current time); *prediction*—estimating the state beyond the time of the last observation available; and *smoothing*—estimating the state at any time based on all observations available before and after that time. It is most natural and certainly rigorous to develop the estimation procedure using a discrete time history for the state variables and for the observations (the amplitudes, or values, of the states and observations are, however, assumed continuous). The discourse in Chapters 4 through 6 focused on continuous models for the system errors, continuity being a fundamental assumption of physical processes. When we actually wish to estimate the state at any specific time, using also observations available at certain instances of time, we, in effect, sample the processes. Thus, one part of the problem is to *discretize* the error dynamics and make them amenable to our estimation procedure. Of course, a continuous estimation development exists and will be presented, but as a generalization of the discrete approach, rather than the discrete approach being a specialization of the continuous case.

Filtering is the most important aspect of the estimation problem because it is the process by which data from various sources, external and internal to the INS, and with different statistical characterizations are combined to yield the estimate of the current system states. Prediction is merely the propagation (or *transition*) of the states from one epoch to the next based on the system dynamics model and the a priori probabilities; while smoothing is a generalization of filtering in which observations before and after the desired estimation epoch are included. With certain assumptions, the filtering algorithm may be developed in recursive form (this was one of the major contributions of Kalman), implying that all information needed to proceed to the next time epoch is available at the current epoch. The resulting estimate recursively computed at any time will be the result of all observations available up to that time. A recursive estimation scheme obviously has immense computational benefits, especially for real-time applications, but also in a post-mission environment where a time history of thousands of estimates may be needed.

The estimator of a system state variable should be optimal in some sense; the conditions of optimality must be specified and may depend in part on the available probability density information. For the moment we consider only linear estimators; nonlinear estimation will be mentioned later. The problem is, therefore, one of linear optimal estimation. In essence, we seek an estimator of the state that is *unbiased*, is *best* according to some measure, and is *consistent*. Unbiasedness implies

that the expected value of the estimator equals the expected value of the state being estimated. Optimality is achieved in the Bayesian sense by minimizing the probabilistic cost incurred by not choosing the true value; no other unbiased estimator has a smaller cost. Finally, consistency is needed to ensure that ultimately as the number of observations increases, the cost approaches zero, or the estimate approaches the true value.

The next section is devoted to the optimal estimation of a random variable, first in general terms and then for the case that an observation of a linear function of the variable is available. The probability density of the observation noise is assumed known, as is the probability density of the variable prior to the observation. In this way the Bayesian approach to estimation can be utilized. It is not the only way to proceed, but has a strong intuitive appeal in terms of information theory. The subsequent section derives a recursive algorithm (the discrete Kalman filter) that utilizes this estimation procedure. Ultimately, the corresponding estimation is also developed in the continuous domain.

## 7.2 Bayesian Estimation

The Bayesian concept applied to our estimation problem is the propagation of the conditional probability density of the state variable from one epoch to the next under the condition of the given probability density of the observations. In addition to the linearity already assumed, we make a further seemingly sweeping proposition. It is that the stochastic processes associated with the system dynamics and the observations are all driven by independent Gaussian random variables. Upon some reflection, however, we may argue that this is not an overly restrictive assumption. The usual justification is that the noise either of the system or of the observation results from many minor random fluctuations, whose sum total is normally distributed according to the *Central Limit Theorem* of statistics (Dudewicz, 1976). In any case, the probability densities of the stochastic processes generally would otherwise not be known; although the first two moments (the mean and standard deviation) can be estimated in many circumstances. Therefore, one might as well assume the Gaussian distribution, it being completely determined by its first two moments. Finally, if for no other reason, this assumption not only simplifies the mathematics, but also makes the solution to our problem tractable.

That the noise variables of the system and observation should be independent is also not an unreasonable assumption in our case since the two arise in completely different regimes, one in the internal workings of the INS sensors, the other associated with an external system, e.g., GPS. Later, when developing the recursive estimation algorithm, we will further assume (in fact, without loss in generality) that the noise sources are white noise processes. This is a reasonable assumption based on the close observed agreement between physical random processes and modeled linear systems driven by white noise. It is certainly only an approximation, one that, strictly speaking, is not physically realizable as illustrated in Section 6.4. However, the mathematical abstraction that defines white noise can easily be attuned to the

real world by restricting our interest to a finite band of system frequencies, which is always sufficiently adequate.

### 7.2.1 Optimal Estimation Criteria

We start with the optimization criterion in our estimation problem from a general viewpoint. In essence, we wish to minimize the risk of choosing the wrong estimate. Risk is formalized by first defining the cost, or penalty, of selecting a value other than the true value. Let  $J(x, \hat{x})$  be the *cost function*, assigning the cost attributable to choosing the estimate  $\hat{x}$  when  $x$  is the true value. (A comment on notation is in order, here. We used upper case letters in Chapter 6 to denote a random variable whose realization is denoted by the corresponding lower case letter. Here, we use lower case letters to denote the random variable, and we tacitly sidestep the formality of a separate notation for its realization, making it explicit only when absolutely necessary. This will allow the distinction to be continued between matrices (upper case) and vectors (still in bold style), that was followed in Chapters 1 through 5.)

By definition, the cost is always non-negative:  $J(x, \hat{x}) \geq 0$ ; but, otherwise, generally, we cannot compute values of the cost function because it is a stochastic quantity, depending on the random variable,  $x$ . Therefore, we introduce a new entity, the *risk*, which is defined to be the expected value of the cost function, based on the probability density,  $f(x)$ , of the variable,  $x$ . With (6.15), the *best estimate* is the one that minimizes this so-called *Bayes' risk*:

$$\hat{x}_{\text{opt}} = \arg \left( \min_{\hat{x}} \mathcal{E}(J(x, \hat{x})) \right) = \arg \left( \min_{\hat{x}} \int_{\Pi} J(x, \hat{x}) f(x) dx \right), \quad (7.1)$$

where  $\arg()$  stands for “argument of” and, in this case, is the value of the estimate,  $\hat{x}$ , among all such estimates, that minimizes the expectation of the cost function, that is, the risk. The probability space of the variable is denoted  $\Pi$ .

The cost function is quite general; for example, one could define it to be (for continuous variables)

$$J(x, \hat{x}) = 1 - \delta(x - \hat{x}), \quad (7.2)$$

where  $\delta$  is the delta function (6.54), meaning that all (non-zero) errors,  $\hat{x} - x$ , in the estimate carry the same maximum penalty of 1. But if  $\hat{x} = x$ , then the cost disappears (by definition any non-positive cost is identical to zero cost). Substituting (7.2) into (7.1), we have

$$\begin{aligned} \hat{x}_{\text{opt}} &= \arg \left( \min_{\hat{x}} \int_{\Pi} (1 - \delta(x - \hat{x})) f(x) dx \right) \\ &= \arg \left( \min_{\hat{x}} (1 - f(\hat{x})) \right), \end{aligned} \quad (7.3)$$

using (6.8) and (6.54); and we see that the optimal estimate in this case is the value

of the variable that minimizes the negative of the probability density of  $x$ . In other words,  $\hat{x}_{\text{opt}}$  is the “mode”, or the value that maximizes  $f(x)$ :

$$\hat{x}_{\text{opt}} = \arg \left( \max_{\hat{x}} f(\hat{x}) \right). \quad (7.4)$$

It is known as the *most probable estimate* (MPE) of  $x$ . Clearly, the probability density of  $x$  must be known, to some extent at least, in order to determine its maximum.

The cost function can also be defined by some measure of the difference between the estimate and the true value, e.g., the absolute value (magnitude), or the squared magnitude, or some other norm of the error. In the case of a random vector,  $x$  (which we assume henceforth), the error is  $\hat{x} - x$ , and we will consider the cost function to be given by the quadratic form:

$$J(x, \hat{x}) = (\hat{x} - x)^T Q (\hat{x} - x), \quad (7.5)$$

where  $Q$  is a given matrix that assigns weights to the products of the errors. We will assume that  $Q$  is symmetric and positive definite. If the expectation of  $J$  (i.e., the risk), as a function of the estimate  $\hat{x}$ , is minimum when  $\hat{x} = \hat{x}_{\text{opt}}$ , then necessarily

$$\frac{d}{d\hat{x}} \mathcal{E}(J(x, \hat{x}))|_{\hat{x}=\hat{x}_{\text{opt}}} = \mathbf{0}. \quad (7.6)$$

The right side is a vector of zeros. Performing the differentiation on the integral in (7.1), written for the vector variable using (7.5), yields

$$\begin{aligned} \frac{d}{d\hat{x}} \mathcal{E}(J(x, \hat{x}))|_{\hat{x}=\hat{x}_{\text{opt}}} &= \int (Q(\hat{x}_{\text{opt}} - x) + Q^T(\hat{x}_{\text{opt}} - x)) f(x) dx \\ &= 2Q\hat{x}_{\text{opt}} \int f(x) dx - 2Q \int x f(x) dx \\ &= 2Q(\hat{x}_{\text{opt}} - \mathcal{E}(x)), \end{aligned} \quad (7.7)$$

by the assumed symmetry of  $Q$ . Note that the integration is with respect to all the components of the vector,  $x$ , and the implied notation is equivalent to (6.22). Since  $Q$  is also positive definite, equations (7.6) and (7.7) not only imply that

$$\hat{x}_{\text{opt}} = \mathcal{E}(x), \quad (7.8)$$

but also it can be shown that (7.8) is a *sufficient* condition for minimizing the expected cost function. That is, the expected value of the random variable indeed minimizes Bayes' risk function with cost given by (7.4). This result is independent of the particular weight matrix,  $Q$ , (as long as it is symmetric and positive definite), and it is also independent of the particular form of the probability density of  $x$  (of course, it depends on where its first moment is located). The estimate (7.8) is called the *minimum mean square error* (MMSE) estimate of  $x$ . If  $x$  is a Gaussian variable, then the expected value is the value where the probability density is maximum (the mean equals the mode; see Figure 6.1), and the MMSE estimate is also the MPE, equation (7.4).

### 7.2.2 Estimation with Observations

So far, the discussion did not include any observations; and, indeed, without them, the estimation is rather dull, being wholly dependent on some assumptions about the probability density of the random variable,  $x$ . But these optimal estimation concepts are completely general with respect to the type of probability density of  $x$ . In particular, it may be the conditional density of  $x$ , given observations,  $y$ :  $f(x|y)$ . Then, the optimal estimate, analogous to (7.1), is defined by

$$\hat{x}_{\text{opt}} = \arg \left( \min_{\hat{x}} \mathcal{E}(J(x, \hat{x})|y) \right) = \arg \left( \min_{\hat{x}} \int_{\Pi} J(x, \hat{x}) f(x|y) dx \right). \quad (7.9)$$

Technically,  $\hat{x}_{\text{opt}}$  is the optimal *estimator*. It is a random variable since the observations are random; when the observations are realized and substituted into the estimator we obtain the optimal *estimate*, that is, a value.

The MMSE estimate is obtained by following the same derivation as in (7.6) through (7.8) with (7.5) as cost function, but  $f(x|y)$  as probability density. It is clear that the MMSE estimate is the *conditional mean*:

$$\hat{x}_{\text{MMSE}} = \mathcal{E}(x|y), \quad (7.10)$$

which requires some knowledge about the conditional density,  $f(x|y)$ . According to *Bayes' Rule* (6.5), the needed density, known as the *a posteriori density*, that is, the density of  $x$ , given that the observations are  $y$ , is

$$f(x|y) = \frac{f(y|x)f(x)}{f(y)}, \quad (7.11)$$

where for any given observations,  $y$ , the value of the density,  $f(y)$ , can be viewed as a constant, not affecting the shape (only the scale) of the density,  $f(x|y)$ . In other words, it will not be necessary to know the value of this density when determining the best estimate of  $x$ , because the minimization (7.1) of the expected value of the cost function is independent of its scale. However, we do need to specify  $f(y|x)$ , the density of the observations, given the random variables.

Similarly, once  $f(x|y)$  is known, its maximum value decides the MPE, analogous to (7.4), given by:

$$\hat{x}_{\text{MPE}} = \arg \left( \max_{\hat{x}} f(\hat{x}|y) \right). \quad (7.12)$$

In this case of an estimate based on an observation, it is also known as the *maximum a posteriori* estimate; it is the same as the MMSE if the densities are Gaussian.

The estimation of variables may also be formulated in the absence of probabilistic information either about the variables or about the observations. First, suppose we have some idea about the density,  $f(y|x)$ , which describes the probability of the observations, given that the variables take on their true values, but know nothing about the variables. Then, it is reasonable to define the best estimate as the value that maximizes this density:

$$\hat{\mathbf{x}}_{\text{opt}} = \arg \left( \max_{\hat{\mathbf{x}}} f(\mathbf{y} | \hat{\mathbf{x}}) \right). \quad (7.13)$$

$f(\mathbf{y} | \mathbf{x})$  is also known as the *likelihood function*, and the estimate becomes the *maximum likelihood estimate* (MLE).

Moreover, if no probability statement can be made regarding the observations, one could simply define the best estimate as the value that minimizes the (possibly weighted) sum of squared residuals:

$$\hat{\mathbf{x}}_{\text{opt}} = \arg \left( \min_{\hat{\mathbf{x}}} (\mathbf{y} - \mathcal{E}(\mathbf{y} | \hat{\mathbf{x}}))^T S^{-1} (\mathbf{y} - \mathcal{E}(\mathbf{y} | \hat{\mathbf{x}})) \right), \quad (7.14)$$

where the expected value of the observations can be found from the specified observation model (see Section 7.3.1), and where  $S^{-1}$  is a suitable (positive definite) weight matrix. The best estimate in this case is called the *least-squares estimate*. If the covariance matrix of the observation errors is known, it should be used for  $S$ ; if it is further known that the probability distribution of the observation errors is Gaussian, the least-squares estimate is the same as the maximum likelihood estimate. Indeed, minimizing the quadratic in (7.14) is then equivalent to maximizing  $f(\mathbf{y} | \mathbf{x})$ , as seen by (6.31) applied to  $\mathbf{y}$  (given  $\mathbf{x}$ ).

Furthermore, if the probability density of  $\mathbf{x}$  is almost constant (meaning that it is virtually flat and close to zero), then by Bayes' Rule (7.11), the MPE (7.12) and the MLE (7.13) are almost the same. In this case, if all densities are Gaussian, then all estimates: MMSE, MPE, MLE, and the least-squares estimate, are the same.

We will not be concerned explicitly with the least-squares and maximum likelihood estimators since we will always know, or presume to know, something about the probabilities of the variables, that is, the states of our system. This is because the system is generally endowed with some driving noise that constitutes the basis for the random character of the states. The noise is usually identified as Gaussian which implies Gaussianity for the system states, as will be shown.

### 7.2.2.1 A Posteriori Density Function

We now consider more explicitly the determination of the *a posteriori* density function,  $f(\mathbf{x} | \mathbf{y})$ , that is, the density of the variables,  $\mathbf{x}$ , conditioned on the observations,  $\mathbf{y}$ . At a point in time when an observation is introduced, it is assumed that the probability density of  $\mathbf{x}$ ,  $f(\mathbf{x})$ , is known; this is called the *a priori density*. We wish to estimate the vector  $\mathbf{x}$  ( $\dim \mathbf{x} = m$ ) on the condition that the vector of observations  $\mathbf{y}$  ( $\dim \mathbf{y} = n$ ) has yielded certain values based on an assumed linear relationship to  $\mathbf{x}$ :

$$\mathbf{y} = H\mathbf{x} + \mathbf{v}, \quad (7.15)$$

where  $H$  is an  $n \times m$  constant matrix,  $\mathbf{v}$  is a vector of observation errors, and either  $f(\mathbf{y} | \mathbf{x})$  or  $f(\mathbf{v})$  is known. These two density functions are equivalent if  $\mathbf{v}$  and  $\mathbf{x}$  are independent, which is assumed henceforth, because then

$$f(\mathbf{y} | \mathbf{x}) = f(\mathbf{v} = \mathbf{y} - H\mathbf{x} | \mathbf{x}) = f(\mathbf{v} = \mathbf{y} - H\mathbf{x}). \quad (7.16)$$

The density on the right side of (7.16) is the density of  $\mathbf{v}$ , but in a coordinate system shifted with respect to that of  $\mathbf{y}$  by  $H\mathbf{x}$ .

As discussed at the start, we suppose that the densities of the a priori probability function of the random variable and the probability function of the observation error are both Gaussian. Then the a posteriori density is also Gaussian. This will now be proved. We have from (6.31):

$$\mathbf{x} \sim \mathcal{N}(\boldsymbol{\mu}_0, P_0) \Rightarrow f(\mathbf{x}) = c_x \exp\left(-\frac{1}{2}(\mathbf{x} - \boldsymbol{\mu}_0)^T P_0^{-1}(\mathbf{x} - \boldsymbol{\mu}_0)\right), \quad (7.17)$$

where the constant  $c_x$  is given by:

$$c_x = |P_0|^{-1/2}(2\pi)^{-m/2}, \quad (7.18)$$

and  $\boldsymbol{\mu}_0$  and  $P_0$  are, respectively, the a priori mean and covariance matrix of the random vector  $\mathbf{x}$ , and where  $\exp(\cdot) \equiv e^{(\cdot)}$ . Similarly, for the observation noise:

$$\mathbf{v} \sim \mathcal{N}(\mathbf{0}, R) \Rightarrow f(\mathbf{v}) = c_v \exp\left(-\frac{1}{2}\mathbf{v}^T R^{-1}\mathbf{v}\right), \quad (7.19)$$

where the constant,  $c_v$ , is

$$c_v = |R|^{-1/2}(2\pi)^{-n/2}. \quad (7.20)$$

The observation noise is supposed to be a zero-mean, Gaussian, random process with covariance matrix,  $R$ . Also,  $\mathbf{x}$  and  $\mathbf{v}$  are assumed to be independent.

From (7.16) and (7.19), we have immediately

$$f(\mathbf{y}|\mathbf{x}) = c_v \exp\left(-\frac{1}{2}(\mathbf{y} - H\mathbf{x})^T R^{-1}(\mathbf{y} - H\mathbf{x})\right). \quad (7.21)$$

Now, the a posteriori density is obtained by substituting (7.17) and (7.21) into Bayes' rule (7.11):

$$f(\mathbf{x}|\mathbf{y}) = c' \exp\left(-\frac{1}{2}(\mathbf{y} - H\mathbf{x})^T R^{-1}(\mathbf{y} - H\mathbf{x}) - \frac{1}{2}(\mathbf{x} - \boldsymbol{\mu}_0)^T P_0^{-1}(\mathbf{x} - \boldsymbol{\mu}_0)\right) \quad (7.22)$$

where  $c' = c_x c_v / f(\mathbf{y})$ . Expanding the exponent in (7.22) yields

$$\begin{aligned} & -\frac{1}{2}(\mathbf{y}^T R^{-1} \mathbf{y} + \boldsymbol{\mu}_0^T P_0^{-1} \boldsymbol{\mu}_0 + \mathbf{x}^T (P_0^{-1} + H^T R^{-1} H) \mathbf{x} \\ & - \mathbf{x}^T (H^T R^{-1} \mathbf{y} + P_0^{-1} \boldsymbol{\mu}_0) - (\mathbf{y}^T R^{-1} H + \boldsymbol{\mu}_0^T P_0^{-1}) \mathbf{x}), \end{aligned} \quad (7.23)$$

where it is noted that the first two terms are also constants, once the observations are given; and therefore, the exponent, itself, is a quadratic in  $\mathbf{x}$ , indicating that the a posteriori density is, indeed, Gaussian.

Explicitly, suppose we write, in agreement with the now proved Gaussianity of  $\mathbf{x}|\mathbf{y}$ :

$$\begin{aligned} f(\mathbf{x}|\mathbf{y}) &= c \exp\left(-\frac{1}{2}(\mathbf{x} - \boldsymbol{\mu})^T P^{-1}(\mathbf{x} - \boldsymbol{\mu})\right) \\ &= c \exp\left(-\frac{1}{2}(\boldsymbol{\mu}^T P^{-1} \boldsymbol{\mu} + \mathbf{x}^T P^{-1} \mathbf{x} - \mathbf{x}^T P^{-1} \boldsymbol{\mu} - \boldsymbol{\mu}^T P^{-1} \mathbf{x})\right), \end{aligned} \quad (7.24)$$

where  $\mu$  and  $P$  are, respectively, the *a posteriori* mean and covariance matrix of the variable,  $x$ ; and  $c$  is a constant that could be expressed in terms of these and other previously defined constants. Comparing the  $x$ -dependent parts of the exponent in (7.24) and of the expression (7.23), which must be the same for all  $x$ , we see that the statistics  $\mu$  and  $P$  are given, respectively, by

$$P^{-1}\mu = (H^T R^{-1}y + P_0^{-1}\mu_0), \quad \text{or} \quad \mu = P(H^T R^{-1}y + P_0^{-1}\mu_0); \quad (7.25)$$

and

$$P = (P_0^{-1} + H^T R^{-1}H)^{-1}. \quad (7.26)$$

According to (7.10), the a posteriori mean,  $\mu$ , is the best (MMSE) estimate of  $x$ , given the observations,  $y$ . Note that the a posteriori covariance matrix,  $P$ , is independent of the a priori mean,  $\mu_0$ , and it is also independent of the observations,  $y$ . This means that the covariance can be computed without any knowledge of the observations; only the covariances of the a priori variable and of the observation noise are needed. This has important consequences in the analysis of the error dynamics of the INS. For any time, the covariance associated with the estimated system state (the estimated INS errors) can be determined in a recursive manner without having to estimate the states or make observations. We only need to assume Gaussian probabilities for the a priori variable and for the observations, and the probabilistic nature for the entire time history of the system state is known (we will also need to assume whiteness in the noise processes).

### 7.2.2.2 A Posteriori Estimate and Covariance

To compute the a posteriori mean,  $\mu$ , according to (7.25) and (7.26) requires three matrix inversions, two of which are of  $m \times m$  matrices. This can be avoided by rewriting the formulas as follows. Subtract and add  $PH^T R^{-1}H\mu_0$  to the right side of (7.25) to find that

$$\begin{aligned} \mu &= P(P_0^{-1} + H^T R^{-1}H)\mu_0 + PH^T R^{-1}(y - H\mu_0) \\ &= \mu_0 + PH^T R^{-1}(y - H\mu_0) \\ &= \mu_0 + K(y - H\mu_0), \end{aligned} \quad (7.27)$$

where (7.26) was used, and we define  $K$  as

$$K = PH^T R^{-1}. \quad (7.28)$$

Also, from (7.26), we have

$$P^{-1} = P_0^{-1} + H^T R^{-1}H. \quad (7.29)$$

Post-multiplying both sides by  $P_0 H^T$  yields

$$P^{-1} P_0 H^T = H^T R^{-1} (H P_0 H^T + R). \quad (7.30)$$

And, now, multiplying both sides by appropriate inverses we get:

$$P_0 H^T (H P_0 H^T + R)^{-1} = P H^T R^{-1}. \quad (7.31)$$

Substitute this into (7.28) to obtain an alternative form of  $K$ :

$$K = P_0 H^T (H P_0 H^T + R)^{-1}. \quad (7.32)$$

With this form of  $K$ , the a posteriori mean (7.27) becomes computationally more manageable since it does not require the a posteriori covariance,  $P$ . Finally,  $P$  can also be reformulated in terms of  $K$  using the basic definition (6.27):

$$P = \text{cov}(\mathbf{x}, \mathbf{x}) = \mathcal{E}((\mathbf{x} - \boldsymbol{\mu})(\mathbf{x} - \boldsymbol{\mu})^T). \quad (7.33)$$

With (7.15) inserted into (7.27) we have

$$\begin{aligned} \mathbf{x} - \boldsymbol{\mu} &= \mathbf{x} - \boldsymbol{\mu}_0 - K(H\mathbf{x} + \mathbf{v} - H\boldsymbol{\mu}_0) \\ &= (I - KH)(\mathbf{x} - \boldsymbol{\mu}_0) - K\mathbf{v}. \end{aligned} \quad (7.34)$$

And this, put into (7.33), gives with the assumed independence of  $\mathbf{x}$  and  $\mathbf{v}$ , and with (7.17), (7.19):

$$\begin{aligned} P &= \mathcal{E}((I - KH)(\mathbf{x} - \boldsymbol{\mu}_0)(\mathbf{x} - \boldsymbol{\mu}_0)^T(I - KH)^T) + \mathcal{E}(K\mathbf{v}\mathbf{v}^T K^T) \\ &= (I - KH)P_0(I - KH)^T + KRK^T. \end{aligned} \quad (7.35)$$

Though it appears more complicated than (7.26), equation (7.35) for  $P$  involves just one inverse, in (7.32), of a matrix of size  $n \times n$ . Furthermore, (7.35) has the computational advantage of being the sum of two symmetric (and under appropriate conditions, positive definite) matrices, thus ensuring symmetry when calculating the resulting matrix (see the next section on the recursive application of these formulas). This form of the a posteriori covariance matrix is known as the *Joseph form*.

In summary, given the a priori mean and covariance matrix,  $\boldsymbol{\mu}_0$  and  $P_0$ , of the random variable,  $\mathbf{x}$ , and given observations,  $\mathbf{y}$ , linearly related to  $\mathbf{x}$  by (7.15), the a posteriori mean and covariance matrix of  $\mathbf{x}$  are obtained from

$$\boldsymbol{\mu} = \boldsymbol{\mu}_0 + K(\mathbf{y} - H\boldsymbol{\mu}_0) \quad (7.36)$$

and

$$P = (I - KH)P_0(I - KH)^T + KRK^T, \quad (7.37)$$

where

$$K = P_0 H^T (H P_0 H^T + R)^{-1}. \quad (7.38)$$

Using (7.25) and (7.26) and with  $P_0^{-1} = 0$  we find a special form of the a posteriori mean and its covariance matrix:

$$\boldsymbol{\mu} = (H^T R^{-1} H)^{-1} H^T R^{-1} \mathbf{y}, \quad (7.39)$$

$$P = (H^T R^{-1} H)^{-1}. \quad (7.40)$$

This is the familiar least-squares formulation of the estimate of unknown parameters,  $\mathbf{x}$ , also linearly related to observation,  $\mathbf{y}$ , (7.15), but derived on the basis of (7.14).

Apart from (7.26) and (7.37), one may derive alternative forms of the a posteriori covariance matrix,  $P$ , that lead to insightful interpretation of the observation's influence on the covariance of the random variables,  $\mathbf{x}$ . Expanding (7.37) and using (7.38) yields:

$$\begin{aligned} P &= P_0 - KHP_0 - P_0H^TK^T + K(HP_0H^T + R)K^T \\ &= P_0 - KHP_0 \\ &= (I - KH)P_0. \end{aligned} \quad (7.41)$$

This is a particularly simple form of  $P$ , but is rarely used because of inherent numerical instabilities (it is the product of a symmetric matrix and a non-symmetric matrix; this means that numerically, symmetry of the resulting matrix is not ensured, nor is the positive definiteness). With (7.38) for the  $K$  matrix, we obtain

$$P = P_0 - P_0H^T(HP_0H^T + R)^{-1}HP_0. \quad (7.42)$$

$P$ ,  $P_0$  and  $R$  are covariance matrices with positive diagonal elements (the variances). It is readily seen that the second term in (7.42) is also a matrix with positive diagonal elements. Thus, whatever the observation, the a posteriori *variance* is never larger than the a priori *variance*. That is, the observation, even if completely worthless, will never “remove information” as expressed by the second-order statistics of the random variable,  $\mathbf{x}$ .

The concept of information can be formalized using covariances as follows. The a posteriori covariance was expressed in terms of its inverse according to (7.29), repeated here for convenience:

$$P^{-1} = P_0^{-1} + H^TR^{-1}H. \quad (7.43)$$

Thus, the inverse of the covariance matrix propagates very simply from the a priori to the a posteriori states. The influence of the observation on the a posteriori covariance is even more apparent. Large observation noise (small  $R^{-1}$ ) only slightly increases the inverse of the covariance; while small observation noise can substantially increase this inverse, or equivalently reduce the covariance of the variable. The inverse covariance matrix is also known as the *Fisher Information Matrix*. Formula (7.43) then says that the a posteriori information equals the a priori information plus the new information from observations. This method of propagating the covariance matrix also has some numerical advantages as will be seen later.

## 7.3 Discrete Kalman Filter

In a dynamical system, such as the INS, there are many variables that we would like to estimate for many epochs in time. These variables may be the errors in position, in velocity, and in orientation as modeled in (5.66), and any other random parameters that are included in the error models of the inertial sensors, such as in (6.107) and (6.109). In navigational practice these errors should be estimated in real time, if possible; in geodetic applications, it may suffice to estimate them after the mission

has been completed. In that case, one could construct one large batch estimation procedure where all errors (potentially, for each epoch!) are estimated at once, given all observations, as well as all the relevant statistics among them. This would have to be the procedure if we could *not* make the following fundamental assumption. We will assume that the total information accumulated by the system up to any time,  $t_k$ , is completely captured by the system state variable, the vector  $\mathbf{x}_k$ , at that time; indeed, we may use this statement as a formal definition of a system state variable. No information about the system prior to this time would add to or improve our ability to predict the future state of the system. This is exactly the Markovian property already encountered in Section 6.5.3. In probabilistic terms, it is formulated as

$$\mathcal{P}(\mathbf{x}_{k+1}|\mathbf{x}_k, \mathbf{x}_{k-1}, \dots, \mathbf{x}_0) = \mathcal{P}(\mathbf{x}_{k+1}|\mathbf{x}_k). \quad (7.44)$$

That is, the conditional probability density of the state based on all past values of the state is the same as the conditional density based only on the most recent value of the state. In addition, the statistics of an observation,  $\mathbf{y}_k$ , at the current time also are independent of all former observations if the current value of the state is known:

$$\mathcal{P}(\mathbf{y}_k|\mathbf{x}_k, \mathbf{y}_{k-1}, \dots, \mathbf{y}_1) = \mathcal{P}(\mathbf{y}_k|\mathbf{x}_k). \quad (7.45)$$

The time epochs, here and henceforth, are denoted by a subscript on the random variables. These do not have to represent constantly spaced time increments, but for simplicity we assume

$$t_k - t_{k-1} = \Delta t = \text{constant}, \quad (7.46)$$

with  $k = 0, 1, \dots$ . We note that it is quite natural at this point to view the state of the system in terms of discrete time epochs.

The conditions (7.44) and (7.45) are fulfilled if the noise driving the system and the noise associated with the observation are both not correlated with the state variable at all times, and if each noise process is, itself, an uncorrelated, or white noise, process. In Section 7.5.1 we will show how the system can be modified to meet these conditions if the noise processes are correlated. Let  $\mathbf{w}_k$  denote the system driving noise variable at time  $t_k$ , and let  $\mathbf{v}_j$  be the observation noise variable at time  $t_j$ . For now, we assume that

$$\begin{aligned} \mathcal{E}(\mathbf{x}_k \mathbf{w}_j^T) &= 0, \quad \text{for all } j, k; \\ \mathcal{E}(\mathbf{x}_k \mathbf{v}_j^T) &= 0, \quad \text{for all } j, k; \\ \mathcal{E}(\mathbf{w}_k \mathbf{w}_j^T) &= 0, \quad \text{for } j \neq k; \\ \mathcal{E}(\mathbf{v}_k \mathbf{v}_j^T) &= 0, \quad \text{for } j \neq k; \end{aligned} \quad (7.47)$$

where the right hand sides are all zero *matrices* with dimensions appropriate to the dimensions of  $\mathbf{w}_k$ ,  $\mathbf{v}_j$ , and  $\mathbf{x}_k$ . Note that each noise process at any time may have any probability distribution function, but we will assume henceforth that they are Gaussian, based on previous elaborations.

### 7.3.1 Observation Model

It is timely at this point in the exposition to digress and be more specific about the exact meaning of an observation of the state variable. In the previous section, it is assumed that the observation is linearly related to the state variable, as in (7.15). In general, the relationship, or model, is non-linear and must, therefore, be reformulated with a suitable linearization, as shown below. The state of the system, in our case, constitutes the set of errors in position, velocity, orientation, and various parameters of the IMU error model. An observation is information brought to the system from a source external to the INS; for example, a GPS observation of position, or an observation of attitude of the platform relative to the stars using a stellar camera. An observation of position, of course, is not immediately a direct observation of the error; but it can be viewed as such, indirectly, according to the following development using a slightly different notation in order to distinguish between the total quantity and its error.

Let  $\mathbf{x}$  be a dynamically varying vector quantity, such as the position coordinates of the INS. Let  $\tilde{\mathbf{x}}$  be the vector of sensed values of  $\mathbf{x}$  as obtained from the IMU sensor (e.g., integrated accelerometer output). The true error state corresponding to the quantity,  $\mathbf{x}$ , is denoted

$$\delta\mathbf{x} = \tilde{\mathbf{x}} - \mathbf{x}. \quad (7.48)$$

Now let  $\tilde{\mathbf{y}}$  be a vector of external observations of the vector quantity,  $\mathbf{y}$ , that is related to  $\mathbf{x}$  according to:

$$\mathbf{y} = \mathbf{h}(\mathbf{x}), \quad (7.49)$$

where  $\mathbf{h}$  is a known vector function. Then, if  $\mathbf{v}$  is the observation noise vector, we have

$$\tilde{\mathbf{y}} = \mathbf{h}(\mathbf{x}) + \mathbf{v}. \quad (7.50)$$

The difference between what  $\mathbf{y}$  would be if the sensor were correct and what was actually observed is denoted

$$\begin{aligned} \delta\mathbf{y} &= \mathbf{h}(\tilde{\mathbf{x}}) - \tilde{\mathbf{y}} \\ &= \mathbf{h}(\tilde{\mathbf{x}}) - \mathbf{h}(\mathbf{x}) - \mathbf{v}. \end{aligned} \quad (7.51)$$

Therefore, a linear approximation of  $\delta\mathbf{y}$  is given by

$$\delta\mathbf{y} \approx H\delta\mathbf{x} - \mathbf{v}, \quad (7.52)$$

where

$$H = \left. \frac{\partial \mathbf{h}}{\partial \mathbf{x}} \right|_{\mathbf{x}=\tilde{\mathbf{x}}} \quad (7.53)$$

is a matrix of partial derivatives evaluated at the sensed values of  $\mathbf{x}$ .

That is, according to (7.52),  $\delta\mathbf{y}$  is an “observation” of the error state vector,  $\delta\mathbf{x}$ , with the same noise (except for the sign) as the actual observation,  $\tilde{\mathbf{y}}$ . Hence, we loosely speak of observing the state of the system, when (in our case) the state comprises

errors, such as in position. The observation is really the difference between the externally observed value of position and the position indicated by the system, but we simply call it an observation of the error. We now return to the notation earlier defined for the state variable and the observations, without the  $\delta$ 's; and the model for the observation is given by (7.15).

### 7.3.2 Optimal State Vector Estimation

Our problem is to estimate the state of the system at time  $t_k$  based on observations at this time as well as all prior information, that by our assumptions is captured in the state at time  $t_{k-1}$ . Then, an estimation at a subsequent time,  $t_{k+1}$ , is obtained recursively using this estimate at  $t_k$  and any new information up to the new time. Provided the system and the observations are linear in the variables and provided that the probabilities are Gaussian, we clearly have at each epoch the type of estimation developed in the Section 7.2.2. We need to include only one additional step for those times when no observations are made. In this case, the estimate of the state is predicted on the basis of the system dynamics model. This algorithm for recursively estimating the state of the system as time progresses on the basis of external observations is known as the (*discrete*) *Kalman filter* (introduced by Kalman (1960); the *Kalman-Bucy filter*, published a year later by Kalman and Bucy (1961) refers to the continuous filter, see Section 7.7).

The state variables at time  $t_k$  comprise an  $m \times 1$  vector,  $\mathbf{x}_k$ . By condition (7.44), the presumably linear dynamics of the system are modeled (see also (6.78) generalized to vectors and specialized to first order) according to:

$$\mathbf{x}_k = \Phi(t_k, t_{k-1})\mathbf{x}_{k-1} + G_k \mathbf{w}_k, \quad (7.54)$$

where  $\Phi(t_k, t_{k-1})$  is an  $m \times m$  matrix, known as the *state-transition matrix*, that (for the present case) is assumed constant over the time interval,  $\Delta t$ , given by (7.46). In addition to the deterministic element, the system is assumed to be driven, or excited, by a random component,  $G_k \mathbf{w}_k$ , where  $G_k$  is a constant (over the interval  $\Delta t$ )  $m \times \ell$  matrix, and the  $\ell \times 1$  vector,  $\mathbf{w}_k$ , consists of Gaussian, zero-mean, white noise processes, in accordance with (7.47):

$$\mathbf{w}_k \sim \mathcal{N}(0, Q_k), \quad (7.55)$$

where  $Q_k$  is the covariance matrix of the noise processes at the time  $t_k$ . Again, it is assumed that this noise vector and the state variables are independent for all epochs.

At time  $t_k$ , there are  $n$  observations linearly related to the state variables (as discussed, above) through the  $n \times m$  matrix  $H_k$ :

$$\mathbf{y}_k = H_k \mathbf{x}_k + \mathbf{v}_k. \quad (7.56)$$

Also,  $\mathbf{v}_k$  is a vector of Gaussian, zero-mean, white noise processes:

$$\mathbf{v}_k \sim \mathcal{N}(0, R_k), \quad (7.57)$$

where the condition (7.47) applies. The estimation of the state using the observations is called an *update*; it is independent (because of (7.47)) of the estimation based solely on the system dynamics from  $t_{k-1}$  to  $t_k$ , which is called the *prediction*.

The zero-mean assumptions for both processes  $w_k$  and  $v_k$  are easy to enforce—if either process has a non-zero mean, simply modify the appropriate model (7.54) or (7.56) by adding a state variable that represents the mean of the process and replace it with the corresponding mean-shifted process. Therefore, we can assume, without loss in generality, as far as the driving noise processes are concerned, that the system states are modeled according to (7.54) and that the observation model is given by (7.56). The covariance matrices,  $Q_k$  and  $R_k$  are assumed known and the latter should have full rank. These covariance matrices may, or may not, depend on time. In the former case, the interpretation must be that the process has changed to a new process (e.g., with a different variance), not that it is nonstationary, a property that would violate the assumption of white noise. If there is reason to suspect time-correlation in the noise, then the observation model would have to be altered (see Section 7.5.1). If properly modeled, the matrices  $Q$  and  $R$  usually are constant for long intervals.

In these state dynamics and observation models the time epochs have been denoted by a common index,  $k$ , for the sake of convenience only; in fact, the associated time intervals for the state and the observation may be dissimilar. For example, the constancy of  $\Phi$  may be valid for intervals of only 1 minute, but the observations may enter at intervals of 10 minutes. This more general situation requires more elaborate notation, but no new theory.

An estimate of the state variable is denoted with the symbol “ $\hat{\cdot}$ ”. But we require a further distinction as to whether at a particular epoch an observation has already been included, or not. Let  $\hat{x}_k$  be the estimate at time  $t_k$ , just *after* the inclusion of an observation  $y_k$ ; and let  $\hat{x}_k^-$  denote the estimate just *prior* to the inclusion of the observation.

Finally, some information is needed to begin the recursive algorithm. Usually we do not know the true values of the state variables at  $t_0$ , but in accordance with the estimation premise established in Section 7.2, we assume to know the mean of the process, which is thus our initial optimal estimate, according to (7.8):

$$\hat{x}_0 = \mathcal{E}(\mathbf{x}_0). \quad (7.58)$$

Furthermore, we assume to know the initial covariance of the process:

$$\text{cov}(\mathbf{x}_0, \mathbf{x}_0) = P_0, \quad (7.59)$$

where  $P_0$  is a full-rank (invertible) matrix.

It is sometimes simpler to deal in terms of errors in our estimation. Thus let:

$$\mathbf{e}_0 = \hat{\mathbf{x}}_0 - \mathbf{x}_0, \quad (7.60)$$

where the error,  $\mathbf{e}_0$ , by (7.58) and (7.59) is a zero-mean random process with covariance,  $P_0$ . Considering the discussion of Section 7.2, we may presume the process,  $\mathbf{x}_0$ , or  $\mathbf{e}_0$ , to be Gaussian:

$$\mathbf{e}_0 \sim \mathcal{N}(0, P_0). \quad (7.61)$$

We note also that trivially, by definition, the estimate, interpreted as an estimator,

at  $t_0$  is unbiased:

$$\mathcal{E}(\hat{\mathbf{x}}_0) = \mathcal{E}(\mathbf{x}_0). \quad (7.62)$$

With these preliminaries, we are ready to consider the prediction and filtering steps in sequence.

### 7.3.2.1 Prediction

The state at any time,  $t_k$ , propagates according to the state transition matrix,  $\Phi$ , and driving noise,  $\mathbf{w}_k$ , as given by the model (7.54). In the absence of observations, we seek the best estimate at time  $t_k$ , being, as always, the expected value conditioned on all prior information. Thus

$$\begin{aligned}\hat{\mathbf{x}}_k &= \mathcal{E}(\mathbf{x}_k) \\ &= \Phi(t_k, t_{k-1})\mathcal{E}(\mathbf{x}_{k-1}) - G_k\mathcal{E}(\mathbf{w}_k) \\ &= \Phi(t_k, t_{k-1})\hat{\mathbf{x}}_{k-1},\end{aligned}\quad (7.63)$$

where the expected value of the white noise process is zero. This is known as *prediction*. Certainly, at some initial time, e.g.,  $t_0$ , an estimate of the state must be given, as in (7.58), to start the recursive prediction algorithm. Subsequent (best) estimates are computed according to (7.63). For example, if initially zero, the *predicted* estimates, for all time, in the absence of observations, will be zero. By our choice of optimal estimator, the prediction estimate trivially is always unbiased, just like at the initial time, as shown in (7.62). For convenience, the notation  $\hat{\mathbf{x}}_k^-$  is not yet used since no observations enter the discussion.

The covariance of the estimation error is propagated similarly. Let the error of the estimated state be

$$\mathbf{e}_k = \hat{\mathbf{x}}_k - \mathbf{x}_k. \quad (7.64)$$

Then, from (7.63) and (7.54)

$$\mathbf{e}_k = \Phi(t_k, t_{k-1})\mathbf{e}_{k-1} - G_k\mathbf{w}_k. \quad (7.65)$$

Because the noise process,  $\mathbf{w}_k$ , at time  $t_k$  is supposed to be uncorrelated with any process at other times, we note that

$$\mathcal{E}(\mathbf{e}_{k-1}\mathbf{w}_k^T) = 0, \quad (7.66)$$

and obtain the covariance matrix for  $\mathbf{e}_k$  according to:

$$\begin{aligned}P_k &= \mathcal{E}(\mathbf{e}_k\mathbf{e}_k^T) \\ &= \Phi(t_k, t_{k-1})\mathcal{E}(\mathbf{e}_{k-1}\mathbf{e}_{k-1}^T)\Phi^T(t_k, t_{k-1}) + G_k\mathcal{E}(\mathbf{w}_k\mathbf{w}_k^T)G_k^T \\ &= \Phi(t_k, t_{k-1})P_{k-1}\Phi^T(t_k, t_{k-1}) + G_kQ_kG_k^T,\end{aligned}\quad (7.67)$$

with starting covariance matrix given by  $P_0$ , equation (7.59).  $P_{k-1}$  has non-negative diagonal elements, as does  $Q_k$ ; hence, the variances of the system states do not decrease with prediction, but generally increase, depending on the driving noise variances. Prediction adds no information to the system.

If we assume Gaussianity for  $w_k$  and  $e_0$ , the probability density of  $e_k$  is also Gaussian. This is easily proved by mathematical induction. Indeed, by the inductive hypothesis we assume that  $e_{k-1} \sim \mathcal{N}(0, P_{k-1})$  and note from (7.65) and (7.55) that  $e_k$  is the linear combination of two Gaussian random variables (that are also independently distributed). Gaussianity is preserved under linear transformation (see (6.35)), so that  $e_k$  is also a Gaussian random variable with covariance  $P_k$  and zero mean:

$$e_k \sim \mathcal{N}(0, P_k). \quad (7.68)$$

This completes the case of simple prediction. The estimate (7.63) is the “best” we can do based on the available information, which in this case is just the model (7.54) with initial condition (7.58). Under the given assumptions of Gaussianity in the various stochastic processes, the probability density of the error is completely determined.

### 7.3.2.2 Filtering

The results of the previous section on prediction are analogous to straightforward applications of error propagation analysis, but are not of principal interest in our estimation problem. Rather, once we introduce external observations, equation (7.56), it is desired to find the estimate that makes optimal use of this new information. This is known loosely as *filtering* (see also Section 7.1) because we wish to remove components of the error of prediction that can be observed at (or, up to) that time. Under the recursive hypothesis, we assume that at time  $t_{k-1}$  the estimate,  $\hat{x}_{k-1}$ , of the state vector and the statistics of the error are known to the extent possible on the basis of all information (system dynamics and observations) up to and including the epoch  $t_{k-1}$ . The estimate and error statistics at the subsequent time,  $t_k$ , are obtained in two steps: a prediction from  $t_{k-1}$  to  $t_k$ , just prior to the observation, followed by an estimation, the update, based on the new information, the observation at  $t_k$ . This update is performed optimally according to the estimation theory developed in Section 7.2.

The prediction is given by the estimate (7.63) and the covariance of the error is (7.67), where now the special notation is used to indicate that the observation has not yet been included:

$$\hat{x}_k^- = \Phi(t_k, t_{k-1})\hat{x}_{k-1}, \quad (7.69)$$

$$P_k^- = \Phi(t_k, t_{k-1})P_{k-1}\Phi^T(t_k, t_{k-1}) + G_k Q_k G_k^T. \quad (7.70)$$

$\hat{x}_k^-$  and  $P_k^-$  are, respectively, the a priori expected value and error covariance of the state variables.

Now, the best estimate at time  $t_k$ , on the condition of including the observation,  $y_k$ , is given, according to (7.10), by the conditional expectation,  $\mathcal{E}(x_k | y_k)$ . This MMSE estimate of the state variables is the a posteriori mean as defined in (7.25):

$$\hat{x}_{\text{MMSE}_k} = \mathcal{E}(x_k | y_k) = \mu_k. \quad (7.71)$$

For convenience we omit the MMSE notation and note that  $\hat{x}_k$  should be inter-

preted as an estimator, whose value, the estimate, depends on the realization of the observations, and it is thus a random variable. Identifying the a priori best estimate,  $\hat{x}_k^-$ , with  $\mu_k^-$  (equivalent to  $\mu_0$  in the notation of Section 7.2.2.1), the best a posteriori estimate of the state variables based on the observation at time  $t_k$  is then given with appropriate index notation by (7.36)–(7.38):

$$\hat{x}_k = \hat{x}_k^- + K_k(y_k - H_k \hat{x}_k^-), \quad (7.72)$$

$$P_k = (I - K_k H_k) P_k^- (I - K_k H_k)^T + K_k R_k K_k^T, \quad (7.73)$$

where

$$K_k = P_k^- H_k^T (H_k P_k^- H_k^T + R_k)^{-1}. \quad (7.74)$$

Equations (7.69)–(7.74) including both prediction and filtering constitute the *Kalman filter*.

Since from (7.63)  $\hat{x}_k^- = \mathcal{E}(\mathbf{x}_k)$ , and  $\mathcal{E}(y_k) = H\mathcal{E}(\mathbf{x}_k)$  from (7.56), the estimate (7.72) is also unbiased:

$$\mathcal{E}(\hat{x}_k) = \mathcal{E}(\mathbf{x}_k). \quad (7.75)$$

Since we have assumed explicitly that the underlying a priori process is Gaussian, the a posteriori process is also Gaussian, as was shown by (7.22) and (7.23); and the complete probability distribution of the state variable, or the estimation error, is determined:

$$\mathbf{x}_k \sim \mathcal{N}(\hat{x}_k, P_k). \quad (7.76)$$

Another discerning interpretation of the a posteriori estimate, according to (7.25), is as the weighted sum of the a priori mean and the observations. The weights sum to the identity matrix, when  $y$  is scaled to the units of  $x$ . This can be seen specifically for the case that  $H$  is a non-singular matrix (a generalization exists for arbitrary  $H$ ). The transformation to  $x$ -like units is  $H^{-1}y$ , and the a posteriori estimate according to (7.25) is

$$\hat{x}_k = P_k(P_k^-)^{-1}\hat{x}_k^- + P_k H_k^T R^{-1} H_k (H_k^{-1}y_k). \quad (7.77)$$

Equation (7.26) then demonstrates that the sum of the weights of  $\hat{x}_k^-$  and  $H_k^{-1}y_k$  is unity.

The matrix,  $K_k$ , is known as the *Kalman gain matrix*. Loosely, it may be interpreted as the ratio of new information provided by the observation relative to the prior information. The difference  $y_k - H_k \hat{x}_k^-$  is known as the *innovation*; it is the difference between the observation and its expected value. The gain determines how much of the innovation should be added to the a priori estimate. If the observation is not very accurate, i.e.,  $R_k$  is large (compared to  $P_k^-$ ), then according to (7.74) the gain will be small and little of the innovation is added; that is, an inaccurate observation will have only a small influence on the estimate. If the observation is very accurate then  $R_k$  is small and the a posteriori estimate will largely be determined by the observation, no matter what the a priori estimate was. That is, the a priori estimate may be very poor and the observation, if accurate, will pull the estimate of

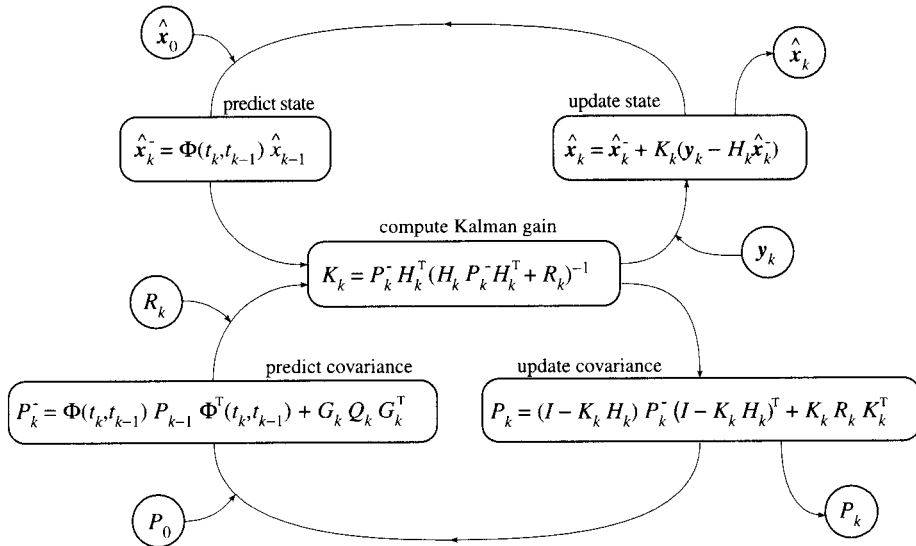


Figure 7.1: Kalman filter loops.

the variable “back to reality.” This is readily seen by considering the special case where  $H_k = I$ ; then, as  $R_k \rightarrow 0$ ,  $K_k \rightarrow I$ , and  $\hat{x}_k \rightarrow y_k$ .

Note, again, that the computation of the covariances for the prediction and update steps are independent of the estimates and the observations, as is the computation of the Kalman gain matrix. Figure 7.1 gives an algorithmic view of the prediction and update steps of the estimation process. The covariance computation is seen to be a loop independent of the estimates and observations. Note also the important initial conditions, given by (7.61).

Even though the forms (7.70) and (7.73) of the a priori and a posteriori covariances help ensure the required symmetry and positive definiteness of the computed matrices, it is prudent to replace the computed  $P_k^-$  and  $P_k$  at each step,  $k$ , by

$$P_k^- \leftarrow \frac{1}{2}(P_k^- + (P_k^-)^T), \quad P_k \leftarrow \frac{1}{2}(P_k + P_k^T). \quad (7.78)$$

This artifice at least forces symmetry in the covariance matrices. The long-term numerical stability of the Kalman recursion algorithm also depends on the system noise function and the observation updates (See Section 7.7.1.3). Other stability enhancing numerical techniques include the *square-root* (of  $P_k$ ) formulation, an algorithm based on the factorization of  $P_k$  into upper triangular and diagonal matrices (*U-D factorization*), and hybridizations of these algebraic devices (Bierman, 1977).

### 7.3.2.3 Smoothing

The smoothing problem with discrete observations is expressed as the estimation of the state vector at some time  $t_k$  based on a set of observations before *and after* this

time. Historically, there are three types of smoothers (Meditch, 1973; Anderson and Moore, 1979). As before, we denote by  $\hat{x}_k$  the estimate of the state vector at time  $t_k$ :

1. *Fixed-point smoothing* is concerned with the estimate  $\hat{x}_j$  at a fixed point  $j$  while  $k$  ( $k > j$ ) increases as new observations become available. For example, this would apply to the initial alignment problem (Chapter 8) using external velocity observations after  $t = 0$ . In this case, the fixed point  $j$  represents the beginning point.

2. *Fixed-lag smoothing* results in the smoothed state  $\hat{x}_{k-M}$  for a fixed time delay  $M \Delta t$ , based on observations up to time  $t_k$ ,  $k = M, M+1, \dots$ . In real-time data processing, this type of smoothing is possible if the delay time is smaller than other significant delays in the system.

3. *Fixed-interval smoothing* yields an estimate  $\hat{x}_{k/N}$  for any time  $t_k$  within an interval over which observations are available:  $k \in [0, 1, \dots, N]$ . This type of smoothing can be done only in post-mission data processing. The subscript notation “ $k/N$ ” refers to the estimate of the state vector at time  $t_k$  on the basis of all observations in the interval (i.e. from  $t_0$  to  $t_N$ ).

An important (post-mission) application of integrated INS/GPS is the optimal interpolation, using INS, of positions between discrete GPS observation updates (Section 10.3). This fits exactly into the fixed-interval smoothing category, which we consider primarily. There exist several versions of the smoothing algorithm. They are based essentially on the combination of a forward-in-time filter (the usual Kalman filter already discussed) and a backward-in-time filter starting from the last time of the interval and predicting and updating backward to a point within the interval. The basic algorithm is often associated with Rauch, Tung, and Striebel (1965) and thus is called the RTS algorithm. Alternatives and variations on this have been derived by Fraser (1967) and Bierman (1973), among others. We present the Fraser algorithm (see also Maybeck, 1982) since it is simplest to derive from the foregoing presentation.

To compute the smoothed estimate,  $\hat{x}_{k/N}$ , we perform the usual Kalman filter up to  $t_k$ , obtaining  $\hat{x}_k$  and its error covariance,  $P_k$ ; this represents the best estimate based on all information up to and including that time. We then perform a backward filter using initial estimates of the state vector and its error covariance just after the time  $t_N$  of the last observation. With careful implementation of time indices, the same Kalman filter equations can be used, ensuring that the state transition matrix incorporates the proper direction of time (see Figure 7.2). Denoting the backward

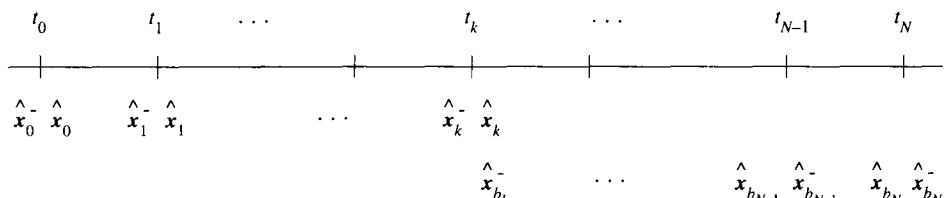


Figure 7.2: Time line and notation for Kalman filter/smusher estimates.

filter estimates with a subscript,  $b$ , we have analogous to (7.72), (7.73), and (7.74), for  $j = N, N-1, \dots, k+1$ , the backward update:

$$\hat{\mathbf{x}}_{b_j} = \hat{\mathbf{x}}_{b_j}^- + K_{b_j}(\mathbf{y}_j - H_j \hat{\mathbf{x}}_{b_j}^-), \quad (7.79)$$

$$P_{b_j} = (I - K_{b_j} H_j) P_{b_j}^- (I - K_{b_j} H_j)^T + K_{b_j} R_j K_{b_j}^T, \quad (7.80)$$

where

$$K_{b_j} = P_{b_j}^- H_j^T (H_j P_{b_j}^- H_j^T + R_j)^{-1}, \quad (7.81)$$

and the initial quantities are  $\hat{\mathbf{x}}_{b_N}^-$  and  $P_{b_N}^-$ . Similar to (7.63) and (7.67), the backward prediction is:

$$\hat{\mathbf{x}}_{b_{j-1}}^- = \Phi(t_{j-1}, t_j) \hat{\mathbf{x}}_{b_j}, \quad (7.82)$$

with associated error covariance:

$$P_{b_{j-1}}^- = \Phi(t_{j-1}, t_j) P_{b_j} \Phi^T(t_{j-1}, t_j) + G_{j-1} Q_{j-1} G_{j-1}^T. \quad (7.83)$$

Note that  $\hat{\mathbf{x}}_{b_{j-1}}^-$  and  $P_{b_{j-1}}^-$  refer to predictions just to the *right* of epoch  $t_{j-1}$ . In other words, the result of this second filter is  $\hat{\mathbf{x}}_{b_k}^-$ , being the backward estimate of the states that has not yet incorporated the observation at  $t_k$ , together with its error covariance,  $P_{b_k}^-$ . The two estimates, from the forward filter,  $\hat{\mathbf{x}}_k$ , and from the backward filter,  $\hat{\mathbf{x}}_{b_k}^-$ , are then combined as follows. We interpret the estimate,  $\hat{\mathbf{x}}_k$ , as “a priori” estimate and interpret the backward estimate,  $\hat{\mathbf{x}}_{b_k}^-$ , as an observation of the entire state vector. In this case the  $H$ -matrix is the identity matrix and (7.25) yields the “a posteriori”, or smoothed, estimate:

$$\hat{\mathbf{x}}_{k/N} = P_{k/N} (P_k^{-1} \hat{\mathbf{x}}_k + (P_{b_k}^-)^{-1} \hat{\mathbf{x}}_{b_k}^-), \quad (7.84)$$

where, from (7.26)

$$P_{k/N} = (P_k^{-1} + (P_{b_k}^-)^{-1})^{-1}. \quad (7.85)$$

The principal difficulty with this two-filter formulation is that the initial backward estimate,  $\hat{\mathbf{x}}_{b_N}^-$ , of the state vector at time  $t_N$  is not known. This is consistent with the condition that the covariance matrix,  $P_N$ , for the forward estimate at  $t_N$  must equal the covariance matrix,  $P_{N/N}$ , for the smoothed estimate at  $t_N$  since both estimates at that time are based on the same information. We then have from (7.85)

$$(P_{b_N}^-)^{-1} = 0, \quad (7.86)$$

indicating that no information is available prior to incorporating the observation at  $t_N$ . Even after incorporating this observation, not all states may be estimated, meaning that the inverse covariance matrix (the Fisher information matrix) is still singular (we slightly abuse the notation here by retaining the inverse symbol,  $-1$ , on a matrix that is not invertible). It is, however, possible to reformulate the backward filter in terms of information matrices; this is also known as the *inverse covariance filter* and could also be applied in the forward sense in the case that the initial covariance is infinite (does not exist). That is, the subsequent derivations assume full rank for all covariance matrices, but the resulting filter equations involve only information matrices, which in the end may be allowed to possess less than full rank.

We start with a transformation of the backward states to a new set of states:

$$\mathbf{z}_j = (\mathbf{P}_{b_j})^{-1} \mathbf{x}_{b_j}. \quad (7.87)$$

Although not known, the initial estimate,  $\hat{\mathbf{x}}_{b_N}^-$ , is assumed to be bounded, so that with (7.86),

$$\hat{\mathbf{z}}_N^- = \mathbf{0}. \quad (7.88)$$

Because of (7.86), there is no uncertainty in this; and so the error covariance of the initial estimate,  $\hat{\mathbf{z}}_N^-$ , is

$$\mathcal{E}((\hat{\mathbf{z}}_N^- - \mathbf{z}_N^-)(\hat{\mathbf{z}}_N^- - \mathbf{z}_N^-)^T) = \mathcal{E}(\mathbf{z}_N^-(\mathbf{z}_N^-)^T) = D_N = 0. \quad (7.89)$$

In general, the error covariance matrix of  $\hat{\mathbf{z}}_j$  is given by

$$D_j = \text{cov}(\mathbf{z}_j, \mathbf{z}_j) = \mathbf{P}_{b_j}^{-1} \mathbf{P}_{b_j} \mathbf{P}_{b_j}^{-1} = \mathbf{P}_{b_j}^{-1}, \quad (7.90)$$

which is easily derived with (6.27) and (7.87).

The recursive update equations for the estimates of  $\mathbf{z}_j$  follow simply by substituting (7.87) into (7.25) and noting that, as before,  $\mu \equiv \hat{\mathbf{x}}$  and  $\mu_0 \equiv \hat{\mathbf{x}}^-$ :

$$\hat{\mathbf{z}}_j = \mathbf{H}_j^T \mathbf{R}_j^{-1} \mathbf{y}_j + \hat{\mathbf{z}}_j^-; \quad (7.91)$$

and the a posteriori information matrix of  $\hat{\mathbf{x}}_{b_j}$ , from (7.43), is given by:

$$\mathbf{P}_{b_j}^{-1} = (\mathbf{P}_{b_j}^-)^{-1} + \mathbf{H}_j^T \mathbf{R}_j^{-1} \mathbf{H}_j. \quad (7.92)$$

With this, the a posteriori estimate,  $\hat{\mathbf{x}}_{b_j}$ , can be computed from (7.87) and (7.91), provided the information matrix is invertible.

The recursive prediction equations require slightly more algebra. In order to obtain the prediction information matrix,  $(\mathbf{P}_{b_j}^-)^{-1}$  (being the error covariance matrix of  $\hat{\mathbf{z}}_j^-$ ), we require the following useful matrix inverse identity (Henderson and Searle, 1981):

$$(\mathbf{A} + \mathbf{B}^T \mathbf{C})^{-1} = \mathbf{A}^{-1} - \mathbf{A}^{-1} \mathbf{B}^T (\mathbf{I} + \mathbf{C} \mathbf{A}^{-1} \mathbf{B}^T)^{-1} \mathbf{C} \mathbf{A}^{-1}, \quad (7.93)$$

where  $\mathbf{A}$  is a nonsingular matrix and  $\mathbf{B}$  and  $\mathbf{C}$  are arbitrary matrices. Let

$$\mathbf{A}_j = \Phi(t_{j-1}, t_j) \mathbf{P}_{b_j} \Phi^T(t_{j-1}, t_j); \quad (7.94)$$

and with  $\mathbf{B}^T = \mathbf{G}_{j-1} \mathbf{Q}_{j-1}$  and  $\mathbf{C} = \mathbf{C}_{j-1}^T$  apply (7.93) to (7.83) to obtain:

$$(\mathbf{P}_{b_{j-1}}^-)^{-1} = \mathbf{A}_j^{-1} - \mathbf{A}_j^{-1} \mathbf{G}_{j-1} \mathbf{Q}_{j-1} (\mathbf{I} + \mathbf{G}_{j-1}^T \mathbf{A}_j^{-1} \mathbf{G}_{j-1} \mathbf{Q}_{j-1})^{-1} \mathbf{G}_{j-1}^T \mathbf{A}_j^{-1}, \quad (7.95)$$

where, using (2.55), we have

$$\Phi^{-1}(t_{j-1}, t_j) = \Phi(t_j, t_{j-1}); \quad (7.96)$$

and hence,

$$\mathbf{A}_j^{-1} = \Phi^T(t_j, t_{j-1}) \mathbf{P}_{b_j}^{-1} \Phi(t_j, t_{j-1}). \quad (7.97)$$

Now let

$$\mathbf{S}_j = \mathbf{A}_j^{-1} \mathbf{G}_{j-1} \mathbf{Q}_{j-1} (\mathbf{I} + \mathbf{G}_{j-1}^T \mathbf{A}_j^{-1} \mathbf{G}_{j-1} \mathbf{Q}_{j-1})^{-1}. \quad (7.98)$$

The prediction information matrix is then given by

$$(P_{b_{j-1}}^-)^{-1} = A_j^{-1} - S_j G_{j-1}^T A_j^{-1}. \quad (7.99)$$

A computationally more stable form is the Joseph form:

$$(P_{b_{j-1}}^-)^{-1} = (I - S_j G_{j-1}^T) A_j^{-1} (I - S_j G_{j-1}^T)^T + S_j Q_{j-1}^{-1} S_j^T, \quad (7.100)$$

which may be verified by expanding the first term on the right side and making use of (7.97). In this case,  $Q_{j-1}$  must be non-singular.

Also, the prediction of the state can be formulated solely in terms of information matrices starting with (7.82), rewritten as

$$(P_{b_{j-1}}^-)^{-1} \hat{x}_{b_{j-1}}^- = (P_{b_{j-1}}^-)^{-1} \Phi(t_{j-1}, t_j) P_{b_j} P_{b_j}^{-1} \hat{x}_{b_j}. \quad (7.101)$$

With (7.87), (7.94), and (7.96) we have

$$\begin{aligned} \hat{z}_{j-1}^- &= (P_{b_{j-1}}^-)^{-1} \Phi(t_{j-1}, t_j) P_{b_j} \hat{z}_j \\ &= (P_{b_{j-1}}^-)^{-1} \Phi(t_{j-1}, t_j) P_{b_j} \Phi^T(t_{j-1}, t_j) \Phi^T(t_j, t_{j-1}) \hat{z}_j \\ &= (P_{b_{j-1}}^-)^{-1} A_j \Phi^T(t_j, t_{j-1}) \hat{z}_j. \end{aligned} \quad (7.102)$$

Finally, substituting (7.99) yields the backward prediction of  $\hat{z}_{j-1}$ :

$$\hat{z}_{j-1}^- = (I - S_j G_{j-1}^T) \Phi^T(t_j, t_{j-1}) \hat{z}_j. \quad (7.103)$$

Note that the transition matrix appearing in (7.103) is for the *forward* direction. Also, as before,  $\hat{x}_{b_j}^-$  can be computed from (7.87) at those times when  $(P_{b_j}^-)^{-1}$  is invertible.

With the backward filter thus formulated in terms of information matrices, the smoothed estimate at time  $t_k$  becomes, from (7.84):

$$\hat{x}_{k/N} = P_{k/N} (P_k^{-1} \hat{x}_k + \hat{z}_k^-). \quad (7.104)$$

where  $P_{k/N}$  is given by (7.85) and  $(P_{b_k}^-)^{-1}$  by (7.100).

In summary, the computation of the smoothed estimate and its error covariance at any time,  $t_k$ , in the interval  $[t_0, t_N]$ , based on all observations within this interval, requires two recursive filters. To save computations in the case that a smoothed estimate is required for many points in the interval one could compute the backward filter first, saving the values of the estimates,  $\hat{z}_j$ , and their error covariances, and follow this by the forward filter using the saved values immediately to compute the smoothed estimate throughout the interval. For long intervals and many states, the computer memory required for this approach may be prohibitive. In addition, two inverses of covariance matrices, in equation (7.85), must be computed for each smoothed estimate. The procedure may turn unstable if these matrices become near-singular.

The RTS algorithm (Gelb, 1974) similarly consists of a forward recursive sweep (filtering) followed by a backward sweep (smoothing). In this case, all forward estimates and covariances are saved, and the smoothed estimates and their error co-

variances are computed recursively in the backward sweep. This algorithm requires that all forward values be saved even if only a single smoothed estimate is sought in the interval; and thus, it is less suited to that particular application. Bierman's (1973) *modified Bryson-Frazier* (mBF) algorithm is similar to the Fraser algorithm derived above, but avoids the computation of covariance matrix inverses.

We note that a simple-minded algorithm for fixed-point smoothing ensues from the fixed-interval smoothing algorithm if we decide on a limit,  $N$ , to the number of observations. In that case the fixed-point smoothed estimate is simply  $\hat{x}_{0/N}$  with error covariance  $P_{0/N}$ . However, this is not a recursive algorithm since it precludes the inclusion of further observations (after time  $t_N$ ). Recursive algorithms much more amenable to estimation analysis may be found, e.g., in (Maybeck, 1982) and (Gelb, 1974).

## 7.4 Discrete Linear Dynamics Model

Section 7.3 established a recursive algorithm for computing the best estimate of the system state variables at time  $t_k$ . It was natural to assume a *discrete* transition model for the system states based on the recursive hypothesis (7.44), and the estimation algorithm proceeds in a discrete, recursive, computationally convenient fashion. Yet, the description of the INS system errors and their dynamics was ascertained from physical principles and was given in the form of linear differential equations for differentiable (hence, continuous) functions (see (5.66)). Fundamentally, all developments arose from Newton's Second Law of Motion (1.5), where the system variables, position and velocity, are governed by strictly physical laws that hold for continuous time,  $t$ . Therefore, although at the most elemental level the sensor and measurement systems inherently are quantized, our model for the system states is based on continuous, rather than discrete functions of time.

In order to transform the continuous system description (linear differential equations) into its discrete counterpart (linear *difference* equations), we formally solve the differential equations over the generic incremental time interval,  $\Delta t$ . In this way the solution is discretized (or sampled) at the end of each time interval, where it then also serves as the initial condition for the subsequent interval. Certain approximations may be incorporated to simplify the computational implementation; and, the result is a discrete transition model for the system states identical to that proposed in (7.54).

We start with a continuous system, assumed to be a set of linear, non-homogeneous, first-order (ordinary) differential equations:

$$\dot{\mathbf{x}}(t) = F(t)\mathbf{x}(t) + D(t)\mathbf{s}(t) + G(t)\mathbf{w}(t), \quad (7.105)$$

where  $\mathbf{x}(t)$  is a vector of random system variables (stochastic processes), depending on time,  $t$ , with mean and covariance at  $t_0$  presumed given.  $F$ ,  $D$ , and  $G$  are (possibly) time-dependent and well defined matrices;  $\mathbf{s}(t)$  is a given vector function of  $t$ ; and  $\mathbf{w}(t)$  is a continuous, zero-mean, white noise, Gaussian, vector process. As such,

the non-homogeneous part of the equation, that which drives, or forces, the system, consists of a deterministic component,  $s(t)$ , and a stochastic component,  $w(t)$ . The former is also known as the *control input*, since it is specified and used to force a definite dynamic behavior on the system.

We will leave control theory to other texts (e.g., Brogan, 1974) and set  $s(t) = \mathbf{0}$ ; thus the forcing term is purely stochastic, in a sense, “out of control”:

$$\dot{x}(t) = F(t)x(t) + G(t)w(t). \quad (7.106)$$

The explicit dependence on  $t$  distinguishes the random variables  $x(t)$  and  $w(t)$  notationally from their discrete analogues. At each time,  $t$ , these two processes are assumed to be independent. We might consider higher-order linear differential equations to describe the system dynamics, but these can always be reduced to first-order equations by appropriately augmenting the vector of variables, as shown in Section 2.2.

Linear, first-order systems of differential equations, like (7.106), are relatively easy to solve for  $x(t)$ . The equation has the form (2.12) and its solution, the sum of the homogeneous solution and a particular solution determined by the method of variation of parameters, is given by (2.70):

$$x(t) = \Phi(t, t_0)x(t_0) + \int_{t_0}^t \Phi(t, t')G(t')w(t') dt', \quad (7.107)$$

where the matrix function  $\Phi$  is called the *state transition matrix* and for fixed  $t'$  satisfies the differential equation (2.57):

$$\frac{d}{dt} \Phi(t, t') = F(t)\Phi(t, t'). \quad (7.108)$$

Note that the solution (7.107) includes the initial value,  $x(t_0)$ .

At this point, the solution to the differential equation (7.106) has really only been written in terms of a new quantity, the state transition matrix, which still has to be determined by solving a differential equation. However, for sufficiently small time intervals or for systems that have reached a stationary state (no transients remain), the dynamics matrix,  $F$ , is constant, or nearly so. For time-invariant  $F$ , the solution to (7.108) is straightforward, given by (2.58):

$$\Phi(t, t') = e^{F(t-t')} = I + F(t-t') + \frac{1}{2!}(F(t-t'))^2 + \frac{1}{3!}(F(t-t'))^3 + \dots, \quad (7.109)$$

where (2.35) was used. As discussed in Section 2.3.1.2, it may be possible to solve (7.106) even if  $F$  is not constant and the solution still has the form (7.107), but  $\Phi$  is not then given by (7.109).

Formally, we are in a position to discretize the continuous system. Identifying  $t_0 = t_{k-1}$  and substituting  $t = t_k$  into (7.107) yields, with the notation  $x_k \equiv x(t_k)$ :

$$x_k = \Phi(t_k, t_{k-1})x_{k-1} + u_k, \quad (7.110)$$

where

$$\mathbf{u}_k = \int_{t_{k-1}}^{t_k} \Phi(t, t') G(t') \mathbf{w}(t') dt'. \quad (7.111)$$

This is the form (7.54) with  $\mathbf{u}_k$  taking the place of  $G_k \mathbf{w}_k$ . However, we must be very careful in the interpretation of the white noise in (7.54) vis-à-vis the white noise in (7.111); in the first place, they have different units (see below).

The random process  $\mathbf{u}_k$  is a Gaussian, zero-mean, *discrete* white noise process as required in (7.54). Indeed, it is white since  $\mathbf{w}(t)$  is white and the intervals  $[t_{k-1}, t_k]$  do not overlap, thus precluding correlations of  $\mathbf{u}_k$  between epochs. It is a Gaussian process because of the linear relationship between  $\mathbf{w}$  and  $\mathbf{u}$  (Section 6.2.1). Since,  $\mathcal{E}(\mathbf{w}(t)) = \mathbf{0}$ , we have

$$\mathcal{E}(\mathbf{u}_k) = \mathbf{0}; \quad (7.112)$$

and the covariance matrix is given by

$$\mathcal{E}(\mathbf{u}_k \mathbf{u}_k^T) = \int_{t_{k-1}}^{t_k} \int_{t_{k-1}}^{t_k} \Phi(t, t') G(t') \mathcal{E}(\mathbf{w}(t') \mathbf{w}(t'')) G^T(t'') \Phi^T(t, t'') dt' dt''. \quad (7.113)$$

The covariance of the white noise process, formally, is a Dirac delta function with amplitude being the power spectral density of the process, see (6.55):

$$\mathcal{E}(\mathbf{w}(t') \mathbf{w}(t'')) = Q \delta(t' - t''), \quad (7.114)$$

where  $Q$  is the matrix of auto- and cross-power spectral densities for the white noise processes in the vector  $\mathbf{w}(t)$ . Making use of the properties of the delta function (6.54) in the integral, equation (7.113) then becomes

$$\Theta_k = \mathcal{E}(\mathbf{u}_k \mathbf{u}_k^T) = \int_{t_{k-1}}^{t_k} \Phi(t, t') G(t') Q G^T(t') \Phi^T(t, t') dt'. \quad (7.115)$$

Since  $\mathbf{u}_k$  and  $\mathbf{x}_k$  (or, equivalently, the error  $\mathbf{e}_k$ ) are uncorrelated, the matrix  $\Theta_k$  takes the place of  $G_k Q_k G_k^T$  in (7.67), giving

$$P_k = \Phi(t_k, t_{k-1}) P_{k-1} \Phi^T(t_k, t_{k-1}) + \Theta_k \quad (7.116)$$

for the propagated error covariance matrix associated with the estimated states.

The rigorous calculation of the covariance matrix  $\Theta_k$  requires an integration of the transition matrix and the  $G$ -matrix, as indicated in (7.115). However, for a sufficiently short integration interval,  $G$  may be considered a constant matrix and the first-order approximation  $\Phi(t, t') \approx I + F(t - t')$  may hold. In this case, neglecting terms on the order of  $\Delta t^2$ , equation (7.115) simplifies to

$$\Theta_k \approx G_k Q \Delta t G_k^T. \quad (7.117)$$

Matrix  $G$  is still associated with the time  $t_k$  since the time-invariance is assumed only for the interval  $\Delta t$ .

We note a conceptually important distinction between the quantities  $Q \Delta t$  and  $Q / \Delta t$ . According to (6.61),  $\mathcal{E}(\mathbf{w}_k \mathbf{w}_k^T) = Q / \Delta t$  is the covariance of the white noise process

averaged over the interval  $\Delta t$ , where

$$\mathbf{w}_k = \frac{1}{\Delta t} \int_{t_{k-1}}^{t_k} \mathbf{w}(t) dt \quad (7.118)$$

is the usual discretization of white noise; see (6.59). On the other hand,  $G_k Q \Delta t G_k^T$  is the (approximate) covariance of  $G(t)\mathbf{w}(t)$  accumulated over the interval  $\Delta t$ . In that sense, we cannot identify (nor approximate)  $\mathbf{u}_k$  with  $G_k \mathbf{w}_k$  since the white noise in  $\mathbf{u}_k$  is the accumulated, not averaged, white noise. In view of (7.117), a comparison of (7.116) and (7.67) yields the covariance for the (accumulated) white noise in our discretized state dynamics model:

$$Q_k = Q \Delta t. \quad (7.119)$$

## 7.5 Modifications

The derivation of the Kalman filter restricts its application to systems that are excited by white noise and observations that also are corrupted by white noise, only. In addition, it is assumed that the system dynamics are linear with respect to the states. Nevertheless, most systems do not operate under the influence of uncorrelated noise and, likewise, the observations may exhibit temporal correlations. It is noted that correlations among observations at a single epoch are allowed under the previous derivation of the filter, meaning simply that the  $R$ -matrix may be a full covariance matrix. Similarly, the  $Q$ -matrix of covariances among the input noise sources at a single epoch may be a full matrix. But correlations between epochs are not permitted. These limitations are readily alleviated in many cases, as is the requirement for linearity of the system dynamics.

This has particular application in the estimation of states of an inertial navigation system, where the accelerometer and gyro errors that drive the system error dynamics are composed of random biases, scale factor errors, and correlated noise, in addition to the white noise, as exemplified in (6.107) and (6.109). Also, observation updates, like GPS-derived positions or velocities, are correlated in time due, for example, to environmental factors such as tropospheric refraction. Finally, we recall that the error dynamics equations (Section 5.3) are the result of a linearization. As error states grow in value with time, second-order terms neglected in the linearization may adversely affect the validity of the estimation model.

### 7.5.1 Augmented State Vector

The basic continuous system dynamics model (7.106) requires that the process  $w(t)$  be white noise and Gaussian. If the noise process consists also (or only) of time-correlated errors, the system states may be augmented by states that describe this correlation. Specifically, this is possible if the driving noise of the original system dynamics can be modeled according to a linear differential equation (or reduced to such an equation) driven, potentially, by white noise. For example, the model

(7.106) would now be

$$\dot{\mathbf{x}}(t) = F(t)\mathbf{x}(t) + B(t)\mathbf{c}(t) + G\mathbf{w}(t), \quad (7.120)$$

where the correlated noise,  $\mathbf{c}(t)$ , satisfies the augmented model

$$\dot{\mathbf{c}}(t) = F_c(t)\mathbf{c}(t) + G_c(t)\mathbf{w}_c(t), \quad (7.121)$$

and  $\mathbf{w}_c(t)$  is a vector of zero-mean, Gaussian, white noise processes with power spectral density matrix,  $Q_c$ . Also, it is assumed as before that  $\mathbf{w}_c(t)$  is not correlated with either  $\mathbf{c}(t)$  or  $\mathbf{x}(t)$ . We may augment the state vector,  $\mathbf{x}(t)$ , with  $\mathbf{c}(t)$ , now treated as a state vector, to form the following expanded system dynamics equation:

$$\frac{d}{dt} \begin{pmatrix} \mathbf{x}(t) \\ \mathbf{c}(t) \end{pmatrix} = \begin{pmatrix} F(t) & B(t) \\ 0 & F_c(t) \end{pmatrix} \begin{pmatrix} \mathbf{x}(t) \\ \mathbf{c}(t) \end{pmatrix} + \begin{pmatrix} G(t) & 0 \\ 0 & G_c(t) \end{pmatrix} \begin{pmatrix} \mathbf{w}(t) \\ \mathbf{w}_c(t) \end{pmatrix}, \quad (7.122)$$

where the zeros in (7.122) are appropriately dimensioned matrices with only zero elements. This model, of course, is in the form of (7.106), satisfying all associated conditions regarding the driving noise processes, and can be discretized as described in the previous section, thus making it amenable to discrete Kalman filtering. We note that in this and the original system dynamics model it is certainly permitted to have  $G(t) = 0$  or  $G_c(t) = 0$ , if that is demanded by the error characteristics. The Kalman prediction and update equations then simplify accordingly.

A second instance of augmenting the state vector arises if the observation model includes time-correlated noise. Again, we assume that the correlated noise can be modeled such that it satisfies a linear differential equation driven by white noise. The observation model (7.15) now may be written as

$$\mathbf{y} = H\mathbf{x} + A\mathbf{r} + \mathbf{v}, \quad (7.123)$$

where the correlated noise,  $\mathbf{r}$ , is given by

$$\dot{\mathbf{r}}(t) = F_r(t)\mathbf{r}(t) + G_r(t)\mathbf{w}_r(t), \quad (7.124)$$

and  $\mathbf{w}_r(t)$  is a vector of zero-mean, Gaussian, white noise processes with power spectral density matrix,  $Q_r$ . As always, the independence of  $\mathbf{w}_r(t)$  and  $\mathbf{x}(t)$  is assumed.

Augmenting  $\mathbf{x}(t)$ , that satisfies (7.106), with  $\mathbf{r}(t)$ , yields the total system dynamics model:

$$\frac{d}{dt} \begin{pmatrix} \mathbf{x}(t) \\ \mathbf{r}(t) \end{pmatrix} = \begin{pmatrix} F(t) & 0 \\ 0 & F_r(t) \end{pmatrix} \begin{pmatrix} \mathbf{x}(t) \\ \mathbf{r}(t) \end{pmatrix} + \begin{pmatrix} G(t) & 0 \\ 0 & G_r(t) \end{pmatrix} \begin{pmatrix} \mathbf{w}(t) \\ \mathbf{w}_r(t) \end{pmatrix}, \quad (7.125)$$

which reverts to the basic form of (7.106). The observation model is rewritten as

$$\mathbf{y} = (H \quad A) \begin{pmatrix} \mathbf{x} \\ \mathbf{r} \end{pmatrix} + \mathbf{v}, \quad (7.126)$$

thus returning it to the form of (7.15) in terms of the augmented state vector. If the noise model in the observation is assumed to contain no white noise, only correlated noise, then we may set  $R$ , the covariance matrix of  $\mathbf{v}$ , to zero in the Kalman filter

equations, provided that the matrix  $HP^{-}H^T$  in (7.74) is nonsingular ( $H$  and  $P^{-}$  must have full rank).

A cautionary note is in order here. While the system dynamics and observation models should be as true as possible to the real situation under investigation, thus including a representative and/or requisite number of states, the *observability* of these states depends on their interrelationships within the dynamics model, as well as on the external observations. Loosely expressed, we expect the observations to yield better estimates of the states, that is, their variances should decrease as we add more information to the system. Too many states and an inadequate set of observations may result in no improvement over initial conditions (see also Section 7.7.2.2). We have already encountered one example where certain states may not be observable. These are the accelerometer bias and orientation error, that in a north-slaved, local level mechanization appear inseparable in the dynamics model, equations (5.77); and external observations of position or velocity will not yield independent estimates of these states (see also Chapter 8).

### 7.5.2 Closed-Loop Estimation

As shown in Chapter 5, the trajectory indicated by an inertial navigation system in terms of position coordinates will usually depart significantly from the true trajectory as time progresses because of a number of sensor errors, such as gyro drifts. With the Kalman filter, one estimates these errors using occasional externally provided observations, and the filter algorithm also gives a variance for the estimate. However, even if that variance is small, indicating that we have a good estimate of the error (usually due to an accurate external observation), the error itself (both the estimate and the true value) may be quite large. That is, unless the INS is specifically corrected, its indicated position will continue to drift away from the true trajectory; the observation simply affords us an estimation of its errant way.

This situation would be tolerable if the error dynamics and, in particular, the observation model were linear in the system states. Indeed, the Kalman filter algorithm was built on the fundamental assumption of linearity. But in many applications, the linear models are derived from linearizations of nonlinear functional relationships. Such is the case in deriving the error dynamics for the inertial navigation system (Chapter 5). Similarly, we derived the observation model (7.52) with a linearization of a more general relationship to the error states. Clearly, the growth in the values of the error states may cause neglected second-order terms to become significant to the extent that this would invalidate the model.

Since our observations give us (presumably) good estimates of the errors, it makes sense to provide these estimates as information to the system that is responsible for generating the errors, in our case the inertial navigation system. This is called closing the loop, or *closed-loop* estimation. It is usually also called the *extended* Kalman filter. As soon as we obtain an estimate of the error after an observation update, the indicated system variable (e.g., the position or velocity of the INS) is corrected by our estimate so that, hopefully, the indicated position forthwith more

closely follows the true trajectory (or, one that is approximately consistent with the observations).

In order to illustrate the mechanics of closed-loop estimation, we again adopt the  $\delta$ -notation already used in Section 7.3.1 to develop the observation model. As in that Section we let  $x$  be the vector of dynamically varying quantities (e.g., position coordinates), and  $\tilde{x}$  is the vector of corresponding sensed or indicated values, so that the true error is given by  $\delta x = \tilde{x} - x$ . Initially, at  $t_0$ , we have an unbiased estimate of  $x_0$ , say  $\hat{x}_0$ , with error covariance matrix  $P_0$ . It is assumed that, initially, the sensor can be adjusted to read  $\tilde{x}_0 = \hat{x}_0$ , and the initial error estimate is, therefore,

$$\delta \hat{x}_0 = \tilde{x}_0 - \hat{x}_0 = \mathbf{0}, \quad (7.127)$$

with error covariance,  $P_0$ .

We now assume further that the error estimate, based on all observations up to time  $t_{k-1}$  can be used to adjust the sensor so that the estimated error at this time is also zero. We denote this error estimate of the “corrected” sensor with a superscript ‘+’:

$$\delta \hat{x}_{k-1}^+ = \mathbf{0}. \quad (7.128)$$

Now, at time  $t_k$  the sensor indicates  $\tilde{x}_k$ , but there is also an external observation,  $\tilde{y}_k$ , as modeled by (7.50). We use the sensed value to compute the observed error

$$\delta y_k = H_k \tilde{x}_k - \tilde{y}_k, \quad (7.129)$$

as in (7.51). The estimated error according to the (linearized) Kalman filter, including prediction and update is given by (7.69) and (7.72):

$$\delta \hat{x}_k^- = \Phi(t_k, t_{k-1}) \delta \hat{x}_{k-1}^+ = \mathbf{0}, \quad (7.130)$$

$$\delta \hat{x}_k = \delta \hat{x}_k^- + K_k (\delta y_k - H_k \delta \hat{x}_k^-) = K_k \delta y_k. \quad (7.131)$$

The quantity  $\delta \hat{x}_k$  yields estimated corrections to the indicated values,  $\tilde{x}_k^-$ , and we adjust the sensor (“close the loop”) so that the sensor now indicates

$$\tilde{x}_k^+ = \hat{x}_k = \tilde{x}_k^- - \delta \hat{x}_k. \quad (7.132)$$

The first equality in (7.132) is consistent with the new estimated error being

$$\delta \hat{x}_k^+ = \tilde{x}_k^+ - \hat{x}_k = \mathbf{0}. \quad (7.133)$$

Since closing the loop means only that the sensed, or indicated quantities are adjusted, the covariance matrix of the estimated errors has the same expression as in the open loop formulation. Note that the observed error, (7.29), in closed-loop Kalman filtering relates to  $\tilde{x}_k$  obtained from the adjusted sensor.

Clearly the same procedure of closing the loop may be applied to augmented states such as constants or Gauss-Markov processes that are not associated with particular sensors. In that case one simply defines an artificial sensor that behaves according to the assumed dynamics. For example, the indicated value of a “constant sensor” is always the same as the initial or corrected value. One should be selective, however, in deciding which states should be estimated in closed-loop fashion since the procedure may be unprofitable or even detrimental to the filter if the observa-

tion yields no significant improvement in the variance of the estimate. For those states, it may be best to retain *open-loop* estimation, that is, the sensed variables are not reset by the error estimates.

As a concluding note, the extended Kalman filter, or closed-loop estimation, is still linear estimation that only attempts to reduce the magnitude of the states in order to satisfy better the linear approximation. Non-linear optimal estimation addresses more fully the nonlinearity of the model, for example, by using a standard type of Newton-Raphson iterative algorithm to converge to the best nonlinear solution at each *fixed* observation epoch (Gelb, 1974).

## 7.6 A Simple Example

Consider the one-dimensional trajectory of a vehicle whose system dynamics are described by the following model:

$$\ddot{x} = a; \quad x(0) = 0, \quad \dot{x}(0) = 0. \quad (7.134)$$

This corresponds to the model (4.69) in the *i*-frame, without a gravitational field. The corresponding error dynamics are given by

$$\delta\ddot{x} = \delta a. \quad (7.135)$$

As in Chapter 5, we use the  $\delta$ -notation to denote errors, and they are regarded as the states of the system. The accelerometer error,  $\delta a$ , consists of an unknown random bias and white noise according to the model:

$$\delta a = b + w, \quad (7.136)$$

where

$$w \sim \mathcal{N}(0, q = 0.01 \text{ (m}^2/\text{s}^4)/\text{Hz}). \quad (7.137)$$

For the purpose of simulation, the indicated position and velocity are given by

$$\begin{aligned} \tilde{x}_k &= \tilde{x}_{k-1} + \tilde{\dot{x}}_{k-1} \Delta t + \frac{1}{2}(a + b + w_k)\Delta t^2, \quad \tilde{x}_0 = 0; \\ \tilde{\dot{x}}_k &= \tilde{x}_{k-1} + (a + b + w_k)\Delta t, \quad \tilde{\dot{x}}_0 = 0; \end{aligned} \quad (7.138)$$

where the true values  $a = 2 \text{ m/s}^2$ ,  $b = 1 \text{ m/s}^2$  are used, and values for  $w_k$  are obtained from a random number generator.

Including the bias as a system state to be estimated, having dynamics model (6.63), the total error dynamics as a set of first-order linear differential equations are given by

$$\frac{d}{dt} \begin{pmatrix} \delta\dot{x} \\ \delta x \\ b \end{pmatrix} = \begin{pmatrix} 0 & 0 & 1 \\ 1 & 0 & 0 \\ 0 & 0 & 0 \end{pmatrix} \begin{pmatrix} \delta\dot{x} \\ \delta x \\ b \end{pmatrix} + \begin{pmatrix} 1 \\ 0 \\ 0 \end{pmatrix} w. \quad (7.139)$$

To convert this to a discrete set of difference equations, we note that the dynamics

matrix,  $F$ , in (7.139), is constant and  $F^3 = 0$ . Hence, from (7.109), we have an exact expression for the state transition matrix:

$$\Phi = \begin{pmatrix} 1 & 0 & \Delta t \\ \Delta t & 1 & \frac{1}{2} \Delta t^2 \\ 0 & 0 & 1 \end{pmatrix}. \quad (7.140)$$

The corresponding discrete noise covariance  $1 \times 1$  matrix is given, according to (7.119), by

$$Q_k = q \Delta t. \quad (7.141)$$

Our initial estimates of the system states and their error covariance matrix are assumed to be

$$\begin{pmatrix} \hat{\delta}\dot{x} \\ \hat{\delta}x \\ \hat{b} \end{pmatrix}_0 = \begin{pmatrix} 0 \\ 0 \\ 0 \end{pmatrix}; \quad P_0 = \begin{pmatrix} 1 \text{ m}^2/\text{s}^2 & 0 & 0 \\ 0 & 1 \text{ m}^2 & 0 \\ 0 & 0 & 1 \text{ m}^2/\text{s}^4 \end{pmatrix}. \quad (7.142)$$

Thus, without further information in the form of external observations, the estimated errors propagate according to (7.63):

$$\begin{pmatrix} \hat{\delta}\dot{x} \\ \hat{\delta}x \\ \hat{b} \end{pmatrix}_1 = \begin{pmatrix} 0 \\ 0 \\ 0 \end{pmatrix}; \quad \begin{pmatrix} \hat{\delta}\dot{x} \\ \hat{\delta}x \\ \hat{b} \end{pmatrix}_2 = \begin{pmatrix} 0 \\ 0 \\ 0 \end{pmatrix}; \quad \begin{pmatrix} \hat{\delta}\dot{x} \\ \hat{\delta}x \\ \hat{b} \end{pmatrix}_3 = \begin{pmatrix} 0 \\ 0 \\ 0 \end{pmatrix}; \quad (7.143)$$

with covariances, according to (7.67), given by

$$P_1 = \begin{pmatrix} 2.01 \text{ m}^2/\text{s}^2 & 1.5 \text{ m}^2/\text{s} & 1 \text{ m}^2/\text{s}^3 \\ 1.5 \text{ m}^2/\text{s} & 2.25 \text{ m}^2 & 0.5 \text{ m}^2/\text{s}^2 \\ 1 \text{ m}^2/\text{s}^3 & 0.5 \text{ m}^2/\text{s}^2 & 1 \text{ m}^2/\text{s}^4 \end{pmatrix}; \quad P_2 = \begin{pmatrix} 5.02 & 6.01 & 2 \\ 6.01 & 9.01 & 2 \\ 2 & 2 & 1 \end{pmatrix};$$

$$P_3 = \begin{pmatrix} 10.03 & 16.53 & 3 \\ 16.53 & 30.3 & 4.5 \\ 3 & 4.5 & 1 \end{pmatrix}; \quad (7.144)$$

where we used  $\Delta t = 1$  s. The units for  $P_2$  and  $P_3$  are the same as shown for  $P_1$ . Note that the rapid increase in uncertainty in position (and velocity) arises in this example from the initial uncertainties, not from the noise of the accelerometer.

Now, at  $t = 3 \Delta t$ , we have an external observation of position that, compared to the position indicated by our system, yields a discrepancy:  $\delta y$ . We assume that this observed error is related to the system states according to the model (7.52):

$$\delta y = (0 \quad 1 \quad 0) \begin{pmatrix} \hat{\delta}\dot{x} \\ \hat{\delta}x \\ b \end{pmatrix} - v, \quad (7.145)$$

where the noise,  $v$ , is white and Gaussian:

$$v \sim \mathcal{N}(0, 0.09 \text{ m}^2). \quad (7.146)$$

These observations are simulated according to (7.51) using (7.138):

$$\delta y_k = \tilde{x}_k - \frac{1}{2} a t_k^2 - v_k. \quad (7.147)$$

Since  $H = (0 \ 1 \ 0)$  and  $R = 0.09 \text{ m}^2$ , the Kalman gain at  $t = 3 \Delta t$ , according to (7.74), is the vector

$$K_3 = \begin{pmatrix} 0.54393 \text{ s}^{-1} \\ 0.99704 \\ 0.14808 \text{ s}^{-2} \end{pmatrix}. \quad (7.148)$$

From (7.72) and (7.73), the a posteriori error estimates and covariance matrix are given, respectively, by

$$\begin{pmatrix} \hat{\delta x} \\ \hat{\delta \dot{x}} \\ \hat{b} \end{pmatrix}_3 = \begin{pmatrix} 2.44224 \text{ m/s} \\ 4.47670 \text{ m} \\ 0.66486 \text{ m}^2/\text{s}^2 \end{pmatrix}; \quad P_3 = \begin{pmatrix} 1.03885 & 0.04895 & 0.55232 \\ 0.04895 & 0.08973 & 0.01333 \\ 0.55232 & 0.01333 & 0.33366 \end{pmatrix}. \quad (7.149)$$

Clearly, the position error estimate reflects the observation and its uncertainty. More accurate estimation of the accelerometer bias requires further external observations.

Figure 7.3 shows the standard deviations of the position, velocity, and bias error estimates, assuming that at intervals of 3 s an observation of position error, with

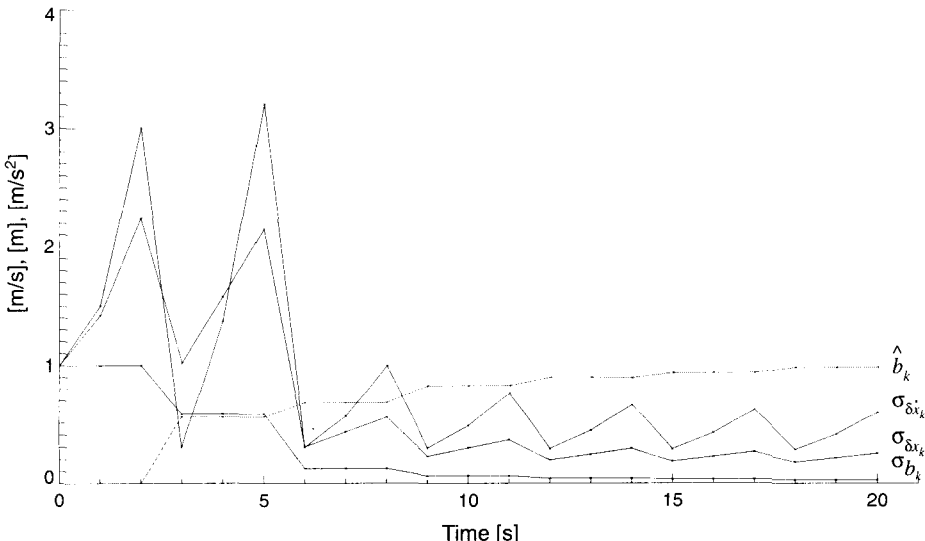


Figure 7.3: Standard deviations of the Kalman filter estimates and also the bias estimate for the example in the text.

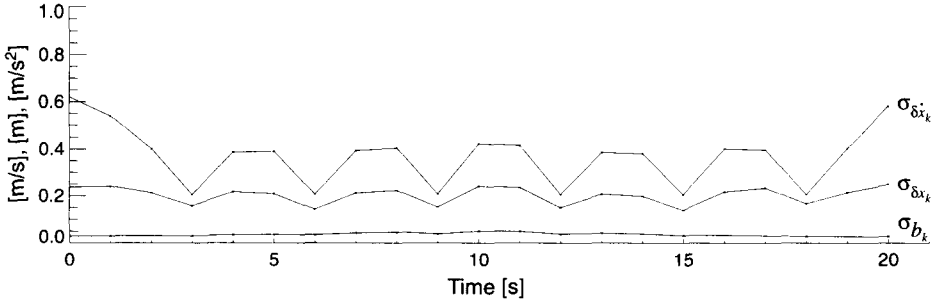


Figure 7.4: Standard deviations of the Kalman smoothed estimates for the example in the text.

noise given by (7.146), is introduced. The characteristic saw-tooth pattern for the position and velocity errors reflects the drift of the indicated position from the true trajectory; this drift is estimated periodically with the help of an external observation which immediately reduces the standard deviations in the position and velocity error estimates. Note that the lines in Figure 7.3 are included only for clarity; the standard deviations are calculated only at discrete points. Also included in this figure is the estimate of the bias,  $\hat{b}_k$ , which approaches the true value ( $b = 1$ ) after several external observations. Due to the non-linear nature of the model, it was necessary to close the loop (Section 7.5.2) on the indicated position and velocity in order to obtain this estimate.

Applying the smoothing algorithm (Section 7.3.2.3) yields standard deviations shown in Figure 7.4. Note the difference in vertical scale. Also, according to equation (7.85), the standard deviations at the observation points are less than in Figure 7.3, because now all observations, past and future, contribute to the estimated errors.

## 7.7 Continuous Kalman Filter

The Kalman filter equations, (7.69) through (7.74), originally were developed for the case of discrete observations that enter into the estimation of the state variables at discrete times  $t_k$ . Alternatively, the observations could be continuous as with an analog measuring device, or they might be considered nearly continuous if the data rate is very fast (or relatively fast compared to the dynamics of the system). Also, in some cases the statistical behavior of the system can be determined in closed, analytical form if formulated as a continuous process, thus perhaps leading to further insight. Therefore, it is of consequence to derive a continuous version of the Kalman filter equations. As the discreteness vanishes into continuity, the prediction and update steps combine into one optimal estimation procedure, which, incidentally, we could also do for the discrete Kalman filter. Specifically, we combine (7.69) and (7.72) to get

$$\hat{\mathbf{x}}_k = \Phi(t_k, t_{k-1})\hat{\mathbf{x}}_{k-1} + K_k(y_k - H_k\Phi(t_k, t_{k-1})\hat{\mathbf{x}}_{k-1}), \quad (7.150)$$

where the Kalman gain matrix is, as before, given by (7.74).

The transition to a continuous filter is now done formally in the limit as the time interval between *observations* approaches zero (see also the original exposition by Kalman and Bucy (1961); whence the continuous Kalman filter is sometimes called the Kalman-Bucy filter). We note that the discrete system model (7.110) was obtained by sampling the solution of the states of a continuous system (7.106). The continuous Kalman filter, on the other hand, refers to the continuity of the observations. Though not completely rigorous, the following derivations have at least a heuristic value in that they allude to concepts and results already presented.

It is necessary first to derive the continuous observation model from the discrete formulation (7.56). The continuous observation model is defined to be the model that when suitably sampled yields the discrete observation model. In essence, an appropriate relationship between the continuous and discrete noise processes must be found. Since, without loss in generality, the observation noise process is assumed to be white, we adopt the correspondence (6.59) between discrete and continuous white noise processes, where the former is a time average of the latter.

Assuming, as before, that the continuous observation model is linear in the system variables with additive white noise, we write:

$$\mathbf{y}(t) = H(t)\mathbf{x}(t) + \mathbf{v}(t). \quad (7.151)$$

Now consider a short time interval,  $\delta t$ . We define the noise process,  $\mathbf{v}(t)$ , as the average of continuous white noise,  $\mathbf{v}(t')$ , over this interval:

$$\mathbf{v}(t) = \frac{1}{\delta t} \int_{t-\delta t}^t \mathbf{v}(t') dt', \quad (7.152)$$

where  $\mathbf{v}(t)$  has power spectral density matrix,  $R$ . If the observation model thus defined is sampled at the discrete times,  $t = t_k$ , with  $t_k - t_{k-1} \geq \delta t$ , then the resulting discrete noise process,  $\mathbf{v}_k$ , is white (no overlapping integrals). In this way we obtain the discrete time model (7.56).

The covariance of the continuous noise process is given in terms of the power spectral density matrix,  $R$  (see (6.55)):

$$\mathcal{E}(\mathbf{v}(t)\mathbf{v}^T(t')) = R\delta(t - t'), \quad (7.153)$$

and is related to the discrete time covariance matrix, according to (6.61), as

$$R_k = \frac{1}{\delta t} R. \quad (7.154)$$

Now, from (7.108) and the definition of the derivative, we have

$$\begin{aligned} \frac{d}{dt} \Phi(t, t') &= \lim_{\delta t \rightarrow 0} \frac{\Phi(t + \delta t, t') - \Phi(t, t')}{\delta t} \\ &= F(t)\Phi(t, t'). \end{aligned} \quad (7.155)$$

For sufficiently small  $\delta t$ , this yields the following approximation:

$$\Phi(t + \delta t, t') - \Phi(t, t') \approx F(t)\Phi(t, t')\delta t; \quad (7.156)$$

and, therefore,

$$\Phi(t + \delta t, t')(\Phi(t, t'))^{-1} \approx I + F(t)\delta t. \quad (7.157)$$

Making use of (2.69), we obtain

$$\Phi(t + \delta t, t) \approx I + F(t)\delta t, \quad (7.158)$$

which finally leads to

$$\Phi(t, t - \delta t) \approx I + F(t - \delta t)\delta t. \quad (7.159)$$

Now, using this and  $t \equiv t_k$ , as well as  $\delta t = t_k - t_{k-1}$ , we write the discrete time Kalman filter estimate (7.150) with explicit time dependence:

$$\hat{x}(t) = (I + F(t - \delta t)\delta t)\hat{x}(t - \delta t) + K(t)(y(t) - H(t)(I + F(t - \delta t)\delta t)\hat{x}(t - \delta t)). \quad (7.160)$$

Similarly, the Kalman gain matrix (7.74) becomes with (7.154):

$$\begin{aligned} K(t) &= P^-(t)H^T(t)\left(H(t)P^-(t)H^T(t) + \frac{1}{\delta t}R\right)^{-1} \\ &= \delta t P^-(t)H^T(t)(H(t)P^-(t)H^T(t)\delta t + R)^{-1}. \end{aligned} \quad (7.161)$$

Substituting (7.161) into (7.160), rearranging terms, and dividing by  $\delta t$  yields

$$\frac{\hat{x}(t) - \hat{x}(t - \delta t)}{\delta t} = F(t - \delta t)\hat{x}(t - \delta t) + \mathcal{K}(t)(y(t) - H(t)(I + F(t - \delta t)\delta t)\hat{x}(t - \delta t)), \quad (7.162)$$

where

$$\mathcal{K}(t) = P^-(t)H^T(t)(H(t)P^-(t)H^T(t)\delta t + R)^{-1}. \quad (7.163)$$

Finally, we note that the a priori covariance is related approximately to the a posteriori covariance of the previous step by

$$P^-(t) \approx P(t - \delta t) + \dot{P}^-(t)\delta t. \quad (7.164)$$

And, in the limit we have

$$\lim_{\delta t \rightarrow 0} P^-(t) = P(t). \quad (7.165)$$

Therefore, also taking the limit of (7.162), as  $\delta t \rightarrow 0$ , we find that the state estimate,  $\hat{x}$ , satisfies the differential equation:

$$\frac{d}{dt}\hat{x}(t) = F(t)\hat{x}(t) + \mathcal{K}(t)(y(t) - H(t)\hat{x}(t)), \quad (7.166)$$

where the Kalman gain, (7.163), in the limit is given, with (7.165), by

$$\mathcal{K}(t) = P(t)H^T(t)R^{-1}. \quad (7.167)$$

Equations (7.166) and (7.167) represent the continuous Kalman filter for the system states based on continuous observation updates. Equation (7.166) is a set of non-homogeneous, linear differential equations (with time-varying coefficients) that may be interpreted as the dynamics model of the states. For some simple models, they can be integrated analytically. Formally, the solution is given by (2.70):

$$\hat{\mathbf{x}}(t) = \vartheta(t, t_0)\hat{\mathbf{x}}(t_0) + \int_{t_0}^t \vartheta(t, t')\mathcal{K}(t')\mathbf{y}(t') dt', \quad (7.168)$$

where for fixed  $t'$ , from (2.57),

$$\frac{d}{dt}\vartheta(t, t') = (F(t) - \mathcal{K}(t)H(t))\vartheta(t, t'). \quad (7.169)$$

Note, however, that it is necessary to know the covariance function  $P(t)$ .

### 7.7.1 Covariance Function

The covariance matrix associated with the estimates of the continuous Kalman filter is a function of  $t$  and its dynamics equation is derived in two steps. We first note that the continuous Kalman filter equations revert to the continuous system dynamics equation for the prediction estimate if no observation updates are available. This corresponds to the special case when  $R^{-1} = 0$ . Then from (7.165),  $\mathcal{K}(t) = 0$ ; and, comparing (7.169) with (7.108),  $\vartheta = \Phi$ . The solution for the prediction estimate from (7.168) is thus

$$\hat{\mathbf{x}}(t) = \Phi(t, t_0)\hat{\mathbf{x}}(t_0). \quad (7.170)$$

Moreover, since the discrete dynamics equations of Section 7.4 were merely evaluations of the continuous equations, it is evident that the covariance function of the error, in this case  $\mathbf{e}(t) = \hat{\mathbf{x}}(t) - \mathbf{x}(t)$ , is given by (7.116) with (7.115). Identifying  $t_k \equiv t$  and  $t_{k-1} \equiv t_0$ , we find

$$P(t) = \Phi(t, t_0)P(t_0)\Phi^T(t, t_0) + \int_{t_0}^t \Phi(t, t')G(t')QG^T(t')\Phi^T(t, t') dt', \quad (7.171)$$

where  $P(t_0)$  is the error covariance matrix associated with  $\mathbf{x}(t_0)$ .

The differential equation for the covariance matrix at time  $t$  can be obtained by taking the time derivative of (7.171). Making use of Leibnitz's rule for differentiating the integral, we obtain

$$\dot{P}(t) = F(t)P(t) + P(t)F^T(t) + G(t)QG^T(t), \quad (7.172)$$

where (7.108) was also used. The initial condition is contained in  $P(t_0)$ . Equation (7.172) is called the *linear variance equation*; it describes the dynamics of the continuous state error covariance under the premise of prediction only (no observation updates). Of course, the exact solution to this differential equation is given by (7.171); but an approximate solution, accurate to first order in  $\Delta t = t - t_0$ , can be obtained with (7.117):

$$P(t) \approx \Phi(t, t_0)P(t_0)\Phi^T(t, t_0) + G(t)Q\Delta t G^T(t). \quad (7.173)$$

Proceeding to the continuous prediction/update case, the covariance matrix satisfies a nonlinear differential equation that will be derived next. We start with the equation of the *inverse* of the error covariance (Fisher information matrix) for the *discrete* updates occurring at small intervals,  $\delta t = t_k - t_{k-1}$ . From (7.43), we have:

$$P_k^{-1} = (P_k^-)^{-1} + H_k^T R_k^{-1} H_k. \quad (7.174)$$

The following approximations hold for small time intervals,  $\delta t$ , analogous to (7.164):

$$\begin{aligned} (P_k^-)^{-1} - (P_{k-1})^{-1} &\approx \frac{d}{dt} (P^-(t))^{-1} \Big|_{t=t_k} \delta t, \\ (P_k)^{-1} - (P_{k-1})^{-1} &\approx \frac{d}{dt} (P(t))^{-1} \Big|_{t=t_k} \delta t. \end{aligned} \quad (7.175)$$

In accordance with the continuous nature of the filter in this discussion, no distinction is made at  $t_{k-1}$  between  $P_{k-1}$  and  $P_k^-$ . Substituting expressions (7.175) into (7.174), we obtain

$$\frac{d}{dt} (P(t))^{-1} \Big|_{t=t_k} \approx \frac{d}{dt} (P^-(t))^{-1} \Big|_{t=t_k} + H_k^T (R_k \delta t)^{-1} H_k. \quad (7.176)$$

The following identity is easily proved by applying the time derivative to  $PP^{-1} = I$  and using the chain rule for differentiation:

$$\frac{d}{dt} (PP^{-1}) = 0 \quad \Rightarrow \quad \frac{d}{dt} P^{-1} = -P^{-1} \left( \frac{d}{dt} P \right) P^{-1}. \quad (7.177)$$

We now apply this identity to each of the derivatives in (7.176) and then substitute (7.174). The result is:

$$P_k^{-1} \frac{d}{dt} P(t) \Big|_{t=t_k} P_k^{-1} \approx (P_k^-)^{-1} \frac{d}{dt} P^-(t) \Big|_{t=t_k} (P_k^-)^{-1} - H_k^T R^{-1} H_k. \quad (7.178)$$

Upon including (7.172) for the time-derivative of the a priori covariance on the right-hand side and taking the limit as  $\delta t \rightarrow 0$ , using (7.165) and  $t_k \equiv t$ , we finally get

$$\dot{P}(t) = F(t)P(t) + P(t)F^T(t) + G(t)QG^T(t) - P(t)H^T(t)R^{-1}H(t)P(t). \quad (7.179)$$

This is known as the *matrix Riccati equation*. It is the differential equation for the a posteriori error covariance of the continuous Kalman filter. It reduces to the differential equation for the continuous prediction error covariance given by (7.172) (the linear variance equation) if there are no observation updates ( $R^{-1} = 0$ ). Note that the equation (7.179) is nonlinear in  $P$  if  $R^{-1} \neq 0$ . Also the forcing terms that drive the dynamics of the error covariance are due to the system noise,  $Q$ , that generally increases the covariance, and due to the observation noise,  $R$ , that generally decreases the covariance. This is evident from (7.179) by the plus and minus signs, respectively, preceding each of the terms  $G(t)QG^T(t)$  and  $P(t)H^T(t)R^{-1}H(t)P(t)$ , which have positive diagonal elements.

### 7.7.2 Solution to Matrix Riccati Equation

A solution to equation (7.179) yields the time evolution of the error variances and covariances of the state variables which may provide useful interpretive analysis of the system. Such analysis includes determining the controllability and observability of system states, as well as their steady state behavior (Gelb, 1974). Unfortunately, completely analytic solutions to the Riccati equation are rarely possible, being restricted to very simple system dynamics. Usually, standard numerical integration must suffice as a viable alternative. For example, the discrete solution given by the combination of (7.70) and (7.73) is one such numerical technique. We do not examine the analysis applications of the solutions in detail, but give formal solutions for three special cases that contribute insight to the INS alignment problem treated in Chapter 8.

#### 7.7.2.1 Constant Coefficient Matrices

If  $F$ ,  $G$ , and  $H$  are constant matrices in (7.179) (or, at least constant over the interval of integration), then the non-linear nature of the corresponding differential equation

$$\dot{P}(t) = FP(t) + P(t)F^T + GQG^T - P(t)H^T R^{-1} HP(t) \quad (7.180)$$

can be eliminated by introducing a pair of auxiliary matrix functions, called  $U(t)$  and  $V(t)$ , related to  $P(t)$  as follows. If  $P$  is an  $n \times n$  matrix, then by definition so are both  $U$  and  $V$ . Let  $U(t)$  be the matrix function that satisfies the first-order, *linear* differential equation

$$\dot{U}(t) = -F^T U(t) + H^T R^{-1} HP(t)U(t). \quad (7.181)$$

Also, let  $V(t)$  be the matrix function defined by

$$V(t) = P(t)U(t). \quad (7.182)$$

It is assumed that both  $U(t)$  and  $V(t)$  are nonsingular for all  $t$ , so that, for example,

$$P(t) = V(t)(U(t))^{-1}. \quad (7.183)$$

The corresponding differential equation for  $V$  is found by differentiating (7.182) and using (7.180) and (7.181):

$$\begin{aligned} \dot{V}(t) &= \dot{P}(t)U(t) + P(t)\dot{U}(t) \\ &= (FP(t) + P(t)F^T + GQG^T - P(t)H^T R^{-1} HP(t))U(t) \\ &\quad - P(t)(F^T U(t) - H^T R^{-1} HP(t)U(t)) \\ &= FP(t)U(t) + GQG^T U(t) \\ &= FV(t) + GQG^T U(t), \end{aligned} \quad (7.184)$$

which is linear in  $U$  and  $V$ . Combining (7.181), (7.182), and (7.184), we obtain a first-order, linear system of differential equations

$$\begin{pmatrix} \dot{U}(t) \\ \dot{V}(t) \end{pmatrix} = \begin{pmatrix} -F^T & H^T R^{-1} H \\ GQG^T & F \end{pmatrix} \begin{pmatrix} U(t) \\ V(t) \end{pmatrix}, \quad (7.185)$$

where the coefficient matrix is a  $2n \times 2n$  constant matrix. The solution to (7.185) is found from (2.54) as

$$\begin{pmatrix} U(t) \\ V(t) \end{pmatrix} = \begin{pmatrix} \Phi_{UU}(t, t_0) & \Phi_{UV}(t, t_0) \\ \Phi_{VU}(t, t_0) & \Phi_{VV}(t, t_0) \end{pmatrix} \begin{pmatrix} U(t_0) \\ V(t_0) \end{pmatrix}, \quad (7.186)$$

where the transition matrix, partitioned into four  $n \times n$  blocks for convenience, is given by (cf. (7.109))

$$\begin{pmatrix} \Phi_{UU}(t, t_0) & \Phi_{UV}(t, t_0) \\ \Phi_{VU}(t, t_0) & \Phi_{VV}(t, t_0) \end{pmatrix} = \exp \left[ \begin{pmatrix} -F^T & H^T R^{-1} H \\ GQG^T & F \end{pmatrix} (t - t_0) \right] \\ = \begin{pmatrix} I & 0 \\ 0 & I \end{pmatrix} + \begin{pmatrix} -F^T & H^T R^{-1} H \\ GQG^T & F \end{pmatrix} (t - t_0) \\ + \frac{1}{2!} \begin{pmatrix} -F^T & H^T R^{-1} H \\ GQG^T & F \end{pmatrix}^2 (t - t_0)^2 + \dots \quad (7.187)$$

Writing out the individual solutions for  $U$  and  $V$ , from (7.186), and using (7.182), we get with obvious abbreviated notation

$$\begin{aligned} U &= (\Phi_{UU} P_0^{-1} + \Phi_{UV}) V_0, \\ V &= (\Phi_{VU} + \Phi_{VV} P_0) U_0. \end{aligned} \quad (7.188)$$

Now, substituting these into (7.183), we have with  $P_0^{-1} = U_0 V_0^{-1}$

$$P(t) = (\Phi_{VU}(t, t_0) + \Phi_{VV}(t, t_0) P(t_0)) (\Phi_{UU}(t, t_0) + \Phi_{UV}(t, t_0) P(t_0))^{-1}. \quad (7.189)$$

This is the solution to the matrix Riccati equation with constant coefficient matrices. Clearly  $P(t_0)$  has to be known. In principle, there are no approximations in this solution; in practice, only a finite (presumably sufficient) number of terms can be included in the series expression (7.187) (in some simple cases, the series may be summable to analytic form).

### 7.7.2.2 No System Process Noise

In the case that the system states are not excited by random noise, that is,  $Q = 0$ , then we have the simplified Riccati equation given by

$$\dot{P}(t) = F(t)P(t) + P(t)F^T(t) - P(t)H^T(t)R^{-1}H(t)P(t). \quad (7.190)$$

This can be “linearized” by changing it to a differential equation for the Fisher information matrix (see (7.43)), using (7.177):

$$\frac{d}{dt} P^{-1}(t) = -P^{-1}(t)F(t) - F^T(t)P^{-1}(t) + H^T(t)R^{-1}H(t). \quad (7.191)$$

This equation is analogous to the differential equation (7.172) whose solution is given by (7.171). Therefore, the solution to (7.191) has a similar form; in fact:

$$P^{-1}(t) = \Phi^T(t_0, t)P^{-1}(t_0)\Phi(t_0, t) + \int_{t_0}^t \Phi^T(\tau, t)H^T(\tau)R^{-1}H(\tau)\Phi(\tau, t) d\tau, \quad (7.192)$$

which can also be verified, as usual, by direct differentiation.  $\Phi$  is the state transition matrix defined by (7.108), where, in this case, the reverse order of the arguments should be noted. If we have no prior information about the states, that is  $P^{-1}(t_0) = 0$ , then the homogeneous part of the solution is absent.

If the initial information matrix is zero, but  $0 < |P^{-1}(t)| \leq c < \infty$  for some  $t > t_0$  and some bounding constant,  $c$ , then the system is said to be (stochastically) *observable*. That is, external observations in this case provide information on the system states.

The error covariance matrix,  $P(t)$ , for the states can be determined by inverting the information matrix (if the inverse exists). If the coefficient matrices  $F$  and  $H$  are constant then the integration in (7.192) (formally) can be done analytically; or, the solution for the covariance matrix is obtained directly from (7.189) with  $\Phi_{VU}(t, t_0) = 0$  (i.e.,  $Q = 0$ ):

$$P(t) = \Phi_{VV}(t, t_0)P(t_0)(\Phi_{UU}(t, t_0) + \Phi_{UV}(t, t_0)P(t_0))^{-1}. \quad (7.193)$$

#### 7.7.2.3 No Observations

If no observations are available (or, the observations have infinite variance), that is  $R^{-1} = 0$ , we, again, have a simplified Riccati equation:

$$\dot{P}(t) = F(t)P(t) + P(t)F^T(t) + G(t)QG^T(t). \quad (7.194)$$

This is the linear variance equation (7.172), whose solution was already found as (7.171). An alternative is given by (7.189) if the coefficient matrices  $F$  and  $G$  are constant, where now  $\Phi_{UV}(t, t_0) = 0$ :

$$P(t) = (\Phi_{VU}(t, t_0) + \Phi_{VV}(t, t_0)P(t_0))\Phi_{UU}^{-1}(t, t_0). \quad (7.195)$$

If the initial covariance of the system states is zero, but the system noise drives it to a positive definitive matrix, while keeping it bounded, i.e.,  $0 < |P(t)| \leq c < \infty$  for some  $t > t_0$  and some bounding constant,  $c$ , the system is said to be (stochastically) *controllable*. That is, the states are affected by system noise and could be controlled with suitable deterministic inputs. Controllability and observability of a system influence the dynamic *stability* of the Kalman filter in the long term (see Maybeck, 1979).

For the practical computation of (7.189), (7.193), and (7.195), for longer times,  $t$ , with respect to  $t_0$ , the solution is usually broken into smaller intervals so that the series (7.187) may be truncated at a reasonable level. The solution for the end of one interval then serves as the initial value for the subsequent interval. Although the solution in each case is exact (to the extent of the truncation of (7.187)), its numerical stability depends on the accumulation of round-off errors in the computations. Here, as also in the discrete Kalman filter algorithm, it is a good idea to ensure symmetry in the covariance matrix by replacing it at each step with  $(P(t) + P^T(t))/2$ .

# 8 INS Initialization and Alignment

## 8.1 Introduction

Before an INS is ready to navigate various initial conditions must be imposed or determined that remove ambiguities, define the navigation frame, and resolve certain systematic errors. Inertial navigation is based on the integration of accelerations; and, the positions and velocities thus obtained are associated with integration constants. Intuitively, it is clear that these constants must be supplied by external sources. But the initial processing of the IMU data encompasses more than that. Besides setting the initial position and velocity, one must determine the initial alignment of the inertial sensors. For the strapdown mechanization this means that the direction cosines between the body frame and the navigation frame must be established before navigation can commence; and, this alignment serves as a starting point (or, another set of integration constants) for the subsequent determination of the attitude based on the integration of the gyro angular rates. For example, we saw how these orientation angles can be obtained by integrating equation (4.19), where the set of integration constants (the initial alignment of the system) must be specified. Similarly, one needs to initialize the prescribed alignment of the platform of a stabilized system with respect to the navigation frame. This is achieved mechanically through appropriate rotations of the platform gimbals.

The initial position and velocity required as integration constants in the primary navigation equations (e.g., (4.77)) are simply inserted into the system as input data. When the system is stationary its velocity (relative to the Earth) is known and presumably it is positioned over a point with known coordinates. For a moving system, very accurate position and velocity are now available from external sources, such as the Global Positioning System (GPS, see Chapter 9), among other radar navigation systems. However, orientation is considerably more difficult to initialize because it requires knowing, for example, the directions of “down” and “north”, that often are not readily available from external observations. Aside from the alignment, the initialization process may also involve the determination of systematic errors in the sensors, to the extent that it is possible to do so. These are the errors that cannot be determined in the laboratory by standard calibration techniques and generally have a stochastic nature; for example, they are the random constants that characterize the biases of the sensors that may change from turn-on to turn-on of the system.

The INS can be initialized and aligned with various levels of accuracy, and the manufacturers build into the system an array of modes that provide flexibility to account for different circumstances and accuracy requirements. Simply keeping the sensors at rest with respect to the Earth, prior to navigation, allows them to respond to known directions of acceleration and angular rate vectors (gravity and Earth’s rotation) that aid in aligning the system. However, the need to account for and attempt an estimation of the gyro bias errors extends the time needed to perform an

accurate alignment. Generally, the more accuracy that is needed, the more parameters must be solved. Also, if less external information is available, it takes longer to prepare the system for navigation. Since a key benchmark figure for many military systems is the amount of time the INS needs to achieve readiness for navigation, considerable effort goes into devising fast, but accurate alignment and initialization procedures.

We consider in detail only the analytics of the basic alignment achieved with external velocity and possibly orientation (primarily azimuth) information either while the system is stationary or when it is moving. Attitude information may come from optical methods of alignment whereby angles are transferred to the system from determinations of accurate external optical sightings. This could be an optical azimuth determination of the system relative to an external reference while it is stationary; or a stellar camera can be used to observe the orientation of the system in flight relative to a set of stars with known celestial coordinates. The latter method also serves to (re)calibrate the gyro errors en route for enhanced navigation performance. Methods such as these, however, require expensive optical equipment and are not suited for all types of weather conditions.

In some situations a set of alignment angles is available from a previous alignment that was stored in the navigation computer. This assumes, of course, that the vehicle has not moved since the last alignment of its inertial sensors. The *stored alignment* method is particularly useful for initializing the heading (azimuth) which is the most difficult to achieve autonomously. A related method is the *transfer alignment* (Kayton and Fried, 1997), whereby an inertial system is aligned relative to another inertial system of higher accuracy, such as aircraft systems relative to an aircraft carrier system, or a missile system relative to an aircraft system.

The subject matter of this chapter is limited to the case where the navigation frame is the local-level frame (*n*-frame or *w*-frame), although by inference and with a slight change in notation the discussion easily could be extended to other frames. Furthermore, while the local-level stabilized mechanization will be mentioned to provide an additional conceptualization, the focus is on strapdown systems; see (Britting, 1971; Kayton and Fried, 1969; and Chatfield, 1997) for more elaborate discussions of the stabilized system. In fact, the difference between the two is almost transparent in terms of the numerical analysis, as it was in the case of the navigation error dynamics (but, of course, there are implementational differences). The usual environment prescribed for initialization and alignment puts the navigation system at rest with respect to the Earth. With accurate external positioning systems available (such as GPS), the methodologies naturally extend to the initialization and alignment of the INS in the kinematic mode.

The alignment can be performed coarsely, at first, based on information such as magnetic north (standard compass) and leveling using bubble vials. This gives at least crude first values for the attitude angles that subsequently may be refined using techniques based on linear estimation. Other coarse alignment techniques are discussed below. The *fine alignment* techniques are either self correcting processes that rely on the fact that the vehicle is stationary on a rotating Earth, or they are based

on aiding information from external positioning or navigation sources (applicable if the vehicle is moving). The difficulty of accurate heading or azimuth determination, mentioned above, was already alluded to in the discussion of the navigation error equations (Section 5.4.1), where it was shown that the vertical gyro error (e.g., bias) is only weakly coupled to the velocities that would serve as external information for the purpose of alignment and calibration of biases.

This and other essential principles of alignment and initialization will be demonstrated analytically and illustrated with simple error analyses performed using the linear estimation theory developed in Chapter 7. Emphasis is placed on the estimation of orientation errors and the calibration of gyro and accelerometer biases, these being the most crucial for accurate inertial navigation. In this respect, the principal states of the system are the attitude errors, as well as the parameters of the unresolved systematic sensor errors, and other states that connect the external information to the attitude errors. While perhaps not the most elaborate of alignment schemes, the purpose of this presentation is to elucidate the essential concepts and limitations. More comprehensive analyses, especially for the in-flight alignment and calibration of one inertial navigation system relative to another may be found in (Bazw and Leondes, 1972a,b).

## 8.2 Coarse Alignment

Instead of using approximate externally provided directions (such as from a compass and leveling bubbles or precomputed angles), a stationary inertial navigation system can align itself by exploiting directions physically defined by the Earth, namely, the direction of gravity and the direction of the Earth's spin axis. The *coarse alignment* of the sensor assembly provides a quick orientation of the platform (stabilized or strapdown) with respect to the navigation frame using the accelerations and angular rates obtained directly from the sensors without consideration of their errors. A subsequent *fine alignment* improves upon this with estimates of uncompensated accelerometer and gyro biases and other systematic errors, in conjunction with the orientation errors. These estimates are obtained from a Kalman filter, thus allowing for the proper statistical treatment of the system and observation noise.

Conceptually, leveling a gimbaled platform is accomplished by monitoring the output of two mutually perpendicular accelerometers with their input axes parallel to the platform. If the platform has zero velocity (is stationary) with respect to the Earth, then the accelerometers sense only components of the *reaction* to the gravity acceleration vector,  $\bar{g}^n$  (see (4.91) with  $v^n = \mathbf{0}$ ). The platform is level when its vertical axis is aligned with the direction of gravity; then the horizontal accelerometers on the platform sense zero specific force. Thus, an approximate leveling ensues by rotating the platform pitch and roll gimbals using the servo motors (Figure 4.4) such that the output of each horizontal accelerometer vanishes. The accuracy of this procedure is limited by the accuracy of the servo motors, the stability of the vehicle, and the accuracy of the accelerometers and of their physical alignment relative to

the platform. We note that alignment to the usual local-level navigation frame (vertical along the ellipsoid normal) requires accounting for the deflection of the vertical (Figure 6.9). On the other hand, neglecting this deflection is equivalent to assuming a bias in the accelerometer output (both cause a misalignment of the system in the  $n$ -frame); and, as noted in Section 5.4.1, such biases are canceled in the navigation solution by the effects of the consequent platform tilt in the case of the north-slaved, local-level, stabilized platform.

Analogously, the alignment of the platform in azimuth is achieved by monitoring the commanded rate of the gyro whose designated input axis lies along the east horizontal direction. According to (4.10) with velocities set to zero, the *east-pointing* gyro on a north-slaved, level platform would have zero commanded rate:

$$\omega_{\text{com}} = (\omega_e \cos \phi \quad 0 \quad -\omega_e \sin \phi)^T, \quad (8.1)$$

assuming no gyro error. Thus, rotating the platform about the vertical (azimuth servo motor) until the (horizontal) gyro output is zero, directs its input axis toward the east, and the axis orthogonal to it in the horizontal plane points north. Similarly, in the wander-azimuth mechanization (zero rate about the vertical), the commanded rate, from (4.14), is

$$\omega_{\text{com}} = (\omega_e \cos \phi \cos \alpha \quad \omega_e \cos \phi \sin \alpha \quad 0)^T, \quad (8.2)$$

and the ratio of the rates for the east and north gyros yields the azimuth,  $\alpha$ , of the  $w$ -frame, which is defined as being parallel to the platform frame. In either case, the gyros provide a heading or azimuth reference based on and in relation to the rotation vector of the Earth. This procedure recalls the original purpose for which the gyro was invented (Section 4.1) and is appropriately called *gyrocompassing*.

In practice, the alignment of the local-level stabilized system is done with the accelerometers and gyros working in concert to achieve both leveling and alignment in azimuth. Assuming the platform gyros are torqued to maintain level on the rotating Earth, then if the east gyro is *not* pointing east, its output, being non-zero, will cause the platform to rotate about the east axis (signal to the platform gimbal servos). A signal is produced in the north accelerometer, that is now not level, and this signal commands the platform to turn in azimuth, until the east gyro and north accelerometer both sense null. This physical alignment is more accurately called *acceleration-coupled gyrocompassing*. The feedback system usually includes specific damping and gain factors, as well as bias compensations derived from a Kalman filter of other external information. These enhancements belong to the class of fine alignment procedures (Section 8.3).

For the strapdown system, a course alignment can be done in a similar, though strictly analytical and numerical fashion. We confine the discussion to the wander-azimuth navigation frame, where specialization to the  $n$ -frame requires only an appropriate stipulation of the wander azimuth and its rate. Again assuming a stationary system ( $\mathbf{v}^w = \mathbf{0}$ ), the accelerometer output with (4.78) and (4.107) is expressed as

$$\mathbf{a}^b = C_w^b \mathbf{a}^w = -C_w^b \bar{\mathbf{g}}^w = -\bar{\mathbf{g}}^b; \quad (8.3)$$

and the gyro output, according to (4.127) with  $\omega_{wb}^b = \mathbf{0}$  (stationary vehicle), is given by

$$\omega_{ib}^b = C_w^b \omega_{iw}^w. \quad (8.4)$$

The object of the alignment is to determine the direction cosines of the transformation from the body frame to the wander-azimuth navigation frame, i.e., the elements of  $C_b^w$ , using the accelerometer and gyro outputs.

Consider one more vector, orthogonal to both naturally defined directions,  $\bar{\mathbf{g}}^w$  and  $\omega_{ie}^w$ ; and, call it  $\mathbf{c}^w$ :

$$\mathbf{c}^w = \bar{\mathbf{g}}^w \times \omega_{ie}^w = \bar{\mathbf{g}}^w \times \omega_{bw}^w, \quad (8.5)$$

where the second equality follows because  $\omega_{we}^w = \mathbf{0}$  if the vehicle is stationary (and if that implies  $\dot{\alpha} = 0$ ). Since the 3-axis of the  $w$ -frame is aligned with the vertical, the gravity vector has only one non-zero component (we neglect the deflection of the vertical; see Figure 6.9):

$$\bar{\mathbf{g}}^w = (0 \quad 0 \quad \bar{g})^T, \quad (8.6)$$

where  $\bar{g}$  is the magnitude of gravity. From (4.13) with zero velocity, we have

$$\omega_{iw}^w = \begin{pmatrix} \omega_e \cos \phi \cos \alpha \\ -\omega_e \cos \phi \sin \alpha \\ \omega_e \sin \phi + \dot{\alpha} \end{pmatrix}. \quad (8.7)$$

Putting these into (8.5) yields

$$\mathbf{c}^w = \begin{pmatrix} \bar{g} \omega_e \cos \phi \sin \alpha \\ \bar{g} \omega_e \cos \phi \cos \alpha \\ 0 \end{pmatrix}. \quad (8.8)$$

Now, using the notation  $[\mathbf{g}^w \times]$  to denote a skew-symmetric matrix, as in (5.48), we have

$$\begin{aligned} \mathbf{c}^b &= C_w^b \mathbf{c}^w \\ &= C_w^b [\bar{\mathbf{g}}^w \times] \omega_{iw}^w = C_w^b [\bar{\mathbf{g}}^w \times] C_b^w C_w^b \omega_{iw}^w = [\bar{\mathbf{g}}^b \times] \omega_{iw}^b \\ &= -\mathbf{a}^b \times \omega_{iw}^b = -\mathbf{a}^b \times (\omega_{ib}^b + \omega_{bw}^b) \\ &= -\mathbf{a}^b \times \omega_{ib}^b, \end{aligned} \quad (8.9)$$

where (1.17) was used in the second line. Then, combine (8.3), (8.4), and (8.9) into one matrix equation to obtain

$$(\mathbf{a}^b \quad \omega_{ib}^b \quad -\mathbf{a}^b \times \omega_{ib}^b) = C_w^b (-\bar{\mathbf{g}}^w \quad \omega_{iw}^w \quad \mathbf{c}^w). \quad (8.10)$$

Solving for  $C_w^b$ , taking the transpose, and using the  $w$ -frame coordinatized quantities (8.6), (8.7), and (8.8), we get

$$C_b^w = \begin{pmatrix} 0 & 0 & -\bar{g} \\ \omega_e \cos \phi \cos \alpha & -\omega_e \cos \phi \sin \alpha & -\omega_e \sin \phi + \dot{\alpha} \\ \bar{g} \omega_e \cos \phi \sin \alpha & \bar{g} \omega_e \cos \phi \cos \alpha & 0 \end{pmatrix}^{-1} \begin{pmatrix} (\mathbf{a}^b)^T \\ (\omega_{ib}^b)^T \\ (-\mathbf{a}^b \times \omega_{ib}^b)^T \end{pmatrix}. \quad (8.11)$$

The IMU sensors yield the quantities in the vector on the right side, while the matrix to be inverted requires the latitude of the platform, as well as its wander-azimuth definition. For example, one might specify the azimuth of the  $w$ -frame and the azimuth rate to be  $\alpha = 0$  and  $\dot{\alpha} = 0$ , which is the same as specifying the  $n$ -frame coordinatization. One then obtains the initial transformation from the  $b$ -frame to the  $n$ -frame:

$$C_b^n = \begin{pmatrix} 0 & 0 & -\bar{g} \\ \omega_e \cos \phi & 0 & -\omega_e \sin \phi \\ 0 & \bar{g}\omega_e \cos \phi & 0 \end{pmatrix}^{-1} \begin{pmatrix} (\mathbf{a}^b)^T \\ (\omega_{ib}^b)^T \\ (-\mathbf{a}^b \times \omega_{ib}^b)^T \end{pmatrix}. \quad (8.12)$$

In this case, the azimuth of the  $b$ -frame is given by the yaw angle (see (1.90)), determined using (1.23). The coefficient matrix in (8.11) or (8.12) is invertible as long as the gravity vector and the Earth's spin axis are not parallel (for otherwise the cross-product,  $\mathbf{c}^w$  defined in (8.5), would be zero). This pathological case occurs only near the poles.

Equations (8.11) and (8.12) show that the output of the accelerometers and gyros of a stationary strapdown INS can be used to determine the body-frame-to-navigation-frame transformation matrix. However, this method is based on an idealization in which there are no accelerometer and gyro errors (and no deflection of the vertical). In reality, of course, both accelerometer and gyro output data have errors, especially the gyros may have large rate biases. Also, even though the vehicle is stationary, it is not rigidly fixed to the Earth and motions due to wind gusts or other disturbances cause inaccurate accelerometer and gyro outputs. Finally, the method above yields no information on the accuracy of the orientation, nor does it apply appropriate weights to the data based on the statistical characteristics of the sensor noise.

### 8.3 Fine Alignment and Calibration

A coarse alignment in leveling and azimuth (achievable in a matter of a few seconds) presumably leaves only small angle differences between the indicated and ideal alignments. These differences are caused, in part, by systematic errors in the sensors that cannot be calibrated in the laboratory, particularly biases that have different values each time the system is turned on. As indicated in Section 5.2, gyro biases are especially detrimental to the accuracy of the navigation solution, most notably in the heading, where the azimuth reference is established using the east gyro, while the change in heading comes from the output of the vertical gyro.

The alignment is refined under the assumption that external information provides a means to estimate the systematic instrument errors. At least gyro biases, but also accelerometer biases need to be considered. However, we already found that these are not readily distinguished in a north-slaved, local-level, stabilized system. Therefore, the gyro biases, if observable at all, can only be estimated to the accuracy of the unknown accelerometer biases. Accelerometer biases in this type of mechaniza-

tion, per se, generally do not affect the navigation solution; but in a strapdown mechanization they do and should be estimated. The calibration then proceeds on the basis of external observations (position and velocity) in a Kalman filter, where the accelerometer error states decouple from the orientation errors as the orientations change with appropriate vehicle maneuvers.

We consider the fine alignment of strapdown systems from a purely analytical perspective which frees us from the particular frame mechanization to some extent. The aim is to provide a more quantitative visualization of the couplings between instrument biases and the initial alignment of the system (as heuristically discussed in Chapter 5) using the estimation techniques developed in Chapter 7.

### 8.3.1 Acceleration Observations

As a first example of a refined alignment procedure, we consider the following method for leveling, that assumes no errors in the gyros (systematic or otherwise), and only white noise in the accelerations. In that sense it is only a more sophisticated coarse leveling procedure with somewhat more realistic weights (gains) for the orientation estimates. It is assumed that the system has already undergone a coarse alignment as described above and that only a small angular perturbation exists due to imperfect acceleration output. This could be due to accelerometer white noise or random movements of the vehicle due to external perturbations (wind gusts, etc.).

To simplify the analysis only the  $n$ -frame mechanization will be treated. From equation (5.62) we have for a stationary system ( $\omega_{en}^n = \mathbf{0}$ )

$$\dot{\psi}^n = -\omega_{in}^n \times \psi^n = -\omega_{ie}^n \times \psi^n, \quad (8.13)$$

since the gyros are assumed to have no error ( $\delta\omega_{is}^s = \mathbf{0}$ ), and the position and velocity of the INS, likewise, are assumed errorless ( $\delta\omega_{in}^n = \mathbf{0}$ ). The elements of the vector  $\psi$  are the orientation errors and constitute the state variables of the system. They are assigned an initial covariance,  $P_0$ , that may be assumed to be a diagonal matrix. With  $\omega_{ie}^n$  from (4.99), equation (8.13) can be put into the usual form, (7.106), of a linear set of differential equations:

$$\frac{d}{dt} \begin{pmatrix} \psi_N \\ \psi_E \\ \psi_D \end{pmatrix} = \begin{pmatrix} 0 & -\omega_e \sin \phi & 0 \\ \omega_e \sin \phi & 0 & \omega_e \cos \phi \\ 0 & -\omega_e \cos \phi & 0 \end{pmatrix} \begin{pmatrix} \psi_N \\ \psi_E \\ \psi_D \end{pmatrix}, \quad (8.14)$$

where the  $G$ -matrix is zero because of the assumed absence of noise driving this system.

The external information brought to the alignment problem is the postulated horizontal acceleration of the vehicle, presumed to be stationary. In terms of perturbations, according to (7.51), the external observations are the differences between the accelerometer output values and the supposed horizontal acceleration of the INS, ideally, zero. Small random accelerations of the vehicle due to wind gusts, or other environmental effects, as well as random noise of the accelerometer are lumped together in the noise vector,  $v^n$ . For the sake of simple illustration, we assume that

these noise components are decoupled along the  $n$ -frame directions. Thus, the model relating the observations to the states, according to (5.61), is given by:

$$\delta \mathbf{a}^n = \mathbf{a}^n \times \boldsymbol{\psi}^n + \mathbf{v}^n. \quad (8.15)$$

Since  $\mathbf{a}^n \approx (0 \ 0 \ -\bar{g})^T$ , we have the required linear relationship as in (7.52):

$$\begin{pmatrix} \delta a_N \\ \delta a_E \end{pmatrix} = \begin{pmatrix} 0 & \bar{g} & 0 \\ -\bar{g} & 0 & 0 \end{pmatrix} \begin{pmatrix} \psi_N \\ \psi_E \\ \psi_D \end{pmatrix} + \begin{pmatrix} v_N \\ v_E \\ v_D \end{pmatrix}. \quad (8.16)$$

We assume that the observations are available on a practically continuous basis. Therefore, to analyze the performance of this alignment procedure, we examine the covariance matrix for the continuous Kalman filter. The matrix Riccati equation describes the dynamics of this covariance matrix; and, because we assumed zero process noise ( $G = 0$ ), it is convenient to use the solution (7.192) that determines the Fisher information matrix as a function of time. The variances of the states (as a function of time) are then the diagonal elements of its inverse.

Because the dynamics of the orientation states, (8.14), depend only on Earth's rate of rotation, with a period of 24 hours that is long compared to the alignment process, we can neglect the  $F$ -matrix and assume that the state transition matrix, (7.109), is the identity matrix. Then (7.192) becomes

$$P^{-1}(t) = P^{-1}(t_0) + \int_{t_0}^t H^T(\tau) R^{-1} H(\tau) d\tau. \quad (8.17)$$

Assigning a nominal variance,  $\sigma_a^2$ , to each observation, the psd matrix of the now continuous white noise vector  $(v_N \ v_E)^T$  is given according to (6.61) by

$$R = \begin{pmatrix} \sigma_a^2 & 0 \\ 0 & \sigma_a^2 \end{pmatrix} \Delta t. \quad (8.18)$$

Also the  $H$ -matrix (see (8.16)) is a constant and the integration in (8.17) is easily performed analytically, resulting in:

$$P^{-1}(t) = \begin{pmatrix} \sigma_N^{-2} & 0 & 0 \\ 0 & \sigma_E^{-2} & 0 \\ 0 & 0 & \sigma_D^{-2} \end{pmatrix} + \begin{pmatrix} \bar{g}^2 \sigma_a^{-2} & 0 & 0 \\ 0 & \bar{g}^2 \sigma_a^{-2} & 0 \\ 0 & 0 & 0 \end{pmatrix} \frac{t - t_0}{\Delta t}, \quad (8.19)$$

where  $\sigma_{N,E,D}^2$  are the initial variances associated with the orientation errors. At time  $t_k = t_0 + k\Delta t$ , these variances are the diagonal elements of

$$P(t_k) = \text{diag} \left( \frac{\sigma_a^2}{kg^2} \frac{1}{1 + \frac{\sigma_a^2}{kg^2} \frac{1}{\sigma_N^2}}, \frac{\sigma_a^2}{kg^2} \frac{1}{1 + \frac{\sigma_a^2}{kg^2} \frac{1}{\sigma_E^2}}, \sigma_D^2 \right). \quad (8.20)$$

Note that the variance of the azimuth error remains unchanged since the horizontal accelerometers perform only the leveling function. If the initial variances,  $\sigma_{N,E}^2$ , are

very large compared to  $\sigma_a^2/g^2$ , they first ( $k = 1$ ) decrease to that level and then propagate in time essentially as  $(\sigma_a^2/g^2)/k$ , decreasing in accordance with the law of averages. Thus more accurate leveling is achieved over time provided the random motions of the vehicle (and the accelerometer errors) are really random (white).

One could also include gyro white noise in the analysis. This would add system process noise to the dynamics equation (8.14), and  $Q \neq 0$ . The covariance matrix of the orientation states is then given by the solution (7.189) to the matrix Riccati equation, which under simplifying assumptions can also be reduced to interpretable analytic form (left as an exercise to the reader).

### 8.3.2 Velocity and Azimuth Observations

In addition to the improved estimation of the leveling errors, we consider next the determination of the azimuth reference, as well as the calibration of the gyro biases. As before, the navigation system is stationary with respect to the Earth, the position of the system is assumed known without error, and the observations are based on the idealization of no system motion. However, while in the previous section, this static condition was reflected in the “observation” of zero horizontal acceleration, here we use zero velocity which tends to give a stronger solution. In addition, an external azimuth determination may be available; for example, an optical system (stellar camera, or other optical sighting to a known reference), or directional radar systems (LORAN, OMEGA, differential GPS, etc.). This provides direct observability of the vertical orientation error and subsequently of the vertical gyro bias. In the absence of an external azimuth observation, the alignment (then known as a *self-alignment*) and calibration of the vertical orientation must depend entirely on the system’s sensitivity to Earth’s rotation; that is, it requires a much longer time to determine these errors. The fine alignment and calibration with the above assumptions can be explored with the following numerical example.

The state vector in this case comprises the orientation errors, the gyro biases, and the velocity errors (although these are “observed”, they enter also explicitly in the differential equation for the orientation error states, as seen below). The dynamics model for the orientation error states is, again, given by (5.62):

$$\dot{\psi}^n = -\omega_{ie}^n \times \psi^n - C_s^n \delta\omega_{is}^s + \delta\omega_{in}^n. \quad (8.21)$$

We assume that  $\delta\omega_{is}^s$  consists of gyro biases only and identify the combination  $C_s^n \delta\omega_{is}^s$  as a vector of  $n$ -frame gyro biases,  $\Delta\omega$ , in as (5.75). This constitutes no loss in generality if the vehicle is stationary. Therefore, let the dynamics of these biases be formulated simply as random constants:

$$\Delta\dot{\omega} = \frac{d}{dt} \begin{pmatrix} \Delta\omega_N \\ \Delta\omega_E \\ \Delta\omega_D \end{pmatrix} = \mathbf{0}. \quad (8.22)$$

In addition, we have from (5.63) with (5.58), setting position errors equal to zero and  $r = R_\phi + h$ :

$$\delta\omega_{in}^n = \begin{pmatrix} \frac{\delta v_E}{r} \\ \frac{-\delta v_N}{r} \\ \frac{-\delta v_E}{r} \tan \phi \end{pmatrix}. \quad (8.23)$$

The dynamics of the velocity errors are given by (5.71), where now we neglect the accelerometer errors, gravity errors, and vertical velocity error:

$$\begin{aligned} \frac{d}{dt} \delta v_N &= -2\omega_e \sin \phi \delta v_E + \bar{g}\psi_E, \\ \frac{d}{dt} \delta v_E &= 2\omega_e \sin \phi \delta v_N - \bar{g}\psi_N. \end{aligned} \quad (8.24)$$

Equations (8.21), (8.22), and (8.24) are combined to form one set of linear differential equations. We let the system state vector be denoted by  $\varepsilon$ :

$$\varepsilon = (\psi_N \ \psi_E \ \psi_D \ \Delta\omega_N \ \Delta\omega_E \ \Delta\omega_D \ \delta v_N \ \delta v_E)^T. \quad (8.25)$$

Then

$$\dot{\varepsilon} = F\varepsilon, \quad (8.26)$$

where, with (8.23), the dynamics matrix is

$$F = \begin{pmatrix} 0 & -\omega_e \sin \phi & 0 & -1 & 0 & 0 & 0 & \frac{1}{r} \\ \omega_e \sin \phi & 0 & \omega_e \cos \phi & 0 & -1 & 0 & -\frac{1}{r} & 0 \\ 0 & -\omega_e \cos \phi & 0 & 0 & 0 & -1 & 0 & \frac{1}{r} \tan \phi \\ 0 & 0 & 0 & 0 & 0 & 0 & 0 & 0 \\ 0 & 0 & 0 & 0 & 0 & 0 & 0 & 0 \\ 0 & \bar{g} & 0 & 0 & 0 & 0 & 0 & -2\omega_e \sin \phi \\ -\bar{g} & 0 & 0 & 0 & 0 & 0 & 2\omega_e \sin \phi & 0 \end{pmatrix}. \quad (8.27)$$

Note that because of our simplifying assumptions, there is no random noise driving this system ( $G = 0$ ).

The observations that are used to estimate the states are the horizontal velocity components, each being the difference between velocity indicated by the system and the evident (Earth-referenced) velocity of the system (ideally zero, if the vehicle is stationary). The accuracy associated with these observations may be derived approximately from knowledge about environmental disturbances, such as wind gusts, or the quantization errors in the indicated velocity. The azimuth observation is the difference between the azimuth indicated by the system, as derived from the indicated direction cosine elements (cf. (1.90) and (1.23)), and the azimuth determined by the externally observed horizontal angle of the system with respect to

true north. Thus, the azimuth error observation is a direct manifestation of  $\psi_D$ . The linear relationship between observations and states is given by

$$\mathbf{y} = \mathbf{H}\boldsymbol{\varepsilon} + \mathbf{v}, \quad (8.28)$$

where the matrix  $H$  is

$$\mathbf{H} = \begin{pmatrix} 0 & 0 & 0 & 0 & 0 & 0 & 1 & 0 \\ 0 & 0 & 0 & 0 & 0 & 0 & 0 & 1 \\ 0 & 0 & 1 & 0 & 0 & 0 & 0 & 0 \end{pmatrix}, \quad (8.29)$$

and  $\mathbf{v} \sim \mathcal{N}(0, R)$ , where

$$\mathbf{R} = \begin{pmatrix} \sigma_{\text{vel}}^2 & 0 & 0 \\ 0 & \sigma_{\text{vel}}^2 & 0 \\ 0 & 0 & \sigma_{\text{az}}^2 \end{pmatrix} \Delta t, \quad (8.30)$$

with  $\sigma_{\text{vel}}$  and  $\sigma_{\text{az}}$  representing the standard deviations of the velocity and azimuth observations.

With the assumption of no internal driving noise components (no process noise), the system state variances can be analyzed using the simplified Riccati equation (7.190), whose solution in terms of the Fisher information matrix is given by (7.192). We will use this solution recursively for small increments of time,  $\Delta t$ . As such, the state transition matrix inside the integral of (7.192) is approximated as the identity matrix, while for the first term we approximate  $\Phi$  with just the linear term in (7.109). We thus have the following recursion for the information matrix:

$$\mathbf{P}_k^{-1} = (\mathbf{I} - \mathbf{F}\Delta t)^T \mathbf{P}_{k-1}^{-1} (\mathbf{I} - \mathbf{F}\Delta t) + \mathbf{H}^T \mathbf{R}^{-1} \mathbf{H} \Delta t, \quad (8.31)$$

with starting values given by the inverse of  $\mathbf{P}_0$ , which is a diagonal matrix with elements:

$$\mathbf{P}_0 = \text{diag}(\sigma_{\psi_N}^2, \sigma_{\psi_E}^2, \sigma_{\psi_D}^2, \sigma_{\Delta\omega_N}^2, \sigma_{\Delta\omega_E}^2, \sigma_{\Delta\omega_D}^2, \sigma_{\delta v_N}^2, \sigma_{\delta v_E}^2). \quad (8.32)$$

These are the initial variances of the states; for the orientation errors they could be guessed from the result of a coarse alignment; and for the gyro biases they would be the values corresponding to the repeatability stated in the instrument specification.

In our numerical example, we choose the following values for the standard deviations in (8.30) and (8.32):

$$\begin{aligned} \sigma_{\psi_N} &= \sigma_{\psi_E} = \sigma_{\psi_D} = 1^\circ, \\ \sigma_{\Delta\omega_N} &= \sigma_{\Delta\omega_E} = \sigma_{\Delta\omega_D} = 0.1^\circ/\text{hr}, \\ \sigma_{\delta v_N} &= \sigma_{\delta v_E} = 0.1 \text{ m/s}, \\ \sigma_{\text{vel}} &= 0.01 \text{ m/s}, \\ \sigma_{\text{az}} &= 5 \text{ arcsec}. \end{aligned} \quad (8.33)$$

The results displayed in Figures 8.1–8.6 were computed using (8.31) and (8.33) with the additional set of values

$$\begin{aligned}\bar{g} &= 9.8 \text{ m/s}^2; \quad \omega_e = 7.292 \times 10^{-5} \text{ rad/s}, \quad r = 6371000 \text{ m}, \\ \phi &= 45^\circ, \quad \Delta t = 1 \text{ s.}\end{aligned}\quad (8.34)$$

For an easier interpretation of the results of the calculations, we repeat (8.21) and (8.24) here as one set of equations:

$$\frac{d}{dt} \delta v_N = -2\omega_e \sin \phi \delta v_E + \bar{g} \psi_E, \quad (8.35a)$$

$$\frac{d}{dt} \delta v_E = 2\omega_e \sin \phi \delta v_N - \bar{g} \psi_N, \quad (8.35b)$$

$$\frac{d}{dt} \psi_N = -\omega_e \sin \phi \psi_E + \frac{\delta v_E}{r} - \Delta \omega_N, \quad (8.35c)$$

$$\frac{d}{dt} \psi_E = \omega_e \sin \phi \psi_N + \omega_e \cos \phi \psi_D - \frac{\delta v_N}{r} - \Delta \omega_E, \quad (8.35d)$$

$$\frac{d}{dt} \psi_D = -\omega_e \cos \phi \psi_E - \frac{\delta v_E}{r} \tan \phi - \Delta \omega_D. \quad (8.35e)$$

Figures 8.1–8.3 show results if no azimuth observation is available; that is, only the velocity observations enter the estimation and  $1/\sigma_{az} = 0$ . Referring to equations (8.35a,b) and Figure 8.1, we see that accurate velocity information yields rapid estimation of the east and north orientation errors,  $\psi_E$ ,  $\psi_N$ , since they are coupled directly to the change in velocity errors. The down orientation error,  $\psi_D$ , however,

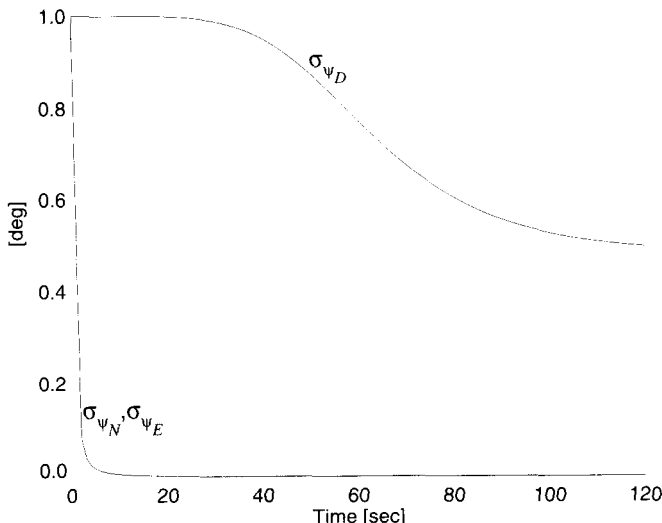


Figure 8.1: Standard deviations of orientation errors versus time. No azimuth observation is used.

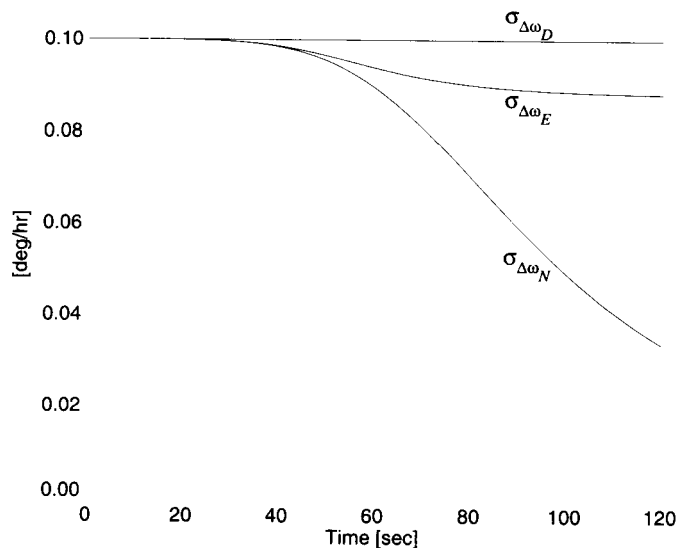


Figure 8.2: Standard deviations of gyro bias errors versus time. No azimuth observation is used.

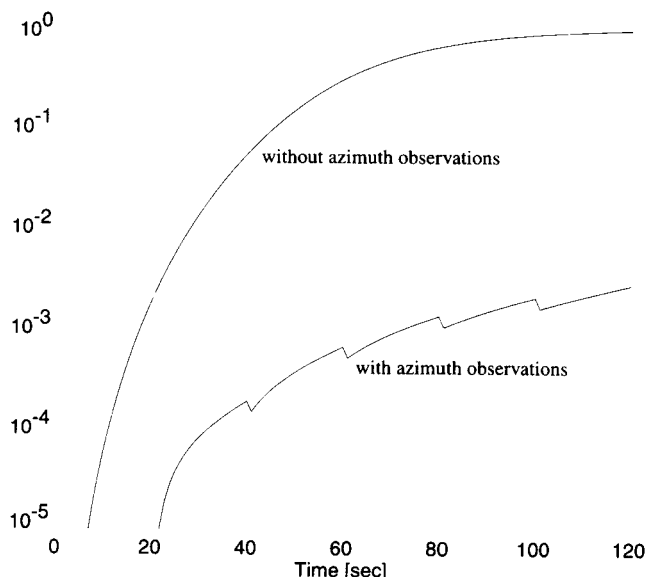


Figure 8.3: Correlation between east gyro bias and down orientation error versus time.

affects only the east orientation error (8.35d) and is not linked directly to the observations. Furthermore, in equation (8.35d) the term  $\omega_e \cos \phi \psi_D$  is indistinguishable from the east gyro bias,  $\Delta\omega_E$ . Therefore, neither the down orientation error nor the east gyro bias is determined well (Figure 8.2); also these two states become highly correlated as seen in Figure 8.3. The limiting standard deviations shown in Figures 8.1 and 8.2 for  $\psi_D$  and  $\Delta\omega_E$  are consistent and depend essentially on the minimum of their respective initial standard deviations:

$$\sigma_{\psi_D}(t_{\max}) = \frac{1}{\omega_e \cos \phi} \sigma_{\Delta\omega_E}(t_{\max}) \approx 0.5^\circ \approx \min \left( \sigma_{\psi_D}, \frac{1}{\omega_e \cos \phi} \sigma_{\Delta\omega_E} \right)_{t=0}. \quad (8.36)$$

The north gyro bias,  $\Delta\omega_N$ , on the other hand is more readily estimated since it is coupled to the east velocity error through the north orientation error; see (8.35c). This more indirect coupling however, extends the time required for accurate estimation. The fact that (8.35c) also contains the east orientation error,  $\psi_E$ , presents no difficulty in estimating  $\Delta\omega_N$  because the former can be estimated independently using the north velocity error observation. Finally the down gyro bias,  $\Delta\omega_D$ , is hardly estimable, being linked only to the down orientation error,  $\psi_D$ , which is not estimated very accurately.

Now, suppose that we include an observation of the azimuth at intervals of 20 seconds. Corresponding results are shown in Figures 8.4 and 8.5. The down orientation error,  $\psi_D$ , is determined immediately to the accuracy of the azimuth observation, which also implies a relatively quick determination of the down gyro bias,  $\Delta\omega_D$  (see Figures 8.4 and 8.5). The east gyro bias,  $\Delta\omega_E$ , is now also determined as

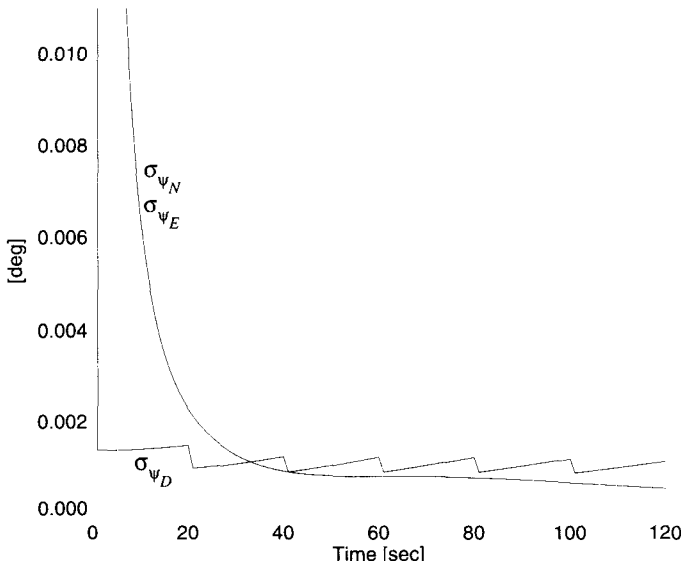


Figure 8.4: Standard deviation of orientation errors versus time. Azimuth observation is used at 20-sec intervals.

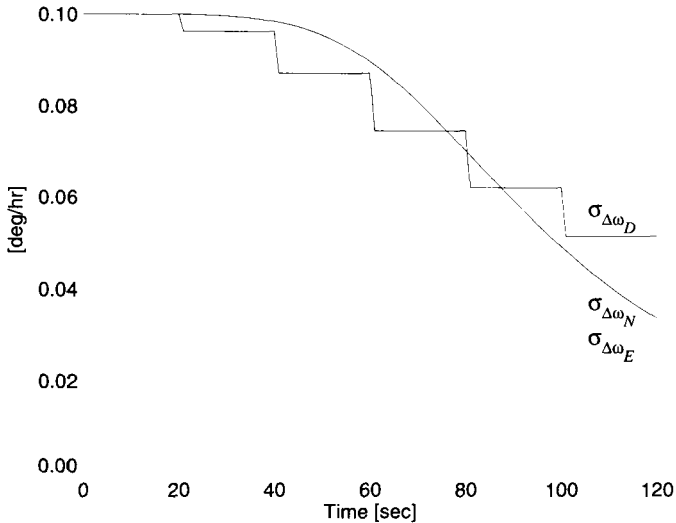


Figure 8.5: Standard deviations of gyro bias errors versus time. Azimuth observation is used at 20-sec intervals.

rapidly as the north gyro bias,  $\Delta\omega_N$  (compare Figures 8.2 and 8.5), and is practically uncorrelated with the down orientation error,  $\psi_D$  (Figure 8.3).

We conclude that without an accurate external azimuth reference, only the north gyro bias can be calibrated well using the velocity information implied by a stationary inertial navigation system. In practice, a gimbaled platform mechanization allows each gyro to be slewed or tumbled, in turn, such that its input axis points in the north direction. In this way, during the alignment process, the rate bias of each gyro can be calibrated. Clearly, this procedure is cumbersome at best and impractical in most situations for the strapdown mechanization.

### 8.3.3 Kinematic Alignment

If an external navigation system, such as the Global Positioning System, provides very accurate velocity information to a *moving* system, then clearly the velocity-based alignment procedure described in Section 8.3.2 may be used, as well. If the velocities are large, then a more rigorous model is required for the dynamics of the orientation and velocity error states (see Chapter 5). Furthermore, this en route, or in-flight, alignment allows calibration of both level gyro biases of a strapdown system using appropriate maneuvers of the vehicle that let each level gyro point northward. The calibration of the down gyro bias is still problematic, although the estimability of  $\Delta\omega_N$  and  $\Delta\omega_E$  now decouples them from the leveling errors,  $\psi_{N,E}$ , that then are able to bring velocity information to the down orientation error,  $\psi_D$ , thus improving its estimability. This is confirmed in the following extension of the

numerical example that includes a vehicle maneuver. Further examples of alignment analysis with external (GPS) velocity aiding, especially for the in-flight mode, can also be found in (Greenspan, 1996).

The error states for the stationary vehicle alignment (Section 8.3.2) did not include accelerometer biases since, as discussed in Section 5.4.1, we know that they are inseparable from the leveling errors. However, accurate velocity information in the kinematic mode separates these errors in the strapdown mechanization if the accelerometers are maneuvered out of their initial orientation in the  $n$ -frame.

The error dynamics model (8.24) is now augmented to include the level accelerometer biases,  $\Delta a_N$  and  $\Delta a_E$ . From (5.71) we have:

$$\begin{aligned}\frac{d}{dt} \delta v_N &= -2\omega_e \sin \phi \delta v_E + \bar{g} \psi_E + \Delta a_N, \\ \frac{d}{dt} \delta v_E &= 2\omega_e \sin \phi \delta v_N - \bar{g} \psi_N + \Delta a_E,\end{aligned}\quad (8.37)$$

where the accelerometer errors in the  $n$ -frame,  $\Delta a_N$  and  $\Delta a_E$ , are given by (5.72) and comprise only biases that, therefore, have the following assumed dynamics in the  $b$ -frame:

$$\frac{d}{dt} \begin{pmatrix} \Delta a_1^b \\ \Delta a_2^b \end{pmatrix} = \begin{pmatrix} 0 \\ 0 \end{pmatrix}. \quad (8.38)$$

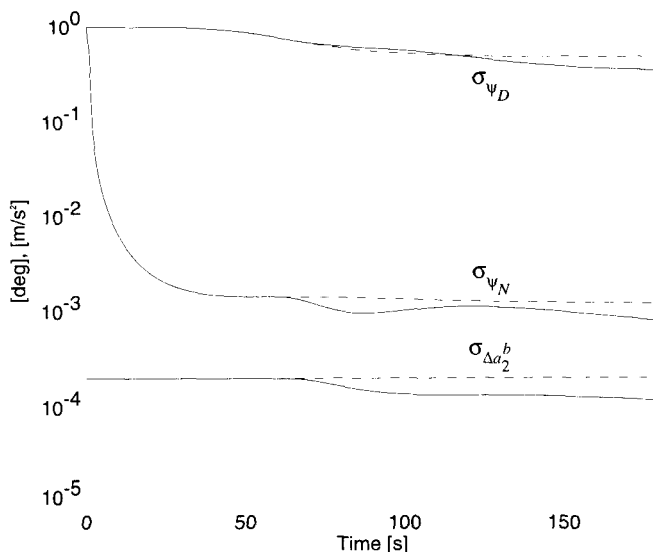


Figure 8.6: Standard deviations of orientation and accelerometer bias errors versus time. The effects of a 90° change in vehicle heading at  $t = 60$  s are shown by the solid line. The dashed lines correspond to no heading change.

The error state vector (8.25) now becomes

$$\boldsymbol{\varepsilon} = (\psi_N \ \psi_E \ \psi_D \ \Delta\omega_1^b \ \Delta\omega_2^b \ \Delta\omega_3^b \ \delta v_N \ \delta v_E \ \Delta a_1^b \ \Delta a_2^b)^T, \quad (8.39)$$

where also the gyro biases are coordinatized in the  $b$ -frame that is allowed to rotate with respect to the  $n$ -frame. Thus, the dynamics matrix,  $F$ , must be modified appropriately, increasing its size to account for the extra states and including elements of the rotation matrix,  $C_b^n$ , to simulate rotations of the vehicle (and the strapdown system). We may still use the zero-velocity approximation in the dynamics matrix, as justified in Section 5.4.

We now consider only horizontal velocity information, so that the observation matrix,  $H$ , and the observation covariance matrix,  $R$ , have only two rows. Still without process noise, the covariance matrix of the system states may be obtained from the solution, (8.31), to the Riccati equations. Using an initial standard deviation of  $\sigma_{\Delta a} = 20$  mgal for the accelerometer biases, the results for the orientation errors,  $\psi_N$  and  $\psi_D$ , and the accelerometer bias,  $\Delta a_2^b$ , are shown in Figure 8.6. Initially the  $b$ -frame is aligned with the  $n$ -frame ( $C_b^n = I$ ) and with no change in vehicle orientation, the standard deviations of the north orientation error and east accelerometer bias, as shown by the dashed lines, do not improve beyond the smaller of their initial values (when brought to common units), in this case  $0.0012^\circ$  or 20 mgal. At approximately  $t = 60$  s the vehicle is turned by  $90^\circ$  so that the east accelerometer and gyro now point north. This improves the estimation of the accelerometer bias as well as the leveling error, as shown by the solid lines. Also, the azimuthal orientation estimate improves eventually as a result of the maneuver, as predicted above.

## 9 The Global Positioning System (GPS)

### 9.1 Introduction

A positioning and navigation system that is entirely different from the inertial system described in Chapter 3 is the Global Positioning System (GPS) of satellites. Instead of dynamic principles like inertial reactions that are at the core of inertial measurement units, this system is based essentially on *geometry* in the classic tradition of geodesy. Specifically and simply put, when using GPS one measures distances. The Global Positioning System belongs to a large class of radio navigation systems that allow the user to determine his range and/or direction (in essence, using two antennas) from a known signal-transmitting station by measuring the differential time of travel of the signal, whose speed is close to the speed of light.

Terrestrial (ground-based) radio navigation systems predate the satellite systems and include systems such as VOR (VHF Omnidirectional Range) and DME (Distance Measuring Equipment) for civilian aviation; the military equivalent, Tacan (Tactical Air Navigation); and low-frequency, long-range systems such as LORAN (Long range navigation) and OMEGA. Motivated by military needs during World War II and rapidly developed afterwards, these systems still provide an essential navigational aid to aviation and marine applications. Details on operational characteristics, instrumentation, implementation, and accuracies may be found in (Beck, 1971) and (Kayton and Fried, 1969, 1997).

Satellite-based navigation systems naturally evolved from these terrestrial systems using much the same radio electronics technology, where the transmitter with known position is the satellite. In addition (in some cases, exclusively), they were used for static geodetic positioning to provide global ties between different national geodetic datums (positioning reference systems), and, in reverse, they provided a means to determine the orbits of satellites from known ground tracking stations. Early systems of the 1960's and 1970's included the Goddard Space Flight Center Range and Range Rate (GRARR) system, the U.S. Army's Sequential Collation of Range (SECOR) system, and the Navy Navigation Satellite System (known as TRANSIT). The latter, based on the Doppler effect of propagating signals, was developed initially as an all-weather navigation system for the U.S. Navy, but contributed significantly to commercial marine navigation and civilian geodetic applications. It is the immediate forerunner of the Global Positioning System and was terminated at the end of 1996. NGSP (1977) provides detailed descriptions of these early systems, mostly for geodetic applications (see also Seeber, 1993). Aside from GPS, modern systems include DORIS (Doppler Orbitography and Radio Positioning Integrated by Satellites) developed by the French and PRARE (Precise Range and Range Rate Experiment) and its extensions developed by the Germans. The primary utilization of these systems is satellite orbit determination (Seeber, 1993). Also of considerable importance is Russia's equivalent to GPS, the Global

Orbiting Navigation Satellite System (GLONASS); see Seeber (1993), Leick (1995), Kayton and Fried (1997).

The Global Positioning System, officially also known as the NAVSTAR (Navigation Satellite Timing and Ranging) system, is a satellite-based navigation system developed in the 1970's and 1980's by the U.S. Department of Defense; and, because of its versatility under myriad conditions and its strong civilian component, it is today, and likely in the foreseeable future, the most widely used positioning and navigation system of its or any other kind. GPS currently enjoys apparently unending and ever increasing worldwide utility because of its inherent comprehensive design and the decentralization of the user segment. Indeed, it has revolutionized positioning and navigation of all sorts, including geodetic static positioning, as well as kinematic positioning and navigation of moving vehicles (ground, marine, air navigation, and satellite orbit determination).

GPS comprises a set of orbiting satellites that may be thought of as active beacons at known locations in space whose signals are observed on the Earth (or anywhere in space where the satellite signals are "in view") and provide information about the distance between the satellite and the observer. With favorable geometry among the satellites and the observer, and with error-free and time-synchronized instrumentation, three distances to distinct satellites having known positions provide sufficient information to solve for the observer's three-dimensional position by the method of intersection (Figure 9.1). Already by the pre-conditions included in the last state-

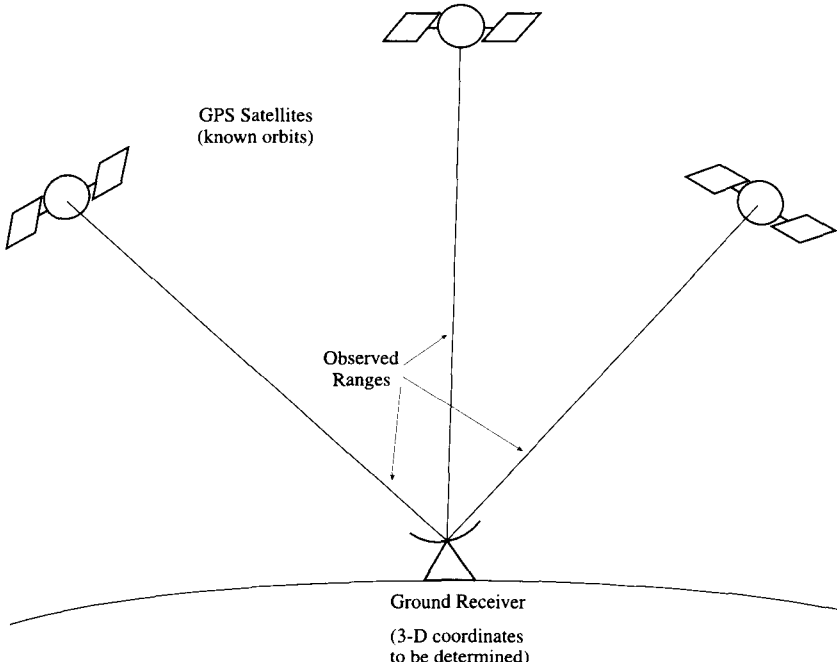


*Figure 9.1:* Ideal principle of positioning using observed satellite ranges.

ment, one may expect some essential difficulties with this type of positioning due to the timing of the signals. These are overcome mostly with both simple and ingenious methods; and GPS, since its inception, has evolved to become the most readily accessible, effortless, and accurate system for positioning (static and kinematic applications) and navigation (real-time application) available to users of all kinds.

The system is designed so that a minimum of four satellites is always in view anywhere in the world to provide continual positioning capability. This is accomplished with 24 satellites distributed unevenly (to maximize satellite availability) in six orbital planes arranged symmetrically in inertial space (Figure 9.2). The orbit of each satellite is approximately circular (eccentricity of the order of 0.006) with geocentric radius approximately equal to 26560 km, yielding an orbital period of about 12 hours. The orbital planes, each occupied by four satellites, are inclined to the Earth's equator at approximately  $55^\circ$  and spaced along the equator at  $60^\circ$  intervals (right ascensions of the ascending node are approximately  $12^\circ, 72^\circ, \dots, 312^\circ$ ).

The applications of GPS range from its original primary intent, military navigation, to commercial operations in monitoring and guiding the location of vehicles (fleet management) and to recreational and sporting activities. GPS receivers are now commonly found on commercial and private airplanes, ships, and boats, and are making an appearance on many other vehicles of different kinds (e.g., earth-moving equipment); few low-Earth-orbit satellites are now launched without GPS tracking capability. The most profound application from the scientific viewpoint is the extremely precise geodetic measurement of baselines (*relative* positioning) varying in length from several meters to hundreds of km, and more. Such precise determinations of baselines (with accuracy in the parts per ten million and higher) can and not only do supplant traditional geodetic measurements of distances between points in local, regional, and national geodetic networks, but also provide, through repeated observations, easy monitoring of crustal deformation associated with vulcanism, earthquakes, tectonic plate motion, and subsidence and rebound, both naturally or anthropogenically induced. This static mode of operation serves the original geodetic interest in GPS as a continuation of satellite geodetic methods, in general. However, with the development of the full constellation of GPS satellites and appropriate modification of GPS geodetic receivers, GPS also yields geodetic quality in the determination of positions of a moving vehicle.

With such wide applicability, why should one bother with any other kind of navigation or positioning system, like the INS? This question is quite serious where both accuracy and reliability are concerned (such as aircraft traffic control, approach and landing systems, as well as collision avoidance systems), or where GPS is not continually available, such as for submarines and vehicles in shadowed environments, like city "canyons". In fact, however, there was a time when GPS was thought to threaten the inertial navigation system with virtual obsolescence, relegating it to just a few very esoteric applications. And, indeed, many commercial and private aircraft, as well as ships and boats now use GPS for navigation instead of (or as pri-

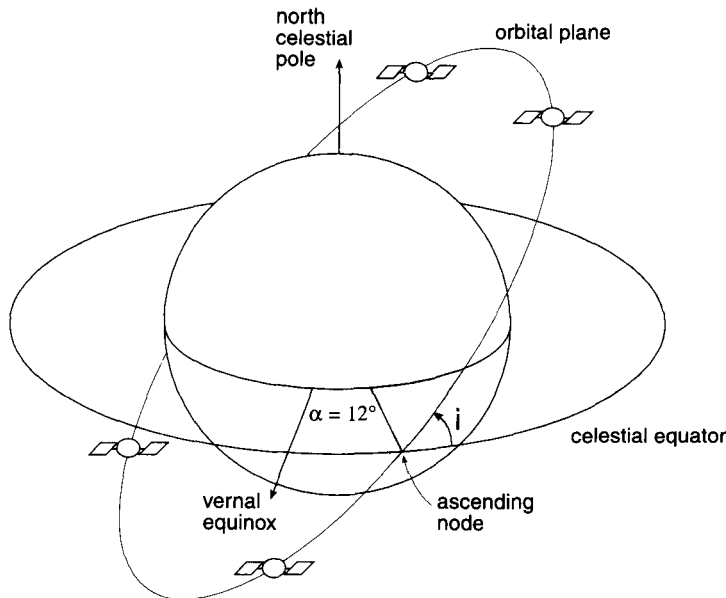


Figure 9.2: Four GPS satellites in one orbital plane with inclination,  $i = 55^\circ$ , and right ascension of ascending node,  $\alpha = 12^\circ$

mary navigation system in addition to) INS or other ground based systems, such as LORAN-C.

But GPS is not without problems and limitations. In the first place, it is not a self-contained, autonomous system like INS. The user must be able to “see” (in the sense of being able to receive transmitted signals from) the GPS satellites. Usually this is no problem, but satellite visibility may be obstructed locally by intervening buildings, foliage, mountains, bridges, and tunnels. This is because the carrier signal that the satellite transmits and that conveys positioning codes and the navigation message has a wavelength only 19 cm long ( $\sim 1.6$  GHz signal) and so will be severely attenuated even with light to moderate foliage and completely blocked by most larger structures. Certainly, direct underwater applications of GPS are completely impossible.

Although this signal shadowing is the most restrictive limitation, other problems with GPS prevent it from realizing the required accuracy and resolution in many kinematic applications. One of these arises from the effects of electronic interference or brief obstructions that may cause the receiver to miss one or more cycles of the carrier wave (this matters only if the carrier phase rather than the code is used for positioning). In fact, jamming and sustained electronic interference are general problems. The frequency of the data output in most receivers is often 1 Hz, rarely greater than 2 Hz without significant increase in the noise levels. This may not yield sufficient resolution or accuracy for airborne platforms that collect scientific data at a higher rate or at random intervals not precisely coincident with the GPS epochs.

Most of the error in GPS positioning comes from medium propagation effects that are unpredictable or difficult to model, including multipath (reflection of the signal before it finds the antenna) and tropospheric refraction.

If one considers the basic error and operational characteristics of the INS, then a clear complementarity to GPS emerges. INS is very precise in the short term and yields data rates much higher than GPS. It is self-contained (autonomous), except for initialization, and operates in any environment. On the other hand, GPS positioning is very accurate in the long term (drifts can be eliminated largely through data processing), it depends on a space segment that provides accurate orbit information, GPS data rates are only moderately high, and the operational environment may limit the positioning capability. The integration of GPS and INS is the subject of Chapter 10; while, in the present chapter we review the essentials of obtaining observations with the Global Positioning System, aiming primarily at kinematic applications.

It is beyond the present scope to expound in detail on the many aspects of the Global Positioning System including the broad range of applications, and the reader is referred to several excellent texts (Parkinson and Spilker, 1996; Hofmann-Wellenhof et al., 1994; Leick, 1995; Seeber, 1993; Teunissen and Kleusberg (1998)).

## 9.2 Global Positioning System

### 9.2.1 Clocks and Time

There are several quantities that may be observed with a GPS receiver; not all are routinely provided by every receiver. However, in one way or another, these observables are all connected to time, and time on board the satellite and in the receiver is kept by clocks that are, in fact, generators oscillating at a particular frequency. These oscillators are also responsible for generating the signals that are used to form the observables. Thus, fundamentally, it is necessary to start with the relationship between phase,  $\phi$ , frequency,  $f$ , and time:

$$f(t) = \frac{d\phi(t)}{dt}, \quad (9.1)$$

where  $t$  represents (true) time. The phase of an oscillating signal is the angle it sweeps out over time; often only the fractional part of a full cycle is distinguishable ( $0 \leq \phi \leq 2\pi$ ). The frequency of the signal is the rate at which the phase changes in time (the rate at which it sweeps through the cycles). An equivalent relationship is given by the integral of (9.1):

$$\phi(t) = \phi(t_0) + \int_{t_0}^t f(t') dt', \quad (9.2)$$

where  $t_0$  is some initial time. In a sense, the variation of the phase of a signal also represents a clock or a passing of time; it is only a matter of changing the units to change the phase into a time-like quantity. The phase has units of cycles and the

frequency has units of Hertz (cycles per second). Thus, let  $\tau$  denote the indicated time related to the phase:

$$\tau(t) = \frac{\phi(t) - \phi_0}{f_0}, \quad (9.3)$$

where  $f_0$  is some nominal (constant) frequency, and where an arbitrary phase offset,  $\phi_0$ , is allowed since the initial indicated time does not coincide with the initial phase (that is,  $\phi(t_0) \neq \phi_0$ ).

With (9.3) we make the firm distinction between the time,  $\tau$ , indicated by the oscillator clock and the “true” time,  $t$ , both in scale (differences are due to drift) and in origin (they are offset initially by a constant amount). The world’s keeper of true time was, until 1988, the *Bureau International de l’Heure* (BIH), in Paris, and now the *Bureau International de Poids et Mesures*, Sèvres, France, which by international agreement coordinates and combines the times kept by various observatories around the world who keep time as generated by very precise atomic clocks. This resulting atomic time, officially adopted on 1 January 1972, is known as TAI (Temps Atomique International) and replaces time as inferred from the apparent motion of the sun. From TAI a civil time is generated, known as UTC (Coordinated Universal Time) which differs from TAI by a precisely defined offset that is changed occasionally (often annually) by so-called leap seconds in order to keep the pace (within  $\pm 0.7$  s) of the time scale inferred from Earth’s rotation rate (which varies because of geodynamic phenomena). The GPS control segment, likewise, maintains an atomic time scale, called *GPS time*, that is adjusted to differ by no more than 1  $\mu$ s from the constant atomic time scale of the U.S. Naval Observatory (one of the observatories that contribute to TAI). On 6 January 1980, GPS time was offset from TAI (it is later than TAI) by 19 seconds and coincided with the civil time, UTC(USNO). However, GPS time does not participate in the leap-second adjustments and represents a constant time scale (differing in 2000 by 13 s from UTC). The difference between GPS time and the USNO atomic time scale is available to an accuracy of about 90 ns.

Returning now to our clocks, the reference to  $t$  as *true* time reflects the fact that the times indicated on satellite and receiver clocks are not perfectly uniform and must be calibrated by master clocks on the Earth. The atomic time scale of GPS time, though not offset from TAI by a strictly constant amount, serves the purpose of a calibrating standard within the context of GPS data processing; and we will designate GPS time as the true time,  $t$ . Substituting (9.3) into (9.2) we get:

$$\tau(t) = \tau(t_0) + \frac{1}{f_0} \int_{t_0}^t f(t') dt'. \quad (9.4)$$

If the frequency,  $f$ , is close to the nominal frequency, we may write

$$f(t) = f_0 + \delta f(t). \quad (9.5)$$

And, putting this into the integral in (9.4), we have the relationship between the

“phase-time”,  $\tau$ , and the true time,  $t$ :

$$\tau(t) = t - t_0 + \tau(t_0) + \delta\tau(t), \quad (9.6)$$

where the perturbation in phase-time in conformity with (9.2) and (9.3) is defined by

$$\delta\tau(t) = \frac{1}{f_0} \int_{t_0}^t \delta f(t') dt'. \quad (9.7)$$

Thus the difference between true time and time indicated by the phase of a signal generator is due to a constant synchronization error at  $t_0$  (the difference,  $\tau(t_0) - t_0$ ) and the perturbation in the frequency,  $\delta f$ . If the oscillator that generates the signal phase does so with constant frequency (i.e., the oscillator frequency is equal to the nominal frequency), then the indicated measure of time differs from the true time only by a constant offset.

In general, we may say that a particular clock, keeping time with a frequency generator, deviates from true time according to the equation (9.6) written in abbreviated form as

$$\tau(t) = t + \Delta\tau(t), \quad (9.8)$$

where  $\Delta\tau(t)$  represents the error of the clock, including a constant offset and the frequency perturbation effect that is a function of time.

### 9.2.2 GPS Signals

The signals transmitted by the GPS satellites are rather complex mixtures of codes and messages that convey the needed information to determine a range, that is, a distance, between the satellite and the receiver antenna. The complexity of the signal design was borne of a need to satisfy diverse user positioning requirements, to allow corrective techniques that counter some media propagation delays, to keep the necessary receiver technology relatively simple, and to provide some measure of protection from electronic interference.

In essence, the signal is a carrier wave (sinusoidal wave) modulated in phase by binary codes that represent interpretable data, as well as other certain predefined sequences of binary, or normal/reverse states. Mathematically, the signal (or one component of it) may be represented by

$$S(t) = AC(t)D(t) \cos(2\pi ft), \quad (9.9)$$

where  $f$  is the frequency of the carrier wave and  $A$  is the amplitude of the signal. The code sequence is denoted by  $C(t)$  and may be represented as a sequence, or step function, of positive ones (+1) and negative ones (-1); the elements of this sequence of altering states are also known as *chips*. (Some textbooks use the analogy of bits, or zeros and ones, but then the above mathematical equation for the signal is only a heuristic representation, where the first multiplication is really modulo-2 addition and the second multiplication really stands for a phase change depending on the result of the modulo-2 addition). Each chip has the same length in time that

is fundamentally related to the wavelength of the carrier since both are generated by the same oscillator.

Similarly,  $D(t)$  represents a data message also generated as a sequence of chips, but with a much longer wavelength. Each satellite transmits a different code (actually two codes, see below) and a data message; but the carrier frequency is the same for all satellites, so the GPS receiver can discriminate between satellites only by using the codes and data messages. (The Russian analogue to GPS, the Global Orbiting Navigation Satellite System (GLONASS), also consists of 24 satellites that transmit similar codes and data but on carrier waves of uniquely different frequencies that serve in discriminating between the satellites.)

Since the code function,  $C(t)$ , and the data function,  $D(t)$ , conceptually have values of either positive one or negative one, so does their product. When this product changes from positive one to negative one (or vice versa) the phase of the carrier changes from  $0^\circ$  to  $180^\circ$  (or, vice versa). Thus the carrier is modulated in phase by the code and data sequences and thereby carries information in the form of  $180^\circ$  phase reversals from the satellite transmitter to the receiver. This is called *binary biphase modulation*. Before discussing the extraction of this information, it is necessary to provide some details about the codes and data messages.

Each GPS satellite actually transmits two different codes, the *C/A* (coarse acquisition) code and the *P*-code (precision code); and, in fact, the *P*-code and the data message are transmitted on two separate *L*-band carriers (in the microwave region). The transmission on two frequencies allows approximate computation of the delay of the signal due to ionospheric refraction. The L1 and L2 carrier frequencies are given by

$$\begin{aligned}f_1 &= 1575.42 \text{ MHz} = 154 \cdot 10.23 \text{ MHz}, \\f_2 &= 1227.60 \text{ MHz} = 120 \cdot 10.23 \text{ MHz}.\end{aligned}\tag{9.10}$$

Using the speed of light,  $c = 2.99792458 \times 10^8 \text{ m/s}$ , the wavelengths of the carriers, respectively, are (approximately)

$$\begin{aligned}\lambda_1 &= \frac{c}{f_1} = 0.1903 \text{ m}, \\ \lambda_2 &= \frac{c}{f_2} = 0.2442 \text{ m}.\end{aligned}\tag{9.11}$$

Each chip of the *C/A*-code has a duration of exactly  $(1/1.023) \times 10^{-6} \text{ s}$ , or almost a microsecond. The corresponding “chipping rate” is 1.023 Mbps (mega-bits per second); and the length of each chip, determined from this rate by the speed of light is defined to be its *wavelength*: 293.052 m. Exactly 1540 waves of the carrier fit into one *C/A*-code chip. The *P*-code chipping rate is exactly 10 times higher: 10.23 Mbps, corresponding to a wavelength of 29.305 m.

The data or navigation message,  $D(t)$ , is a sequence of chips that is generated at the very slow rate of 50 bps. The message contains information in binary form about the satellite and is 37,500 bits long; so it takes 12.5 minutes to transmit the complete

message. Certain important information, including satellite clock error models, relativistic corrections, and time transfer parameters, the satellite ephemeris (orbital parameters), ionospheric model parameters, and other signal information is repeated every 1500 seconds within the message. The orbital information in the message constitutes the so-called *broadcast ephemeris* of the satellite.

The total signal transmitted by the satellite is given by the sum of three sinusoids, two for the two codes (*C/A* and *P*) on the L1 carrier and one for the *P*-code on the L2 carrier. To keep the *C/A* and *P*-code modulations distinguishable on L1 (after all, the wavelength of the *C/A* code is exactly ten times that of the *P*-code and the *C/A*-code transitions the phase at the same time that the *P*-code does), the two are superimposed separately on sinusoids that are 90° out of phase, that is, on cosine and sine wave carriers. The data message is included on both L1 and L2 carriers. In addition, because GPS was designed firstly for military purposes, the *P*-code, representing the more accurate positioning capability (because of its shorter wavelength and, therefore, higher resolution), is encrypted. This is done by multiplying it by a so-called *W*-code which is available only to authorized users in the form of a “key” whose use requires specially equipped receivers. The product of the *P* and *W*-codes is known as the *Y*-code; and implementing this restriction in positioning capability falls under the general procedures of *anti-spoofing* (AS). With AS turned on (since 31 January 1994), the total signal transmitted by a GPS satellite is given by

$$\begin{aligned} S^P(t) = & A_P P^P(t) W^P(t) D^P(t) \cos(2\pi f_1 t) \\ & + A_C C^P(t) D^P(t) \sin(2\pi f_1 t) + B_P P^P(t) W^P(t) D^P(t) \cos(2\pi f_2 t), \end{aligned} \quad (9.12)$$

where  $A_P$ ,  $A_C$ , and  $B_P$  represent amplitudes of the corresponding codes,  $C$  and  $P$  represent the *C/A* and *P*-codes in the form of sequences of positive and negative ones,  $D$  likewise represents the data message, and superscript  $p$  identifies a particular satellite.

Several techniques have been developed, however, to circumvent the restriction imposed by AS, without having to know the *W*-code. The most successful of these is so-called *Z*-tracking (Hofmann-Wellenhof et al., 1994), whereby the encryption code is estimated and subsequently removed on the basis of the correlation of the incoming signal (*Y*-code) with the receiver-generated *P*-codes. This is possible since the *W*-code has significantly lower chipping rate (about 500 kbps) compared to the *P*-code and thus an estimate of the *W*-code ensues in a filter of the correlated components. Since modern geodetic receivers usually have this feature, we will assume that *P*-codes are generally available and correspondingly develop the analysis on that basis.

### 9.2.3 GPS Receiver

Before the signal is processed by the receiver it is pre-amplified and filtered at the antenna, and subsequently down-shifted in frequency to a more manageable level for processing. This is accomplished by the down-converter component of the receiver (Figure 9.3) using the simple artifice of multiplying, or *mixing*, the signal

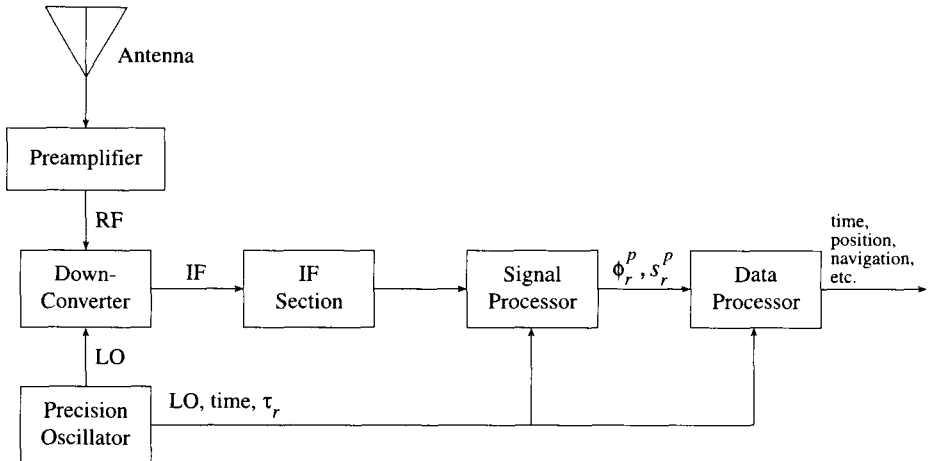


Figure 9.3: Essential components of a GPS receiver.

with a pure sinusoid generated by the receiver oscillator. If  $S_r(t)$  is that sinusoid with local oscillator frequency,  $f_{LO}$ , and  $S^P(t)$  is the satellite signal with frequency,  $f_s$ , and phase,  $\Phi(t)$ , then the mixed signal is given by

$$\begin{aligned}
 S_r(t)S^P(t) &= A \cos(2\pi f_{LO}t) \cos(2\pi f_s t + \Phi(t)) \\
 &= \frac{A}{2} \cos(2\pi(f_s - f_{LO})t + \Phi(t)) + \frac{A}{2} \cos(2\pi(f_s + f_{LO})t + \Phi(t)),
 \end{aligned} \tag{9.13}$$

where  $A$  is an amplitude factor. This signal consists of sinusoids at two vastly different frequencies and so the high-frequency component,  $(f_s + f_{LO})$ , is easily filtered out using a low-pass filter. The remaining signal is like a carrier with a much lower frequency,  $(f_s - f_{LO})$ , that is modulated, however, with the same phase as the original signal; i.e., the modulation of the signal is preserved in the mixing operation.

Once downshifted to an intermediate frequency (IF), the satellite signal is preconditioned in the IF Section to reject interfering, out-of-band signals with appropriate filters and to further increase and control the amplitude of the signal for subsequent processing. The signal then passes to the main signal processing part of the receiver: the tracking loops. To understand their function it is first necessary to examine the phase modulations in more detail.

The  $C/A$ - and  $P$ -codes do not convey any decipherable information, as such. Instead, these codes consist of unique sequences of binary states that are generated using a pseudorandom noise (PRN) algorithmic process. They are random in the sense that their autocorrelation function (Section 6.3.1) is close to zero for non-zero lags. But these sequences are not strictly random because a precise mathematical

formula is used to generate them. In fact, the random sequence for the  $C/A$ -code, which is significantly different for each satellite, repeats every millisecond; it is 1023 chips long. The pseudorandom sequence for the  $P$ -code is much longer, repeating only after 38 weeks. However, each satellite uses only one distinct week's worth of the code, and the code is re-initialized after one week. In this way, the satellites are distinguished by the codes, both  $C/A$  and  $P$ , rather than by frequency—the carrier waves for all satellites are the same.

The codes serve two operational purposes. The first is for determining the range between the satellite and receiver. This is accomplished by generating the same PRN codes in the receiver and comparing the incoming code with the receiver-generated code. The comparison is made under the presumption that the receiver time is synchronized with the satellite time, so that if the two codes do not match it is because one of them, the received code, was delayed due to the time of its transit from the satellite to the receiver. The comparison is done by a correlator in a delay lock feedback loop, where the receiver-generated code is delayed or advanced in time until the correlator matches it to the incoming satellite-generated code. The total time delay is a measure of the transit time of the code plus, in the actual situation, any differences between the satellite and receiver clocks. Using the speed of light the delay is converted to the distance, or range, between the satellite, at time of transmission, and the receiver, at time of reception. It is not the true range if the satellite and receiver clocks differ; and therefore, the calculated range is called the *pseudorange*; it is the range with a bias (primarily) due to clock error. The significance of the clock error is demonstrated by noting, in accordance with the speed of light, that an error of one microsecond causes a range error of about 300 meters. Once the correlator achieves maximum correlation, the codes are locked and tracked continually.

The second main purpose of the codes is to spread the signal over a large frequency bandwidth, thus permitting small antennas on the Earth to gather the transmitted signal that has attenuated significantly over the distance from the satellite. In fact, the power of the signal by the time it reaches Earth is well below the power of the ambient noise. The spreading over frequency is the result of the code having a short wavelength, where the *bandwidth* (or spread) of frequencies is roughly inversely proportional to the wavelength. The short wavelength of the chips implies large bandwidth. Multiplying the spectrally spread incoming signal with a synchronized code generated by the receiver effectively removes the code since  $C(t)^2 = 1$ , for all  $t$ . The result is a signal modulated only by the navigation message; and, because of the message's very large wavelength, the signal now has very small bandwidth. Correspondingly, the power level increases substantially, being concentrated in the narrow bandwidth of the navigation message, and enabling the receiver to track the signal. This method of *direct sequence spread spectrum communication* has additional benefits. In the de-spreading of the navigation message, other extraneous signals are actually spread (as a result of multiplication by the receiver-generated code) out to lower power levels, which can be filtered from the desired signal. This reduces the effects of electronic interference and *multipath* (the reflection of the GPS signal from nearby objects prior to entering the antenna).

A second tracking loop, the phase lock loop, is used to compare the incoming phase of the carrier wave with that of the receiver-generated wave oscillating at the nominal frequency  $f_1$  or  $f_2$ . Once locked by appropriately adjusting the phase of the receiver oscillator, the phase is continually tracked, and the navigation message can be extracted using standard demodulation techniques. As a by-product, the fractional phase difference needed to lock the receiver-generated wave to the incoming wave can be measured. Together with a simple count of the full cycles of the receiver-generated wave that elapse over time, a history of the varying range between receiver and satellite is created. The total range, however, is not obtained from this phase difference measurement until the initial number of full cycles between receiver and satellite has been determined—it cannot be accomplished directly by the receiver.

### 9.3 GPS Observables

The delay of the incoming satellite codes with respect to the identical codes generated by the receiver represents the time of transit of the satellite codes from the satellite to the receiver. Multiplied by the speed of light, this observable includes time lapses due to clock errors, propagation medium effects, multipath, and receiver electronic delays and, thus, is not the true range, but the pseudorange, between receiver and satellite. Disregarding these errors, the observed code delay is the range between the satellite at the point in its orbit when it transmits the signal and the receiver at the point on the rotating Earth when it receives the signal. The pseudorange is time-tagged by the receiver clock.

If  $t$  represents the true time (GPS time) of signal reception, then let  $\tau_r(t)$  be the indicated time of reception of the signal at the  $r^{\text{th}}$  receiver, and let  $\tau^p(t - \Delta t_r^p)$  be the time of transmission of that same signal as indicated on the clock of the  $p^{\text{th}}$  satellite. If the satellite clock were error-free, it would indicate this to be the true time of reception minus the actual time of transit of the signal,  $\Delta t_r^p$ . Notationally, it is convenient as well as conventional to let superscripts identify quantities referring to satellites and to let subscripts identify quantities referring to receivers. Quantities with both superscript and subscript depend on both satellite and receiver.

Because the receiver and satellite clocks (frequency generators) are responsible for generating the codes and the carrier signals, the measured delay is the difference between the *indicated* times; consequently the pseudorange, denoted by  $s_r^p$ , is given by:

$$s_r^p(\tau_r) = c(\tau_r(t) - \tau^p(t - \Delta t_r^p)) + \varepsilon_{p,r}^p, \quad (9.14)$$

where  $\varepsilon_{p,r}^p$  represents pseudorange observation error (it is different for each satellite-locking channel of the receiver). Using (9.8), we have

$$s_r^p(\tau_r) = c(t + \Delta\tau_r(t) - (t - \Delta t_r^p) - \Delta\tau^p(t - \Delta t_r^p)) + \varepsilon_{p,r}^p. \quad (9.15)$$

The time of transit,  $\Delta t_r^p$ , is affected by the retarding influence of the media through which the signal must travel. These include the ionosphere and the troposphere

which cause the signal to travel slower than in a vacuum and also to bend away from the straight geometric connection between transmitter and receiver (the latter generally is a much smaller effect). The troposphere and ionosphere have different *indices of refraction* and are generally treated separately, because for the ionosphere, the refractive index depends on the frequency. In addition the total transit time may be affected by reflections the signal experiences prior to reception as it bounces off nearby objects (also to some extent at the satellite). This is called the *multipath* effect. Then, there are small but finite travel times between the receiver and satellite electronics and their respective antennas that further falsify the true transit time. Finally, the receiver antenna has an unknown center offset and the satellite antenna is offset from the center of mass. The actual transit time (multiplied by the speed of light) thus may be represented by:

$$c \Delta t_r^p = \rho_r^p + \Delta \rho_{\text{offset},r}^p + \Delta \rho_{\text{iono},r}^p + \Delta \rho_{\text{tropo},r}^p + \Delta \rho_{m,\text{path},r}^p + \Delta \rho_{\text{equip},r}^p, \quad (9.16)$$

where  $\rho_r^p$  is the true range between the satellite at time of transmission and the receiver at time of reception, and its various distortions are made evident by the subscripted abbreviations.

It is important to note that the true range,  $\rho_r^p$ , corresponds to the true time of reception,  $t$ , while the pseudorange observation is tagged by the indicated time,  $\tau_r(t)$ . It will, however, be useful to use the indicated time as the independent variable in kinematic positioning, since it is usually accurate enough ( $\pm 1 \mu\text{s}$ ; or  $\pm 1 \text{ ms}$ , if not continually synchronized to GPS time) for whatever other application is to be registered by the positioning solution. To linear approximation, we have from (9.8)

$$\rho_r^p(t) = \rho_r^p(\tau) - \dot{\rho}_r^p \Delta \tau_r(t), \quad (9.17)$$

where, since  $|\dot{\rho}_r^p| < 1000 \text{ m/s}$  and if  $|\Delta \tau_r(t)| < 10^{-6} \text{ s}$ , the true ranges at true and indicated times differ by less than one millimeter. This is not significant, especially when compared to other potentially large errors in (9.16), even if some of the latter are estimated.

Putting (9.16) and (9.17) into (9.15), the pseudorange now becomes

$$\begin{aligned} s_r^p(\tau_r) = & \rho_r^p(\tau_r) + c(\Delta \tau_r(t) - \Delta \tau^p(t - \Delta t_r^p)) - \dot{\rho}_r^p \Delta \tau_r(t) \\ & + \Delta \rho_{\text{offset},r}^p + \Delta \rho_{\text{iono},r}^p + \Delta \rho_{\text{tropo},r}^p + \Delta \rho_{m,\text{path},r}^p + \Delta \rho_{\text{equip},r}^p + \varepsilon_{p,r}^p. \end{aligned} \quad (9.18)$$

Note that some of the systematic error terms, as listed, depend inseparably on both receiver and satellite, such as the atmospheric effects and multipath. Equipment delays and offsets could be written in terms of separate receiver and satellite effects. Some of these errors can be calibrated or compensated fairly readily, using different frequencies or models. Others, in particular the multipath error, are notoriously difficult to deal with.

A pseudorange observable, as shown in (9.18), is available for each of the transmitted codes, the *C/A* code, as well as the *P*-codes on the L1 and L2 carriers, on appropriately equipped receivers. The *P*-code is only available on those receivers that either have the encryption key or use special processing techniques to overcome

the AS effect. Note, also, that the pseudorange observables are associated with receiver indicated times,  $\tau_r$ .

The other type of observable available on all geodetic receivers is the difference between the phase of the receiver-generated carrier signal at the time of reception and the phase of the satellite signal at the time of transmission (which arrives at the receiver unaltered except for the propagation effects that similarly corrupt the code measurement). Actually, the phase tracking loop of the receiver, when it first locks onto the signal, has no way of knowing the integer number of full cycles that constitute the total difference in phases due to the transit of the signal. Therefore, the absolute range to the satellite cannot be determined directly on the basis of the phase measurement. On the other hand, once acquired, the signal is tracked continuously and the complete cycles are counted and added to the measurement of the fractional phase difference.

The phase observable can be expressed as follows

$$\phi_r^P(\tau_r) = \phi_r(\tau_r(t)) - \phi^P(\tau^P(t - \Delta t_r^P)) - N_r^P + \varepsilon_{\phi,r}^P, \quad (9.19)$$

where  $\phi_r$  is the receiver-generated phase (in units of cycles) and  $\phi^P$  is the satellite-generated phase,  $N_r^P$  is the integer representing the unknown number of full cycles at the *initial* time of phase lock, and  $\varepsilon_{\phi,r}^P$  is the phase observation error.  $N_r^P$  is called the *carrier phase ambiguity*, and  $\phi_r^P$  is called the *accumulated carrier phase observable*, or also the *delta range*.

Since the phases are created by the clocks, or frequency generators, of the receiver and satellite, it is somewhat redundant to write  $\phi_r(\tau_r(t))$  instead of  $\phi_r(t)$ , since oscillator phase is equivalent to indicated time (this is consistent with our previous interpretation (9.3) of the generated phase as a time). Therefore, we can simplify the notation with the understanding that the phase, while a function of true time, is indicated (or, tagged) by receiver time (similarly for the satellite phase). Using (9.3) and (9.8), we have for the receiver-generated phase

$$\phi_r(t) = f_0(t + \Delta\tau_r(t)) + \phi_{0,r}, \quad (9.20)$$

and for the satellite-generated phase

$$\phi^P(t - \Delta t_r^P) = f_0(t - \Delta t_r^P + \Delta\tau^P(t - \Delta t_r^P)) + \phi_0^P. \quad (9.21)$$

Substituting these into (9.19) yields the phase observable in terms of the time interval of transit:

$$\phi_r^P(\tau_r) = f_0 \Delta t_r^P + f_0(\Delta\tau_r(t) - \Delta\tau^P(t - \Delta t_r^P)) + \phi_{0,r} - \phi_0^P - N_r^P + \varepsilon_{\phi,r}^P. \quad (9.22)$$

It is noted that in addition to the arbitrary phase offsets  $\phi_{0,r}$  and  $\phi_0^P$  of the receiver and satellite frequency generators, the clock errors  $\Delta\tau_r$  and  $\Delta\tau^P$  contain, besides drifts and drift rates appropriate to the quality of the clocks, constant time offsets according to (9.6). The phase offsets and constant clock errors are treated separately because the same clock error appears in the pseudorange, which, however, does not have the phase offset.

As with the pseudoranges, the time interval of transit of the phases is fraught with errors due to atmospheric refraction, multipath, equipment delays, and geometric

offsets of the phase center from the geometric center of the receiver antenna, and the offset of the satellite antenna from the center of mass. In terms of phase effects, we can write  $\Delta t_r^p$  analogous to (9.16) and substitute this into (9.22) to get

$$\begin{aligned}\phi_r^p(\tau_r) = & \frac{f_0}{c} \rho_r^p(\tau_r) + f_0(\Delta\tau_r(t) - \Delta\tau^p(t - \Delta t_r^p)) + \phi_{0,r} - \phi_0^p - N_r^p - \frac{f_0}{c} \dot{\rho}_r^p \Delta\tau_r(t) \\ & + \Delta\phi_{\text{offset},r}^p + \Delta\phi_{\text{iono},r}^p + \Delta\phi_{\text{tropo},r}^p + \Delta\phi_{m,\text{path},r}^p + \Delta\phi_{\text{equip},r}^p + \varepsilon_{\phi,r}^p.\end{aligned}\quad (9.23)$$

The use of  $\Delta\phi$  instead of  $\Delta\rho$  as in (9.18) distinguishes the influence of a particular effect on the phase from that on the pseudorange. A carrier phase observable such as given in (9.23) holds for both L1 and L2 carriers, where, of course, the nominal frequency,  $f_0$ , as well as the phase error terms are different in each case. Again, as for the pseudorange, it is more convenient to associate the true range with the indicated time,  $\tau_r(t)$ , which is used also to tag the observed phase.

The integer phase ambiguity,  $N_r^p$ , is the leading impediment to range determination using phases. Technically, one would have to know the position of the receiver relative to the satellite at the initial epoch (at time of phase lock) to better than one wavelength (19 cm, for L1) in order to resolve this integer. A multitude of algorithms exist that can be used to determine this integer from information gathered from other GPS observables over some (small) period of time. Not infrequently, however, the phase lock loop momentarily loses its lock on the carrier, causing the count of full cycles to be interrupted. This is called a *cycle slip* and means that the integer ambiguity initially determined is no longer valid—a new value must be found. It is recovered most easily if positioning information already accumulated can be used to predict the position at the epoch of signal re-acquisition. For mobile platforms, the INS has been looked upon as a viable extrapolator in these situations (see Section 10.3).

## 9.4 GPS Errors

Table 9.1 gives a broad overview of typical position equivalent errors caused by the system and environmental errors contained in equations (9.18) and (9.23). By far the largest error is due to the receiver clock (usually a quartz crystal oscillator with a typical stability in frequency of about  $10^{-8}$ ). *P*-code receivers have the wherewithal to synchronize their clocks more accurately to GPS time since the navigation message contains the relationship between GPS time and the *P*-code. This synchronization can be done to an accuracy of about 1  $\mu$ s. The relatively large receiver clock errors must be determined in the navigation solution (a fourth unknown for the receiver location) by observing an additional satellite; or, it is usually recommended to eliminate the receiver clock error by an appropriate differencing of ranges between satellites (see Section 9.5).

The satellite clocks are monitored by the GPS control segment with very stable laboratory atomic clocks. The difference between these is modeled as a second-degree polynomial whose coefficients are also part of the navigation message. The

Table 9.1: Error sources in GPS positioning.

| Error Source                        | Typical Magnitude   |
|-------------------------------------|---|
| Receiver clock error (synchronized) | 1 $\mu$ s (300 m)   |
| Residual satellite clock error      | 20 ns (6 m)   |
| Satellite synchronization to UTC    | 100 ns (30 m)   |
| Selective availability              | 100 m   |
| Orbit error (precise, IGS)          | 20 cm   |
| Tropospheric delay                  | <30 m   |
| Ionospheric delay                   | <150 m  |
| Multipath                           | <5 m (P-code); <5 cm (phase)                              |
| Receiver noise                      | 1 m ( <i>C/A</i> code); 0.1 m (P-code); 0.2 mm (L1 phase) |

residual error represents lack of synchronization between satellites. This and the synchronization error with respect to UTC are given in Table 9.1.

In order to restrain accurate, real-time, absolute GPS positioning, the broadcast satellite ephemeris and the frequency stability of the satellite clock were, until recently, degraded intentionally to a level of accuracy known as Selective Availability (SA) that is consistent with original projections of positioning accuracy of about 100 m thought to be obtainable with the *C/A* code (without SA, positioning with *C/A* code processing turned out to yield 20-30 m accuracy). These restrictions could be overcome completely if only post-mission absolute positioning or relative positioning are required. The IGS (International GPS Service, IGS Central Bureau (1999)) publishes precise orbits ( $\pm 15$  cm) and satellite clock errors ( $\pm 1$  ns) with two weeks' delay and for 900-second intervals; clock errors at 30-second intervals are available from the Jet Propulsion Laboratory. Also, it is noted that the satellite clock errors can be estimated on the basis of accurate orbit determinations and known ground receiver coordinates (Zumberge et al., 1998). With SA discontinued as of May 2000, all users have access to the uncorrupted broadcast ephemeris.

The next significant error sources arise in the medium through which the signal must travel. This includes the ionosphere, a layer enveloping the Earth from an altitude of about 50 km to about 1000 km, which contains a large number of ionized atoms (due to their interaction with solar radiation) and consequently many free electrons. Closer to the Earth the signal encounters the (electrically neutral) stratosphere and troposphere with atmospheric density increasing until it reaches the receiver. The important effect on the electromagnetic signal in both zones is the departure of its propagation speed from the speed,  $c$ , of a signal in vacuum.

The ratio of  $c$  to the signal's speed in a medium,  $v$ , is called the *refractive index*:

$$n = \frac{c}{v}. \quad (9.24)$$

In traveling through the medium, the signal will be delayed, and so,  $n \geq 1$ . Since distance equals the product of speed and time, the delay can be expressed as the difference in travel times, computed by integrating the reciprocal velocities:

$$\Delta t = \int \frac{1}{v} dS - \int \frac{1}{c} dS, \quad (9.25)$$

where  $S$  represents the path and the geometric difference in corresponding paths in the medium and in vacuum has been neglected. In terms of a range difference,  $\Delta\rho = c\Delta t$ , we have, with (9.24)

$$\Delta\rho = \int (n - 1) dS. \quad (9.26)$$

The GPS signal comprises both a carrier wave and a modulation of the carrier by the codes. The modulation can be thought of as the result of the sum (or interference) of several carrier waves having slightly different frequencies, so as to produce a beat frequency, that of the modulation. The velocity of this wave group (the beat) has a velocity that differs from the phase velocity of the carrier, if the latter depends on the frequency. This is the case in the ionosphere which is a *dispersive* medium, where the refractive index, and hence the speed of propagation, depends on the frequency of the signal. As a consequence one must distinguish between the *group refractive index*,  $n_g$ , that refers to the modulations of the carrier, and the *phase refractive index*,  $n_\phi$ , that refers to the phase of the carrier. The two are related in a homogeneous and isotropic medium according to (Leick, 1995, p. 293; see also Richtmyer et al., 1969)

$$n_g = n_\phi + f \frac{dn_\phi}{df}, \quad (9.27)$$

where  $f$  is the frequency of the carrier.

Under simplifying assumptions (such as a first-order approximation), it can be shown that the phase refractive index depends directly on the density of free electrons in the ionosphere,  $N_e$ , and inversely on the square of frequency (see Hartmann and Leitinger, 1984):

$$n_\phi = 1 - \kappa \frac{N_e}{f^2}, \quad (9.28)$$

where, if  $N_e$  has units of electrons per cubic meter and  $f$  has units of Hz, the constant is  $\kappa = 40.28$ . Note that  $n_\phi < 1$  which implies that the phase of the carrier is advanced by the dispersive nature of the ionosphere. (This does not violate Einstein's principle that  $c$  is the maximum speed, since only the wave group transmits information in the form of energy, and the phase velocity has no such physical significance, i.e., total phases are not measurable, as noted before.) Substituting (9.28) into (9.26) yields the corresponding shortening of the distance:

$$\Delta\rho_{\text{iono}}^\phi = -\kappa \frac{\text{TEC}}{f^2}, \quad (9.29)$$

where TEC is the total electron content along the path, that is,  $\text{TEC} = \int N_e dS$ .

For the group refractive index we obtain from (9.27) and (9.28):

$$n_g = 1 + \kappa \frac{N_e}{f^2}; \quad (9.30)$$

and, therefore, with (9.26) the group delay is given in terms of distance by

$$\Delta\rho_{\text{iono}}^g = \kappa \frac{\text{TEC}}{f^2}. \quad (9.31)$$

To simplify the notation, we define the group delay (in units of distance):  $I \equiv \Delta\rho_{\text{iono}}^g$ ; then the ionospheric effects in (9.18) and (9.23) are given by:

$$\begin{aligned} \Delta\rho_{\text{iono},r}^p &= I, \\ \Delta\phi_{\text{iono},r}^p &= -\frac{f_0}{c} I; \end{aligned} \quad (9.32)$$

where the phase advance is in cycles.

Through the TEC, these effects depend on the elevation angle of the satellite; hence they are minimum when the satellite is at the zenith and the path length is shortest. In addition, they depend on the degree of solar activity and the amount by which the path through the ionosphere is exposed to the solar radiation and which thus depends on the season, the time of day, and the observer's location. Empirical models for TEC based on monthly average conditions were developed by Klobuchar (1987) and the corresponding parameter values are transmitted as part of the GPS data message. These models generally account for about 50% of the delay at mid-latitudes. Alternatively, the first-order effect, as given by (9.31), can be eliminated with the use of dual-frequency observations (Section 9.5.1). Models for higher-order effects (that cannot be eliminated in this way, but are less than 5 cm in the range) were developed by Bassiri and Hajj (1993).

The ionospheric effect can be ignored in the case of differencing observations at two ends of a short (<15 km) baseline (Section 9.5.2), since the path from the satellite to each receiver is then approximately the same. For longer baselines, the differenced ionospheric effect must be eliminated using dual-frequency observations or it may be treated as a time-varying stochastic parameter to be solved.

The troposphere, containing mostly electrically neutral particles, is a non-dispersive medium ( $dn_\phi/df = 0$  in (9.27)), and the refractive index for both phase and modulation is the same. The index of refraction depends on the temperature as well as the atmospheric pressures of both its dry ( $p_d$ ) and wet ( $p_w$ ) components, where the latter two are linearly identifiable in the following model (Hofmann-Wellenhof et al., 1994, p. 110; and Leick, 1995, p. 308):

$$n_t - 1 = 7.764 \times 10^{-5} \frac{p_d + p_w}{T} - 1.296 \times 10^{-5} \frac{p_w}{T} + 0.373 \frac{p_w}{T^2}. \quad (9.33)$$

$T$  is temperature in units of Kelvin degrees, and partial pressures  $p_d$  and  $p_w$  are in units of mbar. It turns out that about 90% of the tropospheric delay is accounted for by the first term in (9.33), the so-called dry component. More elaborate models for this refraction component have been developed; see (Hofmann and Wellenhof et al., 1994, pp. 113–117). The wet component is more difficult to model and requires measurements or estimates of water vapor along the path of the signal.

The corresponding tropospheric delays in pseudorange and phase are obtained by substituting refraction models, such as (9.33), into (9.26). Clearly, the delays then also depend on the elevation angle of the satellite (minimum at zenith). Any residual effects not modeled must be treated as an error, or possibly as a stochastic parameter to be estimated (e.g., Tralli and Lichten, 1990).

Other errors in the GPS observables include the multipath error, equipment delays and biases, antenna eccentricities (phase center variations), and the thermal noise of the receiver. The multipath error depends on the reflectivity of the immediate environment and the quality of the receiver processing electronics. It can be minimized to some extent by judiciously selecting antenna locations. The receiver noise depends primarily on the signal-to-noise ratio of the signal entering the receiver and the bandwidth of the tracking loop. The signal-to-noise ratio is defined as the ratio of the power of the signal to the power density of the ambient noise due to thermally agitated electrons in the antenna, transmission cables, and pre-amplifier. Simplified models of the standard deviation of the corresponding jitter in the code delay and the carrier phase are given, respectively, by (Langley, 1998):

$$\sigma_s = \lambda_c \left[ \frac{\alpha B_D}{C/N_0} \right]^{1/2}, \quad (9.34)$$

and

$$\sigma_\phi = \frac{1}{2\pi} \left[ \frac{B_P}{C/N_0} \right]^{1/2}, \quad (9.35)$$

where  $\sigma_\phi$  is in units of cycles,  $\alpha$  is a unitless factor characterizing the code correlator,  $B_D$  is the bandwidth of the delay-lock-loop,  $B_P$  is the bandwidth of the phase-lock-loop,  $C/N_0$  is the signal-to-noise ratio, and  $\lambda_c$  is the wavelength of the code (293.052 m for the  $C/A$  code, 29.305 m for the  $P$  code). Typical values for the bandwidths range from less than 1 Hz to 10 Hz and must be sufficiently large to accommodate the dynamics of the receiver antenna (if on a moving vehicle). The signal-to-noise ratio usually is greater than  $3 \times 10^4$  Hz ( $C$  in Watts and  $N_0$  in Watts per Hz). With this value of  $C/N_0$  and  $B_D = 0.8$  Hz,  $B_P = 2$  Hz, and  $\alpha = 0.5$ , we obtain the values for the receiver noise listed in Table 9.1. A more thorough discussion of receiver noise may be found in (Van Dierendonck, 1996).

## 9.5 Combinations of Observations

Inspecting the observation equations, (9.18) and (9.23), for the pseudorange and carrier phase, one sees some errors that do not change in time, such as clock biases and the phase ambiguity, or that change more slowly or have a long correlation time, such as tropospheric delays. In addition, there are some error terms common to different observations that correspond to different receiver-satellite combinations. Depending on accuracy requirements, it is sometimes not necessary to account for all errors. On the other hand, the larger errors, such as clock biases, must usually be considered. With simultaneous observations of pseudoranges or carrier phases from

several different satellites one solves for these and other unknown error terms to the extent possible using an optimal estimation technique, such as a least-squares adjustment. This procedure is known as *absolute positioning*, or *point positioning*, since the total position vector of the observer is to be determined from GPS observations independent of any other point. Alternatively, what usually turns out to be more accurate in a relative sense, one uses differences between simultaneous observations from different receivers, thus canceling the common mode terms and greatly reducing the effects of some slowly varying error terms. This procedure is known as *relative positioning*, or *differential positioning*, and yields only the differences in coordinates between two points. That is, the position of one receiver is determined relative to another with presumably known coordinates (or, perhaps only the difference in coordinates is of interest). If the absolute coordinates of one point are known, then certainly, relative positioning also yields subsequently the absolute coordinates of the other point. The advantages of relative positioning are not unequivocal, however, in all situations and for all tolerances in accuracy. For example, the longer the baseline is between the two receivers, the less is the cancellation of certain correlated errors, such as tropospheric and ionospheric delays and satellite orbit error (that is, they become uncorrelated).

To investigate the relationships between particularly significant errors and the observations, or combinations thereof, consider again the pseudorange, given by (9.18) and repeated here with some of the error terms excluded:

$$s_r^p(\tau_r) = \rho_r^p(\tau_r) + c(\Delta\tau_r(t) - \Delta\tau^p(t - \Delta t_r^p)) + \Delta\rho_{\text{iono},r}^p + \varepsilon_{\rho,r}^p. \quad (9.36)$$

The excluded error terms are the tropospheric delay, the equipment and antenna offsets, the multipath error, and the time registration error in the true range due to the receiver clock error. These effects either are considered negligible or have to be modeled or calibrated by the user for increased positioning accuracy. Similarly, the phase observable (9.23) simplifies to

$$\phi_r^p(\tau_r) = \frac{f_0}{c} \rho_r^p(\tau_r) + f_0(\Delta\tau_r(t) - \Delta\tau^p(t - \Delta t_r^p)) + \phi_{0,r} - \phi_0^p - N_r^p + \Delta\phi_{\text{iono},r}^p + \varepsilon_{\phi,r}^p. \quad (9.37)$$

Clearly, the observables are functions of the range between the receiver and the satellite, as well as additional so-called *nuisance* parameters (systematic errors), including the clock errors, the ionospheric delay, and (in the case of the phase observable) the phase offsets and initial phase ambiguity. The nuisance parameters need to be solved or eliminated from the positioning problem. Unfortunately, in the observation equations above, only the phase ambiguity and offsets are constants; the other parameters change in value with time. Therefore, each new observation in effect carries with it a new set of unknown parameter values. They can be determined only if sufficient information in the form of independent observations is available. Alternatively, some parameters can be eliminated with suitable combinations (differences) of those observations that mutually contain them. Positioning with these differenced observables is still possible either absolutely or relatively depending on the strength of the geometric content of the corresponding range differences. Often some combination of these strategies is used.

Additional information comes in many forms. In an ideal world, only three receiver-to-satellite ranges would be needed to solve for the receiver's three-dimensional position. By observing additional ranges to other satellites, the receiver clock error can be solved for each time epoch. Equivalently, one can form the difference of observations between (more than 3) satellites and thus eliminate the common receiver clock error from the problem. Modern geodetic receivers are capable of tracking the code and carrier signals on both L1 and L2 frequencies. This additional information allows solving for the first-order ionospheric delay, as described in Section (9.5.1). It also helps in solving for the phase ambiguity.

Differencing the observables with respect to time effectively yields only rates of change in the range, and thus loses some geometric strength, but also eliminates the phase ambiguity and all constant clock errors. Differencing the observables with respect to those of another receiver (usually stationary, but not required to be) that observes the same satellites yields essentially only relative positions, but also eliminates the satellite clock error and reduces effects of orbit error and atmospheric delays.

Finally, as an introduction to the next chapter, it is worth mentioning that an INS also provides additional information, although it is only in the form of relative positions and includes several additional systematic errors. Yet, with proper modeling, integrating INS into the GPS kinematic positioning problem enhances, or in some cases enables, achieving the required resolution and the accuracy and recovery from the inevitable cycle slips.

### 9.5.1 Dual-Frequency Pseudorange and Phase

Some of the artifices noted above for dealing with significant errors are described here first before introducing the INS in Chapter 10. To simplify the presentation, one often combines the true range with the clock errors and the phase offsets with the phase ambiguity. We denote the resulting intermediate pseudorange by

$$\rho^{*p}(\tau_r) = \rho_r^p(\tau_r) + c(\Delta\tau_r(t) - \Delta\tau^p(t - \Delta t_r^p)), \quad (9.38)$$

and the modified phase ambiguity (now *not* an integer!) by

$$N_r^{*p} = N_r^p + \phi_{0,r}^p - \phi_{0,r}. \quad (9.39)$$

With (9.32) describing the ionospheric delays, we thus have the following combined set of observation equations from (9.36) and (9.37):

$$\begin{aligned} s1_r^p(\tau_r) &= \rho^{*p}_r(\tau_r) + I_r^p + \varepsilon_{\rho1,r}^p, \\ s2_r^p(\tau_r) &= \rho^{*p}_r(\tau_r) + \alpha I_r^p + \varepsilon_{\rho2,r}^p, \\ \phi1_r^p(\tau_r) &= \frac{1}{\lambda_1} \rho^{*p}_r(\tau_r) - \frac{1}{\lambda_1} I_r^p - N1_r^{*p} + \varepsilon_{\phi1,r}^p, \\ \phi2_r^p(\tau_r) &= \frac{1}{\lambda_2} \rho^{*p}_r(\tau_r) - \frac{\alpha}{\lambda_2} I_r^p - N2_r^{*p} + \varepsilon_{\phi2,r}^p, \end{aligned} \quad (9.40)$$

where the numbers, 1, 2, refer to the nominal L1 and L2 frequencies, given by (9.10), with  $\lambda_1$  and  $\lambda_2$  given by (9.11); and where

$$\alpha = \frac{f_1^2}{f_2^2} = \frac{\lambda_2^2}{\lambda_1^2} \approx 1.647. \quad (9.41)$$

The combination of observables (9.40) represents for any epoch a system of four equations that could be solved for the four unknowns:  $\{\rho_r^{*p}, I_r^p, N1_r^{*p}, N2_r^{*p}\}$ . In matrix form, we have

$$\begin{pmatrix} s1_r^p(\tau_r) \\ s2_r^p(\tau_r) \\ \phi1_r^p(\tau_r) \\ \phi2_r^p(\tau_r) \end{pmatrix} = \begin{pmatrix} 1 & 1 & 0 & 0 \\ 1 & \alpha & 0 & 0 \\ 1/\lambda_1 & -1/\lambda_1 & -1 & 0 \\ 1/\lambda_2 & -\alpha/\lambda_2 & 0 & -1 \end{pmatrix} \begin{pmatrix} \rho_r^{*p}(\tau_r) \\ I_r^p \\ N1_r^{*p} \\ N2_r^{*p} \end{pmatrix} + \begin{pmatrix} \varepsilon_{\rho1,r}^p \\ \varepsilon_{\rho2,r}^p \\ \varepsilon_{\phi1,r}^p \\ \varepsilon_{\phi2,r}^p \end{pmatrix}, \quad (9.42)$$

showing, indeed, that the coefficient matrix (call it  $H$ ) is non-singular and the unknowns, in theory, are estimable. However, the accuracy of the estimates depends on the errors in the observables. With the values for the standard deviations of receiver noise given in Table 9.1 (appropriately scaled for the L1 and L2 phases according to (9.35)), the covariance matrix of the parameter estimation errors is given by (7.43) as:

$$P = (H^T R^{-1} H)^{-1} = \begin{pmatrix} 0.089 & -0.063 & 0.798 & 0.790 \\ -0.063 & 0.048 & -0.583 & -0.581 \\ 0.798 & -0.583 & 7.262 & 7.205 \\ 0.790 & -0.581 & 7.205 & 7.154 \end{pmatrix}, \quad (9.43)$$

where it is assumed that the observations are uncorrelated ( $R$  is a diagonal matrix) and the a priori covariance of the parameters is infinite (no a priori information). The standard deviations of the estimated cycle ambiguities are  $\sqrt{7.2} \approx 2.7$  cycles (roughly 50–60 cm); and, therefore, because the estimated ambiguity cannot resolve the full cycle count, the phase observables are practically ineffectual in the estimation of the range. Moreover, the range accuracy,  $\pm\sqrt{0.089}$  m, is three times the standard deviation of the pseudorange noise. This is due to the high correlations among all estimated parameters; from the off-diagonal elements of the covariance matrix, the normalized correlations are found to be all very close to 1 indicating that these individual parameters are not well estimated (separable) on the basis of these observations.

The inability to resolve the cycle ambiguities (to a small fraction of a cycle) lies with the noise in the pseudorange observation. This improves as time progresses since subsequent epochs yield four additional observations, but only two additional unknowns—the modified phase ambiguities,  $N1_r^{*p}, N2_r^{*p}$ , which are constants, and once solved hold for all epochs. Therefore, as more pseudorange observations are incorporated (e.g., via a Kalman filter; Chapter 7), the estimates of the ambiguities become more accurate; however, the convergence is slow. Alternatively, one can consider a less demanding problem, that of determining the difference of ambi-

guities defined in the difference in L1 and L2 phase observables:

$$\begin{aligned}\phi w_r^p(\tau_r) &= \phi l_r^p(\tau_r) - \phi 2_r^p(\tau_r) \\ &= \frac{1}{\lambda_w} \rho^*_r(\tau_r) - \frac{1 - \sqrt{\alpha}}{\lambda_1} I_r^p - Nw_r^{*p} + \varepsilon_{\phi w, r}^p,\end{aligned}\quad (9.44)$$

where  $\lambda_w$  is the wavelength of the *wide-lane* signal (the part of a mixed signal corresponding to the difference of frequencies, cf. (9.13)) having frequency  $f_w = f_1 - f_2$ :

$$\lambda_w = \left( \frac{1}{\lambda_1} - \frac{1}{\lambda_2} \right)^{-1} = 0.8619 \text{ m.} \quad (9.45)$$

The wide-lane ambiguity is defined by

$$Nw_r^{*p} = N1_r^{*p} - N2_r^{*p}. \quad (9.46)$$

The standard deviation of the receiver noise for the wide-lane phase,  $\varepsilon_{\phi w, r}^p$ , is  $\sqrt{2}$  times that of the L1 phase (in cycles).

Replacing the L2 phase and ambiguity in the model (9.42), respectively, with the wide-lane phase and ambiguity, according to (9.44) (also, appropriately modifying the matrix  $R$ ), the covariance matrix of the estimates becomes

$$P = \begin{pmatrix} 0.089 & -0.063 & 0.798 & 0.0087 \\ -0.063 & 0.048 & -0.583 & -0.0022 \\ 0.798 & -0.583 & 7.262 & 0.058 \\ 0.0087 & -0.0022 & 0.058 & 0.0068 \end{pmatrix}. \quad (9.47)$$

The wide-lane ambiguity estimate is now practically independent of the other estimates (as a computation of the normalized correlations will confirm), and its standard deviation is a mere  $\sqrt{0.0068} \approx 0.08$  cycles (7 cm) (this value is sensitive to the noise in the pseudorange observation). The L1 ambiguity is still not well determined; however, the estimability of the wide-lane ambiguity becomes significant in the case that an additional constraint can be enforced, namely that it is an integer. This is possible with another type of combination of observables: the double difference, discussed in the next section. In this case, also, the L1 ambiguity can be solved if the ionospheric effect is not considered significant, as in the case of short baselines.

Due to its dependence on frequency, it is sometimes useful to eliminate the first-order ionospheric effect using a linear combination of either phase or pseudorange with respect to the two carrier frequencies. The so-called ionosphere-free ("ion-free") observations in pseudorange and phase are

$$\begin{aligned}(s_{\text{ion-free}})_r^p(\tau_r) &= \frac{1}{1 - \alpha} s2_r^p(\tau_r) - \frac{\alpha}{1 - \alpha} s1_r^p(\tau_r) \\ &= \rho^*_r(\tau_r) + \frac{1}{1 - \alpha} \varepsilon_{\rho 2, r}^p - \frac{\alpha}{1 - \alpha} \varepsilon_{\rho 1, r}^p,\end{aligned}\quad (9.48)$$

and

$$\begin{aligned}
(\phi_{\text{ion-free}})^p_r(\tau_r) &= \frac{\sqrt{\alpha}}{1-\alpha} \phi 2^p_r(\tau_r) - \frac{\alpha}{1-\alpha} \phi 1^p_r(\tau_r) \\
&= \frac{1}{\lambda_1} \rho^{*p}_r(\tau_r) - \frac{1}{1-\alpha} (\sqrt{\alpha} N 2^{*p}_r - \alpha N 1^{*p}_r) \\
&\quad + \frac{\sqrt{\alpha}}{1-\alpha} \varepsilon_{\phi 2, r}^p - \frac{\alpha}{1-\alpha} \varepsilon_{\phi 1, r}^p,
\end{aligned} \tag{9.49}$$

where in each case the first equation is a definition and the second a consequence of the model (9.40). The coefficients for each linear combination are chosen to eliminate the first-order ionospheric effect as given by (9.32) and to ensure that the scaling of  $\rho^*$  is the same as in (9.18) and (9.23), respectively. Alternative sets of coefficients may be used; for example, the wide-lane, ion-free phase is defined as

$$\begin{aligned}
(\phi_{w\text{ion-free}})^p_r(\tau_r) &= \frac{\sqrt{\alpha}}{1+\alpha} \phi 1^p_r(\tau_r) - \frac{1}{1+\sqrt{\alpha}} \phi 2^p_r(\tau_r) \\
&= \frac{1}{\lambda_w} \rho^{*p}_r(\tau_r) - \frac{1}{1+\sqrt{\alpha}} (\sqrt{\alpha} N 1^{*p}_r - N 2^{*p}_r) \\
&\quad + \frac{\sqrt{\alpha}}{1+\alpha} \varepsilon_{\phi 1, r}^p - \frac{1}{1+\sqrt{\alpha}} \varepsilon_{\phi 2, r}^p,
\end{aligned} \tag{9.50}$$

where the second equation follows from (9.40) and the wide-lane wavelength,  $\lambda_w$ , is given by (9.45). Note that the standard deviation of the noise in the ion-free observations increases approximately by a factor of 3; while for the ion-free, wide-lane phase, it decreases by  $\sqrt{2}$ . Indeed, assuming uncorrelated observations on L1 and L2, and using (9.34) and the value of  $\alpha$  in (9.41), we obtain the following variances,  $\sigma^2(\cdot)$ :

$$\begin{aligned}
\sigma^2(\varepsilon_{\phi_{\text{ion-free}}, r}^p) &= \frac{\alpha(1+\alpha)}{(1-\alpha)^2} \sigma^2(\varepsilon_{\phi 1, r}^p) = 10.3 \sigma^2(\varepsilon_{\phi 1, r}^p), \\
\sigma^2(\varepsilon_{\rho_{\text{ion-free}}, r}^p) &= \frac{\alpha(1+\alpha)}{(1-\alpha)^2} \sigma^2(\varepsilon_{\rho 1, r}^p) = 10.3 \sigma^2(\varepsilon_{\rho 1, r}^p), \\
\sigma^2(\varepsilon_{\phi_{w\text{ion-free}}, r}^p) &= \frac{1+\alpha}{(1+\sqrt{\alpha})^2} \sigma^2(\varepsilon_{\phi 1, r}^p) = \frac{1}{1.97} \sigma^2(\varepsilon_{\phi 1, r}^p).
\end{aligned} \tag{9.51}$$

Even though the ion-free, wide-lane noise is lower (in standard deviation) than that of the ion-free noise by a factor of  $\sqrt{20.3}$ , the signal,  $\rho^{*p}_r/\lambda_w$ , is also lower by the same factor (i.e., the signal-to-noise ratio is the same).

### 9.5.2 Single and Double Differences

One way to eliminate most of the receiver clock error from the intermediate pseudorange,  $\rho^{*p}_r$ , in (9.38) is by differencing observations between two satellites at each epoch. The receiver clock error is common to each observation and cancels in their difference. With the same assumptions as in (9.40), equations (9.18) and (9.23) then

become

$$\begin{aligned}\Delta s_r^{p,q}(\tau_r) &= \Delta\rho_r^{*p,q}(\tau_r) + \Delta I_r^{p,q} + \Delta\varepsilon_{\rho,r}^{p,q}, \\ \Delta\phi_r^{p,q}(\tau_r) &= \frac{1}{\lambda} \Delta\rho_r^{*p,q}(\tau_r) - \frac{1}{\lambda} \Delta I_r^{p,q} - \Delta N_r^{*p,q} + \Delta\varepsilon_{\phi,r}^{p,q};\end{aligned}\quad (9.52)$$

where

$$\begin{aligned}\Delta s_r^{p,q}(\tau_r) &= s_r^p(\tau_r) - s_r^q(\tau_r), \\ \Delta\phi_r^{p,q}(\tau_r) &= \phi_r^p(\tau_r) - \phi_r^q(\tau_r), \\ \Delta\rho_r^{*p,q}(\tau_r) &= \rho_r^p(\tau_r) - \rho_r^q(\tau_r) - c(\Delta\tau^p(t - \Delta t_r^p) - \Delta\tau^q(t - \Delta t_r^q)), \\ \Delta I_r^{p,q} &= I_r^p - I_r^q, \\ \Delta N_r^{*p,q} &= N_r^p - N_r^q + \phi_0^p - \phi_0^q, \\ \Delta\varepsilon_{\rho,r}^{p,q} &= \varepsilon_{\rho,r}^p - \varepsilon_{\rho,r}^q, \quad \Delta\varepsilon_{\phi,r}^{p,q} = \varepsilon_{\phi,r}^p - \varepsilon_{\phi,r}^q.\end{aligned}\quad (9.53)$$

A similar set of equations and definitions holds for the quantities referring to the second frequency, taking due care of the scaling of the ionospheric term. Note that the term  $-(\dot{\rho}_r^p - \dot{\rho}_r^q)\Delta\tau_r(t)$  should be added to  $\Delta\rho_r^{*p,q}$  if the receiver clock error is significant, in accordance with (9.17). Also, wide-lane and ion-free differences may be defined as follows from (9.44) and (9.48), (9.49):

$$\Delta\phi_{w_r}^{p,q}(\tau_r) = \frac{1}{\lambda_w} \Delta\rho_r^{*p,q}(\tau_r) - \frac{1 - \sqrt{\alpha}}{\lambda_1} \Delta I_r^{p,q} - \Delta N w_r^{*p,q} + \Delta\varepsilon_{\phi,w,r}^{p,q}, \quad (9.54)$$

with appropriate definitions for the wide-lane ambiguity and noise terms; and

$$\begin{aligned}(\Delta s_{\text{ion-free}})_r^{p,q}(\tau_r) &= \Delta\rho_r^{*p,q}(\tau_r) + \frac{1}{1 - \alpha} \Delta\varepsilon_{\rho 2,r}^{p,q} - \frac{\alpha}{1 - \alpha} \Delta\varepsilon_{\rho 1,r}^{p,q}, \\ (\Delta\phi_{\text{ion-free}})_r^{p,q}(\tau_r) &= \frac{1}{\lambda_1} \Delta\rho_r^{*p,q}(\tau_r) - \frac{1}{1 - \alpha} (\sqrt{\alpha} \Delta N 2_r^{*p,q} - \alpha \Delta N 1_r^{*p,q}) \\ &\quad + \frac{\sqrt{\alpha}}{1 - \alpha} \Delta\varepsilon_{\phi 2,r}^{p,q} - \frac{\alpha}{1 - \alpha} \Delta\varepsilon_{\phi 1,r}^{p,q}.\end{aligned}\quad (9.55)$$

The intermediate pseudorange parameter now contains no receiver clock error; and the modified cycle ambiguity,  $\Delta N_r^{*p,q}$ , contains no receiver phase offset, though it is still not an integer. Therefore, these so-called *single-difference, between-satellite observations* are useful in that they eliminate the receiver biases, otherwise nothing has changed. On the other hand, this is somewhat easier than, although equivalent to (Schaffrin and Grafarend, 1986), including the receiver clock error as a parameter to be solved as part of the positioning problem. Of course, the statistics of the single-difference observation errors must be defined properly. In particular, we see that the standard deviation of the single-difference noise,  $\Delta\varepsilon_{\rho,r}^{p,q}$  and  $\Delta\varepsilon_{\phi,r}^{p,q}$ , has increased in each case by a factor of  $\sqrt{2}$ , assuming that the undifferenced observation noise terms are uncorrelated. Correlations must be considered among those single-difference observations that share a satellite; e.g.  $\Delta\phi_r^{p,q}(\tau_r)$  and  $\Delta\phi_r^{q,v}(\tau_r)$ .

The receiver and satellite clock and phase biases can be eliminated altogether (approximately) by differencing the single-difference observations from two receivers. In this case, not having to know the satellite clock errors is traded for obtaining only coordinate differences relative to the coordinates of one of the receivers. Two subscripts,  $r, s$ , are used to signify the between-receiver difference. Differencing two single-difference observation sets, like (9.52), yields the so-called *double-difference* pseudorange and phase observations:

$$\begin{aligned}\Delta s_{r,s}^{p,q}(\tau) &= \Delta\rho_{r,s}^{p,q}(\tau) + \Delta I_{r,s}^{p,q} + \Delta\varepsilon_{\rho,r,s}^{p,q}, \\ \Delta\phi_{r,s}^{p,q}(\tau) &= \frac{1}{\lambda} \Delta\rho_{r,s}^{p,q}(\tau) - \frac{1}{\lambda} \Delta I_{r,s}^{p,q} - \Delta N_{r,s}^{p,q} + \Delta\varepsilon_{\phi,r,s}^{p,q};\end{aligned}\quad (9.56)$$

where

$$\begin{aligned}\Delta s_{r,s}^{p,q}(\tau) &= s_r^p(\tau_r) - s_r^q(\tau_r) - s_s^p(\tau_s) + s_s^q(\tau_s), \\ \Delta\phi_{r,s}^{p,q}(\tau) &= \phi_r^p(\tau_r) - \phi_r^q(\tau_r) - \phi_s^p(\tau_s) + \phi_s^q(\tau_s), \\ \Delta\rho_{r,s}^{p,q}(\tau) &= \rho_r^p(\tau) - \rho_r^q(\tau) - \rho_s^p(\tau) + \rho_s^q(\tau), \\ \Delta I_{r,s}^{p,q} &= I_r^p - I_r^q - I_s^p + I_s^q, \\ \Delta N_{r,s}^{p,q} &= N_r^p - N_r^q - N_s^p + N_s^q, \\ \Delta\varepsilon_{\rho,r,s}^{p,q} &= \varepsilon_{\rho,r}^p - \varepsilon_{\rho,r}^q - \varepsilon_{\rho,s}^p + \varepsilon_{\rho,s}^q, \quad \Delta\varepsilon_{\phi,r,s}^{p,q} = \varepsilon_{\phi,r}^p - \varepsilon_{\phi,r}^q - \varepsilon_{\phi,s}^p + \varepsilon_{\phi,s}^q.\end{aligned}\quad (9.57)$$

The doubly differenced cycle ambiguity,  $\Delta N_{r,s}^{p,q}$ , now contains no phase offset; and, it is an *integer!* The argument for the double-difference observations is specified as the *indicated* time,  $\tau$ , under the premise that the indicated times on both receivers are the same by definition:  $\tau = \tau_r = \tau_s$ . On the other hand, the true ranges refer to different true times since the receivers are not synchronized perfectly. The corresponding range errors, given for each range by the time-misregistration term,  $\dot{\rho}_r^p \Delta\tau_r$  (see (9.17)), is omitted here as in the case of single differences, (9.53).

In addition, the satellite clock errors do not cancel completely because they refer to different times of transmission; however, the net effect is small and is also excluded in (9.57). Indeed, using (9.38), the doubly differenced satellite clock error in  $\Delta\rho_{r,s}^{p,q}$  is given by

$$c(\Delta\tau^p(t - \Delta t_r^p) - \Delta\tau^q(t - \Delta t_r^q) - \Delta\tau^p(t - \Delta t_s^p) + \Delta\tau^q(t - \Delta t_s^q)). \quad (9.58)$$

The degree to which these terms cancel depends on the stability of the satellite clocks during the differential transit times of the signal from the satellite to each of the receivers,  $r$  and  $s$ . Assuming linear variation in the clock error, it can be shown that (9.58) is equivalent to

$$c \left[ \frac{\Delta f^p}{f_0} (\Delta t_r^p - \Delta t_s^p) - \frac{\Delta f^q}{f_0} (\Delta t_r^q - \Delta t_s^q) \right], \quad (9.59)$$

where  $\Delta f^p$  is the difference between the instantaneous satellite frequency and a nominal value (it is the satellite clock error in terms of frequency). The difference

in transit times,  $\Delta t_r^p - \Delta t_s^p$ , from a satellite to receivers 300 km apart is less than 0.001 s; the frequency stability,  $\Delta f^p/f_0$ , of the satellite clocks with SA is about  $10^{-8}$  (Hofmann-Wellenhof et al., 1994, p. 140); and hence, (9.59) typically amounts to about  $c(10^{-11}$  s), or 3 mm in range error, which is negligible.

For short baselines (<15 km), the doubly differenced ionospheric effect is relatively small and in many cases negligible. Therefore, aside from tropospheric, multipath, and a host of minor equipment-related errors, the double differences yield the simplest and most straightforward relationship between observables and unknown coordinates, being free of the troublesome clock errors of the receiver and satellite (in particular, the former intentional frequency dithering associated with Selective Availability). In addition, the nature of the double-difference ambiguity being an integer adds an important constraint in its determination.

Finally, although precise orbits are available from the IGS within a relatively short period (two weeks), larger orbit errors cancel in the double-difference observables over short baselines. Geometric consideration of the triangle  $\Delta r_{sp}$  formed by the satellite,  $p$ , and the terrestrial baseline between the two receivers,  $r$  and  $s$ , yields the following heuristic relationship between orbit error,  $d\rho$ , and baseline length error,  $db$ :

$$\frac{d\rho}{\rho} = \frac{db}{b}, \quad (9.60)$$

where  $\rho$  is the range to the satellite and  $b$  is the baseline length. Since  $\rho > 2 \times 10^7$  m, a requirement in relative positioning accuracy of 1 cm over a 10-km baseline can tolerate 20 m of orbit error (roughly the error of the broadcast ephemeris with SA).

Analogous to (9.54) and (9.55), wide-lane and ion-free double-differences may also be defined as follows:

$$\Delta\phi w_{r,s}^{p,q}(\tau) = \frac{1}{\lambda_w} \Delta\rho_{r,s}^{p,q}(\tau) - \frac{1 - \sqrt{\alpha}}{\lambda_1} \Delta I_{r,s}^{p,q} - \Delta N w_{r,s}^{p,q} + \Delta\epsilon_{\phi w,r,s}^{p,q}, \quad (9.61)$$

and

$$\begin{aligned} (\Delta s_{\text{ion-free}})^{p,q}_{r,s}(\tau) &= \Delta\rho_{r,s}^{p,q}(\tau) + \frac{1}{1 - \alpha} \Delta\epsilon_{\rho 2,r,s}^{p,q} - \frac{\alpha}{1 - \alpha} \Delta\epsilon_{\rho 1,r,s}^{p,q}, \\ (\Delta\phi_{\text{ion-free}})^{p,q}_{r,s}(\tau) &= \frac{1}{\lambda_1} \Delta\rho_{r,s}^{p,q}(\tau) - \frac{1}{1 - \alpha} (\sqrt{\alpha} \Delta N 2_{r,s}^{p,q} - \alpha \Delta N 1_{r,s}^{p,q}) \\ &\quad + \frac{\sqrt{\alpha}}{1 - \alpha} \Delta\epsilon_{\phi 2,r,s}^{p,q} - \frac{\alpha}{1 - \alpha} \Delta\epsilon_{\phi 1,r,s}^{p,q}. \end{aligned} \quad (9.62)$$

Again, the wide-lane, double-difference ambiguity is an integer. The linear combination of ambiguities for the ion-free, double-difference phase is not an integer, but also not an arbitrary real number.

Note that for any of these double-difference observables the noise term is a combination of single phase or pseudorange receiver noises. For example, the wide-lane,

double-difference phase noise is given by

$$\Delta e_{\phi w,r,s}^{p,q} = [(e_{\phi 1,r}^p - e_{\phi 2,r}^p) - (e_{\phi 1,r}^q - e_{\phi 2,r}^q)] - [(e_{\phi 1,s}^p - e_{\phi 2,s}^p) - (e_{\phi 1,s}^q - e_{\phi 2,s}^q)]. \quad (9.63)$$

Its standard deviation is  $\sqrt{8}$  times the value given by (9.35) if all the individual errors are uncorrelated. As in the case of between-satellite single-differences, correlations must be accounted for where they exist among the double-difference observations that share a satellite.

## 9.6 Kinematic Positioning

The GPS measurements are made in a dynamic environment. Even if the receivers are stationary on the Earth, the distances to the satellites are constantly changing because of their orbital motion and because of Earth's rotation. Nevertheless, one distinguishes between *static* positioning and *kinematic* positioning. As the name implies, static positioning involves placing the receiver at a fixed location on the Earth and determining the position of that point. Kinematic positioning, on the other hand, refers to determining the position of a vehicle or platform that is moving continually with respect to the Earth. One could attempt this either in real time, that is, instantaneously, or usually with higher accuracy in a post-mission mode. We use the term *navigation* to refer to the real-time processing of the positioning data, while *kinematic positioning* is reserved for the post-processing of the data (as computers become more powerful and data links more efficient, the distinction may become rather nebulous). There is an intermediate mode of positioning, known as *semi-kinematic* positioning, whereby the moving receiver (and antenna) is temporarily brought to rest at those points to be positioned, before moving to the next point, at all times maintaining signal lock. It is a rapid form of static surveying that is amenable to vehicles that are able to stop at each survey point.

We will consider only kinematic GPS positioning, as defined above, because in a general sense it encompasses the semi-kinematic mode as a special case that includes explicit constraints. The observation equations, in fact, do not differ even from the static case; after all, the coarse dynamics of the receiver-satellite configuration hardly change if the receiver's velocity relative to the satellite differs because of a relative velocity of the vehicle with respect to the Earth. There are differences in performance with respect to static positioning, however, including the loss of the benefit of time averaging that yields higher accuracy per point, and the need to increase the bandwidth of the tracking loop to accommodate the high-frequency dynamics of the vehicle. The latter implies an increase in the noise variance; see (9.34) and (9.35). (On the other hand, we will not be interested in very high-dynamic vehicles, such as military fighter aircraft.) In addition, kinematic GPS positioning often is burdened by a more restrictive and changing environment in terms of visible satellites, interference from passing structures, and multipath. This, of course, is one of the motivations for integrating GPS and INS, since the latter is insensitive to its geographic and electromagnetic environment.

As in the static case, we define *absolute* kinematic positioning in which the position of the vehicle is determined on the basis of a single receiver on board the vehicle,

and *relative* kinematic positioning where the position of the moving receiver, called the *rover*, is determined by differencing techniques with respect to a stationary receiver, called the *base* receiver. One might contemplate the interesting application where both receivers are moving with respect to each other (e.g., two satellites following each other in a low Earth orbit, such as the *Gravity Recovery and Climate Experiment*, GRACE, Jekeli 1999). It would only mean that the position of neither receiver can be determined absolutely, while in the former case of one stationary receiver, the roving receiver's position can be determined absolutely if the base station coordinates are known. To provide additional strength to the relative kinematic solution, or as a means of testing consistency, one often employs multiple base receivers in the area of the rover's operation.

At the end of the previous section the unknown parameter of primary interest was identified simply as the range; but the actual unknowns, of course, are the coordinates of the receiver (more precisely, the antenna). Toward determining these, one must examine the true range, for example,  $\rho_r^p$ , between the receiver and the  $p^{\text{th}}$  satellite. It is given, in terms of the true time of reception, explicitly by

$$\rho_r^p(t) = |\mathbf{x}^p(t - \Delta t_r^p) - \mathbf{x}_r(t)|, \quad (9.64)$$

where  $\mathbf{x}^p(t - \Delta t_r^p)$  is the true vector of coordinates of the satellite at the true time of signal transmission and  $\mathbf{x}_r(t)$  is the true vector of coordinates of the receiver at the true time of reception.

Also, no mention of a specific coordinate frame for the satellite and receiver coordinates has been made so far and there should be no confusion that the superscript notation used here refers to satellites and not coordinate frames as in earlier chapters. But, care is needed in the proper interpretation of (9.64) where the position vectors of the satellite and receiver refer to different epochs; and, for the subtraction to make sense, they must reside in the same coordinate frame. As such the coordinate frame is not arbitrary, even though the distance, itself, does not depend on the frame. Because the time arguments are different, (9.64) is mathematically correct only if the common frame does not rotate in time; that is, it must be the inertial frame.

Although satellite ephemerides are often coordinatized in the inertial frame, the GPS navigation message provides information that allows computation of *e-frame* (ECEF) coordinates of the transmitting satellite. Also, the coordinates of the receiver, if on a terrestrial platform, are preferred in the *e-frame*. Therefore, the satellite coordinates, if given for the time of transmission in the *e-frame*, must be transformed to the time of reception in order to account for Earth's rotation during the time of transit. That is, the signal does not travel in an Earth-fixed coordinate frame and the two position vectors, in essence, refer to different ECEF frames, one rotated (delayed) by  $\Delta t_r^p \omega_e$  with respect to the other, where  $\omega_e$  is Earth's rate of rotation. To achieve consistency, the satellite coordinates must be rotated forward to the time of reception. Only a single rotation about the 3-axis is involved; and, we have for the case of *e-frame* coordinates:

$$\mathbf{x}^p(t - \Delta t_r^p)|_t = R_3(\Delta t_r^p \omega_e) \mathbf{x}^p(t - \Delta t_r^p). \quad (9.65)$$

Note that this is not a propagation of coordinates according to the dynamics of the satellite motion—the coordinates still refer to the time of transmission; but now they are in an  $e$ -frame that is rotating with the Earth at the time of reception. In terms of  $e$ -frame coordinates, the satellite-receiver range now is given by

$$\rho_r^P(t) = |R_3(\Delta t_r^P \omega_e) \mathbf{x}^P(t - \Delta t_r^P) - \mathbf{x}_r(t)|. \quad (9.66)$$

The notational complexity of introducing an explicit reference to the frame with a further superscript is not necessary if one restricts the derivations to the premise that henceforth *all position vectors are assumed to be coordinatized in the  $e$ -frame*.

### 9.6.1 Dynamics Model

Because of the usual plenitude of visible satellites (often at least 5, well distributed), the number of unknown parameters is smaller than the number of observations; and this calls for a least-squares solution based on minimizing the square of residuals between observations and corresponding adjusted observations. It is noted that the case of static positioning is overwhelmed by observations, their number increasing with time, while the number of unknown parameters remains small. However, in the present context of kinematic positioning the coordinates of the rover depend on time, and thus the number of unknown parameters (the rover's coordinates) increases in step with the number of observations and is at least three times the total number of observation epochs. This suggests a *recursive* linear least-squares approach, or analogously, the Kalman filter algorithm (Chapter 7). It has the added benefit that unknown parameters, or states, of the system may be added or deleted as time progresses and as warranted by the situation, always with rigorous propagation of the error covariances. In all cases, we will assume a linear model for the relationship between the unknowns and the observables. Where this relationship is patently non-linear, for example, for the unknown  $e$ -frame coordinates,  $\mathbf{x}_r$ , in (9.64), a linearization must be performed.

Following the approach of the Kalman filter, it is first necessary to identify the states of the system and to specify a model for their dynamics. Among the states, one naturally includes the position coordinate errors; also the velocity errors, the clock errors, cycle ambiguities (for phase measurements), and assorted perturbing effects due to atmosphere, multipath, and electronic delays may be included, provided sufficient external observations are anticipated to enable their estimation. For each state variable, one must define a (linear) dynamics model, with appropriate statistical information, as presumed in (7.54). For example, in the case of undifferenced pseudorange observations the states may be limited to the coordinate errors and the receiver clock error (see Section 9.6.3). Other errors must then either be neglected or corrected using auxiliary information (e.g., satellite clock corrections provided by the broadcast ephemeris). Or, as an extension to the basic error dynamics model, they could also be modeled stochastically.

Among the nuisance parameters, the initial cycle ambiguity is the most important in the case of phase observables. It is modeled as a (random) constant; however, once it is solved to sufficient accuracy (especially if it can be fixed to an integer value), it

need no longer enter as a state of the system until a cycle slip or loss of signal lock occurs (or a new satellite comes into view). Besides application of the straightforward model (9.42), usually amended by (9.44), many other and related strategies have been devised to solve for the ambiguity, either to improve the numerical efficiency or to deal with fewer types of observables or other inseparable effects (such as the ionospheric delay). Ambiguity search algorithms have been developed both for static positioning (used also to initialize the phase in a kinematic campaign) and for “on-the-fly” (OTF) ambiguity recovery during a vehicle’s journey. OTF algorithms aim to ensure the high positioning accuracy afforded by the phase observables after the occurrence of cycle slips or loss of signal lock. It is beyond the scope of this text to cover these techniques and the interested reader is referred to Hofmann-Wellenhof et al. (1994) for a review and to Teunissen (1998) for a theoretical treatment, among other texts in geodetic applications of GPS, such as by Leick (1995).

The dynamics model for the other nuisance parameters is either straightforward or left to the reasoned imagination of the user. As a motivation to the integration with INS (Chapter 10), we consider primarily the dynamics of the receiver coordinate errors. The nuisance states, such as clock errors, ionospheric delays, and ambiguities can be augmented in the usual way (Section 7.5.1). It is sometimes assumed that the dynamics of the coordinate errors can be described by a white noise model for the acceleration error, which we take up later in this section. A simpler assumption is that the coordinate errors essentially are completely unknown, that is, they are states with arbitrarily large driving white noise. The dynamics model then loses its significance, and, lacking a more definitive one, we may assume the errors are simply and completely unknown (non-stochastic) at each epoch prior to the observations.

Thus, restricting the system to the coordinate error states, let them be represented by the  $3 \times 1$  vector,  $\delta x_k$ . The receiver subscript,  $r$ , has been omitted since only the coordinate errors of the roving receiver are to be estimated; while the subscript,  $k$ , refers, as before, to the time epoch. In order to make use of the previously developed Kalman filter formulation, we define the “dynamics model” of this state vector, as per above assumption, by

$$\delta x_k = w_k, \quad (9.67)$$

where  $w_k$  is a  $3 \times 1$  white noise vector with

$$w_k \sim \mathcal{N}(0, Q_k), \quad (9.68)$$

and where the non-stochastic nature of the states is simulated (in a qualitative sense) by arbitrarily large uncertainty:

$$Q_k = \begin{pmatrix} \infty & 0 & 0 \\ 0 & \infty & 0 \\ 0 & 0 & \infty \end{pmatrix}. \quad (9.69)$$

The model (9.67) implies that the state transition matrix,  $\Phi$ , is zero (cf., 7.54). The a priori values of the states also are defined to equal zero. It is noted that the

true position errors are the differences between the coordinates “indicated” by the system, in this case, selected approximate values at epoch  $t_k$ , denoted by  $\tilde{\mathbf{x}}_k$ , and the true coordinates:

$$\delta\mathbf{x}_k = \tilde{\mathbf{x}}_k - \mathbf{x}_k. \quad (9.70)$$

Without any correlative stochastic information on the error states, the model (9.67) requires that adequate observations be available at every epoch in order to estimate the error states. In general, this is the case with continuously operating GPS receivers, barring the occurrence of cycle slips or loss of signal lock.

More sophisticated models for the coordinate errors could be developed to bridge possible gaps in the GPS data if one could assume, for example, that the error at time  $t_k$  is correlated with the position error at time  $t_{k+1}$ , as described by a reasonable variance for the velocity error or acceleration error. For instance, one might assume that the acceleration errors are (continuous) white noise processes, which is equivalent to assuming that the velocity errors are random walk processes (see Section 6.5.2). The dynamics model for the position errors in this case is given by

$$\frac{d}{dt} \begin{pmatrix} \delta\mathbf{x} \\ \delta\dot{\mathbf{x}} \end{pmatrix} = \begin{pmatrix} 0 & I \\ 0 & 0 \end{pmatrix} \begin{pmatrix} \delta\mathbf{x} \\ \delta\dot{\mathbf{x}} \end{pmatrix} + \begin{pmatrix} \mathbf{0} \\ \mathbf{w} \end{pmatrix}, \quad (9.71)$$

where the elements of the dynamics matrix are the  $3 \times 3$  identity and zero matrices, respectively. The covariance matrix of the entire  $6 \times 1$  noise vector on the right side is given by:

$$\begin{pmatrix} 0 & 0 \\ 0 & \mathcal{E}(\mathbf{w}(\tau)\mathbf{w}(\tau')) \end{pmatrix} = \begin{pmatrix} 0 & 0 \\ 0 & \text{diag}[\mathbf{q}]\delta(\tau - \tau') \end{pmatrix}, \quad (9.72)$$

where  $\text{diag}[\mathbf{q}]$  is a  $3 \times 3$  diagonal matrix with diagonal elements being the noise power spectral density values, comprising vector  $\mathbf{q}$ , that characterize the acceleration errors,  $\delta\ddot{\mathbf{x}}$ .

The discrete form of the model (9.71) is obtained in the usual way. Specifically, from (7.109), the state transition matrix is found to be (the series terminates in this case with the second term):

$$\Phi(t_k, t_{k-1}) = \begin{pmatrix} I & \Delta t I \\ 0 & I \end{pmatrix}, \quad (9.73)$$

where  $\Delta t = t_k - t_{k-1}$ . Therefore, (7.110) prescribes the discrete dynamics model as:

$$\begin{pmatrix} \delta\mathbf{x}_k \\ \delta\dot{\mathbf{x}}_k \end{pmatrix} = \begin{pmatrix} I & \Delta t I \\ 0 & I \end{pmatrix} \begin{pmatrix} \delta\mathbf{x}_{k-1} \\ \delta\dot{\mathbf{x}}_{k-1} \end{pmatrix} + \mathbf{u}_k. \quad (9.74)$$

The  $6 \times 1$  vector  $\mathbf{u}_k$  formally is given by (7.111). In practice, only its covariance matrix is needed:

$$Q_k = \mathcal{E}(\mathbf{u}_k \mathbf{u}_k^T) = \begin{pmatrix} \frac{1}{3} \Delta t^3 \text{diag}[\mathbf{q}] & \frac{1}{2} \Delta t^2 \text{diag}[\mathbf{q}] \\ \frac{1}{2} \Delta t^2 \text{diag}[\mathbf{q}] & \Delta t \text{diag}[\mathbf{q}] \end{pmatrix}. \quad (9.75)$$

A first-order approximation would neglect all but the lower right submatrix,  $\Delta t \text{diag}[\mathbf{q}]$ , in accordance with (7.117).

For additional elaborations and analyses of these models, see (Schwarz et al., 1989); and for an example of a model tuned more specifically to the dynamics of a vehicle (the motion of a ship in this case), see (Sennott et al., 1996). The assumption of white-noise acceleration errors can be replaced by a much more accurate model if the accelerations are actually sensed. This is the case with an on-board inertial navigation system that, therefore, leads to more accurate extrapolation of the position error states over extended periods (at least several minutes) of GPS outages and facilitates on-the-fly ambiguity recovery, while also increasing the overall resolution of the kinematic positioning solution. It is one of the topics of Chapter 10.

### 9.6.2 Observation Equations

The observations are either pseudoranges or phases, or both, for a number of satellites at each epoch. Each depends non-linearly on the position coordinates and linearly on a variety of other states. It is convenient to set up a general structure for the observation equation and subsequently to specialize this to the different types of observations. To allow a more comprehensive set of system states, let the true  $m \times 1$  state vector at epoch  $k$  be represented by  $\varepsilon_k$ . It is, as exemplified by (9.70), the difference between the vector of “indicated” parameter values, such as position coordinates, but generally, let us say  $\tilde{\mathbf{z}}_k$ , and the corresponding vector of true values,  $\mathbf{z}_k$ :

$$\varepsilon_k = \tilde{\mathbf{z}}_k - \mathbf{z}_k. \quad (9.76)$$

The indicated values are initial guesses if the “states” are non-stochastic; otherwise they are obtained on the basis of a formal expectation or an updated estimate from a closed-loop evaluation (Section 7.5.2).

At any particular epoch, the observation equation relates the  $m$  states,  $\varepsilon_k$ , to  $n$  differences between observed and corresponding calculated quantities. In accordance with the notation of Section 7.3.1, let  $\tilde{\mathbf{y}}_k$  be the  $n \times 1$  vector of observations at epoch  $k$ , being the sum of the true vector function,  $\mathbf{h}(\mathbf{z}_k)$ , depending on the true parameters, and discrete white noise,  $\mathbf{v}_k$  (cf. (7.50)):

$$\tilde{\mathbf{y}}_k = \mathbf{h}(\mathbf{z}_k) + \mathbf{v}_k. \quad (9.77)$$

The difference,  $\delta \mathbf{y}_k$ , between the vectors of calculated values and observations is given in linear approximation by (7.52):

$$\delta \mathbf{y}_k \approx H_k \varepsilon_k - \mathbf{v}_k, \quad (9.78)$$

where (cf. (7.53))

$$H_k = \left. \frac{\partial \mathbf{h}}{\partial \mathbf{z}} \right|_{\mathbf{z}=\tilde{\mathbf{z}}_k} \quad (9.79)$$

is a  $n \times m$  matrix of evaluated partial derivatives. Elements of the vector functions,  $\mathbf{h}(\mathbf{z}_k)$ , were developed in the previous sections, and it remains only to find the ap-

propriate partial derivatives for specific sets of system states. Several relevant cases are elaborated in the following sections.

### 9.6.3 Single-Receiver Case

Positioning with a single receiver anywhere in the world was the original intent of the Global Positioning System, and it is still one of the principal applications in military as well as civil and commercial navigation and kinematic positioning. Primarily it is accomplished with the pseudoranges, but we will assume as well that the phase of the carrier signal is an observable, this being the case for all precision receivers. This means that, in principle, a more accurate positioning solution is obtained since the wavelength of the carrier signal is much shorter than that of the code signal. On the other hand, additional unknowns enter the problem, specifically, the initial cycle ambiguity. In seeking higher accuracy, the model must also include other parameters to account for systematic effects, such as ionospheric and tropospheric delays. This requires additional information, for example, observations at a second frequency, as provided by dual frequency receivers.

In the following, we consider first a simplified illustrative example where only the pseudorange observable at a single frequency (L1) is available. Formulations of more complicated combination observables of pseudorange and phase are then easily extrapolated. Even though there is only one receiver, the receiver subscript,  $r$ , is retained for the sake of uniformity in notation and clarity in denoting receiver-satellite differences.

Assuming the satellite clock error has been corrected, ignoring the ionospheric effect in (9.36) (or suppose it has been removed with a TEC model), and using (9.66), we have the following pseudorange observation:

$$s_r^p(\tau) = |R_3(\Delta t_r^p \omega_e) \mathbf{x}^p(\tau - \Delta t_r^p) - \mathbf{x}_r(\tau)| + c \Delta \tau_r + \varepsilon_{p,r}^p. \quad (9.80)$$

The system state vector includes the receiver coordinate errors and the receiver clock error (scaled by  $c$  to yield units of distance) at epoch  $t_k$ :

$$\varepsilon_k = \begin{pmatrix} \delta \mathbf{x}_r(\tau_k) \\ \delta(c \Delta \tau)_k \end{pmatrix}. \quad (9.81)$$

A linear perturbation of the model in terms of the system states yields:

$$\tilde{s}_r^p(\tau) = -\frac{1}{\rho_r^p(\tau)} [R_3(\Delta t_r^p \omega_e) \mathbf{x}^p(\tau - \Delta t_r^p) - \mathbf{x}_r(\tau)]^T \delta \mathbf{x}_r(\tau) + \delta(c \Delta \tau_r) + \varepsilon_{p,r}^p. \quad (9.82)$$

The coefficients of the perturbations on the right side are the partial derivatives needed in (9.79). Evaluating these at the indicated (approximate) values of the parameters, we obtain the  $n_p \times m$  observation matrix,  $H_k$ , where  $n_p$  is the number of observed satellites at epoch  $t_k$ , and in the present case  $m = 4$ . To simplify the notation, let

$$\tilde{\mathbf{e}}_r^p(\tau_k) = \frac{1}{\tilde{\rho}_r^p(\tau_k)} [R_3(\Delta t_r^p \omega_e) \mathbf{x}^p(\tau_k - \Delta t_r^p) - \tilde{\mathbf{x}}_r(\tau_k)], \quad (9.83)$$

which, incidentally, is the unit vector in the direction of the vector connecting the satellite and the receiver at the approximate coordinates,  $\tilde{\mathbf{x}}_r$ . These coordinates are used also to calculate the range,  $\tilde{r}_r^p(\tau_k)$ , where from (9.66):

$$\tilde{r}_r^p(\tau_k) = |R_3(\Delta t_r^p \omega_e) \mathbf{x}^p(\tau_k - \Delta t_r^p) - \tilde{\mathbf{x}}_r(\tau_k)|. \quad (9.84)$$

Note that the interval  $\Delta t_r^p$  also depends on the epoch,  $\tau_k$ . The  $n_p \times 4$  observation matrix then contains the following rows,  $p = 1, \dots, n_p$ :

$$(H_k)_p = [-[\tilde{\mathbf{e}}_r^p(\tau_k)]^T, 1], \quad (9.85)$$

$$\text{where } H_k = ((H_k)_1^T \quad (H_k)_2^T \quad \cdots \quad (H_k)_{n_p}^T)^T.$$

The  $n_p \times 1$  observation vector is given by the difference between calculated and observed pseudorange:

$$\delta \mathbf{y}_k = [\tilde{s}_r^p(\tau_k) - s_r^p(\tau_k)]_{p=1, \dots, n_p}, \quad (9.86)$$

where  $\tilde{s}_r^p$  is calculated from (9.80) on the basis of the approximate (or “system-indicated”) coordinates. The  $n_p \times 1$  white noise vector in (9.77) is

$$\mathbf{v}_k = [\varepsilon_{p,r}^p(\tau_k)]_{p=1, \dots, n_p}. \quad (9.87)$$

The calculation of  $H_k$  and  $\tilde{s}_r^p$  requires the coordinates of the satellites which are obtained from their respective ephemerides. But to know the epoch for these coordinates requires that the signal transit time,  $\Delta t_r^p$ , be known; this can be calculated if the receiver and satellite positions are known. This apparently circular problem is easily overcome with an iterative procedure. Only one iteration is required since the convergence is rapid. Indeed, let  $\varepsilon_\rho$  be the error in the computed range due to an initial position error for either receiver or satellite. The corresponding error in transit time is given by  $\varepsilon_{\Delta t} = \varepsilon_\rho/c$ , which translates into an error in computed satellite coordinates approximately given by

$$\varepsilon_{x_i^p} < |\dot{\mathbf{x}}^p| \varepsilon_{\Delta t} = 1.3 \times 10^{-5} \varepsilon_\rho, \quad (9.88)$$

since  $|\dot{\mathbf{x}}^p| \approx 3900$  m/s. Thus, even an initial 500 m position error causes an error in computed satellite coordinates of less than 1 cm due to the corresponding transit time uncertainty.

The covariance matrix,  $R_k$ , of the observation noise vector,  $\mathbf{v}_k$ , at epoch  $k$ , is a diagonal  $n_p \times n_p$  matrix of pseudorange error variances, under the assumption that the errors in tracking the various satellites at an epoch are uncorrelated (negligible interchannel biases in the receiver). It is further assumed that the errors from epoch to epoch are uncorrelated. Correlations could be included as necessary by adding appropriate error states, as developed in Section 7.5.1.

The estimates of the system states and their covariance matrix at epoch  $k$  are given by (7.72) and (7.73) with obvious notational substitutions ( $\varepsilon$  for  $\mathbf{x}$ , etc.). The covariance matrix can also be written in the form (7.43):

$$P_k^{-1} = (P_k^-)^{-1} + H_k^T R_k^{-1} H_k^{-1}, \quad (9.89)$$

which expresses the increase in information as a result of the innovation. If there is

no statistical capability to predict a position from the previous estimate, as in (9.69) ( $Q_k \rightarrow \infty$ ), then the a priori information,  $(P_k^-)^{-1}$ , is zero; and, the covariance of the estimate depends entirely on the information provided by the observations:

$$P_k = (H_k^T R_k^{-1} H_k)^{-1}. \quad (9.90)$$

Assuming all observation errors have equal variance,  $\sigma_{p,k}^2$ , we have

$$P_k = \sigma_{p,k}^2 (H_k^T H_k)^{-1}. \quad (9.91)$$

To estimate the three receiver coordinate errors and the clock error ( $m = 4$  states) requires at least four observations ( $n_p \geq 4$ ). However, it is the geometry of the satellites relative to the receiver, as embodied in the matrix,  $H_k$  (containing the unit vectors, (9.83)), that is critical to the magnitudes of the variances and correlations of the estimated states, where high correlation implies that corresponding states are not independently estimable. If the satellite geometry is such that the matrix  $H_k^T H_k$  approaches near singularity, then the variances of the estimated states become large. Formally, this *dilution of precision* (DOP) due to unfavorable satellite geometry is measured by the diagonal elements of the unitless matrix,  $(H_k^T H_k)^{-1}$ . The *geometric dilution of precision* (GDOP) is the square root of the trace of this  $4 \times 4$  matrix:

$$\text{GDOP}_k = \sqrt{\text{tr}(H_k^T H_k)^{-1}}. \quad (9.92)$$

Other specific DOP's may be defined; for example, the *position dilution of precision* (PDOP) is the square root of the sum of the first three diagonal elements of  $(H_k^T H_k)^{-1}$ ; and the *time dilution of precision* (TDOP) is the square root of the fourth diagonal element of  $(H_k^T H_k)^{-1}$ . Knowing the range error variance and the PDOP, one can quickly judge the corresponding positioning accuracy.

Other types of GPS observables, such as the phase and combinations of phase or pseudorange, are processed similarly in kinematic positioning. For example, one could use the ion-free, single-difference phases to obtain precise positioning if the satellite clock errors are known (and other systematic effects, such as tropospheric refraction and multipath can be modeled or are negligible). In this case, the modified cycle ambiguity (9.39) must be established initially with methods, such as described by Mader (1992), or as a random constant in a Kalman filter as shown here.

The observation model for the ion-free, single-difference pseudoranges and phases is given from (9.55) by

$$\begin{aligned} (\Delta s_{\text{ion-free}})_r^{p,q}(\tau_k) &= \Delta \rho_r^{p,q}(\tau_k) + \Delta \varepsilon_{\rho_{\text{ion-free}}, r}^{p,q}, \\ (\Delta \phi_{\text{ion-free}})_r^{p,q}(\tau_k) &= \frac{1}{\lambda_1} \Delta \rho_r^{p,q}(\tau_k) - \Delta N_{\text{ion-free}}^{*p,q} + \Delta \varepsilon_{\phi_{\text{ion-free}}, r}^{p,q}, \end{aligned} \quad (9.93)$$

where the range differences have already been corrected for satellite clock errors, and

$$\Delta N_{\text{ion-free}}^{*p,q} = \frac{1}{1 - \alpha} (\sqrt{\alpha} \Delta N2_r^{*p,q} - \alpha \Delta N1_r^{*p,q}) \quad (9.94)$$

is a constant for each pair of satellites,  $p$  and  $q$ . The cycle length of the ion-free

phase is  $\lambda_1$ , but the pseudorange observations may help, at least initially, to solve for the ambiguity (note that it can not be constrained as an integer).

The states in the Kalman filter are now

$$\boldsymbol{\varepsilon}_k = \begin{pmatrix} \delta \mathbf{x}_r(\tau_k) \\ \vdots \\ \Delta N_{\text{ion-free}}^{*(p,q)} \\ \vdots \end{pmatrix}. \quad (9.95)$$

The dimension of this vector is  $3 + n_{p,q}$ , depending on the number,  $n_{p,q}$ , of satellite pairs tracked per epoch. The notation assumes that the initial state value of the ion-free ambiguity is zero (i.e., no  $\delta$ -notation), meaning that most of the total cycle count comes immediately from the pseudorange observation. The dynamics of the position error states were discussed in Section 9.6.1 and the ion-free ambiguity is modeled as a random constant (independent of the time,  $\tau_k$ ).

The observation matrix corresponding to the linearized form of (9.93) is easily obtained analogous to previous developments. From the difference of ranges, given by (9.66), we find:

$$\begin{aligned} \frac{\partial(\Delta s_{\text{ion-free}})^{p,q}(\tau)}{\partial \mathbf{x}_r} &= \frac{-1}{\rho_r^p(\tau)} [\mathbf{R}_3(\Delta t_r^p \omega_e) \mathbf{x}^p(\tau - \Delta t_r^p) - \mathbf{x}_r(\tau)]^T \\ &\quad + \frac{1}{\rho_r^q(\tau)} [\mathbf{R}_3(\Delta t_r^q \omega_e) \mathbf{x}^q(\tau - \Delta t_r^q) - \mathbf{x}_r(\tau)]^T, \end{aligned} \quad (9.96)$$

and a similar expression for the ion-free, single-difference phase:

$$\frac{\partial(\Delta \phi_{\text{ion-free}})^{p,q}(\tau)}{\partial \mathbf{x}_r} = \frac{1}{\lambda_1} \frac{\partial(\Delta s_{\text{ion-free}})^{p,q}(\tau)}{\partial \mathbf{x}_r}. \quad (9.97)$$

From these we construct the  $2n_{p,q} \times (3 + n_{p,q})$  observation matrix,  $H_k$ , with  $n_{p,q}$  submatrices, each having dimension  $2 \times (3 + n_{p,q})$  and the form:

$$(H_k)_{p,q} = \begin{pmatrix} -[\tilde{\mathbf{e}}_r^{p,q}(\tau_k)]^T & \cdots 0 \cdots & 0 & \cdots 0 \cdots \\ -\frac{1}{\lambda_1} [\tilde{\mathbf{e}}_r^{p,q}(\tau_k)]^T & \cdots 0 \cdots & -1 & \cdots 0 \cdots \end{pmatrix}; \quad (9.98)$$

that is, the right-hand side is a representative set of two rows in  $H_k$  for the satellite pair  $(p, q)$ . The symbol  $\cdots 0 \cdots$  in each row denotes a string of zeros, its length depending on the ordering of the satellite pairs; and, from (9.83),

$$\tilde{\mathbf{e}}_r^{p,q}(\tau_k) = \tilde{\mathbf{e}}_r^p(\tau_k) - \tilde{\mathbf{e}}_r^q(\tau_k). \quad (9.99)$$

(It is not a unit vector.)

The covariance matrix for the observations is most easily determined with the rule for propagation of covariances (exemplified for the Gaussian case by (6.33) and (6.35), but holding in general). Let

$$\mathbf{\Lambda} = (\cdots \ s1_r^p \ s2_r^p \ \cdots \ \phi1_r^p \ \phi2_r^p \ \cdots)^T \quad (9.100)$$

be the  $4n_p \times 1$  vector of pseudoranges and phases for all  $n_p$  satellites; and let

$$\Xi = A\Lambda \quad (9.101)$$

be the  $n_{p,q} \times 1$  vector of combination observables. The rows of the  $n_{p,q} \times 4n_p$  matrix,  $A$ , have zeros except in those columns corresponding to a pseudorange or phase observable that is used in the combination. In that case the row element is the appropriate coefficient determined from (9.48), (9.49), and (9.53). The covariance matrix is then:

$$R = \mathcal{E}(\Xi\Xi^T) = AW\Lambda A^T, \quad (9.102)$$

where

$$W = \mathcal{E}(\Lambda\Lambda^T) = \text{diag}(\dots \sigma_{s1}^2 \sigma_{s2}^2 \dots \sigma_{\phi1}^2 \sigma_{\phi2}^2 \dots) \quad (9.103)$$

is the  $4n_p \times 4n_p$  diagonal matrix of variances of the presumably uncorrelated errors in  $\Lambda$ .  $R$  is not diagonal if different combinations share an observed pseudorange or phase.

#### 9.6.4 Multiple-Receiver Case

Relative kinematic positioning involves more than one receiver, the objectives being to eliminate the satellite clock errors (particularly the effect of SA), as well as to cancel other common systematic errors; the latter is especially successful for small baselines. We consider only two receivers, where one receiver is the rover and the other is either the base receiver or another moving receiver. An obvious generalization of this concept expands the number of stationary and moving receivers to more than two; and it is only a matter of careful bookkeeping to accommodate this situation in the Kalman filter estimation procedure.

For (any) two receivers, one forms double differences by differencing two single-difference observables, as defined in (9.56), (9.61), and (9.62). The geometry of the receivers and satellites is only sufficiently strong to determine coordinate differences,  $\mathbf{x}_{r,s} = \mathbf{x}_r - \mathbf{x}_s$ , between receivers. Corresponding errors in  $\mathbf{x}_{r,s}$  now enter as system states; however, if the base station coordinates are assumed fixed, they are equivalent to errors in the coordinates of the roving receiver:

$$\delta\mathbf{x}_{r,s}(\tau_k) = \delta(\mathbf{x}_r - \mathbf{x}_s)(\tau_k) = \delta\mathbf{x}_r(\tau_k). \quad (9.104)$$

This means that the partial derivatives in the observation matrix,  $H_k$ , associated with the coordinate difference errors are the same as for the single-receiver case; for example:

$$\frac{\partial\Delta s_{r,s}^{p,q}(\tau)}{\partial\mathbf{x}_{r,s}} = \frac{\partial\Delta s_{r,s}^{p,q}(\tau)}{\partial\mathbf{x}_r} = \frac{\partial\Delta s_r^{p,q}(\tau)}{\partial\mathbf{x}_r}, \quad \frac{\partial\Delta\phi_{r,s}^{p,q}(\tau)}{\partial\mathbf{x}_{r,s}} = \frac{\partial\Delta\phi_{r,s}^{p,q}(\tau)}{\partial\mathbf{x}_r} = \frac{\partial\Delta\phi_r^{p,q}(\tau)}{\partial\mathbf{x}_r}. \quad (9.105)$$

One strategy to deal with the phase ambiguities in this case takes advantage of the fact that the doubly differenced ambiguity is an integer. This provides a powerful constraint that allows the observed phases to yield their full precision potential. For short baselines (e.g., at the beginning of a trajectory when the rover and base station

are close), the differential ionospheric delay,  $\Delta I_{r,s}^{p,q}$ , may be omitted, and the doubly differenced (L1) pseudorange and wide-lane phase,

$$\begin{aligned}\Delta s_{r,s}^{p,q}(\tau_k) &= \Delta \rho_{r,s}^{p,q}(\tau_k) + \Delta \varepsilon_{\rho,r,s}^{p,q}, \\ \Delta \phi w_{r,s}^{p,q}(\tau_k) &= \frac{1}{\lambda_w} \Delta \rho_{r,s}^{p,q}(\tau_k) - \Delta N w_{r,s}^{p,q} + \Delta \varepsilon_{\phi w,r,s}^{p,q},\end{aligned}\quad (9.106)$$

can be used to solve for the wide-lane, double-difference ambiguity,  $\Delta N w_{r,s}^{p,q}$ . The  $1 + n_{p,q}$  system states during this first stage of data processing are simply

$$\boldsymbol{\varepsilon}_k = \begin{pmatrix} \delta \Delta \rho_{r,s}^{p,q}(\tau_k) \\ \vdots \\ \Delta N w_{r,s}^{p,q} \\ \vdots \end{pmatrix}. \quad (9.107)$$

The  $2n_{p,q} \times (1 + n_{p,q})$  observation matrix,  $H_k$ , is represented by the  $2 \times (1 + n_{p,q})$  submatrix:

$$(H_k)_{p,q} = \begin{pmatrix} 1 & \cdots 0 \cdots & 0 & \cdots 0 \cdots \\ \frac{1}{\lambda_w} & \cdots 0 \cdots & -1 & \cdots 0 \cdots \end{pmatrix}. \quad (9.108)$$

The ambiguities are set to the integer values nearest the corresponding estimates determined by the Kalman filter.

Subsequently, with these resolved, the wide-lane phase observables (9.61) are processed a second time in a Kalman filter with the following states (the ambiguities are now absent)

$$\boldsymbol{\varepsilon}_k = \begin{pmatrix} \delta \mathbf{x}_{r,s}(\tau_k) \\ \vdots \\ \Delta I_{r,s}^{p,q} \\ \vdots \end{pmatrix}, \quad (9.109)$$

where the ionospheric delays may be modeled as stochastic processes with assumed correlation functions (e.g., the first-order Gauss-Markov process). The observation matrix,  $H_k$ , in this case consists of the following  $n_{p,q}$  rows, each containing  $3 + n_{p,q}$  elements:

$$(H_k)_{p,q} = \left( -\frac{1}{\lambda_w} [\tilde{\mathbf{e}}_r^{p,q}(\tau_k)]^T \quad \cdots 0 \cdots \quad \frac{1 - \sqrt{a}}{\lambda_1} \quad \cdots 0 \cdots \right), \quad (9.110)$$

with due consideration of (9.105). As in the single-receiver case, the noise vector,  $\mathbf{v}_k$ , of the combination observables and its covariance matrix,  $R$ , must represent the corresponding combinations of pseudorange and phase noises; see (9.102). The results of this second stage of processing are the position errors of the roving receiver at epoch,  $t_k$ .

As an alternative approach, one could try to resolve the L1 ambiguity, as well, during an intermediate processing stage using the ion-free, double-difference phases, re-formulated from (9.62) and with  $\Delta Nw = \Delta N1 - \Delta N2$ :

$$(\Delta\phi_{\text{ion-free}})^{p,q}_{r,s}(\tau_k) = \frac{1}{\lambda_1} \Delta\rho^{p,q}_{r,s}(\tau_k) - \frac{\sqrt{\alpha}}{1-\alpha} ((1-\sqrt{\alpha}) \Delta N1^{p,q}_{r,s} - \Delta Nw^{p,q}_{r,s}) + \Delta\varepsilon^{p,q}_{\phi_{\text{ion-free}}, r,s}, \quad (9.111)$$

where now the wide-lane ambiguity is already known. Once the L1 ambiguity is resolved, the final stage of processing makes full use of the phase (either ion-free or with stochastic models for the ionospheric delay) as a very precise measurement of range to solve for the vehicle's position.

Many other strategies have been employed to resolve the ambiguities and to proceed with the data processing for precise kinematic positioning. Only a few options were presented here to illustrate the basic problems. Often different schemes must be tested to adapt to the particular circumstances of the vehicle's trajectory. In particular, frequent cycle slips or loss of lock will cause the most serious degradation in positioning accuracy, especially if the ambiguities cannot be resolved on the fly in a timely manner. Once the ambiguities are resolved, of course, they can be applied backward in time to the point where the cycle slip or loss of lock occurred.

# 10 Geodetic Application

## 10.1 Introduction

Previous chapters described the inertial navigation system (INS), its component sensors and how they operate, the mathematics behind the solution for position and velocity, and the associated errors and methods to estimate them on the basis of stochastic models. In essence, we showed how the basic sensors of an INS, the accelerometers, measure accelerations of the vehicle carrying the INS, and how the gyroscopes provide the necessary orientation of the measured accelerations in the navigation coordinate frame. Given initial conditions for the position and velocity of the vehicle, the measured accelerations are integrated in time to yield a navigation solution, that is, the vehicle's position and velocity, for all subsequent times of its trajectory. As such, the INS is a self-contained, autonomous navigation system, requiring only an initialization that supplies the integration constants. The errors in positioning grow with time and the rate of growth is a function of the accuracy of the sensors, primarily the gyros. Occasionally, external position or velocity information may be used to re-calibrate the sensor errors using optimal estimation techniques and thus reduce or bound the positioning errors.

Depending on the breadth of definition of geodesy, inertial navigation systems inherently are geodetic instruments. Geodesy is the science of the measurement and mapping of the Earth's surface, of which determining coordinates of points on the Earth's surface is the ultimate objective. That is precisely what an INS does for a moving vehicle; it determines the coordinates of the vehicle along its trajectory. The two-fold integration of sensed acceleration to determine coordinate differences with respect to a starting point deviates only in concept from the more traditional surveying technique of running a traverse by measuring distances with tape or with electronic distance meters and directions (and angles) with a theodolite (or both range and angles using a total station surveying apparatus). Even the earliest motivation for developing the gyroscope, that of providing a reference direction for marine navigation, was essentially geodetic in nature. On the other hand, modern geodesy deals with positional accuracy on the order of 10 cm or often much better; whereas, the INS by itself, because of the cumulative character of its errors, is generally consigned to applications requiring accuracy worse by three or four orders of magnitude, if operated autonomously for periods as short as one hour. Historically, these applications resided mostly in coarse navigational needs, where accuracy in destination would suffice at the level of a kilometer. This distinguishes the INS from traditional geodetic instrumentation. Also, its primary purpose of real-time operation further deprives it of the usual, post-mission, constrained adjustment of errors that is the hallmark of geodesy.

In fact, real-time navigation and guidance were the principal motivations to develop the INS. Precise geodetic positioning (post-mission) was rarely the stimulus to drive the inertial technology because throughout INS development, geodesy already had

many established methods of much higher accuracy at its disposal; and, therefore, no immediate need existed to incorporate the INS into its arsenal of position determination techniques. Yet the INS possesses some advantages not easily duplicated by traditional geodetic methods. These include the speed with which the INS yields measurements and the freedom from the dependence on lines of sight between survey points. The labor of field surveying is the single most expensive aspect of geodesy, and the prospect of saving man-hours of work in surveying a single point was enough to motivate several investigators to consider the utility of adapting the INS to geodetic surveying applications.

The burgeoning development of the Global Positioning System (GPS) over the last two decades has all but displaced every other positioning and navigation system, whether radio system or inertial system, in most commercial, recreational, and many military applications. Furthermore, because of its relatively low cost to the user, its high accuracy of better than 100 m (and even much better without Selective Availability; Section 9.4) in absolute positioning, and orders of magnitude more accurate in relative positioning, GPS offers broad capabilities not easily duplicated with other systems, both in real time and especially in post-mission trajectory determination.

In terms of the proportion of activity within a single discipline, GPS arguably has had the most profound impact in geodesy. However, even here GPS cannot fill all kinematic positioning needs in spatial data referencing and geodetic surveying. It is limited to areas that have a clear “view” of a sufficient number of GPS satellites. Thus, for example, GPS is useless or nearly so under water (ocean floor positioning), in tunnels, and in thickly foliated regions, very rugged terrain, and areas of densely constructed high-rise buildings. Difficulties can arise also near strong electromagnetic fields and radiation areas, such as high-tension wires, radio and television towers, and in areas replete with multipath sources, that is, large reflecting nearby structures. In addition, navigation and guidance developers, especially for aviation (military and commercial) and missile systems, would rather not rely exclusively on a navigation system that could easily be turned off (intentionally) or electronically jammed (intentionally or not).

These and other less severe encumbrances (such as the pervasive cycle slip in the GPS phase signal) offer an advantageous, if limited, niche for the inertial navigation system as an aid to or a temporary replacement of the positioning and navigation utility derived from GPS. The INS is essentially autonomous, its operation depending neither on signal transmissions nor receptions from an external source. Only initial and possibly occasional external velocity or position updates are needed to calibrate its errors. In many other ways the INS and GPS are complementary devices that together, in an integrated fashion, yield a more robust positioning and navigation system.

GPS and INS are functionally also quite distinct and this fact can be used, for example, to measure the gravity field or to provide three-dimensional orientation in addition to position of the vehicle. In particular, the gravimetric application has significant implications in regional geoid determination and in geophysical problems including mineral and oil exploration. These diverse facets of the INS in geodesy, its

utilization as a supplement to traditional surveying methods, its integration with GPS for precise positioning, and its combination with GPS for gravimetry are the subjects of this chapter.

## 10.2 Inertial Survey System

As the name implies, an *inertial survey system* is designed for precise determination of point coordinates in a geodetic network rather than for real-time trajectory determination, or navigation. Thus, while the sensor assembly is an IMU (often adapted from an INS) and the system dynamics model is based on the usual navigation equations for an INS, the data are analyzed and processed with a sufficient amount of external information to maintain tight control on the well known accumulation of errors (Chapter 5) in order to achieve geodetic levels of accuracy. The usual application is the determination of the three-dimensional coordinates of points along a traverse that connects two points with known coordinates. The points along the traverse may be visited by a land-vehicle or by a helicopter, and the time spent to cover such a traverse typically ranges from under one up to two or three hours. Many traverses may be combined to survey a longer traverse or an area network of points. Although preliminary solutions for the coordinates can be determined in near real-time in the field using a Kalman filter or smoother, best results are obtained with a post-mission least-squares adjustment of the entire network. Thus, the inertial survey incorporates several aspects or stages of error control and optimization.

### 10.2.1 Historical Developments

The origins of the inertial survey system can be traced back to efforts by the U.S. Army Engineer Topographic Laboratories (USAETL) that in the early 1960's began supporting research and development of systems to measure precise positions (three-dimensional) and azimuth in the field in near real time. Fortunately, this development just followed the formulation and application of the Kalman filter that is now the essence of optimal error control in linear dynamic systems. It was immediately applied to control the inertial survey system errors using external information such as velocity or position updates.

The first successful geodetic inertial surveyor, the Position and Azimuth Determination System (PADS), was developed by Litton Guidance and Control Systems, Inc., in the early 1970's (Huddle and Maughmer, 1972) in response to USAETL military requirements. The goal with this system was to demonstrate positioning accuracy of 10 m in elevation and about 20 m in horizontal position for missions up to 6 hours in duration. Also, the accuracy of the estimated azimuth was to remain under 1 arcmin during that time. Originally outfitted with an odometer and a laser velocimeter as external sensors to control the growth of errors, the occasional full stop of the system for short duration proved to be a sufficient, as well as more efficient, technique for estimating errors of the system and thus bounding the INS

position errors. This allowed the system to operate otherwise in the free-inertial mode. The so-called ZUPT's (zero-velocity updates) would become a standard operational procedure for all land-vehicle and helicopter inertial surveying systems.

The IMU of the PADS consisted of two TDF, air-bearing gyros and three force-rebalance accelerometers on a Schuler-tuned (local-level), north-slaved (NED) stabilized platform. The horizontal and vertical position coordinates were obtained from the usual navigation equations, such as (4.91). Note that because of the damping in the vertical channel using the velocimeter and (or only, but then more frequent) ZUPT's, positioning is possible in all three dimensions (see Section 5.2). The error dynamics model used in the Kalman filter controller was simplified by eliminating most of the cross-coupling terms that have negligible effect during the relatively short duration of free-inertial navigation between ZUPT's, or that would masquerade as existing sensor errors and thus could be treated as inseparable from them. In particular, only those interactions between platform orientation errors were retained that contribute to azimuth misalignment error. Also, because of the external control on navigation errors, the effect of the accumulation of position error on the dynamics model could be neglected, as could the Foucault oscillation terms. Finally, the platform tilt errors that enter as vertical acceleration errors (first two elements of the sixth row of the error dynamics matrix,  $F''$ , equation (5.67)) were accommodated implicitly within the accelerometer error states. Through these types of considerations and analyses, the design of the dynamics matrix reduced the number of couplings between the nine navigation error states from 34 to 13. These simplifications, moreover, completely decoupled the horizontal and vertical channels, and the system errors could be controlled by two independent Kalman filters, one for horizontal position and orientation and the other for vertical position. Clearly, the motivation for this design was strictly one of computational efficiency which, with today's computing capability, may no longer be as important an issue.

The sensor errors as well as the effects of unknown gravity components were modeled with additional states as described in Chapter 6. The accelerometer error model included a (non-repeatable, or random) bias and first-order Gauss-Markov correlated noise. The model for the gravity error also assumed the characterization of an exponentially correlated noise, but with correlation time varying with the speed of the vehicle. The gyro error models comprised a (non-repeatable) rate bias, scale factor error, and first-order Gauss-Markov correlated noise. Other error sources associated with the accelerometer (velocity quantization error) and with the odometer and velocimeter (scale factor errors and misalignments) that could be interpreted as stochastic in nature were similarly modeled.

The demonstrated success of the militarily oriented PADS and its predicted high accuracy with additional external error control spurred the development of inertial surveying systems for applications more specifically applicable to surveys of high geodetic quality, meaning position accuracies of the order of 10 cm, or better. The Litton PADS evolved under different names associated with different users (e.g., Inertial Positioning System (IPS), U.S. Defense Mapping Agency; Inertial Surveying System (ISS), Canadian Department of Energy, Mines, and Resources;

and Rapid Geodetic Survey System (RGSS), USAETL and U.S. Defense Mapping Agency; among others). In addition, other leading manufacturers of inertial navigation systems introduced inertial surveying systems. Honeywell, Inc., developed the Honeywell Geo-Spin system, a *space*-stabilized system whose orientation was maintained by two electrically suspended TDF gyros (Hadfield, 1978). Also, Ferranti Ltd., of Scotland, in the later 1970's developed the Ferranti Inertial Land Surveyor (FILS), being a descendant of its own PADS built for the British military (Hagglund and Hittel, 1977). Like the Litton system it uses local-level stabilization and the IMU consists of three viscous damped accelerometers and three SDF floated, rate-integrating gyros.

A fixed-wing airborne survey system was developed by the Charles Stark Draper Laboratory (Hursh et al., 1977). Comprising a gimbaled IMU for positioning, a laser tracker for error control (observation updates), and a laser altimeter profiling system, the positioning technology of this so-called Aerial Profiling of Terrain System (APTS) was a precursor to systems that today are developed exclusively around GPS, though perhaps aided by INS; see Section 10.3.

The Kalman filter designs for each system were similar in that they incorporated the usual set of position, velocity, and orientation error states (5.64), as well as several states for the IMU errors, such as accelerometer biases, scale factor errors, gyro drifts, gravity disturbance components, and sensor misalignments, or a linear combination thereof (owing to the non-estimability of individual effects), and external sensor errors as appropriate. Despite these elaborate system error dynamics models, however, it was recognized that to achieve geodetic accuracies of even better than ten meters, one cannot rely on the Kalman filter alone to remove or estimate all systematic errors using ZUPT's. We have already found in Chapter 8 (Fig. 8.1) that the azimuth (down orientation) error is rather poorly estimated with velocity updates; but azimuth error affects the north velocity and hence north position error through the east orientation error (see (5.71) and (5.74)). This is particularly serious in traverses that are L-shaped (or contain significant turns). To control this error requires additional information in the form of external azimuth transfers or known coordinates at both endpoints of the traverse.

The processing of data from an inertial survey system thus developed into two or three distinct stages. The first stage deals with the system errors and their estimability through the Kalman filter based on a presumed model of the system error dynamics and zero-velocity updates along the trajectory. The second stage improves upon this with some form of optimal smoothing where further systematic errors are accounted for using all information for the traverse, such as known endpoint coordinates. Finally, if more than one traverse constitutes a survey network, a third stage can be applied wherein additional constraints imposed by the geometry of the traverses are used to eliminate any remaining inconsistencies. For example, two traverses crossing the same point clearly should yield the same set of coordinates for that point. These constraints, such as provided by the cross-over points and repeated runs of the same traverse, as well as other external observations (for example, distances between points of the same or different traverses) are used in

a final post-mission least-squares adjustment. The second and third stages can be combined in one unified adjustment.

### 10.2.2 Estimation Methods

It is known that such comprehensive adjustments of many data, and especially the determination of reliable standard deviations for the coordinate estimates, depend on appropriate weighting factors for the data, which derive from their covariance matrix. However, especially in the first stage of data processing, such covariance matrices were rarely available for intermediate points of the traverse, since by its recursive nature the Kalman filter has no need to retain a covariance history of its states. Most of the inertial survey system analyses and software developments by users, therefore, concentrated on smoothing procedures and post-mission adjustments. These were based largely on parametric models of systematic errors deemed as still remaining in the Kalman-filtered solution. A unified approach in terms of least-squares adjustments may be developed that generally expresses both the smoothing procedures and the network coordinate adjustments (Schwarz, 1985). Least-squares adjustment formulas are well known in geodesy (Koch, 1987; Leick, 1995) and are based essentially on the criterion (7.14). Under the assumption of normally distributed observation errors, the least-squares estimation formulas are those for a single observation update cycle in the Kalman filter; and, this provides the basis of the following discussions.

#### 10.2.2.1 Models and Observations

Two types of parameters enter into the adjustment, position coordinate errors,  $\delta\mathbf{x}$ , and system error parameters,  $\mathbf{s}$ , that could not be estimated with the initial Kalman filter of the first stage of data processing. The coordinate errors further fall into two categories: those associated with control point coordinates and those without any external control. Also, it is assumed that the remaining systematic error parameters, though stochastic, do not behave as stochastic processes, since only a single (non-recursive) adjustment will be performed (however, their effect on coordinate errors may be modeled as a function of time, as illustrated below). As such, the remaining errors are essentially empirical in nature, being represented by simple functions thought to describe their variation along the traverse. For the  $\ell^{\text{th}}$  traverse, the *total* coordinate errors at any point are assumed to be related to the empirical system errors according to the model

$$\delta\mathbf{x}_{\text{tot},\ell} = \delta\mathbf{x}_\ell + H_{s,\ell}\mathbf{s}_\ell, \quad (10.1)$$

where  $\mathbf{s}_\ell$  may be a different set of parameters for each traverse and  $H_{s,\ell}$  is an appropriate coefficient matrix. The coordinate errors,  $\delta\mathbf{x}_\ell$ , are those that remain after the system errors have been removed.

A typical set of systematic error parameters may be based, for example, on gyro drift biases and initial velocity errors. The latter would account for the effect of an accelerometer scale factor error,  $\kappa_a$ , during the initial acceleration,  $a$ , of the vehicle after a ZUPT. The initial velocity error is then  $\delta v = \kappa_a a \delta t$ ; and if  $\delta t$  is a short time

interval and  $a = \text{constant}$  during this interval, the velocity error propagates into position error according to (5.12) or (5.13):

$$\delta x = \delta v \sin \omega_S \Delta t \approx \delta v \omega_S \Delta t, \quad (10.2)$$

where  $\omega_S$  is the Schuler frequency and  $\Delta t$  is the time from the last ZUPT. The approximation in (10.2) is accurate to better than a part in a thousand if  $\Delta t$  is less than fifteen minutes. Similarly, an initial orientation error in azimuth,  $\psi_D$  (or, equivalently, a non-orthogonality between the horizontal accelerometer input axes), causes an initial velocity error,  $\delta v = \psi_D a \delta t$ , again leading to the type of position error given by (10.2). On the other hand, a drift error,  $\delta \omega_G$ , in the east or north gyro, representing a forcing error term, leads to a position error of the type (5.24), which with (5.26) becomes:

$$\delta x \approx \frac{g}{6} \delta \omega_G \Delta t^3. \quad (10.3)$$

From (5.71) and (5.74), we see that north and east position errors, as implied by corresponding velocity errors, are cross-coupled; and all gyro drift biases eventually couple into each position error. Thus, for example, the latitude (north coordinate) error,  $\delta \phi \approx \delta x / R$ , depends, through the terms involving  $\Delta t$ , not only on the latitude displacement of the vehicle,  $\Delta \phi$  ( $\Delta t \approx R \Delta \phi / v_N$ , if  $v_N$  is approximately constant; see (4.103)), but also on the longitude displacement,  $\Delta \lambda$  ( $\Delta t \approx R \Delta \lambda \cos \phi / v_E$ ), along the traverse. In general, one might consider an error model for  $H_{s,\ell,s}$ , based on theoretical considerations, as above, or based on empirical analyses of a particular system operated in a controlled survey environment. In the latter case the errors could be modeled as linear or higher-order polynomials in coordinate or time differences, thus representing a variety of combined residual systematic sensor and navigation algorithm errors. An example of such an empirical model was determined by Hannah (1982a) for the IPS, where

$$\mathbf{s}_\ell = (s_{\phi 1} \ s_{\phi 2} \ s_{\phi 3} \ s_{\lambda 1} \ s_{\lambda 2} \ s_{\lambda 3} \ s_{h 1} \ s_{h 2} \ s_{h 3})_\ell^T, \quad (10.4)$$

and the parameter coefficient matrix is given by  $H_{s,\ell} = (\cdots \ (H_{s,\ell})_j^T \ \cdots)^T$ , where

$$(H_{s,\ell})_j = \begin{pmatrix} \Delta \phi_j & \Delta \lambda_j & \Delta \lambda_j^2 & 0 & 0 & 0 & 0 & 0 & 0 \\ 0 & 0 & 0 & \Delta \phi_j & \Delta \lambda_j & \Delta \lambda_j^2 & 0 & 0 & 0 \\ 0 & 0 & 0 & 0 & 0 & 0 & \Delta \phi_j & \Delta \lambda_j & \Delta t_j \end{pmatrix}, \quad (10.5)$$

for the  $j^{\text{th}}$  point in the traverse. The  $\Delta$ 's designate differences between a point in the traverse and its previous ZUPT point. Similar models were reviewed and examined by Schwarz (1981), Schwarz and Gonthier (1981), and Hannah (1982b).

At the  $j^{\text{th}}$  point of the  $\ell^{\text{th}}$  traverse, the errors in coordinates (relative to some initial point) are  $\delta \mathbf{x}_{\ell,j} = ((M + h)\delta \phi, (N + h) \cos \phi \delta \lambda, -\delta h)_{\ell,j}^T$  (see (5.53)), and in total,  $\delta \mathbf{x}$ , comprises the errors of coordinates for all points along all traverses where it is desired that the system indicate a position. At non-control points, the initial estimate of the error cannot be improved since no external observations of coordinates are available. Therefore, in the following, we restrict the estimation to errors,  $\delta \mathbf{x}_c$ , in coordinates of control points within the geodetic network to be surveyed.

At these control points, we compute the differences between coordinates indicated by the inertial survey system after the filtering (closed-loop mode, Section 7.5.2) of the first stage of processing and the coordinates obtained by some external means (e.g., with GPS, or from conventional surveys). We assume in accordance with (7.52) that the parameters,  $\delta\mathbf{x}_c^T = (\dots \quad \delta\mathbf{x}_{c,\ell}^T \quad \dots)$  and  $\mathbf{s}^T = (\dots \quad \mathbf{s}_\ell^T \quad \dots)$ , are related linearly to these observations:

$$\mathbf{y} = (H_{x_c} \quad H_{s_c}) \begin{pmatrix} \delta\mathbf{x}_c \\ \mathbf{s} \end{pmatrix} + \mathbf{v}, \quad (10.6)$$

where  $H_{s_c} = (\dots \quad H_{s_c,\ell}^T \quad \dots)^T$ , only for control points, and  $\mathbf{v} \sim \mathcal{N}(0, R)$ . The observation error, presumed to be white noise, is due to the inaccuracy of the externally provided control point coordinates, as well as noise in the registration of the inertial survey system relative to the ground marker.  $H_{x_c}$  is the identity matrix if the total coordinate error vector is observed directly.

We may assume that we have some a priori estimates for these parameters, say  $\delta\mathbf{x}_c^-$  (from the Kalman filter) and  $\mathbf{s}^-$ , consistent with our earlier notation for linear recursive estimation; and we suppose the existence of a priori covariance matrices, where the two sets of initial estimates are uncorrelated:

$$\text{cov}\left(\begin{pmatrix} \delta\mathbf{x}_c^- \\ \mathbf{s}^- \end{pmatrix} ((\delta\mathbf{x}_c^-)^T \quad (\mathbf{s}^-)^T)\right) = \begin{pmatrix} P_{x_c}^- & 0 \\ 0 & P_s^- \end{pmatrix}. \quad (10.7)$$

$P_{x_c}^-$  is the covariance matrix of the Kalman-filtered estimates of coordinates at control points along the traverse.  $P_s^-$  is a model for the covariance of the system error parameters that must be chosen suitably.

### 10.2.2.2 Parameter Estimation

The a posteriori estimates of the parameters are given by (7.72), where the Kalman gain matrix is, from (7.74)

$$K = \begin{pmatrix} P_{x_c}^- & 0 \\ 0 & P_s^- \end{pmatrix} \begin{pmatrix} H_{x_c}^T \\ H_{s_c}^T \end{pmatrix} (H_{x_c} P_{x_c}^- H_{x_c}^T + H_{s_c} P_s^- H_{s_c}^T + R)^{-1}. \quad (10.8)$$

With the assumption that the initial estimates are  $\delta\mathbf{x}_c^- = \mathbf{0}$  (closed-loop filtering) and  $\mathbf{s}^- = \mathbf{0}$ , the a posteriori estimates, in the form of (7.72), are

$$\hat{\delta}\mathbf{x}_c = P_{x_c}^- H_{x_c}^T (H_{x_c} P_{x_c}^- H_{x_c}^T + H_{s_c} P_s^- H_{s_c}^T + R)^{-1} \mathbf{y}, \quad (10.9)$$

$$\hat{\mathbf{s}} = P_s^- H_{s_c}^T (H_{x_c} P_{x_c}^- H_{x_c}^T + H_{s_c} P_s^- H_{s_c}^T + R)^{-1} \mathbf{y}. \quad (10.10)$$

The covariance matrix of these estimates is given by (7.42) or (7.73). Using the former, we have

$$\begin{pmatrix} P_{x_c} & P_{x_c s} \\ P_{s x_c} & P_s \end{pmatrix} = \begin{pmatrix} P_{x_c}^- & 0 \\ 0 & P_s^- \end{pmatrix} - \begin{pmatrix} P_{x_c}^- H_{x_c}^T \\ P_s^- H_{s_c}^T \end{pmatrix} (H_{x_c} P_{x_c}^- H_{x_c}^T + H_{s_c} P_s^- H_{s_c}^T + R)^{-1} \times (H_{x_c} P_{x_c}^- \quad H_{s_c} P_s^-). \quad (10.11)$$

Note that the parameter estimates,  $\delta\hat{x}_c$  and  $\hat{s}$ , do not depend on each other, but their errors are correlated. This formulation breaks down if the a priori *information* matrix,  $(P_{x_c}^-)^{-1}$ , is partially, or wholly, equal to zero; or equivalently, if some or all of the coordinate errors are to be treated as non-random unknowns.

The following two matrix identities hold for non-singular matrices  $A$  and  $D$  (Henderson and Searle, 1981) and are used to transform the expressions for the estimates to slightly more convenient forms involving the information matrix,  $(P_{x_c}^-)^{-1}$ :

$$AB^T(BAB^T + D)^{-1} = (B^TD^{-1}B + A^{-1})^{-1}B^TD^{-1}, \quad (10.12)$$

$$(BAB^T + D)^{-1} = D^{-1} - D^{-1}B(B^TD^{-1}B + A^{-1})^{-1}B^TD^{-1}. \quad (10.13)$$

Let

$$C = H_{s_c} P_s^- H_{s_c}^T + R; \quad (10.14)$$

then, applying (10.12) with  $B = H_x$  and  $D \equiv C$  to (10.9) we find that

$$\delta\hat{x}_c = (H_{x_c}^T C^{-1} H_{x_c} + (P_{x_c}^-)^{-1})^{-1} H_{x_c}^T C^{-1} y. \quad (10.15)$$

Similarly, applying (10.13) to (10.10), we also find:

$$\begin{aligned} \hat{s} &= P_s^- H_{s_c}^T C^{-1} (I - H_{x_c} (H_{x_c}^T C^{-1} H_{x_c} + (P_{x_c}^-)^{-1})^{-1} H_{x_c}^T C^{-1}) y \\ &= P_s^- H_{s_c}^T C^{-1} (y - H_{x_c} \delta\hat{x}_c), \end{aligned} \quad (10.16)$$

where (10.15) was inserted. Corresponding covariance matrices are obtained similarly using (10.13) in (10.11) with  $D \equiv (P_{x_c}^-)^{-1}$  and  $D \equiv C$ , respectively:

$$\begin{aligned} P_{x_c} &= (H_{x_c}^T C^{-1} H_{x_c} + (P_{x_c}^-)^{-1})^{-1}, \\ P_s &= P_s^- - P_s^- H_{s_c}^T C^{-1} (I - H_{x_c} (H_{x_c}^T C^{-1} H_{x_c} + (P_{x_c}^-)^{-1})^{-1} H_{x_c}^T C^{-1}) H_{s_c} P_s^-. \end{aligned} \quad (10.17)$$

The formulations (10.15)–(10.17) clearly show the importance of the a priori coordinate error information in estimating the system error parameters. Suppose the observation matrix for the coordinate errors is the identity matrix ( $H_{x_c} = I$ ). If there is no prior information from the inertial system, then the external observation is used entirely to compute the error estimate,  $\delta\hat{x}_c$ ; and no improvement in the system parameters ensues:

$$(P_{x_c}^-)^{-1} = 0 \Rightarrow \delta\hat{x}_c = y \Rightarrow \hat{s} = \mathbf{0}, P_s = P_s^-. \quad (10.18)$$

### 10.2.3 Final Adjustments

The adjustment can proceed in several ways. The most rigorous and straightforward approach is to estimate the control point coordinate errors and system parameter errors for all traverses simultaneously using observations of all control point coordinates in the network. Then the coordinate error estimates at all points of the  $\ell^{\text{th}}$  traverse are given with (10.15) and (10.16) and (10.1) by

$$\delta\hat{x}_{tot,\ell} = \delta\hat{x}_\ell + H_{s,\ell} \hat{s}_\ell, \quad (10.19)$$

where  $\delta\hat{x}_\ell = \mathbf{0}$  at the non-control points,  $\delta\hat{x}_\ell = \delta\hat{x}_{c,\ell}$  at the control points, and  $H_{s,\ell}$

comprises  $[H_{s,\ell}]_j$ , as shown in (10.5), for all points of the traverse. The covariance matrix of the total estimated error,  $\delta\hat{x}_{\text{tot}}$ , at all control points distributed throughout the network can be computed using the covariances and cross-covariances determined with (10.11):

$$\begin{aligned} P_{\text{tot},c} &= H_{s_c} P_s H_{s_c}^T + H_{s_c} P_{sx_c} + P_{sx_c} H_{s_c}^T + P_{x_c}, \\ P_{\text{tot},nc} &= H_{s_{nc}} P_s H_{s_{nc}}^T + P_{x_{nc}}, \end{aligned} \quad (10.20)$$

where the subscript “*nc*” signifies non-control points. For the latter, the cross-covariance terms are absent and  $P_{x_{nc}} = P_{x_{nc}}^-$ .

Alternatively, the adjustment procedure may be separated into two steps. First, only a smoothing takes place for each individual traverse and no attempt is made to estimate the parameters,  $\delta\hat{x}$ , or combine traverses within a network. The advantage of such a procedure is that the removal of remaining systematic effects from individual traverses is done quickly in the field and may indicate blunders or deficiencies that warrant an immediate re-survey of the traverse. The observation model (10.6) reduces to observed misclosures at control points of a particular traverse:

$$\mathbf{y}_\ell = H_{s_c,\ell} \mathbf{s}_\ell + \mathbf{v}_\ell, \quad \mathbf{v}_\ell \sim \mathcal{N}(0, R_\ell); \quad (10.21)$$

and the total coordinate error estimates at all points of the traverse, as a result of smoothing, are given with  $H_{x_c} = 0$  in (10.10) by

$$\delta\hat{x}_{\text{tot},\ell}^- = H_{s,\ell} \hat{\mathbf{s}}_\ell = H_{s,\ell} (P_{s,\ell}^-) (H_{s_c,\ell}^T P_{s,\ell}^- H_{s_c,\ell}^T + R_\ell)^{-1} \mathbf{y}_\ell. \quad (10.22)$$

Also, the covariance matrix from (10.11) is given by

$$P_{\text{tot},\ell}^- = H_{s,\ell} (P_{s,\ell}^- - P_{s,\ell}^- H_{s_c,\ell}^T (H_{s_c,\ell}^T P_{s,\ell}^- H_{s_c,\ell}^T + R_\ell)^{-1} H_{s_c,\ell} P_{s,\ell}^-) H_{s,\ell}^T. \quad (10.23)$$

The minus sign as superscript on the left sides of (10.22) and (10.23) denotes the preliminary nature of these estimates and their covariance. Note that the system parameter estimation does not depend on the a priori information,  $(P_{x_c}^-)^{-1}$ , nor on an abundance of control points (as little as one end point is possible) because of the stochastic constraint imposed by  $(P_{s,\ell}^-)^{-1}$ , which, therefore, requires some care in selecting.

Once the coordinates of each traverse have been smoothed by applying the estimated errors (10.22), a subsequent adjustment of all traverses of the network is performed on the basis of the observation model

$$\mathbf{y} = H_{x_c} \delta\mathbf{x}_c + \mathbf{v}_x, \quad (10.24)$$

where now the observation at each control point is the difference between the coordinates indicated by the inertial system, corrected by  $\delta\hat{x}_{\text{tot},\ell}^-$ , and the externally observed coordinates. Presumably no systematic errors remain in these coordinate differences, and the covariance matrix of the noise,  $\mathbf{v}_x$ , is given by (10.23), restricted to the control points. The final adjustment serves primarily to distribute random noise optimally among all the coordinate error estimates at control points. The final coordinate error estimates are obtained from an adaptation of (10.15), with  $H_{s_c} = 0$  in (10.14):

$$\delta \hat{x}_c = (H_{x_c}^T (P_{tot,c}^-)^{-1} H_{x_c} + (P_{x_c}^-)^{-1})^{-1} H_{x_c}^T (P_{tot,c}^-)^{-1} y, \quad (10.25)$$

where  $(P_{x_c}^-)^{-1}$  contains a priori stochastic information from the Kalman filter, if available, as in the previous case. The covariance of the estimates is given by

$$P_{x_c} = (H_{x_c}^T (P_{tot,c}^-)^{-1} H_{x_c} + (P_{x_c}^-)^{-1})^{-1}. \quad (10.26)$$

For additional discussions and alternative adjustment strategies and their comparative advantages, the reader may consult Schwarz (1985) and Schwarz and Arden (1985).

#### 10.2.4 Typical Results

Several test surveys were conducted in the 1970's and early 1980's to analyze the operational procedures and performance of inertial surveying systems. One such extensive test of the RGSS in the White Sands area of New Mexico, operated both on a road vehicle and on a helicopter, is described by Todd (1981) and by Hannah (1982b). Networks consisting of crossing traverses 90 minutes to three hours in duration were surveyed in 1980 and 1981 (see Figure 10.1). A typical traverse using either road vehicle or helicopter began with up to one hour of pre-mission align-

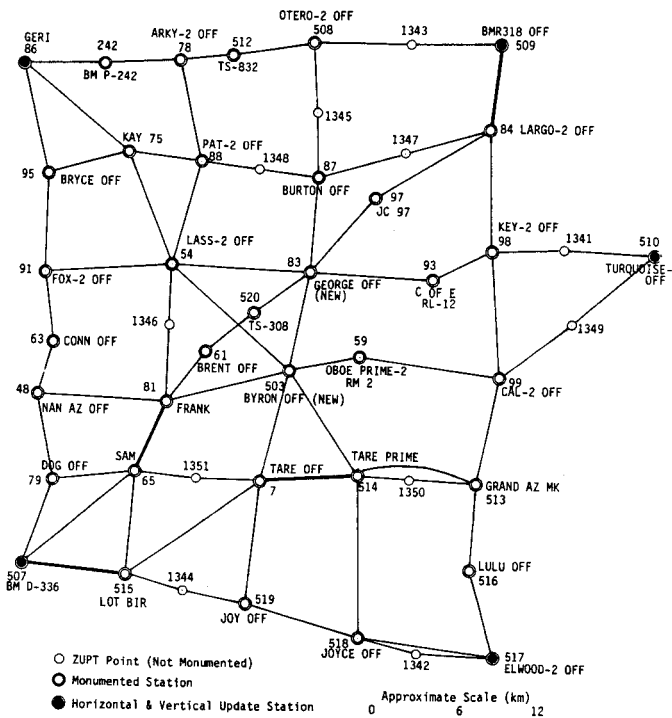


Figure 10.1: Network at White Sands Missile Range, New Mexico, surveyed by the RGSS (Hannah, 1982b).

ment and calibration, followed by several 3–4 minute periods of travel between ZUPT's. The system remained at rest during the ZUPT (it was removed from the helicopter, but not the road vehicle) for about one minute. Traverses were run both in forward and reverse directions so that the ensuing redundancy could be used to estimate errors. The traverses generally maintained constant heading, however, L-shaped and U-shaped traverses were also tested to determine the affect of significant azimuth changes. Hannah (1982b) reported the results of full network adjustments, concluding that the horizontal coordinates of ZUPT points can be determined to an accuracy of about 10 cm (errors in heights were on the order of 30 cm).

A review of similar tests and procedures with other systems was prepared by Huddle (1985). The assessment of the state-of-the-art reached at that time indicated that both ZUPT's and cross-over points of traverses are essential to achieve high accuracy in inertial surveying. Moreover, relatively simple empirical error models employed in the methods of smoothing and filtering, as described above, generally are sufficient in the control of systematic errors. Finally, as noted earlier, the reliable estimation of errors depends on realistic error models (statistical covariances) of all (control) observations.

It is worth mentioning already here that inertial survey systems ultimately were viewed not just as position survey systems but as gravity vector measurement systems (see Section 10.4). In that case more care is required in modeling the gravity error (that now becomes a signal to be estimated).

The inertial surveying system, though holding much promise, was never so widely deployed as to lay claim to the niche of rapid and accurate geodetic surveying. Therefore, it is not entirely appropriate to say that the inertial methods were *replaced* by kinematic positioning using the Global Positioning System (GPS). Before inertial technology could be developed to yield a cost-effective and accurate surveying tool, GPS had already quickly emerged as the clear choice that, better than any other technique, offered ease of use, accuracy, and low cost. Today, GPS quite literally has replaced or is replacing conventional surveying in most applications. There remain some instances, of course, where inertial techniques are still useful if not indispensable, such as for submarine and subterranean surveys, and it provides important aiding functions in kinematic GPS positioning. Both the RGSS and the IPS currently are operated by the National Imagery and Mapping Agency at the White Sands Missile Range and Holloman Air Force Base, New Mexico.

### 10.3 GPS/INS Integration

In Section 9.6.1, where GPS observations were used in a Kalman filter algorithm to estimate errors in kinematic positions, we hesitated to provide a dynamics model for the position error because we lacked information on its stochastic or dynamic behavior between GPS updates. However, known characteristics of the motion might be used to describe the errors both stochastically and deterministically. For example, such models derive from the known aerodynamics of an aircraft (*phugoid*

motion) or the fact that the platform (on the aircraft) is moving more or less at constant altitude and constant heading. Simple models that assume first-order correlations, such as the Gauss-Markov process, often provide the stochastic element. This type of modeling may lead to more accurate interpolation between GPS epochs and can be quite effective in dynamically benign cases.

On the other hand, the problem of maintaining precise continuous positioning of a moving platform is illustrated tellingly with Galileo's Law,  $\delta s = 0.5\delta a t^2$ , that predicts, for example, a variation in position,  $\delta s = 2.5$  cm, given a change in acceleration,  $\delta a = 0.2$  m/s<sup>2</sup>, over a time interval,  $t = 0.5$  s. The relatively low data output rate of GPS receivers (usually once per second or lower) could pose a challenge in maintaining accuracy when interpolating between GPS-derived kinematic positions accurate at the centimeter level. One geodetic application in which this is particularly critical is aerial photogrammetry, where the shutter opening of the camera does not necessarily coincide with the epoch of the GPS-derived position. Some form of interpolation is required if GPS positioning should determine the coordinates of the camera at the time of exposure.

The problem becomes even more serious when one considers the potential temporary loss of a GPS signal (due to shadowing, for example, by banked aircraft wings) or the introduction of phase ambiguity resulting from cycle slips. Although with sufficient GPS data the cycle ambiguity may be resolved on the fly, this procedure generally requires several data epochs (up to 10, or more), depending on the receiver type and the satellite configuration geometry. Once re-determined, the full-cycle count may be extrapolated backward (in post-mission processing) to the time of the cycle slip, thus rendering the latter inconsequential. However, repeated cycle slips that span a time interval too short to enable resolution of the full-cycle ambiguity effectively cause a loss of signal over that interval. Such losses in the GPS signal temporarily reduce the number of tracked satellites and weakens (or even precludes) the positioning solution.

Suppose that in addition to GPS we have a second instrument or sensor that could provide directly the dynamics of the motion between GPS epochs at high temporal resolution. This would complement the discrete nature of GPS and aid the positioning solution in the events of cycle slips and losses in the signal. This is precisely what an inertial navigation system (INS) offers. The error dynamics are quite complicated as we have already seen; yet, because of the high short-term precision and resolution of INS data, it is the closest we can come to the true continuous dynamics of the motion. These contrasting characteristics expressly motivate the integration of GPS and INS for precise positioning applications. As summarized in Table 10.1, the essential properties of GPS and INS, both viewed as positioning devices, are almost diametrically opposite, making these systems complementary rather than competitive.

Because positioning with INS requires the integration with respect to time of accelerations and angular rates, the measurement noise accumulates and results in long-wavelength errors. GPS positioning derives from a more direct measure of distances, where errors generally do not accumulate, but in the short term, without

Table 10.1: Essential characteristics of GPS and INS as precision positioning devices.

|                         | GPS                              | INS                               |
|-------------------------|----------------------------------|-----------------------------------|
| measurement principle   | distances from time delays       | inertial accelerations            |
| system operation        | reliance on space segment        | autonomous                        |
| output variables        | positions, time                  | positions, orientation angles     |
| long-wavelength errors  | low                              | high                              |
| short-wavelength errors | high                             | low                               |
| data rate               | low ( $\leq 1$ Hz)               | high ( $\geq 25$ Hz)              |
| instrument cost         | low (\$20,000, geodetic quality) | high (\$100,000, med/high accur.) |

the benefit of averaging, they are relatively larger and the measurements have poorer resolution. Being completely autonomous (except requiring initial position and velocity), the INS is not susceptible to the vagaries of external support as is the GPS receiver that must track satellite transmissions. For these reasons, from the geodetic point of view, we may consider INS as aiding GPS positioning, both as an interpolator and as a stopgap device. In addition, because of the orientation output from an INS, the possibility exists to determine the complete rotational motion of the vehicle. The only drawback is the cost of this aiding apparatus, which can be many times the cost of the primary positioning device. However, the cost of the INS ultimately is a function of the required accuracy. Low-cost systems that emphasize short-term precision over long-term accuracy would suffice, for example, if only rapid cycle slip recovery is a concern.

Geodetic applications of the integrated GPS/INS for enhanced positioning capability have focused on the *mobile mapping system* and similar systems that, with both ground vehicles and aircraft, perform remote sensing and land data acquisition through multispectral imaging. Critical to creating a viable data base of such geographical information is accurate spatial referencing of the data which can be accomplished by knowing the position of the mapping system. Several systems have been developed around the world; see, e.g., (Linkwitz and Hangleiter, 1995), also (El-Sheimy and Schwarz, 1998) and (Grejner-Brzezinska, 1999) for illustrative performance analyses.

### 10.3.1 Integration Modes

The types of system integration are characterized in two ways: by the extent to which data from each component aid the other's function, that is, by the mechanization or the architecture of the system; and, by the method of combining or fusing the data to obtain position coordinates (Greenspan, 1996). Although, to some extent, the method of data blending actually reflects the mechanization imposed by the hardware configuration, different levels of processing may be applied to a particular mechanization. In fact, clear distinctions between mechanizations and methods of data processing fade as the system integration becomes tighter.

More descriptively, the mechanization is referred to as a coupling, where no coupling (*uncoupled* integration) implies no data feedback from either instrument to the other for the purpose of improving its performance; and, in *tight coupling* the sensors are treated as belonging to a single system producing several complementary types of data that are processed simultaneously and optimally and used to enhance the function of individual sensor components where possible. In a *loosely coupled* system processed data from one instrument are fed back in an aiding capacity to improve the utility of the other's performance, but each instrument still has its own individual data processing algorithm.

The real-time feedback of INS velocities to the GPS receiver enables an accurate prediction of GPS pseudorange and phase at the next epoch, thus allowing a smaller bandwidth of the receiver tracking loop in a high-dynamic environment with a subsequent increase in accuracy (see equations (9.34) and (9.35)). Conversely, inertial navigation improves if the GPS solution functions as an update in a Kalman filter estimation of the systematic errors in the inertial sensors. Similarly, GPS positions and velocities may be used to aid the INS solution in a high-dynamic situation by providing a better reference for propagating error states based on the linear approximation (see Sections 5.3 and 7.5.2). Also, one may consider the possibility of using an INS to aid in the determination of a three-dimensional positioning or navigation solution from a set of GPS satellites having unfavorable geometry or being partially blocked from view, thus helping to bridge GPS outages or improve solutions with poor GDOP.

In geodetic applications, we are less concerned with real-time kinematic positioning (navigation) and usually are able to integrate systems only off-the-shelf, that is, without significant hardware coupling between them. Furthermore, most applications are in a dynamically benign environment and it is enough to concentrate on integrating the data processing algorithms. Embedded GPS/INS systems represent the ultimate in coupled systems, where the GPS receiver is added to an inertial system as an integral hardware component (a single electronic circuit card). Currently being manufactured primarily for military and civil applications, in the future, these systems may also be directed to precision geodetic applications.

The processing algorithms fall into two basic categories: centralized and decentralized. As the name implies, *centralized* processing is usually associated with tight system integration wherein the raw sensor data are combined optimally using one central processor (e.g., a Kalman filter or smoother) to obtain a position solution. *Decentralized* processing is characterized by a sequential approach to processing, where processors of individual systems provide solutions that subsequently are combined with various degrees of optimality by a master processor. Other terms occur in the literature to describe decentralized integration, such as cascaded and federated integration. Also, various degrees of this loose type of integration may be designed and employed. In principle, if the statistics of the errors are correctly propagated, the optimal decentralized and centralized methods should yield identical solutions. However, certain aspects, such as system fault detection, isolation, and correction capability and the relative computational simplicity generally favor

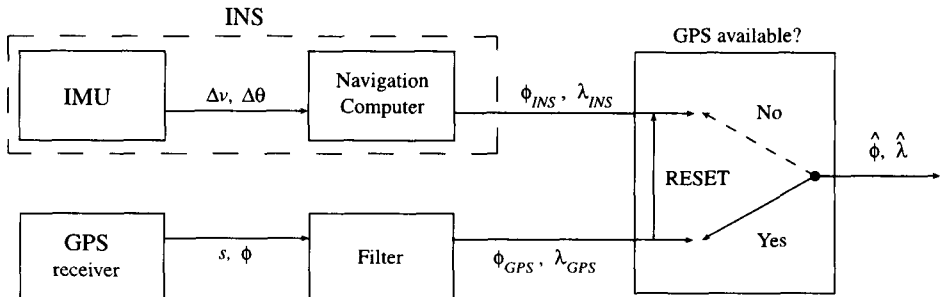


Figure 10.2: Uncoupled, decentralized GPS/INS integration with no INS error calibration.

the decentralized approach (Gao et al., 1993). The centralized approach is considered to yield the best performance in the navigation and positioning solutions, especially since error statistics can be most rigorously modeled and propagated within the single Kalman filter (smoother).

The following examples illustrate some of the possible processing schemes for an integrated positioning system comprising a GPS receiver (and antenna) and an IMU assembly, either alone or as part of an INS. Combining distinct subsystems in this way implies either uncoupled or loosely coupled system integration and represents a typical mode for geodetic applications. The degree of centralization in the data processing depends on the level of the data product available from each system—the closer the data are to the raw measurements of the sensors, the more centralization is possible.

### 10.3.1.1 Decentralized Integration

Consider first the uncoupled, decentralized GPS/INS integrated system, as shown in Figure 10.2, where the INS and GPS receiver independently collect and process position data. The IMU data, comprising velocity and angle increments,  $\Delta v$  and  $\Delta\theta$ , are integrated by the navigation computer of the INS as described, for example, in Chapter 4, yielding position coordinates,  $\phi_{INS}$  and  $\lambda_{INS}$ , as well as corresponding velocity components, and orientation angles. Standard deviations of the errors may or may not accompany these computed values; however, no attempt is made within the INS to estimate its errors, which were calibrated last during the initialization of the system (usually at the start of the mission).

Likewise, pseudoranges and phases,  $s$  and  $\phi$ , measured by the GPS receiver are processed to yield coordinates,  $\phi_{GPS}$  and  $\lambda_{GPS}$ ; usually error estimates are also provided. The estimation may be formulated with a Kalman filter, as discussed in Section 9.6, where observations such as the wide-lane phases, (9.61), are used to update coordinates predicted on the basis of modeled velocities, for example, the dynamics model (9.71). Other states may be included in the Kalman filter, such as cycle ambiguities or ionospheric effects (see (9.95) and (9.109)).

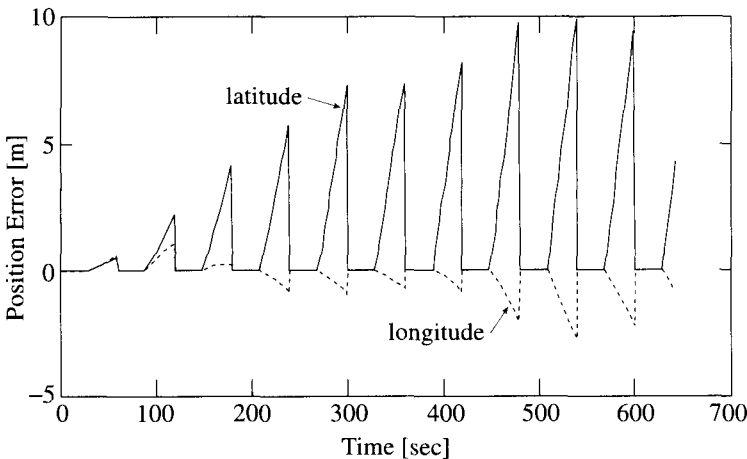


Figure 10.3: Differences between INS and GPS coordinates during GPS outages for uncoupled, decentralized processing and no INS error calibration.

The data integration of the two systems may be accomplished with a simple decision algorithm that uses one or the other system output depending on the availability of GPS; that is, GPS serves as the primary system because of its long-term stability. A reset of INS coordinates to current GPS coordinates within the integration processor bounds the relatively substantial increase in INS errors (but does not affect their rate of increase!). The integration algorithm is given by:

$$\begin{bmatrix} \hat{\phi}(t_k) \\ \hat{\lambda}(t_k) \end{bmatrix} = \begin{cases} \begin{bmatrix} \phi_{\text{GPS}}(t_k) \\ \lambda_{\text{GPS}}(t_k) \end{bmatrix}, & \text{if GPS solution is available;} \\ \begin{bmatrix} \phi_{\text{INS}}(t_k) + (\phi_{\text{GPS}}(t_0) - \phi_{\text{INS}}(t_0)) \\ \lambda_{\text{INS}}(t_k) + (\lambda_{\text{GPS}}(t_0) - \lambda_{\text{INS}}(t_0)) \end{bmatrix}, & \text{if GPS solution is not available;} \end{cases} \quad (10.27)$$

where  $t_0$  is the most recent time that a GPS solution was available. Figure 10.3 illustrates the differences between  $\hat{\phi}(t)$ ,  $\hat{\lambda}(t)$  calculated from (10.27) and  $\phi_{\text{GPS}}(t)$ ,  $\lambda_{\text{GPS}}(t)$  derived from GPS during periods when INS presumably takes over as a free-inertial system without error compensation (except the reset). Note the rapid divergence of the free-inertial solution. This example was constructed from data obtained by an airborne GPS/INS positioning system tested in central Ohio. In this and the next case, the height coordinate is not available from INS unless its internal solution is aided (coupled) with GPS or barometric (or other type of) altimeter observations.

At this point it must be noted that the location of the GPS antenna, to which the GPS positioning solution refers, does not coincide with the computation point for the inertial navigation solution. The offset can amount to several decimeters, up to a few meters, obviously depending on where the antenna is installed relative to the INS. It is readily measured in terms of Cartesian coordinates in the body-frame of the particular vehicle. To obtain corresponding coordinate differences in the navi-

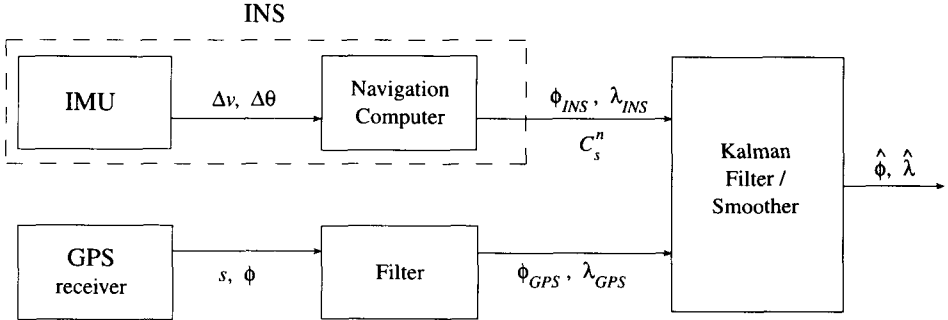


Figure 10.4: Loosely coupled, decentralized GPS/INS integration with INS error calibration.

gation frame requires knowledge of the rotation matrix,  $C_b^n$ , given by (1.90) and, in principle, available from the gyros through the inertial navigation solution (or from the platform gimbals of a stabilized system). However, the accuracy of the angles need not be great; if the offset in any coordinate is less than 1 m, then orientation uncertainty of  $10^{-3}$  rad ≈ 3 arcmin causes less than 1 mm of error in the computed offset. We will assume henceforth that this offset correction is an integral part of the integrated processing of GPS and INS data.

Improved results are obtained if the data integration method takes advantage of the updating information contained in the GPS position solution to estimate (some of) the errors of the IMU. Again, there is no tight coupling of INS and GPS functionality. Each system independently collects and determines a position solution, as illustrated schematically in Figure 10.4. However, the position solution obtained from INS during GPS outages may be compensated by the estimates of IMU errors that are obtained with a Kalman filter (or smoother) on the basis of the prior accumulated GPS positioning information. This case is completely analogous to the first stage of data processing used in inertial surveying, where now kinematic GPS positions take the place of ZUPT's. As seen in the error estimation formulas below, the direction cosine matrix,  $C_s^n$ , from sensor to navigation frame must also be provided by the navigation computer in the case of a strapdown system (for a local-level, north-slaved, stabilized system,  $C_s^n = I$ ).

For short periods of time and conventional velocities ( $\leq 200$  m/s), we may abbreviate the IMU error dynamics equation, similar to equation (5.82), formulated in the NED frame without the height variables:

$$\frac{d}{dt} \begin{bmatrix} \psi_N \\ \psi_E \\ \psi_D \\ \delta\phi \\ \delta\lambda \\ \delta\dot{\phi} \\ \delta\ddot{\phi} \end{bmatrix} = \begin{bmatrix} 0 & -\omega_e \sin \phi & 0 & 0 & \cos \phi & -\omega_e \sin \phi & 0 \\ \omega_e \sin \phi & 0 & \omega_e \cos \phi & -1 & 0 & 0 & 0 \\ 0 & -\omega_e \cos \phi & 0 & 0 & -\sin \phi & -\omega_e \cos \phi & 0 \\ 0 & \frac{-a_3^n}{r} & \frac{a_2^n}{r} & 0 & -\omega_e \sin 2\phi & 0 & 0 \\ \frac{a_3^n}{r \cos \phi} & 0 & \frac{-a_1^n}{r \cos \phi} & 2\omega_e \tan \phi & 0 & 0 & 0 \\ 0 & 0 & 0 & 1 & 0 & 0 & 0 \\ 0 & 0 & 0 & 0 & 1 & 0 & 0 \end{bmatrix} \begin{bmatrix} \psi_N \\ \psi_E \\ \psi_D \\ \delta\phi \\ \delta\lambda \\ \delta\dot{\phi} \\ \delta\ddot{\phi} \end{bmatrix} + \begin{bmatrix} \delta\omega_{GN} \\ \delta\omega_{GE} \\ \delta\omega_{GD} \\ \delta\alpha_{AE} \\ 0 \\ 0 \end{bmatrix}. \quad (10.28)$$

The sensor errors in the right-most term could be modeled, for example, as comprising a drift bias and white noise for each gyro, respectively represented by the sensor-frame vectors,  $\mathbf{d}$  and  $\mathbf{w}_G$  (see (5.75) and (6.109)):

$$\delta\omega_G = C_s^n \delta\omega_{is}^s = C_s^n (\mathbf{d} + \mathbf{w}_G), \quad (10.29)$$

and a bias, scale factor error, and white noise for each accelerometer, denoted by the vectors  $\mathbf{b}$ ,  $\boldsymbol{\kappa}_A$ , and  $\mathbf{w}_A$  in the  $s$ -frame (see (5.72) and (6.107)):

$$\delta\mathbf{a}_A = D^{-1} C_s^n \delta\mathbf{a}^s = D^{-1} C_s^n (\mathbf{b} + \text{diag}(\mathbf{a}^s) \boldsymbol{\kappa}_A + \mathbf{w}_A), \quad (10.30)$$

where  $\text{diag}(\mathbf{a}^s)$  represents a diagonal matrix of sensed acceleration components and  $D$ , given by (5.69), transforms from geodetic to local Cartesian differential elements.

Denoting the navigation error states by

$$\boldsymbol{\varepsilon}_1 = [\psi_N \ \psi_E \ \psi_D \ \delta\dot{\phi} \ \delta\dot{\lambda} \ \delta\phi \ \delta\lambda]^T, \quad (10.31)$$

and assuming the systematic error parameters

$$\boldsymbol{\varepsilon}_2 = [\mathbf{d}^T \ \mathbf{b}^T \ \boldsymbol{\kappa}_A^T]^T \quad (10.23)$$

are all random constants, satisfying (6.63), the augmented error dynamics differential equation (10.28) is given by (see also Section 7.5.1):

$$\frac{d}{dt} \begin{pmatrix} \boldsymbol{\varepsilon}_1 \\ \boldsymbol{\varepsilon}_2 \end{pmatrix} = \begin{pmatrix} F_1 & F_2 \\ 0 & 0 \end{pmatrix} \begin{pmatrix} \boldsymbol{\varepsilon}_1 \\ \boldsymbol{\varepsilon}_2 \end{pmatrix} + \begin{pmatrix} G \\ 0 \end{pmatrix} \begin{pmatrix} \mathbf{w}_G \\ \mathbf{w}_A \end{pmatrix}, \quad (10.33)$$

where  $F_1$  is the error dynamics matrix in (10.28), and

$$F_2 = \begin{pmatrix} C_s^n & 0_{3 \times 3} & 0_{3 \times 3} \\ 0_{2 \times 3} & JD^{-1} C_s^n & JD^{-1} C_s^n \text{diag}(\mathbf{a}^s) \\ 0_{2 \times 3} & 0_{2 \times 3} & 0_{2 \times 3} \end{pmatrix}, \quad G = \begin{pmatrix} C_s^n & 0_{3 \times 3} \\ 0_{2 \times 3} & JD^{-1} C_s^n \\ 0_{2 \times 3} & 0_{2 \times 3} \end{pmatrix},$$

$$J = \begin{pmatrix} 1 & 0 & 0 \\ 0 & 1 & 0 \end{pmatrix}, \quad (10.34)$$

where all zero matrices have their dimensions indicated.

Since position coordinates derived from GPS are used as updates, the observation equation (cf., equation (7.52)) is given by

$$\mathbf{y} = H\boldsymbol{\varepsilon} + \mathbf{v}, \quad (10.35)$$

with  $\boldsymbol{\varepsilon}^T = (\boldsymbol{\varepsilon}_1^T \ \boldsymbol{\varepsilon}_2^T)^T$  and

$$H = \begin{pmatrix} 0 & I_{2 \times 2} & 0_{2 \times 9} \end{pmatrix}. \quad (10.36)$$

The GPS observations of  $\phi, \lambda$  are obtained as in the previous example using a separate Kalman filter. The assumption in (10.35) of temporally uncorrelated observation noise coming from this filter is rarely satisfied and the model for the final

Kalman filter (or smoother) should in theory be augmented, as described in Section 7.5.1, by additional GPS error parameters, if they are distinct in their statistical behavior from the error states already included. Also, the INS solution should be reset, as in the previous example, by the most recent GPS solution (closed-loop operation, Section 7.5.2) in order to maintain fidelity in the linear approximation of the error models.

With appropriate statistical information for the noise processes,  $w_G$ , and  $w_A$ , as well as a priori covariances for the error states, these models and observations are processed by a discrete Kalman filter (Section 7.3.2.2) and/or smoother (Section 7.3.2.3) to yield estimates  $\hat{\phi}$  and  $\hat{\lambda}$  for all epochs of interest. From (7.132), the position coordinate estimates for all  $t_k$  are then

$$\begin{aligned}\hat{\phi}(t_k) &= \phi_{\text{INS}}(t_k) - \delta\hat{\phi}(t_k), \\ \hat{\lambda}(t_k) &= \lambda_{\text{INS}}(t_k) - \delta\hat{\lambda}(t_k).\end{aligned}\quad (10.37)$$

The verity of the corresponding covariances, extracted from the matrix,  $P_k$ , given by equation (7.73), depends on the accuracy of the error models, including the covariances of the GPS noise vector,  $v$ .

At the update epochs the coordinate estimates are close to the coordinates (the observations) derived from the presumably much more accurate GPS solution. These estimates are also used to reset the INS-indicated coordinate values. At other times, the coordinates come from the INS solution corrected for sensor errors estimated on the basis of the updates. In other words, the IMU errors have been calibrated (to the extent possible from the GPS updates; see Chapter 8). Applying the same test-flight data as used for Figure 10.3 to this loosely-coupled integration scheme, the differences  $\hat{\phi}(t) - \phi_{\text{GPS}}(t)$  and  $\hat{\lambda}(t) - \lambda_{\text{GPS}}(t)$  were computed during periods when the calibrated free-inertial INS solution supposedly takes over from GPS (i.e., there are no GPS updates during these periods). The results are shown in Figure 10.5 and demonstrate an order of magnitude improvement over the uncalibrated solution; the corresponding Kalman-smoothed solution yields a further reduction by a factor of two.

### 10.3.1.2 Centralized Integration

A third example illustrates the centralized integration of IMU and GPS data as shown schematically in Figure 10.6. It represents an almost tight coupling of GPS and INS as conventionally defined, since there is no feedback from the processor to the GPS receiver tracking loops. The essential difference between this integration and the decentralized configuration shown in Figure 10.4 lies in the processing of the data. The data available to the integration algorithm from both the IMU and GPS are now assumed to be the raw incremental angles and velocities, respectively,  $\Delta\theta$  and  $\Delta v$ , from the gyros and accelerometers, as well as the phases and pseudoranges from the GPS receiver. All positioning error states and error parameters corresponding to both systems are estimated simultaneously with one Kalman filter. Instead of GPS-derived coordinates providing updates to the inertial navigation

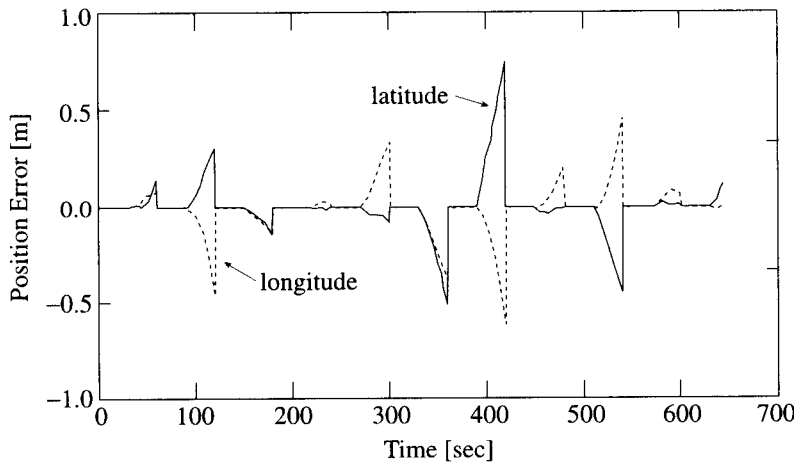


Figure 10.5: Differences between INS and GPS coordinates during GPS outages for loosely coupled, decentralized processing and INS error calibration.

solution, the ranges and range differences or, even at a more elemental level, the phases and pseudoranges and their differences (Section 9.5.2) now serve that function.

The sensor error states for the IMU are those considered before; however, in this example, we formulate the dynamics in the  $e$ -frame, since the centralized processing approach intrinsically provides vertical channel damping of the vertical IMU position and velocity errors through the three-dimensional GPS updates. This allows

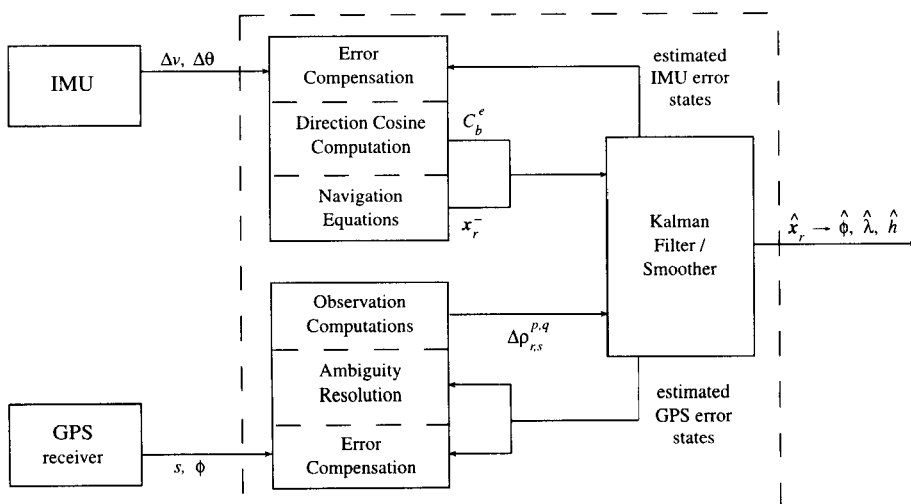


Figure 10.6: Centralized GPS/INS (strapdown) integration.

utilization of the considerably simpler error dynamics equations for the strapdown IMU in the  $e$ -frame, which is also the primary coordinate frame for GPS observations. Moreover, we now include additional states to model correlated sensor errors and/or unknown gravity disturbance components (e.g., Gauss-Markov processes; Section 6.6.3).

The GPS error states may include the cycle ambiguity terms, as well as ionospheric and tropospheric delays. For the moment we consider the ambiguities already determined using an on-the-fly (OTF) algorithm aided by the INS, as described in the next section. Once these are estimated with sufficient accuracy, they are assigned fixed values (integers in the case of doubly differenced phases) and may be deleted from the system state vector (see Section 9.6.4). Also, the tropospheric delay is considered as largely modeled outside the Kalman filter and in the form of a correction to the GPS observations (see also Section 9.4). The total state vector is divided into the standard 9-element navigation error state vector, a vector of IMU sensor parameters, and a vector of GPS-related parameters, as follows:

$$\boldsymbol{\varepsilon} = (\boldsymbol{\varepsilon}_1^T \quad \boldsymbol{\varepsilon}_2^T \quad \boldsymbol{\varepsilon}_3^T)^T, \quad (10.38)$$

where

$$\begin{aligned} \boldsymbol{\varepsilon}_1 &= ((\boldsymbol{\psi}^e)^T \quad (\delta \dot{\mathbf{x}}_r)^T \quad (\delta \mathbf{x}_r)^T)^T, \\ \boldsymbol{\varepsilon}_2 &= (\mathbf{d}^T \quad \mathbf{b}^T \quad \boldsymbol{\kappa}_A^T \quad \mathbf{c}^T)^T, \\ \boldsymbol{\varepsilon}_3 &= (\dots \quad \Delta I_{r,s}^{p,q} \quad \dots)^T, \end{aligned} \quad (10.39)$$

and where the frame-designating superscript on the position and velocity errors has been omitted as in Section 9.6 with the understanding that these are vectors in the  $e$ -frame. Compared to (10.32) the state vector,  $\boldsymbol{\varepsilon}_2$ , now also accommodates correlated errors modeled as first-order Gauss-Markov processes (see (6.69)):

$$\dot{\boldsymbol{\varepsilon}} = -\text{diag}(\boldsymbol{\beta})\boldsymbol{\varepsilon} + \mathbf{w}_c, \quad (10.40)$$

where  $\text{diag}(\boldsymbol{\beta})$  is a diagonal matrix whose diagonal elements are the correlation parameters,  $\boldsymbol{\beta}^T = (\beta_1 \quad \beta_2 \quad \beta_3)^T$ , of the processes and have known values, and  $\mathbf{w}_c$  is a vector of white noise processes with known variances.

The dimension of the last component of (10.38),  $\boldsymbol{\varepsilon}_3$ , is dynamic and depends at any epoch on the number of satellites being tracked. Each state corresponds to a double difference (in this example) of the ionospheric effect between two satellites,  $p$  and  $q$ , and two GPS receivers,  $r$  and  $s$ , one roving and the other presumably stationary. The dimension of  $\boldsymbol{\varepsilon}_3$  is  $n_{p,q}$ , the number of doubly-differenced ionospheric delays; and, each of these states may be modeled as a random walk (Grejner-Brzezinska et al., 1998) or other type of stochastic process. Considering the former, we have

$$\frac{d}{dt} \Delta I_{r,s}^{p,q} = w_I. \quad (10.41)$$

If other error parameters are to be included in the state vector, such as tropospheric delays, their stochastic models should be distinct from those already incorporated,

otherwise statistically they would not be estimable and should simply be subsumed within the existing models.

The dynamics model for the states in this example is

$$\frac{d}{dt} \begin{pmatrix} \varepsilon_1 \\ \varepsilon_2 \\ \varepsilon_3 \end{pmatrix} = \begin{pmatrix} F_{11} & F_{12} & 0_{9 \times 2n_{p,q}} \\ 0_{12 \times 9} & F_{22} & 0_{12 \times 2n_{p,q}} \\ 0_{2n_{p,q} \times 9} & 0_{2n_{p,q} \times 12} & 0_{2n_{p,q} \times 2n_{p,q}} \end{pmatrix} \begin{pmatrix} \varepsilon_1 \\ \varepsilon_2 \\ \varepsilon_3 \end{pmatrix} + \begin{pmatrix} G_1 \\ G_2 \\ G_3 \end{pmatrix} \begin{pmatrix} w_G \\ w_A \\ w_C \\ w_I \end{pmatrix}, \quad (10.42)$$

where  $F_{11}$  is given by the dynamics matrix in (5.51), and

$$F_{12} = \begin{pmatrix} C_b^e & 0_{3 \times 3} & 0_{3 \times 3} & 0_{3 \times 3} \\ 0_{3 \times 3} & C_b^e & C_b^e \text{ diag}(\alpha^s) & C_b^e \\ 0_{3 \times 3} & 0_{3 \times 3} & 0_{3 \times 3} & 0_{3 \times 3} \end{pmatrix}, \quad F_{22} = \begin{pmatrix} 0_{9 \times 9} & 0_{9 \times 3} \\ 0_{3 \times 9} & -\text{diag}(\beta) \end{pmatrix}. \quad (10.43)$$

Also, from models analogous to (10.29) and (10.30), but in the  $e$ -frame, and from (10.40) and (10.41), it is easily verified that

$$G_1 = \begin{pmatrix} C_b^e & 0_{3 \times 3} & 0_{3 \times (3+n_{p,q})} \\ 0_{3 \times 3} & C_b^e & 0_{3 \times (3+n_{p,q})} \\ 0_{3 \times 3} & 0_{3 \times 3} & 0_{3 \times (3+n_{p,q})} \end{pmatrix}, \quad G_2 = \begin{pmatrix} 0_{9 \times 6} & 0_{9 \times 3} & 0_{9 \times n_{p,q}} \\ 0_{3 \times 6} & I_{3 \times 3} & 0_{3 \times n_{p,q}} \end{pmatrix}, \quad G_3 = \begin{pmatrix} 0_{n_{p,q} \times 9} & I_{n_{p,q} \times n_{p,q}} \end{pmatrix}. \quad (10.44)$$

The GPS observables are doubly differenced wide-lane phases given by (9.61), where the ambiguity, as already mentioned, is determined outside the filter. The observation matrix,  $H$ , now becomes a  $n_{p,q} \times (21 + n_{p,q})$  matrix with each row given, similar to (9.110), by

$$(H)_{p,q} = \begin{pmatrix} 0_{1 \times 6} & -\frac{1}{\lambda_w} (\tilde{e}_r^{p,q})^T & 0_{1 \times 12} & \dots 0 \dots & \frac{1 - \sqrt{\alpha}}{\lambda_1} & \dots 0 \dots \end{pmatrix}, \quad (10.45)$$

where, as in (9.98), the symbol  $\dots 0 \dots$  denotes a string of zeros of appropriate length depending on the ordering of the satellite pairs,  $(p, q)$ ; and  $\tilde{e}_r^{p,q}$  is given by (9.99). The covariance matrix,  $R$ , is similar to (9.102), taking into account the combination of phase errors (9.63) for each double-difference observation. It is noted that the final three-dimensional position estimate in Cartesian coordinates can easily be transformed into geodetic coordinates using (1.84).

Comparing the decentralized and centralized integrations, we see that their basic architecture is quite similar, where the IMU provides the reference trajectory, while GPS serves as the updating system. The difference is the point in the GPS processing when the filtering takes place; that is, double-difference ranges rather than solved coordinates are used as updates. As before, the inertial navigation solution takes advantage of corrected sensor data. In principle, the results should be equivalent if the error models in both types of integration are identical and the propagation of

error statistics is accomplished rigorously. For example, the full covariance matrix from the stand-alone GPS filter should be used in the decentralized integration, as well as any epoch-to-epoch correlations.

Clearly, the centralized integration is more forgiving to losses in the GPS signals. In the decentralized integration a position solution depends on a sufficient number of tracked satellites (at least four). Without this minimum condition, no solution is obtained; and, therefore, it is not available as update to the free-inertial solution (unless specialized filters are constructed to compute degraded, or lower dimensioned solutions in such cases). On the other hand, the centralized integration makes use of any GPS signal, even if it is only a single double-difference.

For these reasons, one generally prefers the centralized approach. However, there are also advantages to the decentralized integration. Should there be a sensor failure or other significant unforeseen degradation in either system, the decentralized integration, operating essentially on two independent solutions, is more likely to detect these faults or consequent outliers and is better able to take appropriate remedial action. A second advantage concerns the computational complexity of the integration. Processing two low-order state filters in the cascaded, or decentralized approach, requires fewer calculations than processing a single high-order state filter. However, in post-mission processing, especially in high-accuracy geodetic applications, this advantage fades with the potential loss of rigorous propagation of error statistics. Even in real-time processing, this advantage is becoming less important as computational capability continues to rise exponentially.

### 10.3.2 Cycle Ambiguity Determination

Aside from providing higher resolution to the positioning solution of a moving platform, as well as bridging periods of GPS signal outages, the inertial system is particularly suited to the en route detection and recovery of cycle ambiguities in the GPS phase observable. Although efficient search algorithms exist to determine these, both in the static and kinematic (on-the-fly, OTF) modes, their performance degrades with the baseline length, the severity of atmospheric effects, the roughness of vehicle dynamics, and the unavailability of accurate *P*-code tracking (anti-spoofing). The determination of cycle ambiguities is required not just in the event of a cycle slip, but also as new satellites rise to supplement or replace others in the kinematic positioning solution.

If a solution is already possible on the basis of a minimum number of satellites with good geometry, then the cycle ambiguity of the phase signal of any additional satellite is easily determined using the position coordinates of the vehicle and the satellite. Otherwise, the position implied by the IMU data might be used either to calculate or to recover the cycle count or to detect an erroneous count (a cycle slip), depending on the accumulated level of free-inertial navigation error. With precise, well calibrated inertial measurements, the ambiguity can easily be determined within a few seconds, as long as the INS accuracy deteriorates by less than half the wavelength of the carrier (10 cm for L1, and 43 cm for the widelane signal).

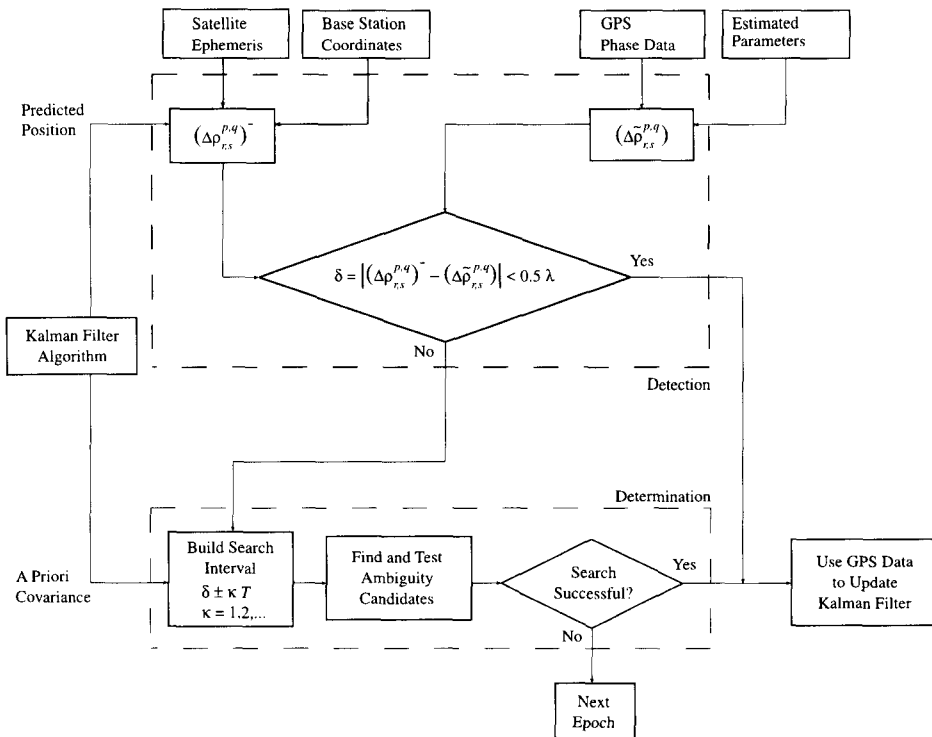


*Figure 10.7: Cycle ambiguity detection and determination in centralized GPS/INS integration.*

Figure 10.7 depicts a typical flow of logic to detect and resolve cycle ambiguities in an integrated system. Illustrated for relative kinematic GPS positioning based on doubly differenced phase observables, the essential logic would not differ in the case of single-receiver, absolute positioning. At each epoch the integrity of the double-difference phase is examined by calculating the ranges according to (9.66), and doubly differenced according to (9.57), from the position of the vehicle as *predicted* by the Kalman filter algorithm and from the positions of the relevant satellites and base station. This predicted range,  $(\Delta\rho_{r,s}^{p,q})^-$ , is comparable to the combination of a doubly differenced phase (observed L1, wide-lane, or ion-free phase, *including* the phase error) and the corresponding full cycle count, and possibly an ionospheric effect; for example; for the wide-lane phase, (9.61), we have:

$$(\Delta\phi_{r,s}^{p,q})^- - \varepsilon_{\Delta\rho} = \lambda_w (\Delta\phi w_{r,s}^{p,q} - \Delta\phi_{\psi W, r,s}^{p,q}) + \frac{\lambda_w}{\lambda_1} (1 - \sqrt{\alpha}) \Delta I_{r,s}^{p,q} + \lambda_w \Delta N w_{r,s}^{p,q}, \quad (10.46)$$

where  $\varepsilon_{\Delta\rho}$  is the error in the predicted range. From the observed phase,  $\Delta\phi^{w_r, q}_{r,s}$ , and the estimated ionospheric effect and previous cycle count (presumed constant), one can calculate, again from (9.61):

$$\Delta\tilde{\rho}_{r,s}^{p,q} = \lambda_w \Delta\phi w_{r,s}^{p,q} + \frac{\lambda_w}{\lambda_1} (1 - \sqrt{\alpha}) \Delta\hat{I}_{r,s}^{p,q} + \lambda_w \Delta N w_{r,s}^{p,q}|_0. \quad (10.47)$$

Assuming that the prediction,  $(\Delta\rho_{r,s}^{p,q})^-$ , and estimate,  $\Delta\hat{I}_{r,s}^{p,q}$ , are sufficiently accurate, any significant difference between  $(\Delta\rho_{r,s}^{p,q})^-$  and  $\Delta\tilde{\rho}_{r,s}^{p,q}$ :

$$\begin{aligned} \frac{1}{\lambda_w} ((\Delta\rho_{r,s}^{p,q})^- - \Delta\tilde{\rho}_{r,s}^{p,q}) &= \frac{\varepsilon_{\Delta\rho}}{\lambda_w} - \Delta\varepsilon_{\phi w, r,s}^{p,q} + \frac{(1 - \sqrt{\alpha})}{\lambda_1} (\Delta I_{r,s}^{p,q} - \Delta\hat{I}_{r,s}^{p,q}) \\ &\quad + \Delta N w_{r,s}^{p,q} - \Delta N w_{r,s}^{p,q}|_0 \\ &= T + \Delta N w_{r,s}^{p,q} - \Delta N w_{r,s}^{p,q}|_0, \end{aligned} \quad (10.48)$$

as compared to a tolerance,  $T$ , based on estimated standard deviations of the errors, is attributable to an incorrect value of  $\Delta N_{r,s}^{p,q}|_0$ .

Equation (10.48) not only serves to detect a cycle slip, but can also be used immediately to compute the ambiguity,  $\Delta N w_{r,s}^{p,q}$ , if  $T$  is less than 0.5 cycles. Such a small value of  $T$  depends mostly on the standard deviation of  $\varepsilon_{\Delta\rho}$ , that reflects the accuracy of the predicted range based on the inertially derived position. If  $T > 0.5$  cy (e.g., because the predicted range has degraded due to an extended GPS outage), standard search techniques should be attempted to find the correct value of the ambiguity, which may take several epochs to converge. We note that once a cycle ambiguity is determined it is valid backward in time to the epoch of the cycle slip, or the start of satellite tracking.

## 10.4 Moving-Base Gravimetry

GPS and INS are integrated primarily for applications in positioning and navigation, as shown in the previous sections, because of their complementary error characteristics and consequent mutual aiding abilities. There is another type of integration that has attracted the geodetic and geophysical communities in their efforts to measure the gravity field. It is based directly on the fundamental equation, (1.7), that is, Newton's second law of motion. With a slight rearrangement, we have simply

$$\mathbf{g}^i = \ddot{\mathbf{x}}^i - \mathbf{a}^i, \quad (10.49)$$

which holds in the  $i$ -frame and says that the gravitational vector is the difference between the total acceleration, e.g., as determined kinematically by differentiating GPS-derived positions, and the specific force, as measured by an accelerometer. In fact, this is not an integration or blending of GPS and INS, but a collocation of two distinct sensors whose functional dissimilarity is the essence of the combination that, at the same time, suffers from their contrasting error characteristics. That is, since neither system aids the other, their errors combine. We know that INS errors accumulate with time and thus are significant primarily in the long term. Assuming GPS position errors are mostly white, the corresponding errors in the derived acceleration are large at high frequencies, or in the short term. Consequently, there is

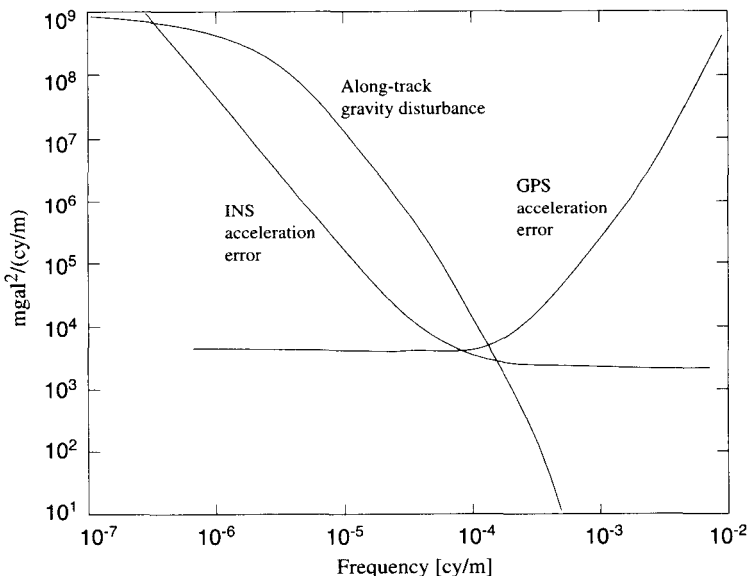


Figure 10.8: Spectral window for gravity disturbance estimation using INS and GPS.

only a potentially small window within which the gravitational signal may be discerned. This is shown graphically in Figure 10.8 (see also Schwarz et al., 1992) in terms of along-track power spectral densities (power per frequency). The window depends also on the speed of the vehicle and moves to the right relative to the gravity signal with decreasing speed.

It is noted that all gravimetry, whether static or on a moving platform, derives fundamentally from Newton's law, (10.49). In the static case, a gravimeter, being a very precise vertical accelerometer, senses the reaction (a specific force) of Earth's surface on the stationary platform due to the gravitational acceleration plus the small effect of the centrifugal acceleration from Earth's rotation. On a moving platform, such as an airplane, the gravimeter senses the lift exerted on the wings, as well as reactions to centrifugal and Coriolis accelerations. In both cases, vertical gravitation can be extracted from the gravimeter measurements only if the vertical component of the total acceleration,  $\ddot{x}^i$ , of the platform is obtained independently (which in the static case is just a component of the centrifugal acceleration). Because of the measurement principles associated with force-rebalance (and vibrating-beam) accelerometers (Sections 3.3.3 and 3.3.4), we also realize that these sensors yield accelerations only relative to some initial calibrated value and, as such, are suitable only for *relative* gravimetry.

We develop the concepts of INS/GPS gravimetry from the general three-dimensional perspective, thus easily allowing the consideration of special cases, such as vertical gravimetry (e.g., using a relative gravimeter). Correspondingly, a distinction is also made between *vector gravimetry*, the determination of the entire

vector of gravity (or at least more than a single component), and *scalar gravimetry*, referring to the measurement of (usually) the down component or the magnitude of the vector. Furthermore, we distinguish between the method of *accelerometry*, based on direct measurements of acceleration, and an approach, already indicated in Section 10.2, based on positioning, where an inertial system, such as the inertial surveying system, may be used to obtain estimates of the gravity vector components.

The accelerometric approach is a straightforward, literal application of (10.49). The acceleration (specific force) of the platform is taken from the output of the inertial sensors (accelerometers) and properly oriented by the gyros. The kinematic acceleration must be calculated independently by numerical differentiation with respect to time of positions determined by GPS, or radar or laser altimetry in the case of scalar (vertical) gravimetry. Subsequently, gravitational components are estimated from the difference of these two types of accelerations.

In the case of inertial positioning, the accelerometer measurements are integrated numerically once with respect to time to obtain velocity and again to obtain positions, thus yielding

$$\mathbf{x}^i = \mathbf{x}_0^i + (t - t_0)\dot{\mathbf{x}}_0^i + \int_{t_0}^t \int_{t_0}^t (\mathbf{a}^i + \mathbf{g}^i) dt dt, \quad (10.50)$$

in accordance with the basic equation (10.49). A more complicated formula ensues in the *n*-frame, derivable from (4.91); but the principle is the same. These inertially indicated positions or velocities are compared to external updates of kinematic positions or velocities (such as ZUPT's) and will differ from them because an incorrect value of gravitation was used in (10.50) (or (4.91)). The observed discrepancy may then lead to an estimation of the correct gravitation using an appropriate procedure, such as the Kalman filter. In comparison to accelerometry, this indirect type of determination punctuates a fundamental difference in the approaches to gravity field estimation with inertial instrumentation. Both techniques use the same sensor data, but the data processing differs, involving a numerical differentiation in the first case and a numerical integration in the second. These approaches are sufficiently distinct to imply profound theoretical as well as numerical subtleties; in fact, both have merit, as well as disadvantages.

One aspect of vector gravimetry that is common to all approaches is the strong coupling of uncompensated gyro errors into the horizontal acceleration components. Consider the north component whose velocity error dynamics equation (5.71) is repeated here:

$$\frac{d}{dt} \delta v_N = -2\omega_e \sin \phi \delta v_E - a_D \psi_E + a_E \psi_D + \delta a_{AN} + \delta \bar{g}_N, \quad (10.51)$$

where now we have taken  $\mathbf{a}^n$  from (4.101). There are four acceleration terms forcing the dynamics of the velocity error, all potentially of similar magnitude. The gravity disturbance component typically has a magnitude on the order of 40 mgal; and uncompensated accelerometer biases in medium-to-high accuracy systems are only

somewhat smaller. The term,  $-a_D\psi_E$ , couples the dynamics of the east orientation error into acceleration errors in the ratio  $a_D \approx -\bar{g} \approx 10 \text{ m/s}^2$ , or about 1 mgal per  $10^{-6}$  rad ( $\approx 0.2$  arcsec) of orientation error. The down orientation error is less influential since for low dynamics of the vehicle,  $|a_E| \ll \bar{g}$ .

It is possible to isolate the gravity disturbance from the other acceleration terms only if its signal, transformed into the time domain using the velocity of the vehicle, is sufficiently distinct in character. More precisely, those *spectral* components of  $\delta\bar{g}_N$  can be estimated that are separable from the effects of the system errors. With benign vehicle dynamics, the accelerometer biases essentially remain biases in the navigation frame. And, if the dynamics of the orientation error,  $\psi_E$ , as a consequence of stable motion are governed largely by gyro drifts (see (5.75) and (5.74)), then the corresponding acceleration error,  $-a_D\psi_E$ , is uniform and resembles a trend. In this case, bias-removal and detrending techniques allow estimation of at least the short wavelengths of the horizontal gravity components. On the other hand, it is clear that because of the term,  $-a_D\psi_E$  (and, similarly,  $a_D\psi_N$  for the east component), the orientation accuracy is extremely critical in vector gravimetry, especially since the gyro errors tend to dominate in inertial navigation systems.

In addition, velocity errors also affect the estimation accuracy through the Coriolis terms. For example, errors as little as 10 cm/s in any component already cause acceleration errors on the order of 1 mgal, as seen in (10.51) with  $\phi = 45^\circ$  (see also (5.71)).

The following discussions address only moving-base terrestrial systems (thus excluding space-borne systems which are now in development (Jekeli, 1999), but including airborne systems). Furthermore, it is assumed that gravity field determination is restricted to the gravity disturbance vector, usually defined as the residual to the normal gravity vector, as in (6.95). The discussion easily holds, however, if the reference gravity field is a higher-degree, approximating, truncated, spherical harmonic series, analogous to (6.99). The reference field, whether represented by normal gravity or a higher-degree model, always includes the centrifugal acceleration due to Earth's rotation, so that the gravity disturbance components are pure gravitational accelerations (but we retain the over-bar notation for consistency).

#### 10.4.1 Gravitation from Inertial Positioning

Oddly, implementation of the method of inferring the (horizontal) gravity disturbance components from the errors associated with inertial positioning preceded the more natural and direct approach of measuring them with accelerometers. The reasons for this, however, are clear: a mechanism already existed to deal with INS errors using optimal estimation techniques (e.g., the Kalman filter); and, it was difficult or impossible to obtain reliable kinematic accelerations, that is,  $\ddot{\mathbf{x}}$ , by differentiating position coordinates in time.

The error dynamics model that includes the gravity disturbance as an error state of the system was derived in Section 5.3. In the  $n$ -frame coordinatization it is equation (5.66), and the relevant components of the forcing term,  $G^n\mathbf{u}$ , belonging to the

velocity error dynamics are obtained from (5.65) and (5.68) as

$$[G^n \mathbf{u}]_{\text{rows } 4,5,6} = D^{-1}(C_s^n \delta \mathbf{a}^s + \delta \bar{\mathbf{g}}^n). \quad (10.52)$$

It is noted however that the instability of free inertial navigation in the vertical direction (Section 5.2) makes the estimation of the vertical gravity disturbance component rather problematic with this method. That is, in principle, we require both GPS and INS to act as independent sensors in order to extract the gravitational signal. It exceeds the capability of GPS to serve reasonably in that function and also provide the vertical damping required for precise inertial vertical positioning. Therefore, we exclude vertical position and velocity errors from the system state vector, and consequently restrict gravity estimation to the horizontal components.

In order to apply a Kalman filter to the errors, each of the components,  $\delta \mathbf{a}^s$  and  $\delta \bar{\mathbf{g}}^n$ , must further be expressed as a linear model of stochastic parameters. For the accelerometer error, we could choose (10.30), and the gravity disturbance elements might be represented as Gauss-Markov processes. We then have

$$[G^n \mathbf{u}]_{\text{rows } 4,5} = JD^{-1} C_s^n (\mathbf{b} + \text{diag}(\mathbf{a}^s) \boldsymbol{\kappa}_A + \mathbf{w}_A) + JD^{-1} \delta \bar{\mathbf{g}}^n, \quad (10.53)$$

where  $\mathbf{J}$  is defined in (10.34),  $\mathbf{D}$  in (5.69), and where each element of  $\delta \bar{\mathbf{g}}^n$ , if modeled as a third-order process, satisfies a differential equation of the type (6.104) and introduces two extra parameters. The total state vector in this case is given by (10.31) and (10.32), augmented by the states of the gravity disturbance models:

$$\begin{aligned} \boldsymbol{\varepsilon}_1 &= (\psi_N \quad \psi_E \quad \psi_D \quad \delta \dot{\phi} \quad \delta \dot{\lambda} \quad \delta \phi \quad \delta \lambda)^T, \\ \boldsymbol{\varepsilon}_2 &= (\mathbf{d}^T \quad \mathbf{b}^T \quad \boldsymbol{\kappa}_A^T)^T, \\ \boldsymbol{\varepsilon}_3 &= (\delta \bar{g}_N \quad \delta \bar{g}_E \quad c_{N1} \quad c_{E1} \quad c_{N2} \quad c_{E2})^T, \end{aligned} \quad (10.54)$$

where, again, the gyro error is modeled as a drift plus white noise, (10.29) and the parameters  $c_{N1}$ ,  $c_{N2}$ ,  $c_{E1}$ ,  $c_{E2}$  belong to the third-order Gauss-Markov processes. Clearly, alternative models for the sensor errors and the gravity disturbance components could reduce or increase the number of parameters in the total state vector of the system, and a judicious choice must be made to ensure estimability, as explained below. For example, with strapdown systems on level flights (or with level-stabilized platforms) the vertical accelerometer bias and scale factor play no role in the following procedure and are not estimable.

The error dynamics equation becomes, analogous to (10.33),

$$\frac{d}{dt} \begin{pmatrix} \boldsymbol{\varepsilon}_1 \\ \boldsymbol{\varepsilon}_2 \\ \boldsymbol{\varepsilon}_3 \end{pmatrix} = \begin{pmatrix} F_{11} & F_{12} & F_{13} \\ 0 & 0 & 0 \\ 0 & 0 & F_{33} \end{pmatrix} \begin{pmatrix} \boldsymbol{\varepsilon}_1 \\ \boldsymbol{\varepsilon}_2 \\ \boldsymbol{\varepsilon}_3 \end{pmatrix} + \begin{pmatrix} G_1 \\ 0 \\ G_3 \end{pmatrix} \begin{pmatrix} \mathbf{w}_G \\ \mathbf{w}_A \\ \mathbf{w}_{\delta g} \end{pmatrix}, \quad (10.55)$$

where  $F_{11}$  is the same as  $F_1$  in (10.33) and is given by the  $7 \times 7$  matrix in (10.28); also  $F_{12}$  is the same as  $F_2$ , given in (10.34), and

$$F_{13} = \begin{pmatrix} 0 & 0 \\ 3 \times 2 & 3 \times 4 \\ JD^{-1}J^T & 0 \\ 0 & 2 \times 4 \\ 0 & 0 \\ 2 \times 2 & 2 \times 4 \end{pmatrix}, \quad (10.56)$$

$$F_{33} = \begin{pmatrix} 0 & I & 0 \\ 2 \times 2 & 2 \times 2 & 2 \times 2 \\ 0 & 0 & I \\ 2 \times 2 & 2 \times 2 & 2 \times 2 \\ -v^3 \text{ diag}(\beta_N^3, \beta_E^3) & -3v^2 \text{ diag}(\beta_N^2, \beta_E^2) & -3 \text{ diag}(\beta_N, \beta_E) \end{pmatrix}.$$

The speed of the vehicle is  $v$ , and the two parameters,  $\beta_N$ ,  $\beta_E$ , with specified values correspond, respectively, to each of the two Gauss-Markov models, as given in (6.103). Also, the white noise processes associated with these models are contained in the  $2 \times 1$  vector,  $w_{\delta g}$ . Analogous to (10.34), we have in this case

$$G_1 = \begin{pmatrix} C_s^n & 0 & 0 \\ 3 \times 3 & 3 \times 2 \\ 0 & JD^{-1}C_s^n & 0 \\ 2 \times 3 & 2 \times 2 \\ 0 & 0 & 0 \\ 2 \times 3 & 2 \times 3 & 2 \times 2 \end{pmatrix}, \quad G_3 = \begin{pmatrix} 0 & 0 \\ 4 \times 6 & 4 \times 2 \\ 0 & I \\ 2 \times 6 & 2 \times 2 \end{pmatrix}. \quad (10.57)$$

The observations that serve as updates are the differences (7.51) between the indicated geodetic coordinates obtained by integrating the inertial navigation equations and the externally obtained geodetic coordinates, such as from GPS. Analogous to (10.36), the observation matrix is given by

$$H = \begin{pmatrix} 0 & I & 0 \\ 2 \times 5 & 2 \times 2 & 2 \times 15 \end{pmatrix}. \quad (10.58)$$

Again, as discussed in Section 10.3.1, the difference in location between the GPS antenna and the INS should be taken into account with a simple offset correction that depends also on the orientation of the body-frame with respect to the navigation frame. Alternatively, one could introduce these offsets, that vary with the dynamics of the vehicle, as additional stochastic parameters in the state vector.

The Kalman filter then distributes these observed discrepancies among the various error parameters with optimal weights according to given stochastic information, as in (7.72). Two of these parameters are the gravity disturbance components whose estimates are also accompanied by a covariance matrix (the appropriate diagonal block in (7.73)). This estimation procedure is shown schematically in Figure 10.9.

The efficacy of this method, therefore, relies on specifying reasonable stochastic models, not only for the usual systematic errors of the inertial sensors, but also for the gravitational disturbance components. The models and the states they represent must be sufficiently distinct in order to achieve estimability of the disturbances as individual “errors” that are not lumped inseparably with other errors. That is, the inseparability of accelerometer bias and tilt error (caused by gyro drift), already examined in Section 5.4, extends to the gravity disturbance components, as dis-

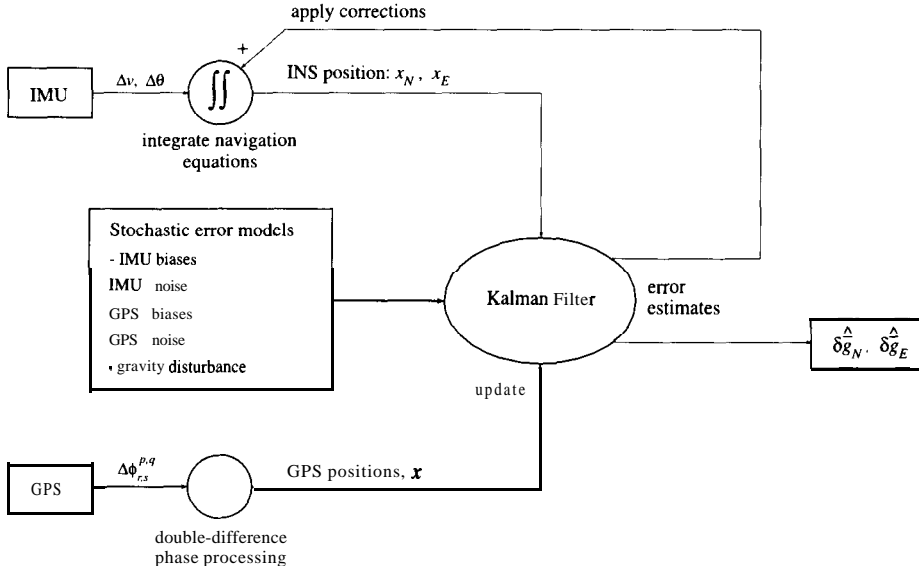


Figure 10.9: Basic gravity disturbance estimation procedure with inertial positioning approach.

cussed above. The stochastic nature of the latter must be different from that of the sensor errors so that the filter yields accurate estimates.

This reliance of the gravity disturbance estimation on stochastic models elicits several criticisms (see also Schwarz and Li, 1996). In the first place, that it is possible to interpret the gravity disturbance as a stochastic process may be argued both ways. It is clear, however, that the estimation is sensitive to the chosen model (Jekeli, 1995), thus diminishing the robustness of the method. This is compounded by the additional shortcomings, elaborated in Section 6.6.3, of stochastically modeling the gravity disturbance vector. That is, it cannot be done with complete infallibility since the Kalman filter is one-dimensional and the models are of finite order, neither of which applies to the gravity field; and, correlations among different components usually are neglected for the sake of simplicity.

There are some advantages, however; primarily, the updates are in the form of observed positions (or velocities), both of which are relatively easy to obtain kinematically. The classic example is the ZUPT, but, of course, GPS now offers accurate kinematic positioning of moving platforms almost continuously. Also, the fact that inertial navigation involves integration with respect to time means that the random errors of the IMU's tend to shift towards the lower frequencies thus producing a smoother result. Finally, the estimation is optimal and includes a covariance determination, but this is valid only if the models are reasonably accurate.

Demonstrations of inertial vector gravimetry go back to Rose and Nash (1972), who used ship-borne INS with position and velocity updates obtained from

LORAN. The method was studied and applied mostly to inertial survey systems (Schwarz, 1980; Huddle, 1986) because of the strong and frequent updates in the form of ZUPT's. Still, the most serious impediment is the gyro drift error that combines directly with the horizontal gravity disturbance component in the positioning error, as illustrated in (10.51). To solve these problems some “gravity updates” (externally measured deflections of the vertical, (6.98)) were included at control stations to help separate the drift error from the horizontal components along the survey trajectory. The obvious impracticality of ZUPT's with a fixed-wing airborne system motivated Northrop Corporation (1986) to use a stellar camera collocated with the INS to update the orientation angles with observed directions to known stars, thus continually controlling the drift error of the gyros (see also (Mangold, 1997)). An alternative to this rather expensive and environment-limited solution is to measure attitude by three or more GPS antennas on the aircraft. Tests have shown, however, that the flexure of the needed long baselines (several meters) may preclude adequate orientation control for airborne vector gravimetry.

#### 10.4.2 Gravitation from Accelerometry

The more direct approach to vector gravimetry is the straightforward generalization of scalar gravimetry based on acceleration measurements with accelerometers (usually a gravimeter in the scalar case) and kinematic accelerations observed from precise positioning. The success of airborne vertical gravimetry is attributable primarily to the ability of GPS to provide kinematic positioning with both sufficient accuracy and resolution to compute kinematic vertical accelerations, as well as horizontal velocities (Brozena and Peters, 1992; Hein, 1995). Other systems such as radar and laser altimetry and LORAN have also yielded good results, but GPS clearly dominates current operations. The same concept may be extended to vector gravimetry. It is noted that the problem of orientation errors coupling the strong vertical acceleration into horizontal acceleration errors does not disappear with this approach, but there is no inherent dependence on a stochastic interpretation or modeling of the gravity disturbance vector, as in the previous approach.

In terms of the specific force,  $\mathbf{a}^s$ , in the sensor frame and the kinematic acceleration,  $\ddot{\mathbf{x}}^i$ , in the  $i$ -frame, the gravitation vector is expressed from (10.49) in the  $n$ -frame as follows:

$$\mathbf{g}^n = C_i^n (\ddot{\mathbf{x}}^i - C_s^i \mathbf{a}^s). \quad (10.59)$$

In the case of stabilized platform systems, the transformation matrices,  $C_i^n$  and  $C_s^i$ , are combined mechanically with  $\mathbf{a}^s$  to yield directly the accelerations in the mechanized frame (e.g., the  $n$ -frame, or also, with appropriate modifications, the wander azimuth frame). However, we consider only strapdown IMU's where the sensor frame is the same as the body frame. The gravity disturbance vector is obtained by removing from  $\mathbf{g}^n$  the normal gravity vector corrected for Earth's centrifugal acceleration (compare (4.89) and (6.95)):

$$\begin{aligned}\delta\bar{\mathbf{g}}^n &= \bar{\mathbf{g}}^n - \gamma^n = \mathbf{g}^n - C_e^n \Omega_{ie}^e \Omega_{ie}^e \mathbf{x}^e - \gamma^n \\ &= C_i^n (\ddot{\mathbf{x}}^i - C_b^i \mathbf{a}^b) - (\gamma^n + C_i^n \Omega_{ie}^i \Omega_{ie}^i \mathbf{x}^i),\end{aligned}\quad (10.60)$$

where  $\Omega_{ie}^e = C_i^e \Omega_{ie}^i C_e^i$ , whose non-zero components are  $\pm \omega_e$ , according to (1.77).

All quantities on the right side of (10.60) are measured or computed. The accelerometers yield  $\mathbf{a}^b$ , and the transformation matrix,  $C_b^i$ , from the body frame to the inertial frame is obtained directly from the output of the gyros,  $\boldsymbol{\omega}_{ib}^b$ , by integrating the corresponding differential equation for the quaternions, (4.21) (see Section 4.2.3.1). Gyro errors here will affect the computation of  $C_b^i \mathbf{a}^b$ , as discussed above. The transformation matrix,  $C_i^n = C_e^n C_i^e$ , given by (1.87) and (1.78), is readily calculated from the position of the vehicle using the transformation (1.84) from Cartesian Earth-fixed to geodetic coordinates (where, of course,  $\mathbf{x}^e = C_e^e \mathbf{x}^i$ ). An error in these coordinates represents a misregistration error of the gravity disturbance vector. The magnitude of this error depends on the gradients of the gravity disturbance components, which are small enough (usually much less than 0.1 mgal/m) to allow several meters of position error. The height determination is the most critical, affecting the calculation of the vertical component,  $\gamma_h$ , of the normal gravity vector to the extent of 0.31 mgal per meter of error (reflecting the vertical gradient of gravity). However, all positioning requirements for registration of computed and estimated quantities are easily achieved with GPS.

What demands much more precision, however, is the position,  $\mathbf{x}^i$ , that must be differentiated to obtain the kinematic acceleration:

$$\ddot{\mathbf{x}}^i = \frac{d^2}{dt^2} \mathbf{x}^i. \quad (10.61)$$

Many standard numerical techniques exist to calculate the acceleration from positions, among them fitting each component of  $\mathbf{x}^i$ , as a function of time, to cubic splines. An approximate relationship between the accuracy in position and the corresponding acceleration accuracy is obtained by considering a simple least-squares fit to Galileo's law:

$$x_j^i(t) = \frac{1}{2} a_j t^2, \quad j = 1, 2, 3, \quad t = \Delta t, 2\Delta t, \dots, n\Delta t; \quad (10.62)$$

where  $a_j$  represents the  $j^{\text{th}}$  component of the acceleration vector to be estimated over some integration (averaging) time,  $\tau = n\Delta t$ . The unweighted least-squares estimate of  $a_j$  is given by (7.39)

$$\hat{a}_j = (H^T H)^{-1} H^T \mathbf{y}_j, \quad (10.63)$$

where

$$H = \frac{\Delta t^2}{2} (1^2 \quad 2^2 \quad \cdots \quad n^2)^T, \quad \mathbf{y}_j = (x_j^i(\Delta t) \quad x_j^i(2\Delta t) \quad \cdots \quad x_j^i(n\Delta t))^T. \quad (10.64)$$

The variance of the estimate is given by

$$\begin{aligned}\sigma_{a_j}^2 &= (H^T H)^{-1} H^T \mathcal{E}(y_j y_j^T) H (H^T H)^{-1} = \sigma^2(x_j^i) (H^T H)^{-1} \\ &= \sigma^2(x_j^i) \frac{4}{\Delta t^4} \left( \sum_{k=1}^n k^4 \right)^{-1},\end{aligned}\quad (10.65)$$

where it is assumed that the errors in the position coordinates are uncorrelated (the covariance matrix,  $\mathcal{E}(y_j y_j^T)$ , is diagonal) and all have the same variance,  $\sigma^2(x_j^i)$ . An approximate formula for the sum of many consecutive integers to the  $q^{\text{th}}$  power is

$$\sum_{k=1}^n k^q \approx \frac{n^{q+1}}{q+1}, \quad (n \gg 1). \quad (10.66)$$

Therefore, with  $q = 4$ , (10.65) becomes

$$\sigma_{a_j}^2 \approx \frac{20 \Delta t}{\tau^5} \sigma^2(x_j^i). \quad (10.67)$$

Taking  $\Delta t = 1$  s and an averaging time of  $\tau = 60$  s, a standard deviation in position of 6 cm translates into an acceleration accuracy of about 1 mgal. Examples of acceleration computations from GPS-derived position coordinates are found in (Wei and Schwarz, 1995) and (Jekeli and Garcia, 1997).

Because the GPS antenna and the INS do not occupy the same location on or in the vehicle, the computed and sensed accelerations refer to different points in space. However, these points presumably are rigidly connected and the accelerations are related by the lever-arm effect derived in Section 3.3.1. Adapting (3.98) to the present circumstances, where the case in Figure 3.13 is the vehicle ( $b$ -frame) and  $\mathbf{b}^b$  represents the coordinate vector of the GPS antenna with respect to the origin of the  $b$ -frame (taken to be the location of the IMU), we have

$$\ddot{x}_{\text{antenna}}^i = \ddot{x}_{\text{IMU}}^i + C_b^i (\omega_{ib}^b \times \mathbf{b}^b + \dot{\omega}_{ib}^b \times (\omega_{ib}^b \times \mathbf{b}^b)), \quad (10.68)$$

with subscripts “antenna” and “IMU” indicating the locations of the GPS antenna and IMU, respectively.  $\ddot{x}_{\text{antenna}}^i$  is the acceleration computed from GPS position coordinates and  $\ddot{x}_{\text{IMU}}^i$  is the acceleration required in (10.59). The angular rate,  $\omega_{ib}^b$ , of the vehicle with respect to the  $i$ -frame, embodied in the corresponding transformation matrix,  $C_b^i$ , comes directly from the gyros (as noted above); and, the angular acceleration,  $\dot{\omega}_{ib}^b$ , could be obtained by numerical differentiation. However, this Coriolis term, in particular, and also the centrifugal term require significant smoothing to reduce the high-frequency errors generated by the white noise of the gyros. We note that (3.96) and (3.97) also yield the lever-arm effect in the forms

$$\begin{aligned}\ddot{x}_{\text{antenna}}^i - \ddot{x}_{\text{IMU}}^i &= \frac{d^2}{dt^2} (C_b^i \mathbf{b}^b), \\ \ddot{x}_{\text{antenna}}^i - \ddot{x}_{\text{IMU}}^i &= \frac{d}{dt} (C_b^i \omega_{ib}^b \times \mathbf{b}^b).\end{aligned}\quad (10.69)$$

In practice, the numerical differentiation (with smoothing) of the bracketed terms on the right-hand sides of (10.69) may yield more stable results.

#### 10.4.2.1 Kalman Filter Approaches

It may be desirable or even necessary to estimate the major errors associated with the IMU in the direct accelerometric approach. A Kalman filter can be formulated very simply in which the kinematic acceleration serves as external update. The error states of the system are now limited to the IMU error parameters and the orientation errors, which link the gyro and accelerometer errors; and in accordance with the traditional approach, one may include the gravity disturbance components in the state vector. For illustrative purposes, as in (10.54), we restrict the sensor errors to biases and accelerometer scale factor errors; however, in actual situations a different set of parameters may be chosen depending on their estimability.

Thus, let the system state vector be

$$\boldsymbol{\varepsilon} = ((\boldsymbol{\psi}^i)^T \quad \boldsymbol{\varepsilon}_2^T \quad \boldsymbol{\varepsilon}_3^T)^T, \quad (10.70)$$

where  $\boldsymbol{\psi}^i$  is the vector of orientation errors that are committed in realizing the inertial frame; and the vectors  $\boldsymbol{\varepsilon}_2$  and  $\boldsymbol{\varepsilon}_3$ , given in (10.54), respectively contain the sensor error states and the state variables associated with the models for the gravity disturbance components. The dynamics of the orientation errors are given by the first equation in (5.46); and, as before, the sensor errors are assumed to be random constants, whose dynamics are given by (6.63). The three gravity disturbance components could each be represented (usually in the  $n$ -frame) by a third-order Gauss-Markov process, satisfying (6.81); that is,  $\boldsymbol{\varepsilon}_3$  now contains nine elements:

$$\boldsymbol{\varepsilon}_3 = (\delta\bar{g}_N \quad \delta\bar{g}_E \quad \delta\bar{g}_D \quad c_{N1} \quad c_{E1} \quad c_{D1} \quad c_{N2} \quad c_{E2} \quad c_{D2})^T. \quad (10.71)$$

With  $\delta\omega_{ib}^b = \mathbf{d} + \mathbf{w}_G$ , similar to (10.29), we have:

$$\frac{d}{dt} \begin{pmatrix} \boldsymbol{\psi}^i \\ \boldsymbol{\varepsilon}_2 \\ \boldsymbol{\varepsilon}_3 \end{pmatrix} = \begin{pmatrix} 0 & F & 0 \\ 0 & 0 & 0 \\ 0 & 0 & F_{33} \end{pmatrix} \begin{pmatrix} \boldsymbol{\psi}^i \\ \boldsymbol{\varepsilon}_2 \\ \boldsymbol{\varepsilon}_3 \end{pmatrix} + \begin{pmatrix} G_1 \\ 0 \\ G_3 \end{pmatrix} \begin{pmatrix} \mathbf{w}_G \\ \mathbf{w}_{\delta_g} \end{pmatrix}, \quad (10.72)$$

where

$$F = \begin{pmatrix} -C_b^i & 0 \\ 0 & 3 \times 6 \end{pmatrix}, \quad G_1 = \begin{pmatrix} -C_b^i & 0 \\ 0 & 3 \times 3 \end{pmatrix}, \quad G_3 = \begin{pmatrix} 0 & 0 \\ 0 & I \\ 3 \times 3 & 3 \times 3 \end{pmatrix}, \quad (10.73)$$

and  $F_{33}$ , analogous to (10.56), is

$$F_{33} = \begin{pmatrix} 0 & I & 0 \\ 0 & 0 & I \\ -v^3 \text{diag}(\beta_N^3, \beta_E^3, \beta_D^3) & -3v^2 \text{diag}(\beta_N^2, \beta_E^2, \beta_D^2) & -3 \text{diag}(\beta_N, \beta_E, \beta_D) \end{pmatrix}. \quad (10.74)$$

Corresponding to (7.51), the observation update is given by the difference between the acceleration sensed by the IMU and the comparable externally observed acceleration obtained from the kinematic acceleration and gravitation, according to  $\mathbf{a}^i = \ddot{\mathbf{x}}^i - \mathbf{g}^i$ . In this case, we presume to know only the normal gravity,  $\gamma^i$  (plus centrifugal acceleration), where (see also (10.60))

$$\mathbf{g}^i = \gamma^i + \Omega_{ie}^i \Omega_{ie}^i \mathbf{x}^i + \delta\bar{\mathbf{g}}^i, \quad (10.75)$$

and  $\delta\bar{\mathbf{g}}^i$  is the gravity disturbance vector in the  $i$ -frame. Therefore, the observation model becomes

$$\mathbf{y} = \tilde{\mathbf{a}}^i - (\tilde{\mathbf{x}}^i - (\gamma^i + \Omega_{ie}^i \Omega_{ie}^i \mathbf{x}^i)), \quad (10.76)$$

where the tilde, “~”, signifies observations or quantities indicated by the sensor. The registration error (due to incorrect position coordinates) in the normal gravity (plus centrifugal part) is of no concern with reasonably accurate positioning, as discussed above. Again, the computed acceleration,  $\tilde{\mathbf{x}}^i$ , refers to the reference point of the IMU and should include the lever-arm effect, indicated in (10.68) or (10.69).

The observations,  $\mathbf{y}$ , reflect the errors in the sensed and computed accelerations:

$$\begin{aligned} \tilde{\mathbf{a}}^i &= \mathbf{a}^i + \delta\mathbf{a}^i, \\ \tilde{\mathbf{x}}^i &= \dot{\mathbf{x}}^i + \delta\dot{\mathbf{x}}^i. \end{aligned} \quad (10.77)$$

These errors are given by the combination of (5.35), specialized to the  $i$ -frame, and  $\delta\mathbf{a}^b$  from (10.30), as well as by an assumed white noise,  $\mathbf{w}_K$ , for the kinematic acceleration:

$$\begin{aligned} \delta\mathbf{a}^i &= C_b^i \delta\mathbf{a}^b - \Psi^i C_b^i \mathbf{a}^b \\ &= C_b^i (\mathbf{b} + \text{diag}(\mathbf{a}^b) \boldsymbol{\kappa}_A + \mathbf{w}_A) + \mathbf{a}^i \times \boldsymbol{\psi}^i, \\ \delta\dot{\mathbf{x}}^i &= \mathbf{w}_K. \end{aligned} \quad (10.78)$$

The latter is an idealization that is reasonably approximated with sufficient smoothing to reduce the high-frequency errors generated by the numerical differentiation. Substituting (10.77) into (10.76) and considering (10.49) and (10.75), the observation model becomes

$$\mathbf{y} = \delta\mathbf{a}^i - \delta\dot{\mathbf{x}}^i - \delta\bar{\mathbf{g}}^i. \quad (10.79)$$

With (10.78), it can be expressed in terms of the system states as

$$\mathbf{y} = H\boldsymbol{\varepsilon} + \mathbf{v}, \quad (10.80)$$

where the observation matrix is

$$H = ([\mathbf{a}^i \times] \quad 0 \quad C_b^i \quad C_b^i \text{diag}(\mathbf{a}^b) \quad -C_n^i \quad 0 \quad 0), \quad (10.81)$$

and the noise vector is

$$\mathbf{v} = C_b^i \mathbf{w}_A - \mathbf{w}_K. \quad (10.82)$$

Assuming the errors  $\mathbf{w}_A$  and  $\mathbf{w}_K$  are uncorrelated and have respective covariance

matrices  $R_A$  and  $R_K$ , the covariance matrix of  $\nu$  is given by

$$R = C_b^T R_A C_b + R_K. \quad (10.83)$$

The estimate of the state parameter vector,  $\varepsilon$ , which includes the gravity disturbance components is computed recursively by (7.72) with covariance matrix given by (7.73). In contrast to the solution of Section 10.4.1, this approach yields estimates for all three components of  $\delta\bar{g}^n$  since it is not based on determining an inertial navigation solution. However, the method still requires a stochastic model for the gravity disturbance which, as discussed in Sections 10.4.1 and 6.6.3 is a problematic construct.

An alternative that was applied with some success by Jekeli and Kwon (1999) removes the gravity disturbance vector from the error parameters which are then represented by

$$\hat{\varepsilon} = ((\psi^i)^T \quad \varepsilon_2^T)^T, \quad (10.84)$$

with a corresponding simplification in the dynamics equation (10.72):

$$\frac{d}{dt} \begin{pmatrix} \psi^i \\ \varepsilon_2 \end{pmatrix} = \begin{pmatrix} 0 & F \\ 0 & 0 \end{pmatrix} \begin{pmatrix} \psi^i \\ \varepsilon_2 \end{pmatrix} + \begin{pmatrix} G \\ 0 \end{pmatrix} w_G. \quad (10.85)$$

The observation model (10.80) now *formally* becomes

$$\hat{y} = y + \delta\bar{g}^i = \hat{H} \hat{\varepsilon} + \nu, \quad (10.86)$$

where the observation matrix is

$$\hat{H} = ([\alpha^i \times] \quad 0 \quad C_b^i \quad C_b^i \text{ diag}(\alpha^b)). \quad (10.87)$$

The covariance matrix for the noise is still given by (10.83).

Applying the Kalman filter to the system states, (10.84), dynamically varying according to (10.85) and updated with observed values,  $y$ , computed by (10.76), yields corresponding estimates of these states:

$$\hat{\varepsilon} = \hat{\varepsilon} + \delta\hat{\varepsilon}, \quad (10.88)$$

where

$$\delta\hat{\varepsilon} = ((\delta\psi^i)^T \quad \delta d^T \quad \delta b^T \quad \delta \kappa_A^T)^T \quad (10.89)$$

are the respective true errors in the estimates. The parameter estimates,  $\hat{\varepsilon}$ , lead to an *adjusted* observation given by

$$\hat{y} = \hat{H} \hat{\varepsilon}. \quad (10.90)$$

The *residual* of this adjusted observation relative to the observed value is derived as follows, using, consecutively, equations (10.90), (10.88), (10.86), and (10.89):

$$\begin{aligned} v &= y - \hat{y} \\ &= y - \hat{H} \hat{\varepsilon} \end{aligned}$$

$$\begin{aligned}
&= \mathbf{y} - \widehat{\mathbf{H}}(\widehat{\boldsymbol{\varepsilon}} + \delta\widehat{\boldsymbol{\varepsilon}}) \\
&= \mathbf{y} - (\mathbf{y} + \delta\bar{\mathbf{g}}^i - \mathbf{v} + \widehat{\mathbf{H}}\delta\widehat{\boldsymbol{\varepsilon}}) \\
&= -\delta\bar{\mathbf{g}}^i - C_b^i(\delta\mathbf{b} + \text{diag}(\mathbf{a}^b)\delta\boldsymbol{\kappa}_A) - \mathbf{a}^i \times \delta\boldsymbol{\psi}^i + C_b^i\mathbf{w}_A - \mathbf{w}_K. \quad (10.91)
\end{aligned}$$

The residual is computed using (10.76) and (10.90) according to the first equation of (10.91); but as seen in the last equation, it contains the gravity disturbance vector as well as the true errors in the estimates of the system parameters and the noise of the IMU sensors and observed kinematic acceleration (the gyro errors enter through  $\delta\boldsymbol{\psi}^i$ ). If one can assume that the latter are all small compared to the gravity disturbance vector, then the (negative) residual estimates it:

$$\mathbf{v} \approx -\delta\bar{\mathbf{g}}^i. \quad (10.92)$$

Clearly, once determined in the  $i$ -frame,  $\delta\bar{\mathbf{g}}^i$  can easily be transformed to the  $n$ -frame using  $C_i^n$ , obtained from the position coordinates of the vehicle. The overall estimation procedure is shown schematically in Figure 10.10.

This rather unconventional method of determining the gravity disturbance vector, while simultaneously estimating the sensor errors, is based on the customary technique of detecting outliers in a least-squares adjustment by inspecting the residuals corresponding to the adjusted observations. More generally, significant systematic behavior in the residuals usually indicates faulty or deficient modeling. In our case, the observation model was approximated by the right side of (10.86).

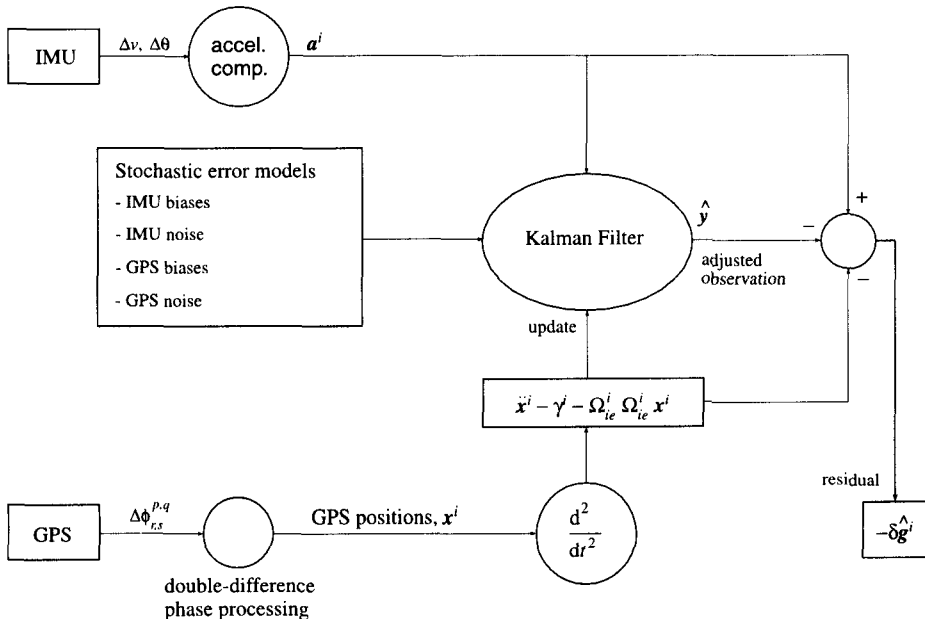


Figure 10.10: Gravity disturbance vector estimation procedure with accelerometric approach.

Of course, there are serious caveats that must accompany this method. Those parts of the gravity disturbance signal that (when transformed into the time domain by the velocity of the vehicle) exhibit the same signal characteristics as the sensor errors will be absorbed by the corresponding estimates in the Kalman filter. This means that the *true errors* in the estimates,  $\delta\hat{\epsilon}$ , can be large and thus may vitiate the result (10.92). In essence, the feasibility of the method depends on the separability of the gravity disturbance signal from the effects of sensor errors on the accelerations in the navigation frame (e.g., the  $i$ -frame). But this is the case with any of these approaches, again, highlighting the fundamental problem of moving-base vector gravimetry.

Other types of gravity modeling may be attempted (e.g., Salychev, 1995, 1998), but in the end, successful vector gravimetry depends on inertial sensors with predictably stable systematic errors and low angular and linear dynamics of the moving platform.

#### 10.4.2.2 Scalar Gravimetry

Measuring the vertical component of the gravity disturbance is far less sensitive to the coupling of  $\bar{g}_D$  with the leveling error,  $\psi$ , of the platform. In this case, the accelerometer measurement is  $\bar{g}_D$  scaled by  $\cos\psi$  and the corresponding error is only of second order:

$$\bar{g}_D \cos\psi \approx \bar{g}_D - \bar{g}_D\psi^2/2. \quad (10.93)$$

(As noted in (10.51), horizontal components are affected by first-order errors:  $\bar{g}_D \sin\psi \approx \bar{g}_D\psi$ .) This fact and precise height determination with GPS, radar, or laser altimetry have enabled airborne (scalar) gravimetry to become a viable and operational undertaking that is exploited throughout the world for geophysical exploration and scientific purposes.

Although most airborne gravimetry systems use gravimeters (traditional static instruments modified to operate in dynamic environments), the vertical accelerometer of an inertial navigation system is also a gravimeter; in principle, they are identical sensors. The following discussion, therefore, holds for both types of systems. From (4.91), the gravity vector,  $\bar{g}^n$ , in the  $n$ -frame is related to the specific force,  $\mathbf{a}^n$ , according to

$$\bar{g}^n = \frac{d}{dt} \mathbf{v}^n - \mathbf{a}^n + (\Omega_{in}^n + \Omega_{ie}^n) \mathbf{v}^n. \quad (10.94)$$

Substituting the geodetic coordinate rates, given by (4.103), into (4.102), which is the equivalent component form of (10.94), the expression for the vertical component can be extracted and becomes

$$\delta\bar{g}_D = -\gamma_D - \ddot{h} - a_D + 2\omega_e v_E \cos\phi + \frac{v_N^2}{M+h} + \frac{v_E^2}{N+h}, \quad (10.95)$$

where  $\gamma_D$  is the vertical (down) component of normal gravity in the NED frame (see (6.96) and (6.93)) and is computed from known latitude and height using (6.90).

Note that  $\ddot{h}$  is the vertical kinematic acceleration in the upward direction, while  $a_D$  is the down component of the specific force, obtained from the presumably vertical accelerometer. The last three terms on the right side of (10.95) together form the so-called *Eötvös correction*, where the last two terms are usually combined with  $R_\phi$  from (5.57) to yield the approximation:  $v^2/(R_\phi + h)$ , where  $v$  is the total horizontal speed of the vehicle.

The Eötvös correction and the vertical kinematic acceleration,  $\ddot{h}$ , can be computed by differentiating the geodetic coordinates,  $(\phi, \lambda, h)$ , obtained from a GPS solution, and making use of (4.97). A simpler and equivalent formula for  $\delta\bar{g}_D$  that bypasses the conversion of GPS-derived  $i$ -frame coordinates to geodetic coordinates and velocities is found by extracting the third component directly from (10.60):

$$\delta\bar{g}_D = [C_i^n(\ddot{\mathbf{x}}^i - \Omega_{ie}^i \Omega_{ie}^i \mathbf{x}^i)]_3 - a_D - \gamma_D, \quad (10.96)$$

where the subscript on the bracketed vector on the right identifies the vertical (positive down) component.

We can use (5.52) to determine the effects of orientation error on the measurement of  $a_D$ , as well as the effects of velocity and position errors on the computation of the Eötvös correction. Specifically, with the help of (5.67), the third component of (5.52) is expressed as follows:

$$\begin{aligned} \delta\ddot{h} &= a_2^n \psi_N - a_1^n \psi_E + 2\dot{\phi}\delta v_N + 2\dot{\ell}_1 \cos\phi \delta v_E \\ &\quad - (\lambda\dot{\ell}_2 \sin 2\phi + \bar{\Gamma}_{31}^n) r \delta\phi - \bar{\Gamma}_{32}^n r \cos\phi \delta\lambda + (\dot{\phi}^2 + \lambda\dot{\ell}_2 \cos^2\phi + \bar{\Gamma}_{33}^n) \delta h. \end{aligned} \quad (10.97)$$

The left side should not be confused with the error in the *kinematically* observed vertical acceleration; it simply represents the acceleration errors due to the effects just mentioned and listed on the right side. The first two terms produce significant errors if the vertical accelerometer (or gravimeter) either is not stabilized in the horizontal or its orientation is not known to sufficient accuracy. Note that an azimuth error,  $\psi_D$ , has no direct effect (to first order). However, the velocity, especially the east component because of Earth's spin rate, requires accurate determination; an error of 0.1 m/s in east velocity at  $\phi = 45^\circ$  produces an error of 1 mgal in acceleration. Thus, the heading (azimuth) indirectly becomes an important parameter if only the total horizontal speed can be measured accurately. Errors in the latitude and longitude of the vehicle must be as large as several arcminutes (several kilometers) before they affect the acceleration accuracy at the level of 1 mgal. On the other hand, the vertical gradient of gravity,  $\bar{\Gamma}_{33}^n \approx 0.3086$  mgal/m, makes the determination of  $\delta\bar{g}_D$  rather sensitive to vertical position errors (registration error).

Inspecting the expression (10.96), the effect of the lever-arm,  $\mathbf{b}^i = \mathbf{x}_{\text{antenna}}^i - \mathbf{x}_{\text{IMU}}^i$ , is found to be simply the vertical (third) component of the vector

$$C_i^n((\ddot{\mathbf{x}}_{\text{antenna}}^i - \ddot{\mathbf{x}}_{\text{IMU}}^i) - \Omega_{ie}^i \Omega_{ie}^i C_b^i \mathbf{b}^b), \quad (10.98)$$

where the difference,  $\ddot{\mathbf{x}}_{\text{antenna}}^i - \ddot{\mathbf{x}}_{\text{IMU}}^i$ , is obtained, e.g. from (10.69), and the term depending on  $\mathbf{b}^b$  is negligible because Earth's rotation rate is small.

## References

- Abramowitz, M. and I.A. Stegun (eds.) (1972): *Handbook of Mathematical Functions*. Dover Publications, New York.
- AFSC (1992): Specification for USAF Standard Form, Fit, and Function (F3) Medium Accuracy Inertial Navigation Unit. SNU 84-1, Rev. D, Aeronautical Systems Division, Air Force Systems Command, Wright-Patterson AFB, OH.
- Anderson, B.D.O. and J.B. Moore (1979): *Optimal Filtering*. Prentice-Hall, Englewood Cliffs, NJ.
- Arfken, G. (1970): *Mathematical Methods for Physics*. Academic Press, New York.
- Babuska, I., M. Prager, and E. Vitasek (1966): *Numerical Processes in Differential Equations*. John Wiley & Sons, Ltd., London.
- Barbour, N. and G. Schmidt (1998): Inertial sensor technology trends. Proceedings of the IEEE Symposium on Autonomous Underwater Vehicle Technology, pp. 55–62, 20–21 August 1998, Cambridge, Massachusetts.
- Bassiri, S. and G.A. Hajj (1993): Higher-order ionospheric effects on the Global Positioning System observables and means of modeling them. *Manuscripta Geodaetica*, **18**(5), 280–289.
- Baziw, J. and C.T. Leondes (1972a): In-flight alignment and calibration of inertial measurement units—part I: general formulation. *IEEE Transactions on Aerospace and Electronic Systems*, **AES-8**(4), 439–449.
- Baziw, J. and C.T. Leondes (1972b): In-flight alignment and calibration of inertial measurement units—part II: experimental results. *IEEE Transactions on Aerospace and Electronic Systems*, **AES-8**(4), 450–465.
- Beck, G.E. (1971): *Navigation Systems*. Van Nostrand Reinhold, London.
- Bierman, G.J. (1973): Fixed interval smoothing with discrete measurements. *Int. J. Control.*, **18**(1), 65–75.
- Bierman, G.J. (1977): *Factorization Methods for Discrete Sequential Estimation*. Academic Press, New York.
- BIPM (1991): Le Système International d’Unités (SI). Bureau International des Poids et Mesures, Sèvres.
- Borkowski, K.M. (1989): Accurate algorithms to transform geocentric to geodetic coordinates. *Bulletin Géodésique*, **63**, 50–56.
- Bortz, J.E. (1971): A new mathematical formulation for strapdown inertial navigation. *IEEE Trans. Aerospace and Electronic Systems*, **AES-7**(1), 61–66.
- Boyce, W.E. and R.C. DiPrima (1969): *Elementary Differential Equations and Boundary Value Problems*. John Wiley & Sons, Inc., New York.
- Britting, K.R. (1971): *Inertial Navigation Systems Analysis*. Wiley Interscience, Wiley & Sons, New York.
- Brogan, W.L. (1974): *Modern Control Theory*. Quantum Publ., Inc., New York.
- Brown, R.G. and P.Y.C. Hwang (1992): *Introduction to Random Signals and Applied Kalman Filtering*. John Wiley and Sons, Inc., New York.
- Broxmeyer, C. (1964): *Inertial Navigation Systems*. McGraw Hill Book Company, New York.
- Burdess, J.S., A.J. Harris, J. Cruickshank, D. Wood, G. Cooper (1994): Review of vibratory gyroscopes. *Engineering Science and Education Journal*, **3**(6), 249–254.
- Chatfield, A.B. (1997): *Fundamentals of High Accuracy Inertial Navigation*. American Institute of Aeronautics and Astronautics, Inc., Reston, Virginia.

- Chapin, D. (1998): Gravity instruments: past, present, future. *The Leading Edge*, **17**(1), 100–112.
- Chow, W.W., J. Gea-Banacloche, L.M. Pedrotti, V.E. Sanders, W. Schleich, and M.O. Scully (1985): The ring laser gyro. *Reviews of Modern Physics*, **57**(1), 61–104.
- Conte, S.D. and C. de Boor (1965): *Elementary Numerical Analysis*. McGraw-Hill Book Co., New York.
- Craig, R.J.G. (1972a): Theory of operation of an elastically supported, tuned gyroscope. *IEEE Transactions on Aerospace and Electronic Systems*, **AES-8**(3), 280–288.
- Craig, R.J.G. (1972b): Theory of errors of a multigimbal, elastically supported, tuned gyroscope. *IEEE Transactions on Aerospace and Electronic Systems*, **AES-8**(3), 289–297.
- Cressie, N.A.C. (1993): *Statistics for Spatial Data*. John Wiley and Sons, Inc., New York.
- Dudewicz, E.J. (1976): *Introduction to Statistics and Probability*. Holt, Rinehart, and Winston, New York.
- El-Sheimy, N. and K.P. Schwarz (1998): Navigating urban areas by VISAT—a mobile mapping system integrating GPS/INS/Digital cameras for GIS applications. *Navigation, Journal of the Institute of Navigation*, **45**(4), 275–285.
- Eissfeller, B. and P. Spietz (1989): Shaping filter design for the anomalous gravity field by means of spectral factorization. *Manuscripta Geodaetica*, **14**, 183–192.
- Everitt, C.W.F. (1988): The Stanford relativity gyroscope experiment (A): History and Overview. In: *Near Zero: New Frontiers of Physics*, edited by J.D. Fairbanks et al., W.H. Freeman and Co., New York.
- Feissel, M. and F. Mignard (1998): The adoption of ICRS on 1 January 1998: Meaning and consequences. *Astronomy and Astrophysics*, **331**(3), L33–L36.
- Forsberg, R. (1987): A New Covariance Model for Inertial Gravimetry and Gradiometry. *J. Geophys. Res.*, **92**(B2), 1305–1310.
- Fraser, D.C. (1967): A new technique for the optimal smoothing of data. Report No. T-474, M.I.T. Instrumentation Lab, Cambridge, Massachusetts.
- Gao, Y., E.J. Krakiwsky, and M.A. Abousalem (1993): Comparison and analysis of centralized, decentralized, and federated filters. *Navigation, Journal of the Institute of Navigation*, **40**(1), 69–86.
- Gear, C.W. (1971): *Numerical Initial Value Problems in Ordinary Differential Equations*. Prentice-Hall, Inc., Englewood, NJ.
- Gelb, A., 1974: *Applied Optimal Estimation*. M.I.T. Press., Cambridge, Massachusetts.
- Goldstein, H. (1950): *Classical Mechanics*. Addison-Wesley Pub. Co., Reading, MA.
- Goursat, E. (1945): *Differential Equations*. Dover Pub., New York.
- Greenspan, R.L. (1995): Inertial navigation technology from 1970–1995. *Navigation, Journal of the Institute of Navigation*, **42**(1), 165–185.
- Greenspan, R.L. (1996): GPS and inertial integration. In *Global Positioning System: Theory and Practice*, vol. II, by B.W. Parkinson and J.J. Spilker (eds.), pp. 187–220, American Institute of Aeronautics and Astronautics, Inc., Washington, DC.
- Grajner-Brzezinska, D.A., R. Da, and C. Toth (1998): GPS error modeling and OTF ambiguity resolution for high-accuracy GPS/INS integrated system. *Journal of Geodesy*, **72**(11), 626–638.
- Grajner-Brzezinska, D.A. (1999): Direct exterior orientation of airborne imagery with GPS/INS system: performance analysis. *Navigation, Journal of the Institute of Navigation*, **46**(4).
- Hadfield, M.J. (1978): Location, navigation and survey-adaptability of high precision ESG inertial systems in the 1980's. IEEE PLANS 1978, Position, Location and Navigation Symposium, 6–9 November, San Diego.

- Hagglund, J.E. and A. Hittel (1977): Evolution of the Ferranti Inertial Survey System. Proceedings of the First International Symposium on Inertial Technology for Surveying and Geodesy, 12–14 October 1977, Ottawa, pp. 257–277.
- Hannah, J. (1982a): The development of comprehensive error models and network adjustment techniques for inertial surveys. Report No. 330, Department of Geodetic Science and Surveying, Ohio State University, Columbus.
- Hannah, J. (1982b): Inertial Rapid Geodetic Survey System (RGSS) error models and network adjustment. Report No. 332, Department of Geodetic Science and Surveying, Ohio State University, Columbus.
- Hartmann, G.K. and R. Leitinger (1984): Range errors due to ionospheric and tropospheric effects for signal frequencies above 100 MHz. *Bulletin Géodésique*, **58**(2), 109–136.
- Hein, G.W. (1995): Progress in airborne gravimetry: solved, open and critical problems. Proceedings of IAG Symposium on Airborne Gravity Field Determination, IUGG XXI General Assembly, Boulder, CO, 2–14 July 1995, pp. 3–11.
- Heiskanen, W.A. and H. Moritz (1967): *Physical Geodesy*. W.H. Freeman, San Francisco.
- Heller, W.G. and S.K. Jordan (1979): Attenuated White Noise Statistical Gravity model. *J. Geophys. Res.*, **84**(B9), 4680–4688.
- Helmholtz, F.R. (1880): *Die Mathematischen und Physikalischen Theorien der höheren Geodäsie*. Teubner, Leipzig.
- Henderson, H.V. and S.R. Searle (1981): On deriving the inverse of a sum of matrices. *SIAM Review*, **23**(1), 53–60.
- Hobson, E.W. (1965): *The Theory of Spherical and Ellipsoidal Harmonics*. Chelsea Publishing, New York.
- Hofmann-Wellenhof, B., H. Lichtenegger, and J. Collins (1994): *Global Positioning System, Theory and Practice*. Springer-Verlag, Wien.
- Hotate, K. (1997): Fiber-optic gyros. In: *Optical Fiber Sensors, vol. 4, Applications, Analysis, and Future Trends*, edited by J. Dakin and B. Culshaw, pp. 167–206, Artech House, Inc., Boston.
- Huddle, J.R. (1985): Historical perspective and potential directions for estimation in inertial surveys. Proceedings of the Third International Symposium on Inertial Technology for Surveying and Geodesy, 16–20 September 1985, Banff, Canada, pp. 215–239.
- Huddle, J.R. (1986): Historical perspective on estimation techniques for position and gravity survey with inertial systems. *J. Guidance and Control*, **9**(3), 257–267.
- Huddle, J.R. and R.W. Maughmer (1972): The application of error control techniques in the design of an advanced inertial surveying system. Presented at the 28th Annual Meeting of the Institute of Navigation, West Point, New York, June 1972.
- Hursh, J.W., G. Mamon, J.A. Stoltz (1977): Aerial Profiling of Terrain. Proceedings of the First International Symposium on Inertial Technology for Surveying and Geodesy, 12–14 October 1977, Ottawa, pp. 121–130.
- IEEE (1984): IEEE Standard Inertial Sensor Terminology. IEEE Std 528-1984, New York.
- Ignagni, M.B. (1990): Optimal strapdown attitude integration algorithms. *Journal of Guidance*, **13**(2), 363–369.
- Ignagni, M.B. (1998): Duality of optimal strapdown sculling and coning compensation algorithms. *Navigation*, **45**(2), 85–96.
- IGS Central Bureau (1999): International GPS Service, Information and Resources. Report produced by Jet Propulsion Laboratory, Pasadena, CA.
- Jekeli, C. (1995): Airborne vector gravimetry using precise, position-aided inertial measurement units. *Bulletin Géodésique*, **69**(1), 1–11.
- Jekeli, C. (1999): The determination of gravitational potential differences from satellite-to-satellite tracking. *Celestial Mechanics and Dynamical Astronomy*, **75**(2), 85–100.

- Jekeli, C. and R. Garcia (1997): GPS phase accelerations for moving-base vector gravimetry. *Journal of Geodesy*, **71**, 630–639.
- Jekeli, C. and J.H. Kwon (1999): Results of airborne vector (3-D) gravimetry. *Geophysical Research Letters*, **26**(23), 3533–3536.
- Jiang, Y.F. and Y.P. Lin (1992): Improved strapdown coning algorithms. *IEEE Trans. Aerospace and Electronic Systems*, **28**(2), 484–489.
- Jordan, S.K. (1972): Self-consistent statistical models for the gravity anomaly, vertical deflection, and undulation of the geoid. *Journal of Geophysical Research*, **77**(20), 3660–3670.
- Kalman, R.E. (1960): A new approach to linear filtering and prediction problems. *Trans. ASME J. Basic Eng.*, **82**, 34–45.
- Kalman, R.E. and R.S. Bucy (1961): New results in linear filtering and prediction theory. *Trans. ASME J. Basic Eng.*, **83**, 95–108.
- Kayton, M. and W.R. Fried (1969): *Avionics Navigation Systems*. John Wiley & Sons, Inc., New York.
- Kayton, M. and W.R. Fried (1997): *Avionics Navigation Systems*. Second edition. John Wiley & Sons, Inc., New York.
- Kim, B.Y. and H.J. Shaw (1986): Fiber-optic gyroscopes. *IEEE Spectrum*, **23**(3), 54–60.
- Klobuchar, J.A. (1987): Ionospheric time-delay algorithm for single-frequency GPS users. *IEEE Trans. Aerospace and Electronic Systems*, **AES-23**(3), 325–331.
- Koch, K.R. (1987): *Parameter Estimation and Hypothesis Testing in Linear Models*. Springer Verlag, Berlin.
- Lang, S. (1971): *Linear Algebra*. Addison-Wesley Pub. Co., Reading, MA.
- Langley, R.B. (1998): GPS receivers and the observables. In *GPS for Geodesy* (2nd ed.), by P.J.G. Teunissen and A. Kleusberg (eds.), pp. 151–185, Springer-Verlag, Berlin.
- Lawrence, A. (1998): *Modern Inertial Technology: Navigation, Guidance, and Control*. Springer-Verlag, New York.
- Lefèvre, H. (1993): *The Fiber-Optic Gyroscope*. Artech House, Boston.
- Leick, A. (1995): *GPS Satellite Surveying*. John Wiley & Sons, Inc., New York.
- Lemoine, F.G. et al. (1998): The development of the joint NASA GSFC and the National Imagery Mapping Agency (NIMA) geopotential model EGM96. NASA Technical Report NASA/TP-1998-206861, Goddard Space Flight Center, Greenbelt, Maryland.
- Leondes, C.T. (ed.) (1963): *Guidance and Control of Aerospace Vehicles*. McGraw-Hill Book Company, New York.
- Linkwitz, K. and U. Hangleiter (eds.) (1995): *High Precision Navigation 95*. Proceedings of the Third International Workshop on High Precision Navigation, Dümmler Verlag, Bonn.
- Lipa, J.A. and G.M. Keiser (1988): The Stanford relativity gyroscope experiment (B): Gyroscope development. In *Near Zero: New Frontiers of Physics*, J.D. Fairbanks et al. (eds.) (W.H. Freeman and Co., New York), pp. 640–658.
- Mader, G.L. (1992): Rapid static and kinematic Global Positioning System solutions using the ambiguity function technique. *Journal of Geophysical Research*, **97**(B3), 3271–3283.
- Madsen, S.N., H.A. Zebker, and J. Martin (1993): Topographic mapping using radar interferometry: processing techniques. *IEEE Trans. Geoscience and Remote Sensing*, **31**(1), 246–256.
- Mangold, U. (1997): Theory and performance prediction for continuous vector gravimetry based on a DGPS augmented rate bias inertial navigation system and a star tracker. *Navigation, Journal of The Institute of Navigation*, **44**(3), 329–345.
- Mansour, W.M. and C. Lacchini (1993): Two-axis dry tuned-rotor gyroscopes: design and technology. *J. Guidance, Control, and Dynamics*, **16**(3), 417–425.
- Marple, S.L. (1987): *Digital Spectral Analysis with Applications*. Prentice-Hall, Inc., Englewood Cliffs, New Jersey.

- Martin, J.L. (1988): *General Relativity, A Guide to its Consequences for Gravity and Cosmology*. Ellis Horwood Ltd., Chichester.
- Maybeck, P.S. (1979): *Stochastic Models, Estimation, and Control (vol. I)*. Academic Press, New York.
- Maybeck, P.S. (1982): *Stochastic Models, Estimation, and Control (vol. II)*. Academic Press, New York.
- McCarthy, D.D. (1996): IERS Conventions (1996). IERS Tech. Note 21, Observatoire de Paris, Paris.
- Meditch, J.S. (1973): A survey of data smoothing for linear and nonlinear dynamic systems. *Automatica*, **9**, 151–162.
- Meydan, T. (1997): Recent trends in linear and angular accelerometers. *Sensors and Actuators, A: Physical*, **59**(1–3), 43–50.
- Moritz, H. (1992): Geodetic Reference System 1980. *Bulletin Géodésique*, **66**(2), 187–192.
- Moritz, H. (1980): *Advanced Physical Geodesy*. H. Wichmann Verlag, Heidelberg.
- Moritz, H. and I.I. Mueller (1987): *Earth Rotation, Theory and Observation*. Ungar Pub. Co., New York.
- Morse, P.M. and H. Feschbach (1953): *Methods of Theoretical Physics*. McGraw-Hill Book Company, Inc., New York.
- Nerem, R.S., C. Jekeli, and W.M. Kaula (1995): Gravity Field Determination and Characteristics: Retrospective and Prospective. *Journal of Geophysical Research*, **100**(B8), 15053–15074.
- NIMA (1997): Department of Defense World Geodetic System 1984. Tech. Report TR-8350.2, third edition, National Imagery and Mapping Agency, Bethesda, MD.
- NGSP (1977): National Geodetic Satellite Program, Parts I and II. Report SP-365, Scientific and Technical Information Office, NASA, Washington, DC.
- Northrop Corporation, Electronics Division, 1986: Gravity Compensation for INS Demonstration Program, Volume 4—Operational Testing, Report No. AFWAL TR-85-1156, AF Wright Aeronautical Laboratories, Wright-Patterson AFB, Ohio.
- O'Donnell, C.F. (ed.) (1964): *Inertial Navigation, Analysis and Design*. McGraw-Hill Book Company, New York.
- Paik, H.J. (1996): Superconducting accelerometers, gravitational-wave transducers, and gravity gradiometers. In *SQUID Sensors: Fundamentals, Fabrication and Applications*, H. Weinstock (ed.), Kluwer Academic, Dordrecht, pp. 569–598.
- Papoulis, A. (1991): *Probability, Random Variables, and Stochastic Processes*. McGraw Hill, New York.
- Parkinson, B.W. and J.J. Spilker (eds.) (1996): *Global Positioning System: Theory and Application, Volumes I and II*. American Institute of Aeronautics and Astronautics, Inc., Washington, DC.
- Post, E.J. (1967): Sagnac effect. *Reviews of Modern Physics*, **39**(2), 475–493.
- Priestley, M.B. (1981): *Spectral Analysis and Time Series Analysis*. Academic Press, New York.
- Rauch, H.E., F. Tung, C.T. Striebel (1965): Maximum likelihood estimates of linear dynamic systems. *AIAA J.*, **3**, 1445–1450.
- Richtmyer, F.K., E.H. Kennard, and J.N. Cooper (1969): *Introduction to Modern Physics*. McGraw-Hill Book Company, New York.
- Rose, R.C. and R.A. Nash (1972): Direct recovery of deflections of the vertical using an inertial navigator. *IEEE Transactions on Geoscience and Electronics*, **GE-10**(2), 85–92.
- Sagnac, G. (1913): L'éther lumineux démontré par l'effet du vent relatif d'éther dans un interféromètre en rotation uniforme. *Compte-rendus de l'Académie des Sciences*, **95**, 708–710.

- Salychev, O.S. (1995): *Inertial Surveying: ITC Ltd. Experience*. Bauman MSTU Press, Moscow.
- Salychev, O.S. (1998): *Inertial Systems in Navigation and Geophysics*. Bauman MSTU Press, Moscow.
- Savage, P.G. (1978): Strapdown sensors. In: *Strapdown Inertial Systems*, AGARD Lecture Series 95, NATO, Neuilly-sur-Seine, France.
- Savet, P.H. (ed.) (1961): *Gyroscopes: Theory and Design*. McGraw-Hill Book Co., Inc., New York.
- Schaffrin, B. and E. Grafarend (1986): Generating classes of equivalent linear models by nuisance parameter elimination. *Manuscripta Geodaetica*, **11**, 262–271.
- Schwarz, K.P. (1980): Gravity field approximations using inertial survey systems. *The Canadian Surveyor*, **34**(4), 383–395.
- Schwarz, K.P. (1981): A comparison of models in inertial surveying. Proceedings of the Second International Symposium on Inertial Technology for Surveying and Geodesy, 1–5 June 1981, Banff, Canada, pp. 61–76.
- Schwarz, K.P. (1983): Inertial surveying and geodesy. *Reviews of Geophysics and Space Physics*, **21**(4), 878–890.
- Schwarz, K.P. (1985): A unified approach to post-mission processing of inertial data. *Bulletin Géodésique*, **59**, 33–54.
- Schwarz, K.P. and M. Gonthier (1981): Analysis of the heading sensitivity in the Litton Inertial Survey System. Proceedings of the Second International Symposium on Inertial Technology for Surveying and Geodesy, 1–5 June 1981, Banff, Canada, pp. 399–413.
- Schwarz, K.P. and D.A.G. Arden (1985): A comparison of adjustment and smoothing methods for inertial networks. Proceedings of Third International Symposium on Inertial Technology for Surveying and Geodesy, 16–20 September 1985, Banff, Canada, pp. 257–272.
- Schwarz, K.P., M.E. Cannon, and R.V.C. Wong (1989): A comparison of GPS kinematic models for the determination of position and velocity along a trajectory. *Manuscripta Geodaetica*, **14**, 345–353.
- Schwarz, K.P., O.L. Colombo, G. Hein, E.T. Knickmeyer (1992): Requirements for airborne vector gravimetry. Proc. IAG Symp., From Mars to Greenland: Charting Gravity with Space and Airborne Instruments, General Assembly of the IUGG, Vienna, 1991, Springer Verlag, New York, pp. 273–283.
- Schwarz, K.P., M.A. Chapman, M.W. Cannon, and P. Gong (1993): An integrated INS/GPS approach to the georeferencing of remotely sensed data. *Photogrammetric Engineering & Remote Sensing*, **59**(11), 1667–1674.
- Schwarz, K.P., J.M. Brozena, and G.W. Hein (eds.) (1995): Airborne Gravimetry. Proc. IAG Symp. on Airborne Gravity Field Determination, IUGG XXI General Assembly, Boulder CO, 2–14 July 1995.
- Schwarz, K.P. and Z. Li (1996): An introduction to airborne gravimetry and its boundary value problems. International Summer School of Theoretical Geodesy, Como, 26 May–7 June 1996.
- Seeber, G. (1993): *Satellite Geodesy*. Walter deGruyter & Co., Berlin.
- Sennott, J., I.S. Ahn, and D. Pietraszewski (1996): Marine Applications. In *Global Positioning System: Theory and Practice*, vol. II, by B.W. Parkinson and J.J. Spilker (eds.), pp. 303–325, American Institute of Aeronautics and Astronautics, Inc., Washington, DC.
- Shortley, G. and D. Williams (1971): *Elements of Physics*. Prentice-Hall, Inc., Englewood Cliffs, New Jersey.
- Schuler, H. (1923): Die Störung eines Pendels und eines Kreiselgerätes infolge Beschleunigung des Fahrzeugs. *Physikalische Zeitschrift*, Band 24, Kiel.

- Stieler, B and H. Winter (1982): *Gyroscopic Instruments and their Application to Flight Testing*. AGARD-AG-160, vol. 15, Advisory Group for Aerospace Research and Development, NATO, Neuilly sur Seine, France.
- Teunissen, P.J.G. (1998): GPS carrier phase ambiguity fixing concepts. In *GPS for Geodesy* (2nd ed.), by P.J.G. Teunissen and A. Kleusberg (eds.), pp. 319–388, Springer-Verlag, Berlin.
- Teunissen, P.J.G. and A. Kleusberg (eds.) (1998): *GPS for Geodesy* (2nd ed.). Springer-Verlag, Berlin.
- Thomson, W.T. (1960): *Laplace Transformation*. Prentice-Hall, Inc., Englewood, NJ.
- Todd, M.S. (1981): Rapid Geodetic Survey System (RGSS) White Sands tests for position, height, and the anomalous gravity vector components. Proc. Second International Symposium on Inertial Technology for Surveying and Geodesy, 1–5 June 1981, Banff, Canada, pp. 373–385.
- Torge, W. (1989): *Gravimetry*. Walter de Gruyter, Berlin.
- Torge, W. (1991): *Geodesy*, 2nd edition. Walter de Gruyter, Berlin.
- Tralli, D.M. and S.M. Lichten (1990): Stochastic estimation of tropospheric path delays in Global Positioning System geodetic measurements. *Bulletin Géodésique*, **64**(2), 127–159.
- Van Dierendonck, A.J. (1996): GPS receivers. In *Global Positioning System: Theory and Practice*, vol. I, by B.W. Parkinson and J.J. Spilker (eds.), pp. 329–407, American Institute of Aeronautics and Astronautics, Inc., Washington, DC.
- Vassiliou, A.A. and K.P. Schwarz (1987): Study of the High-Frequency Spectrum of the Anomalous Gravity Potential, *J. Geophys. Res.*, **92**(B1), 609–617.
- Walter, P.L. (1997): History of the accelerometer. *Sound and Vibration*, **31**(3), 16–22.
- Walter, P.L. (1999): Trends in accelerometer design for military and aerospace applications. *Sensors (Peterborough, NH)*, **16**(3), 44–51.
- Wei, M., and K.P. Schwarz (1995): Analysis of GPS-derived accelerations from airborne tests. In: *Airborne Gravimetry*, by K.P. Schwarz, J.M. Brozena, and G.W. Hein (eds.), Proceedings of IAG Symposium G4, XXI General Assembly of IUGG, pp. 175–188.
- Wilson, H.K. (1971): *Ordinary Differential Equations*. Addison-Wesley Pub. Co., Reading, MA.
- Yazdi, N., F. Ayazi, and K. Najafi (1998): Micromachined inertial sensors. *Proceedings of the IEEE*, **86**(8), 1640–1658.
- Zumberge, J.F., M.M. Watkins, and F.H. Webb (1998): Characteristics and applications of precise GPS clock solutions every 30 seconds. *Navigation, Journal of the Institute of Navigation*, **44**(4), 449–456.

# Index

- a posteriori
  - covariance 206
  - density 202–203
  - estimate 205
  - mean 205
- a priori
  - covariance 204
  - density 203
  - mean 204
- acceleration
  - centrifugal 127, 153, 186, 188, 321, 331
  - Coriolis 4, 53, 321
  - gravitational 3–4, 87–88, 141, 186, 320
  - kinematic 322, 328–330, 333, 335
- accelerometer 8, 51–53, 86, 240–241
  - bias 93, 99–100, 109, 144–145, 160–161, 181, 192, 229, 240, 243, 253–254, 298–300, 313, 322–325
  - bias stability 52
  - cryogenic 52
  - errors 99–100
  - force-rebalance 90, 94
  - frame 8
  - micro-machined 94
  - pendulous 90, 93–94
  - pendulous integrating gyro (PIGA) 94
  - scale factor 98–99
  - scale factor error 99–100, 106, 195, 299–300, 313, 330
  - scale factor stability 52
  - vibrating beam 96, 99
- accelerometry 322
- accumulated carrier phase observable 268
- aerial photogrammetry 307
- Aerial Profiling of Terrain System (APTS) 299
- a-frame 124, 148
- aircraft navigation 101
- aircraft rotations 12, 25–26
- algorithm error 118, 122, 137
- alignment 238–242
  - coarse 239–240, 243
  - fine 239–240, 243–244
- kinematic 252
- optical methods 239
- self- 246
- stored 239
- transfer 239
- ambiguity 268–269, 274–276, 280–281, 284–285, 292, 318–320
- modified 275–276, 279
- wide-lane 277
- angular momentum 54–56
- angular rate 19, 25, 53, 73
- angular velocity 19–20, 55, 57
- anisoelasticity error 64, 99
- anisoinertia error 63, 70
- anti-spoofing (AS) 263
- attitude and heading reference system (AHRS) 104
- attitude rates 27
- autoregressive model 184
- averaging operator 176
- axial vector 18–19
- axis
  - coordinate 1
  - input 51, 53, 56
  - output 51, 56, 59, 61
  - pendulous 91
  - pendulous reference 91
  - reference input 92
  - semi-major 23
  - semi-minor 23
  - spin 60
  - spin reference 56
- azimuth 110, 161, 239, 243, 246, 248
- wander 110, 131, 133
- backscattering 80
- bandwidth 265, 273
- Bayes' risk 200
- Bayes' rule 166, 198
- Bayesian approach 199
- bias
  - accelerometer 93, 99–100, 109, 144–145, 160–161, 181, 192, 229, 240, 243, 253–254, 298–300, 313, 322–325
  - clock 265, 273, 280

- bias (*Continued*)**
  - gyro drift 63, 65, 80, 86, 130, 146, 238, 243, 246, 248, 251–252, 254, 298–301, 313, 327
  - Faraday 80
  - frequency 79
  - magnetic 78–79
  - modulation 85
  - optical 79
  - phase 84
  - random 181, 223
  - receiver 279
  - sensor 113, 238, 243
  - stability 52, 79, 86
- b-frame** 8, 25, 112
- binary biphasic modulation** 262
- body frame** 8, 22, 26, 105, 112, 114, 122, 130, 134, 238, 242, 327–328
- Brillouin scattering** 81
- broadcast ephemeris** 263, 270
- Bureau International de l'Heure (BIH)** 260
- Bureau International des Poids et Mesures (BIPM)** 9, 260
- C/A code** 262–265, 267, 270
- calibration** 54, 64–65, 100, 113, 197, 238, 240, 243–244, 246
  - gyro error 161, 252
- carouseling** 134
- carrier phase** 268, 273
  - ambiguity 268–269, 274, 276, 285
  - ambiguity, wide-lane 277
  - error 269
- carrier signal** 258
- carrier wave** 261
- cascaded integration** 309
- center of mass, Earth** 5–6
- centralized processing** 309, 314–315, 317–318
- centrifugal acceleration** 127, 153, 186, 188, 321, 331
- characteristic polynomial** 36
- chips** 261
- clock** 259, 261, 268
  - error 261, 266, 268–270, 274, 284–285
  - receiver error 268–270, 275, 279, 288
  - satellite error 268–270, 275, 280, 290, 292
- closed loop** 61, 85–86, 302
  - estimation 225–226
  - operation 314
- code** 265
  - C/A 262–265, 267, 270
  - function 262
  - P 262–265, 267
  - sequence 261
  - W 263
  - Y 263
- commanded**
  - platform 107–111, 241
  - rate 109–111, 130, 132, 241
  - torque 61–63, 69–70, 91, 112
- commutativity error** 118
- complex exponential** 28
- complex number** 14–15
- coning error** 105, 118
- control input** 221
- control point** 302, 304
- control segment, GPS** 269
- controllability** 237
- Coordinated Universal Time (UTC)** 260
- coordinates**
  - axis 1
  - Cartesian 1–2, 6
  - curvilinear 2, 6
  - frame 2–3
  - geodetic 6
  - indicated 314
  - local 6
  - north-east-down (NED) 6, 25
  - rectangular 1
  - spherical polar 16
  - system 1–2
  - transformation 22
  - traverse 297
- Coriolis**
  - acceleration 4, 53, 321
  - law 21, 56, 90, 124
- correlation function** 173, 264
- correlation time** 174
- correlator** 265
- cost function** 200–201
- covariance** 168
- covariance function** 173, 233
  - auto- 175
  - cross- 175
  - empirical 193
- covariance matrix** 175, 207, 211, 302
  - auto- 170

- covariance matrix (*Continued*)  
 — cross- 170  
 cross-coupling error 63, 70  
 cross-variance 175  
 cycle 259, 269  
 — ambiguity 307, 316, 318, 319–320  
 — slip 269, 285, 294, 307, 318, 320
- data function 262  
 data message 262  
 decentralized processing 309–310, 312, 317–318  
 deflection of the vertical 157, 190, 327  
 delay lock feedback loop 265  
 differential equation 20, 31  
 — homogeneous 34  
 — linear 32–33  
 — matrix 37, 42  
 — numerical solution 44  
 — ordinary 31  
 — partial 31  
 — solution 33–34  
 — system 32, 45  
 dilution of precision (DOP) 290  
 — geometric (GDOP) 290, 309  
 — position (PDOP) 290  
 — time (TDOP) 290  
 Dirac delta function 178  
 direct sequence spread spectrum  
   communication 265  
 direction cosine 9–10, 15, 17–18  
 direction cosine matrix 11, 16  
 discretization 198  
 dispersive medium 271  
 disturbing potential 189  
 dither 79  
 double-difference 277  
 — phase 280, 293  
 — pseudorange 280, 293  
 drift bias, gyro 63, 65, 80, 86, 130, 146, 238, 243, 246, 248, 251–252, 254, 298–301, 313, 327  
 dynamical tuning 66  
 dynamics  
   — accelerometer 88, 93, 98  
   — navigation errors 147–148  
   — navigation system 125  
   — SDF gyroscope 59–60  
   — TDF gyroscope 69–70  
 dynamics model 139–140, 195, 198, 210, 220–221, 224, 233, 246–247, 253, 284–286, 297, 306, 313, 317, 323–324, 330, 332
- Earth-centered-Earth-fixed frame 6  
 Earth Gravity Model 1996  
   (EGM96) 191  
 Earth rotation 19, 53, 238, 240, 243, 246, 283  
 — rate 22, 186–187  
 eccentricity  
   — first 24, 188, 257  
   — second 132  
 e-frame 6, 22, 122, 126, 283  
 eigenvalue 36–38, 162  
 — multiplicity 39  
 eigenvector 36  
 ellipsoid 6–7, 22–25  
 — height 6  
 — normal 186  
 — normal to 157  
 embedded GPS/INS system 309  
 ensemble statistics 176  
 Eötvös correction 335  
 equipotential surface 186, 188–189  
 equivalence principle 87  
 ergodic process 176, 180  
 error  
   — estimation 197–198, 207–208, 225, 299–300, 312, 316  
   — clock 261  
   — GPS 269–270  
   — registration 328, 331, 335  
   — state 209, 225, 244, 246, 252–254, 285–287, 298–299, 313, 315–316, 323, 330  
 error dynamics equations 139–140, 220, 312  
 — e-frame 152  
 — i-frame 151  
 — n-frame 153  
 error dynamics model 195–196, 246–247, 253, 284–286, 313, 317, 323–324, 330, 332  
 error model 165, 172–173, 195, 301, 313  
 — accelerometer 99–100  
 — FOG 86  
 — RLG 80–81  
 — SDF gyro 64–65  
 — stochastic 179  
 — TDF gyro 70  
 estimability 276

- estimator 197, 202, 211
  - unbiased 198, 212, 214
- Euclidean system 3
- Euler angle 9, 11–13, 25, 114
- Euler equation 14, 56
- Euler method 48
- event 165
  - independent 166
- existence theorem 34
- expected value 168–170, 199–201
- external information (observation, control) 123, 139, 145, 166, 197–198, 209–210, 213, 225, 238–241, 243–244, 252, 295–300, 322, 330
- Faraday effect 79, 85
- Faraday rotator 79–80
- federated integration 309
- feedback 60–61, 85, 105, 130, 158, 241, 309
- filtering 198, 213
- Fisher information matrix 207, 236
- flattening 23
- flexure bars 66, 68
- force 87–88
- force-rebalance 90, 92–93, 95–96, 98
- forced harmonic oscillator 43
- forcing function 43
- Foucault oscillation 158, 163
- Fourier series 28
- Fourier transform 27, 29
- Fourier transform pair 29
- fractional phase 266, 268
- frame
  - arbitrary 124
  - body 112
  - gimbal 57
  - instrument 51
  - navigation 112
  - non-inertial 89
  - wander-azimuth 110, 131
- Fraser algorithm 216
- free-fall 5
- free-inertial dynamics matrix 156
- free-inertial navigation 123, 298, 311
- free spectral range 77
- frequency 28, 259
  - carrier 262
  - intermediate 264
- frequency lock-in 77–78
- fringe pattern 73, 76
- function
  - differentiable 31
  - forcing 43
  - periodic 27, 29, 35
  - scalar 31
  - vector 32, 49
- fundamental matrix 40
- fundamental set of solutions 39–40
- Galileo’s law of falling bodies 144, 328
- Gaussian mean radius 154
- Gaussian probability distribution 170–171, 199, 202–204, 208, 210
- Gauss-Markov model 182, 193–194, 298, 307, 316, 324–325, 330
  - first-order 183
  - second-order 184
  - third-order 184
- geodesy 3, 295–296
  - applications 295, 309–310
  - coordinates 23
  - datum 6
  - height 3
  - latitude 3, 6, 23, 128
  - longitude 3, 6, 23, 128
  - surveying 296, 306
- geodetic
  - reference system 6
- Geodetic Reference System 1980 (GRS80) 24, 187
- geoid 6
  - undulation 186
- g-frame 57
- gimbal 56–58, 62, 65–66, 91, 95, 105
  - angle 59–63, 66, 69, 105
  - dynamics 59
  - frame 57
- gimbal/rotor assembly 57, 63, 67, 70
- gimbaled platform 54, 62, 105, 240, 252
- gimbaled system 8, 299
- Global Orbiting Navigation Satellite System (GLONASS) 255, 262
- Global Positioning System (GPS) 255–59, 296, 306
  - characteristics 308
- gravimeter 86, 321, 334
- gravimetry 54, 296, 321
  - airborne 323
  - approaches 322

- gravimetry, moving-base 320–321, 334
  - relative 321
  - scalar 322, 334
  - static 321
  - vector 321–322, 326–327
  - vertical 321, 327
- gravitation 5, 127
  - gravitational
    - acceleration 3–4, 87–88, 141, 186, 321
    - disturbance vector 148
    - gradient 142
    - mass 4
    - vector 4
  - gravity 127, 147, 153, 160, 186, 238, 240, 242
    - disturbance 153, 316, 322–323, 325–327, 333
    - disturbance vector 189, 194
    - gradient 153, 157, 335
    - signal 321, 334
    - vector 323
- Gravity Recovery and Climate Experiment (GRACE) 283
- group velocity 271
- gyrocompassing 107, 241
  - accelerometer-coupled 241
  - gyroscope (gyro) 8, 51–53, 241
    - calibration 64–65, 161, 243–244, 246, 252
    - differential laser 79
    - dry 62
    - dry, tuned 65
    - error 63–65, 70, 73, 77, 80, 85, 161
    - error model 64–65, 70, 80–81, 86
    - fiber-optic (FOG) 81
    - floated 62
    - frame 8
    - interferometric fiber-optic 81
    - mechanical 54
    - multioscillator RLG 79
    - optical 70
    - rate 61–62
    - rate-integrating 62–63, 105
    - ring laser (RLG) 73
    - scale factor 62, 80, 83
    - scale factor error 63–65, 80, 86, 195
    - scale factor stability 52, 85–86
    - single-degree-of-freedom (SDF) 56
    - tuned, two-degree-of-freedom 67
  - two-degree-of-freedom (TDF) 65–67
  - zero-lock 80
- Hamilton 14
- harmonic oscillator 43, 108
- height
  - ellipsoid 6, 128, 188
  - error 162, 306
  - geoid 186
- homogeneous solution 34–35, 143
- Hooke's law 88
- i-frame 5, 22, 51, 122, 126
- imaginary unit 14
- index of refraction 267, 270, 272
- inertia tensor 54–55
- inertial
  - frame 3–5, 55
  - guidance 104
  - navigation 7, 9, 51–54, 62, 106, 148, 238, 240
    - navigation, free 123, 192, 298, 311
    - navigation, horizontal 107, 109, 189
    - navigation, vertical 145, 161
  - sensors 52
  - system 3–4
- inertial measurement unit (IMU) 4, 18, 51–53, 101, 238, 298
- inertial navigation system (INS) 3, 8, 27, 31, 51, 53, 101–104, 123, 139, 182, 192, 197, 223, 240, 257, 259, 269, 295–296, 287, 334
  - accuracy 102
  - characteristics 308
  - Inertial Positioning System (IPS) 298
  - inertial surveying system 297, 306, 322
  - Inertial Surveying System (ISS) 298
  - initial conditions 34, 121, 238
  - initialization 107, 121, 197, 238–240
  - innovation 214
  - input axis 51, 91
  - instrument frame 9
  - integration
    - GPS/INS 306–308, 310, 320
    - loosely coupled 309, 312
    - tightly coupled 309, 314
    - uncoupled 309–310
  - integration algorithm
    - functions 50
    - INS/GPS 311, 314

- integration algorithm (*Continued*)
  - navigation 134
  - quaternions 114
- integration modes 308
- International Atomic Time (TAI) 260
- International Celestial Reference System (ICRS) 5
- International Earth Rotation Service (IERS) 5
- International GPS Service (IGS) 270, 281
- International Terrestrial Reference Frame (IRTF) 6
- International Terrestrial Reference System (ITRS) 5–6
- inverse Fourier transform 29
- ionosphere 266, 270–272, 274
- ionospheric delay 275, 285, 316
- isotropy 193, 195
- Joseph form 206, 219
- Kalman filter 61, 199, 215, 223, 240, 244, 284, 298–300, 323, 325, 330
  - augmented 314
  - continuous 230, 233, 245
  - discrete 210
  - extended 225
  - inverse covariance 217
  - square-root formulation 215
- Kalman gain matrix 214
- Kalman-Bucy filter 231
- Kerr effect 79, 85
- kinematic forces 4
- L-band 262
- L1 carrier frequency 262
- L2 carrier frequency 262
- Langmuir flow 77
- Laplace transform 35
- laser 73, 77, 81
- Law of Coriolis 21, 56, 90, 124
- law of conservation of angular momentum 4, 55
- laws of motion 3, 51, 86, 96, 320
- least-squares
  - adjustment 284, 300, 304, 333
  - collocation 193
  - estimate 203, 206
- lever-arm 55
  - effect 90, 329, 335
- likelihood function 203
- linear momentum 3
- linear variance equation 233–234
- lock-in range 79
- magnetic bias 78–79
- marine navigation 101
- Markovian property 184, 208
- mass unbalance 64–65
- matrix identity 303
- maximum a posteriori estimate 202
- maximum likelihood estimate 203
- mechanization 101, 104
  - local-level stabilized 106–107, 109, 113, 159–160
  - local-level stabilized, north-slaved 107, 110, 241
  - local-level stabilized, wander-azimuth 107, 110
  - space-stabilized 106
  - stabilized 101, 104
  - stabilized platform 238, 252
  - strapdown 54, 62, 101, 104, 112–113, 118, 161, 238–239, 241, 243, 253
  - wander-azimuth 241
- micro-machining 52
- milligal (mgal) 195
- minimum mean square error 201, 213
- misalignment 64, 79, 100, 109, 143, 241, 298–299
- mixing, signal 263
- mobile mapping system 308
- modified Bryson-Frazier algorithm 220
- moments of inertia 55, 63
- most probable estimate 201
- multipath 259, 265, 267–268, 273
- NAVSTAR 256
- navigation 1, 3, 6, 7, 52, 282, 296
  - equations 123, 131, 139
  - equations, solution 134
  - frame 6–8, 18, 124, 126, 239, 241
  - inertial 7, 9, 51–54, 62, 106, 148, 238, 240
  - message 262, 265, 269
  - satellite 101, 255–256
- National Imagery and Mapping Agency 306
- Newton, Isaac 3
  - first law of motion 3, 5

- Newton, Isaac (*Continued*)  
 — gravitational constant 4  
 — law of gravitation 4  
 — laws of motion 3, 51, 86, 96, 320  
 — second law of motion 3, 4, 88  
 n-frame 7, 25, 107, 110, 112, 126, 253  
 noise  
 — time-correlated 224  
 — white 22, 177, 199, 208, 231  
 non-reciprocity error 77, 85  
 normal  
 — ellipsoid 186  
 — gravity 188–189  
 — gravity field 186–187  
 — probability distribution 170–171, 199, 202–204, 208, 210  
 north-east-down (NED) 6, 25  
 nuisance parameters 274, 284  
 numerical integration 50, 114, 134  
 numerical integrator 118, 122, 134  
 observability 225, 237, 246  
 observation 166, 197–198, 284, 287, 303–304  
 — acceleration 244, 327  
 — azimuth 246–248, 251  
 — combination 273  
 — continuous 231, 245  
 — covariance 204, 207, 211, 214, 223–224, 231, 237, 254, 289, 291–293, 317, 332  
 — difference 268, 276, 278  
 — double-difference 280  
 — external 209–210, 213, 225, 238, 244–246, 299, 301, 303  
 — GPS 252, 266, 274  
 — ionosphere-free 277  
 — matrix of partial derivatives 209, 245, 248, 287, 302, 317, 325, 331  
 — single-difference, between-satellite 279  
 — update 210, 213, 215–216, 223, 225, 233, 299–300, 310, 325–326, 331  
 — velocity 246–249, 252  
 on-the-fly (OTF) algorithm 285, 316, 318  
 open-loop 98  
 — estimation 227  
 optical bias 79  
 optical path 73, 75, 77, 79–80, 85  
 orientation error 240, 244–246, 249, 251–252, 254, 301, 323, 335  
 orthogonal projection 1, 10  
 orthogonal transformation 11, 18  
 oscillator 259  
 — receiver 264  
 output axis 51, 91  
 — equation 60  
 — rotation error 63, 70  
 parameter  
 — deterministic 172–173, 193  
 — ellipsoid 6, 24  
 — estimate 206, 276, 300, 302–303, 332–333  
 — Gauss-Markov model 183–185, 193, 324–325  
 — normal gravity field 186–188  
 — nuisance 274, 284  
 — random (stochastic) 207, 272–273, 324  
 — variation of 40–41, 221  
 particular solution 34, 40–41, 143  
 path lengthening 71  
 path shortening 72  
 P-code 262–264, 267  
 pendulosity 93  
 pendulous axis 91  
 pendulous reference axis 91  
 pendulum 99  
 phase 259  
 — ambiguity 268–269, 274–275, 280–281, 284–285, 292, 318–320  
 — ambiguity, modified 275–276, 279  
 — biasing 84  
 — double-difference 280, 294, 319  
 — double-difference, wide-lane 293, 317  
 — fiber-optic gyro 81, 83–85  
 — ion-free 277, 290–291, 294  
 — modulator (modulation) 84–85, 261–262, 264  
 — nulling 85  
 — observable 268–269, 274, 277, 284, 319  
 — offset 268, 274–275, 280  
 — refractive index 271  
 — ring laser gyro 73, 76, 79–80  
 — signal generator 261, 268  
 — single-difference, between-satellite 279, 290–291  
 — time 261, 268  
 — velocity 271  
 — wide-lane 277, 293, 319  
 — wide-lane, ion-free 278, 281

- phase lock loop 266, 268–269, 273
- photon shot noise 85
- pitch 25, 240
- platform frame 9, 109– 110, 241
- polarized beams 80
- Position and Azimuth Determination System (PADS) 297-299
- positioning 3, 53-54, 123, 153, 296
  - absolute 274, 288
  - absolute kinematic 282
    - aiding 296, 307, 309
  - differential 274
  - inertial 322-323
  - kinematic 282, 284, 290, 307, 309, 319
    - point 274
  - relative 257, 274
    - relative kinematic 283, 292
  - semi-kinematic 282
  - static 282, 284
- power spectral density 175
- precession 5, 60
- prediction 198, 210, 212-213
- principal axes of inertia 55
- principle of equivalence 4-5
- probability 165-167
  - conditional 166
  - probability density function 166
    - conditional 167
  - conditional moments 169
  - joint 167
    - marginal 167
  - moments 168
- probability distribution function 167
- Gaussian (normal) 170-171, 199, 202-204, 208, 210
- products of inertia 55
- proof mass 56, 87, 94, 99
- pseudorandom noise (PRN) 264
- pseudorange 265-267
  - double-difference 280, 293
  - intermediate 275, 279
  - ion-free 277, 279, 281, 290
  - observable 267, 273-274, 288-289
    - single-difference, between-satellite 278-279
- quantization error 77
- quasi-inertial frame 5
- quaternion 9, 13, 15-18, 21, 27, 114, 117-123
- radio navigation system 255
- radius of curvature 23, 154, 158
- random constant 180
- random (stochastic) variable 165-166, 172
  - independent 167
  - uncorrelated 169
  - vector 169
- random walk 181
- range 267, 283
- Rapid Geodetic Survey System (RGSS) 299, 305
- Rayleigh** scattering 85
- reaction force 5, 89-90
- reaction torque 9 1-92
- realization
  - event 165
  - stochastic process 172, 176, 179-181, 193
  - system 2
- rebalance loop 61-64, 66, 85-86
- receiver
  - clock error 268-270, 275, 279, 288
  - GPS 263, 269
    - noise 273
- reference input axis 92
- refractive index 270
  - group 271
  - phase 271
- relative positioning 257, 274
- residual 332-333
- Riccati equation 234-236, 245, 248, 254
- ring resonator 73
- roll 25, 240
- rotation matrix 12
- rotation vector 16
- rotational transformation 19-20
- rotor 56, 66
  - spin axis 56, 58-60, 63-64, 67
  - spin rate 58
- rotor/gimbal assembly 57, 63, 67, 70
- RTS (**Rauch**, Tung, Striebel)
  - algorithm 216, 219
- Runge-Kutta method 45-46, 114, 118
  - fourth-order 49
- Sagnac effect 51, 70, 73-74, 81
- sample space 165
- satellite clock 266, 269-270
  - error 263, 265, 268, 275, 280, 290, 292
- satellite geometry 256, 290

- satellite-based navigation system 101, 255–256
- scale factor 80, 83, 98–99
  - error 63–65, 80, 86, 99–100, 106, 195, 223, 298–300, 313, 330
  - stability 52, 85–86
- torquer 62
- Schuler
  - feedback loop 113, 130, 158, 163–164
  - frequency 108–109, 143, 147, 163, 301
  - period 109, 161
  - tuning 107, 130, 149, 298
- sculling error 105, 137
- Selective Availability (SA) 270, 281
- semi-major axis 23
- semi-minor axis 23
- sensor frame 8, 148, 158
- servo motors 61–62, 95, 105, 107, 109–110, 112–113, 118, 240
- signal
  - generator 56
  - GPS 261, 263
  - modulation 264
  - shadowing 258, 307
  - wide-lane 277
- signal-to-noise ratio 273
- Simpson's rule 50
- single-step method 44
- skew symmetric matrix 13
- small-angle rotation 19
- smoothing 198, 215, 299–300, 304, 314
  - fixed-interval 216, 220
  - fixed-lag 216
  - fixed-point 216, 220
- specific force 5, 88
- spectral density 30
- spectrum 28, 30
- speed of light 262, 271
- spherical harmonic series 191
- spin axis
  - Earth 5–6
  - rotor 56, 58–60, 63–64, 67
- stabilization
  - local-level 54, 70, 106–107, 109, 113, 159–160
  - local-level, north-slaved 107, 110, 241
  - local-level, wander-azimuth 107, 110
  - space 106, 110
- stabilized platform 62, 105, 238, 240, 252
- stable element 105
- standard deviation 168
- state 197, 210, 240, 254, 298
  - augmented 223
  - error 330
  - system 284
  - transition matrix 210, 212, 219, 221, 228, 236–237, 245, 248, 285–286
- stationary process 173–177, 180, 182–183, 221
- gravity 193
- stellar camera 327
- stochastic model 165, 326
- stochastic process 172
  - gravity 192–193
- strapdown mechanization 8, 54, 62, 70, 101, 104–105, 112–113, 118, 161, 238–239, 241, 243, 253
- system error 106, 139, 155, 197–198, 220, 297–300, 302–303, 323
- system error dynamics 106, 139, 220, 223
- test survey 305–306
- tilt error 109, 113, 146, 157, 159–161, 163–164, 298, 325
- time 259
  - atomic 260
  - dynamic 5
  - GPS 260
  - indicated 260, 268
  - true 260
- torque 54–55
  - applied 60–61
  - commanded 61–63, 69–70, 91, 112
  - damping 62, 92
  - error 61
  - pendulous 95
  - reaction 61
  - rebalance 61–62, 69, 91, 93, 99
  - scale factor 62
- torque generator 56, 109
- torque rebalance loop 61–64, 69–70, 85
- total electron content (TEC) 271–272
- tracking loop 264, 266, 268
- transformation 3, 9, 20
  - b-frame to n-frame 25
  - i-frame to e-frame 23
  - n-frame to e-frame 25
  - orthogonal 11, 18
  - rotational 19–20
- transformation matrix 11–12, 21, 114

- transit time 267, 289
- transition matrix 40, 43, 210, 212, 219, 221, 228, 236–237, 245, 248, 285–286
- troposphere 270, 272
- tropospheric effect 259, 266, 272
- U.S. Army Engineer Topographic Laboratories (USAETL) 297
- U.S. Defense Mapping Agency 298
- unbiased 198, 212, 214
- uniqueness theorem 34
- unit vector 1, 11
- update 210, 213, 215, 223, 225–226, 230, 233–234, 306, 309
  - acceleration 330–331
  - backward 217
  - coordinates 313–314, 325
  - velocity/position 296–297, 326
  - zero-velocity 298–299, 306, 326–327
- variance 168, 176, 197
  - conditional 169
  - cross- 175
  - Gauss-Markov process 183–185
  - gravity disturbance 193–194
  - Normal distribution 171
  - random constant 180
  - random walk 182
  - stationary process 173–174
  - white noise 177–179
- variation of parameters 40–41, 221
- velocity 7
  - Vening-Meinesz equations 192
  - vertical channel 130, 298
    - damping 145, 315
  - vibrating
    - element 51, 86, 96
- beam accelerometer 96, 99
- string 96–98
- vibropendulous error 93, 99
- wander azimuth 110, 131, 133
- wavelength 28, 97
  - C/A code 262–263, 265, 273
  - carrier signal 258, 288
  - data message 262, 265
  - errors 308
  - light 73
  - P-code 262–263, 265, 273
  - wide-lane signal 277
- wavenumber 28
- W-code 263
- w-frame 110, 131, 242
- white noise 22, 177, 199, 208, 210–211, 222–223, 285
  - accelerometer 100, 195–196, 244, 313
  - approximation 183
  - covariance 178, 231
  - discrete 179, 231
  - Gaussian 179, 182–183
  - gyro 64, 80, 195–196, 313
  - variance 177–179
- Wiener (Brownian-motion) process 182
- World Geodetic System 1984
  - (WGS84) 24
- yaw 25
- Y-code 263
- zero-lock gyro 80
- zero-velocity assumption 157–158, 162
- zero-velocity update (ZUPT) 298–299, 306, 326–327
- Z-tracking 263